Flood and Megaflood Processes and Deposits: Recent and Ancient Examples

Special Publication Number 32 of the
International Association of Sedimentologists
Edited by I. Peter Martini, Victor R. Baker and Guillermina Garzón
and published by Blackwell Science

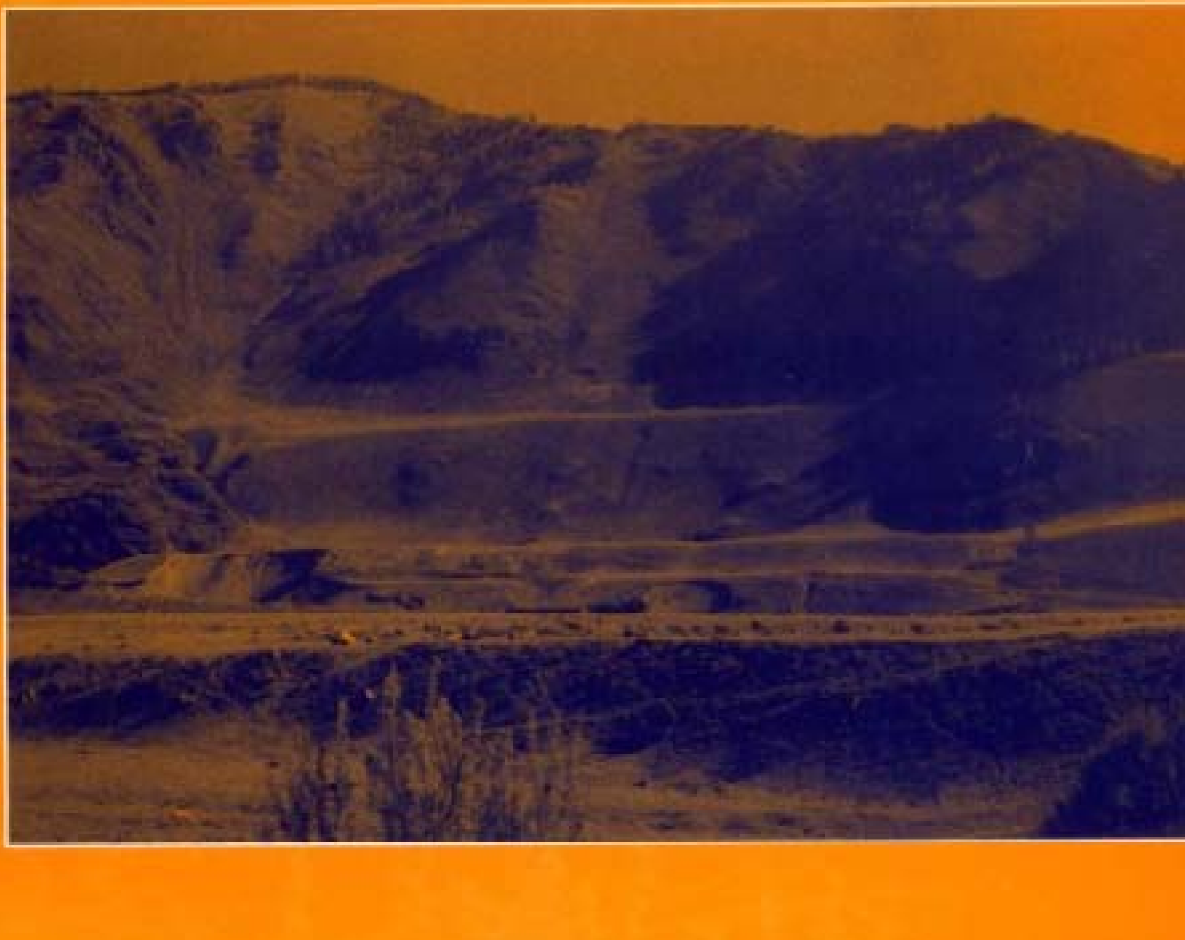

FLOOD AND MEGAFLOOD PROCESSES AND DEPOSITS: RECENT AND ANCIENT EXAMPLES

Flood and Megaflood Processes and Deposits: Recent and Ancient Examples. Edited by I. Peter Martini, Victor R. Baker and Guillermina Garzón © 2002 International Association of Sedimentologists. ISBN: 978-0-632-06404-5

SPECIAL PUBLICATION NUMBER 32 OF THE
INTERNATIONAL ASSOCIATION OF SEDIMENTOLOGISTS

Flood and Megaflood Processes and Deposits: Recent and Ancient Examples

EDITED BY
I. PETER MARTINI, VICTOR R. BAKER
AND GUILLERMINA GARZÓN

Blackwell
Science

Blackwell Science Ltd
Editorial Offices:
Osney Mead, Oxford OX2 0EL
25 John Street, London WC1N 2BS
23 Ainslie Place, Edinburgh EH3 6AJ
350 Main Street, Malden
MA 02148-5018, USA
54 University Street, Carlton
Victoria 3053, Australia
10, rue Casimir Delavigne
75006 Paris, France

Other Editorial Offices:
Blackwell Wissenschafts-Verlag GmbH
Kurfürstendamm 57
10707 Berlin, Germany

Blackwell Science KK
MG Kodenmacho Building
7–10 Kodenmacho Nihombashi
Chuo-ku, Tokyo 104, Japan

Iowa State University Press
A Blackwell Science Company
2121 S. State Avenue
Ames, Iowa 50014-8300, USA

First published 2002

Set by Graphicraft Limited, Hong Kong
Printed and bound in Great Britain
by MPG Books Ltd, Bodmin, Cornwall

DISTRIBUTORS

Marston Book Services Ltd
PO Box 269
Abingdon, Oxon OX14 4YN
(*Orders*: Tel: 01235 465500
Fax: 01235 465555)

The Americas
Blackwell Publishing
c/o AIDC
PO Box 20
50 Winter Sport Lane
Williston, VT 05495-0020
(*Orders*: Tel: 800 216 2522
Fax: 802 864 7626)

Australia
Blackwell Science Pty Ltd
54 University Street
Carlton, Victoria 3053
(*Orders*: Tel: 3 9347 0300
Fax: 3 9347 5001)

A catalogue record for this title is available from the British Library

ISBN 0-632-06404-8

Library of Congress
Cataloging-in-Publication Data

Flood and megaflood processes and deposits: recent and ancient examples/edited by I. Peter Martini, Victor R. Baker & Guillermina Garzón.
p. cm. —
(Special publication number 32 of the International Association of Sedimentologists)
ISBN 0-632-06404-8
1. Floods. 2. Sedimentation and deposition.
I. Martini, I. P. (Ireneo Peter), 1935– II. Baker, Victor R.
III. Garzón, G. (Guillermina)
IV. Special publication . . . of the International Association of Sedimentologists; no. 32.

GB1399 .F54 2001
551.48′9—dc21

2001035125

For further information on Blackwell Science, visit our website:
www.blackwell-science.com

Contents

Preface

This special publication consists of 17 papers, some delivered at the homonymous symposium held during the IAS 15th International Sedimentological Congress in southern Spain in 1998, and others submitted specifically for this publication. The goal of the symposium and of this publication is the understanding of large floods and their impact on the Earth's surface. The major objectives are:

1 to take a second look at what constitutes a megaflood that the principle of uniformitarianism is at some loss to explain;

2 try to determine what could happen in such large floods by analysing those that occur in front of glaciers, in alluvial-fans and in alluvial valleys.

In so doing, the products of such floods are presented in terms of sedimentary deposits, erosional features and damage to human activities. For convenience, the papers are included under the headings of (1) megafloods, (2) glacial outwash floods, (3) alluvial-fan floods, (4) alluvial valley floods and (5) special cases.

1 The megaflood section includes a general perspective paper followed by two others dealing with the account and the effects of megafloods, one in Siberia where the record is primarily a sedimentary one consisting mainly of very large (100 m high) side-valley bars, and one in northern Iceland where the record is primarily the downcutting of a deep narrow gorge.

2 The glacial outwash floods section contains three papers analysing the events and the deposits of the 1996 large meltwater flood in southern Iceland in some detail. A similar event and related deposits have been recorded from the South Island of New Zealand and they are reported here in a fourth paper.

3 Alluvial-fan floods are analysed in the third section, first in two papers dealing with recent cases in California and the Italian Alps: the events are described and the resulting depositional facies are presented. Two other papers dealing with ancient deposits in Italy and Spain take the opposite approach: from analysis of depositional facies, the possible flood and sedimentary gravity-flow events have been reconstructed. Both approaches—study of the recent and of the ancient—have intrinsic validity and also are valuable in assessing risk and hazards of floods and debris-flow-prone areas.

4 The alluvial valley floods papers of the fourth section deal with a variety of subjects, ranging from floods induced by spills from a hydroelectric reservoir in distal reaches of a subarctic river, to the effects of changing climate and human interference on rivers in Spain and The Netherlands. Another paper presents a remote sensing method for monitoring floods and their effect, utilizing images taken either during the flood itself and/or soon after.

5 Finally the special cases section may at first appear a bit odd for a sedimentological publication, because sediments *per se* are not described. However, one paper deals with potential reasons for a scanty sedimentary record in an area where it ought to have been abundant. This is explained not so much by erosion but by the uneven sedimentation of floods in ephemeral streams that may have developed in front of an unstable Pleistocene glacier terminus in Germany. The second paper presents a good description of an area of the Himalayas in front of the Tibetan plateau where meltwater and monsoon-rain floods have occurred and are recorded in some deposits, but, perhaps more novel, also where megafloods are likely to have occurred during deglaciation, and have eroded high-altitude regions and covered the lower lands with thick deposits.

The editors would like to thank the many reviewers of the papers. In most cases, their efforts went beyond the normal task of trying to improve the various contributions. We thank the authors themselves who, most of the time, graciously accepted and responded positively to the criticisms of the reviewers and the picky editors. The final reading by Guy Plint helped considerably in removing the last inconsistencies, particularly from the figures. This project has taken a long time to complete, some authors having their papers finalized in the first year, some last week. This, however, is the nature of special publications. We hope that this collection of papers serves not only as a record of what has been done and thought, but also as a source of ideas on how and where to work to advance sedimentology and the field of environmental science. There is indeed a great potential for sedimentological contribution to the safe settlement of troubled lands.

I.P. MARTINI
University of Guelph, Canada
V.R. BAKER
University of Arizona, USA
G. GARZÓN
Univ. Complutense, Madrid, Spain

Plate 2. Photograph of sediment plume into the Canterbury Bight (Pacific Ocean) and breaching of the gravel beach, Rangitata River, 10 January 1994. The normal exit channel for the river (under equilibrium conditions) is to the left and out of view, landward of the barrier beach. A small fishing community occurs at the right (south bank of the river) for scale. (Photograph by John Bisset, The Timaru Herald.)

Plate 3. Mouth of the Ashburton River under normal flow (equilibrium) conditions. The mouth of the river is deflected north, landward of the gravel barrier beach. The beach is formed by strong north-directed longshore drift. (Photograph by L. Homer, Landscape Photographer—Lloyd Homer Ltd.)

Flood and Megaflood Processes and Deposits: Recent and Ancient Examples. Edited by I. Peter Martini, Victor R. Baker and Guillermina Garzón © 2002 International Association of Sedimentologists. ISBN: 978-0-632-06404-5

(A)

(B)

Plate 1. The Rangitata River at Arundel Bridge (see Fig. 1), under (A) normal flow conditions (discharge approximately 100 cumecs) and (B) during the January 1994 flood event. Discharge peaked at 2640 cumecs during the 1994 flood. Note the rip-rap blocks on the true right bank as a reference point in both photographs.

Megafloods

Flood and Megaflood Processes and Deposits: Recent and Ancient Examples. Edited by I. Peter Martini, Victor R. Baker
and Guillermina Garzón © 2002 International Association of Sedimentologists. ISBN: 978-0-632-06404-5

Spec. Publs int. Ass. Sediment. (2002) **32**, 3–15

High-energy megafloods: planetary settings and sedimentary dynamics

V. R. BAKER

Department of Hydrology and Water Resources, University of Arizona, Tucson, AZ 85721–0011, USA
(Email: baker@hwr.arizona.edu)

ABSTRACT

High-energy megafloods usually occur in relatively narrow and deep, confined reaches supplied by large volumes of water. Examples of planetary settings include modern and ancient glacial outburst floods (jökulhlaups) of Iceland, glacial lake spillways south of the Pleistocene Laurentide Ice Sheet, the Channeled Scabland of the north-western USA, mountain lake bursts from central Asia, spillways connecting Pleistocene lake basins in Asia, and the immense outflow channels of Mars. The palaeohydraulic analyses of all these floods indicate that they generate values of stream power per unit area (> 10^3 W m^{-2}) and bed shear stress (> 10^3 N m^{-2}) that are two orders of magnitude larger than are typical for floods on large alluvial rivers such as the Amazon and Mississippi. Flood discharges can be comparable to flows in ocean currents, indicating important short-term roles in planetary water and sediment fluxes.

Significant sedimentary processes in the confined reaches for megafloods include streamlining (and related bar formation), scour around obstacles and giant current ripple (dune) formation. Sediment transport involves the entrainment of large boulders and phenomenally high loading of the flow with extremely coarse suspended and wash load. The outflux of high-energy, sediment-charged megafloods from confined continental settings to ocean basins results in hyperpycnal flows, and unusually powerful turbidity currents. These have been documented recently for the Pleistocene Missoula floods that formed the Channeled Scabland. They also were probably very important for the Martian outflow channel floods, which may have exerted the primary trigger for climatic change during Mars' geological history.

INTRODUCTION

Geologists have long applied a pragmatic method of studying modern Earth processes and their effects for the purpose of understanding unobservable past processes. Although this actualism serves as a most useful tool, it can be abused when enshrined as an epistemological or substantive principle (Baker, 1998). Nature is not obligated to display uniformity of process such that the meagre time sample of the present will adequately represent the rare, great cataclysmic processes of the past. There is also a very practical reason to study evidence of the processes and effects of the greatest ancient cataclysmic flood processes. The modern record affords ample opportunities to study frequent, small-scale flood processes that can be sampled over relatively short time periods (Baker, 1988). These processes are measured with instruments, samples taken, and generalizations made. However, cataclysmic processes occur with energy levels so great that instruments are destroyed, and sampling becomes impossible. These more rare processes do, nevertheless, determine much of the geological record (Ager, 1993), and they may cause great damage to human constructions. Does one understand them solely by upward extrapolation from measurements made on processes of far lower intensity and smaller scale? Any such extrapolation can be hypothetical only; to be scientific, hypotheses must be tested. Because direct testing is impractical, actualism leads to a dilemma.

Fortunately, rare, great cataclysmic processes generate long-lasting impacts on landscapes and sediments. By analysing these impacts in physical terms, one can reconstruct the causative processes (Baker, 1996a). The scale of the processes and the quality of the recorded indicators may be such as to afford

Flood and Megaflood Processes and Deposits: Recent and Ancient Examples. Edited by I. Peter Martini, Victor R. Baker and Guillermina Garzón ISBN: 978-0-632-06404-5

considerable accuracy. One can compare the results to upward extrapolations from the small-scale measured processes, thereby testing the process generalizations.

The above strategy is now being realized in the scientific study of cataclysmic megafloods. Rare, high-discharge floods in narrow, deep bedrock channels generate remarkably high values of bed shear stress and stream power per unit area (Baker & Costa, 1987; Baker & Kochel, 1988; Baker & Kale, 1998). When applied for sufficient duration (Costa & O'Connor, 1995) these conditions contribute to spectacular work of erosion and sediment transport. In contrast, even the largest alluvial rivers, such as the Amazon, produce stream power per unit area values of about 10 W m^{-2} and bed shear stress values of 10 N m^{-2} or less. The floods of interest in this paper generally will have power and stress values two or more orders of magnitude larger than those of floods in the Amazon, Mississippi, and similar large rivers. Thus, it is important to recognize that high-energy megafloods comprise a class of phenomena very different than the flooding described in much of the process literature.

PLANETARY SETTINGS

The largest known terrestrial floods are associated with glaciation (Baker, 1996b). These floods exerted major short-term influences on global fluxes of water and sediment (Baker, 1994). Much of the evidence for the past occurrences of such megafloods is erosional, developed from studies such as those in the Channeled Scabland and the north-western USA (Bretz, 1928; Bretz *et al*., 1956; Baker, 1973a,b). However, recent work has tied the influence of megafloods to sedimentation in nearby marine basins. Also, evidence for the largest known megafloods and their deposits has now been documented for Mars. The following examples illustrate the variety of high-energy megaflood settings.

Iceland

Iceland constitutes a largely volcanic plateau lying just south of the Arctic Circle on a broad rise of the North Atlantic sea floor between Greenland and Europe. Active volcanic rifts, extensions of the Mid-Atlantic Ridge, bisect the island. These are flanked by large shield volcanoes, several of which are capped by ice sheets ('jökull' in Icelandic). Europe's largest glacier, Vatnajökull, occurs in this setting near the south-east coast of the island. Like other Icelandic glaciers, it is subject to the episodic release of immense amounts of stored water through catastrophic outburst floods. The 4–5 November 1996 outburst ('jökulhlaup' in Icelandic) was generated from meltwater stored at the Grimsvötn subglacial volcano. The outburst released about 3.4 km^3 water at a peak flow of 52 000 m^3 s^{-1}, which is typical for large jökulhlaups from this source (Gudmundsson *et al*., 1995). The Vatnajökull outbursts move about 50 km beneath ice from Grimsvötn to surface at Skeiðarársandur, where they produce an extensive complex of fan deposits (Russell and Knudsen, this volume, pp. 67–83) prior to entering the North Atlantic.

The largest historical jökulhlaup is that of 12 October 1918, produced when about 0.5 km^3 of magma surfaced in the 10-km diameter Katla caldera of south central Iceland (Tómasson, 1996). Several cubic kilometres of water and ice were transported by the outburst below Mydalsjökull, at a peak discharge of about 300 000 m^3 s^{-1} (Tómasson, 1996). The sedimentology of the sandur deposits generated by this flooding is discussed by Maizels (1989, 1993), who estimates the Katla flood peak at 1.5×10^6 m^3 s^{-1} (Maizels, 1995).

An extremely large palaeoflood was generated from the northern margin of Vatnajökull between 2500 and 2000 yr ago, following Jökulsá á Fjöllum. Peaking at 0.7×10^6 m^3 s^{-1}, this flood produced scabland-like features, including large gravel bars, giant current ripples and huge water-transported boulders (Waitt, this volume, pp. 37–51). Much larger floods may have been generated at full-glacial time, when extensive ice sheets covered nearly all of Iceland. In the Iceland Basin of the sea floor, 500 km south of Iceland, a large submarine fan complex consists of turbidites rich in volcanoclastic glass shards derived from Iceland (Haraldur Sigurdssen, personal communication, 2000). H. Sigurdssen (personal communication, 2000) interprets the turbidites to indicate jökulhlaup sources at least an order of magnitude more energetic than those of today.

North America

The late-glacial sedimentary environments of North America were dominated by the influence of the Laurentide Ice Sheet. The weight of this great ice dome produced topographic sags that filled with meltwater, especially along the southern ice-margin. As water levels rose in these marginal sags, the lakes overspilled, and outburst floods eroded prominent spillways (Kehew & Teller, 1994). The spillways were part of a glacial drainage pattern that dominated the

Mississippi and St Lawrence outlets to the world ocean (Teller, 1990).

The mid-continent glacial meltwater spillways of North America contain assemblages of landforms produced by high-energy water flow (Kehew & Lord, 1986). These landforms are recognized because of the extensive work done to document the effects of cataclysmic flooding along the southern margins of the Cordilleran Ice Sheet. Covering the Rocky Mountains, west of the Laurentide Ice Sheet, the Cordilleran Ice Sheet delivered meltwater into intermontane valleys. The largest lake thus formed was Glacial Lake Missoula (Fig. 1), in which about 2500 km^3 water was impounded behind a lobe of the Cordilleran Ice Sheet (Pardee, 1942). Failure of this ice dam, which impounded water 600 m deep, produced the high-energy floodwater that eroded the scabland of eastern Washington State (Bretz, 1928, 1959; Baker & Nummedal, 1978; Baker, 1981). The long controversy over the catastrophic flood origin of the Channeled Scabland region (Baker, 1978a, 1981) illustrates the philosophical impediments to the geological study of high-energy megafloods mentioned above in the introduction.

The late-glacial flooding from Lake Missoula delivered a peak flow of about 1×10^7 m^3 s^{-1} from the Wallula Gap area (Fig. 1) to the lower Columbia River valley below the Channeled Scabland (O'Connor & Baker, 1992). The floodwater had immense power (Benito, 1997) and was charged with coarse sediment in suspension. The latter point is confirmed by the emplacement of 100–160 m of graded beds in a submarine rift valley 1000 km from the mouth of the Columbia River (Brunner *et al*., 1999; Zuffa *et al*., 2000). Long-distance transport of Missoula Flood sediments across the abyssal Pacific Ocean floor is indicated by the lithology of pebbles recovered from the Blanco Fracture Zone (Fig. 1) (Griggs *et al*., 1970). However, the data from Ocean Drilling Program sites 1037 and 1038 provide clear evidence that sediment-charged Missoula floodwater entered the ocean close to the heads of Astoria and Willapa Canyons on the Astoria Fan, when sea level was about 60–70 m below present (Fig. 1) (Zuffa *et al*., 2000). The sediments seem to have been emplaced by hyperpycnal gravity flows (Mulder & Syvitski, 1995) which induced turbidity currents that reached the distant rift valley (Zuffa *et al*., 2000).

Central Asia

Various reconstructions of late Pleistocene Eurasian ice sheets (Grosswald, 1980, 1998) envision spectacular damming of north-flowing Siberian rivers, with associated spillovers and drainage diversions (Fig. 2). Alternative reconstructions (Velichko *et al*., 1989) involve less ponding and diversion, but incomplete field mapping and geochronology precludes a scientific preference for either of these alternatives. However, the Manych spillway, which connected the late Pleistocene Caspian Sea to the Black Sea, shows evidence of late Pleistocene cataclysmic flooding, including streamlined hills, elongate depressions (now lakes) and scabland erosion. Other spillway systems connected enlarged Pleistocene lakes in the basins of the modern Aral Sea, Ob River, and Yenisei River (Fig. 2).

A second type of megaflood association in central Asia involves ice-dammed lakes that formed in the mountain systems lying along the boundary between the former Soviet Union, China and Mongolia. Examples include the late Pleistocene palaeofloods of Issyk-kul (Grosswald *et al*., 1994), the Altai (Rudoy, 1988; Baker *et al*., 1993; Rudoy & Baker, 1993; Carling *et al*., this volume, pp. 17–35) and Tuva (Grosswald, 1999).

Late-glacial floodwater from the Manych spillway entered the basin of the modern Black Sea. There it joined with meltwater discharges from the ice sheet in northern Europe to create an immense freshwater lake, the 'New Euxine' (Chepalyga, 1984). According to one interpretation, the recession of the Eurasian ice sheets redirected drainage westward along their southern margin, cutting off the south-flowing drainage toward the Black Sea. Meltwater was directed toward the modern North Sea. There, another spillway may have formed by floodwater breaching a chalk barrier at the site of the present Dover Strait in late Pleistocene time (Smith, 1985).

There is considerable unresolved controversy concerning the timing of the southward-directed flows toward the Black Sea and Mediterranean (Arkhipov *et al*., 1995) and the magnitude and extent of ice-sheet-related flooding (Grosswald, 1999). Moreover, there is a provocative scenario whereby the diversion of the meltwater away from the Black Sea led to evaporative lowering of the latter during the latest Pleistocene and early Holocene, at the same time that the world ocean was rising because of shrinking ice sheets (Ryan *et al*., 1997). According to this model, at 7.6 ka the Mediterranean rose to a spill point from the Sea of Marmara to cut the channel now known as the Bosporus Strait. The resulting massive saltwater inundation of the New Euxine Basin displaced a sizeable human population, whose memories came to comprise

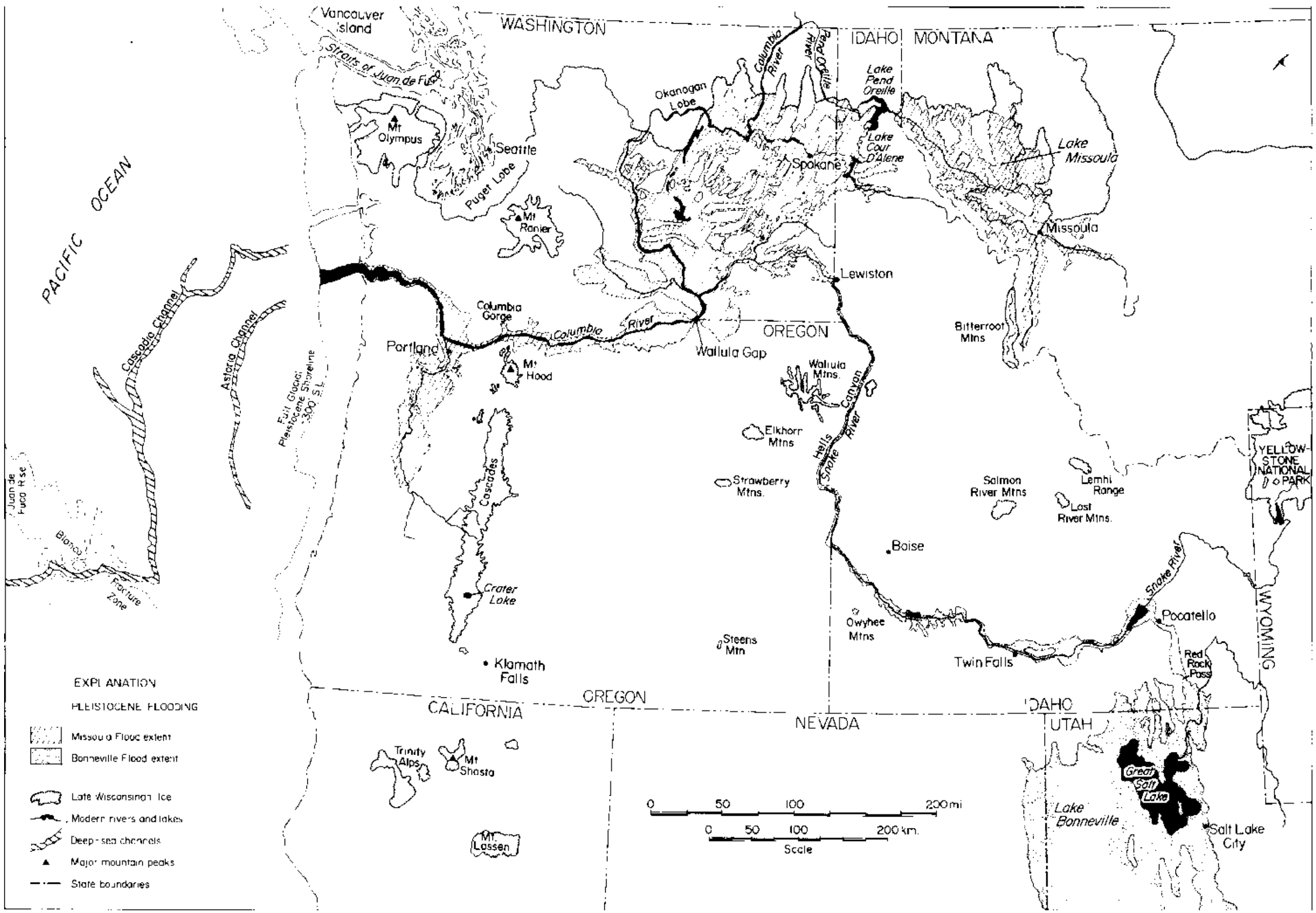

Fig. 1. Generalized map showing features related to cataclysmic late Pleistocene flooding in the north-western USA.

Fig. 2. Generalized map showing the extent of late Pleistocene flood-related features of Asia. The stippled area shows a controversial interpretation of the maximum hypothesized extent of glaciation (Grosswald, 1998). The black arrows indicate areas of mountain megafloods; white arrows indicate spillway floods between glacially enlarged lakes (shaded), marginal ice drainage, and outlets of meltwater to the world oceans (darkest shading).

various flood stories of the Middle East, including the Biblical tale of Noah (Ryan & Pittman, 1998).

Mars

The largest known high-energy megafloods occurred on the planet Mars. The ancient floods of Mars are inferred from the study of the landform assemblages associated with large-scale complexes of fluid-eroded troughs, including channel patterns, bedforms, streamlined uplands, grooves and scour marks (Fig. 3) (Baker, 1982; Mars Channel Working Group, 1983; Baker *et al.*, 1992). The inferred flows emanated from discrete collapse zones at the heads of the troughs, which are named 'outflow channels' to emphasize this relationship (Sharp & Malin, 1975). Because of similarities of the flow-related landforms to features in the Channeled Scabland, catastrophic flooding emerged as the leading hypothesis to explain the fluid-flow landforms and the large-scale erosion of the troughs (Baker & Milton, 1974; Baker, 1978a, 1982).

The largest Martian outflow channels emanate from the Tharsis volcanic province and adjacent equatorial uplands (Fig. 4). Their immense discharges (see next section) were directed toward the northern lowlands of the planet. The latter are hypothesized to have constituted a temporary ocean (Parker *et al.*, 1989, 1993) named 'Oceanus Borealis' (Baker *et al.*, 1991). The relationship of channels to the ocean is considered genetic by Baker *et al.* (1991), who also inferred a connection to the global water cycle and climate change for the planet.

PALAEOHYDRAULICS

Early attempts to estimate discharges for high-energy megafloods relied upon the Chezy and Manning equations. Bretz (1925) made an estimate for Missoula flooding on this basis. This was improved upon by slope-area procedures (Baker, 1973a). The most recent estimates use step-backwater modelling of energy-balanced water-surface profiles. This technique was applied to Bonneville flooding of the Snake River (Fig. 1) by Jarrett & Malde (1987) and by O'Connor (1993). O'Connor & Baker (1992) applied the method to Missoula flooding, and Baker *et al.* (1993) applied it to the Altai megaflooding in Siberia.

Enough palaeodischarge data have now accumulated to compare many of the known megafloods. Using additional data on flow widths and depths, it is also possible to compare other hydraulic variables. These include bed shear stress, τ

$$\tau = \rho g D S \tag{1}$$

where ρ is the fluid density, g is the acceleration of gravity, D is depth and S is slope. They also include stream power per unit area, ω

$$\omega = \rho g Q S / W = \tau V \tag{2}$$

where Q is discharge, W is width and V is mean flow velocity. Of course, the hydraulic variables are also related by continuity

$$Q = W D V \tag{3}$$

where the variables are all defined as above. Finally, O'Connor (1993) found that high-energy megaflooding tended to erode channels such that mean flow velocities did not exceed a critical Froude number of 1.0, such that

$$V^2 < g D \tag{4}$$

All of the above considerations, and published data, were used to construct Table 1, which approximates many of the high-energy megafloods in the various

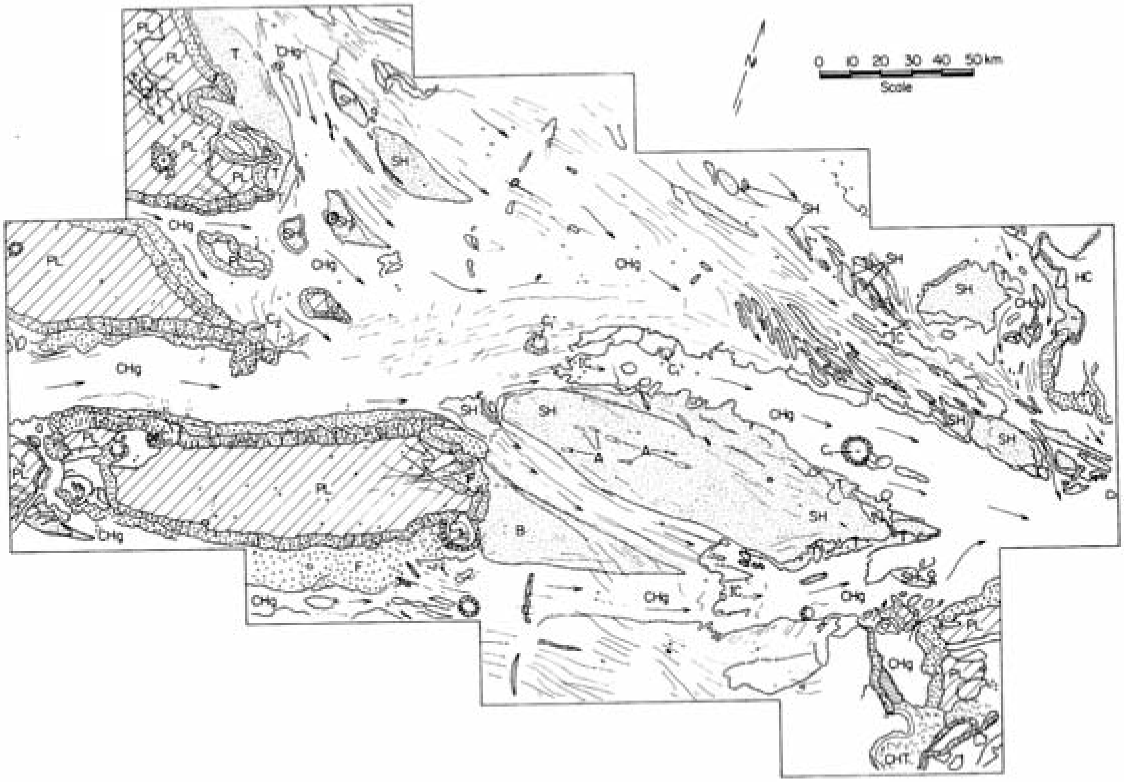

Fig. 3. Sketch map showing cataclysmic flood landforms associated with Kasei Vallis, Mars. Features indicating high-energy flows include grooved channel floors (CHg and lineations) in an overall anastomosing pattern (arrows), inner channel cataracts (IC), and streamlined hills (SH). Other features include heavily cratered uplands (HC), impact craters (C_1, C_2, C_3), plateau uplands (PL), post-flood fans (F), terraces (T), chaotic terrain (CHT), aeolian wind streaks (A) and (B) probable depositional bar. More detailed discussion of these relationships is found in Baker (1978a, 1982).

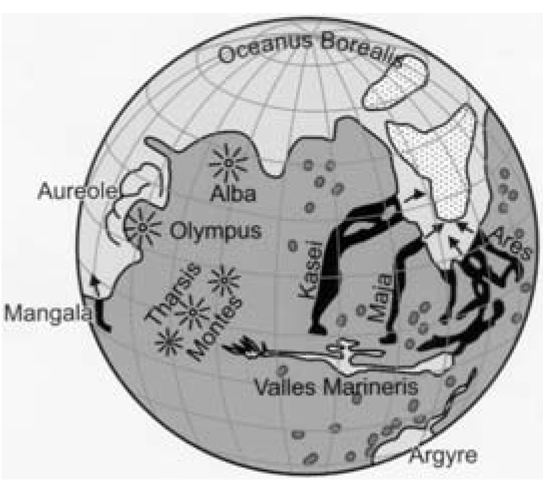

Fig. 4. Relationship of Martian outflow channels (black) to cratered uplands and Tharsis volcanic province (heavy shading). The black arrows show flow directions of cataclysmic discharges to the northern plains, which temporarily constituted the Oceanus Borealis (Baker *et al.*, 1991). Inferred areas of deposition by turbidity current flows are indicated by the stippled pattern.

settings described above. Shown for comparison are oceanic flows, including the hypothesized early Holocene overflow of the Mediterranean into the Black Sea through the Bosporus (Ryan *et al.*, 1997) and the early Pliocene erosion of the Strait of Gibraltar. The latter terminated the Miocene 'salinity crisis' of the Mediterranean Basin (Hsü *et al.*, 1997). Note that megaflood velocities range from 10 to

Table 1. Dimensions and hydraulics for representative high-energy megafloods compared with ocean currents and spillways. Published values and equations 1–4 were used to construct the table.

Location	Width (km)	Depth (m)	Velocity ($m\ s^{-1}$)	Discharge ($m^3\ s^{-1}$)	Bed shear stress ($N\ m^{-2}$)	Stream power per unit area ($W\ m^{-2}$)	Slope	Reference
Missoula Flood (Rathdrum)	6	150	25	2×10^7	1×10^4	2×10^5	0.01	O'Connor & Baker (1992)
Altai Flooding (Chuja)	2.5	400	25	2×10^7	4×10^4	1×10^6	0.01	Baker *et al.* (1993)
Jökulsá á Fjöllum	5–10	10	10*	7×10^5	–	–	–	Waitt (this volume, pp. 37–51)
Strait of Dover	20	50	13*	1×10^7	–	–	–	Smith (1985)
Gibraltar (Pliocene)	6	300	30*	5×10^7	–	–	–	–
Bosporus	1	100	6	6×10^5	–	–	–	Ryan *et al.* (1997)
Gulf Stream	50–75	1000	1–3	1×10^8	–	–	–	Gross (1987)
Mangala Vallis (Mars)	14	100	14	2×10^7	3×10^3	6×10^4	0.003	Komar (1979)
Maja Vallis (Mars)	80	100	38	3×10^8	2×10^4	8×10^5	0.02	Baker (1982)
Ares Vallis (Mars)	25	500–1000	25–100	5×10^8	1×10^5	3×10^6	0.02–0.0001	Komatsu & Baker (1997)
Kasei Vallis (Mars)	80	400–1300	30–75	$1–2 \times 10^9$	1×10^5	3×10^6	0.01	Robinson & Tanaka (1990)

*Determined from equation (3).

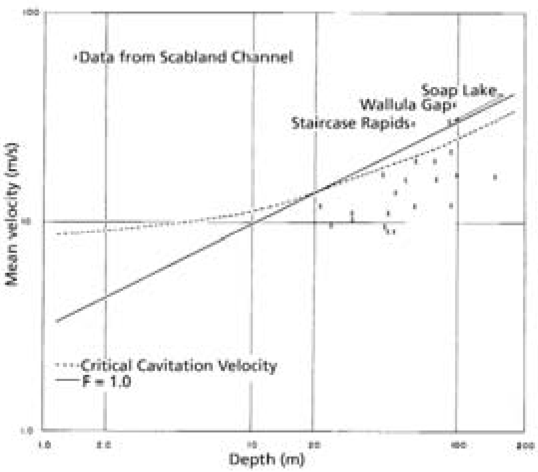

Fig. 5. Calculated mean flow velocities for peak Missoula flood flows in the Channeled Scabland as a function of depth. The solid line shows the critical Froude number of 1.0, and the dashed line shows the critical point for initiating cavitation in the flow. See Baker (1973b) and O'Connor (1993) for more extensive discussion of these relationships.

100 $m\ s^{-1}$ (Fig. 5); discharges range from 10^5 to 10^9 $m^3\ s^{-1}$; bed shear stresses range from 10^3 to 10^5 N m^{-2}; and power per unit area ranges from 10^4 to 10^6 W m^{-2}. The largest, most energetic floods were those of Mars.

MEGAFLOODS AND CLIMATE

The most powerful high-discharge currents in the ocean are the western boundary currents, which include the Gulf Stream in the Atlantic, the Kuroshio in the Pacific, and the Agulhas in the Indian Ocean. These currents usually extend to depths of about 1 km, and they are relatively narrow for oceanic currents, usually less than or equal to 100 km. The Florida Current, part of the Gulf Stream between Cuba and the Bahamas, achieves surface velocities of 1–3 m s^{-1} (Gross, 1987). Discharges of these currents range from 10 to 100 million $m^3\ s^{-1}$ (Olson, 1992), which are comparable to the discharges of many megafloods (Table 1).

The ocean currents are integral to Earth's climate, distributing heat from equatorial latitudes poleward. The comparable magnitudes of megafloods emphasizes their inferred role in climate change on Earth (Teller, 1990; Arkhipov *et al.*, 1995) and on Mars (Baker *et al.*, 1991). Perhaps the most important mechanism for abrupt climate change on Earth is the thermohaline circulation, which is driven by increasing salinity of surface water moving northward in the Atlantic (Broecker & Denton, 1989). As the North Atlantic water becomes cold and dense, it sinks, driving deep, cold, salty water back to the Southern Ocean. Constituting an immense 'conveyor belt', the thermohaline circulation averages on the order of 15×10^6 $m^3\ s^{-1}$ and may take several centuries to complete one global cycle (Broecker, 2000). When the conveyor runs slowly, at low discharge, CO_2 accumulates in the deep sea at the expense of the atmosphere, cooling Earth toward a glacial state. At high discharge, however, the deep ocean ventilates its CO_2 to the atmosphere, increasing global temperatures by the resulting greenhouse warming. On Earth, these processes are hypothesized to amplify insulation changes induced by changes in orbital parameters.

The immense Mars megaflood discharges (Table 1) transferred water and heat from the equatorial Tharsis volcanic province to Oceanus Borealis (Fig. 4). The Martian floods can only have achieved their scale from an immense energy source. A huge release of internal planetary heat would seem to be the only possible source of energy at the necessary scale (Baker *et al.*, 1991). Water, and probably CO_2, released by the heat influx, simultaneously generated Oceanus Borealis and a transient cool–wet climate on the otherwise extremely cold–dry planetary surface. The H_2O–CO_2 atmosphere could not have been stable, however. It would have quickly reacted with surface rocks, flushing bicarbonate-rich water into the permeable upper lithosphere. There the water and CO_2 would be trapped for hundreds of millions of years until another immense planetary heat release could again generate a new episode of megaflooding. This cyclic process probably occurred several times over the 4.6 billion year history of the planet (Baker *et al.*, 1991).

SEDIMENTARY PROCESS OVERVIEW

Quantification of the flow mechanics for high-energy megafloods ultimately resolved a number of enigmas that had troubled various antagonists in the early debates over the origin of the Channeled Scabland (Baker, 1978a, 1981). Bretz's (1928, 1959) interpretation of massive bedrock erosion and gravel bar emplacement by catastrophic flooding could be seen as the natural physical consequence of cataclysmic flooding (Baker, 1973a,b). This section will consider some of the cataclysmic flood processes in the more general context of planetary megafloods, particularly their sedimentary effects.

Streamlining

Large-scale erosional remnants and depositional bars for cataclysmic floods typically develop streamlined forms. As discussed by Baker (1979, 1982) and Komar (1983, 1984), these features evolve toward an equilibrium form that minimizes the resistance to the flood flow. Figure 6 shows how drag reduction is the process that leads to this equilibrium form.

Scour marks

Scour marks develop around obstacles in cataclysmic flow fields. These are common in Icelandic jökulhlaups because immense blocks of glacial ice are stranded on the gravel plains (sandar) that occur at the mouths of glaciers. The outburst floods scour depressions around these obstacles. Baker (1973a) describes a well-developed scour mark around a 20-m diameter

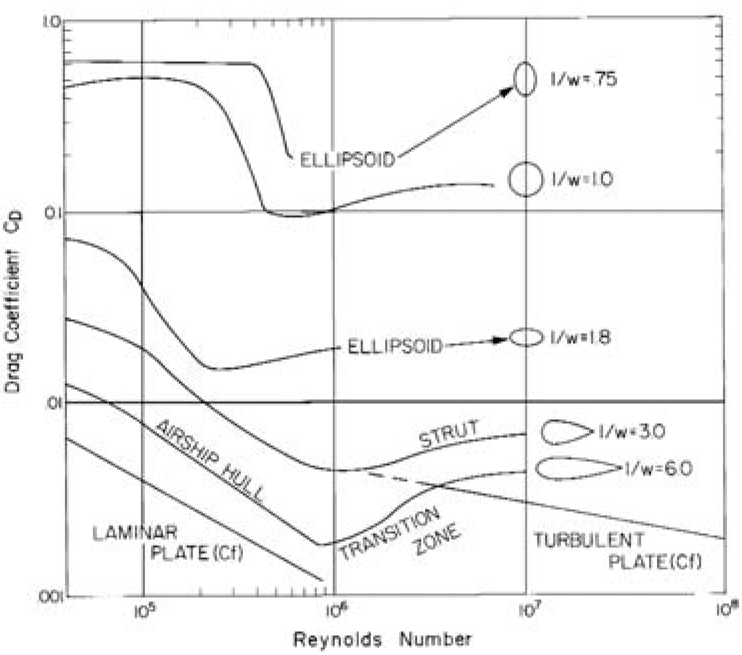

Fig. 6. Relationship of drag (indicated by a drag coefficient) to Reynolds number (proportional to flow velocity) for various shaped flow obstacles. Note the drag reduction for the elongate, streamlined shape with a higher length-to-width ratio (l/w). Drag ultimately is reduced to skin friction, indicated by the friction drag coefficient (Cf) on a flat plate in laminar or turbulent flow regimes.

Fig. 7. A 20-m diameter basalt boulder, one of the largest known to have been transported by Missoula flood flows in the Channeled Scabland. The depression visible immediately behind the vehicle is a scour depression extending downstream from the boulder (Baker, 1973a).

boulder on a flood fan in the Channeled Scabland. A deep scour hole wraps around the upstream side of the boulder, and a broad, shallower depression extends downstream from the boulder (Fig. 7). Baker (1978b) describes similar scour marks in the Martian outflow channels.

Boulder transport

Impressive large boulders have long been noted as evidence of the high competence of high-energy megafloods (Fig. 7). Early work compared the transported boulder sizes to values of velocity and bed shear stress (Baker, 1973a; Baker & Ritter, 1975; Costa, 1983). More recently, emphasis has been placed on hydraulic conditions at the sites of boulder deposition (O'Connor, 1993). Studying the extensive 'Melon gravel' boulder fields emplaced by Lake Bonneville flooding of Snake River Plain, O'Connor (1993) developed the most extensive data set on palaeohydraulic conditions associated with boulders deposited under high-energy flooding conditions.

Giant current ripples (dunes)

Giant current ripples, so named and discovered by Bretz *et al*. (1956), were analysed for the Channeled Scabland by Baker (1973a). They seem to have strong correlations to palaeoflow parameters, and they correspond to the bedform regime of fluvial dunes. More recently, Carling (1996a,b) analysed similar bedforms in the Altai Mountain region of central Asia. Carling (1996a) used the bedform dimensions to estimate flow velocities and discharges for these bedforms. Field examples of giant current ripples (dunes) are shown in Fig. 8.

Sediment transport

A critical megaflood consideration is the range of particle sizes transported as bedload, suspended load and washload. Komar (1980) analysed criteria for these distinctions in high-energy floods using relationships developed by Bagnold (1966). Applying these criteria to the Bonneville Flood, O'Connor (1993) found that above sustained bed shear stresses of 1000 N m^{-2}, which commonly develop in high-energy megafloods, particles as large as 10–20 cm move in suspension, and coarse sand moves as washload. Coarse gravel deposited high above the fluvial channel bed at eddy locations in canyon-wall re-entrants confirmed O'Connor's (1993) prediction of suspended sediment sizes.

Komar (1980) originally developed his transport criteria for application to megafloods on Mars. At a given bed shear stress or mean flow velocity, Martian floods will transport much larger particles as suspended load or washload than can be achieved on Earth. This is because the reduced Martian gravity results in lower particle settling velocities. Komar (1980) did not extend his analysis to particle sizes larger than 10 cm. A conjectural extrapolation of Komar's relationships (Komatsu & Baker, 1997) suggests that Martian outflow channel flows (bed shear stress of 10^4–10^5 N m^{-2}, power per unit area of 10^6 W m^{-2}) could move 10-m diameter particles

Fig. 8. Giant current ripples (dunes) emplaced by megafloods. (a) Ripple field of the Missoula flooding near Spirit Lake, Idaho. These gravel ripples have a spacing of 85 m and a height of 4 m (Baker, 1973a). Pine trees accentuate the ripple troughs. (b) Ripple field of the megaflood in the Kuray Basin of the Altai Mountain area, Siberia (Rudoy & Baker, 1993; Carling, 1996a,b). These dunes reach spacings of as much as 200 m and heights of 10–16 m (photograph by A. Rudoy).

in suspension. Gravel of 10 mm size would move as washload.

Submarine effects of megafloods

Komar (1979) developed a physical analogy between Martian outflow channels and the submarine channels associated with deep-sea turbidity currents. Velocities for the latter on Earth are in the range of 10–20 m s^{-1} (Komar, 1969). Upon emanating from a deep-sea channel, terrestrial turbidity currents spread their deposits over immense areas of sea floor. The mobility of the currents is enhanced by their low densities, 1.1–1.2 g cm^{-3} (Komar, 1977), which imparts a very low effective gravity. Combined with the lower absolute gravity on Mars, transport distances across the flat plains of Mars, such as in Oceanus Borealis, would be greatly enhanced above terrestrial analogues.

Sediment-charged Martian floods from outflow channels would have entered the ponded northern plains water body (Oceanus Borealis) as hyperpycnal flows, thereby creating a plane jet underflow (Moore, 1966) and powerful turbidity currents. The northern plain contains a vast deposit covering 2.7×10^7 km^2, approximately one-sixth of the planet's area (Parker *et al.*, 1993). This unit has a remarkable topographic smoothness (Head *et al.*, 1998, 1999), which is consistent with the hypothesis of submarine emplacement by turbidity current flows. Alternatively, Jöns (1985) and Tanaka (1997) hypothesize subaerial mud or debris flows for emplacing the deposit. However, these authors fail to account for the need to emplace the deposit over immense areas of flat terrain. The extremely high mobility of turbidity current flows, triggered by sediment-charged megafloods, seems to provide the most reasonable physical mechanism to explain this relationship.

The Astoria fan relationships for Missoula flooding show that submarine effects need to be considered more broadly in regard to megafloods. Mutti *et al.* (1996) have already begun this investigation for tectonically active basins.

CONCLUSIONS

Although J Harlen Bretz once thought his discovery of cataclysmic flood effects in the Channeled Scabland to have been unique, it is now clear that high-energy megafloods are general phenomena of considerable geological importance. They were associated with late Pleistocene glacial ice margins in both North America and Asia. They have modern manifestations in Iceland, and their most spectacular effects occur on the planet Mars. Yet, all these examples show similarities of certain erosional and depositional features, as well as similar ranges of flow velocities, bed shear stress and power per unit area.

The accumulating palaeohydraulic data now show that these megafloods compare with the largest water flows of the world ocean. Like ocean currents, they probably had important influences on global climate. For Mars, the megafloods are hypothesized to be the principal cause of climatic change on long, geological time-scales.

Perhaps the most widespread and significant sedimentary effect of high-energy megafloods arises when sediment-charged flows emerge from confined continental valleys to enter adjacent ocean basins. The resulting hyperpycnal flows and turbidity currents have now been documented for the Missoula floods that carved the Channeled Scabland. Physical considerations and geomorphological relationships also suggest that similar processes occurred during an ancient epoch on Mars associated with the outflow channels and Oceanus Borealis.

ACKNOWLEDGEMENTS

Thirty years of research on a topic leave too many colleagues, students and collaborators to thank properly. Paul Komar, in particular, shared many ideas pertinent to this particular paper. Of course, the late 'Doc' Bretz got it all started. This paper is ALPHA contribution number 61.

REFERENCES

Ager, D.V. (1993) *The Nature of the Stratigraphical Record*. Wiley, Chichester.

Arkhipov, S.A., Ehlers, J., Johnson, R.G. & Wright, H.E. Jr (1995) Glacial drainage towards the Mediterranean during the Middle and Late Pleistocene. *Boreas* **24**, 196–206.

Bagnold, R.A. (1966) An approach to the sediment transport problem from general physics. *U.S. geol. Surv. Prof. Pap.* **422-I**, 1–37.

Baker, V.R. (1973a) Paleohydrology and sedimentology of Lake Missoula flooding in eastern Washington. *Geol. Soc. Am. Spec. Pap.* **144**, 1–79.

Baker, V.R. (1973b) Erosional forms and processes for the catastrophic Pleistocene Missoula floods in eastern Washington. In: *Fluvial Geomorphology* (Ed. Morisawa, M.), pp. 123–148. Publications in Geomorphology, State University of New York, Binghamton, NY.

Baker, V.R. (1978a) The Spokane Flood controversy and the Martian outflow channels. *Science* **202**, 1249–1256.

Baker, V.R. (1978b) A preliminary assessment of the fluid erosional processes that shaped the Martian outflow channels. In: *Proceedings of the 9th Lunar and Planetary Science Conference*, pp. 3205–3223. Lunar and Planetary Institute, Houston, TX.

Baker, V.R. (1979) Erosional processes in channelized water flows on Mars. *J. geophys. Res.* **84**, 7985–7993.

Baker, V.R. (1981) *Catastrophic Flooding: the Origin of the Channeled Scabland*. Dowden, Hutchinson and Ross, Stroudsburg, PA.

Baker, V.R. (1982) *The Channels of Mars*. University of Texas Press, Austin, TX.

Baker, V.R. (1988) Cataclysmic processes in geomorphological systems. *Z. Geomorph. Suppl.* **67**, 25–32.

Baker, V.R. (1994) Glacial to modern changes in global river fluxes. In: *Material Fluxes on the Surface of the Earth* (Ed. National Research Council), pp. 86–98. National Academy Press, Washington, DC.

Baker, V.R. (1996a) Discovering Earth's future in its past: Palaeohydrology and global environmental change. In: *Global Continental Changes: the Context of Palaeohydrology* (Eds Branson, J., Brown, A.G. & Gregory, K.J.), Spec. Publ. geol. Soc. London, No. 115, pp. 73–83. Geological Society of London, Bath.

Baker, V.R. (1996b) Megafloods and glaciation. In: *Late Glacial and Postglacial Environmental Changes* (Ed. Martini, I.P.), pp. 98–108. Oxford University Press, NY.

Baker, V.R. (1998) Catastrophism and uniformitarianism: logical roots and current relevance. In: *Lyell: the Past is the Key to the Present* (Eds Blundell, D.J. & Scott, A.C.), Spec. Publ. geol. Soc. London, No. 143, pp. 171–182. Geological Society of London, Bath.

Baker, V.R. & Costa, J.C. (1987) Flood power. In: *Catastrophic Flooding* (Eds Mayer, L. & Nash, P.), pp. 1–21. Allen and Unwin, London.

Baker, V.R. & Kale, V.S. (1998) The role of extreme floods in shaping bedrock channels. In: *Rivers over Rock: Fluvial Processes in Bedrock Channels* (Eds Tinkler, K.J. & Wohl, E.E.), pp. 153–165. Monograph 107, American Geophysical Union, Washington, DC.

Baker, V.R. & Kochel, R.C. (1988) Flood sedimentation in bedrock fluvial systems. In: *Flood Geomorphology* (Eds Baker, V.R., Kochel, R.C. & Patton, P.C.), pp. 123–137. Wiley, NY.

Baker, V.R. & Milton, D.J. (1974) Erosion by catastrophic floods on Mars and Earth. *Icarus* **23**, 27–41.

Baker, V.R. & Nummedal, D. (1978) *The Channeled Scabland*. NASA Planetary Geology Program, Washington, DC.

Baker, V.R. & Ritter, D.F. (1975) Competence of rivers to transport coarse bedload. *Geol. Soc. Am. Bull.* **86**, 975–978.

Baker, V.R., Strom, R.G., Gulick, V.C., Kargel, J.S., Komatsu, G. & Kale, V.S. (1991) Ancient oceans, ice sheets and the hydrological cycle on Mars. *Nature* **352**, 589–594.

Baker, V.R., Carr, M.H., Gulick, V.C., Marley, M.S. & Williams, C.R. (1992) Channels and valley networks. In: *Mars* (Eds Kieffer, H.H., Jakosky, B. & Synder, C.), pp. 493–522. University of Arizona Press, Tucson.

Baker, V.R., Benito, G. & Rudoy, A.N. (1993) Paleohydrology of late Pleistocene superflooding: Altay Mountains, Siberia. *Science* **259**, 348–350.

Benito, G. (1997) Energy expenditure and geomorphic work of the cataclysmic Missoula flooding in the Columbia Gorge, U.S.A. *Earth Surf. Process. Landf.* **22**, 457–472.

Bretz, J H. (1925) The Spokane Flood beyond the Channeled Scabland. *J. Geol.* **17** (97–115), 232–259.

Bretz, J H. (1928) The Channeled Scabland of eastern Washington. *Geograph. Rev.* **18**, 446–477.

Bretz, J H. (1959) Washington's Channeled Scabland. *Washington Div. Mines Geol. Bull.* **45**, 1–57.

Bretz, J H., Smith, H.T.U. & Neff, G.E. (1956) Channeled Scabland of Washington: New data and interpretations. *Geol. Soc. Am. Bull.* **67**, 957–1049.

Broecker, W.S. (2000) Abrupt climate change: Causal constraints provided by the paleoclimate record. *Earth Sci. Rev.* **51**, 137–154.

Broecker, W.S. & Denton, G.H. (1989) The role of ocean-atmosphere reorganizations in glacial cycles. *Geochim. Cosmochim. Acta* **53**, 2465–2501.

Brunner, C.A., Normark, W.R., Zuffa, G.G. & Serra, F. (1999) Deep-sea sedimentary record of the late Wisconsin cataclysmic floods from the Columbia River. *Geology* **27**, 463–466.

Carling, P.A. (1996a) A preliminary palaeohydraulic model applied to Late Quaternary gravel dunes: Altai Mountains, Siberia. In: *Global Continental Changes: the Context of Palaeohydrology* (Eds Branson, J., Brown, A.G. & Gregory, K.J.), Spec. Publ. geol. Soc. London, No. 115, pp. 165–179. Geological Society of London, Bath.

Carling, P.A. (1996b) Morphology, sedimentology and palaeohydraulic significance of large gravel dunes: Altai Mountains, Siberia. *Sedimentology* **43**, 647–664.

Carling, P.A., Kirkbride, A.D., Panachov, S., Borodavko, P.S. & Berger, G.W. (2002) Late glacial catastrophic flooding in the Altai Mountains of south-central Siberia: a synoptic overview and an introduction to flood deposit sedimentology. In: *Flood and Megaflood Processes and Deposits: Recent and Ancient Examples* (Eds Martini, I.P., Baker, V.R. & Garzón, G.), Spec. Publ. int. Ass. Sediment., No. 32, pp. 17–35. Blackwell Science, Oxford.

Chepalyga, A.L. (1984) Inland sea basins. In: *Late Quaternary Environments of the Soviet Union* (Ed. Velichko, A.A.), pp. 229–247. University of Minnesota Press, Minneapolis.

Costa, J.E. (1983) Paleohydraulic reconstruction of flash-flood peaks from boulder deposits in the Colorado Front Range. *Geol. Soc. Am. Bull.* **94**, 986–1004.

Costa, J.E. & O'Connor, J.E. (1995) Geomorphically effective floods. In: *Natural and Anthropogenic Influences in Fluvial Geomorphology* (Eds Costa, J.E., Miller, A.J., Potter, K.W. & Wilcock, P.R.), pp. 45–56. Geophysical Monograph 89, American Geophysical Union, Washington, DC.

Griggs, G.B., Kulm, L.D., Waters, A.C. & Fowler, G.A. (1970) Deep-sea gravel from Cascadia Channel. *J. Geol.* **78**, 611–619.

Gross, M.G. (1987) *Oceanography: a View of the Earth*. Prentice Hall, New Jersey, 406 pp.

Grosswald, M.G. (1980) Late Weichselian ice sheet of northern Eurasia. *Quat. Res.* **13**, 1–32.

Grosswald, M.G. (1998) New approach to the ice age palaeohydrology of northern Eurasia. In: *Palaeohydrology and Environmental Change* (Eds Benito, G., Baker, V.R. & Gregory, K.J.), pp. 199–214. Wiley, Chichester.

Grosswald, M.G. (1999) *Cataclysmic Megafloods in Eurasia and the Polar Ice Sheets*. Scientific World, Moscow. (In Russian.)

Grosswald, M.G., Kuhle, M. & Fastook, J.L. (1994) Wurm glaciation of Lake Issyk-kul area, Tian Shan Mountains: a case study in the glacial history of central Asia. *Geojournal* **33**, 273–310.

Gudmundsson, M.T., Bjornsson, H. & Palsson, F. (1995) Changes in jökulhlaup sizes in Grimsvötn, Vatnajökull, Iceland, 1934–91, deduced from in-situ measurements of subglacial lake volume. *J. Glaciol.* **41**, 263–272.

Head, J.W. III, Kreslavsky, M., Hiesinger, H., Ivanov, M., Pratt, S. & Seibert, N. (1998) Oceans in the past history of Mars: Tests for their presence using Mars Orbiter Laser Altimeter (MOLA) data. *Geophys. Res. Lett.* **25**, 4401–4404.

Head, J.W., Hiesinger, H., Ivanov, M.A., Kreslavsky, M.A., Pratt, S. & Thomson, B.J. (1999) Possible ancient oceans on Mars: Orbiter laser altimeter data. *Science* **286**, 2134–2137.

Hsü, K.J., Garrison, R.E., Montadert, L., *et al*. (1977) History of the Mediterranean salinity crisis. *Nature* **267**, 399–403.

Jarrett, R.D. & Malde, H.E. (1987) Paleodischarge of the late Pleistocene Bonneville Flood, Snake River, Idaho, computed from new evidence. *Geol. Soc. Am. Bull.* **99**, 127–134.

Jöns, H.-P. (1985) Late sedimentation and late sediments in the northern lowlands on Mars. In: *Lunar and Planetary Science XVI*, pp. 404–405. Lunar and Planetary Institute, Houston, TX.

Kehew, A.E. & Lord, M.L. (1986) Origin and large-scale erosional features of glacial-lake spillways in the northern Great Plains. *Geol. Soc. Am. Bull.* **97**, 162–177.

Kehew, A.E. & Teller, J.T. (1994) History of late glacial runoff along the southwestern margin of the Laurentide Ice Sheet. *Quat. Sci. Rev.* **13**, 859–877.

Komar, P.D. (1969) The channelized flow of turbidity currents with application to Monterey deep-sea channel. *J. geophys. Res.* **74**, 4544–4558.

Komar, P.D. (1977) Computer simulation of turbidity current flow and the study of deep-sea channels and fan sedimentation. In: *The Sea*, Vol. 7 (Ed. Goldberg, D.), pp. 603–621. Wiley, New York.

Komar, P.D. (1979) Comparisons of the hydraulics of water flows in Martian outflow channels with flows of similar scale on Earth. *Icarus* **37**, 156–181.

Komar, P.D. (1980) Modes of sediment transport in channelized water flows with ramifications to the erosion of the Martian outflow channels. *Icarus* **42**, 317–329.

Komar, P.D. (1983) Shapes of streamlined islands on Earth and Mars: experiments and analyses of the minimum-drag form. *Geology* **11**, 651–654.

Komar, P.D. (1984) The lemniscate loop: comparisons with the shapes of streamlined landforms. *J. Geol.* **92**, 133–145.

Komatsu, G. & Baker, V.R. (1997) Paleohydrology and flood geomorphology of Ares Vallis, Mars. *J. geophys. Res.* **102**, 4151–4160.

Maizels, J.K. (1989) Sedimentology, palaeoflow dynamics and flood history of jökulhlaup deposits: palaeohydrology of Holocene sediment sequences in southern Iceland sandur deposits. *J. sediment. Petrol.* **59**, 204–223.

Maizels, J.K. (1993) Lithofacies variations within sandur deposits: the role of runoff regime, flow dynamics, and sediment supply characteristics. *Sediment. Geol.* **85**, 299–325.

Maizels, J.K. (1995) Sediments and landforms of modern proglacial terrestrial environments. In: *Modern Glacial Environments* (Ed. Menzies, J.), pp. 365–416. Butterworth-Heinemann, Oxford.

Mars Channel Working Group (1983) Channels and valleys on Mars. *Geol. Soc. Am. Bull.* **95**, 1035–1054.

Moore, D. (1966) Deltaic sedimentation. *Earth Sci. Rev.* **1**, 87–104.

Mulder, T. & Syvitski, P.M. (1995) Turbidity currents generated at river mouths during exceptional discharges to the world oceans. *J. Geol.* **103**, 285–299.

Mutti, E., Davoli, G., Tinterri, R. & Zavala, C. (1996) The importance of ancient fluvio-deltaic systems dominated by catastrophic flooding in tectonically active basins. *Mem. Sci. Geol.* **48**, 233–291.

O'Connor, J.E. (1993) Hydrology, hydraulics and sediment transport of Pleistocene Lake Bonneville flooding on the Snake River, Idaho. *Geol. Soc. Am. Spec. Pap.* **274**, 1–83.

O'Connor, J.E. & Baker, V.R. (1992) Magnitudes and implications of peak discharges from glacial Lake Missoula. *Geol. Soc. Am. Bull.* **104**, 267–279.

Olson, D.B. (1992) Ocean circulation. In: *Encyclopedia of Earth System Science* (Ed. Nierenberg, W.A.), pp. 367–382. Academic Press, San Diego.

Pardee, J.T. (1942) Unusual currents in glacial Lake Missoula, Montana. *Geol. Soc. Am. Bull.* **53**, 1569–1600.

Parker, T.J., Saunders, R.S. & Schneeberger, D.M. (1989) Transitional morphology in the west Deuteronilus Mensae region of Mars: implications for modification of the lowland/upland boundary. *Icarus* **82**, 111–145.

Parker, T.J., Gorsline, R.S., Saunders, R.S., Pieri, D.C. & Schneeberger, D.M. (1993) Coastal geomorphology of the Martian northern plains. *J. geophys. Res.* **98**, 11 061–11 078.

Robinson, M.S. & Tanaka, K.L. (1990) Magnitude of a catastrophic flood event at Kasei Vallis, Mars. *Geology* **18**, 902–905.

Rudoy, A.N. (1988) The regime of intermontane ice-dammed lakes of south Siberia. *Data Glacial Research, Acad. Sci., USSR* **61**, 36–42. (In Russian.)

Rudoy, A.N. & Baker, V.R. (1993) Sedimentary effects of cataclysmic late Pleistocene glacial outburst flooding, Altay Mountains, Russia. *Sediment. Geol.* **85**, 53–62.

Russell, A.J. & Knudsen, O. (2002) The effects of glacier outburst flood flow dynamics on ice-contact deposits: November jökulhlaup, Skeiðarársandur, Iceland. In: *Flood and Megaflood Processes and Deposits: Recent and Ancient Examples* (Eds Martini, I.P., Baker, V.R. & Garzón, G.), Spec. Publ. int. Ass. Sediment., No. 32, pp. 67–83 Blackwell Science, Oxford.

Ryan, W. & Pitman, W. (1998) *Noah's Flood: the New Scientific Discoveries about the Event that Changed History*. Simon and Schuster, New York.

Ryan, W.B.F., Pitman, W.C. III & Major, C.O. (1997) An abrupt drowning of the Black Sea shelf. *Mar. Geol.* **138**, 119–126.

Sharp, R.P. & Malin, M.C. (1975) Channels on Mars. *Geol. Soc. Am. Bull.* **86**, 593–609.

Smith, A.J. (1985) A catastrophic origin for the palaeovalley system of the eastern English Channel. *Mar. Geol.* **64**, 65–75.

Tanaka, K.L. (1997) Sedimentary history and mass flow structures of Chryse and Acidalia Planitia, Mars. *J. geophys. Res.* **102**, 4131–4149.

Teller, J.T. (1990) Meltwater and precipitation runoff to the North Atlantic, Arctic, and Gulf of Mexico from the Laurentide ice sheet and adjacent regions during the Younger Dryas. *Paleoceanography* **5**, 897–905.

Tómasson, H. (1996) The jökulhlaup from Katla in 1918. *Ann. Glaciol.* **22**, 249–254.

Velichko, A.A., Isayesa, L.L., Oreshkin, D.B. & Faustova, M.A. (1989) The last glaciation of Eurasia. In: *The Arctic Seas: Climatology, Oceanography, Geology, and Biology* (Ed. Herman, Y.), pp. 729–758. Van Nostrand Reinhold, New York.

Waitt, R.B. (2001) Great Holocene floods along Jökulsá á Fjöllum, north Iceland. In: *Flood and Megaflood Processes and Deposits: Recent and Ancient Examples* (Eds Martini, I.P., Baker, V.R. & Garzón, G.), Spec. Publ. int. Ass. Sediment., No. 32, pp. 37–51. Blackwell Science, Oxford.

Zuffa, G.G., Normack, W.R., Serra, F. & Brumer, C.A. (2000) Turbidite megabeds in an oceanic rift valley recording jökulhlaups of late Pleistocene glacial lakes of the western United States. *J. Geol.* **108**, 253–274.

Spec. Publs int. Ass. Sediment. (2002) **32**, 17–35

Late Quaternary catastrophic flooding in the Altai Mountains of south–central Siberia: a synoptic overview and an introduction to flood deposit sedimentology

P. A. CARLING*, A. D. KIRKBRIDE†, S. PARNACHOV‡,
P. S. BORODAVKO‡ *and* G. W. BERGER§

**Department of Geography, Highfield, University of Southampton, SO17 1BJ, UK (Email: p.a.carling@soton.ac.uk);*
†Département de Géographie, CP 6128 Succ. Centre Ville, Montreal, Québec H3C 3J7, Canada;
‡Department of Geology and Geography, Tomsk State University, 634050 Tomsk, Russia; and
§Quaternary Sciences Center, Desert Research Institute, 2215 Raggio Parkway, Reno, NV 89512–1095, USA

ABSTRACT

This paper provides an overview of the geography and palaeogeography of the Chuja (Chuya)–Katun river system in the Altai Mountains of south Siberia. In addition, an introduction to the sedimentology of catastrophic flood deposits is provided. Tracts of large gravel dunes and giant gravel bars in the Katun and Chuja river valleys of south-central Siberia are testimony to episodes of catastrophic flooding that occurred owing to the sudden emptying of the ice-impounded glacial lake Kuray–Chuja primarily during the Late Pleistocene (40 ka to 13 ka). Although today there are no substantial water bodies in the Kuray and Chuja basins, glaciolacustrine deposits attest to the former presence of large ice-proximal lakes, whereas multiple strandlines at various elevations around the basin margins indicate former lake levels. Floods were of a scale similar to that recorded for glacial-lake Missoula in North America. A large flood down the main Chuja and Katun river valleys deposited huge quantities of coarse and fine gravels within back-flooded tributary mouths and other valley-side embayments. Today these deposits form giant bars that blanket the valley walls and block each tributary entrance for a distance of over 70 km. While the bars were being deposited, the base of the main valley was infilled to a depth of 60–90 m by coarse-gravel traction deposits. In particular coarse gravel bedload and hyperconcentrated-flow units prograded down-valley beneath flood waters several hundred metres deep. Locally, steeply cross-stratified units, each several decimetres thick attest to steep bar-front progradation similar in style to a Gilbert-type delta.

During individual floods, fine gravel and coarse sand, mostly transported in suspension, was deposited by multiple flood pulses in the entrance to flooded tributaries. The resultant giant bars, up to 5 km long and 120 m in height, temporarily impounded lakes in the tributaries, indicated by local small-scale limnic deposits. Subsequently, tributary streams cut through the bars, draining the small lakes and incising the lacustrine deposits. Later floods down the main river valley again blocked the tributaries with flood gravels such that lakes reformed.

INTRODUCTION

Extensive catastrophic Pleistocene (46 ka to 13 ka) floods in south-central Siberia have been documented recently (Rudoy, 1988, 1990, 1998; Rudoy *et al.*, 1989). These floods produced a suite of diluvial ('great flood') landforms, including large gravel dunes (Carling, 1996a,b), giant bars and flood-scoured channelways on a scale similar to that associated with the draining of glacial Lake Missoula in North America (Baker, 1973; Baker & Bunker, 1985). The morphology and sedimentology of these landforms may be diagnostic of catastrophic floods, and thus detailed description may aid in the interpretation of other ancient landscapes and stratigraphical successions. The sources of the Siberian floods were vast ice-dammed lakes impounded within the intermontane basins of the Altai and Sayan mountains (Fig. 1). Evidence for

Flood and Megaflood Processes and Deposits: Recent and Ancient Examples. Edited by I. Peter Martini, Victor R. Baker and Guillermina Garzón ISBN: 978-0-632-06404-5

Fig. 1. Location map of study area in southern Siberia. The Kuray (K) and Chuja (C) basins are shown in the headwater of the River Chuja.

catastrophic floods has been noted within the headwater valleys of the rivers Ob and Yenisei. For example, the Chulym, Chulyshman, Bashkaus, Biya, Chuja (Chuya) and Katun river valleys, amongst others (Grosswald & Rudoy, 1996; Frechen & Yamskikh, 1999), show evidence of superfloods, but only the Chuja–Katun system has been studied in any detail. The River Chuja, a tributary of the Katun, was the routeway for several very large floods. Brief descriptions of these outburst floods, which emanated from glacially dammed lakes in the Kuray and Chuja basins (Fig. 1), have been provided by Baker *et al.* (1993) and Rudoy & Baker (1993). Baker *et al.* (1993) concluded that there was one major Kuray–Chuja flood and a number of minor floods; the peak flow of the largest was apparently consistent with the sudden collapse of an ice-barrier.

This paper provides a more detailed overview of the region and the palaeogeography, together with an introduction to the sedimentology. Localities mentioned in the text are identified in three ways: by local place name; by latitude and longitude (degrees, minutes and decimal seconds—determined using GPS) and by reference to kilometre road markers (e.g. *km 672*) that give the distance from Novosibirsk. This degree of detail should help other scientific visitors find key localities. The primary objectives are to elucidate the detail of the flood dynamics of the Kuray–Chuja floods, and to define the temporal and spatial sequence of flooding.

PERSPECTIVE

The Altai mountains are part of an extensive, structurally complex succession of individual mountain ranges in central Asia stretching from the Tien Shan in the west to the Aldan range in the east. The Altai Mountains were up-thrust in the Eocene and early Oligocene and the majority of the area has been tectonically active to some degree throughout the Cenozoic (Tapponier & Molnar, 1979). As explained below, it is the distinctive tectonic history that set the scene for Quaternary catastrophic floods. Major subparallel faults trending north-west to south-east intersect subsidiary faults that trend roughly east–west. Increased lateral shearing in the Cenozoic resulted in pronounced off-sets in the north–south fault alignment (Nekhoroshev, 1966). The result is a series of ridges, such as the Kuray Range to the north and the North and South Chujski ranges to the south of the tectonic depressions of the Kuray and Chuja basins (Bogachkin, 1981) (Fig. 2). Vertical relative movement of the order of 2500 m took place, particularly during the Pliocene–Pleistocene transition, enhancing basin development. Further motion occurred again at the beginning of the Mid-Pleistocene and during the Late Pleistocene. During the latter phase, however, uplift in the Altai is believed to have been slight (Zyatkova, 1977; Serebryanny, 1984) and largely occurred following deglaciation (Nekhoroshev, 1966). Enclosed by north-west and east–west trending mountain chains, the depressions bounded by strike-slip faults now form spectacular enclosed intermontane basins. Sedimentation has resulted in up to 0.5 km of Neogene and Quaternary sediment fill in the Kuray Basin and over 1 km of fill in the Chuja Basin. The latter exhibits, in the Chagan River valley (N50°3′15.4″; E88°25′58.78″), one of the most complete and important sections of the Cenozoic within central Asia (Zykin & Kazanskii, 1995). Today these basins contain no significant water bodies and drainage is solely to the north-west via the gorge of the Chuja River (Fig. 3). During the Pleistocene, however, large ice-dammed lakes filled the depressions, as witnessed by lacustrine deposits and palaeoshorelines (Figs 3 & 4).

Within the modern Altai massif, short alpine glaciers, totalling some 909 km^2 in area, descend from small ice-caps around the margins of the intermontane basins of Kuray and Chuja (Fig. 2). Presently, most Altai glaciers are fed by moisture from south-westerly and north-westerly airstreams. However, during the Quaternary, a cold anticyclone developed over central Asia such that the prevailing winds were from the north and north-east (Velichko, 1984; Back & Strecker, 1998). The global Quaternary cooling coupled with the distinctive topography was important in controlling associated glaciations. However, it is not clear how many glacial cycles occurred in the Altai during the Pleistocene (Okishev, 1977). Local terminology varies but, in accord with the system adopted for other central Asian mountain glaciations, the Late Pleistocene may be divided into four units (Archipov, 1998). The oldest is the Kazantsevo interglacial (substage 5e of the ocean isotope scale) which followed a pre-150 ka glaciation: the Tazovo. Two Late Pleistocene glacial phases followed: the Ermakovian (*c.* 100–50 ka) and the Sartan (*c.* 22–13 ka). These latter distinct cold periods were separated by the Karginian mega-interstadial, during which climate ameliorated abruptly (Back & Strecker, 1998) but was punctuated by frequent cold phases (Yamskikh *et al.*, 1999). Together these three younger periods form the Zyriankan glaciation that corresponds to the Würm (Weichselian) of western Europe. During maximum glaciation ice descended to around 1200 m altitude (Vardaniants, 1938; Grosswald, 1998) such that ice-caps covered both mountains and intermontane basins, and the piedmont to the north of the Altai (Grosswald, 1998). The maximum extent of glaciation is well delineated by terminal moraines in the piedmont (Fig. 2). The climatic variability of the Karginian interstadial is seemingly complex; glaciation in the Altai Mountains may have been continuous, with ice retreating from the basin margins during the interstadial. Although Mid and Late Pleistocene ice surrounded the Kuray and Chuja basins, and glaciolacustrine sediment suites demonstrate that locally glaciers were proximal to the lake margins, nevertheless the basins remained ice-free throughout much of the Late Pleistocene (Svitoch & Khorev, 1975). For example, during the final Sartan cold stage, although persistent local ice-caps occurred at higher elevations (Okishev, 1977; Serebryanny, 1984), mountain valley glaciers descended only as far as the basin margins (Fig. 2). During the Late Pleistocene, ice did not extend below 1750 m altitude in the Chuja Basin (Rudoy, 1998). The Sartan stadial maximum occurred around 18 ka when coldest-month temperatures were about –30°C (10°C lower than present), warmest-month temperatures were about +10°C (4°C lower than present) and annual precipitation was about 200–300 mm (around 300 mm lower than present, Tarasov *et al.*, 1999). The associated biome was mainly tundra, but cold steppe and cold deciduous forest occurred locally (Tarasov *et al.*, 1999). From this stadial maximum, the retreat of valley glaciers was punctuated by eight readvances. The sketchy glacial chronology for the Altai is in accord with that for the neighbouring Sayan Mountains and with the detailed chronology from the region around Lake Baikal to the east (Back & Strecker, 1998) and the Tien Shan to the west (Grosswald *et al.*, 1994). On this basis the continental-dominated climatic system for central Siberia shows close similarity to that of west Siberia

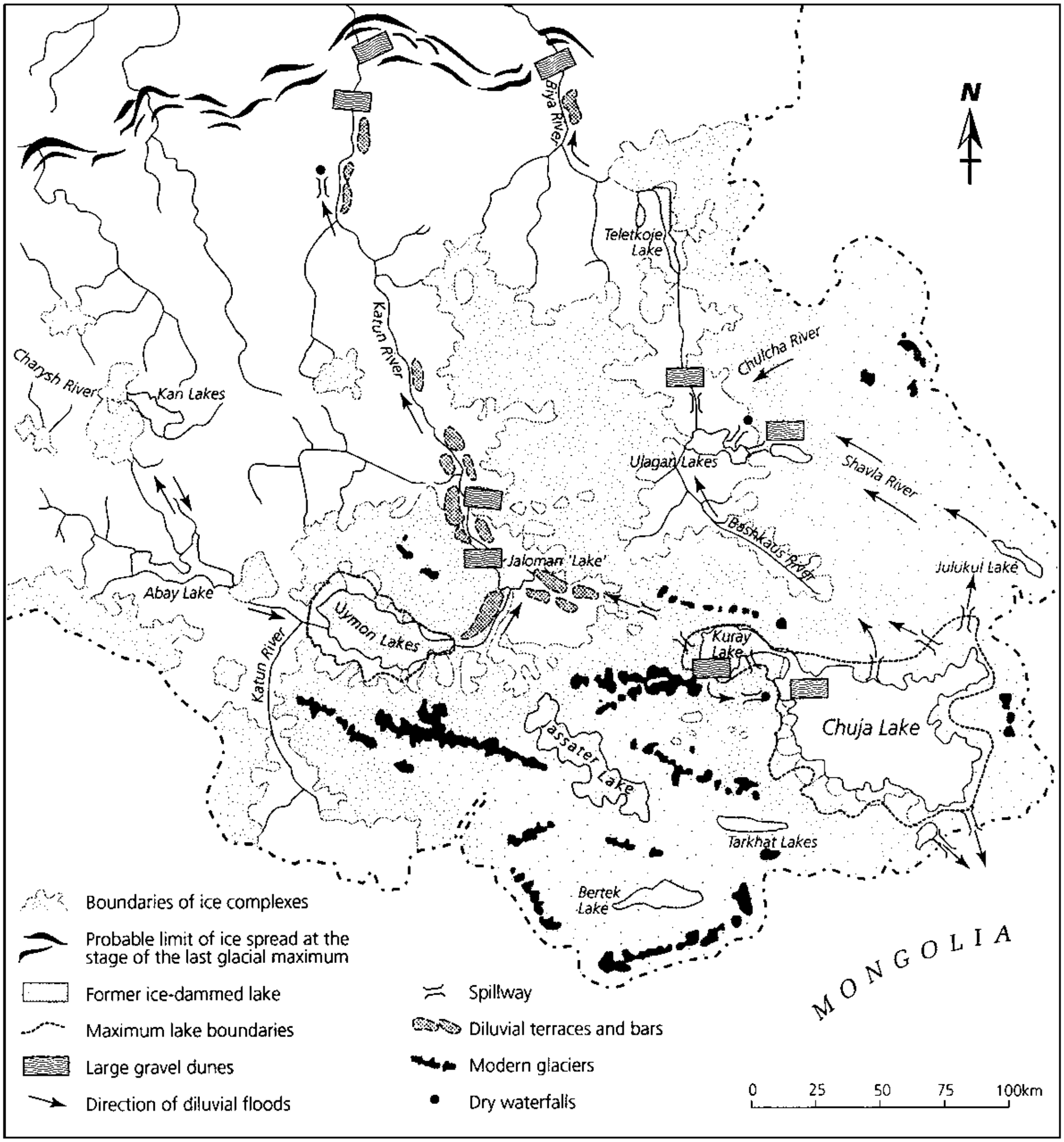

Fig. 2. Schematic palaeogeography of the Altai region during the Late Quaternary (after Rudoy, 1998). Approximate extent of ice-impounded lakes is based on strandline evidence and locations of glaciolacustrine sedimentary complexes. Maximum potential highstands are constrained by the modern altitude of potential outflow channels (spillways) without any correction for tectonic adjustments. Features in the Katun, Chuja and upper Bashkaus valleys and in the Kuray and Chuja basins have been verified by the authors. Note: dunefield in the upper Bashkaus valley reported by Rudoy (1998) could not be located by the authors and appears to be gullied terrain. Maximum extent of ice sheets during the Sartan is based on several Russian studies modified by Rudoy (1998). The Kuray and Chuja basins were ice-free.

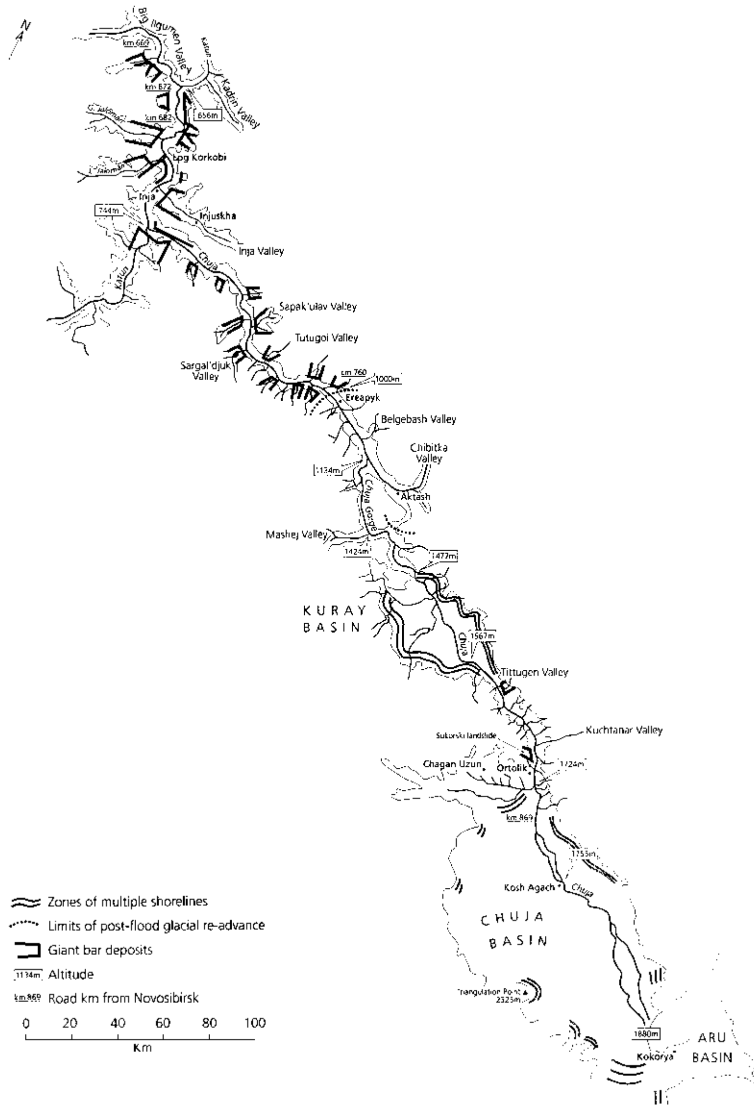

Fig. 3. Map of study area showing key locations and geomorphological features.

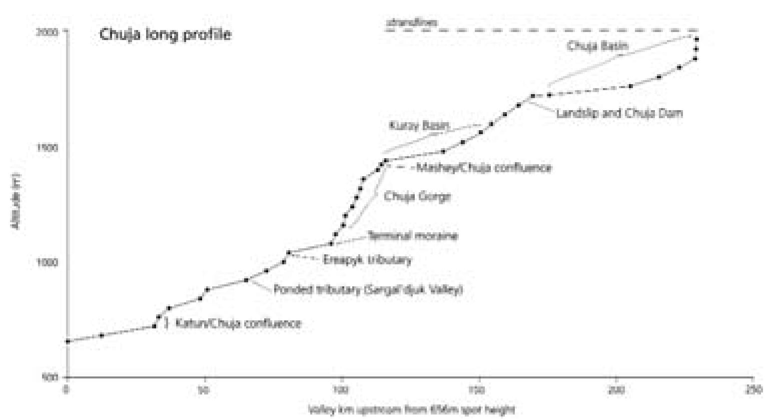

Fig. 4. Long-profile showing altitude of key locations and geomorphological features.

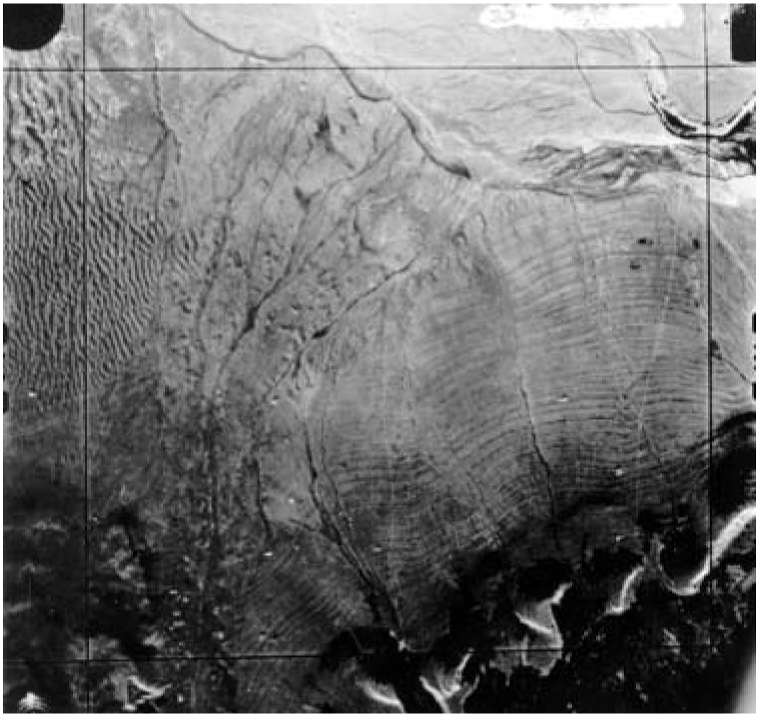

Fig. 5. Aerial view of portion of southern margin of the Kuray Basin. Tree-covered (bottom right) and treeless ridges (bottom left at an altitude of around 1700–1800 m) represent local bedrock outcrops and glacial end-moraines of former valley glaciers, which descended from the Chujski Range to terminate around the basin margins. The altitude of the basin floor (top) is around 1500 m. The subparallel lines (centre and right at an altitude between 1550 and 1650 m) are multiple strandlines representing fluctuations in the level of glacial Lake Kuray. The eastern extremity of the Kuray gravel dunefield can be seen at the top left (Carling, 1996a). Scale: horizontal distance is approximately 5.0 km.

and Europe during the past 130 ka (Archipov, 1998; Frechen & Yamskikh, 1999).

Using a variety of geomorphological evidence, including remnants of moraines (Rudoy, 1998), Baker *et al.* (1993) concluded that the Chuja gorge had been blocked periodically by ice-sheet lobes or large valley-glaciers, which coalesced in the vicinity of the Belgebash, Chibitka and Mashej valleys (Figs 3 & 4). The substantial ice-barriers impeded the only drainage line exiting from the Kuray and Chuja basins, causing the development of a temporal series of large ice-dammed lakes. Numerous wave-built strandlines testify to variation in the lake level and, being best developed on south and south-west basin margins, attest to the direction of the prevailing northerly wind during the Quaternary (Figs 3 & 5).

In the Chagan valley (Fig. 3), thermoluminescence (TL) dating of the most ancient glaciolacustrine moraine complexes (N50°1′7.6″; E88°17′11.25″) indicates a Mid-Pleistocene age (380 ka to 266 ka). More recent glaciolacustrine deposits have been dated at 145 ka and between 32 ka and 25 ka using ^{14}C assay (Svitoch & Khorev, 1975); the latter deposits overlie moraine dated at 58 ka. In addition, the presence of lacustrine dropstones at a number of locations (e.g. near Kokorya: N49°56′49.69″; E89°4′15.97″) and strandlines on the 58 ka moraine attest to the former presence of glacial lakes that were contemporaneous with, or post-date, some glaciolacustrine successions. Notwithstanding tectonic adjustments, strandlines at a range of elevations show that lake levels fluctuated greatly, occasionally attaining depths of several hundred metres. The lowest strandlines (below about 1940 m altitude) in the Chuja Basin are faint, are developed on gently sloping terrain and are widely held to be Late Pleistocene. Distinctive strandlines occur at higher elevations on the northern side of the basin and are most prominent on ‘headlands’ along the southern margin. Here recurved spits at several elevations show that longshore drift was universally from north-west to south-east along this southern shore (Fig. 6). The altitude and longshore gradient of a suite of Chuja strandlines have been surveyed below a triangulation point (*c.* 2137 m N49°48′; E88°56′) located in the south-east of the basin (Fig. 3). Seven distinct accretionary strandlines range between *c.* 2105 m and 1960 m, although locally the elevations are indicated by notches cut in weak bedrock. Several pits dug in the strandlines together with two ground-penetrating radar (GPR) profiles (one shore parallel and one shore

Fig. 6. View looking north across the Chuja Basin from a bedrock 'headland' on the southern margin of the basin. In the immediate foreground (A) is the steep outer margin of a strandline. Below this, running obliquely across the view, is a strandline (B) at a lower elevation. A third lower strandline (C) terminates in a distinctive recurved gravel spit (longshore transport left to right). The central dark area consists of lush vegetation developed on fine sediments deposited within the recurve of the spit. A human figure (arrowed) can be seen immediately right of centre and cow-sheds just beyond the spit provide scale. Additional low-amplitude spits are present top-centre, depicted as light-coloured areas interfingering with darker wetland vegetation to the right.

normal) reveal decimetre-thick units of poorly sorted, angular, pebble gravels interspersed with fine sand lenses, the latter up to several centimetres thick. The lowest of these strandlines has been ^{14}C dated recently to 32 190 ± 260 yr BP (U. Moody, Florida Community College, Jacksonville, personal communication, 2000). Svitoch & Khorev (1975) argue that the highest strandlines (up to 2100 m) are more ancient. Possible high-level spillways at similar elevations (2100 m) have been identified by Rudoy *et al.* (1989). These various surveys yield a potential total lake depth of around 300 m in the Chuja Basin and up to 600 m in the Kuray Basin, giving maximum lake volumes of about 600 km^3 in the Chuja Basin and a volume of around 400 km^3 in the Kuray Basin (Rudoy, 1988; Rudoy *et al.*, 1989). The Kuray strandlines (Fig. 5) have been mapped at elevations between 1615 m and 2000 m and demonstrate longshore gradients of up to a degree or two. High-level strandlines at Kuray penetrate the valley connecting to the Chuja Basin, and low-level strandlines curve around and cut across the entrance to the valley near Tidtugem. Thus at low lake levels a separate lake developed in the Kuray Basin. The Chuja strandlines have subparallel longshore gradients up to 5°, decreasing in altitude towards the north-west. Although previously ascribed to tectonic tilting alone (Svitoch & Khorev, 1975), close inspection shows that some suites of similarly tilted strandlines occur at the same altitude on neighbouring headlands and that the width and height of each accretionary body increases in a south-easterly direction towards the promontory. Thus the tilting in part may be ascribed to depositional processes associated with the residual direction of drift. However, future study clearly is required to couple the history of strandline development to tectonic tilting and physically realistic ice-dam thicknesses.

Two distinct Late Pleistocene moraines (*km 849*) (TL dated *c.* 30 ka and 18–20 ka) demonstrate that a glacier emerging from the Kuehtanar valley (*km 851*) blocked the corridor connecting the Chuja and Kuray basins (Rudoy, 1998), such that lake levels in Chuja and Kuray were at times not necessarily concordant. At the same location a very large landslide complex is found opposite the Kuehtanar valley. This deposit occupies the whole easterly flank of the Sukorski Mountain and may have resulted from over steepening of the valley wall by glaciation, or by floods. Parts of the complex pre-date and post-date the moraines. The orientation of large gravel bedforms near Chagan-Uzun (*km 861*; N50°5′18.25″; E88°22′7.42″; Fig. 3) and Kam-Sugi (*km 869*; N50°35′7″; E88°25′8.78″) show that flood waters flowed from the Chuja Basin to the Kuray Basin. Throughout the length of the corridor, large 'bars' or moraines (?) block the entrance to several tributary rivers between Tidtugem (*km 840*) and *km 848*. Low-level strandlines cut into these deposits demonstrate that the Kuray Lake reformed after glacier retreat and after any major flood from the Chuja Basin.

Detailed studies of terrace deposits in the Yenisei River valley, within the neighbouring Sayan Mountains (Fig. 1), show multiple episodes of glacial flooding from 40 ka extending into the early Holocene (Yamskikh, 1972, 1996; Frechen & Yamskikh, 1999). In part, the flooding in the Yenisei system may have been fed by outburst floods from a glacially dammed lake in the Darkhat Basin of northern Mongolia (Grosswald, 1987; Grosswald & Rudoy, 1996). Such meltwater events may be associated with repeated rapid fluctuations between warm and cold climatic phases (Kind, 1974) and/or with the cyclical refilling of the lake basins by meltwater until the impounding ice-dams failed (Grosswald, 1987; Rudoy, 1998). Repeated breaching and reforming of the ice-barrier(s) impounding the Kuray–Chuja lakes would have resulted in lake-level fluctuations. A series of superfloods would have resulted, routed down the steep course of the Chuja and Katun rivers, with the greatest flood estimated to have peaked at $16–18 \times 10^6$ m^3 s^{-1}, with local flood-water depths reaching 400 m (Baker *et al*., 1993). However, radiocarbon assays of organic material from (active) pingos in the Kuray Basin (N50°11′29.15″; E87°43′37.35″) and at Tebelar village in the Chuja Basin show that any residual lakes had drained by 10 845 ± 80 yr BP (CO AH-2346) and 3810 ± 105 yr BP (CO AH-2146), respectively (Rudoy, 1988, 1998). A palaeosol developed on a low-level strandline in the Chuja Basin has been dated recently to 2580 ± 70 yr BP (U. Moody, Florida Community College, Jacksonville, personal communication, 2000). Svitoch (1978, 1987) placed the Late Pleistocene glacial maximum at 58 ka (± 6.7 ka) with well-established recessional standstills at 32 ka (± 4 ka), 25.6 ka (± 0.6 ka) and 3.2 ka (± 0.6 ka) separated by small readvances. In many areas of the world, including south Siberia (Svitoch & Khorev, 1975), the first stage of late glacial warming was abrupt, with rapid warming over as little as 200–300 yr (Crowley & North, 1991). Such rapid change could account for the catastrophic breaching of glacial barriers and the rapid draining of large ice-dammed lakes world-wide. The global-scale abrupt warming at *c*. 13 ka, followed by a short period of climatic reversal at 11 ka, and renewed warming around 10 ka to 8 ka, is broadly reflected in south Siberia where the moraine sequences indicate that the final deglaciation in the Altai was complex but nevertheless rapid (Svitoch & Khorev, 1975). Similarly, unpublished studies (P.S. Borodavko, Tomsk State University, personal communication, 2000) of Altanian lake cores universally demonstrate development of organic deposits no earlier than 13 ka. Maloletko (1980) sampled alluvial deposits on the Maima terrace 40 m above the modern River Katun in the Altai foothills; two samples provided ^{14}C dates of 13 890 ± 200 yr BP (LG-92) and 12 750 ± 65 yr BP (CO AH-779). Maloletko & Paniechev (1991) obtained four dates, from alluvial terraces close to the Maima terrace, of between 28 730 ± 995 yr BP and 20 500 ± 240 yr BP, whereas Carling (1996a) obtained a TL date for silts in gravel dunes at nearby Platovo (N52°5′44.43″; E85°53′42.18″) of 36 ka (± 4 ka). Such a wide range of dates for alluvial deposits probably attests to the long period of flooding associated with southern Siberia. A.F. Yamskikh (Pedagogical University, Krasnoyarsk, personal communication, 1998), for example, from detailed studies of alluvial deposits in the headwaters of the Yenisei River, identified periods of flooding from 110 ka to as recently as 1.5 ka. However, he believes that two significant Late Pleistocene periods are particularly associated with ice-dam-related flooding. The Karginian interstadial saw the development of boreal forest in the piedmont of the Altai, with periodic cooling, high flood levels and the local development of loess. The period 21 ka to 10.5 ka was the coldest period in the Late Pleistocene, but was characterized by short-period warming, the development of dammed lakes, large floods and accumulation of loess.

MAIN DEPOSITIONAL ASSOCIATIONS

Four main sedimentary associations found in the immediate study area have been identified as relevant to this investigation. These are (i) large gravel dunes and sand dunes; (ii) giant flood bars; (iii) fluvioglacial terraces; and (iv) lacustrine units. Interpretations of the flood history are based on surveys of the bars, lacustrine and fluvioglacial associations described in the text below. Gravel dunes have been described by Carling (1996a,b).

Gravel dunes and sand dunes

Fields of gravel dunes occur at a number of locations within the Katun River valley (such as at Little Jaloman; N50°29′21.4″; E86°37′35.2″) and within the Kuray Basin (e.g. near Kuray village N50°11′4.86″; E87°55′23.65″; Fig. 2). Carling (1996a) considered that the dunefields in the Katun River valley formed as flood waters surged down the valley. In contrast it is probable that the dunefields in the Kuray and Chuja basins formed *beneath* lake waters during the final stages of lake-level drawdown during a lake drainage event. Huggenberger *et al*. (1998) used GPR surveys (calibrated using grain-size analysis and stratigraphical mapping of small sections) to elucidate the internal structures of several two-dimensional dunes. A striking feature was the presence of continuous, subhorizontal reflections in sections parallel to the palaeoflow. These reflections separate sets of inclined reflections, identified as cross-sets consisting of alternate layers of well-sorted open-framework cobbles and bimodal finer gravels. Steeper reflections represent lee-side avalanche sets, whereas low-angle reflectors represent sorting processes associated with bedload sheets on low-angle lee-sides. Sections parallel to and beneath crestlines locally show trough-shaped reflectors indicative of more strongly three-dimensional sedimentary structures associated with lobes or saddles in the dune crestlines. Taken together this evidence is interpreted to represent unsteady downstream migration of two-dimensional dunes, about 2 m in height in an aggradational setting.

As well as the dunefields described by Carling (1996a), additional dunefields were located in 1999 and 2000. Two gravel dunefields occur near Baratel (N50°15′35.84″; E87°44′47.51″) within minor side-valleys close to the Chuja gorge. At an altitude of 1710 m, these bedforms indicate strong currents moving towards the lake outlet into the Chuja valley. At the same location, but at a slightly higher altitude, strandlines terminate abruptly, close to where the ice-dam would have existed. Within the Chuja valley, weakly developed dunes occur on top of a giant bar at Iodro (N50°23′46.5″; E86°59′9.9″). In addition, a group of six immense flow-transverse gravel bedforms (antidunes?) occurs within the exit to the Chuja Basin at *km 861*, close to the village of Chagan-Uzun (Fig. 3); the largest bedform is 20 m high and 300 m long in the direction of the palaeoflow. An extensive field of gravel dunes also occurs at Kam-Sugi (*km 869*)—both these sets of bedforms indicate flow from the Chuja Basin through the corridor to the Kuray Basin. Speransky (1937) and Lungershausen & Rakovets (1958) correctly identified the bedforms in the Kuray Basin as dunes. Latterly many Soviet geologists believed incorrectly that these structures were rogen moraine (or parallel-gullied outwash) owing to the distinct 'ribbed' or 'rippled' planform characteristic of this type of glacial moraine (Hättestrand & Kleman, 1999). Considered together the various bedforms of the Kuray and Chuja basins attest to the former flow direction of lake waters emptying rapidly into the Chuja and Katun river valleys. These floods can be traced into the lower piedmont zone of the Katun River (Fig. 2), where extensive fields of fossil subaqueous gravel and sand dunes have been identified on river terraces (Butvilovsky, 1993). For example, some 2 km to the south of the village of Surtaika, large dunes consisting of fine sand occur on both sides of the road (N52°12′27.5″; E85°53′44.4″). Road-side sections, including a gravel pit at the confluence of the rivers Isha and Katun, show that the dunes overlie a gravel terrace and are themselves covered by up to 0.5 m of loess. Along the course of the River Katun, gravel dunes are found as far north as the town of Chemal. Here a well-defined dunefield (N51°21′9.91″; E86°2′47″) occurs on the top of a giant flood bar close to the confluence of the tributary River Tolgoek and the River Katun (Okishev, 1997; his fig. 2).

Giant bars

Downstream of the Chuja gorge a series of prominent diluvial gravel bars occur within the Chuja River valley from *km 760* near the village of Erbalyk and along the course of the Katun River until *km 672* (Fig. 3). At this point the Katun River turns abruptly to the east into a narrow gorge and the valley width is halved. In addition, the Kadrin River valley (Fig. 3) is known to have contained a glacier, which on occasion extended into the valley of the Katun River. Thus passage of any large flood-wave would have been impeded at this point by the valley constriction (and possibly by the Kadrin glacier) causing temporary 'ponding' of flood water for several kilometres upstream. The surge from the flood in the Katun valley would have run directly into the tributary Big Ilgumen valley (Fig. 3), such that diluvial 'run-up' deposits extend to the north-west at an altitude of 800–840 m near *km 669*.

The most massive of the diluvial bars (N50°21′48.3″; E86°40′44.1″) blocks the Katun River valley at the Chuja River confluence, which demonstrates that the greatest floods came down the Chuja valley from the Kuray Basin. These bars either infill small alcoves that flank the main valley (Fig. 7); or form barriers across larger side-valleys (Fig. 8); or occur on the inside of main valley bends in a similar position to point-bars within river channels (Fig. 9). These bars have steep (outer) margins (see Fig. 11) facing the main valley (typically 20° to 35° slopes; Fig. 7), rise 80–120 m above the highest river terrace, and individually are up to 5 km in length. Often 'run-up' deposits are found (tens of metres higher than the elevation of the bar-top) on the downstream side of the tributary where flood waters surged against the valley flank (see Fig. 11a). In the Chuja valley, distinct benches are cut in the outer margins (e.g. at the Satakular and Tutugoi valley locations; N50°22′39.6″; E87°2′39.8″; Fig. 7). Where bars developed across the entrances to tributary valleys, temporary lakes often formed in the impounded tributaries, as witnessed by lacustrine deposits. The tributaries subsequently cut through the barriers, thus draining the small lakes. However, a small lake still exists behind an intact bar in the Sargal'djuk valley (N50°19′41.1″; E87°3′28.5″; Figs 3 & 4). Later, further main valley floods entered the embayments and deposited more gravel in the areas behind the original bars. These later gravel deposits may be intercalated with lacustrine deposits within the side-valleys.

Fig. 7. Distinct benches cut in a giant gravel bar flanking the Chuja valley (flow right to left). At the extreme right a wedge of (light-coloured) flood gravels (A) can be seen partially filling a right-bank tributary valley. Flood sediments are thin on the rocky ridges, but the benches are well developed in the small alcoves between the ridges. In the centre foreground is the Chuja River incised into the boulder-strewn 'Inja' terrace.

Fig. 8. Aerial view of the Little Jaloman giant bar. Mountain massifs are present far right and bottom left. The Katun River flows northwards from bottom right to top left. A left-bank tributary, the Little Jaloman River, joins the Katun River from centre far-left. The ovoid mass in the centre of the image is the Little Jaloman giant bar developed on the inside curve of the valley. Originally the bar extended across the entrance to the Little Jaloman valley filling the tributary with flood gravels. The tributary has trenched through these deposits, which are now heavily gullied, both along the course of the Little Jaloman River and along the outer margin of the bar within the Katun valley. Pock-marks and sinuous features on the bar top are kettle holes and associated drainage gullies, which resulted from melt-out of stranded ice-blocks (partially obscured by cultivation). Scale: horizontal distance is approximately 5.0 km.

Fig. 9. View from the top of the giant bar blocking the right-bank tributary to the Katun River at the village of Inja (far left). The Inja River breaches the giant bar in a deep narrow defile below the electricity pylon (arrowed). The Katun River in the foreground flows from left to right entrenched in the Inja terrace. Centre-right, the upstream portion of the Little Jaloman giant bar may be seen (A), developed above the terrace level, in the lee of the dark mountain massif (Fig. 8). The 20-m-high pylon and habitation provide scale.

There are two styles of bar deposition related to whether the bars are proximal or distal with respect to the flood source. Bars within the Chuja valley consist largely of deposits of pebble gravels, some 100 m thick, although cobble- or boulder-beds also are very common (Fig. 10). Within each tributary valley, the bars consist primarily of stacks of multiple, subparallel gravel sheets, each some decimetres to 2 m thick. Within the Satakular bar (Fig. 3), individually the sheets form planar surfaces that dip towards the main valley and thus are inclined upwards, and obliquely, into the tributary valley. A well-developed, preferred pebble imbrication also indicates that bedload transport was from the main valley obliquely into the tributary. Together, these observations indicate that the bar was built up by sheets of bedload entering the tributary valley from the flood in the main valley in separated, recirculating flow-cells (Fig. 11). As the bar developed in height, flood water would have continued to wash over the bar top so that some deposits in the inner part of the bar should reflect this overwash process. However, the structure of the inner margins of these Chuja bars is not known, owing to poor exposures, but the present-day inner margins occasionally are extremely steep (including angle-of-repose), forming impressive barriers tens of metres high across the tributaries. Thus, the process of deposition is analogous to that of a barrier-bar process, whereby sediment moves across a planar, low-angle outer-margin to be deposited on a steep overwash lee-side. The Chuja valley is steep and narrow, such that flood velocity would have been very high (Baker *et al.*, 1993). This control, together with the fact that the bar outer-margins dip towards the main valley, probably indicates that the bar sediments never prograded far towards the centre of the main valley. Consequently, the modern morphology of the bars is essentially the same as immediately after the flood episode. However, some benches on the outer-margins of many Chuja bars probably are erosional, reflecting stillstands in the recession of the flood wave (Figs 7 & 11c).

Fig. 10. Proximal bars, within the Chuja valley, consist largely of deposits of pebble gravels some 100 m thick, although cobble- or boulder-beds also are common. This section is marked as (x) in Fig. 11a, and is about 70 m above the Chuja River within the giant bar that blocks the tributary Satakular River (Fig. 3). The view is from the upstream flank (Fig. 11a) of the tributary looking obliquely downstream towards the Chuja valley. The bar consists primarily of stacks of multiple, subparallel gravel sheets, each a few decimetres to 2 m thick. Individually the sheets form planar surfaces that dip obliquely towards the main valley (Fig. 11b).

The largest bars occur in the Katun River valley close to the villages of Inja and Little Jaloman (Fig. 3).

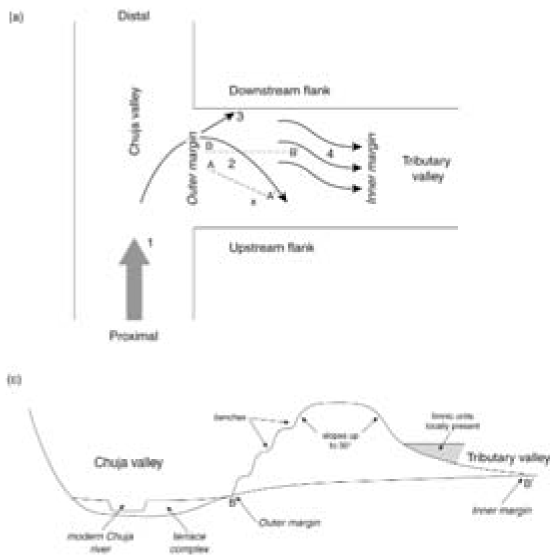

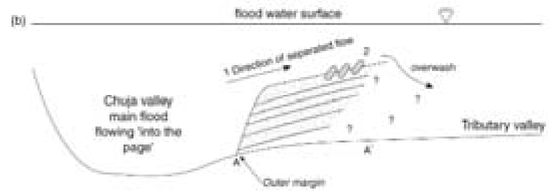

Fig. 11. Cartoon depicting the mechanism by which giant bars were deposited within tributaries to the Chuja River. (a) The flood wave in the main valley (1) generated a giant eddy into the tributary (2) as well as 'run-up' deposits (3) high on the downstream flank. Coarse gravel deposition was confined initially to the immediate tributary mouth, latterly sediments were washed over (4) the developing bar into the ponded tributary valley. (b) The section A–A′ (Fig. 11a) demonstrates how the separated flow (1) within the eddy resulted in primary bedding and imbrication (2) dipping obliquely across the entrance to the tributary. Lateral trimming of the outer margin of the bar caused over-steepening of the outer margin. (c) The section B–B′ (Fig. 11a) shows the characteristic, flat-topped bar-form seen today, characterized by steep inner and outer margins. Benches (Fig. 7) developed on the outer margin during flood draw-down. The effective blocking of the tributary resulted in the development of a small lake, indicated by limnic sediments.

The Inja bar forms a barrier across the Inja River valley (N50°27′25″; E86°38′1.8″) in which there are three lacustrine deposits separated by units of flood gravels. The Little Jaloman bar forms a broad 'point-bar' that extends across the entrance to the Little Jaloman River valley in which there are no lacustrine deposits (Figs 8 & 9). Distinctive cone-shaped hollows with associated drainage gullies on the top of the Little Jaloman bar (Fig. 8), as well as on other bars, are ascribed to melt-out of stranded ice blocks (Maizels, 1977; Syverson, 1998). These features are similar to kettle-holes, and concentrations of large angular boulders in the upstream portions of the bars are indicative of flood flow tearing bedrock from the adjacent valley walls.

In contrast to the coarse pebble gravels in the Chuja valley, down-system fining is such that the Katun valley bars, near Inja and Little Jaloman, consist mainly of fine pebbles and granules. Average grain size further decreases down-valley to granules and sand near *km 672*. In the vicinity of Little Jaloman and Inja, the valley gradient is reduced (Fig. 4), the valley widens, and here the largest bars are found. These bars tend to have steep truncated outer margins (Fig. 8), although the bedding in the outer margin is near-horizontal, or dips gently towards the main valley centre. This stratigraphy indicates that the outer margins originally extended towards the centre of the main valley, but subsequently have been cut back to some degree by lateral erosion.

In contrast to the Chuja valley bars, the bars in the Katun valley often have gentle inner margins, with deposits extending some thousands of metres up the tributaries (Figs 12 & 13). Trenching by streams has resulted in good exposures of the bar sediments at locations near the outer and inner margins of bars within the tributary valleys. The bar-top surface and major bedding planes dip into the tributary valleys at angles of a few degrees to 10°. As a result, deposits pinch-out up-tributary at a distance of some 2 km. Beds are thickest (10–20 m) proximally at the base of the bar, and thin distally, reaching a minimum thickness of about 1–2 m (Fig. 14). The sediment, consisting of fine pebbles and granules, tends to show constant grain size or fines distally, as trough cross-bedded coarse angular sands and granules commonly replace gravels up-tributary.

The bar deposits at Little Jaloman consist of 11 distinct successions (Fig. 15). The facies characteristics of each succession are fundamentally identical one with another except in terms of thickness and local detail. The lowest successions within the proximal deposits (Fig. 14) can be 10–20 m thick, but this decreases

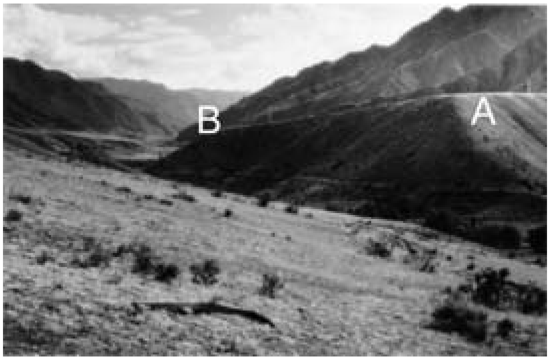

Fig. 12. Oblique view, into the tributary, of the gravel infill on the downstream flank of the Little Jaloman valley. The river has cut a deep defile through the giant bar. The steep outer margin of the bar (A) is sun-lit on the right beneath a 20-m-high pylon. The bar top, on the true left flank of the tributary, slopes back into the valley at a uniform gradient before steepening beyond a second pylon. The inner margin is at (B).

both vertically and towards the inner margin. In view of the distinct repetition, successions can be termed *rhythmites*. The monotonous repetition of the facies in each superimposed succession implies a repetitive flow control rather than vagaries in sediment supply. Within the lower to mid-sequence of the rhythm (not shown) massive coarse gravels give way to smaller scale coarsening or fining-upward sets of subparallel laminae and beds of granules and pebbles, 3 mm to 400 mm thick. Isolated cobbles and boulders in fine gravels are common. Higher in the sequence undulating-, sigmoidal- or cross-beds of very coarse sand and granules occur beneath a cap of coarse fluvial gravel/ debris flow deposits (top of Fig. 15 and see Fig. 16).

Lacustrine successions

Giant bars temporarily impounded small lakes in some of the tributaries until the tributaries cut down

Fig. 13. Oblique view, into the tributary, of the gravel infill on the upstream flank of the Little Jaloman valley (viewed from beneath the pylon in Fig. 12). The bar top is out of sight to the left, from which direction flood water would have entered the tributary from the Katun valley. The sedimentary surface (A) (abutting the flanking mountains), and the bedding of the deposits, slope into the valley at about 10°, finally pinching out 2 km upstream (Fig. 14). Originally the fill would have constituted a continuous surface but the tributary subsequently cut through the deposits.

Fig. 14. Cartoon depicting mechanism by which giant bars were deposited within tributaries to the Katun River. Section extends from the outer margin adjacent to the Katun valley to the inner margin within the tributary. Bedding is often self-similar, forming a series of stacked rhythms (of which only three are depicted here). These rhythms thin distally and in some tributaries interbed with limnic deposits. The separated flood flow (1) entered the tributary above an accreting bar-form, evidence for return currents (2) is weak and flow-direction indicators, such as particle orientation (3), suggest up-tributary flow.

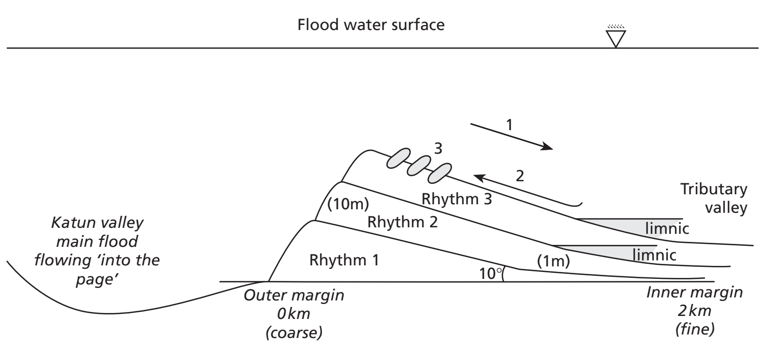

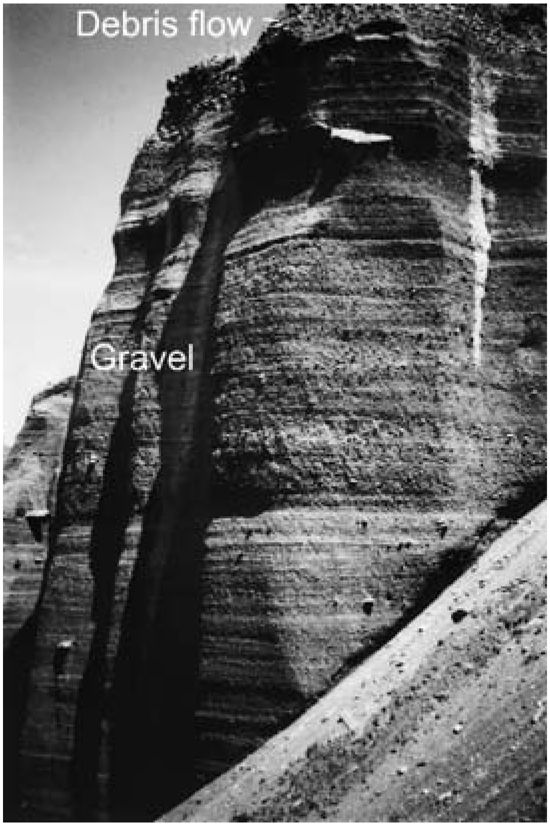

Fig. 15. Eight-metre-high section representing one rhythm of deposition in a stack of 11 self-similar units within giant bar deposits in the Little Jaloman River valley.

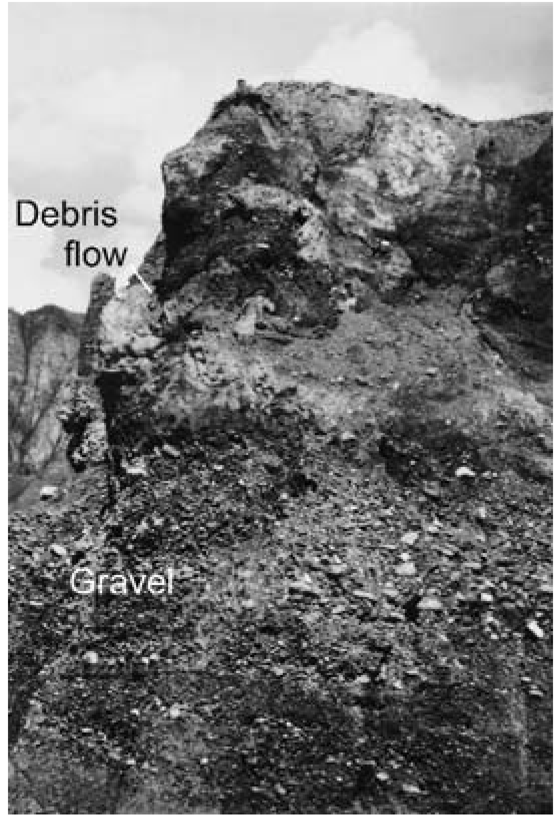

Fig. 16. Two-metre section of coarse fluvial gravel and debris flow deposits at top of rhythm shown in Fig. 15.

and drained the lakes (Figs 11c & 14). Within the Inja valley there is clear evidence for at least three lacustrine units separated by flood-gravel units. Gully sections in giant bar sediments in the Inja valley, adjacent to the village of Injuskha, expose the full 70-m thickness of the sediment pile. The sections show at least three flood-gravel units separated by three episodes of lacustrine deposition. The last and highest lacustrine unit forms the present-day horizontal surface behind the giant bar. The lake sediments are finely laminated or rippled white silts (Munsell 10 YR 8/1) with red staining (Munsell 10 YR 8/8) in some laminae. Worm trails are abundant in the upper lacustrine silts and fish bones have been reported (Ragosin, 1942). Convolution (Fig. 17) and local intercalation of the lacustrine deposits with reworked flood gravels reflect reworking of the earliest lake silts and flood gravels by subsequent floods. In addition, the sediment pile was unconsolidated and slumped as progressive downcutting by the tributary stream breached the bar and trenched the lacustrine fill. Until recently, the age of these Inja deposits was disputed. Ragosin (1942) suggested a Late Mesozoic or Tertiary origin, whereas Svitoch & Khorev (1975) and Svitoch (1987), using radiocarbon and luminescence dating, argue for deposition at the end of the Late Pleistocene during the Karginian interstadial (between 46 ka and 23 ka). Recently, however, the middle and the upper lacustrine units have yielded ^{14}C dates of 23 350 ± 400 yr BP and 22 275 ± 370 yr BP, respectively (Barishnikov, 1992). During this study an infrared stimulated luminescence (IRSL) date of 22.4 ka (± 2.3 ka) was obtained for the middle lacustrine unit by the Desert Research Laboratory in Reno, Nevada. Thus a Sartan stadial date seems appropriate.

Fig. 17. Convoluted laminations of fine white lacustrine silts. Axe is 50 cm long.

Terrace successions

The terrace gravels have not been studied in detail and further stratigraphical and sedimentological investigation is needed. To date only the basic relationships have been recorded. Near Little Jaloman village the sediment-fill in the Katun River valley consists of up to 90-m thickness of terrace gravel (Fig. 5), which thins upstream to less than 60-m thickness in the Chuja River valley (Fig. 6). The modern river has cut a deep narrow trench in this sediment. Two main terrace levels occur: one broad terrace primarily at 80 m above the modern river, is termed the Inja terrace, and another narrower terrace is 5–10 m higher. Minor terracettes, similar to those in braided rivers, occur on the 80-m level and up to six other discontinuous terraces occur along the trench walls. A single TL assay of questionable validity, 55 m above the river near the Chuja–Katun confluence, dates the Inja terrace to 148 ka (± 16.7 ka) such that it was formerly believed that the terrace sequence should be older than the Inja bar (Svitoch, 1978). Despite the TL dating, poor exposures of sediment sections at Log Korkobi and Inja demonstrate that the giant bar gravels extend beneath the terrace gravels towards the centre of the valley. A good exposure at the confluence of the Katun and Chuja rivers shows giant bar sediments on a bedrock surface at the modern river level with debris flow and terrace gravels above. In each example the contact is distinct and unconformable. Consequently, the bar sediments must pre-date the terrace sequences. At Log Korkobi, and at some other locations, the lowest valley-fill, at the base of the terrace gravels, lies on bedrock and consists of a 1-m thickness of grey (Munsell 5Y 6/1) silty sand dated by IRSL to 47.2 ka (± 6.7 ka). This layer is overlain by a 3-m to 10-m thickness of cobbles with a distinctive cream-coloured (Munsell 10 YR 8/2) silt matrix. Above is the rest of the terrace succession. This has not been mapped in detail but consists of trough cross-bedded braided river deposits, conformably and unconformably interspersed with several decametres of very poorly sorted, coarse gravel beds, which include numerous boulders up to 2 m in diameter. These latter coarse beds are interpreted as large-scale grain-flow deposits. Throughout the succession of coarse gravels, several horizontally laminated fine sand and silt beds occur. These beds are up to 1 m thick but pinch-out laterally after several decametres. These sandy units appear to represent temporary small ponds, formed by river inundation of hollows on former braidplain levels. Near Great Jaloman, the terrace succession is capped by a massive boulder-layer consisting of well-rounded, half-metre size boulders forming a single bed up to 3 m thick. Although most terrace gravels are horizontally bedded there are a few locations where a single, thick unit of cross-stratified gravel is in evidence. For example, on the right bank of the Katun River, opposite the confluence of the Little Jaloman River, the terrace gravels consist of a single 30-m-thick unit of cross-stratified gravel in which individual foresets can be traced, dipping steeply (up to 30°) away from the valley margin. A similar 10-m-high unit occurs just downstream of a bridge crossing the Chuja River at the village of Iodro (N50°24′1.0″; E86°58′22.8″). In both cases, the large-scale foresets lie on bedrock at the base of the terrace succession.

The distinctive large-scale gravel foresets noted near Little Jaloman and elsewhere are interpreted as originally constituting a largely unmodified Gilbert-type 'delta', similar to that described for fluvioglacial deposition into standing water (Clemmensen & Houmark-Neilsen, 1981; Smith & Jol, 1997; Plink-Björklund & Ronnert, 1999). This interpretation is reinforced by a distinct upward coarsening from the bottom-set through the foresets to the boulder top-set. The generally gradational contacts between the gravel beds indicate penecontemporaneous deposition of the complete cross-stratified succession.

PRELIMINARY INTERPRETATION OF DEPOSITIONAL ASSOCIATIONS

The interbedded succession of flood gravels and limnic units in the Inja valley demonstrates that at least three large floods in the Katun River valley penetrated the tributary valley of the Inja River. The two later floods overtopped the earlier bar deposits and added flood gravels to the local succession. On the basis of the evidence at Inja it is assumed that the complete suite of giant bars found along the course of the Chuja and Katun rivers are of a similar age range, and in many cases may be compound sedimentary bodies derived from several flood episodes.

The following sequence of events is envisaged. The earliest giant bars were deposited around 23 ka, as indicated by the date of the earliest limnic unit in the Inja valley. At this time the valleys of the Chuja and Katun rivers may have contained little sediment, or the initial flood surge scoured the main valleys to bedrock. The evidence is that only remnants of older deposits are to be found, such as the grey silty sand dated by IRSL to 47.2 ka. These thin remnants are preserved beneath giant bar gravels, which largely sit directly on the bedrock surface close to the altitude of the modern river. Over a total period of several thousand years a number of large floods, some 200 m or more in depth, coursed down the steep Chuja River valley depositing giant bars at each tributary confluence. The primary source of the sediments was material eroded from fluvioglacial fans deposited within the Kuray and Chuja lake basins upstream, but local valley-side bedrock, scree and glacial deposits were also eroded and then redeposited in alluvial successions. In the steep Chuja River valley, flood power was great and the primary sediment source close to hand. Hence the giant bars tend to consist of coarse gravel. Downstream of the confluence of the Chuja and Katun rivers the gradient of the valley is reduced, the valley widens and here flood power was reduced. In addition, flood waters were ponded temporarily by the valley constriction at *km 672* (Fig. 3). Consequently flood waters backed up in the Katun valley, between *km 672* and the Chuja–Katun confluence, depositing several large fine gravel bars, including those at Inja and Log Korkobi. The back-water effect extended up the Katun River valley for about 15 km above the Chuja confluence, infilling the Katun valley with two large bar complexes, which extend from Sok-Yarik (N50°16′35.1″; E86°41′51.9″) to Komdodj (N50°22′26.6″; E86°40′5.1″).

The power of the flood could erode and transport blocks of many metres in diameter from the valley walls (Baker *et al.*, 1993). However, most of the flood gravels in the Katun valley giant bars consist of pebbles and granules. Presumably large blocks were readily fragmented by the flood power (~ 10^5 W m^{-2}; Baker *et al.*, 1993) or were numerically insignificant compared with finer gravels. On the rising limb of a flood, coarse cobble-sized gravels were rapidly deposited in the tributary mouths probably forming an initial deposit, typically 10–20 m high, similar to a coastal spit across each side-valley. As water depths increased during the main flood, the side-valleys became deeply flooded such that finer gravels were deposited above the cobble-sized deposits from a high-concentration suspension; these finer gravels extend further into the tributaries than the cobble gravels. The finer gravels form successions typically between 70 and 200 m high.

In contrast to the fine gravels in the bars, the terrace gravels are much coarser, generally consisting of cobble or boulder gravel, including debris-flow units and large-scale cut-and-fill sequences, the latter typical of braided river deposits. The whole terrace succession often exhibits boulders concentrated at the terrace surface (Fig. 7). The stratigraphical relationship between giant bars and the terrace infill shows that the bars predate the terrace infill. However, the large-scale cross-stratification indicates that at least parts of the terrace succession were deposited as a steep depositional front consisting of Gilbert-type foresets moving down the main valley into a body of water. The best explanation is that some of the terrace infill, i.e. the cross-stratified deposits, was deposited almost conformably with the giant bars. While the giant bars were deposited in lateral locations, largely from suspension, a bed-load dominated large-scale bar-front was prograding downstream into the back-flooded Katun River valley. On the falling stage of the flood, and during subsequent periods, these bar-front deposits were extensively eroded and reworked. Subsequent flow events infilled the valley developing the main (Inja) terrace, such that the present-day terrace surface is most likely a composite of large flood deposits and later reworked material. In time the river cut vertically and laterally forming the low-level terraces, before down-cutting once more to its present level on the bedrock. The controls and timing of the phases of incision are not known.

CONCLUSIONS

Gigantic gravel bars, some 120 m high and up to 5 km in length, developed across the mouths of valleys draining into the Chuja and Katun rivers as a result of Mid to Late Pleistocene superfloods that coursed down the Chuja–Katun system. The origin of the flood waters was the ice-impounded glacial lake Kuray–Chuja, which filled and emptied repeatedly. Geomorphological evidence indicates that the lake was impounded by convergent glaciers in the vicinity of the town of Aktash, and possibly at Kuehtanar. At least three major floods occurred. The first of these floods, for which we have good evidence, occurred around 23 ka and deposited a series of 'primary' bars. Through both erosion and deposition, subsequent floods have modified the bars so that some, such as at Inja, consist of multiple alluvial successions interbedded with limnic deposits. Often modification occurred by flood waters overtopping earlier bars, or by the deposition of additional minor bars set against the outer margins of primary bars. Additionally, where tributary river flow had, over time, breached the primary bars and drained any impounded small lakes, later flood waters entered the tributaries, depositing flood gravels as insets behind the primary bars within the tributary valleys. However, further stratigraphical and sedimentological data, and dating control, are needed to demonstrate the detail of these events.

The overall character of the deposits demonstrates that the bars were formed by recirculating flow within back-flooded tributary mouths. Within the Chuja River valley, close to the ice-dam failure, bars consist of cobble and pebble gravels, but they fine downstream to pebble gravels, granules and coarse sand in the Katun River valley. In the high-gradient Chuja system, bars often have flat tops, very steep inner margins and frequently exhibit benches on the outer margins. In the lower-gradient Katun valley, bars show less evidence of benches, and have tops and inner margins that slope gently for up to 2 km into the tributaries. Limnic deposits in some side-valleys show that the giant bars temporarily impounded tributary inflow after the flood waters had receded; tributaries subsequently cut down through the barriers, draining the small lakes.

The stratigraphical relationship of the giant bars to the sediment-fill within the main valleys is not clear. The main valley-fill locally consists of large-scale cross-stratified units reminiscent of Gilbert-type foresets that prograded down-valley. These deposits have been fluvially reworked to give a series of terrace surfaces. Further investigation is warranted.

ACKNOWLEDGEMENTS

Data were collected during the 1993, 1994, 1995, 1996, 1999 and 2000 Altai Geomorphological Expeditions sponsored by the Royal Society of London, Royal Geographical Society of London, Tomsk State Pedogogical Institute, Tomsk University and the Tomterra Company. Professor A. Rudoy (TSPI) is thanked for introducing us to the diluvial landscapes of the Altai. P.A.C. would like to thank Dr Christoph Siegenthaler and Professor Peter Martini for insightful discussion in the field concerning giant bar sedimentology. Drs Anton and Anatoli Yamskikh provided information on the tectonic history of the Altai region. Dr Juergen Herget kindly provided GPS data and Dr Ula Moody provided unpublished ^{14}C dates. The comments of Professor V.R. Baker, Dr G. Plint and other referees, together with Professor I.P. Martini's careful editorial work, contributed to the final presentation.

REFERENCES

Archipov, S.A. (1998) Stratigraphy and paleogeography of the Sartan glaciation in West Siberia. *Quat. Int.* **45/46**, 29–42.

Back, S. & Strecker, M.R. (1998) Asymmetric late Pleistocene glaciations in the North basin of the Baikal Rift, Russia. *J. geol. Soc. London* **155**, 61–69.

Baker, V.R. (1973) Paleohydrology of catastrophic Pleistocene flooding in eastern Washington. *Geol. Soc. Am. Spec. Pap.* **144**, 1–79.

Baker, V.R. & Bunker, R.C. (1985) Cataclysmic late Pleistocene flooding from glacial Lake Missoula: a review. *Quat. Sci. Rev.* **4**, 1–41.

Baker, V.R., Benito, G.B. & Rudoy, A.N. (1993) Paleohydrology of Late Pleistocene superflooding, Altay Mountains, Siberia. *Science* **259**, 348–350.

Barishnikov, G.Y. (1992) *Development of Landscape in the Transition Zones of the Altai Mountains*. Tomsk University Press, Tomsk, 182 pp.

Bogachkin (1981) *The Neotonics of the Altai Mountains During the Cainozoic*. Nauka Press, Moscow, 132 pp. (In Russian.)

Butvilovsky, V. (1993) *Last glaciation and Holocene palaeogeography of the Altai: cataclysmic model.* Unpublished Monograph, Tomsk State University, Tomsk. (In Russian.)

Carling, P.A. (1996a) Morphology, sedimentology and palaeohydraulic significance of large gravel dunes: Altai Mountains, Siberia. *Sedimentology* **43**, 647–664.

Carling, P.A. (1996b) A preliminary palaeohydraulic model applied to late Quaternary gravel dunes: Altai Mountains, Siberia. In: *Global Continental Changes: the Context of Palaeohydrology* (Eds Branson, J., Brown, A.G. & Gregory, K.J.), Spec. Publ. geol. Soc. London, No. 115, pp. 165–179. Geological Society Publishing House, Bath.

Clemmensen, L.B. & Houmark-Neilsen, M. (1981) Sedimentary features of a Weichselian glaciolacustrine delta. *Boreas* **10**, 229–245.

Crowley, T.J. & North, G.R. (1991) *Palaeoclimatology*. Oxford University Press and Clarendon Press, New York and Oxford.

Frechen, M. & Yamskikh, A.F. (1999) Upper Pleistocene loess stratigraphy in the southern Yenisei area. *J. geol. Soc. London* **156**, 515–525.

Grosswald, M.G. (1987) The Late-glacial of the Sayany–Tuva highland: morphology, and rate of filling of ice-dammed lakes. In: *Interaction of the Glaciation with the Atmosphere and the Ocean* (Eds Kotikov, V.M. & Grosswald, M.G.), pp. 152–170. Academy of Science of the USSR, Nauka Press, Moscow. (In Russian.)

Grosswald, M.G. (1998) New approach to the Ice Age paleohydrology of Northern Eurasia. In: *Palaeohydrology and Environmental Change* (Eds Benito, G., Baker, V.R. & Gregory, K.J.), pp. 199–214. John Wiley and Sons Ltd, Chichester.

Grosswald, M.G. & Rudoy, A.N. (1996) Quaternary glacier-dammed lakes in the mountains of Siberia. *Polar Geogr.* **20**, 180–198.

Grosswald, M.G., Kuhle, M. & Fastook, J. (1994) Würm glaciation of Lake Issyk-kul area, Tien Shan Mts. A case study in glacial history of Central Asia. *Geojournal* **33**(2/3), 273–310.

Hättestrand, C. & Kleman, J. (1999) Ribbed moraine formation. *Quat. Sci. Rev.* **18**, 43–61.

Huggenberger, P., Carling, P.A., Scotney, T., Kirkbride, A. & Parnachov, S.V. (1998) GPR as a tool to elucidate the depositional processes of giant gravel dunes produced by late Pleistocene superflooding, Altai, Siberia. In: *Proceedings of the 7th International Conference on Ground Penetrating Radar, 1,* pp. 279–283. Radar Systems and Remote Sensing Laboratory, University of Kansas, USA.

Kind, N.V. (1974) *Geochronology of the Late Anthropogene Based on Isotope Data*. Nauka Press, Moscow.

Lungershausen, G.F. & Rakovets, O.A. (1958) Some new data about Tertiary sediment stratigraphy of the Altai Mountains. *Work VAGT (All-Union Aerial Geological Trust)* **4**, 79–91.

Maizels, J.K. (1977) Experiments on the origin of kettle-holes. *J. Glaciol.* **18**, 291–303.

Maloletko, A.M. (1980) About the origin of Maima Terrace (Altai). *Questions Geogr. Siberia* **13**, 89–92. (In Russian.)

Maloletko, A.M. & Paniechev, V.A. (1991) Catastrophic flood in the Katun valley: its behaviour and age. In: *Exogenic Processes in the Altai Region*, pp. 45–47. Proceedings of a Scientific Conference, Barnaul University, Barnaul, Russia. (In Russian.)

Nekhoroshev, V.P. (1966) *The Tectonics of the Altai Mountains*. Nedra Press, Moscow, 306 pp. (In Russian.) Reprinted as Nechoroschew, W.P. (1966) Geologie des Altai, pp. 11–157. In: *Fortschritte der Sowjetischen Geologie, 7,* Akademie-Verlag, Berlin. (In German.)

Okishev, P.A. (1977) Dimensions and characteristics of Late Pleistocene glaciation of the Altay Mountains. *Trans. Glaciol. Stud. Chron.* **29**, 203–210. (In Russian.)

Okishev, P.A. (1997) Some questions of the genesis problem of the high Altai terraces. *Questions Geogr. Siberia* **22**, 9–18.

Plink-Björklund, P. & Ronnert, L. (1999) Depositional processes and internal architecture of Late Weichselian ice-margin submarine fan and delta settings, Swedish west coast. *Sedimentology* **46**, 215–234.

Ragosin, L.A. (1942) Middle Katun valley terrace. In: *Investigation and Exploration of the Productive Force of Siberia*, pp. 36–107. Proceedings of a Scientific Conference, Tomsk University, Tomsk. (In Russian.)

Rudoy, A.N. (1988) The regime of intermontane ice-dammed lakes of South Siberia. *Data Glacial Res., Acad. Sci., USSR* **61**, 36–42. (In Russian.)

Rudoy, A.N. (1990) Ice flow and ice-dammed lakes of the Altai in the Pleistocene. *USSR Acad. Sci. Izv. Ser. Geogr.* **120**, 344–348. (In Russian.)

Rudoy, A.N. (1998) Mountain ice-dammed lakes of southern Siberia and their influence on the development and regime of the intracontinental run-off systems of north Asia in Late Pleistocene. In: *Palaeohydrology and Environmental Change* (Eds Benito, G., Baker, V.R. & Gregory, K.J.), pp. 215–234. John Wiley & Sons, Chichester.

Rudoy, A.N. & Baker, V.R. (1993) Sedimentary effects of cataclysmic late Pleistocene glacial outburst flooding, Altay Mountains, Siberia. *Sediment. Geol.* **85**, 53–62.

Rudoy, A.N., Galakhov, V.P. & Danilin, A.L. (1989) Reconstruction of glacial drainage of the Upper Chuja and the feeding of ice-dammed lakes in the Late Pleistocene. *All-Union Geogr. Soc. Proc.* **121**, 236–244. (In Russian.)

Serebryanny, L.R. (1984) Mountain glaciation in the USSR in the Late Pleistocene and Holocene. In: *Late Quaternary Environments of the Soviet Union* (Eds Wright, H.E. & Barnosky, C.W.), pp. 35–41. Longman, Harlow.

Smith, D.A. & Jol, H.M. (1997) Radar structure of a Gilbert-type delta, Peyto Lake, Banff National Park, Canada. *Sediment. Geol.* **113**, 195–209.

Speransky, B.F. (1937) Basic moments of Cainozoic history of the south-eastern Altai. *Vestnik ZSGU (West-Siberian Geological Committee)* **5**, 50–66. (In Russian.)

Svitoch, A.A. (1978) *Sections of the Youngest Deposits of the Altai*. Moscow University Press, Moscow. (In Russian.)

Svitoch, A.A. (1987) *The Palaeogeography of the Pleistocene*. Moscow University Press, Moscow. (In Russian.)

Svitoch, A.A. & Khorev, V.S. (1975) Old glacial deposits and glaciations of the Altay Mountains. *USSR Acad. Sci: Izv. Ser. Geogr.* **4**, 101–108. (In Russian.)

Syverson, K.M. (1998) Sediment record of short-lived ice-contact lakes, Burroughs Glacier, Alaska. *Boreas* **27**, 44–54.

Tapponier, P. & Molnar, P. (1979) Active faulting and Cainozoic tectonics of the Tien Shan, Mongolia and Baikal regions. *J. geophys. Res.* **84**, 3425–3459.

Tarasov, P.E., Peyron, O., Guiot, J., *et al.* (1999) Last Glacial Maximum climate of the former Soviet Union and Mongolia reconstructed from pollen and plant macrofossil data. *Clim. Dyn.* **15**, 227–240.

Vardaniants, L.A. (1938) On the past glaciation of the Altai and Caucasus. *Izv. Gos. Geogr. Ova* **70**(3), 386–404. (In Russian.)

Velichko, A.A. (1984) Late Pleistocene spatial paleoclimatic reconstructions. In: *Late Quaternary Environments of the Soviet Union* (Eds Wright, H.E. & Barnosky, C.W.), pp. 261–285. Longman, London.

Yamskikh, A.F. (1972) The stratigraphy of Cainozoic deposits of the Upper Yenisei river basin. In: *Geology and Geography of Yenisei, Siberia* (ed. Yamskikh, A.F.), pp. 51–82. Krasnoyarsk State University Press, Krasnoyarsk, USSR. (In Russian.)

Yamskikh, A.F. (1996) Late Quaternary intra-continental river palaeohydrology and polycyclic terrace formation: the example of south Siberian river valleys. In: *Global Continental Changes: the Context of Palaeohydrology* (Eds Branson, J., Brown, A.G. & Gregory, K.J.), Spec. Publ. geol. Soc. London, No. 115, pp. 181–190. Geological Society Publishing House, Bath.

Yamskikh, A.F., Yamskikh, A.A. & Brown, A.G. (1999) Siberian-type Quaternary floodplain sedimentation: the example of the Yenisei River. In: *Fluvial Processes and Environmental Change* (Eds Brown, A.G. & Quine, T.A.), pp. 241–252. John Wiley and Sons, Chichester.

Zyatkova, L.K. (1977) *The Structural Geomorphology of the Altai–Sayan Mountainous Region*. Nauka Press, Novosibirsk, USSR. (In Russian.)

Zykin, V.S. & Kazanskii, A.Y. (1995) Stratigraphy of Cainozoic (Pre-Quaternary) deposits of the Chuja depression in Gorny Altai. *Geologiya I Geofizika* **36**(10), 75–84.

Spec. Publs int. Ass. Sediment. (2002) **32**, 37–51

Great Holocene floods along Jökulsá á Fjöllum, north Iceland

R. B. WAITT

U.S. Geological Survey, 5400 MacArthur Blvd., Vancouver, WA 98661, USA (Email: waitt@usgs.gov)

ABSTRACT

Jökulsá á Fjöllum, Iceland's largest glacial river, drains from Vatnajökull icecap northward to the sea along a broad low that includes an active volcanic belt. Geomorphic features along this path reveal an ancient discharge of water large enough to fill the river valley and spill among a plexus of lows in the volcanic landscape. Stratigraphy in most places reveals just one late Holocene great flood down Jökulsá á Fjöllum, between 2500 and 2000 yr ago. Step-backwater computation suggests its peak flow was 0.7 million m^3/s or more. An early scabland-carving great flood had swept down the Ásbyrgi area of lowermost Jökulsá just after deglaciation, 9000–8000 yr ago. Stratigraphy near Vesturdalur reveals at least 16 additional floods, perhaps of moderate discharge, between about 8000 and 4000 yr ago.

Dispersed field evidence of the late Holocene great flood—anastomosing channels whose basalt surfaces are water fluted and half-potholed, in places plucked down to small-scale scabland replete with dry cataracts, huge boulders, long gravel bars, giant current dunes—is traced the length of Jökulsá valley. From Vatnajökull's north margin at Kverkfjöll, water anastomosed through diverse lows of a high-relief landscape. Thus swift release of meltwater from subglacial Kverkfjöll caldera must have been a source of flood. But even this catastrophic outflow was insufficient to constitute the huge discharges evident farther down-valley. Field evidence reveals a yet greater discharge directly from the large outlet glacier Dyngjujökull. There is no evidence that subglacial Bárðarbunga caldera was involved, but subglacial melting during eruption of a more eastern fissure system could be a source of flood.

INTRODUCTION

Ásbyrgi canyon near the lower Jökulsá á Fjöllum canyon, Iceland (Fig. 1) is a huge now-dry abandoned cataract, similar to much larger examples scattered about the extraordinary, vast landscape of the Channeled Scabland in Washington, USA. Sigurður Thórarinsson (1960) recognized Ásbyrgi formed by a giant flood down Jökulsá. From tephra stratigraphy he inferred it to have occurred after deposition of a regional tephra dated at about 2900 ^{14}C yr ago. On aerial photographs Haukur Tómasson (1973) traced some geomorphic effects of this flood abandoned cataracts, broad floodpaths, gravel bars upvalley to Vaðalda and inferred that it had burst from nearby Dyngjujökull, the outlet glacier of Vatnajökull icecap. Kristján Saemundsson (1973) agreed that such a young great flood had swept Ásbyrgi but also inferred a large flood about 9000 yr ago soon after icecap retreat. Sigurvin Elíasson (1977) disagreed on Saemundsson's old flood but from stratigraphy inferred that three great floods between 4600 and 2000 yr BP carved out Ásbyrgi.

Elements of topography in Jökulsá á Fjöllum resemble unusual features along other deeply flood-swept rivers; it has some attributes (but at smaller scale) of the topography of the Channeled Scabland and Snake River Plain in western United States, topography carved by some of Earth's largest fresh-water floods (Bretz, 1925, 1928, 1932; Bretz *et al.*, 1956; Baker, 1973a,b; O'Connor, 1993; Waitt, 1994). The Scabland floods were thought to number one or a few (Bretz, 1969), but stratigraphy shows that they were scores of separate floods (Waitt, 1980, 1984, 1985; Atwater, 1986; Atwater *et al.*, 2000). Back-flooded tributaries preserve the most complete sections of bedded sediment. Might a similar stratigraphical study in sidecanyons reveal a history of repeated floods down Jökulsá á Fjöllum? An Icelandic great flood younger than 3000 yr in any case preserves pristine field

Flood and Megaflood Processes and Deposits: Recent and Ancient Examples. Edited by I. Peter Martini, Victor R. Baker and Guillermina Garzón ISBN: 978-0-632-06404-5

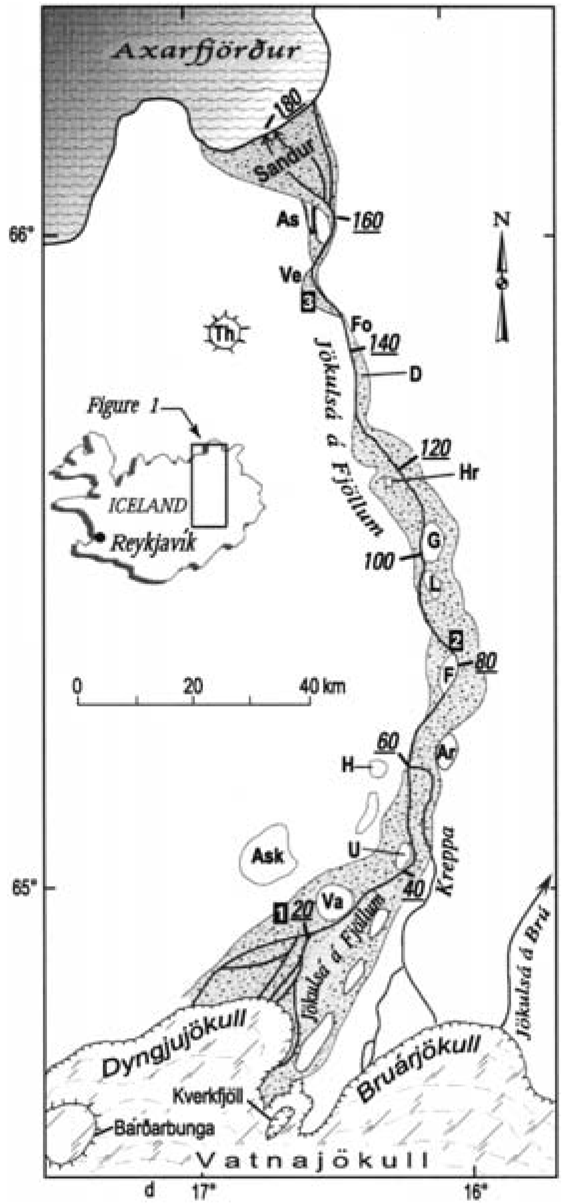

Fig. 1. Generalized map of extent of the late Holocene flood inferred from field evidence. Barbed line delineates margin of source glacier, and wavy lines indicate the sea. Stipple area indicates where late-Holocene flood spilled broadly beyond Jökulsá's canyon. Numbers are valley distances (in kilometres) from source along Jökulsá á Fjöllum. Volcanic highs and other features mentioned in text indicated in letter code: Ar, Arnardalsalda; Ask, Askja; As, Ásbyrgi; D, Dettifoss (Selfoss is 1 km up-valley, Hafragilsfoss 2 km down-valley); F, Ferjufjall; Fo, Forvöð valley; G, Grímsstaðanúper; H, Herðubreið; Hr, Hrossaborg; L, Lambafjöll; Th, Theistareykja; U, Upptyppingar; Va, Vaðalda; Ve, Vesturdalur. Numbered dark squares refer to sites mentioned in text.

evidence for reconstructing the flood's palaeohydrology. Guttormur Sigbjarnarson (1990) has published work on Jökulsá palaeofloods.

Effects of at least 10 historic floods between 1477 and 1729 and in 1902–1903 (Thórarinsson, 1950; Ísaksson, 1985) are evident along Jökulsá but ignored here. Although vastly exceeding Jökulsá's annual floods, they were nonetheless small compared with the great late Holocene flood. Thus at Upptyppingar (*km 40*)[1] (Fig. 1), fine-gravel bars, seemingly of the largest historic flood(s), reach 15 m above the river in a simple channel 1 km wide where the late Holocene flood peaked 40 m deep in a braided channel 9 km wide.

WEICHSEL GLACIATION AND POSTGLACIAL VOLCANISM

Jökulsá á Fjöllum drains the north and northwest of Vatnajökull, Iceland's largest icecap (Fig. 1). The west half of the icecap overlies several active volcanic and geothermal systems—Grímsvötn in the centre, Bárðarbunga caldera in the west, Kverkfjöll in the north, and rift systems between Bárðarbunga and Kverkfjöll. Extending north, a broad north-south rift valley harbouring Jökulsá á Fjöllum is floored by lava flows and vent cones, most of which are mapped as pre-last-glacial but several as Holocene (Saemundsson, 1977; Sigbjarnarson, 1993, 1996).

At its maximum stand, Iceland's Weichsel (late Pleistocene) ice sheet reached north to beyond the present coast (Einarsson, 1968; Norðdahl, 1990). On the northern parts of peninsulas west and east of Axarfjörður (Fig. 1), grooved bedrock and glacially striated cobbles are scarcely weathered, thus of this last glaciation. The ice sheet also glaciated all of lower Jökulsá and Axarfjörður, the valley outlet closer to the ice centre. Upland basalt tracts along Jökulsá are deeply grooved and striated revealing ice flow north and northwest (azimuths 000° to 320°), parallel to the general valley trend. This striated bedrock is overlain

[1] Valley distance, in italics to distinguish from other distances measured in kilometres, along Jökulsá á Fjöllum is ticked off in 5-km increments along the general trend of the river and ignores small in-valley meanders, where *km 0* represents the ice margins at Kverkfjöll and Dyngjujökull, and *km 180* Jökulsá's meeting with the sea (summarized in Fig. 1); river distance measured around every meander would be 10–15 km longer.

by drift[2] containing angular to rounded stones as large as 2.5 m,[3] some of them striated. The drift forms an irregular ground moraine that locally dams ponds and is sparsely cut by ice-marginal channels. According to Norðdahl's (1990) regional reconstructions including radiocarbon dates from Axarfjörður, the ice margin at 10 500 yr BP lay beyond Jökulsá's present mouth at the sea but by 9600 yr BP had retreated 70 km up Jökulsá. From there the glacier retreated rapidly during the regionally warming climate after 10 000 yr BP (Björck *et al.*, 1996). During retreat hanging deltas formed in small tributaries 4–6 km back from Jökulsá (*km 146*) and 120–180 m above the valley floor. A flight of about 20 north-descending moraines and moraine-capped strath terraces across one of the tributaries (*km 145*) shows that they built against the margin of ice downwasting and receding from Jökulsá.

Ages of glacial and postglacial events are estimated in some areas by thickness of overlying aeolian silt and by the enclosed ash layers of known ages. Glaciated surfaces along lower Jökulsá á Fjöllum are overlain by a 1–2.5 m succession of windblown yellowish to brownish silt.[4] The silt is punctuated in downward succession by basaltic tephras including V-1717 and V-1477 and the silicic Hekla tephras H3 (2879 ± 34 ^{14}C yr BP), H4 (3826 ± 12 ^{14}C yr BP), and H5 (*c.* 6100 ^{14}C yr BP) (Fig. 2) (Larsen & Thórarinsson, 1977; Larsen, 1982, 1984; Vilmundardóttir & Kaldal, 1982; Dugmore *et al.*, 1995; Larsen *et al.*, 1998).[5] Calibrated by the CALIB (version 4.2, March 2000) program (Stuiver & Reimer, 1993; Stuiver *et al.*, 1998), tephra H3 is about 3100–3200 yr BP, H4 is 4200–4300 yr BP, and H5 is 6900–7000 yr BP in calendar time. Calendar time is used below. (Thórarinsson's (1971) early 'corrected' dates for these ash layers were similar: 2900, 4500, 7100, respectively.) With an average postglacial silt thickness of 1.5 m, the dates suggest that 1 cm of the aeolian silt accumulates in an average 30–50 yr. Tephra H4 is a distinctive couplet: white silt overlain by black very fine sand.[6] Beneath tephra H4 is 0.5–1 m of the yellowish silt, an interval containing tephra H5. Tephra H5 is thin and difficult to recognize, but where it is visible a few to several decimetres of the yellowish silt underlie it.

[2] 'Drift' in long-standing and current North American usage includes all deposits and landforms of a particular glaciation—e.g. till (morainal or not), sporadic boulders, outwash, kame terraces, eskers (Flint, 1971; p. 147)—a reviewer complained that the term is abandoned in Europe but offers no other simple embracing term.

[3] Glacial and floodborne boulders are recorded here by *intermediate*, not largest, diameter.

[4] By engineering rather than geological definition often called 'soil', but this term would mislead here because the material is a layered series of primary Holocene deposits, not highly weathered older material.

[5] Ash layers as designated by Larsen & Thorarinsson (1977) and Larsen (1982, 1984). 'V-1477' signifies an eruption in Veiðivötn (western Vatnajökull) in AD 1477; 'H4' is 4th Hekla white silicic tephra down from the surface in south Iceland.

Lower Jökulsá valley and Ásbyrgi area

From the large shield Theistareykja, 23 km south-southwest of Ásbyrgi (Fig. 1), a lava surface slopes 24 m/km north-northeast and passes below the sandur of Axarfjörður (Saemundsson, 1977). The near-vertical walls of Ásbyrgi, as high as 30 m, show the lava to be at least 25 stacked flows each variably 1–3 m thick, and at least the upper two surfaces display ropy pahoehoe.

Much of the lava-flow surface is unglaciated, but north of *km 152*, thin, scattered drift atop its lightly fluted and striated surface show that the glacier ice overrode its eastern 1–5 km. A glassy-margined (ice-contact?) lava flow forming the west rim of Jökulsá canyon near *km 151* is cut by small hanging channels ending in fine-gravel hanging deltas. The lava flow and gravel patches are capped by 1–2 m of aeolian silt enclosing the Hekla H3 and H4 ashes (30 cm of silt below H4). The next lower bench closer to Jökulsá is heavily glacially striated and grooved. The glacier thinning from Jökulsá valley must have readvanced and overrode the young-lava margin, while the glacier's drainage left the hanging channels and deltas.

Deeply grooved, striated basalt strewn with perched boulders as large as 2.2 m also lies near Ásbyrgi, at 1.5 km southeast of the canyon head. That surface is overlain by 1.5 m of oxidized aeolian silt containing the Hekla H3 and H4 tephras, 0.5 m of the silt lying beneath H4. Saemundsson (1973) inferred that the Theistareykja basalt flows about Ásbyrgi lay beyond the last-glacial limit and that striations there must have been etched by rock debris carried by glacial floods from a maximal ice margin far south. But striations and other features that lightly embellish these lava flows are of typically glacial form (Fig. 3). The light glacial overprint must be from a brief, late readvance of ice. Saemundsson seems to have distinguished only a deeply scoured glacial landscape from a lightly etched one. Elíasson (1977) too argued that the

[6] Median grain sizes specific in sedimentological (Wentworth) terms (Folk, 1980).

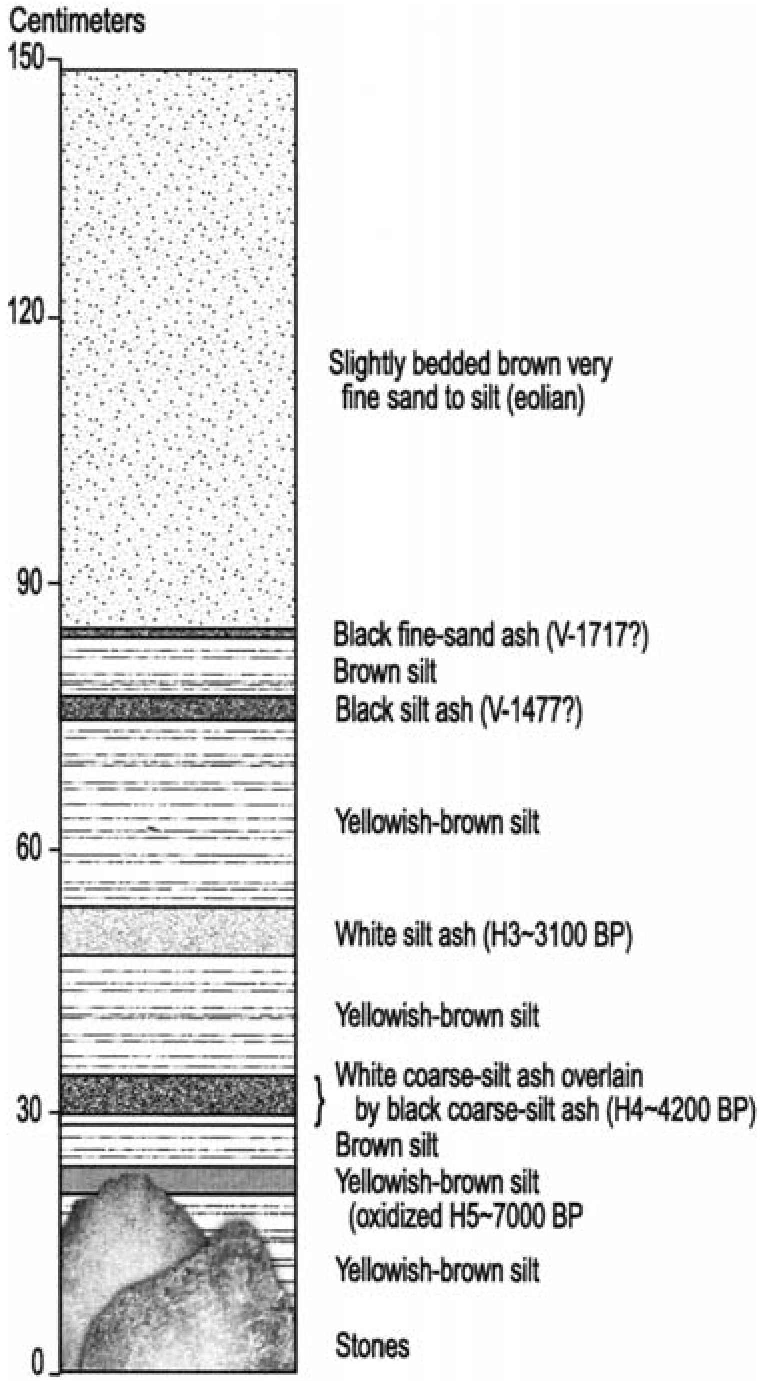

Fig. 2. Aeolian silt and tephra stratigraphy typically overlying glaciated areas throughout the area, here overlying a bare postglacial great-flood gravel atop the 'Eyjan' at Ásbyrgi. Tephras labelled as by Larsen (1982, 1984).

Fig. 3. Southwestward view atop a higher part of the Eyjan showing striated basalt in stoss-and-lee glacial form (ice palaeoflow to the north-northwest (long arrow)). The ground is partly covered by bouldery diamict (glacial till). Knife (short arrow) is 9 cm long.

striae about Ásbyrgi are genuinely glacial; but he inferred the faint ones to have been subsequently muted by blowing sand.

Holocene rifts and volcanism

Lava flows with primary (postglacial) surfaces issued from several fissures near Jökulsá á Fjöllum. From rifted hyaloclastite ridges 10–20 km north of Kverkjökull, lava flows covered a few hundred square kilometres north and northeast. North of Dyngjujökull several other postglacial lava flows cover far larger areas about upper Jökulsá (Fig. 1) (Sigbjarnarson, 1993, 1996).

A north-trending rift-and-graben belt crosses Jökulsá below Dettifoss (*km 138*). Basaltic cinder-and-spatter cones and lava flows erupted from it directly overlie the drift and striated basalt. A metre or more of yellowish aeolian silt including Hekla ash H4 overlies the cinder deposits. Another chain of unglaciated cones overlies a rift along narrow and crooked Jökulsá canyon (*km 148–154*) below the Forvöð valley. Some cones stand unaltered on Jökulsá's rim. Cinders from them fell directly on glacial drift, they underlie Hekla tephra H5, and therefore the eruptions probably occurred 9000 yr BP or a little earlier (Elíasson, 1974; Sigbjarnarson, 1990). Deeply flood-eroded to their interiors, the cones within Jökulsá canyon stand as ragged spines called 'Hljoðaklettar'. An associated intracanyon lava flow fills a 2-km^2 area just west in Vesturdalur.

Preflood Jökulsá canyon

Most of Jökulsá valley seems to have existed in roughly its present form before the Holocene series of floods. Along most of its course, tributary valleys cut into pre-late-glacial basalt fall into mainstem Jökulsá about at grade. They include: Kreppa (*km 60*), Arnardalsá (*km 72*), Skarðsá (*km 98*), Vatnsleysá (*km 122*). Even Landsá (*km 162*) falls only 10 m into lowermost Jökulsá on a fairly gradual grade. These relations indicate long-term approximately graded valley junctions showing little down-cutting of mainstem Jökulsá at these sites by later catastrophic flood.

Late-glacial and postglacial lava flows entered the edges of Jökulsá valley along much of the upper 60 km of its course, abutting from the west uplands such as Vaðalda and Upptyppingar, shoving Jökulsá east into a new course (*km 25–61*), most notably east of Upptyppingar (*km 37–50*) where it flows in a relative canyon.

Much of Jökulsá's canyon section between Selfoss (*km 137*) and Axarfjörður (*km 162*) seems heavily flood-modified, but probably this entire segment also predates the floods. Along an 8-km segment of valley (*km 142–150*) including Forvöð valley, flood effects are nested within a deep valley whose sloping rims are in glacial drift. The steeply encanyoned cataracts segment just above this (*km 137–142*) is clearly deepened and widened by a headcutting late-Holocene great flood (see below).

Some of the Hljoðaklettar cinders lie low inside the Jökulsá canyon, and an affiliated intracanyon lava flow flooded Vesturdalur. These fills show that along this reach (*km 150–154*) Jökulsá had cut a canyon nearly to present depth before the eruptions (before 9000 yr BP).

The late-glacial Theistareykja lava flows (Saemundsson, 1977) apparently diverted lower Jökulsá below Vesturdalur (*km 154–161*) east to the lava-field edge. Even the modern (postflood) canyon there remains steep and narrow. Tributary Vesturdalsá (*km 152*) falls in with a steep 15-m drop, Valagilsá (*km 157*) with a sharp 80-m drop. Saemundsson (1973) considered Ásbyrgi as the former lower end of Jökulsá and that the flood newly carved out the deep canyon to the east and captured the river. But above Ásbyrgi's head there is no valley, only the scabland tract—whose head is *higher* than Vesturdalur upvalley, thus not a viable valley for Jökulsá. There had to have been a preflood Jökulsá canyon between Vesturdalur to where Landsá gradually falls in (*km 161*). This reach may have been narrow, substantially enlarged later by catastrophic floods.

EARLY AND MIDDLE HOLOCENE FLOODS, LOWER JÖKULSÁ

Pre-8000 yr BP flood

In most of lower Jökulsá, stratigraphy of dated ash layers and geomorphologic features reveal two catastrophic floods: one between 8000 and 9000 yr ago (soon after deglaciation), and the other between about 2000 and 2500 yr ago. Field evidence for each flood is similar: sporadic coarse gravel deposits, some of them in the round-topped form of fluvial bars, overlying water-eroded rock surfaces.

Anastomosing around higher points of striated rock overlain by drift just west of Ásbyrgi, and on its Eyjan ('island'), is a network of water-washed surfaces (Fig. 4). A conspicuous sparsely vegetated late Holocene scabland tract leads to Ásbyrgi. Outside this tract, a thickly scrub-vegetated, sinuously braided scabland tract expands 1–2 km west. This anastomosing incipient scabland is extensively cut into the gently north-dipping basalt west of Ásbyrgi and also includes much of the Eyjan ('island') between Ásbyrgi's canyons. It resembles the young tract but is more finely and intricately channelled, and is geomorphically more subtle by its coat of silt and vegetation. It includes an abandoned cataract high on Jökulsá's west rim (Fig. 4). Like nearby glaciated areas, the water-formed surfaces and deposits are overlain by the yellowish aeolian silt and tephra sequence down to below tephra H5 (Fig. 2). This sequence shows the channelled surfaces to be about the same age as glacial surfaces, but being nested below the glaciated surfaces they are slightly younger.

Where locally stripped of vegetation, the lower rock surfaces of the Eyjan are sculpted into smoothly furrowed, scalloped, fluted and half-potholed forms, some with sharp tops (Fig. 5A)—features typically formed beneath turbulent water and described by some observers as 'p-forms' or 's-forms' (Maxon &

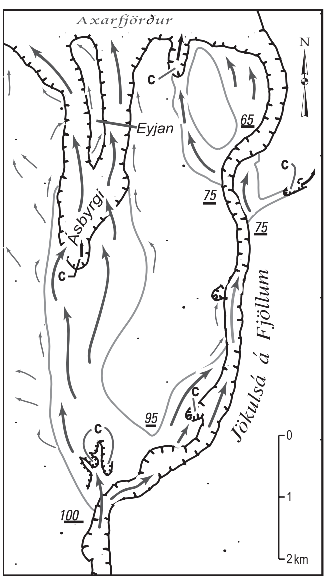

Fig. 4. Geomorphologic sketch map of lowermost Jökulsá and Ásbyrgi area (*km 154–163*). Hachured heavy lines and fine stipple delineate major features—Jökulsá canyon, Ásbyrgi dry cataract, and lesser dry cataracts indicated by 'c' (hachures indicate cliff side). Light lines and blank areas delineate approximate limits of late Holocene flood tracts that overflowed rims of Jökulsá canyon leading to high scabland and the dry cataracts. Numbers are heights (in metres) of peak-flow depth above adjacent floor of Jökulsá.

Fig. 5. Flood erosion and deposits. (A) Low area along east rim of Ásbyrgi's Eyjan showing water-fluted rock partly overlain by sorted gravel and a thick cap of windblown silt containing Hekla tephras (arrow). Shovel on left is 104 cm long. (B) Southward view (upcurrent) of well-rounded boulder gravel along west rim of Ásbyrgi's Eyjan. Compare roundness here with that in Fig. 3. Visible part of shovel is about 1 m.

Campbell, 1935; Dahl, 1965; Allen, 1971, 1982; Gray, 1981, 1984; Baker & Pickup, 1987; Wohl, 1992; Tinkler, 1993; Glasser & Nicholson, 1998; Whipple *et al*., 2000). In low places west of Ásbyrgi and on the Eyjan, the basalt is locally eroded down into a plexus of low-relief butte-and-basin topography (incipient scabland). Scattered over these rock surfaces are patches of sorted, subrounded to rounded cobble to boulder clast-supported, matrix-free gravel (Fig. 5A & B), clearly stream-deposited. Some of these deposits are gently whaleback in shape, the sides descending into moats against bedrock—the form of fluvial bars rather than river terraces (Baker, 1973b; Waitt, 1994). These features reveal a widespread discharge energetic enough not only to remove glacial drift but also to erode the low parts of the bedrock surface into fluted and incipient-scabland forms.

Many floods 8000–4000 yr BP

On most floodswept surfaces along lower Jökulsá, the overlying silt blanket either: (i) is a metre or more thick, yellowish, and contains the tephra sequence to well below the Hekla ashes H4 or H5; or (ii) is thin, brownish, and lacks Hekla H3 and all older tephras. Most floodswept surfaces thus are either older than 7000 yr BP or younger than 2500 yr BP.

Sigurvin Elíasson (1977, Fig. 4) did not recognize the pre-H5 flood but from stratigraphy did infer three great floods at about 4600, 3000 and 2000 yr BP—the last being the young flood all workers acknowledge. Guttomur Sigbjarnarson (personal communication, 1984, 1990, Fig. 8) noted two apparently floodlaid gravel deposits high on Jökulsá's rim east of Vesturdalur, one underlying Hekla H4, the other overlying Hekla H3—corresponding to the oldest and youngest of Elíasson's three great floods.

Stratigraphically much more detailed sand deposits lie about at the upper limit of a late Holocene flood 1.5 km back from and 60 m above Jökulsá's west bank just above Vesturdalur (*km 150*) (Fig. 1, site 3). The lowest sand bed directly overlies glacial drift of angular to rounded stones as large as 0.75 m. As many as 21 sand beds are interrupted by yellow-brown aeolian silt and the Hekla tephras H3 and H4 (Fig. 6). The lower 16 sand beds are brownish grey, strongly rippled medium to fine sand. The ripples are symmetrical to strongly asymmetric climbing ripples of variable dips up to 20° (Fig. 7A). Bed 8 (30–100 cm thick) where thickest comprises: the lower third of medium sand in 'type-A' ripple-drift laminations, the middle third of fine sand where 'type-A' succeeds to 'type B' ripple-drift laminations, the next one-sixth of ripple drapes in fine sand, and the top sixth of plane-bedded very fine sand (Jopling & Walker, 1968; Ashley *et al*., 1982). Other thick sand beds (beds 2, 10, 12, 15) also are normally graded and in places show a similar upward succession of sedimentary structures. Some of the thicker sand beds are internally penetrated by structures crossing up through the primary ripple structure, in plan view appearing as pipes (Fig. 7B), structures widely interpreted as evidence of rapid expulsion of internal water (Allen, 1961, 1982). The ripple cross-laminations in each bed of this high-level site climb

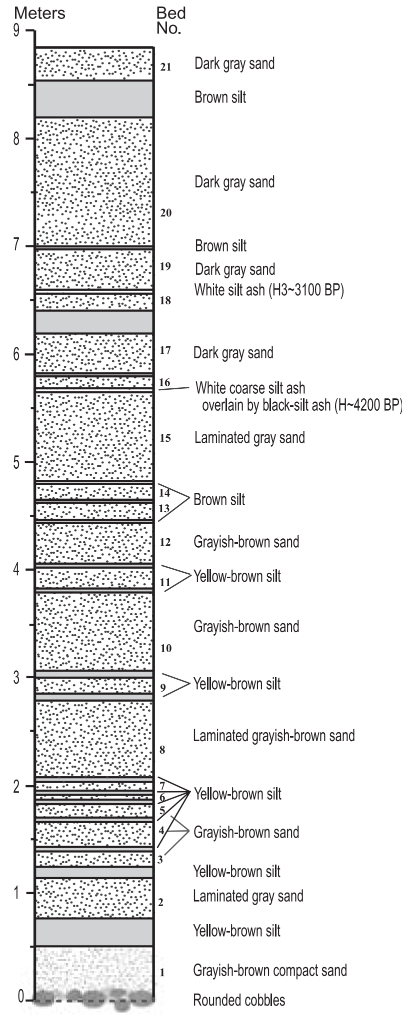

Fig. 6. Section of waterlaid greyish-brown, ripple-drifted sand (beds 1–16) and aeolian black, massive sand (beds 17–21) interlayered with yellowish and brownish silt and tephra high on west side of Vesturdalur (*km 150*).

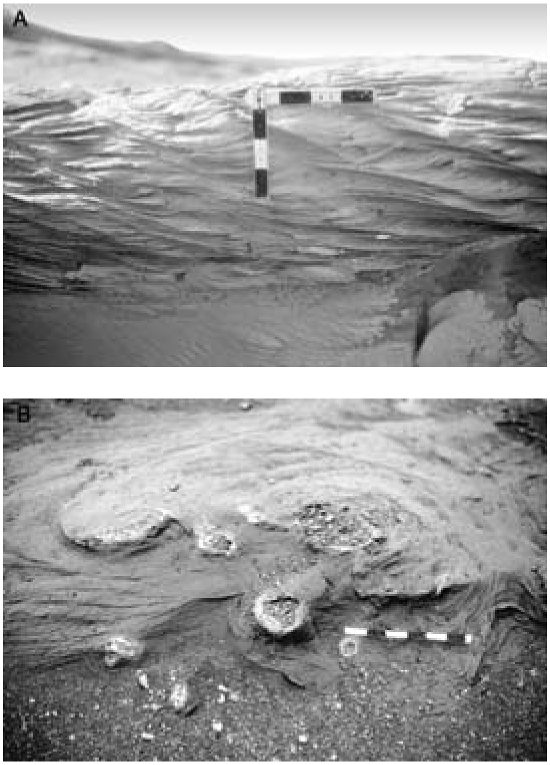

Fig. 7. Details of section of Fig. 6. (A) Section view of ripple-drift cross-laminations in sand bed 8. Palaeocurrent direction toward left (south-southwest), upvalley. Emphasized scale divisions 3 cm. (B) View downward of pipe structures that penetrates ripple-drift laminated sand. Emphasized scale divisions 5 cm.

toward azimuths 160–230° (SSE, S, SSW, SW)—*up*-valley and *away from* Jökulsá main canyon. These palaeocurrents high above Jökulsá record a counter-clockwise eddy circulating along the left side during a succession of 16 or 17 nearly valley-filling floods between 8000 and 4000 yr ago.

In the upper part of the section, above tephra H4, sand beds 17–21 are very different from the others. They are dark grey to black, nearly massive, loose medium to coarse sand. They are thus coarser, far less structured, and looser. They are identical to aeolian-sand deposits in the Jökulsá region, including many far above the limit of flood.

The sand beds of the lower two-thirds (sand beds 1–16) of the exposure above Vesturdalur resemble the stacks of graded beds deposited by giant jökulhlaups in some of the backflooded tributaries off Washington's Channeled Scabland (Waitt, 1980, 1984, 1985). Thus the upward sequence of normal grading and succession of structures described for sand-bed 8 suggests rapid sedimentation during a waning current (Ashley *et al*., 1982), comparing closely with some Missoula backflood beds (Waitt, 1980).

Whereas hundreds of stratigraphic exposures lie in the Washington–Oregon Channeled Scabland, in Jökulsá the Vesturdalur exposure seems unique. The reason may be that voluminous late-glacial and early Holocene lava flows and cones obstructed Jökulsá canyon from Vesturdalur down and kept it narrow, hydraulically retarding and partially ponding early floodflows through this reach. Coursing down a far more restricted Jökulsá canyon than present, mid-Holocene floods of only moderate volumes and discharge might have ponded to these high levels. Only later might the great late Holocene flood have eroded out this reach to its present width and depth.

LATE HOLOCENE FLOOD

Along Jökulsá valley field evidence for a great late flood is widespread, in places spectacular. The aeolian silt that overlies flood-sculpted rock surfaces and bars lacks not only H3 and older Hekla tephras but also part of the brownish silt that elsewhere separates tephras H3 and V-1477 (Fig. 2). Thus this flood occurred after deposition of tephra layer H3, probably between 2500 and 2000 yr BP. Just a few sites along the late Holocene floodpath are summarized below.

Field criteria for catastrophic flood

Extraordinary discharge is evident from numerous unusual features distributed along Jökulsá á Fjöllum nearly from Vatnajökull to the sea:

1 basalt flows broadly stripped of drift and aeolian silt, etched into fluted, quasi-potholed forms, locally eroded down to scabland, and littered with large boulders;

2 long channels cut sharply into basalt;

3 clast-supported gravel, and in the form of large bars—whaleback-shaped mounds tens or hundreds of metres long and with metres of surface relief;

4 giant current dunes ornamenting gravel bars;

5 flood tracts diverging, showing overflow between two or more valleys, in places across low divides;

6 such diversions arcing kilometres beyond the main canyon then returning to it, altogether forming a braided plexus;

7 such features far beyond and above any historic flood (see below).

These features in Jökulsá á Fjöllum, alien to non-flood landscapes, resemble large such features of Washington's Channeled Scabland (Bretz, 1928, 1959; Baker, 1973a,b; Waitt, 1994; O'Connor & Waitt, 1995).

Upper limit of flood

The upper limit of late Holocene flood down any one reach of Jökulsá á Fjöllum lies above the uppermost field evidence of water currents cited above. It lies below the lowest level of clearly unaffected terrain —glacial drift, surfaces overlain by the yellowish aeolian blanket containing the Hekla tephras, passes across a low divide lacking fluvial modification. In most reaches this peak-flood limit can be discerned only to within many metres but in a few places to within just a metre or two.

Fig. 8. Southward view (upcurrent) of gravel bars below scabland channels etched back into lava-flow front (L) (*km 11*). Water issued from upland valley at Kverkfjöll (K). This channel is higher than, isolated from, and 9 km east of the head of Jökulsá at Dyngjujökull. Location shown on Fig. 9.

Sources: Kverkfjöll and Dyngjujökull

Subglacially erupting basaltic lava can melt 14 times its volume of glacier ice (Gudmundsson *et al.*, 1997). Were only 0.5 km^3 of magma to erupt beneath Vatnajökull, some 7 km^3 of ice could melt and the water be trapped temporarily at the glacier bed, poised for catastrophic escape. Some 3.5 km^3 of water are inferred to have escaped in the November 1996 eruption-induced flood south to Skeiðará (Gudmundsson *et al.*, 1997).

Kverkfjöll, a prominent high and a large geothermal area between Vatnajökull's two northern outlet glaciers Brúarjökull and Dyngjujökull (Fig. 1), continues northeastward 25 km from the icecap as subparallel rift ridges of late Pleistocene hyaloclastite and pillow lava (Sigbjarnarson, 1993). Small postglacial lava flows spread along lows between these ridges. In lows northeast of Kverkfjöll some postglacial lava surfaces are polished and cupped to fluted, quasi-potholed forms, in places plucked into incipient scabland. These erosional surfaces are littered with erratic boulders of basalt, in places concentrated to boulder-gravel bars (Fig. 8). The lava flows have been washed by water with enough discharge to overflow low parts of valley rims and braid among adjacent paths, some flood strands dividing again and again to cross minor divides (Fig. 9). The plexus altogether comprises a few dozen separate strands ranging from 10 m to 3 km wide. Simultaneous flow through many broad channels indicates a brief extreme discharge.

One can roughly estimate discharge through a short reach of channel by the product of channel cross-section and a plausible mean velocity. For comparison, the present Jökulsá in July–August typically flows at 150–200 m^3/s. Peak palaeoflows through the channel plexus from Kverkfjöll seem to range from a few tens of cubic metres per second (small separate channels) to several 1000 m^3/s^{-1} (broad combined channels).

Yet even when these channel discharges are summed together, the catastrophic outflow from the Kverkfjöll area seems nearly an order of magnitude too small to constitute the enormous discharge of water that descended Jökulsá valley not far downvalley (Fig. 9, top). Catastrophic flood thus also seems required from the main outlet glacier, Dyngjujökull. If a subglacial eruption occurred at Kverkfjöll caldera, water trapped beneath the ice could have flowed down gradients driven by surface-ice contours not only north from Kverkfjöll but also west to Dyngjujökull (Fig. 1). A large hlaup from Kverkfjöll thus also could escape simultaneously from Dyngjujökull outlet glacier.

Eruptions from rifts farther west beneath Vatnajökull also could yield subglacial water. Björnsson's (1988; map 6) plot of subglacial water gradients shows that had the 1996 Gjálp eruption (Gudmundsson *et al.*, 1997) occurred a few kilometres farther north along that rift, water would have drained northwest to Dyngjujökull and down Jökulsá á Fjöllum, rather than as it did southeast to Grímsvötn and down Skeiðará.

Downvalley course and limits

Above shield volcano Vaðalda (*km 25*), floodwater from two sources took different paths into Jökulsá

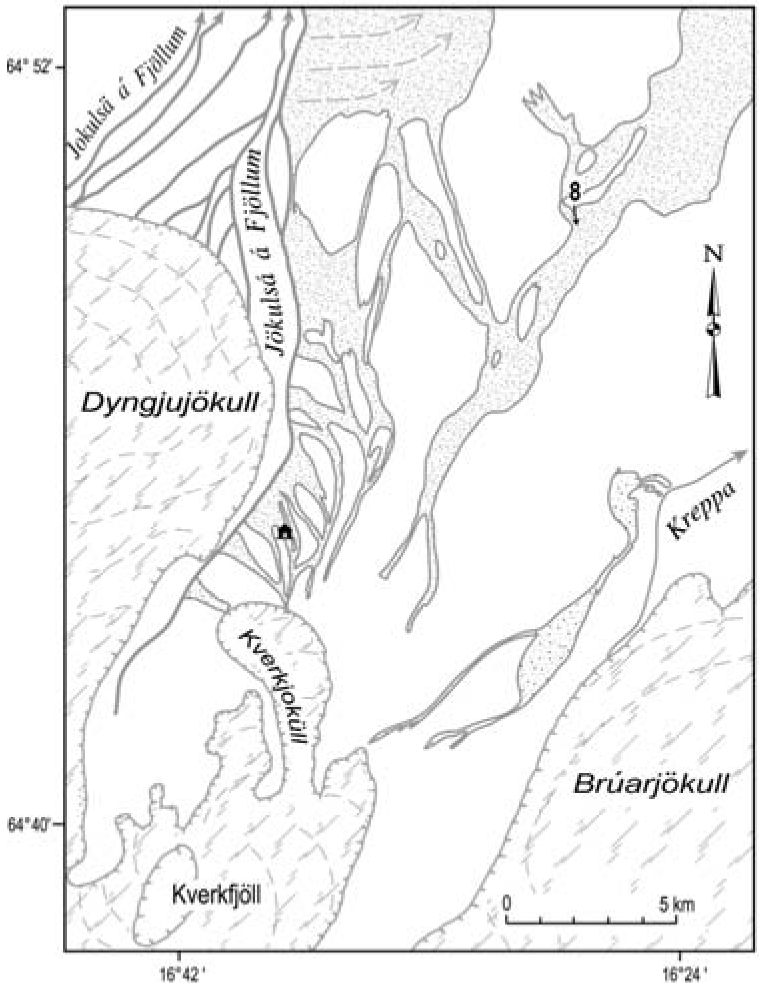

Fig. 9. Sketch map showing divergent–convergent plexus of floodpaths through high-relief landscape issuing from Kverkfjöll area. North-central area (broken arrows) depicts huge eastward overflow from mainstem of Jökulsá á Fjöllum that dominates Jökulsá flood evidence from there down-valley. 8→, view direction of Fig. 8. Building symbol, Kverkfjöll hut.

valley. From there floodwaters channelled into or spread out from one general path (Fig. 1).

Above Vaðalda (km 0–30)

Contrasting the abundant and clear evidence of great flood winding through high-relief topography north of Kverkfjöll, field evidence for evidently enormously greater discharge is far more subtle across the broad, flat, sandy floor of Jökulsá, also swept by large historic floods for some kilometres below the terminus of Dyngjujökull. But starting at about *km 19* the field evidence becomes widespread and unmistakable all the way to the sea.

At the west-margin peak-flood limit at *km 19* (altitude 680–700 m, about 20 m above Jökulsá (Fig. 1, site 1)), basalt surfaces are swept clear of debris and the sharp east edge quarried back into small incipient dry cataracts. Downcurrent, 2–3 m lower, there are several high-level broad bars that trend 055°, are as long as 150 m and as high as 2 m, and comprise boulders as large as 1.1 m (Fig. 10A). Open-framework boulders are imbricated against one another (Fig. 10B), evidence of northeastward flood flow. Jökulsá valley at this level is 10 km across, with a channel cross-sectional area of about 100 000 m^2. If mean velocity were only 5 m/s, palaeoflow discharge would be 0.5 million m^3/s. From here the flood channel divides around the shield Vaðalda (*km 25–35*). The high west channel across lava flows is littered with boulders as large as 4 m and with gravel bars.

A broad floodway east from Jökulsá (*km 24–29*) diverges through a 3-km-wide gap between hills and

Fig. 10. High-level flood deposit directly from Dyngjujökull (site 1 on Fig. 1). (A) View toward azimuth 080° of high flood bar downcurrent from washed surface of postglacial lava flow (foreground), the east edge of which (just out of view) is quarried back into small incipient cataracts. Arrows show flood direction. (B) View toward azimuth 170° of imbricated angular boulders on high flood bar. Palaeocurrent flow toward left (toward azimuth 050°). Visible plane of upper boulder measures about 0.5 m by 1 m.

cascades east down a postglacial lava-flow front 15 m high. It sculpted the lava flow into a scabland with relief 2–8 m, stranding boulders as large as 2.5 m but concentrating into sporadic gravel bars. Straight channels as large as 1 km long and 40 m wide harbour streamlined coarse-gravel bars 50 m long and 5 m high.

Vaðalda to Selfoss (km 30–136)

The 106-km reach from Vaðalda to Selfoss displays widespread scabland. A channel diverging and arcing 3 km from Jökulsá (*km 30–36*) is floored by scabland carved as much as 8 m into basalt and overlain by bouldery gravel bars 1–2 km long. In narrows between hills at its lower end (*km 35.5*) flood-moved boulders reach 5.2 m diameter. This dried-up river channel is continuous on both ends with Jökulsá but is 8–22 m higher, a geomorphic record of great overflow out of and back to Jökulsá.

Along a plain 0–7 km east of Jökulsá (*km 30–35*) a lava flow is locally carved into shallow scabland and is discontinuously strewn with gravel. In a moat east of a lava flow, giant dunes of sorted gravel are 1 m high and spaced 24 m, lying 15 m above Jökulsá. At *km 37* and 6 km east from Jökulsá, the 4-km-wide edge of the lava flow is quarried back into a series of vertically walled horseshoe-shaped dry cataracts, one 500 m long and 150 m wide.

The floodpath divides around Upptyppingar (*km 39–48*), the main Jökulsá channel passing on the east and peak-flood limit about 40 m above the river. The wide, higher western scabland channel leads to a vertically walled horseshoe-shaped cataract 6–8 m deep and 180 m wide, cut back 375 m (Fig. 11). Just downcurrent, a lava-flow front is deeply quarried into

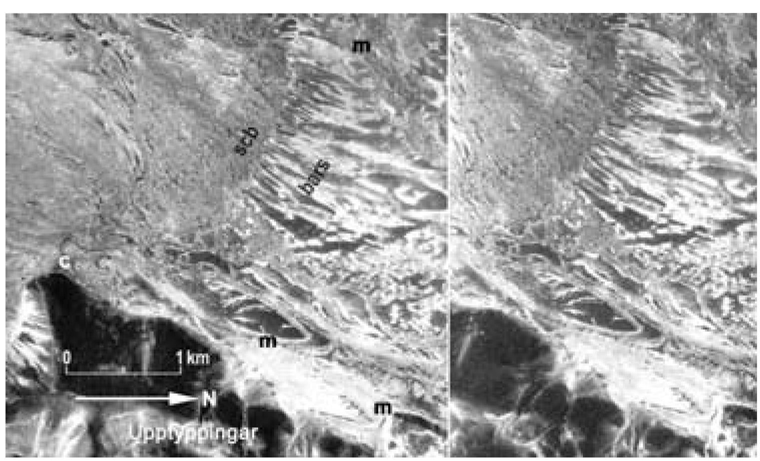

Fig. 11. Stereographic vertical photograph of scabland-channel diversion off Jökulsá (*km 38*) passing west of Upptyppingar (U in Fig. 1). Palaeocurrent toward north (right). Channel forms include dry cataracts (c), steep lava-flow front etched by scabland channels (scb), a suite of gravel bars just downcurrent of these channels. Note moats (m) of non-deposition and erosion bordering not only both sides of scabland channel but also individual whaleback bars.

sharp channels and the flat beyond it strewn with two dozen elongate gravel bars (Fig. 11). Two kilometres farther north, a projecting knoll has scour channels along both sides and a pendant bar downcurrent. No stream flows through this reach today. At *km 77* Jökulsá becomes encanyoned, passing east of Ferjufjall. Yet at *km 78–80* a channel 40 m above Jökulsá diverges: it is 2 km broad and floored by a gravel bar studded with boulders and corrugated by giant dunes spaced 100 m apart. At *km 79* the main channel divides again around Kjalfell (Fig. 1, site 2). The east channel, 1.5–2 km wide is floored by gravel studded with 1–2 m boulders as much as 15 m above Jökulsá. For 8 km along this channel the gravel forms a diverse field of transverse giant-current dunes 1–3 m high and spaced 10–25 m apart. At Lambafjöll, Jökulsá enters a canyon (*km 94–102*) floored by scabland and bars. Just to the west scabland reaches 40 m above the river (*km 95*) and includes a dual dry falls 500 m across and 15 deep. A small arm of flood channelled a gap west 40 m above Jökulsá.

Below Grímsstaðanúpur the floodpath abruptly spread across a plain 7 km wide (*km 106–115*) into a complex of bars of pebble gravel studded with 1-m boulders. The west part flowed around both sides of tuff ring Hrossaborg (*km 115*). A divergent bar built against the upstream side of Hrossaborg has a sharp moat of nondeposition a few metres wide and deep against the obstacle, the deposits thus being convex-up with moated edges—unlike normal river terraces but typical of subaqueous bars. The flood breached the east side of the tuff ring and built a small fan into the crater in water ponded 5 m deep.

Selfoss to Axarfjörður (km 136–162.5)

Dettifoss–Forvöð–Vesturdalur. Below *km 136* Jökulsá plunges over several lava flows as waterfalls Selfoss, Dettifoss, and Hafragilsfoss (*km 136–140*) (Fig. 1). Within 4 km the river is in a narrow canyon 20 m deep. Through this steep-gradient reach, basalt is eroded into scabland buttes, sharp channels, and deep abandoned cataracts; water-moved boulders reach 4 m diameter. Below this steep canyon, Jökulsá widens into Forvöð valley (*km 146–148*) where an upper limit of scabland defines the flood limit 80 m above the valley floor. Glacial drift and aeolian sand at higher levels are overlain by 1.5–2.5 m of yellowish silt and tephra, including Hekla H4. A scabland butte 20 m above the river is capped only by 15–55 cm of brownish silt containing only thin black ashes and no Hekla H3. This and other high scabland thus were swept by late Holocene flood.

Fig. 12. Southeastward view across Vesturdalur area showing surface of postglacial intracanyon lava flow modified into a high boulder-studded low-relief scabland quarried into deep, wide cataract alcove (in centre). East of Jökulsá (J) a high bar (arrow) lies just below peak-flood limit (*km 152–154*).

Vesturdalur (*km 152*) drains around an early Holocene intracanyon lava flow (see above) whose edges have been flood-quarried down to leave a residual rock island (Fig. 12). Its surface 50 m above Jökulsá is etched down into a high scabland sculpted 1–5 m deep and littered with angular boulders as large as 3 m extending 2 km west from Jökulsá. The downcurrent edge is quarried back 300 m into dry cataract 300 m wide and 15 m deep (Fig. 12). These floodswept surfaces are overlain by only 15–20 cm of brown silt containing three black-sand ashes including V-1717. A gravel bar on Jökulsá's east side defines this late Holocene flood limit at 65 m above the river.

Lowermost Jökulsá canyon and Ásbyrgi. Below Vesturdalur, Jökulsá flows in a deep canyon (*km 153–160*) from which divergent high scabland tracts reveal flood overflow of the rim. A conspicuous tract 1–1.5 km wide leads from a sharp bend in Jökulsá (*km 154*) down the sloping basalt surface to Ásbyrgi 3.5 km north. The head of this tract, 95–100 m above the valley bottom, is a scabland bearing four dry-cataract alcoves as high as 10 m with pristine plunge pools and downcurrent bars (Fig. 4). Scabland, bars, and stranded large boulders mark the path to Ásbyrgi. Whereas outside this tract overlying silt is thick and yellowish and contains the Hekla H3, H4, and H5 tephras, along the scabland tract the silt is brown, thin, and lacks Hekla tephras.

Ásbyrgi is a nearly vertical, horseshoe-shaped alcove quarried 2 km back into basalt flows. It is 1 km across, its lower end splitting to two channels separ-

Fig. 13. View northwest along cliff (about 25 m high at near distance) defining west side of Ásbyrgi's Eyjan (right). Ásbyrgi's west arm is floored by bars bearing large boulders (left). A continuous moat of nondeposition as deep as 5 m separates bar from Eyjan wall, evidence of high shear or turbulence along sides of deep wall-to-wall flood flow.

ated by the vertically walled 'Eyjan'. At the head of Ásbyrgi the walls are 30 m high. At base of this drop a closed depression of 15 m delineates the former plunge pool. A continuous moat of nondeposition 5 m deep and 20–50 m wide separates the west wall of the Eyjan from a flat bar studded with large boulders that floors most of Ásbyrgi (Fig. 13). Such features show that floodflow down Ásbyrgi was immense even though fed only by high overflow out of an unblocked lower Jökulsá canyon also discharging immense floodwater.

In Jökulsá canyon just downvalley of the overflow channel to Ásbyrgi, a sand–gravel bar on the east rim lies 100 m above Jökulsá's floor (*km 156*). Below *km 157* Jökulsá canyon becomes shallower and along both rims lie high-level scabland and bars. At *km 160* water overflowed east and west into the heads of tributaries—evidenced by scabland tracts leading to horseshoe-shaped dry cataracts (Fig. 4).

Revision atop the Eyjan. Atop the Eyjan between Ásbyrgi's chasms (Fig. 4), Sigurvín Elíasson (1977; figs 7–9) photographed angular stones said to overlie tephra H3 and which he took as evidence that a great flood swept the Eyjan 2000 yr ago. But I found the stones not a stratigraphic layer but a veneer one stone thick (Fig. 14). They overlie not just H3 but the whole historic tephra sequence. These closely fitted angular stones were merely placed by humans to discourage sheep, a common practice here. Parts of the glaciated Eyjan had been swept by flood, but only the early Holocene pre-H5 one (above, and Fig. 4). There is

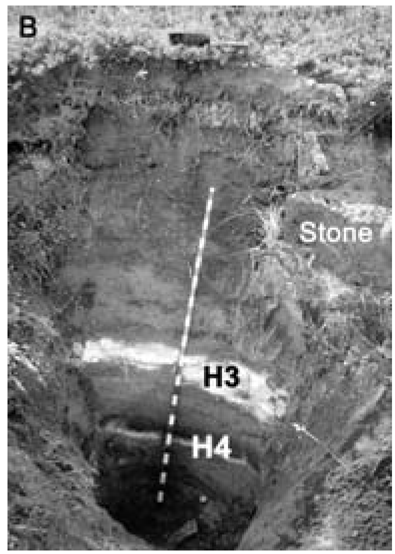

Fig. 14. Exposure along east rim of Ásbyrgi's Eyjan. Scale divisions 3 cm. (A) *In situ* stones sitting on aeolian-silt deposits containing Hekla H3 and H4 tephras. This relationship has been mistaken as evidence that a huge 2000 yr BP flood overtopped the Eyjan (Elíasson, 1977, figs 7 & 8). (B) Photograph revealing true nature of the stones, here removed: they were placed by humans to discourage erosion by sheep's hooves.

no field evidence that the late Holocene flood leapt 25–30 m from Ásbyrgi's floor to overtop the Eyjan.

Inferred hydraulics

In the canyon reach from Selfoss to Axarfjörður (*km 133–162*), peak discharge of the late Holocene flood is computed by HEC-2 version 4.6.2 (Hydrologic Engineering Center, 1991) step-backwater method. Chris Harpel summarized topography in 19 detailed cross sections of this canyon reach and ran the HEC-2 models in 1995 using assumptions (such as values of Manning '*n*') by which peak discharges of many large and even colossal palaeofloods including the Pleistocene Missoula floods have been estimated (detailed explanation in O'Connor, 1993, pp. 12–16; see also O'Connor *et al.*, 1986; O'Connor & Webb, 1988; O'Connor & Baker, 1992; O'Connor & Waitt, 1995; Wohl & Ikeda, 1998; Harpel *et al.*, 2000).

Cross sections for most of Jökulsá's canyon are from 1 : 20 000 topographic maps with 5-m contours (Orkufstofnun, unpublished), but one stretch is only at 1 : 100 000 with 20-m contours. An 'input' discharge of at least 0.7 million m^3/s is needed to bring modelled water-surface profiles up to the field evidence of peak-flood limits. This peak-discharge estimate agrees broadly with Tómasson's (1973) estimate of 0.4–0.5 million m^3/s. Such discharges are three to four orders of magnitude larger than Jökulsá's annual peak flows, typically between 400 and 1000 m^3/s (Helgason, 1987; fig. 11.2).

ACKNOWLEDGEMENTS

Richard S. Williams, Jr. and Michael C. Malin were helpful early informants on Iceland and Jökulsá á Fjöllum. Several of the University of Iceland aided the 1986 field project. Gudmundur Sigvaldasson, Karl Grönvold, and Thorvaldur Thorðarson of Nordic Volcanological Institute, and Leó Kristjánsson and Helgi Björnsson of the Science Institute facilitated logistics. Helgi Björnsson sponsored the project for the National Research Council of Iceland. Field excursions with Jón Jónsson and Thorleifur Einarsson in south Iceland and with Karl Grönvold in Kverkfjöll were most informative. Kristján Saemundsson, Haukur Tómasson, and Guttormur Sigbjarnarson of Orkustofnun (National Energy Authority) discussed their field mapping and/or compilations in Jökulsá; Saemundsson provided copies of unpublished large-scale topographic maps for the HEC-2 modelling. Leó Kristjánsson and Elin Olafsdottir have my heart for their warm hospitality in Reykjavík in 1986. A Gilbert Fellowship (USGS) funded 1986 fieldwork.

In July 2000 Magnus Tumi Gudmundsson helpfully translated parts of Icelandic literature accurately to English, and Andy Russell and Oskar Knudsen collaborated in a brief revisit to four critical areas in Jökulsá. Suggestions by reviewers Jon Major, Jim O'Connor, Andy Russell, and Magnus Tumi Gudmundsson, and by editor I. Peter Martini, much improved the manuscript.

REFERENCES

Allen, J.R.L. (1961) Sandstone-plugged pipes in the lower Old Red Sandstone of Shropshire, England. *J. sediment. Petrol.* **31**, 325–335.

Allen, J.R.L. (1971) Bed forms due to mass transfer in turbulent flows—a kaleidoscope of phenomena. *J. Fluid Mech.* **49**, 49–63.

Allen, J.R.L. (1982) *Sedimentary Structures, their Character and Physical Basis*, Vol. II, pp. 40–48, 137–141, 253–291. Elsevier, New York.

Ashley, G.M., Southard, J.B. & Boothroyd, J.C. (1982) Deposition of climbing-ripple beds—a simulation. *Sedimentology* **29**, 67–79.

Atwater, B.F. (1986) Pleistocene glacial-lake deposits of the Sanpoil River valley, northeastern Washington. *U.S. geol. Surv. Bull.* **1661**, 39 pp.

Atwater, B.F., Smith, G.A. & Waitt, R.B. (2000) Comment on 'The Channeled Scabland: Back to Bretz?'. *Geology* **28**, 574–575 (and GSA Data Repository item 200062).

Baker, V.R. (1973a) Paleohydrology and sedimentology of Lake Missoula flooding in eastern Washington. *Geol. Soc. Am. Spec. Pap.* **144**, 1–79.

Baker, V.R. (1973b) Erosional forms and processes for the catastrophic Pleistocene Missoula floods in eastern Washington. In: *Fluvial Geomorphology* (Ed. Morisawa, M.), pp. 123–148. SUNY Publications in Geomorphology, Binghamton, New York.

Baker, V.R. & Pickup, G. (1987) Flood geomorphology of the Katherine gorge, northern Territory, Australia. *Geol. Soc. Am. Bull.* **98**, 635–646.

Björck, S., Kromer, B., Jóhnsen, S., *et al.* (1996) Synchronized terrestrial atmospheric deglacial records around the North Atlantic. *Science* **274**, 1155–1160.

Björnsson, H. (1988) *Hydrology of Ice Caps in Volcanic Regions*. Vísingdafélag Íslendinga, Reykjavík, pp. 45 + map plates.

Bretz, J H. (1925) The Spokane flood beyond the Channeled Scablands. *J. Geol.* **33** (97–115), 236–259.

Bretz, J H. (1928) The Channeled Scabland of eastern Washington. *Geogr. Rev.* **18**, 446–477.

Bretz, J H. (1932) *The Grand Coulee*. Special Publication 15, American Geographical Society, New York.

Bretz, J H. (1959) Washington's Channeled Scabland. *Washington Div. Mines Geol. Bull.* **45**, 1–57.

Bretz, J H. (1969) The Lake Missoula floods and the Channeled Scabland. *J. Geol.* **77**, 505–543.

Bretz, J H., Smith, H.T.U. & Neff, G.E. (1956) Channeled Scabland of Washington—new data and interpretations. *Geol. Soc. Am. Bull.* **67**, 957–1049.

Dahl, R. (1965) Plastically sculptured detail forms on rock surfaces in northern Nordland, Norway. *Geogr. Ann.* **47**, 83–140.

Dugmore, A.J., Cook, G.T., Shore, J.S., Newton, A.J., Edwards, K.J. & Larsen, G. (1995) Radiocarbon dating tephra layers in Britain and Iceland. *Radiocarbon* **37**, 379–388.

Einarsson, T. (1968) *Jardfrædi—Saga Bergs og Lands*. Mal og Menning, Reykjavik.

Elíasson, S. (1974) Eldsumbrot í Jökulsárgljúfrum. *Náttúrufræðingurinn* **44**, 52–70.

Elíasson, S. (1977) Molar um Jökulsarhlaup og Ásbyrgi. *Náttúrufræðingurinn* **47**, 160–179.

Flint, R.F. (1971) *Glacial and Quaternary Geology*. John Wiley & Sons, New York.

Folk, R.L. (1980) *Petrology of Sedimentary Rocks*. Hemphill Publishing, Austin, TX.

Glasser, N.F. & Nicholson, F.H. (1998) Subglacial meltwater erosion at Loch Treig. *Scott. J. Geol.* **34**, 7–13.

Gray, J.M. (1981) P-forms from the Isle of Mull. *Scott. J. Geol.* **17**, 39–47.

Gray, J.M. (1984) A p-form site on the Isle of Islay, Scottish Inner Hebrides. *Quat. Newsl.* **42**, 17–20.

Gudmundsson, M.T., Sigmundsson, F. & Björnsson, H. (1997) Ice–volcano interaction of the 1996 Gjálp subglacial eruption, Vatnajökull, Iceland. *Nature* **389**, 954–957.

Harpel, C.J., Waitt, R.B. & O'Connor, J.E. (2000) Paleodischarges of the Late Pleistocene Missoula Floods, Eastern Washington, U.S.A. *Extremes of the Extremes Symposium Abstracts,* p. 21. Report OS-2000-036, Orkustofnun, Reykjavík.

Helgason, J. (1987) *Jarðfræðirannsóknir á Vatnasviði Jökulsár á Fjöllum við Möðrudal*. Report OS-87005/VOD-01, Orkustofnun Reykjavík.

Hydrologic Engineering Center (1991) *HEC-2 Water Surface Profiles*. U.S. Army Corps of Engineers, Davis, CA.

Ísaksson, S.P. (1985) Stórhlaup í Jökulsá á Fjöllum á fyrri hluta 18. Aldar. *Náttúrufræðingurinn* **54**, 165–191.

Jopling, A.V. & Walker, R.G. (1968) Morphology and origin of ripple-drift cross-laminations, with examples from the Pleistocene of Massachusetts. *J. sediment. Petrol.* **38**, 971–984.

Larsen, G. (1982) Gjóskutímatal Jökuldals og nágrennis. In: *Eldur er í Norðri*, pp. 51–65. Sögufélag, Reykjavík.

Larsen, G. (1984) Recent volcanic history of the Veidivötn fissure swarm, southern Iceland—an approach to volcanic risk assessment. *J. Volcanol. geotherm. Res.* **22**, 33–58.

Larsen, G. & Thórarinsson, S. (1977) H4 and other acid Hekla tephra layers. *Jökull* **27**, 28–46.

Larsen, G., Gudmundsson, M.T. & Björnsson, H. (1998) Eight centuries of periodic volcanism at the center of the Iceland hotspot revealed by glacier tephrostratigraphy. *Geology* **26**, 943–946.

Maxon, J.H. & Campbell, I. (1935) Stream fluting and stream erosion. *J. Geol.* **43**, 729–744.

Norðahl, H. (1990) Late Weichselian and early Holocene deglaciation history of Iceland. *Jökull* **40**, 27–50.

O'Connor, J.E. (1993) Hydrology, hydraulics, and geomorphology of the Bonneville flood. *Geol. Soc. Am. Spec. Pap.* 274.

O'Connor, J.E. & Baker, V.R. (1992) Magnitudes and implications of peak discharges from glacial Lake Missoula. *Geol. Soc. Am. Bull.* **104**, 267–279.

O'Connor, J.E. & Waitt, R.B. (1995) Beyond the Channeled Scabland—a field trip to Missoula flood features in the Columbia, Yakima, and Walla Walla valleys of Washington and Oregon. *Oregon Geol.* **57**, 51–60, 75–86, 99–115.

O'Connor, J.E. & Webb, R.H. (1988) Hydraulic modeling for paleoflood analysis. In: *Flood Geomorphology* (Eds Baker, V.R., Kockel, R.C. & Patton, P.C.), pp. 393–402. John Wiley & Sons, New York.

O'Connor, J.E., Webb, R.H. & Baker, V.R. (1986) Paleohydrology of pool-and-riffle pattern development—Boulder Creek, Utah. *Geol. Soc. Am. Bull.* **97**, 410–420.

Saemundsson, K. (1973) Straumrákaðar klappir í kringum Ásbyrgi. *Náttúrufræðingurinn* **43**, 52–60.

Saemundsson, K. (1977) *Ísland Jarðfræðikort*, sheet 7 (*Norðausturland*). Scale 1 : 250 000, Museum of Natural History and Iceland Geodetic Survey, Reykjavík.

Sigbjarnarson, G. (1990) Hlaup og hlaupfarvegir. In: *Vatnið of Landið* (Ed. Sigbjarnarson, G.), pp. 129–143. Orkustofnun, Reykjavík.

Sigbjarnarson, G. (1993) Norðan Vatnajökuls, II. Jarðlagaskipan og jarðfræðikort. *Náttúrufræðingurinn* **63**, 201–217.

Sigbjarnarson, G. (1996) Norðan Vatnajökuls III. Eldstöðvar og hraun frá nútíma. *Náttúrufræðingurinn* **65**, 199–212.

Stuiver, M. & Reimer, P.J. (1993) Extended ^{14}C data base and revised CALIB 3.0 ^{14}C-age calibration program. *Radiocarbon* **35**, 215–230.

Stuiver, M., Reimer, P.J. & Braziunas, T.F. (1998) High-precision radiocarbon age calibration for terrestrial and marine samples. *Radiocarbon* **40**, 1127–1151.

Thórarinsson, S. (1950) Jökulhlaup og eldos á jökulvatnasæði Jökulsár á Fjöllum. *Náttúrufræðingurinn* **20**, 113–133.

Thórarinsson, S. (1960) Der Jökulsá-Canyon und Ásbyrgi. *Petermanns geogr. Mitt.* **104**, 154–162.

Thórarinsson, S. (1971) Aldur ljósu gjóskulaganna úr Heklu samkvæmt leiðréttu geislakolstímatali. *Náttúrufræðingurinn* **41**, 99–105.

Tinkler, K.L. (1993) Fluvially sculpted rock bedforms in Twenty Mile Creek, Niagara Peninsula, Ontario. *Can. J. Earth Sci* **30**, 945–953.

Tómasson, H. (1973) Hamfarahlaup í Jökulsá á Fjöllum. *Náttúrufræðingurinn* **43**, 12–34.

Vilmundardóttir, E.G. & Kaldal, I. (1982) Holocene sedimentary sequence at Tráviðarlækur basin, Þjórsárdalur, southern Iceland. *Jökull* **32**, 49–59.

Waitt, R.B. (1980) About forty last-glacial Lake Missoula jökulhlaups through southern Washington. *J. Geol.* **88**, 653–679.

Waitt, R.B. (1984) Periodic jökulhlaups from Pleistocene glacial Lake Missoula—new evidence from varved sediment in northern Idaho and Washington. *Quat. Res.* **22**, 46–58.

Waitt, R.B. (1985) Case for periodic, colossal jökulhlaups from Pleistocene glacial Lake Missoula. *Geol. Soc. Am. Bull.* **96**, 1271–1286.

Waitt, R.B. (with contributions from O'Connor, J.E. & Benito, G.) (1994) Scores of gigantic, successively smaller Lake Missoula floods through Channeled Scabland and Columbia valley. In: *Geologic Field Trips in the Pacific Northwest* (Eds Swanson, D.A. & Haugerud, R.A.), Chapter 1K. Department Geological Sciences, University of Washington, Seattle.

Whipple, K.X., Hancock, G.S. & Anderson, R.S. (2000) River incision into bedrock—mechanics and relative efficacy of plucking, abrasion, and cavitation. *Geol. Soc. Am. Bull.* **112**, 490–503.

Wohl, E.E. (1992) Bedrock benches and boulder bars—floods in the Burdekin gorge of Australia. *Geol. Soc. Am. Bull.* **104**, 770–778.

Wohl, E.E. & Ikeda, H. (1998) Patterns of bedrock channel erosion on the Boso Peninsula, Japan. *J. Geol.* **106**, 331–345.

Glacial outwash floods

Flood and Megaflood Processes and Deposits: Recent and Ancient Examples. Edited by I. Peter Martini, Victor R. Baker and Guillermina Garzón © 2002 International Association of Sedimentologists. ISBN: 978-0-632-06404-5

Spec. Publs int. Ass. Sediment. (2002) **32**, 55–65

November 1996 jökulhlaup on Skeiðarársandur outwash plain, Iceland[1]

Á. SNORRASON, P. JÓNSSON, O. SIGURÐSSON, S. PÁLSSON, S. ÁRNASON, S. VÍKINGSSON *and* I. KALDAL

Hydrological Service, National Energy Authority, Grensásvegi 9, IS-108 Reykjavík, Iceland
(Email for P. Jónsson: pj@os.is)

ABSTRACT

On 30 September 1996, seismological evidence indicated that a volcanic eruption was starting north of the Grímsvötn caldera in the glacier Vatnajökull, Iceland. As the eruption developed during the first half of October, meltwater was collected in the subglacial lake[2] Grímsvötn at a tremendous rate. It was obvious that a catastrophic jökulhlaup could be expected on the outwash plain Skeiðarársandur south of the glacier Skeiðarárjökull, endangering travellers, as well as bridges and roads in the area. This paper describes the events, hydrograph and suspended sediment transport for the catastrophic flood on Skeiðarársandur, following the subglacial eruption.

JÖKULHLAUP CHRONOLOGY (Oddur Sigurðsson, Skúli Víkingsson and Ingibjörg Kaldal)

Jökulhlaups (glacier outburst floods) are more common in Iceland than any other country in the world. Hence, the international scientific community has adopted the Icelandic word 'jökulhlaup' as a term for this natural phenomenon. Jökulhlaups in Iceland are related to several different circumstances:

1 ice-dammed marginal lakes;
2 subglacial, geothermal areas where the water is trapped temporarily in a subglacial lake;
3 depressions in the glacier surface;
4 subglacial volcanic eruptions.

In early November 1996 a jökulhlaup on Skeiðarársandur received international attention and is described here. The course of events of this jökulhlaup is reproduced from the accounts of eyewitnesses, water-level records, video recordings and photographs. The maximum extent of the jökulhlaup was mapped from aerial photographs of the Iceland Geodedic Survey of 6 November, ERS1 radar image of 7 November and oblique aerial photographs.

Skeiðarársandur is the largest glacial outwash plain in Iceland, with an area of approximately 1000 km^2. The rivers Núpsvötn to the west and Skeiðará to the east border it. Its coastline, to the south, is approximately 50 km long, and to the north it is bordered by the glacier Skeiðarárjökull. The shortest distance from the glacier margin to the sea is approximately 20 km (Fig. 1a).

Several rivers flow down the outwash plain, as can be seen in Fig. 1. Farthest to the west is Núpsvötn. A few kilometres east of Núpsvötn is the fairly large river Gígjukvísl, running in a well-defined channel through the moraines south of the Skeiðarárjökull. The largest river on the Skeiðarársandur is Skeiðará, farthest to the east. It is a braided river like Núpsvötn and basically has one outlet between the glacier and the mountain Jökulfell.

The Icelandic Public Road Administration (IPRA) was in charge of the preventive and protective measures taken before the flood. The Hydrological Service (HS) at the National Energy Authority (NEA) was

[1] This paper combines three short contributions presented originally as extended abstracts in the *Proceedings of the XX Nordic Hydrological Conference,* Helsinki, Finland, 1998: Nordic Hydrological Programme, NHP Report no. 44.
[2] Terms such as glacier, river, lake, mountain are used for the benefit of the reader but they are not capitalized because most Icelandic proper names already contain such information.

Flood and Megaflood Processes and Deposits: Recent and Ancient Examples. Edited by I. Peter Martini, Victor R. Baker and Guillermina Garzón © 2002 International Association of Sedimentologists. ISBN: 978-0-632-06404-5

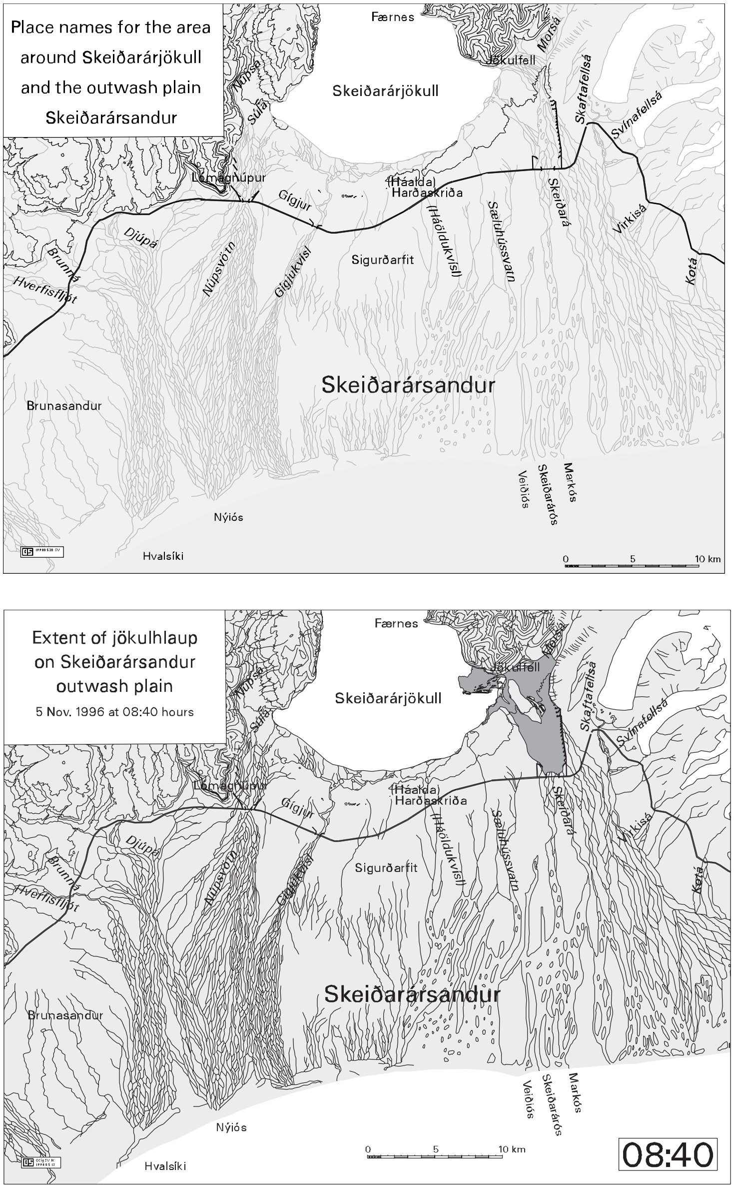

Fig. 1. (a) Map of Skeiðarársandur with the most important place names. (b) Map showing the extent of jökulhlaup on Skeiðarársandur at 0840 hours on 5 November 1996.

responsible for carrying out measurements of water level and discharge of the three major rivers on Skeiðarársandur, Skeiðará, Gígjukvísl and Núpsvötn, before and during the flood. The HS also took samples for chemical analysis and conductivity measurements in co-operation with the Science Institute of the University of Iceland (SIUI). The course of events is described in Snorrason *et al.* (1997) and Sigurðsson *et al.* (1998).

At the beginning of October 1996, a subglacial volcanic eruption under the Vatnajökull ice-cap melted $3\ km^3$ of glacier ice. The meltwater flowed immediately away from the eruption site along the glacier bed, over a 200-m high subglacial ridge and was trapped in a subglacial lake in the now quiescent Grímsvötn caldera, Iceland's most active volcano (Guðmundsson, 1997). During quiescent periods the thermal energy of the Grímsvötn caldera melts on average about $1\ km^3$ of ice in a 5-yr period (Guðmundsson *et al.*, 1995), which subsequently causes a jökulhlaup with a peak discharge of about $3000\ m^3\ s^{-1}$ (Sigurðsson *et al.*, 1992). The jökulhlaups from the Grímsvötn caldera have, through the ages, formed the 1000 km^2 Skeiðarársandur. In 1996, the water level in the lake was rising at a much higher rate than ever observed previously and it became clear that it was only a question of time before the ice-dam holding the water in the lake would break and the water would flush under the glacier Skeiðarárjökull, causing a catastrophic jökulhlaup on the outwash plain Skeiðarársandur, endangering travellers, bridges and roads in the area.

At 2100 hours on 4 November 1996 seismic signals from the nunatak Grímsfjall on the Vatnajökull ice-cap indicated that the ice barrier of the reservoir had failed. Ten hours later, at 0720 hours on 5 November the flood front broke up through 250 m of ice, 50 km down-glacier and 2–3 km from the terminus of the Skeiðarárjökull outlet glacier. This formed an approximately 2-km-long undulating fissure. Timing of the events indicates that the flood front had travelled at a speed of about 5 km h^{-1} beneath the glacier. Later that day the flood broke out successively farther to the west, along the terminus.

A considerable volume of water (of the order 1–2 km^3) was stored below the glacier along the course from Grímsvötn to the terminus of Skeiðarárjökull (Jónsson & Snorrason, 1998a). The process of water forcing its way under the glacier and subsequently breaking vertically and explosively to the surface through 200–300 m of ice resembles the subterranean motion of lava and subsequent fissure eruption.

The first slight indication of rising water level in the Skeiðará was noticed at 0720 hours on the morning of 5 November at the bridge over the Skeiðará river (Fig. 1a & b). At 0800 hours the main flood front hit a water-level gauge below Skaftafell farm and at 0850 hours it reached the bridge, indicating that the flood front had moved at an average speed of 9 km h^{-1} (Fig. 1b; Snorrason & Árnason, 1998). In the Skeiðará the flood course was divided between two main tributaries that join about 5 km downstream of the terminus of the glacier. Which of these tributaries conveyed the initial flood wave is not known owing to darkness, so there is some uncertainty as to the exact travel speed of the flood front. The road on both sides of the Skeiðará river bridge was broken at 0945 hours and the power line south of the bridge collapsed at 0952 hours.

At 1015 hours the flood broke out of the glacier 5 km to the west of Skeiðará river, and split into two river courses, Sæluhússvatn and Gígjukvísl. At 1050 hours the flood front had reached the outlet through the main terminal moraine (Fig. 2a). This outlet was eroded during the flood at widths ranging between about 160 m and 400 m. At 1300 hours the flood front in the Gígjukvísl had reached half way to the coast (Fig. 2b).

In very much the same manner as the initial eruption of the flood water from the glacier surface a few kilometres back from the glacier terminus, there were several subsequent outbreaks gradually farther to the west until the last one appeared at the south-west corner of the Skeiðarárjökull terminus at 1545 hours. At 1615 hours the flood front reached the bridge of the river Núpsvötn (Fig. 3a).

At about 1300 hours a new channel developed 6 km along the eastern edge of the glacier. A similar channel formed along the western edge of the glacier some time after 1530 hours. After dark, the water level in front of the glacier in the middle of the outwash plain had risen about 20 m and reoccupied an abandoned channel, which led to extensive damage of roads.

At 1540 hours the flood issued from the entire 20 km length of the glacier terminus. The flood peaked at about 2300 m^3 s^{-1} in the westernmost channel, the Núpsvötn, at about 1900 hours. In the Skeiðará, a peak discharge of about 22 000 m^3 s^{-1} was reached a little before 2300 hours, and, in the Gígjukvísl, sometime after midnight, the greatest discharge of any individual channel reached about 33 000 m^3 s^{-1} (Jónsson & Snorrason, 1998a).

The flood wave travelled 20–25 km to the coast at a speed of 8–10 km h^{-1}. The jökulhlaup completely swept away the 376-m-long bridge over the Gígjukvísl river in half an hour at 1300 hours, and carried away one-fifth of a 900-m-long bridge over the Skeiðará river between 1600 and 1700 hours. The flood washed away or damaged 12 km of public roads and 7 km of dykes. Twenty-three power-line towers collapsed in the flood.

Fifteen hours after the break-out from the glacier terminus, the combined estimated peak discharge reached more than 50 000 m^3 s^{-1}, the second largest river on Earth at that moment. The total area covered by the flood outside the glacier was about 750 km^2 (Fig. 3b). The coastline advanced up to 800 m in front of the mouth of Gígjukvísl river. The area of the new land was measured to be about 7 km^2. Within 6 months wave action had smoothed this new area along the coast.

MEASUREMENTS OF WATER LEVELS AND TEMPERATURE

(Árni Snorrason and Sigvaldi Árnason)

Water-level recorders and temperature sensors were installed on Skeiðarársandur prior to the jökulhlaup. It was believed to be very important to record the time

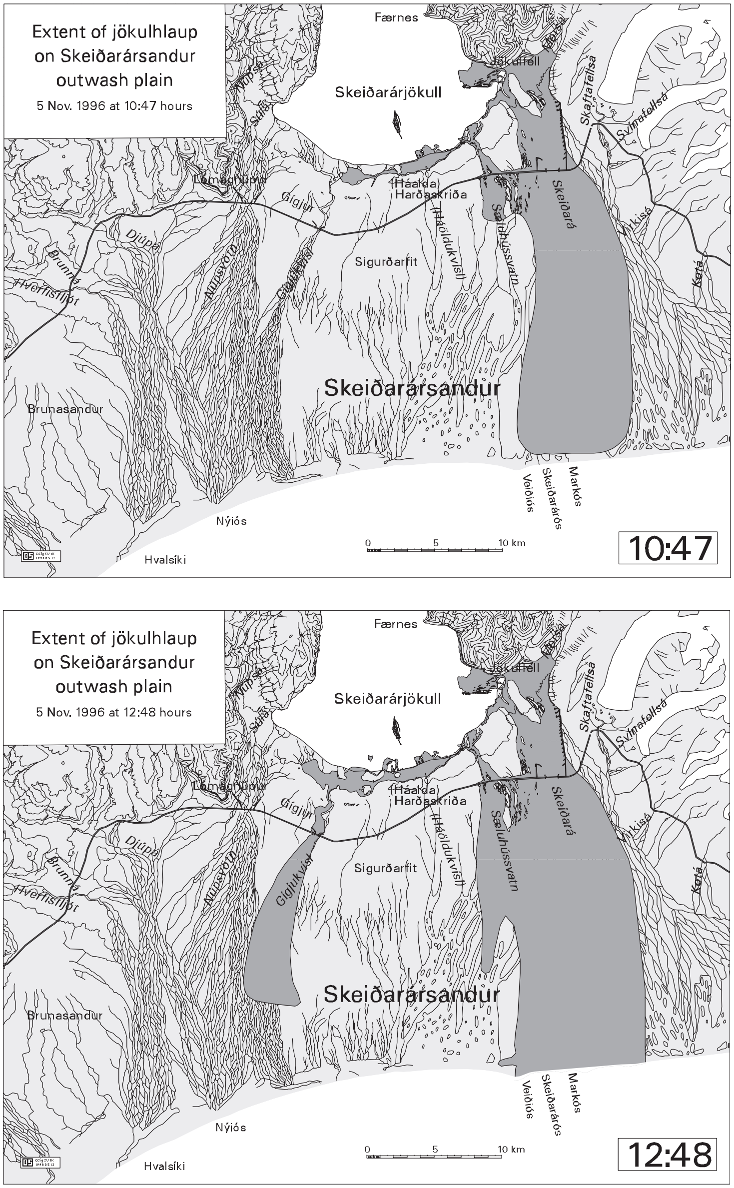

Fig. 2. (a) Map showing the extent of jökulhlaup on Skeiðarársandur at 1047 hours on 5 November 1996. (b) Map showing the extent of jökulhlaup on Skeiðarársandur at 1248 hours on 5 November 1996.

of the very beginning of the jökulhlaup, especially if it occurred during the night. The temperature measurements were expected to make it easier to interpret how the floodwater had travelled under the glacier from the Grímsvötn caldera and how the Skeiðará channels under the glacier had developed during the flood. Two hydrographs were recovered, as well as one record of the temperature of the jökulhlaup water. These data are difficult to interpret, but provide an overview of the development of events in time and therefore are invaluable for further studies of the processes involved.

Two water-level recorders were placed on the banks of the Skeiðará river. One of the water-level recorders was placed about 5 km upstream of the bridge on the main road over the Skeiðarársandur outwash plain and the second one at the eastern end of the bridge. The first one was equipped with a gas pressure gauge system with an electronic pressure sensor and a digital data logger. It was installed on a steep bank along

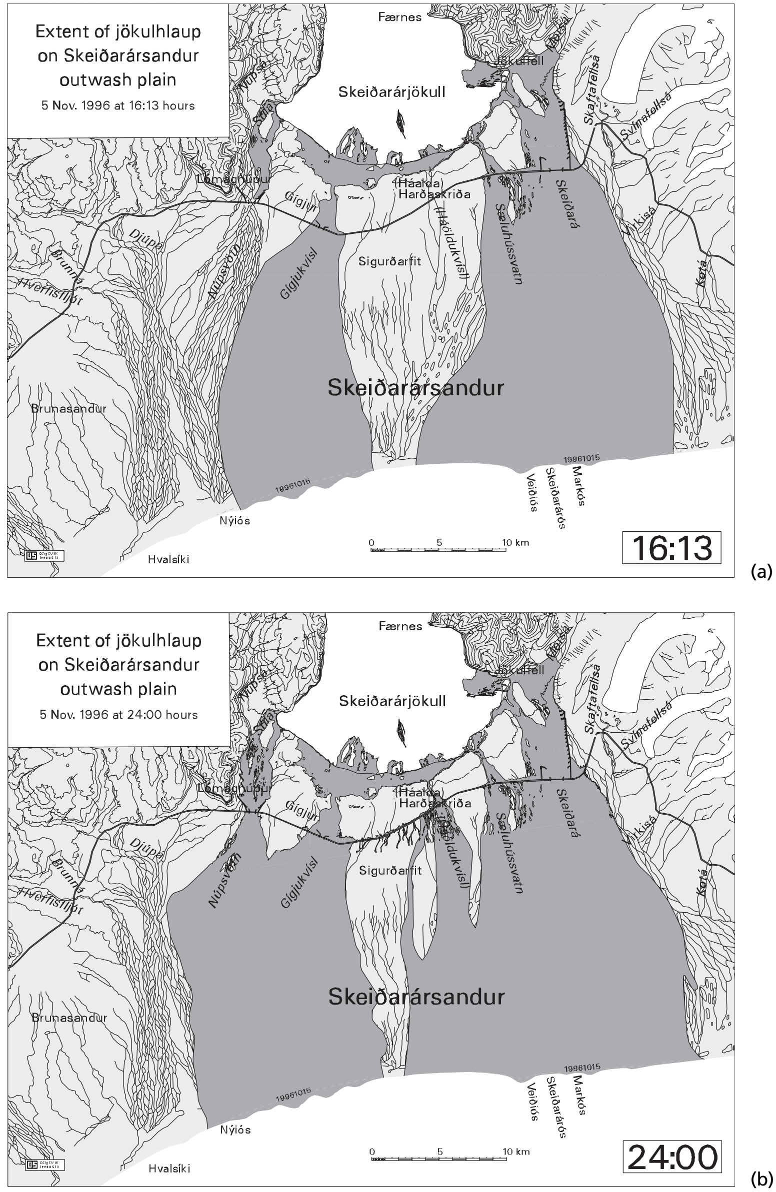

Fig. 3. (a) Map showing the extent of jökulhlaup on Skeiðarársandur at 1613 hours on 5 November 1996. (b) Map showing the extent of jökulhlaup on Skeiðarársandur at 2400 hours on 5 November 1996.

the easternmost channel of Skeiðará at Skaftafell. The second one was a pressure sensor connected to an electronic logger that recorded the water level every 5 min.

The hydrograph for the upstream gauge is shown in Fig. 4a for the whole event, and for the initial phase on Fig. 4b. The initial wave submerged the end of the bubbling system at the first gauge at 0800 hours and reached a maximum of 3.2 m 40 min later. The second reached a peak of over 5 m at about 0920 hours. The water level then declined and reached a minimum level after 1100 hours. The level increased again from 1330 hours to about 1600 hours, but then stayed at relatively the same level until about 2300 hours, when a definite decline starts, indicating subsidence of the jökulhlaup.

The interpretation of the initial phases of the flood are difficult, because flood waves hit the banks at full force, and the water was heavily laden with sediments.

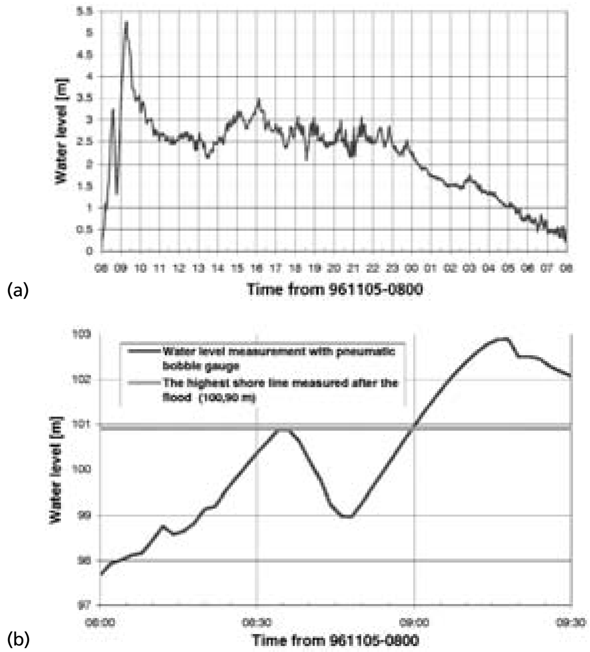

Fig. 4. Diagrams showing water level at Skaftafell (upstream gauge): (a) during the jökulhlaup in November 1996; (b) during the initial phase of the jökulhlaup in November 1996.

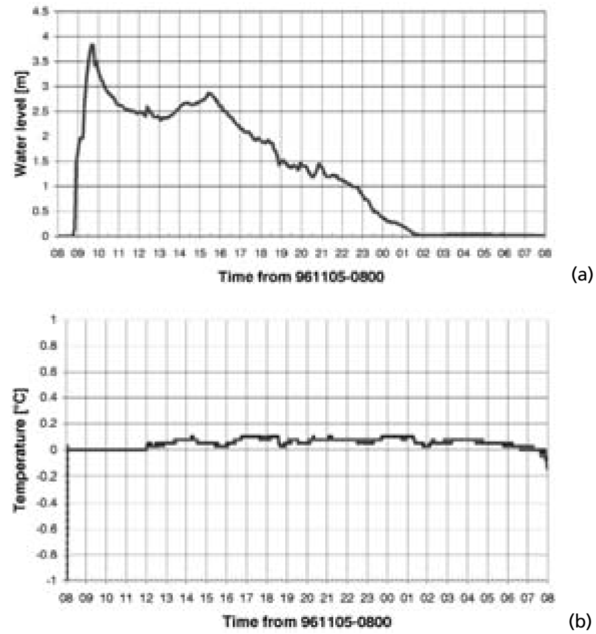

Fig. 5. Diagrams showing measurements during the jökulhlaup in November 1996: (a) water level at Skeiðarársandur (gauge at bridge); (b) water temperature at Skaftafell (upstream gauge).

It also is possible that the bubbling system clogged during the initial flood waves. Water-level analyses after the flood showed that the level reached the height of the first peak. However, these estimates and the behaviour of the gauges are not conclusive, because the density of the fluid in the initial phases of the flood was definitely higher than that of water. In fact, surface samples of the water, taken at the bridge at 0925 hours, showed a concentration of about 120 g L^{-1} (Jónsson & Snorrason, 1998a), which is considered to be a gross underestimation of the mean concentration.

The second gauge was a pressure sensor, installed before the flood on dry land near a lagoon located upstream and east of the bridge over the Skeiðará. During this catastrophic jökulhlaup the pressure sensor gave a continuous, reliable hydrograph of the flood, as shown in Fig. 5a. The sensor was submerged by the initial wave at 0845 hours and at 0940 hours it reached the highest level of almost 4 m above the sensor. At the highest level, the flood wave overtopped the dykes around the lagoon and the eastern side of the bridge, and took about an hour for them to fail and erode away, as can be seen from the water-level record. At about 1500 hours there is another maximum, but the decline in the water levels after that probably is a result of the erosion of the channel itself; it is known from smaller jökulhlaups that very dramatic erosion can take place in localized channels under the bridge. This interpretation is supported by the fact that the eastern part of the bridge failed during the period from just before 1600–1630 hours. The record shows a steady decline after about 2200 hours in the evening, indicating that the discharge was declining. Comparison between the gauge readings and reference measurements during and after the flood showed good agreement. The issue of the density of the liquid is not important in this case, because the gauge was located inside a lagoon, and sediments fell out of suspension rapidly causing the concentration to decrease within the lagoon.

A temperature sensor was placed close to the bubble gauge. As soon as the jökulhlaup started, the sensor was submerged in water and worked continuously during the flood event (Fig. 5b). The temperature of the floodwater for the first 4 h of the flood was exactly 0°C, but it then rose to 0.05–0.10°C. The reason for this is that at the beginning of the flood the water was mixed with ice and ice slush, possibly owing to mechanical erosion and breaking of the ice. This ice had not melted completely before the floodwater reached the location of the sensor, so the water stayed at 0°C. In later stages of the flooding, equilibrium between the widening of the flood channel and the heat in the floodwater was probably reached, resulting in water at 0°C at the glacial outlet. The floodwater then warmed up on the way from the terminus to the sensor because of the change of potential energy into heat owing to the viscosity of the water.

These data are a very valuable record of the development of a major flood and will be the basis for further analysis of the processes involved in these events, and for the interpretation of ancient sedimentary facies.

DISCHARGE AND SEDIMENT TRANSPORT

(Páll Jónsson, Árni Snorrason and Svanur Pálsson)

Hydrograph estimation

In the planning before the jökulhlaup, it was considered important to measure the discharge during the event. However, the flood was of such dimensions and its outburst so violent that as soon as the first flood wave was observed, it was obvious that no traditional discharge measurements could be carried out. Nevertheless, the HS and IPRA made independent estimates of the discharge for each of the three major rivers, Skeiðará, Gígjukvísl and Núpsvötn, several times during the event. The results of these estimates are shown in Table 1, where the last two discharge estimates in the river Núpsvötn are actually calculated from depth and surface velocity measurements (Snorrason *et al*., 1997).

The hydrographs for each of the three major rivers on Skeiðarársandur, Núpsvötn, Gígjukvísl and Skeiðará, were based on the estimates of discharge made during the jökulhlaup. It was assumed that both the growth and the decline of discharge are exponential, following Jónsson & Snorrason (1998b). In all the three rivers, the flood started with a tremendous flood wave, like a dam-break outburst travelling down the river channel from the glacier. The timing of these initial flood waves is well known and used in the construction of the hydrographs. The hydrograph is drawn linearly from zero discharge at the time of the start of the initial flood wave towards the exponential curve describing the growth of the discharge after the initial flood wave, but start of the exponential growth is estimated.

For the Skeiðará and Núpsvötn rivers, the timing of the maximum water level is known, rather than the timing of peak discharge (Snorrason *et al*., 1997; Snorrason & Árnason, 1998). The timing of the peak discharge cannot be established with certainty because when the discharge rate begins to fall, the suspended sediment settles, changing the geometry of the channels and possibly causing the water level to rise even though the discharge is declining. For the Núpsvötn river, the peak discharge is known to be approximately 2500 m^3/s, because the maximum water level was the same as in the jökulhlaup in Núpsvötn in 1986, when the peak discharge was actually measured. The time of peak discharge in Núpsvötn was approximately 1900 hours on 5 November 1996. For the Skeiðará river, its easternmost branch reached peak water level between 2200 and 2300 hours on 5 November 1996. For the Gígjukvísl river, the time of peak is not known. However, during the night between 5 and 6 November, Gígjukvísl flooded an old channel of the Háöldukvísl river, suggesting that it peaked during the night. This is not conclusive, because the channel geometry of the Gígjukvísl river changed dramatically during the event as a result of the heavy sediment load.

The hydrographs for the three rivers are shown in Fig. 6a, together with a hydrograph constructed by adding the three hydrographs together. The estimated discharge according to Table 1 is also shown in the figure. Experience from previous jökulhlaups suggests that the hydrographs are not as peaked as the mathematical model suggests, but are somewhat flattened

Table 1. Estimates of the discharge for the rivers on Skeiðarársandur in November 1996. Numbers in italics indicate direct measurements.

Time	Skeiðará ($m^3 s^{-1}$)	Gígjukvísl ($m^3 s^{-1}$)	Núpsvötn ($m^3 s^{-1}$)	Total ($m^3 s^{-1}$)
1200 hours, 5 November	10 000	10 000	–	20 000
1700 hours, 5 November	15 000	15 000	1 500	31 500
1900 hours, 5 November	–	–	2 300	–
1000 hours, 6 November	1 500	15 000	600	17 100
1900 hours, 6 November	400	5 000	*560*	5 960
0930 hours, 7 November	50	300	*160*	510

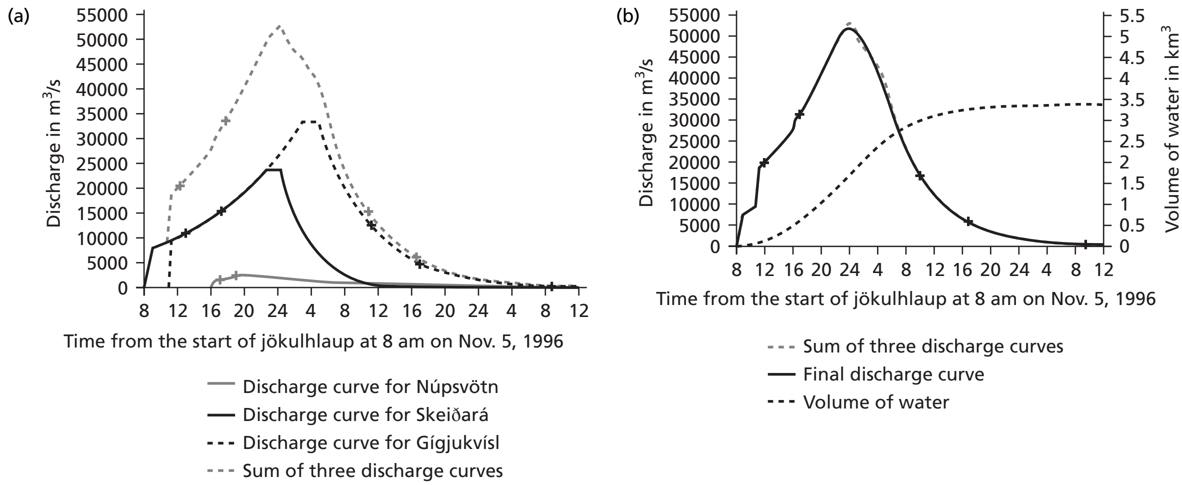

Fig. 6. Jökulhlaup discharges on Skeiðarársandur: (a) estimated hydrographs for the three major rivers; (b) total hydrograph and total volume of water.

at the top. Therefore, the hydrographs for the three rivers were all reduced by cutting 10% off the peak discharge. It is obvious from Fig. 6a that the sum curve is somewhat irregular at the top and also at the times of the initial flood waves. This is because of the 'cutting off' of the peak discharge for the individual curves and because the initial flood waves have been modelled linearly. In order to obtain a final hydrograph for the total jökulhlaup on the Skeiðarársandur outwash plain, this sum curve has been smoothed (Fig. 6b).

Figure 6b shows that the maximum discharge was 52 000 $m^3\ s^{-1}$ shortly after midnight on 5 November 1996. The discharge thus reached a maximum in only 16 h, indicating how violent the event was. The jökulhlaup also declined very rapidly. After only 36 h from the start of the jökulhlaup, the discharge was approximately equal to the maximum discharge of the small jökulhlaup in the spring of 1996, or 3000 $m^3\ s^{-1}$. It is reasonable to conclude that the jökulhlaup was completely over in only two days, which is an exceptionally short duration, compared with accounts of historical jökulhlaups (Þórarinsson, 1974).

Figure 6b also shows the cumulative total volume of water that flooded the outwash plain, as a function of time from the start of the jökulhlaup. The total volume of water that flooded the Skeiðarársandur in the jökulhlaup is estimated from the hydrograph at 3.4 km^3. The SIUI measured the height of the ice-shelf during the jökulhlaup with a barometer and deduced the water level and volume of water in the lake Grímsvötn, estimating that 3.2 km^3 of water flowed from the lake. Furthermore, SIUI estimates from measurements of the glacier surface after the flood showed that approximately 0.4 km^3 of water was melted, by the warm water flowing from the lake Grímsvötn, on the 50-km-long route under the Skeiðarárjökull glacier to the Skeiðarársandur outwash plain. The difference in these two independent estimates is therefore only 0.2 km^3, which is well within all uncertainty limits.

The SIUI also used the measurement of the height of the ice-shelf to construct a hydrograph for the outflow from lake Grímsvötn (Björnsson, 1997). According to this hydrograph, the peak discharge for the outflow was 40 000 $m^3\ s^{-1}$. In addition, the maximum rate of melting of ice on the route from the lake to the outwash plain, as a result of the heat in the water and the loss in potential energy, is estimated to be about 5000 $m^3\ s^{-1}$. This independent estimate is somewhat lower than the peak discharge estimated from the total hydrograph for the flood on the outwash plain. However, it is clear that the long route under the glacier, from the lake down to the outwash plain, has great influence on the hydrograph. The flood broke out from the glacier terminus under great pressure and at different locations, starting at the eastern part and propagating to the west as time passed. This indicates that the water did not follow the traditional channels under the glacier, but rather flooded the whole area under it and the water pressure probably lifted the entire Skeiðarárjökull glacier from lake Grímsvötn down to Skeiðarársandur outwash plain.

The hydrographs for the three rivers, Núpsvötn, Gígjukvísl and Skeiðará, indicate that during the jökulhlaup, 0.2 km^3 of water flowed in the Núpsvötn,

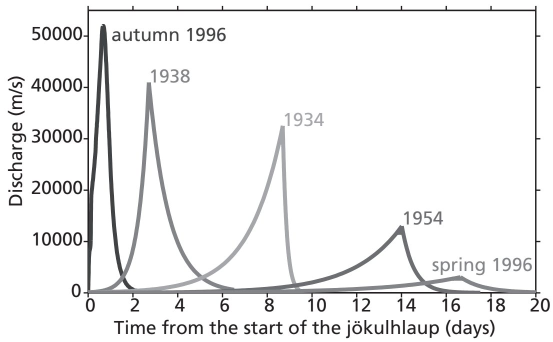

Fig. 7. Discharge curves for jökulhlaups of 1934, 1938, 1954 and 1996, according to the prediction model.

1.2 km^3 in the Skeiðará and 2.0 km^3 in the Gígjukvísl. The volume of water flowing in other rivers on the Skeiðarársandur was insignificant. Assuming that the 3.4 km^3 came down to the Skeiðarársandur in 48 h, the mean discharge was 20 000 m^3 s^{-1}. The cumulative curve in Fig. 6b indicates that the flood was most violent in the 12-h period between 1600 hours on 5 November and 0400 hours on 6 November, and, during that period, about 1.9 km^3 flowed on to the Skeiðarársandur, corresponding to a mean discharge of 44 000 m^3 s^{-1}.

The hydrograph of the jökulhlaup in November 1996 can be compared with estimated hydrographs for historical jökulhlaups in the twentieth century. These hydrographs have been calculated using the prediction model developed by the Icelandic Hydrological Service in October 1996 as part of the preparations made before the jökulhlaup (Snorrason *et al.*, 1997; Jónsson & Snorrason, 1998b). Figure 7 shows that the event of November 1996 is quite extraordinary, both with respect to maximum discharge and the short duration of the flood.

Sediment transport

Measurements of sediment transport in jökulhlaups on Skeiðarársandur include the total concentration of suspended sediment in the floodwater and the grain size distribution. However, no measurements of bedload are available. The sediment is divided into four grain-size categories: clay (< 0.002 mm), fine silt (0.002–0.02 mm), coarse silt (0.02–0.2 mm) and sand (0.2–2.0 mm).

Conditions for taking sediment samples in the jökulhlaup on Skeiðarársandur in November 1996 were extremely difficult, both because of the extreme discharges and also because the floodwater was spread widely over the Skeiðarársandur outwash plain. The samples were taken either with a sediment sampler (U.S. DH-48) into a bottle, or, directly, with a bucket in difficult conditions. Most of the samples were taken from the left bank of the river Skeiðará, but on the second day of the flood, samples were also taken from other channels.

The samples were not depth-integrated and the bucket samples were taken from the surface. Furthermore, the intake nozzle of the sediment sampler was clogged periodically owing to ice formation. From this it is clear that the samples are not representative of the average concentration of suspended sediment and probably they underestimate the average concentrations, especially for the coarser grain sizes. The total sediment transport probably is underestimated by a factor of between two and five.

In the samples taken with the sampler, the mass concentration of sand is only 1–2% of the total suspended sediment transport. For the bucket samples, the mass concentration of sand was zero, except for the first sample taken at the Skeiðará river bridge at 0925 hours on the first day of the jökulhlaup, which had a sand concentration of 1%. This sample was taken at a very important point in time, only half an hour after the initial flood wave hit the bridge over the Skeiðará. It was taken in a bucket and poured into two sediment bottles. The sample in the bottles was filtered for chemical analysis and one of the bottles was sent to the sediment laboratory. This bottle had a large amount of sediment at the bottom, but there was hardly any water left. The mass of the sediment was measured and because it was known that the bottle had been filled when the sample was taken, the concentration of suspended sediment could still be measured. The result of the measurement was an astonishing mass concentration of 121 g L^{-1}, which is an underestimate, because some of the sediment must have been lost both when pouring the sample from the bucket to the bottle and in the filtering process.

In spite of all these difficulties in sampling the measurements can be used to estimate the total mass of suspended sediment transport in the jökulhlaup. Figure 8 shows the estimated jökulhlaup hydrograph for the river Skeiðará, together with the measured mass concentration of suspended sediment. The sediment concentration was weighted with the discharge and integrated to obtain the total amount of suspended sediment transported by the river. Figure 9a shows the total mass of suspended sediment transported in the jökulhlaups in the Skeiðará during the period 1972–1996. These are the only jökulhlaups on

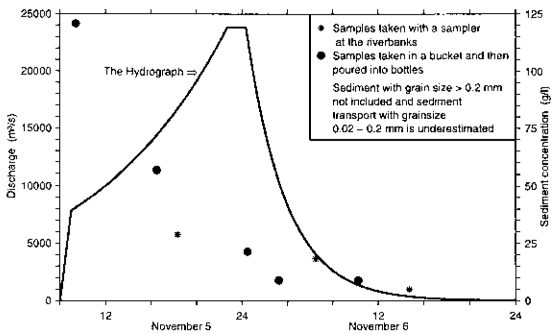

Fig. 8. Diagram showing discharge and concentration of suspended sediment in the jökulhlaup of November 1996.

Skeiðarársandur with reasonably reliable sediment sampling. It is clear that the total mass of suspended sediment estimated to have been transported in the jökulhlaup in November 1996 is exceptionally high, even if grossly underestimated. The total mass of sediment transported in the Skeiðará river alone is estimated to be 63 million tons, compared with the second highest mass of 24 million tons in 1972.

One sample was taken in the Gígjukvísl river, on 6 November, the second day of the jökulhlaup, when the discharge was down to approximately 5000 $m^3 s^{-1}$. The mass concentration was 31 g L^{-1} and 12% of the sample was sand. It is impossible to calculate the total mass of suspended sediment transported by the river Gígjukvísl, based on this sample alone. There were no sediment samples taken from river Núpsvötn. In order to estimate the total mass of suspended sediment transported in the jökulhlaup, the total mass transported in Skeiðará is scaled up in proportion to the 3.4 km^3 of water flowing in the jökulhlaup compared with the 1.2 km^3 in the river Skeiðará alone. This calculation gives 180 million tons for the estimated total mass of suspended sediment transported in the jökulhlaup. As can be seen in Fig. 9b, this mass is approximately six times the second largest mass of sediment transport in the jökulhlaup of 1972, illustrating the extraordinary sediment transport capacity of this jökulhlaup.

CONCLUSION

The jökulhlaup in November 1996 was extraordinary compared with the earlier jökulhlaups in the twentieth century. The initial flood wave was like a dam-break flood breaking out from the terminus of Skeiðarárjökull. The maximum discharge was estimated from hydrographs to be about 50 000 $m^3 s^{-1}$, and although the flood lasted only 48 h, the total volume of water was estimated to be about 3.4 km^3. The measurements of SIUI, on the water level in lake Grímsvötn and on the

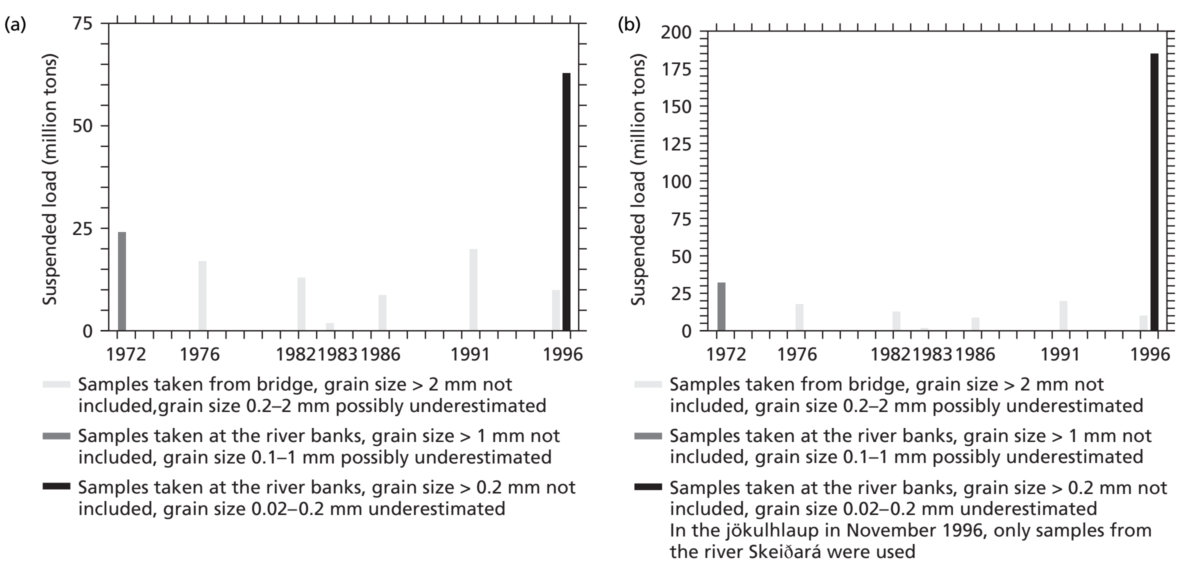

Fig. 9. (a) Diagram showing total mass of suspended sediment in jökulhlaups in the river Skeiðará 1972–1996. (b) Diagram showing total mass of suspended sediment in jökulhlaups from lake Grímsvötn 1972–1996 (Skeiðará, Gígjukvísl and Núpsvötn rivers).

surface of Skeiðarárjökull glacier after the flood, indicate that the maximum outflow from the lake, together with the melting of ice at the outlet from the lake, can be estimated at 45 000 $m^3 s^{-1}$ and the total volume of water at 3.6 km^3.

The total mass of suspended sediment transported during the jökulhlaup was estimated to be 180 million tons, which is grossly underestimated, owing to the problems with sediment sampling during the flood. A flood of such dimensions is bound to influence the morphology of the outwash plain, as events of this magnitude have done in the past.

REFERENCES

Björnsson, H. (1997) Grímsvatnahlaup fyrr og nú. In: *Vatnajökull. Gos og Hlaup 1996 [Vatnajökull. Eruption and Jökulhlaup 1996]* (Ed. Haraldson, H.), pp. 61–77. Vegagerðin, Reykjavík.

Guðmundsson, M.T. (1997) Gosið í Vatnajökli í október 1996. Einkenni, bræðsla íss og breytingar á jöklinum. In: *Vatnajökull. Gos og Hlaup 1996 [Vatnajökull. Eruption and Jökulhlaup 1996]* (Ed. Haraldson, H.), pp. 37–59. Vegagerðin, Reykjavík.

Guðmundsson, M.T., Björnsson, H. & Pálsson, F. (1995) Changes in jökulhlaup sizes in Grímsvötn, Vatnajökull, Iceland, 1934–91, deduced from in-situ measurements of subglacial lake volume. *J. Glaciol.* **41** (138), 263–272.

Jónsson, P. & Snorrason, Á. (1998a) Discharge and sediment transport in the jökulhlaup on Skeiðarársandur in November 1996. In: *XX Nordic Hydrological Conference 1998* (Ed. Kajander, J.), pp. 713–722. Report no. 44, Nordic Hydrological Programme, Helsinki.

Jónsson, P. & Snorrason, Á. (1998b) The prediction model used during the jökulhlaup on Skeiðarársandur in November 1996. In: *XX Nordic Hydrological Conference 1998* (Ed. Kajander, J.), pp. 694–703. Report no. 44, Nordic Hydrological Programme, Helsinki.

Sigurðsson, O., Snorrason, Á. & Zóphóníasson, S. (1992) Jökulhlaupaannáll 1984–88. *Jökull* **42**, 73–80.

Sigurðsson, O., Víkingsson, S. & Kaldal, I. (1998) Course of events of the jökulhlaup on Skeiðarársandur outwash plain, Iceland, in November 1996. In: *XX Nordic Hydrological Conference 1998* (Ed. Kajander, J.), pp. 704–708. Report no. 44, Nordic Hydrological Programme, Helsinki.

Snorrason, Á. & Árnason, S. (1998) Measurements of water levels and temperature during the jökulhlaup on Skeiðarársandur in November 1996. In: *XX Nordic Hydrological Conference 1998* (Ed. Kajander, J.), pp. 709–712. Report no. 44, Nordic Hydrological Programme, Helsinki.

Snorrason, Á., Jónsson, P., Pálsson, S., *et al*. (1997) Hlaupið á Skeiðarársandi haustið 1996. Útbreiðsla, rennsli og aurburður. In: *Vatnajökull. Gos og Hlaup 1996 [Vatnajökull. Eruption and Jökulhlaup 1996]* (Ed. Haraldson, H.), pp. 79–137. Vegagerðin, Reykjavík.

Þórarinsson, S. (1974) *Vötnin stríð. Saga Skeiðarárhlaupa og Grímsvatnagosa*. [Turbulent Waters. The history of Jökulhlaups on Skeiðarársandur and Eruptions in the Grímsvötn caldera.] Bókaútgáfa Menningarsjóðs, Reykjavík.

Spec. Publs int. Ass. Sediment. (2002) **32**, 67–83

The effects of glacier-outburst flood flow dynamics on ice-contact deposits: November 1996 jökulhlaup, Skeiðarársandur, Iceland

A. J. RUSSELL* *and* Ó. KNUDSEN†

**School of Earth Sciences and Geography, Keele University, Keele, Staffordshire ST5 5BG, UK (Email: a.j.russell@keele.ac.uk); and*
†Klettur Consulting Engineers, Bíldshöfða 12, IS 112, Reykjavík, Iceland (Email: ok@isl.is)

ABSTRACT

This study examines the extent to which observed large-scale stage variations are reflected in the proglacial landform and sedimentary record of the November 1996 jökulhlaup, Skeiðarárjökull, Iceland. Discrimination of rising from falling flood stage landforms and deposits usually is based upon the interpretation of the geomorphological and sedimentary record. Sedimentary successions in proglacial environments have been interpreted on the basis of vertical sedimentary characteristics, which are then linked to the flood hydrograph. Spatial segregation of rising and falling stage proglacial outwash during the November 1996 jökulhlaup provided a superb opportunity to examine the role of flow stage in the creation and preservation of distinctive proglacial jökulhlaup landforms and deposits. Rising stage deposits contain finer, more poorly sorted sediment than found in falling stage successions and on erosional surfaces. Rising stage deposits show one or more upward-coarsening successions, characteristic of progressive supply of coarser grained sediment with stage increase, compatible with previous models of rising stage sedimentation. Some rising stage successions, however, show few signs of large-scale grading, and instead contain repeated cycles of sedimentation, recording individual sedimentation pulses. Distinctive upward-coarsening successions on a waning stage outwash fan were generated by sediment winnowing resulting in progressive bed coarsening from matrix-supported gravels to clast-rich armour. The presence of an upward-coarsening succession alone is clearly not diagnostic of rising stage deposition. Conduits occupied by flows on both rising and falling flow stages were characterized by initial rising stage fan deposition followed by falling stage dissection and exhumation of ice blocks and intraclasts deposited on the rising flow stage. Where waning stage flows were routed through a single conduit, high sediment efflux and aggradation rates were maintained late into the waning stage. This study illustrates the geomorphological and sedimentary significance of major within-jökulhlaup sediment reworking and ice-margin erosion over distances of 10^2–10^3 m.

BACKGROUND AND AIMS

Discrimination of rising from falling flood stage landforms and deposits usually is based upon the interpretation of the geomorphological and sedimentary record. Sedimentary successions in proglacial environments have been interpreted as being of jökulhlaup origin on the basis of vertical sedimentary characteristics, which are then linked to specific components of the flood hydrograph (Maizels, 1989a,b, 1991, 1993, 1997; Maizels & Russell, 1992; Russell & Marren, 1998). Assignment of characteristic vertical sedimentary successions to typical transient flow characteristics is common within the literature of flood, hyperconcentrated, debris and turbidite flows (Nemec & Steel, 1984; Pierson & Scott, 1985; Wells & Harvey, 1987; Dietrich *et al*., 1989; Smith, 1993; Sohn, 1997; Cronin *et al*., 1999; Hodgson & Manville, 1999). As such, a vertical sedimentary succession may reflect changing flow and depositional conditions during the passage of sediment-rich floods such as jökulhlaups. However, assumptions have to be made regarding the likely availability of sediment within jökulhlaups. Although non-Newtonian hyperconcentrated flows and debris flows often deposit distinctive sedimentary units, it may be difficult to infer their actual sediment

Flood and Megaflood Processes and Deposits: Recent and Ancient Examples. Edited by I. Peter Martini, Victor R. Baker and Guillermina Garzón ISBN: 978-0-632-06404-5

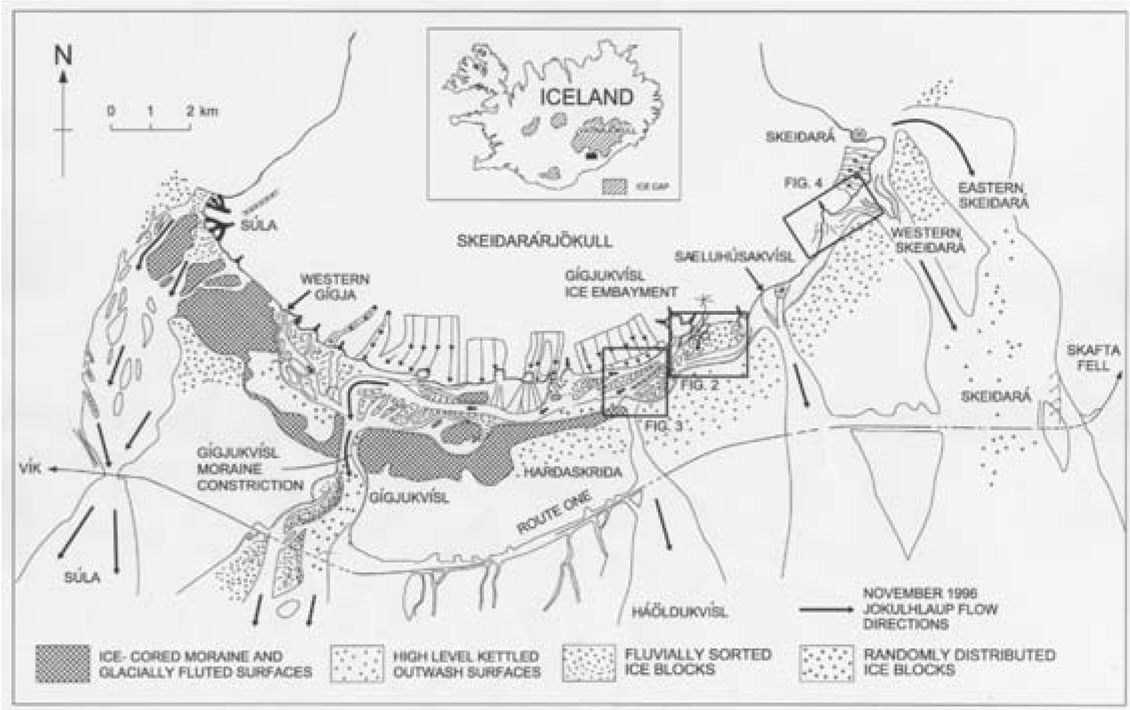

Fig. 1. Map showing the field area within Iceland (inset) and the location of sites discussed in the text.

concentrations from deposits of more fluidal turbulent flows. Although these assumptions can be satisfactorily constrained in modern proglacial environments (Maizels, 1989a,b, 1991, 1993; Russell, 1994; Russell & Marren, 1999), justification of specific sediment supply and flux characteristics becomes more difficult when relict proglacial fluvial systems are considered (Fraser & Bleuer, 1988; Russell, 1995; Russell & Marren, 1998). It is clear that sediment flux may vary considerably between and during floods (Tómasson, 1974; Tómasson *et al.*, 1980; Wells & Harvey, 1987), resulting in complex patterns of within-event sediment reworking (Stewart & La Marche, 1967; Scott & Gravlee, 1968; Russell, 1993). To date, most research on the sedimentology of flood deposits has considered efflux within channels active on both rising and falling flow stage, where the resultant morphology and sedimentology are the product of the temporal variability of both water and sediment flux (Stewart & La Marche, 1967; Scott & Gravlee, 1968; Carling, 1987).

The November 1996 jökulhlaup, Skeiðarárjökull, Iceland, exited the glacier via multiple conduits, each with differing hydrographs (Snorrason *et al.*, 1997; Russell & Knudsen, 1999a,b; Tweed & Russell, 1999) (Fig. 1). Some jökulhlaup outlets were active solely on either the rising or falling flow stage whilst others remained active throughout the rising and falling flow stage (Russell & Knudsen, 1999a; Tweed & Russell, 1999). Well-established spatial segregation of rising and falling stage proglacial outwash during the November 1996 jökulhlaup provides an opportunity to assess the role of flow stage in the creation and preservation of distinctive proglacial jökulhlaup landforms and deposits. Although jökulhlaup flows from each outlet had both rising and falling stages, the fact that some outlets were active predominantly on the rising or falling stage of the flood event as a whole, means that they are likely to be associated with characteristic rising or falling stage flow conditions.

This study examines the extent to which observed large-scale stage variations are reflected in the proglacial landform and sedimentary record. The significance of stage-related geomorphological and sedimentary characteristics of November 1996 proglacial outwash is discussed in relation to previous models of jökulhlaup deposition. Description and discussion of the morphology and sedimentology of November 1996 outwash is subdivided into: (i) rising stage, (ii) falling stage and (iii) combined flow stage deposits.

METHODS

Pre-jökulhlaup, geomorphological mapping and sedimentological studies were undertaken in July, August and October 1996. Post-jökulhlaup field surveys and sedimentological work were carried out during November 1996, May 1997, August 1997, July–August 1998 and July 1999. Aerial photographs taken pre-flood (1992), during the flood (1200 hours, 6 November 1996) and after the flood (July and August 1997) were examined. Observations of jökulhlaup flow conditions were obtained from media footage taken during daylight hours on 5 and 6 November together with airborne video footage taken on 7 November 1996. Oblique aerial photographs taken on 5 and 6 November provided detailed information of flow conditions at various outlets.

THE NOVEMBER 1996 JÖKULHLAUP

A volcanic eruption beneath the Vatnajökull ice-cap began on 30 September 1996 (Guðmundsson *et al.*, 1997). Over the next month meltwater travelled subglacially into the Grímsvötn subglacial caldera lake until it reached a critical level for the drainage of 3.8 km^3 of meltwater into the proglacial zone (Björnsson, 1997). The jökulhlaup began on the most easterly outlet river, the Skeiðará, at 0730 hours on 5 November, and reached a peak discharge of 45 000 $m^3 s^{-1}$ within 14 h, making this the shortest rising limb for any jökulhlaup recorded from the Grímsvötn caldera (Björnsson, 1997; Russell *et al.*, 1999) (Fig. 1). The jökulhlaup also burst from single conduit outlets and crevasses up to 2 km in length (Snorrason *et al.*, 1997; Russell & Knudsen, 1999a,b) (Fig. 1). Although the November 1996 jökulhlaup was the first large flood from Grímsvötn to be observed in detail, similar sized floods have been noted from Skeiðarárjökull at intervals over the last two centuries (Thórarinsson, 1974). Jökulhlaups with multiple outlets are known to have occurred on Skeiðarársandur (Thórarinsson, 1974) and elsewhere (Roberts *et al.*, 2000a,b).

Rising stage efflux

Violent rising stage efflux was observed from the main outlet feeding the Gígjukvísl or Gígja channel from 1047 hours until darkness fell at *c.* 1630 hours on 5 November (Fig. 1). Intermittent video observations until approximately 1630 hours on 5 November show that this conduit expanded rapidly. Large ice blocks up to an estimated 40 m in diameter were observed grounding in front of the outlet on a prominent radial fan. Comparison of pre- and post-jökulhlaup aerial photographs suggest that the glacier margin at the fan apex retreated by up to 200 m. The surface of a well-defined radial fan was observed above the floodwaters on the morning of 6 November (Fig. 2a). However, greater flow depths (*c.* 5 m) were maintained around the flanks of the fan by higher discharge flows exiting the waning stage outlet, which cut diagonally across the axis of the main proglacial trench, thereby providing an effective hydraulic dam (Figs 1 & 3a). Backwater levels fell progressively during 6 November.

Falling stage efflux

Large volumes of water were observed exiting a double-chambered 'embayment' and ice canyon complex, excavated over a distance of nearly 1 km into the glacier surface immediately to the west of the rising stage outlet (Russell & Knudsen, 1999a,b) (Fig. 3a & b). No outlet or fan was seen at this location during daylight hours of 5 November but on the morning of 6 November waning stage flows were observed exiting the ice canyon at a time when all the large ice blocks had already been deposited (Russell & Knudsen, 1999a,b) (Fig. 3a). Flows waned considerably during daylight hours of 6 November.

Multiple stage efflux

Outlets occupied by both rising and falling stage were observed at various locations on the glacier snout; the largest and most active were towards the eastern margin of the glacier, flowing into the Skeiðará, western Skeiðará and Sæluhúsakvísl channels (Fig. 1). Smaller multistage outlets were found at intervals towards the western tributaries of the Gígjukvísl and various channels feeding the Súla. Flows in the western Skeiðará and Sæluhúsakvísl reached their peak early during 5 November and waned noticeably by the onset of darkness (Fig. 4). By contrast, the jökulhlaup only burst from the western margin of the glacier by mid-afternoon of 5 November and was observed to have waned considerably by the morning of 6 November (Snorrason *et al.*, 1997).

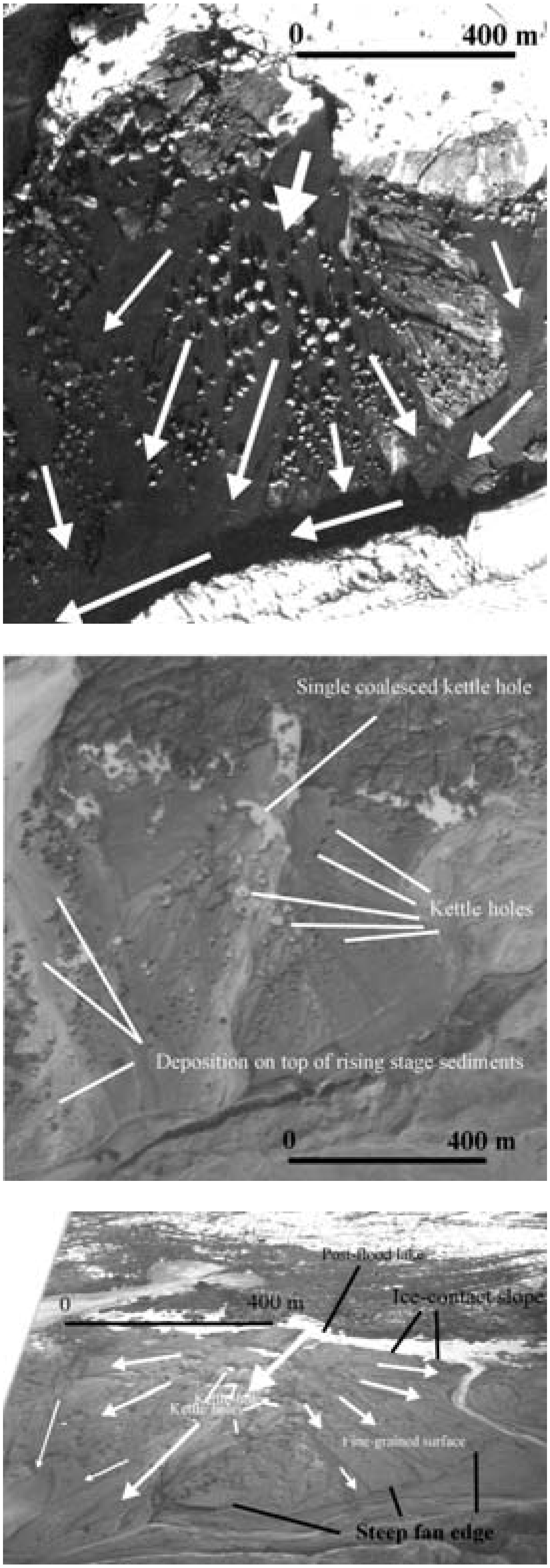

OUTLET TYPES

Rising stage outlet deposits

The rising stage fan axis is orientated in a north–south direction and the fan apex is marked by a 100-m long, 50-m wide lake recessed into the glacier margin (Fig. 2b & c). The depression forming the lake marks the jökulhlaup outlet (Fig. 2b). The fan supports a series of water-filled kettle-scours up to 30 m in diameter with minimum depths of 5 m (Fig. 2b & c). Ice blocks deposited in a line transverse to flow have resulted in a single coalesced kettle hole 130 m wide and 40 m long (Fig. 2b). A central channel runs along the fan axis, away from which the number and size of ice blocks and kettle holes decreases. The eastern and southern margins of the fan are marked by a sharp slope break with an associated drop in elevation of approximately 4 m. The western fan margin consists of a zone where later flows from the waning stage outlet were deposited on top of the fan sediments (Fig. 2b). This zone of waning stage overprinting is also characterized by the deposition of a line of large ice blocks, which appear to have prevented the migration of a series of lobate bar fronts into more tranquil flow conditions over the rising stage fan. Rising stage fan-surface sediment generally is relatively fine grained. The finest sediment is away from the waning stage channel, where the surface is armoured by pebbles and cobbles.

The low-gradient, steep-fronted nature of the rising stage fan indicates that deposition took place in deep water. Topographically controlled backwater conditions were observed on the rising flow stage at this

Fig. 2. Comparison of aerial photographs of the rising stage fan taken (a) during and (b) after the November 1996 jökulhlaup. (a) Relatively tranquil waning stage flows at 1200 hours, 6 November 1996 across the radial-shaped fan surface. Note the rapid decrease in ice-block size with distance from the fan apex and outlet. White arrows show flood flow directions. (b) Post-jökulhlaup fan morphology. Light-grey coloured areas represent coarse-grained, armoured surfaces whereas darker tones represent sand-covered surfaces. Note how the southern and eastern flanks of the rising stage fan have been eroded by flows exiting the glacier to the east. (c) Oblique aerial photograph of the rising stage fan taken during July 1998. White arrows indicate flood flow directions. Note the largest kettle holes are located within the central part of the fan and become smaller with distance from the former tunnel outlet. A series of armoured channels dissect the fan in a radial pattern. The fan has a steep, 3–4 m high front, which in places has been reworked by waning stage flows. Glacier retreat since the 1996 jökulhlaup has resulted in the ponding of a large lake between the ice-contact slope of the fan and the 1998 ice margin.

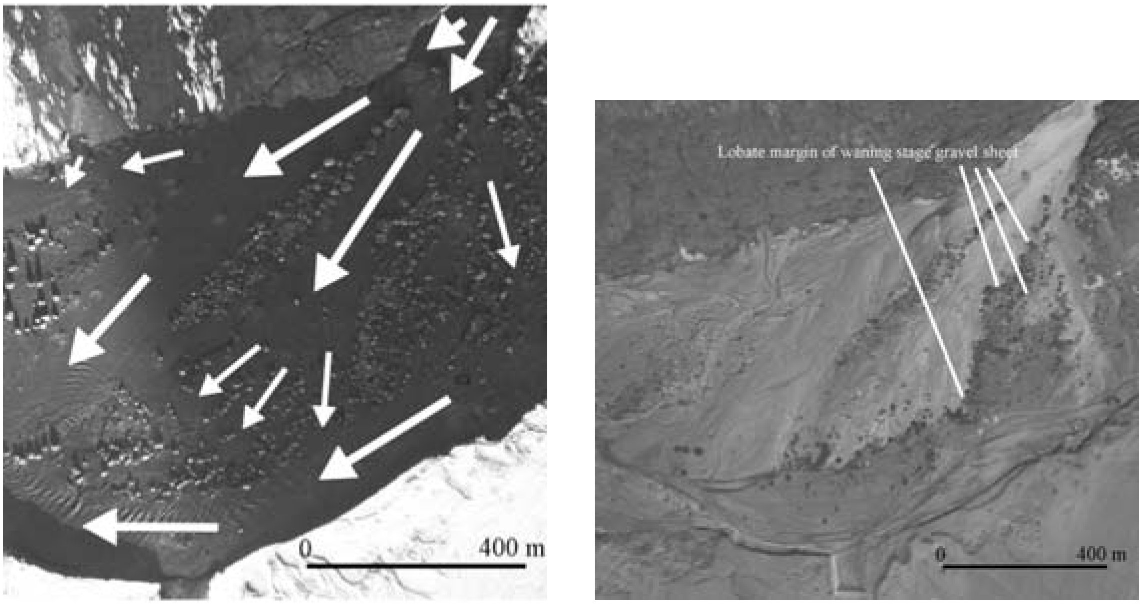

(a) (b)

Fig. 3. Comparison of aerial photographs of the falling stage fan taken (a) during and (b) after the November 1996 jökulhlaup. (a) Waning stage flows exiting the main ice-walled channel (top right). White arrows represent flood flow directions. Flows expand from 150 to 1500 m in width over a downstream distance of less than 2 km. Note large sets of standing waves and the major flow separation and wake effects around stranded ice blocks. Flows are channelled between major shoals of large grounded ice blocks. (b) 1997 post-jökulhlaup morphology of waning stage shows the development of kettle holes and the relatively uniform fan-surface texture. The light grey tone of the fan surface represents a well-armoured surface composed of sediment of gravel to boulder size. Darker-toned areas represent surface sediments of sand size. Section 1 (Fig. 6) is located in the margins of the kettle hole most proximal to the ice-walled channel. Waning stage gravel sheets characterized by lobate fronts can be seen fringing these more sheltered areas.

location during daylight hours of 5 November. The steep southern flanks of the fan are composed of sandy foresets up to 5 m in height dipping away from the fan apex (Russell & Knudsen, 1999a). Individual beds contain climbing ripple sequences deposited as sediment was being transported down the 10° inclined foresets (Russell & Knudsen, 1999a). The presence of backwater effects may explain the simultaneous deposition of both coarse- and fine-grained sediment and the compact fan morphology. Ice blocks on this fan are well embedded and have created a series of well-defined 'kettle-scours' and kettle holes (Fay,

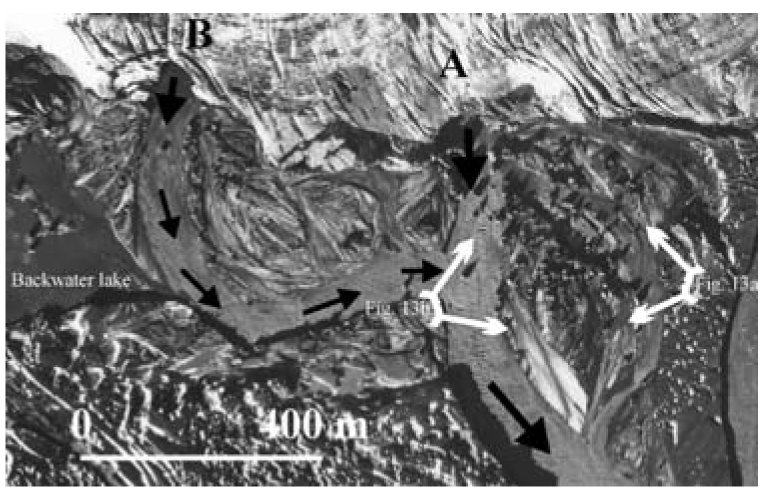

Fig. 4. Aerial photograph taken at 1200 hours on 6 November 1996 shows waning stage flows exiting the western Skeiðará A and B outlets. Black arrows indicate flood flow directions. Note the presence of a backwater lake on the immediate left of the photograph. Standing waves can be seen within the main channels where flows have become confined. White arrows show the locations of the panoramas within Fig. 13 (a & b).

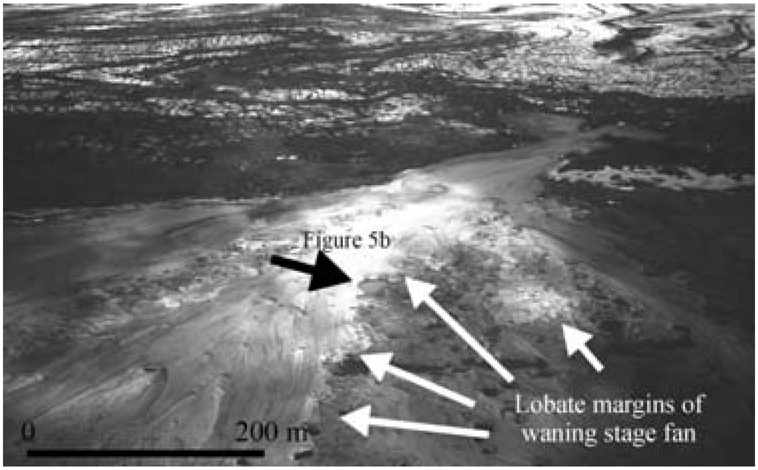

(a)


(b)

Fig. 5. (a) Oblique aerial photograph of the waning stage fan taken in July 1997 shows zones of intensive kettle topography cut by lower elevation waning stage channels displaying numerous ice-block obstacle marks. (b) View of the largest ice blocks deposited on the Gígja fan in April 1997. Note bus for scale. Melting of the largest block in this photograph resulted in the creation of the kettle hole section 3 (Fig. 7).

2002, this volume, pp. 85–97). Although rising stage, topographically controlled backwater conditions were removed later in the flood as a result of channel widening, subsequent outflows from the ice canyon and double embayment acted as a hydraulic dam, thereby maintaining high flow depths covering most of the rising stage fan until the morning of 6 November (Fig. 2a).

Falling stage outlet deposits

The waning stage fan has an elongate appearance radiating out through only 90° and grading fully into the river channel 3 km downstream (Fig. 3a & b). The embayment and fan exit the glacier at an oblique angle to the main proglacial trench, in contrast to other fans (Figs 1 & 3a & b). The fan has a coarse-grained, well-armoured surface, especially in the main channels between the lines of large blocks and subsequent kettle holes (Fig. 5a). The largest accumulation of ice blocks is over 1 km in length and extends up to 300 m in width at its widest (Figs 3a & 5a). The largest blocks are found upstream with a progressive down-cluster reduction in ice-block size (Figs 3a & 5b). Bed elevation in and around the ice block clusters is up to 5 m higher than in the adjacent channels.

Large kettle-scours provide excellent sections; however, the sedimentary structures within most of these sections are strongly controlled by localized flow around these large obstacles (Fay, 2002, this volume). Kettle-hole sections therefore do not provide a representative picture of overall fan sedimentology. Sections used in this study include those from an ice-proximal kettle hole, free from wake effects of upstream ice-block obstacles (section 1; Fig. 6) and a section on the side of a large kettle hole that protruded into a channel area free from large ice blocks (section 3; Fig. 7).

Fig. 6. Section 1 consists of a 4-m-thick coarsening upward succession exposed in the wall of a large kettle hole in the proximal area of the waning stage fan. Finer grained gravel matrix constitutes a continuous aggradation unit. Arrow indicates former flow direction. There is a marked increase in clast clustering and imbrication towards the top of the section. Note ski pole for scale.

Section 1 shows a distinctive coarsening upward succession illustrating a transition from indistinctly horizontally bedded matrix-supported gravels (Gmm/Gh) to gravel and boulder dominated beds containing imbricated (Gm/Bm) and occasionally massive (Gms/Bms) lithofacies (Fig. 6). This face is parallel to the depositional flow direction with former flows from right to left (Fig. 6). Lower units (Gh) are dominated by fine-gravel-sized sediment forming a non-cohesive matrix supporting the largest clasts (Fig. 6). Overlying coarse-grained units show signs of crude horizontal bedding, where the clasts are arranged in clusters occasionally displaying signs of imbrication (Gm/Bm) (Fig. 6). Occasional layers of fine-grained matrix (Gmm/Bmm) occur intermittently and with less frequency towards the top of the succession accompanied by a marked increase in clast concentrations (Fig. 6).

Section 2 is orientated at right angles to the former flow direction and section 1, with former flows out of the face. The overall succession is similar to that described for section 1 with a marked increase in mean clast size and concentration toward the surface, accompanied by a reduction in the frequency of fine-gravel matrix support. Interestingly, a series of shallow trough-shaped erosional structures, up to 20 cm deep, can be seen throughout the succession. Trough bases are commonly floored by single layers of coarser clasts, which become more continuous through the succession. Section 2 shows that coarser layers of clustered sediment also vary from being laterally discontinuous near the base of the section to more continuous near the section surface.

Section 3 is 8 m high in the flank of a large kettle hole on the waning stage outwash fan. The section contains some of the largest boulders observed in any of the November 1996 jökulhlaup deposits (Fig. 7). The base of the section directly underneath the figure contains a large block of glacier ice overlain by an occasionally imbricated boulder unit (Bmm/Bm) (Fig. 7). This unit also contains a series of boulder-sized diamicton intraclasts (Fig. 7). The largest clasts are, in places, contained within a structureless gravel matrix, where their *a*-axes are commonly orientated parallel to palaeoflow and dipping at high angles (Fig. 7). There are more contacts between the largest imbricated clasts towards the top of the section (Fig. 7).

Both sections 1 and 2 reveal upward-coarsening successions characterized by decreasing matrix content and increasing clast content. Progressive armouring associated with increased bed scour and reworking on the waning stage resulted in the deposition of

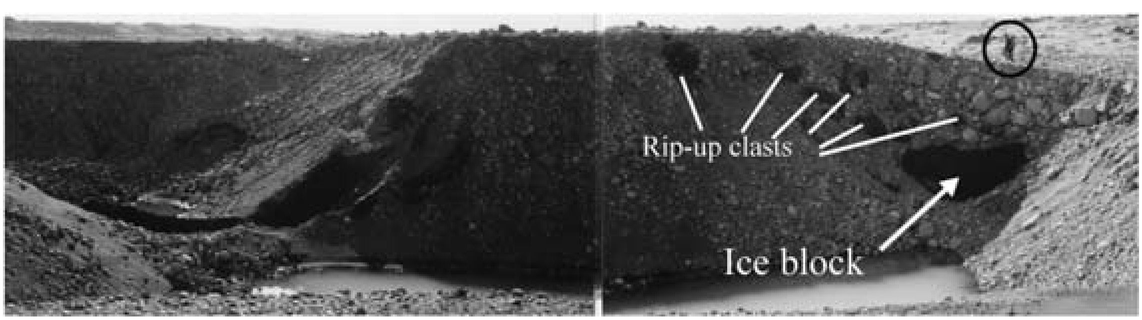

Fig. 7. Panorama of large kettle holes resulting from the meltout of fluvially transported ice blocks on the waning stage fan. Section 3 is seen on the extreme right of the photograph below the 1.8-m-high figure. Flow directions were from right to left. Figures 3b & 5b show the location of this kettle-hole complex in relation to the rising and falling stage fans.

progressively coarser sediment in comparison with the finer grained sediment deposited under high aggradation rates. The presence of increased numbers of shallow troughs floored by larger clasts, which form lags or proto-armoured layers, suggest progressively more episodes of scouring through the succession. These observations are consistent with experimental results reported by Dietrich *et al*. (1989), who suggest that reduced rates of bedload supply in relation to transport capacity promote surface coarsening. Rubin *et al*. (1998) also explain progressive river bed coarsening during a flood with mixed grain-sizes as the product of washing of fines from the bed, leaving progressively coarser bed sediment. Reduction in sediment supply commonly occurs during the waning flow stage owing to sediment supply exhaustion (Østrem, 1975; Gurnell, 1987; Lawson, 1993). The massive matrix-supported nature of the beds is, however, consistent with rapid deposition from a sediment-rich flow. Alternatively, waning stage reworking of coarse-grained sediment within the ice embayment and ice-walled channel system may have released coarse sediment for deposition on the waning stage fan. Russell & Knudsen (1999a) interpreted polymodal matrix-supported sediment as hyperconcentrated flow deposits that, when subsequently reworked, generated individual, locally dense bedload sheets that were emplaced by frictional freezing. Waning stage deposition resulted in thin, occasionally massive units representing rapid deposition by frictional freezing from high-density grain dispersions (Russell & Knudsen, 1999a). Russell & Knudsen (1999b) suggested that material of up to boulder size was transported in suspension within the main Gígja outlet ice-walled channel.

Crude bedding in boulder deposits of section 3 dip in an upstream direction towards the tail of the kettle-scour-forming ice block (Fig. 7). Such stoss-side bedding occasionally is preserved in ephemeral fluvial systems where rapid flow stage reduction prevents wash out (Alexander & Fielding, 1997). Fay (2002, this volume) presents a model indicating that flows around large ice-block obstacles are locally supercritical and result in the presence of standing waves on the flanks of the ice block, under which there is an 'inphase' bedform. This indicates an overall fluidal depositional setting. However, the matrixsupported nature of the boulder deposit, combined with only the presence of high-angle *a*-axis parallel imbrication, suggests rapid deposition from a hyperconcentrated flow. Although intraclasts may have been frozen (Russell & Marren, 1999), intraclasts composed of cohesive sediments are commonly found within non-glacial environments (Karcz, 1972). Many of the Skeiðarársandur intraclasts show evidence of internal deformation and overconsolidation compatible with a subglacial origin. These overconsolidated intraclasts therefore may not need to be frozen in order to be transported for distances of nearly 2 km from the glacier. Indeed many intraclasts are thought to have travelled for considerable distances as suspended load (Russell & Knudsen, 1999b).

Although the waning stage fan was initiated during the late rising stage, aggradation on the lower fan continued through the waning stage as more proximal deposits were reworked. A prolonged waning flow stage promoted widespread armouring and coarsening of the fan surface. Reduction in sediment concentration on the waning flow stage was interrupted by short-lived, hyperconcentrated sediment pulses generated by sudden, localized incision associated with scour around ice blocks.

Multiple stage deposits

Western Gígja

A panoramic photograph taken within a week of the jökulhlaup shows incised fans in the western tributaries of the Gígja, with partially to totally exhumed ice blocks visible along the flanks of the erosional terraces (Fig. 8). During this period there was an absence of steep-sided kettle holes indicative of ice-block meltout. Fans radiate from the supraglacial area immediately behind the ice margin and coalesce with neighbouring fans.

Section 4 shows a 1.5-m-high face in a terrace cut during the jökulhlaup (see Fig. 8 for location). Former flows were from left to right and slightly out of the face (Fig. 9). This section shows a trough structure, above and behind which there is a buried ice block, which can just be seen within the section and on the ground surface behind the section (Fig. 9). The trough is defined by both bedding dipping downwards, and an infill unit that thickens around the block (Fig. 9). Up-flow of the block there is crude bedding of various poorly sorted matrix-supported units (Gmm), some with occasional signs of imbrication (Gmm(i)) (Fig. 9 & Table 1). Imbricate matrix-supported clusters are found within the trough-fill surrounding the ice block. A fining upward set of trough cross-stratified sands and gravels cap the matrix-supported units in the lee of the ice block (Fig. 9).

Section 5 is excavated on the lee of a 6-m-diameter, partially exhumed ice block on the edge of a channel

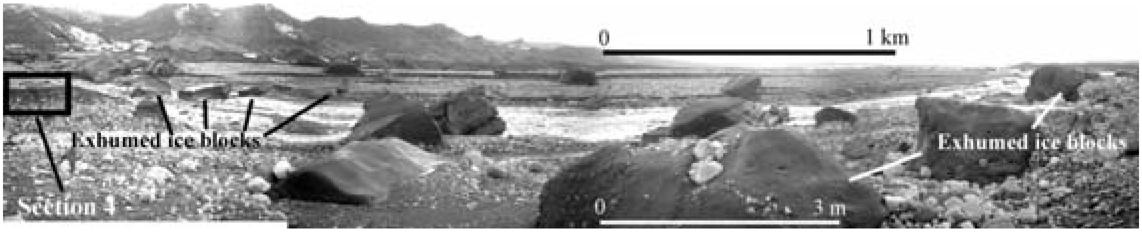

Fig. 8. Panorama showing one of the western Gígja outlets one week after the November 1996 jökulhlaup. Note the stepped morphology consistent with progressive jökulhlaup-fan incision. Within-jökulhlaup incision provided a number of good sedimentary sections (Figs 9 & 10). Reworking of deposits laid down earlier during the jökulhlaup has also re-exposed a number of large ice blocks, which can be seen partially exposed across the sandur surface. Areas of the fan that were reworked have an armoured surface consisting of clusters of clasts up to boulder size.

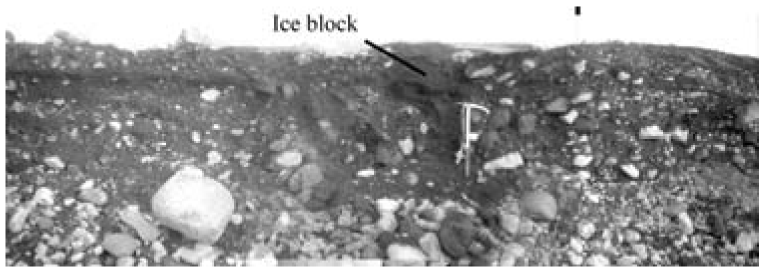

Fig. 9. Section 4 comprises a 1.5-m-high section exposed by waning stage incision on the western Gígja fan. Sedimentary structures were strongly influenced by an almost completely buried ice block. Flow directions were slightly oblique to the face from left to right. This section is dominated by matrix-supported pebble to boulder gravel showing occasional *a*-axis imbrication.

Table 1. Lithofacies codes used in this study for the classification and interpretation of jökulhlaup deposits (after Brennand, 1994; Russell & Marren, 1998, 1999).

Lithofacies code	Description	Interpretation
Bm/Gm (uc)	Poorly sorted, heterogeneous, clast-supported imbricated gravels and boulders: (uc) = upward coarsening	Grain-by-grain deposition from traction load in a turbulent, high-energy flow
Bmm/Gmm (uc)	Massive, poorly sorted, matrix-supported boulders and rip-up clasts: (uc) = upward coarsening; (i) = imbricated	Hyperconcentrated flow deposit
Gms	Massive clast-supported gravel	Non-Newtonian grain dispersion deposits
Gh	Poorly sorted, heterogeneous, horizontally bedded gravel: (uf) = upwards fining; (uc) = upwards coarsening	Deposition from fluidal flows. Transport in turbulent suspension prior to late-stage traction transport (Russell & Knudsen, 1999b)
Gt	Trough cross-stratified gravel	Large-scale gravel bedform migration or channel fills
Gp	Planar cross-stratified gravel	Bar or delta-front advance. Migration of straight-crested gravel bedform

cut by the jökulhlaup. Boulders and ice blocks form a lag in front of the section. An upward-coarsening, massive matrix-supported unit (Gmm/Bmm) is capped by finer grained, crudely stratified, upstream dipping, matrix-supported gravel beds (Gh), forming an inverse to normally graded unit. Non-imbricated coarse clast concentrations increase towards the surface of the massive inverse-graded unit giving the impression of clast-support.

Section 6 comprises a 2-m-high, crudely bedded, upward-coarsening succession exposed in a flow-parallel direction, with former flows from right to left on Fig. 10. Massive and upward-coarsening matrix-supported units are capped by thin (< 20 cm), well-sorted, openwork gravel units (Gms) (Fig. 10). The upper 0.5 m of the section comprises an upward-coarsening unit containing a non-cohesive sand and fine gravel matrix (Gmm(uc)) (Fig. 10). Within the

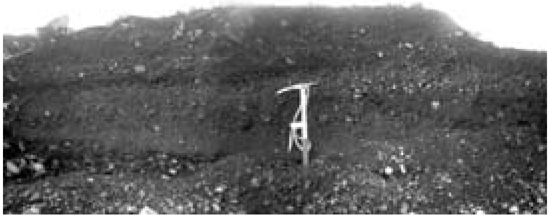

Fig. 10. This 2-m-high section (6a) on the western Gígja fan shows an overall coarsening upward trend. Evidence of repeated flow pulses is provided by the stacking of smaller matrix-rich and clast-rich units. Flow direction was from right to left.

matrix-supported units, some of the larger clasts are arranged with *a*-axis vertical (Fig. 10).

The morphology and sedimentology of exposures within the western Gígja outlets provide a consistent picture of jökulhlaup flow and depositional conditions at this location. Successions in sections 5, 6a and b are characterized by their upward-coarsening trends and by a progressive increase in the thickness of matrix-supported units, suggestive of both the supply of increasingly coarse sediment and a progressive increase in sediment concentrations within the flow. Occasionally imbricated (*a*-axis-parallel) matrix-supported units are indicative of rapid deposition from successive hyperconcentrated bedload 'sheets' (Todd, 1989; Sohn, 1997). Rapidity of deposition is indicated by the complete burial of small (< 2 m) ice blocks resulting in the subsequent development of steep-sided kettle holes. Incorporation of such small ice blocks within a highly concentrated bedload sheet may have resulted in simultaneous deposition of both ice blocks and sediment (Russell & Knudsen, 1999a). Exposed portions of the succession were deposited around much larger ice blocks, 10 m in diameter, which are buried to varying depths. Observations of media video footage from various outlets confirm that the largest ice blocks were deposited during the rising flow stage as conduit mouths enlarged by tunnel collapse. Trough structures developed in section 4 around a partially buried ice block confirm that the largest blocks acted as obstacles to the flow, generating secondary flow cells sufficiently strong to disrupt local flow and depositional patterns (Russell, 1993; Fay, 2002, this volume). Repeated upward-coarsening successions of alternating openwork and matrix-supported facies in section 6 record the passage of rising stage hyperconcentrated sediment pulses. Flows from these outlets had waned considerably by 1200 hours on 6 November, when they were confined to the main channels and many large exhumed ice blocks could be seen above the floodwaters. Fan incision and channel formation therefore took place earlier during either the late rising or falling flow stage.

Sæluhúsakvísl and western Skeiðará A and B

Observations at the eastern Sæluhúsakvísl outlet show a radial outwash fan with a relatively smooth upper surface, dissected by a main channel floored, in places, by an extensive vegetated surface and at other locations floored by very poorly sorted sediment arranged as a series of hummocks (Fig. 11). Occasional large boulders

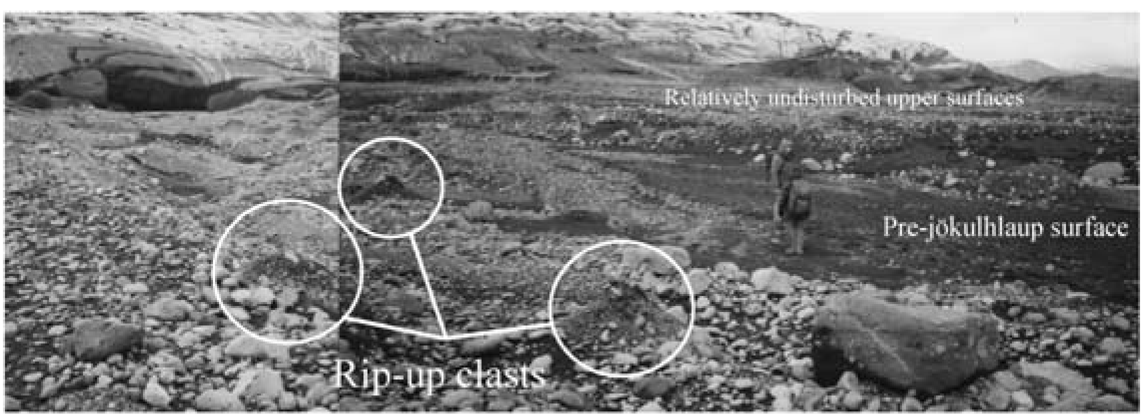

Fig. 11. Panorama of the central Sæluhúsakvísl outwash fan, taken during May 1997. Note the relatively undisturbed upper fan surfaces dissected by a main channel leading from the prominent subglacial conduit (left). Vegetation exposed on the channel floor underlies the jökulhlaup fan and is interpreted as a pre-flood surface exhumed by waning flood stage erosion. The poorly sorted surface within the channel is in contrast with the better sorted, undisturbed upper surfaces (top right and bottom left). We suggest that numerous rip-up clasts and outsized boulders represent waning stage lag deposits.

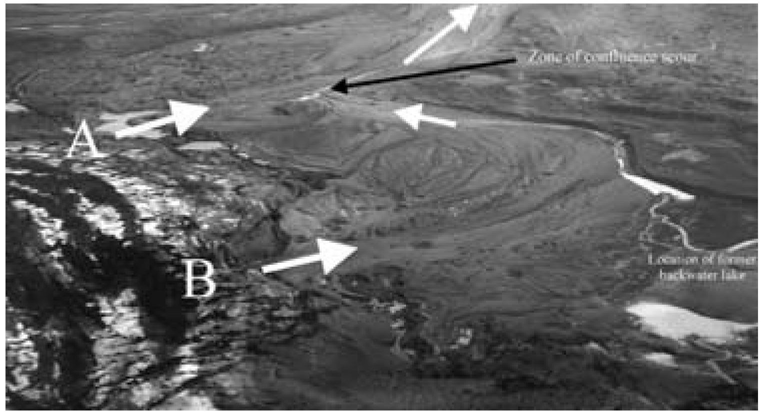

Fig. 12. Oblique aerial photograph of the western Skeiðará outlets taken in July 1998. Compare with Fig. 4, which was taken on 6 November 1996, on the waning flow stage. White arrows represent main flood flow directions. Note how the fan in front of outlet B has a radial morphology and terminates in a series of delta lobes on its western margin, where deposition was into a backwater lake. Flows exiting outlet B joined those from the larger outlet A at right angles, creating a distinctive confluence scour channel.

are seen on the deposit surface. The largest surface grain sizes within the channel consist of rip-up clasts composed of stratified fluvial sediment and a variety of diamictons of probable glacial origin (Fig. 11).

The western Skeiðará was fed by two main outlets during the November 1996 jökulhlaup (Fig. 4). Conduit outlet A drained directly into the large pre-existing western Skeiðará proglacial channel. Flows from this location therefore were relatively unimpeded by topography. By contrast, flows exited conduit B into a lake constrained by high-elevation former outwash surfaces. Flows from conduit B were initially radial, gradually swinging to the east to become confluent with flows exiting conduit A (Figs 4 & 12). These confluences are at right angles, with flow from conduit B entering the junction at a higher level, forming a bar front truncated by waning stage flows from conduit A (Figs 4 & 12).

Jökulhlaup fan A consists of a high-level outer surface containing numerous deeply embedded large ice blocks (Fig. 13a). The western flank of fan A coincides with the confluence zone with flows from conduit B and consists of a low-elevation channel (Figs 4 & 13b). This channel has relatively gentle slopes composed of localized terraces preserved in the lee of large numbers of large ice blocks (Fig. 13b). In May 1997 ice blocks were found resting only on the floor of the channel, and were not embedded to any degree into the channel bed. Channel-bed sediments consisted of a lag of poorly sorted deposits up to boulder size. The largest clasts, up to 5 m in diameter, consisted of rip-ups composed of stratified fluvial sediment and glacial diamicton.

Jökulhlaup efflux from conduit B resulted in the partial infill of a pre-jökulhlaup lake (Fig. 12). Fan B radiates from either side of conduit B, although fan deposits on the eastern flank are much more extensive (Fig. 12). Fan deposits on the western flank of the outlet terminate in a spectacular 4–5 m high delta front, beyond which a 1–2 m thickness of planar and ripple-drift cross-laminated silts and sands are found blanketing the floor of a small lake basin. Flows in this lake persisted well into the waning flow stage as seen from aerial photographs taken at noon on 6 November 1996 (Fig. 4). The main flood channel exiting conduit B is considerably lower than adjacent fan flanks.

The Sæluhúsakvísl and western Skeiðará A outlet fans have similar morphological characteristics consisting of: **1** well-developed upper fan surfaces consisting of well-sorted surface sediment and deeply embedded ice blocks; **2** channels with irregular step-like margins consisting of poorly sorted boulder beds, numerous rip-up clasts, fewer wholly buried ice blocks and fewer kettle-scours. The upper, well-developed fan surfaces are interpreted to preserve rising and high stage deposits. Upper fan sediments at western Skeiðará A contain large numbers of deeply embedded icebergs surrounded by well-sorted coarse gravel and cobble-sized sediment, again suggesting rising and high stage sedimentation. Some of the largest ice blocks have grounded on a pre-jökulhlaup ridge around which thicker rising stage jökulhlaup sediment was deposited and partially buried. Large channels incised into both the western Skeiðará A and Sæluhúsakvísl fans were observed to be occupied by waning stage flows that are thought to have resulted in widespread erosion of rising stage sediments and ice blocks, leaving only large isolated ice blocks and diamict clasts on top of a boulder lag deposit. Extensive pre-jökulhlaup vegetated surfaces on the floor of the Sæluhúsakvísl channel indicate waning stage incision to the pre-jökulhlaup land surface. As such, it is possible that the jökulhlaup also may have incised into pre-jökulhlaup sediment at

Fig. 13. Panoramas of western Skeiðará fan A illustrating contrasts in fan morphology between rising/high stage deposits and waning stage erosional channels. (a) View from east to west across western Skeiðará fan A showing large deeply embedded ice blocks on a well-preserved outwash surface. Flows were from right to left. The ice blocks were buried by rising stage sedimentation fanning out from the main outlet. On the falling flow stage, this area was relatively undisturbed as waning stage flows were concentrated in the western channel (Fig. 13b). (b) Western Skeiðará main outlet waning stage channel (note jeep for scale). Flows were from left to right. View towards the east is uphill towards rising stage deposits (Fig. 13a). Note isolated and well-exposed nature of ice blocks reflecting waning stage scour and exhumation. Presence of cobble lags, megaclusters and exhumed rip-up clasts all point to waning stage sediment erosion.

other locations. The poorly defined, down-fan sloping, terraces on the western Skeiðará fan are interpreted as erosional shadows of sediment preserved in the lee of the largest exhumed ice blocks along the waning stage channel flanks. The western Skeiðará B fan is graded to a local backwater lake resulting in delta-front formation. Grounded ice blocks on western Skeiðará fan B were observed to have already grounded by 1600 hours on 5 November, indicating relatively little waning stage incision. Waning stage incision was inhibited by the persistence of high, backwater-controlled local water levels.

DISCUSSION

Fan morphology

On Skeiðarársandur, outwash fan morphology is highly varied, depending upon jökulhlaup outlet morphology and pre-jökulhlaup proglacial topography. Rising-stage-dominated fan morphology is controlled by the presence of topographically controlled backwater lakes. The flat-topped, steep-sided fan bears similarities to jökulhlaup deltas graded to temporarily raised lake levels (Shakesby, 1985; Russell, 1993, 1994; Russell & Marren, 1999). Jökulhlaup flows within the Gígjukvísl river were confined by a major proglacial trench developed between the active ice-margin and older, high-level outwash surfaces (Russell & Knudsen, 1999a). Channel constrictions on the rising stage allowed backwater conditions to prevail throughout much of the proglacial trench. Erosion of channel constrictions resulted in progressive lowering of backwater levels during the jökulhlaup. Backwater effects could act as a major control on jökulhlaup sedimentation where the active glacier margin was flanked by older, high elevation ice-contact deposits (Russell & Knudsen, 1999a). However, the potential of backwater controls to dominate processes and patterns of sedimentation were greatly reduced as the flood progressed. Reduction in local base levels and increases in flow energy associated with the removal of backwater effects are expected to result in fan reworking and incision.

The Gígjukvísl rising stage fan was well preserved owing to major efflux from the double-chambered embayment that maintained the backwater conditions through the waning stage. Western Skeiðará fan B also was deposited in a topographically controlled backwater zone, partially infilling a pre-jökulhlaup lake. The falling-stage-dominated fan has a uniform surface gradient and grades directly into the main Gígjukvísl jökulhlaup channel. Fan morphology is dominated by two major channels flanked by large shoals of deeply embedded ice blocks. Fan reworking was limited to widespread surficial scouring and winnowing of sediment rather than major localized fan incision. As such, the overall surface morphology of

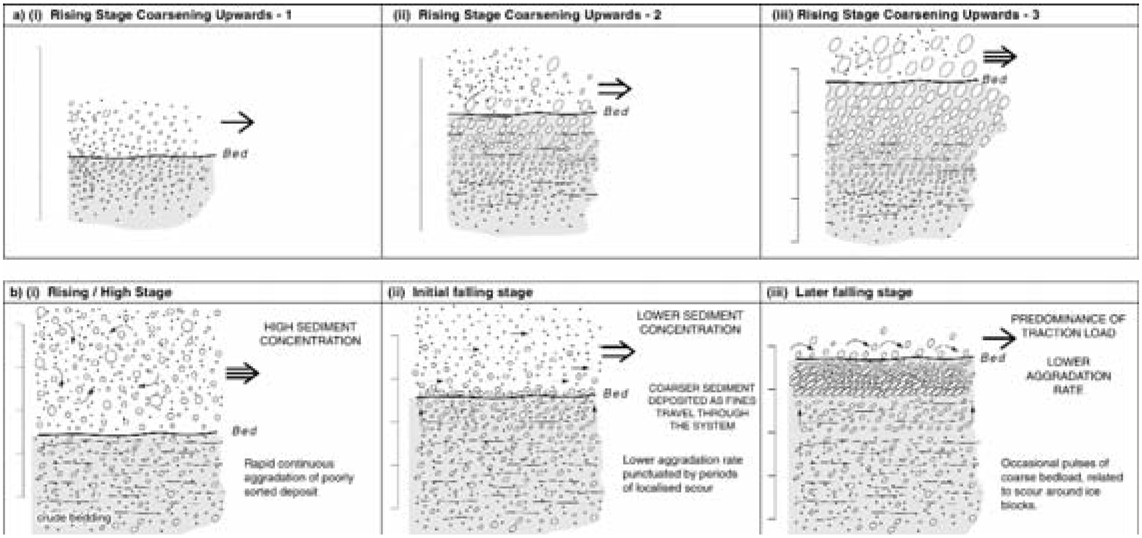

Fig. 14. Schematic diagrams showing the development of an upward-coarsening succession on the rising flow stage related to a competence-related increase in grain size (a) and on the falling flow stage related to a progressive decrease in coarse sediment supply during waning stage flows (b).

this fan is well preserved. Lack of major incision of the waning stage fan is a result of high sediment fluxes being maintained through the waning flow stage (Russell & Knudsen, 1999b; Fay, 2002, this volume). Multiple stage deposits at the Western Gígja, Sæluhúsakvísl and Skeiðará are all characterized by rising stage aggradation and major waning stage incision, creating a distinctive heavily dissected fan morphology. Although ice-contact jökulhlaup deposit morphology is clearly strongly influenced by stage-related variables such as backwater conditions and sediment flux, the unusual migration of the main Gígjukvísl conduit allowed spatial segregation of rising and waning stage flows.

Fan sedimentology

Rising stage deposits characteristically contain finer, more poorly sorted sediment than found in falling stage successions and on erosional surfaces. Backwater-controlled sedimentation results in delta-like foresets containing large amounts of sediment ranging from sand to gravel in size. Rising stage deposits in the western Gígjukvísl show upward-coarsening successions, characteristic of progressive supply of coarser grained sediment with stage increase. This is compatible with models of rising stage sedimentation proposed by Maizels (1989a,b, 1991, 1993, 1995, 1997) and Maizels & Russell (1992). The western Gígjukvísl rising stage successions, however, show few signs of large-scale grading, and instead contain repeated cycles of sedimentation recording individual sedimentation pulses representing either the passage of near-bed sediment pulses (Todd, 1989; Sohn, 1997) or repeated surges of the entire flow (Hodgson & Manville, 1999) (Fig. 14a). Coarsening upward successions on the Gígja waning stage fan were generated by sediment reworking and winnowing rather than increasing flood power and sediment transport capacity, compatible with rising stage flow (Fig. 14b). Waning stage, upward-coarsening successions are not represented in existing models of jökulhlaup sedimentation. Indeed upward-coarsening successions within models presented by Maizels (1989a,b, 1991, 1993, 1997), Russell & Knudsen (1999a) and Russell & Marren (1999) all represent deposition from rising stage flows (Fig. 14a & b). It is now clear, however, that the presence of an upward-coarsening succession alone is not diagnostic of rising flow stage deposition.

Ice blocks and flow stage

Ice-block release from heavily fractured portions of the glacier margin was concentrated mainly on rising and peak flow stages, burial of which subsequently led to the formation of kettle holes. Both rising and falling stage aggradation around large ice blocks results in the formation of 'kettle-scours' or kettle holes that display obstacle mark characteristics (Fay, 2002, this volume). Waning stage reworking of multiple stage, ice-contact deposits resulted in the exhumation of wholly and partially buried ice blocks.

CONCLUSIONS AND WIDER IMPLICATIONS

The morphological and sedimentological record of a single jökulhlaup is highly varied owing to the presence of numerous outlets of varying size active during discrete periods of the jökulhlaup. The main morphological and sedimentological characteristics of ice-contact jökulhlaup fans associated with different flow stages are illustrated by the model in Fig. 15. Conduits occupied by flows on both rising and falling flow stages are characterized by initial rising stage fan deposition, followed by falling stage dissection and exhumation of ice blocks and diamict clasts (Fig. 15c & d). Backwater-controlled and non-backwater-controlled outlets subject to prolonged falling stage flows will be heavily dissected as sediment fluxes decline (Fig. 15c & d). Such erosion removes the finest grain sizes but leaves large rip-up clasts, boulders and ice blocks. Rip-up clasts are thought to be a good indicator of subglacial jökulhlaup erosion (Russell & Knudsen, 1999a).

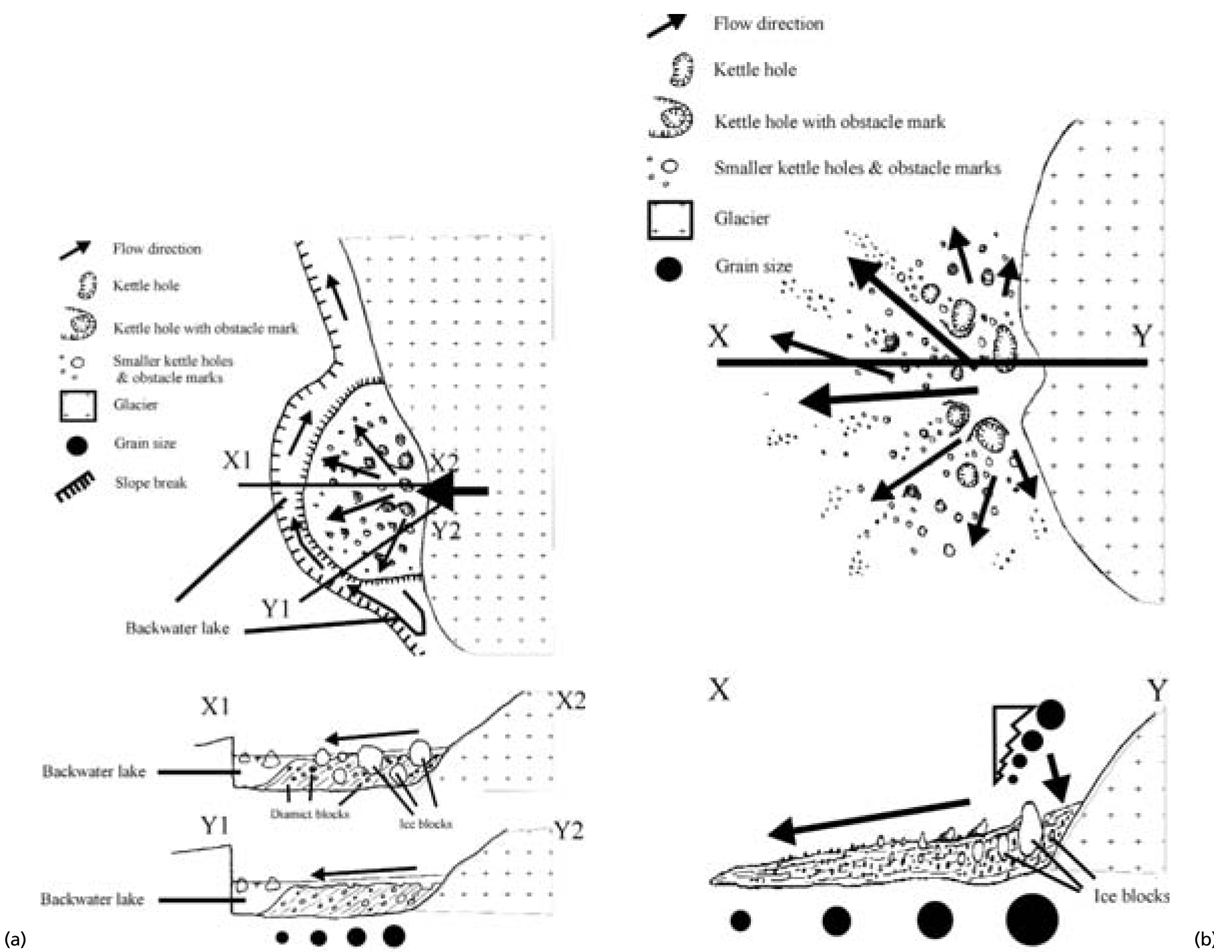

Fig. 15. Diagrams illustrating some of the main morphological and sedimentological characteristics of ice-contact jökulhlaup fans associated with different flow stages. (a) Rising stage deposition into a topographically controlled backwater lake. (b) Unconfined drainage during the jökulhlaup rising stage results in the creation of an outwash fan built by the aggradation of individual sheet-like layers. (*cont'd*)

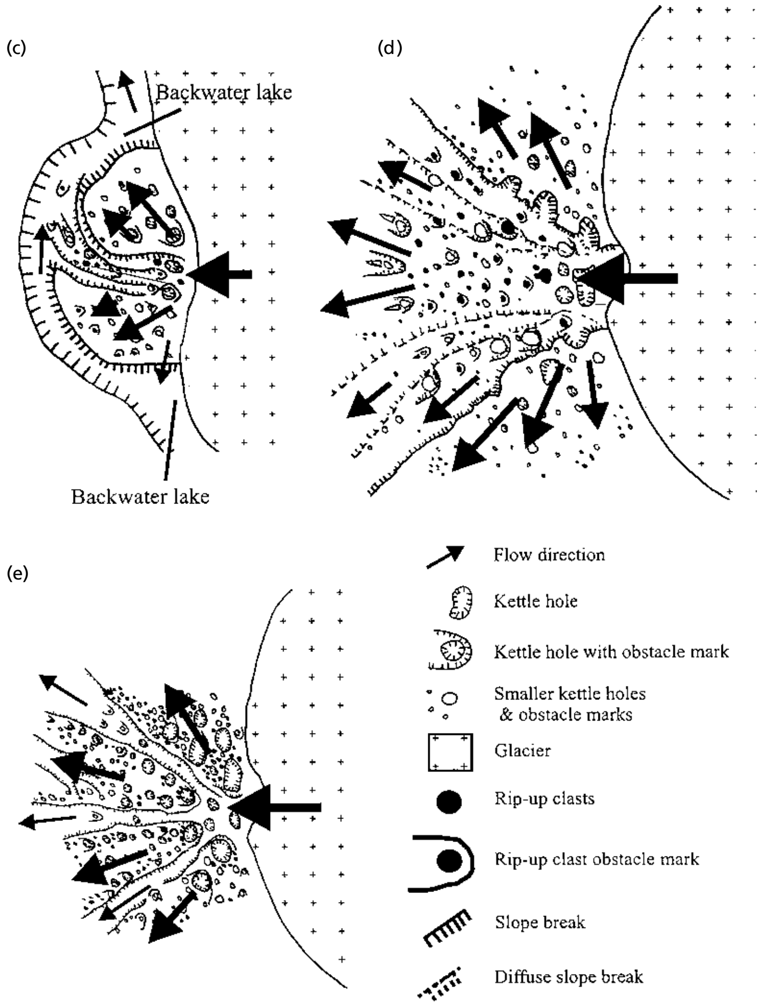

Fig. 15. (*cont'd*) (c) Heavily dissected backwater-controlled and (d) non-backwater-controlled outwash as a result of declining sediment flux on the prolonged falling flow stage. (e) Fans subject to high sediment flux on both rising and falling flow stage can aggrade until the end of the jökulhlaup, when surface armouring and shallow channelization occur.

Rising stage deposition into topographically controlled backwater lakes results in the formation of relatively flat-topped, delta-like, radial outwash fans that show a rapid down-fan decrease in ice-block size (Fig. 15a). Ice blocks completely buried by rising stage flows result in circular kettle holes, which are completely independent of surface topography. Some of the largest ice blocks are only partially buried and give rise to 'kettle-scours' (Fay, 2002, this volume). Rising stage deposits contained both single upward-coarsening successions as well as successions consisting of stacked upward-coarsening and normally graded units (Fig. 15b).

Where waning stage flows are routed through a single conduit, high sediment efflux and aggradation rates are maintained late into the waning stage (Fig. 15e). Rising and falling stage sedimentary successions will be preserved on outwash fans subject to prolonged high sediment fluxes (Fig. 15e). Such fans also will have a much more uniform surface morphology than found on the other fan types. Absence of backwater conditions during jökulhlaup falling stage results in the creation of fans of uniform gradient, built up by the aggradation of individual sheet-like layers. Winnowing and sediment starvation result in progressive bed coarsening from matrix-supported gravels to clast-rich armour (Fig. 15b & e). Careful examination of the abundance of the sand and fine-gravel matrix through the upward-coarsening succession will allow waning stage bed coarsening by winnowing to be distinguished from rising stage coarsening by sediment transport capacity increases.

This study illustrates the significance of major within-jökulhlaup sediment reworking and ice-margin erosion over distances of 10^2–10^3 m. Ill-defined erosional, streamlined terraces reflect exhumation on the flood waning stage (Fig. 15c & e). This landform and sedimentary succession possibly could be confused with the product of fluvial depositional and erosional cycles operating over longer time-scales associated with more sedate rates of glacier retreat within former proglacial areas.

ACKNOWLEDGEMENTS

Research visits immediately before and after the jökulhlaup were funded by a UK NERC grant (GR3/10960) awarded to A.J.R. in October 1996. Fieldwork during 1997 was funded by grants awarded to Ó.K. by the Icelandic Public Roads Administration and the Icelandic Research Council. Fieldwork during 1998 was funded by the Earthwatch Institute (A.J.R.), the Icelandic Public Roads Administration (Ó.K.) and the Icelandic Research Council (Ó.K.). Magnús Tumi Guðmundsson provided us with photographs of the jökulhlaup. We thank all of the 1998 and 1999 Earthwatch volunteers, Helen Fay and Iain Taylor for field assistance and logistic support. Helen Fay and Philip M. Marren, together with reviewers Victor Baker and John Costa, are thanked for their constructive reviews of this manuscript. I. Peter Martini and Guy Plint are thanked for their editorial improvement of this paper. Within Keele University School of Earth Sciences and Geography, Richard Burgess is thanked for photographic reproduction. Peter Greatbach and David Wilde are thanked for their cartography.

REFERENCES

Alexander, J. & Fielding, C. (1997) Gravel antidunes in the tropical Burdekin River, Queensland, Australia. *Sedimentology* **44**, 327–337.

Björnsson, H. (1997) Grímsvatnahlaup Fyrr og Nú. In: *Vatnajökull: Gos og Hlaup 1996* (Ed. Haraldson, H.), pp. 61–77. Vegagerðin, Reykjavik.

Brennand, T.A. (1994) Macroforms, large bedforms and rhythmic sedimentary sequences in subglacial eskers, south-central Ontario: implications for esker genesis and meltwater regime. *Sediment. Geol.* **91**, 9–55.

Carling, P.A. (1987) Hydrodynamic interpretation of a boulder berm and associated debris-torrent deposits. *Geomorphology* **1**, 53–67.

Cronin, S.J., Neall, V.E., Lecointre, J.A. & Palmer, A.S. (1999) Dynamic interactions between lahars and stream flow: a case study from Ruapehu volcano, New Zealand. *Geol. Soc. Am. Bull.* **111**, 28–38.

Dietrich, W.E., Kirchner, J.W., Ikeda, H. & Iseya, F. (1989) Sediment supply and the development of the coarse surface layer in gravel-bedded rivers. *Nature* **340**, 215–217.

Fay, H. (2002) Formation of ice-block obstacle marks during the November glacier outburst flood (jökulhlaup), Skeiðarársandur, southern Iceland. In: *Flood and Megaflood Processes and Deposits: Recent and Ancient Examples* (Eds Martini, I.P., Baker, V.R. & Garzón, G.), Spec. Publs int. Ass. Sediment., No. 32, pp. 85–97. Blackwell Science, Oxford.

Fraser, G.S. & Bleuer, N.K. (1988) Sedimentological consequences of two floods of extreme magnitude in the Late Wisconsinan Wabash valley. *Geol. Soc. Am. Spec. Pap.* **229**, 111–125.

Guðmundsson, M.T., Sigmundsson, F. & Björnsson, H. (1997) Ice–volcano interaction of the 1996 Gjálp subglacial eruption, Vatnajökull, Iceland. *Nature* **389**, 954–957.

Gurnell, A.M. (1987) Suspended sediment. In: *Glaciofluvial Sediment Transfer: an Alpine Perspective* (Eds Gurnell, A.M. & Clarke, M.J.), pp. 305–354. John Wiley & Sons, Chichester.

Hodgson, K.A. & Manville, V.R. (1999) Sedimentology and flow behaviour of a rain-triggered lahar, Mangatoetoenui Stream, Ruapehu volcano, New Zealand. *Geol. Soc. Am. Bull.* **111**(5), 743–754.

Karcz, I. (1972) Sedimentary structures formed by flash floods in southern Israel. *Sediment. Geol.* **7**, 161–182.

Lawson, D.E. (1993) Glaciohydrologic and glaciohydraulic effects on runoff and sediment yield within glacierised basins. *US Army Corps Eng. Cold Regions Res. Eng. Lab. Monogr.* **93–2**, 108 pp.

Maizels, J.K. (1989a) Sedimentology, paleoflow dynamics and flood history of jökulhlaup deposits: paleohydrology of Holocene sediment sequences in southern Iceland sandur deposits. *J. sediment. Petrol.* **59**, 204–223.

Maizels, J.K. (1989b) Sedimentology and palaeohydrology of Holocene flood deposits in front of a jökulhlaup glacier, South Iceland. In: *Floods, Hydrological, Sedimentological and Geomorphological Implications: an Overview* (Eds Bevan, K. & Carling, P.), pp. 239–253. John Wiley & Sons, Chichester.

Maizels, J.K. (1991) Origin and evolution of Holocene sandurs in areas of jökulhlaup drainage, south Iceland. In: *Environmental Change in Iceland: Past and Present* (Eds Maizels, J.K. & Caseldine, C.), pp. 267–300. Kluwer, Dordrecht.

Maizels, J.K. (1993) Lithofacies variations within sandur deposits: the role of runoff regime, flow dynamics and sediment supply characteristics. *Sediment. Geol.* **85**, 299–325.

Maizels, J.K. (1995) Sediments and landforms of modern proglacial terrestrial environments. In: *Modern Glacial Environments: Processes, Dynamics and Sediments* (Ed. Menzies, J.), pp. 365–416. Butterworth-Heinemann, Oxford.

Maizels, J.K. (1997) Jökulhlaup deposits in proglacial areas. *Quat. Sci. Rev.* **16**, 793–819.

Maizels, J.K. & Russell, A.J. (1992) Quaternary perspectives on jökulhlaup prediction. In: *Applications of Quaternary Research* (Ed. Gray, J.M.), pp. 133–153. Quaternary Proceedings No. 2, Quaternary Research Association, London.

Nemec, W. & Steel, R.J. (1984) Alluvial and coastal conglomerates: their significant features and some comments on gravelly mass flow deposits. In: *Sedimentology of Gravels and Conglomerates* (Eds Koster, E.H. & Steel, R.J.), Mem. Can. Soc. petrol. Geol., Calgary, **10**, 1–31.

Østrem, G. (1975) Sediment transport in glacial meltwater streams. In: *Glaciofluvial and Glaciolacustrine Sedimentation* (Eds Jopling, A.V. & MacDonald, B.C.), Spec. Publ. Soc. econ. Paleont. Miner., Tulsa, **23**, 101–122.

Pierson, T.C. & Scott, K.M. (1985) Downstream dilution of a lahar: transition from debris flow to hyperconcentrated streamflow. *Water Resour. Res.* **21**, 1511–1524.

Roberts, M.J., Russell, A.J., Tweed, F.S. & Knudsen, Ó. (2000a) Rapid sediment entrainment and englacial deposition during jökulhlaups. *J. Glaciol.* **46** (153), 349–351.

Roberts, M.J., Russell, A.J., Tweed, F.S. & Knudsen, Ó. (2000b) Ice fracturing during jökulhlaups: implications for floodwater routing and outlet development. *Earth Surf. Process. Landf.* **25**, 1429–1446.

Rubin, D.M., Nelson, J.M. & Topping, D.J. (1998) Relation of inversely-graded deposits to suspended-sediment grain-size evolution during the 1996 flood experiment in Grand Canyon. *Geology* **26**, 99–102.

Russell, A.J. (1993) Obstacle marks produced by flows around stranded ice blocks during a jökulhlaup in West Greenland. *Sedimentology* **40**, 1091–1113.

Russell, A.J. (1994) Subglacial jökulhlaup deposition, Jotunheimen, Norway. *Sediment. Geol.* **91**, 1–14.

Russell, A.J. (1995) Late Devensian meltwater movement and storage within the Ochil Hills, central Scotland. *Scot. J. Geol.* **31**, 65–78.

Russell, A.J. & Knudsen, Ó. (1999a) Controls on the sedimentology of November 1996 jökulhlaup deposits, Skeiðarársandur, Iceland. In: *Fluvial Sedimentology VI* (Eds Smith, N.D. & Rogers, J.), Spec. Publs int. Ass. Sediment., No. 28, pp. 315–329. Blackwell Science, Oxford.

Russell, A.J. & Knudsen, Ó. (1999b) An ice-contact rhythmite (turbidite) succession deposited during the November 1996 catastrophic outburst flood (jökulhlaup), Skeiðarárjökull, Iceland. *Sediment. Geol.* **127**, 1–10.

Russell, A.J. & Marren, P.M. (1998) Younger Dryas (Loch Lomond Stadial) jökulhlaup deposits, Fort Augustus, Scotland. *Boreas* **27**, 231–242.

Russell, A.J. & Marren, P.M. (1999) Proglacial fluvial sedimentary sequences in Greenland and Iceland: a case study from active proglacial environments subject to jökulhlaups. In: *The Description and Analysis of Quaternary Stratigraphic Field Sections* (Eds Jones, A.P., Tucker, M.E. & Hart, J.K.), pp. 171–208. Technical Guide 7, Quaternary Research Association, London.

Russell, A.J., Knudsen, Ó., Maizels, J.K. & Marren, P.M. (1999) Channel cross-sectional area changes and peak discharge calculations on the Gígjukvísl river during the November 1996 jökulhlaup, Skeiðarársandur, Iceland. *Jökull* **47**, 45–58.

Scott, E.M. & Gravlee, G.C. Jr (1968) Flood surge on the Rubicon River, California. Hydrology, hydraulic and boulder transport. *US geol. Surv. Prof. Pap.* **422-M**, 38 pp.

Shakesby, R.A. (1985) Geomorphological effects of jökulhlaups and ice-dammed lakes, Jotunheimen, Norway. *Nor. geogr. Tiddsskr.* **39**, 1–16.

Smith, G.A. (1993) Missoula flood dynamics and magnitudes inferred from sedimentology of slack-water deposits on the Columbia Plateau, Washington. *Geol. Soc. Am. Bull.* **105**, 77–100.

Snorrason, Á., Jónsson, P., Pálsson, S., *et al.* (1997) Hlaupið Á Skeiðarársandi Haustið 1996: Útbreiðsla, rennsli og aurburður. In: *Vatnajökull: Gos og Hlaup 1996* (Ed. Haraldson, H.), pp. 79–137. Vegagerðin, Reykjavik.

Sohn, Y.K. (1997) On traction-carpet sedimentation. *J. sediment. Petrol.* **67**, 502–509.

Stewart, J.H. & La Marche, V.C. (1967) Erosion and deposition produced by the flood of December 1964 on Coffee Creek, Trinity County, California. *US geol. Surv. Prof. Pap.* **422-K**, 22 pp.

Thorarinsson, S. (1974) *Vötnin Strið: Saga Skeiðarárhlaupa og Grímsvatnagosa*. Bókaútgáfa Menningarsjóðs, Reykjavík, 254 pp.

Todd, S.P. (1989) Stream-driven, high-density gravelly traction carpets: possible deposits in the Trabeg Conglomerate Formation, SW Ireland and some theoretical considerations of their origin. *Sedimentology* **36**, 513–530.

Tómasson, H. (1974) Grímsvatnhlaup (1972) mechanism and sediment discharge. *Jökull* **24**, 27–38.

Tómasson, H., Pálsson, S. & Ingólfsson, P. (1980) Comparison of sediment transport load in the Skeiðará jökulhlaups in 1972 and 1976. *Jökull* **30**, 21–33.

Tweed, F.S. & Russell, A.J. (1999) Controls on the formation and drainage of glacier-impounded lakes: implications for jökulhlaup character. *Progr. phys. Geogr.* **23**, 79–110.

Wells, S.G. & Harvey, A.M. (1987) Sedimentologic and geomorphic variations in storm-generated alluvial fans, Howgill Fells, northwest England. *Geol. Soc. Am. Bull.* **98**, 182–198.

Spec. Publs int. Ass. Sediment. (2002) **32**, 85–97

Formation of ice-block obstacle marks during the November 1996 glacier-outburst flood (jökulhlaup), Skeiðarársandur, southern Iceland

H. FAY

Earth Surface Processes Research Group, School of Earth Sciences and Geography, Keele University, Keele, Staffordshire ST5 5BG, UK (Email: ggd25@esci.keele.ac.uk)

ABSTRACT

Glacier outburst floods or 'jökulhlaups' commonly involve the transport of ice blocks released from glacier margins. Very few published studies have focused on the effects of ice blocks on outwash plains during and following jökulhlaups. A volcanic eruption beneath the Vatnajökull ice-cap in southern Iceland generated a jökulhlaup on 5 November 1996 that transported numerous ice blocks as large as 45 m in diameter on to Skeiðarársandur. The morphology and sedimentology of a series of large, coarse grained bedforms formed around large stranded ice blocks during the November 1996 jökulhlaup are examined in relation to flow conditions.

Ice-block obstacle marks were formed both by scour during the flow and by *in situ* melting after the flood receded. Flow separation around ice blocks resulted in the lee of the blocks becoming a locus of rapid deposition and led to the formation of entirely aggradational obstacle shadows. Flow around ice blocks also resulted in the deposition of upstream-dipping strata in sets up to 4 m thick that are interpreted as antidune stoss sides. Evidence of deposition from traction carpets during both rising and waning stages of the flood was preserved around ice blocks. It is suggested that the 1996 jökulhlaup flow was predominantly subcritical, but that locally flow became supercritical around ice blocks.

RATIONALE AND AIMS

Glacier outburst floods or 'jökulhlaups' commonly involve transport of ice blocks released from glacier margins. Scour around stranded ice blocks during a flood often leads to the formation of ice-block obstacle marks (Fahnestock & Bradley, 1973; Elfström, 1987; Russell, 1993; Maizels, 1995, 1997), whereas the melting of buried ice after the flood has receded normally leads to the formation of kettle holes (Klimek, 1972, 1973; Churski, 1973; Galon, 1973a,b; Nummedal *et al.*, 1987; Maizels, 1977, 1992, 1995, 1997). Very few studies focus on the impact of ice blocks on outwash plains during and following jökulhlaups (Scholz *et al.*, 1988; Maizels, 1992; Russell, 1993). Most examinations of obstacle marks formed around naturally occurring obstacles (Peabody, 1947; Sengupta, 1966; Karcz, 1968, 1973; Richardson, 1968; Bluck, 1979; Allen, 1984, 1985) have concentrated on small obstacles in low-flow discharges, such as around pebbles and stranded wood. Karcz (1968), for example, described obstacle marks formed around small pebbles by flow velocities of 6 m s^{-1}. Large-scale obstacle marks observed in marine environments, for example associated with wrecks, are formed by tidal currents and not high-velocity unidirectional flood flow (Werner & Newton, 1975; Caston, 1979). Experimental studies of scour around bridge piers (Carstens & Sharma, 1975) have concentrated on bluff bodies of simple geometry on sandy stream beds.

Previous studies have not examined large obstacle marks in detail or the morphology and lithofacies of bedforms associated with them. The November 1996 jökulhlaup in southern Iceland provided an opportunity to study large (up to 160 m in length) ice-block obstacle marks produced during a high-magnitude flood (Russell & Knudsen, 1999). This study aims to:

1 examine in detail the morphology and sedimentology of bedforms consisting of material up to boulder size, formed around large ice-block obstacles during a high-magnitude jökulhlaup;

2 explain the genetic processes of formation in relation to November 1996 jökulhlaup flow conditions;

Flood and Megaflood Processes and Deposits: Recent and Ancient Examples. Edited by I. Peter Martini, Victor R. Baker and Guillermina Garzón ISBN: 978-0-632-06404-5

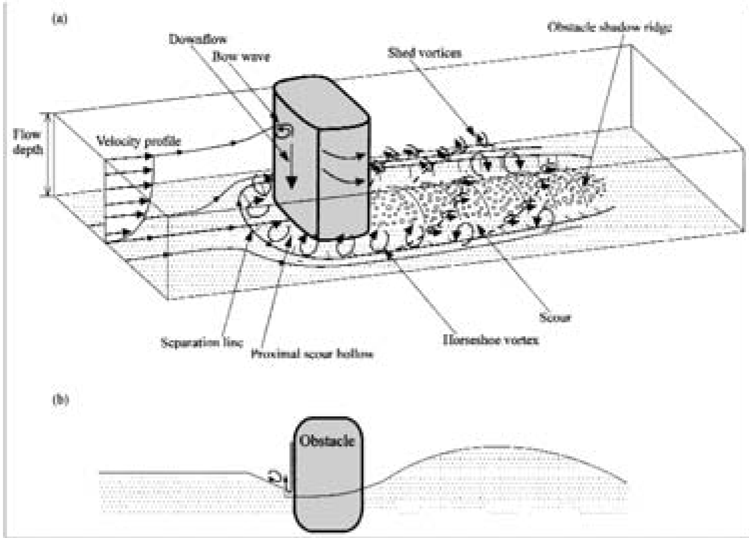

Fig. 1. Schematic representation, (a) oblique and (b) in cross-section, of the patterns of flow acceleration around obstacles such as bridge piers and ice blocks and the association between horseshoe vortices and proximal scour, and between shed vortices and obstacle-shadow deposition (after Bradley & McCutcheon, 1987).

3 assess the importance of ice-block obstacles in creating distinctive jökulhlaup landform and sediment associations.

THE IMPACT OF ICE BLOCKS ON PROGLACIAL OUTWASH PLAINS

Fluid flow around obstacles produces secondary flow cells that are deflected downwards and outwards from the obstacle in the form of a 'horseshoe vortex' (Allen, 1984; Acarlar & Smith, 1987; Best, 1993) (Fig. 1). The enhanced velocities in front and along the sides of the obstacle prevent the deposition of sediment and create a U-shaped scour surrounding the body (Sengupta, 1966; Karcz, 1968; Richardson, 1968; Allen, 1984). Clustering of vortices downstream of the obstacle results in the preferential accumulation of sediment, or the minimization of scour, producing a 'shadow' ridge in the lee of the obstacle (Sengupta, 1966; Karcz, 1968; Richardson, 1968; Baker, 1973a,b, 1978a,b; Carstens & Sharma, 1975; Patton & Baker, 1978; Allen, 1984; Fraser & Bleuer, 1988; Breusers, 1991a,b; Raudkivi, 1991; O'Connor, 1993).

The formation of obstacle marks and kettle holes observed on the Skeiðarársandur, south Iceland (Fig. 2), has been linked to ice blocks deposited during jökulhlaups (Krigström, 1962; Bogacki, 1973; Churski, 1973; Galon, 1973a,b; Klimek, 1973; Nummedal *et al.*, 1987; Maizels, 1992; Russell & Knudsen, 1999). Maizels (1992) investigated the formation of 'rimmed kettles' on Mýrdalssandur, south Iceland, produced by the *in situ* melting of debris-rich ice blocks. Laboratory experiments confirmed that kettle morphology was dependent on the sediment concentration of the ice block and the depth of submergence of the block in the sediment. Excavation of ice-block obstacle shadows, formed during a glacier outburst flood in west Greenland, revealed a predominantly erosional origin for the ice-block obstacle marks (Russell, 1993).

THE NOVEMBER 1996 JÖKULHLAUP

On 30 September 1996, a volcanic eruption began beneath the Vatnajökull ice-cap in southern Iceland (Gudmundsson *et al.*, 1997) (Fig. 2). The resultant jökulhlaup on 5 November 1996 transported large numbers of ice blocks as large as 45 m in diameter on to Skeiðarársandur. The flood occupied all the rivers draining Skeiðarárjökull, reaching its peak of 45 000 $m^3 s^{-1}$ in only 14 h (Björnsson, 1997).

METHODS AND STUDY AREA

Field sites were chosen to provide information on ice-block obstacle marks created exclusively during three different flood stages: rising, rising stage during backwater control and waning stage. Information on jökulhlaup flow was obtained from video film taken on 5 and 6 November 1996 and oblique video film

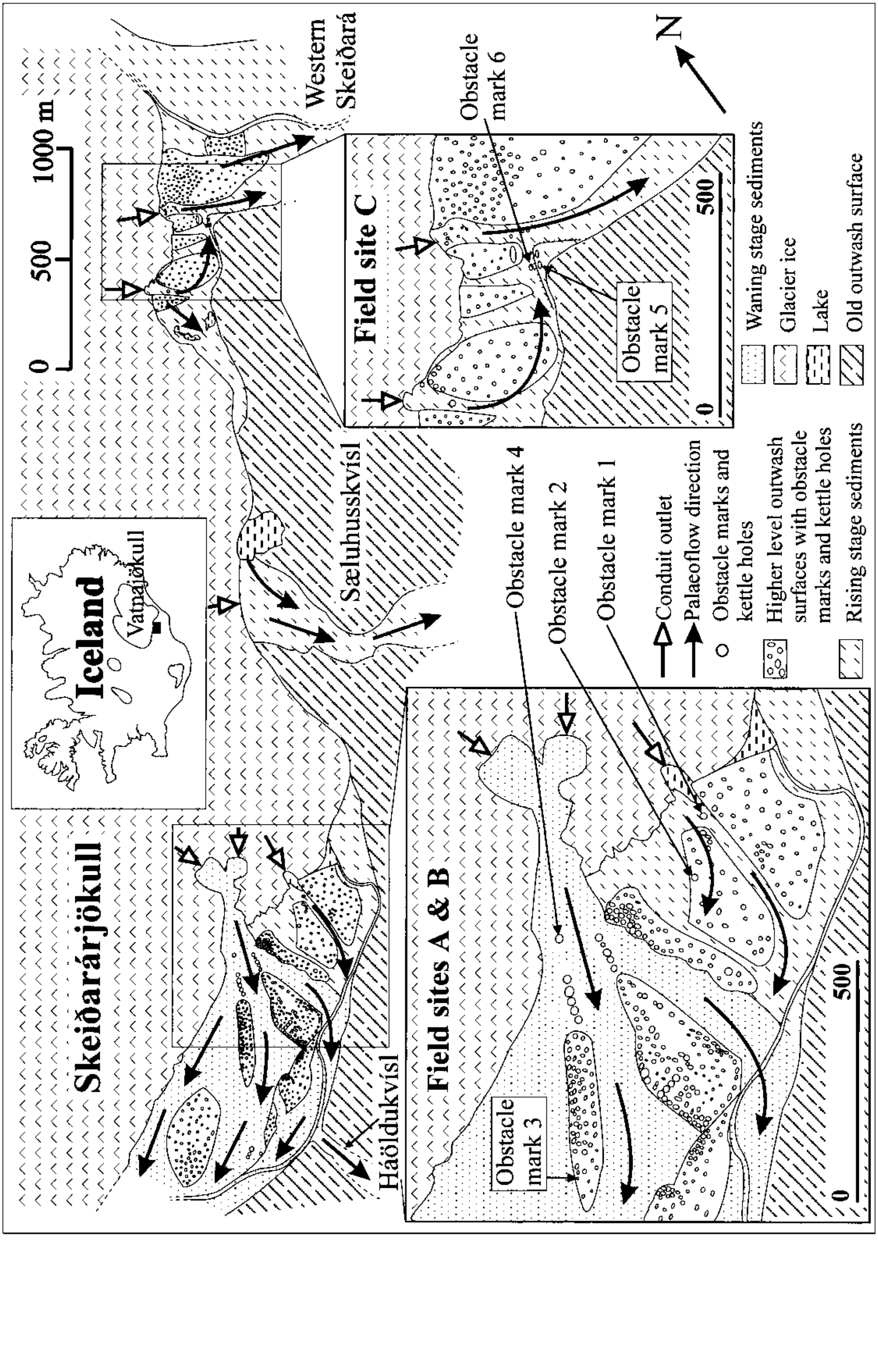

Fig. 2. Location map of the field area in Iceland, the principal field areas, and the location of obstacle marks examined in detail.

Table 1. Lithofacies scheme used in this study after Miall (1978) and Russell & Marren (1999).

Lithofacies codes	Description	Interpretation
Gm	Poorly sorted, massive or crudely stratified, matrix- or clast-supported gravel. Graded: normal or reverse. *a* (p) *a* (i) imbrication. Thin sheets	Hyperconcentrated moving bedload layers *or* 'traction-carpet' deposits (Todd, 1989; Sohn, 1997)
Gs	Well-sorted, massive or stratified, clast-supported gravel. Graded: normal. *a* (t) *b* (i) imbrication	Deposition from fully turbulent fluidal flow with high sediment concentration (Costa, 1988; Todd, 1989)
Sp	Planar cross-bedded sands	Deposition from fluidal flow (Costa, 1988; Todd, 1989)

taken on 7 November 1996. Post-jökulhlaup data were collected in the field during July and August 1998 when sedimentary sections within obstacle marks were examined. The characteristics of the lithofacies present were recorded, in particular: grain size, grading, style of clast support within the sediment (matrix- or clast-supported), sorting, bed thickness and geometry, presence of internal structures of beds and presence of large-scale structures. The lithofacies scheme used in this study was adapted from Miall (1978) and Russell & Marren (1999) (Table 1). Peak jökulhlaup discharge figures for the Gígjukvísl were available from published hydrographs (Snorrason *et al.*, 1997).

Field sites are on Skeiðarársandur (Fig. 2). Site A is located on a proglacial outwash fan formed during the rising stage, graded to backwater conditions. Site B is located on a proglacial outwash fan formed during the waning stage of the flood that lies adjacent to the rising stage fan. Site C is located in rising stage sediments in the east of the proglacial zone, west of the Skeiðará river.

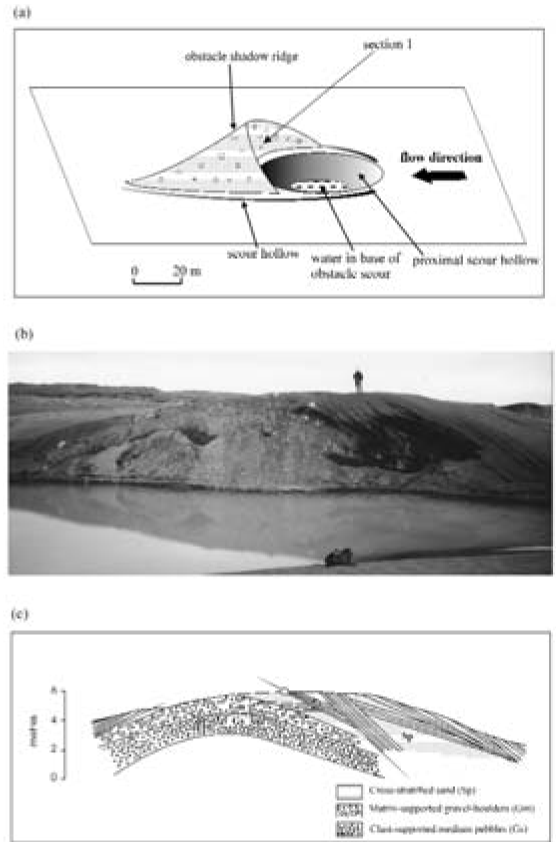

Fig. 3. (a) Morphology of obstacle mark 1. (b) Section 1. View down-current of section 1, which is transverse to the obstacle shadow and is anticlinal in shape. (c) Section 1 lithofacies: clast-supported pebbles (Gs) overlain by matrix-supported gravel with boulders (Gm), in turn overlain by planar, cross-stratified sand (Sp).

RESULTS

Field site A

Section 1, in the lee side of obstacle mark 1, was formed by an ice block 45 m in diameter and has a well-defined obstacle shadow (Fig. 3). Section 2 is in the side wall of obstacle mark 2, also exhibiting a well-defined obstacle shadow (Fig. 4). Obstacle mark 2 is approximately 8 m deep with buried ice at its base and was produced by an ice block 16 m in diameter.

Lithofacies within section 1 consists of beds of well-sorted, medium–coarse, planar cross-stratified sand (Sp), which dip steeply transverse to the general flow direction and are truncated by the stream bed. Sediment underlying the Sp unit is inversely graded

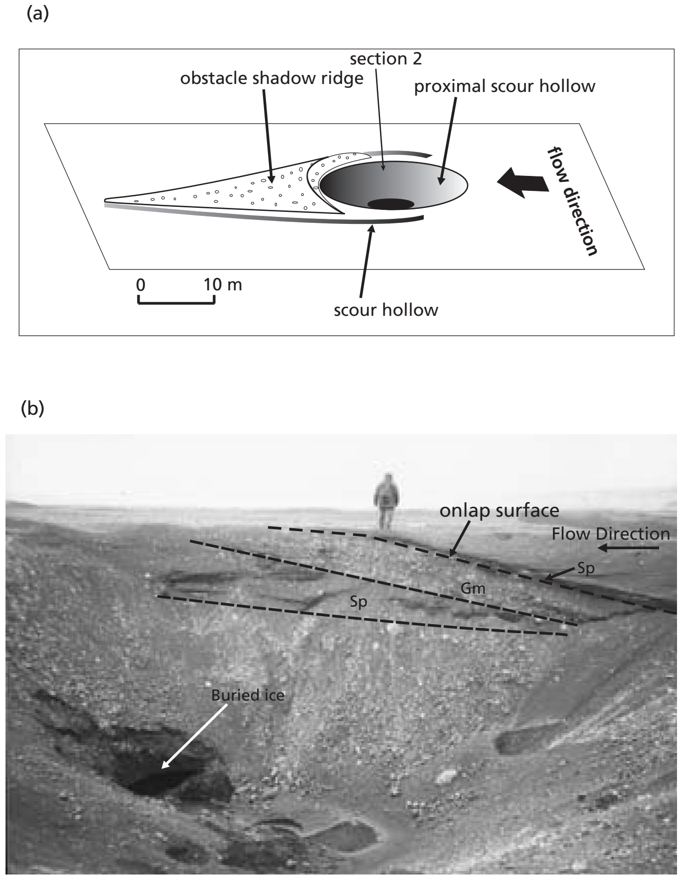

Fig. 4. (a) Morphology of obstacle mark 2. (b) Section 2. Upstream-dipping beds of planar, cross-stratified sand and gravel (Sp) and matrix-supported pebbles and cobbles (Gm) truncated by surface morphology. Planar, cross-stratified sand onlaps the Gm facies.

and structureless, consisting of small pebbles to boulders supported by a finer grained polymodal matrix (Gm). Facies Gm dips upstream, the boulders orientated with *a*-axes parallel to dip direction. The lithofacies association is mirrored on each side of the section, forming an anticlinal-shaped feature. The lower part of this 'anticline' consists of structureless, clast-supported pebble gravel (Gs).

In section 2, facies consist of planar cross-stratified medium sand and gravel (Sp), truncated by an upstream-dipping unit (14°) conformable with the stream bed, which consists of crudely bedded pebbles to cobbles supported by a sand and granule matrix (Gm). Within the Gm facies, beds are normally graded and include imbricated cobble clusters. Clasts in the Gm beds show high-angle *a*-axis imbrication, with the modal class distribution between 20 and 40° from the horizontal plane. Planar cross-bedded medium sand (Sp) overlies the Gm facies and is conformable with the stream bed.

Field site B

Section 3 is in the side wall of obstacle mark 3 (Fig. 5), which was formed by the melting of an ice block 30 m in diameter and has a depth of 3.5 m to water table. Section 4 is located in the side wall of obstacle mark 4 (Fig. 6) formed by an ice block 40 m in diameter. Obstacle mark 4 has a depth of 5.5 m to water table and shows evidence of buried ice at its base. Stoss-side scour hollows and horseshoe-scours of both obstacle marks 3 and 4 are not well developed.

Section 3 shows upstream-dipping, crudely bedded lithofacies consisting of unsorted boulder gravel, supported by a coarse sand matrix (Gm). The boulders are imbricated and in places are clustered. Towards the lee of obstacle mark 3, the upstream-dipping facies (Gm) truncate alternating beds of upward-coarsening gravel supported by a coarse sand matrix (Gm) and clast-supported gravel (Gm), which dip steeply

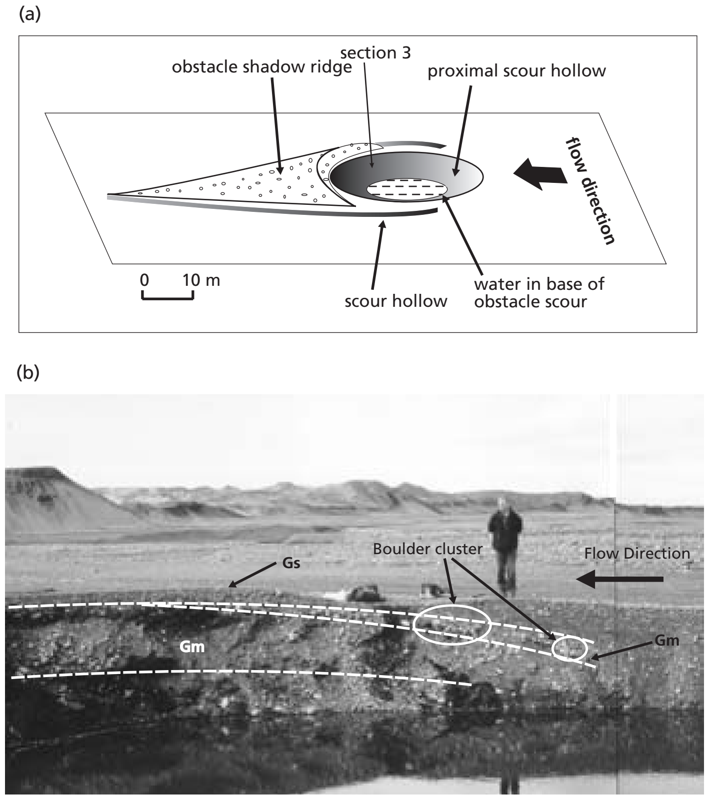

Fig. 5. (a) Morphology of obstacle mark 3. (b) Section 3. Upstream-dipping, crudely bedded, matrix-supported boulder gravel (Gm) truncated by normally graded, clast-supported gravel (Gs). Note the presence of imbricated boulders forming clusters.

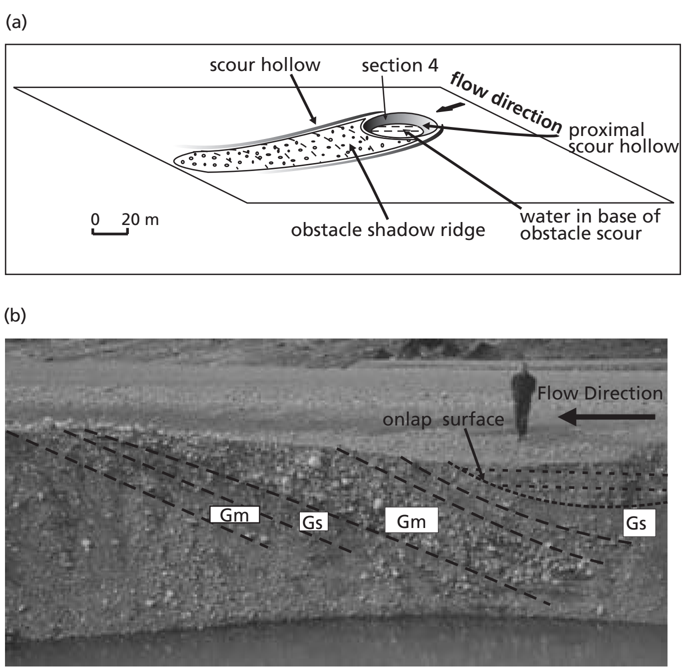

Fig. 6. (a) Morphology of obstacle mark 4. (b) Section 4. Upstream-dipping, openwork, boulder gravel (Gm) and clast-supported pebble gravel (Gs) truncated by surface morphology. A succession of lower angle, upward-fining beds of Gs onlap the Gm.

downstream. The top of the section consists of normally graded, clast-supported gravel (Gs) that truncates the upstream-dipping Gm and is conformable with the stream bed.

In section 4, poorly defined beds of openwork, poorly sorted cobbles and boulders (Gm) dip steeply upstream at 18° and are truncated by the stream bed. The clasts are in places clustered, displaying unidirectional, upcurrent, high-angle *a*-axis imbrication with a modal distribution of 20–40° from horizontal. Lithofacies consisting predominantly of clast-supported granules and pebbles, some cobbles and coarse sand (Gs) can be found as a succession of upward-fining beds that dip upstream and are truncated by Gm. Fining upward beds of Gs also can be seen on the right of the section, dipping upstream at a much lower angle than the Gm facies.

Field site C

Section 5 is in the lee side of obstacle mark 5 (Fig. 7), which has a depth of 5 m down to water table and was formed by an ice block 16 m in diameter. Section 6 is in the side wall of obstacle mark 6 (Fig. 8) and of similar size to obstacle mark 5. Both obstacle marks have poorly defined proximal and lateral scour.

In section 5, beds of poorly sorted cobble and boulder gravel, which include imbricated boulders supported by a medium sand matrix (Gm), are conformable with stream bed morphology. An unconformable, steeply dipping bed of normally graded gravel supported by a coarse sand matrix (Gm) caps this sediment. The latter bed contains boulders of up to 80 cm in size orientated with *a*-axes parallel to flow direction. This facies arrangement creates a large anticlinal-shaped feature, the centre of which is

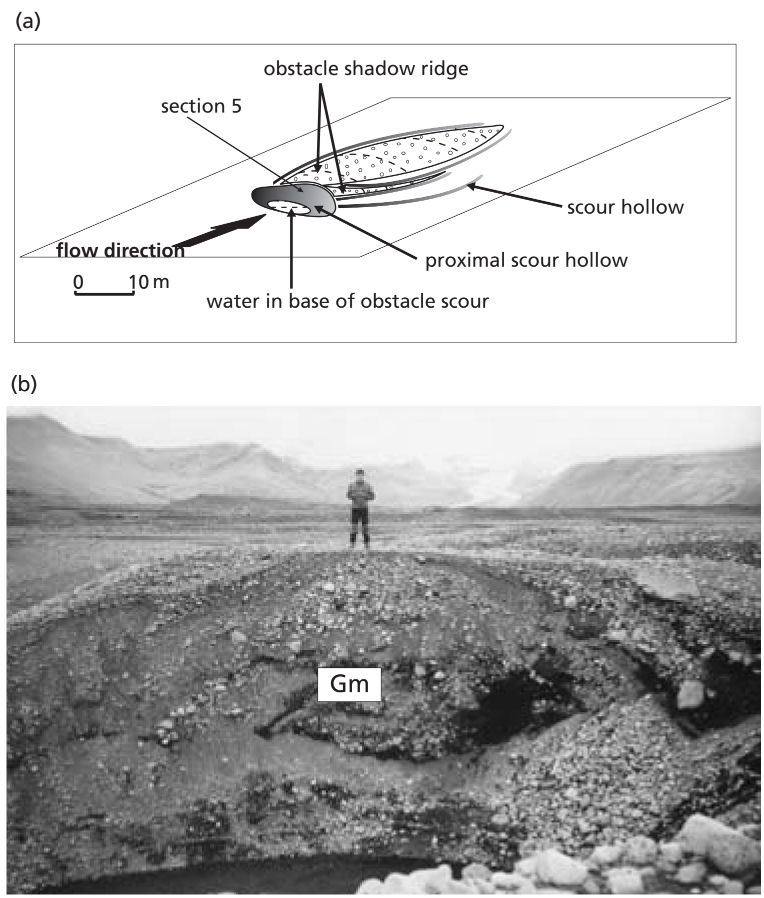

Fig. 7. (a) Morphology of obstacle mark 5. (b) Section 5 is a transverse section, looking downstream, across the obstacle shadow. Lithofacies consist of beds of Gm producing an anticlinal-shaped feature.

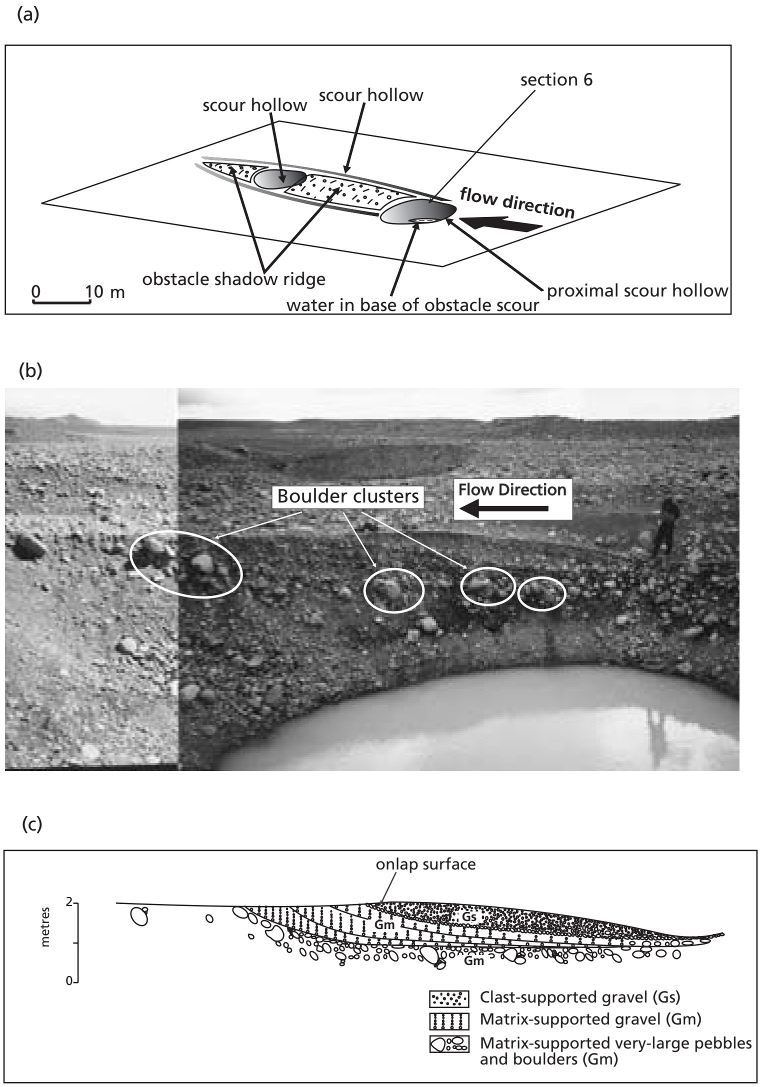

Fig. 8. (a) Morphology of obstacle mark 6. (b) Section 6. Upward-fining succession of upstream-dipping beds. Circles indicate boulder clusters exhibiting high-angle *a*-axis imbrication. (c) Section 6 lithofacies: beds consist of matrix-supported cobbles and boulders (Gm) and matrix-supported pebbles (Gm) truncated by surface morphology. Lower angle upstream-dipping beds of clast-supported granules to medium pebbles (Gs) onlap the Gm.

composed of very poorly sorted, structureless boulder gravel supported by a coarse sand matrix (Gm).

Section 6 shows a crudely upward-fining sequence consisting of upstream-dipping (10°), weakly bedded material up to boulder size that is nonconformable with the stream bed. The middle of the section consists of poorly sorted cobbles and boulders supported by a medium sand matrix (Gm), some boulder clusters exhibiting high-angle (modal distribution 20–40° from horizontal) *a*-axis imbrication. Overlying this succession are several normally graded beds of pebble gravel supported by a coarse sand matrix (Gm) and truncated by the stream bed. Larger material within these beds forms clast-supported clusters that exhibit high-angle *a*-axis imbrication with a modal distribution of 20–40° from horizontal. At the top of the section, a bed of normally graded, relatively well sorted, clast-supported granules to medium pebbles (Gs) displaying imbrication (*a* (t) *b* (i)) dips upstream at a lower angle than the Gm.

INTERPRETATION AND DISCUSSION

At field sites A and B, the large size and steep-sided nature of the obstacle marks and evidence of buried ice blocks indicate that these could not have been created by scour alone. This especially is relevant where stoss-side and horseshoe scour is poorly developed as a result of a high sedimentation rate during the flood (Russell *et al.*, 2001). Russell & Knudsen (1999) suggested that during the November 1996 flood, flows exiting the glacier were sediment rich. This high sediment flux would have reduced the potential for scour. These obstacle marks are interpreted as 'kettle-scours', formed both by scour during the flow and *in situ* melting after the flood had receded.

The absence of well-defined bedding, the poorly sorted and matrix-supported nature, plus the presence of *a*-axis imbrication of lithofacies type Gm in sections 2, 3, 5 and 6 suggest that the sediments were deposited during hyperconcentrated-flow conditions (Kehew & Lord, 1987; Maizels, 1989a,b; Todd, 1989; Kehew, 1993; Russell & Knudsen, 1999; Russell & Marren, 1999). The presence of imbrication clusters within lithofacies type Gm in sections 2, 3 and 6 suggest that 'live-bed' conditions operated (Martini, 1977), and that turbulent water flow processes operated in parts of the flow (Costa, 1988; Maizels, 1997; Russell & Knudsen, 1999). The poorly sorted, crudely bedded, openwork nature and presence of *a*-axis imbrication within lithofacies type Gm in section 4 also suggest deposition during hyperconcentrated-flow conditions, such as those described by Costa (1988). Openwork gravel successions can develop where high-energy traction currents prevent the deposition of finer sediment and deposit lenses of matrix-free gravels (Maizels, 1997), or where parts of the hyperconcentrated flow are more turbulent (Costa, 1988). Inverse grading within the Gm unit in section 1, and the position of the largest clasts at the top of the Gm in sections 1 and 5, indicate that size segregation due to gradients in dispersive stress was occurring within the flow. Inverse grading of the Gm facies suggests deposition from highly concentrated moving bedload layers or 'traction carpets' (Todd, 1989; Sohn, 1997). The traction carpets would develop beneath, and be driven by, turbulent overlying flows. A high waning-stage sediment flux of 156 kg m^{-3} s^{-1} calculated by Russell *et al.* (2001) at the main flood outlet suggests that flows maintained their high concentration through much of the waning stage at field site B. Video film clearly shows that the main flood was dominated by turbulent surface flow on both the rising and waning stages of the flood (Benediktsson & Axelsson, 1996).

The top of the anticlinal sedimentary structures in sections 1 and 5 (Figs 3 & 7) are conformable with the stream bed, which implies that they are entirely aggradational. The very poorly sorted, structureless, coarse-grained, matrix-supported nature of the Gm facies at the base of section 5 is suggestive of rapid deposition from traction carpets. Buried ice in section 2 (Fig. 4) indicates that sedimentation on the rising stage was rapid enough to allow complete burial of some ice. Obstacle shadows in the lee of the ice blocks were formed by flow separation associated with reduced flow velocities and rapid deposition (Baker, 1978b; Komar, 1983; Kehew & Lord, 1986; Kehew, 1993). The shelter provided in the lee of the ice blocks then preserved the shadows (Allen, 1984; Russell, 1993).

In each of the sections 2, 3, 4 and 6, the upstream-dipping strata and the high angle of *a*-axis imbrication (larger than the angle of the depositional slope) are indicative of deposition on the stoss side of an antidune (Allen, 1966; Langford & Bracken, 1987; Yagishita & Taira, 1989; Yagishita, 1994). Yagishita & Taira (1989) measured imbrication angles of between 20 and 30° from the horizontal in a laboratory antidune. Stoss-side beds were deposited while a standing wave, which formed just downstream of the ice block, migrated upstream. The presence of an upstream-migrating surface wave indicates that flow around the ice blocks was within the upper flow regime (Froude number > 1) (Allen, 1984; Barwis & Hayes, 1985; Carling, 1999). Observations made from media footage show flow separation occurring and standing waves forming around ice blocks during the flood (Benediktsson & Axelsson, 1996). Martini (1977), Broome & Komar (1979) and Barwis & Hayes (1985) suggested that flow may become supercritical just down-flow of an obstruction, and a hydraulic jump represented the return to subcritical flow. Flood flow velocities are enhanced in front and along the sides of the obstacle, forming horseshoe vortices (Allen, 1984; Acarlar & Smith, 1987; Best, 1993). The enhanced velocities cause the flow to become supercritical just down-flow of the ice block, producing a hydraulic regime capable of generating an upstream-migrating wave (Prave & Duke, 1990). The standing wave forming the hydraulic jump migrates upstream, depositing stoss beds (Fig. 9) (Allen, 1984; Barwis & Hayes, 1985; Pickering & Hiscott, 1985; Langford & Bracken, 1987). This is largely as a result of the tendency of the associated antidune to move upstream owing to erosion on the lee side where water accelerates and deposition on the stoss side where water decelerates (Middleton, 1965). It is likely that as the standing wave migrated upstream, antidune stoss beds infilled the scour hollow (Fig. 9).

The fact that the upstream-dipping beds in section 2 are conformable with the stream bed indicates that it is unlikely much erosion took place at field site A following the deposition of the antidune bedding. This suggests that at field site A, the current was suddenly reduced. Russell *et al.* (2001) suggested that the main

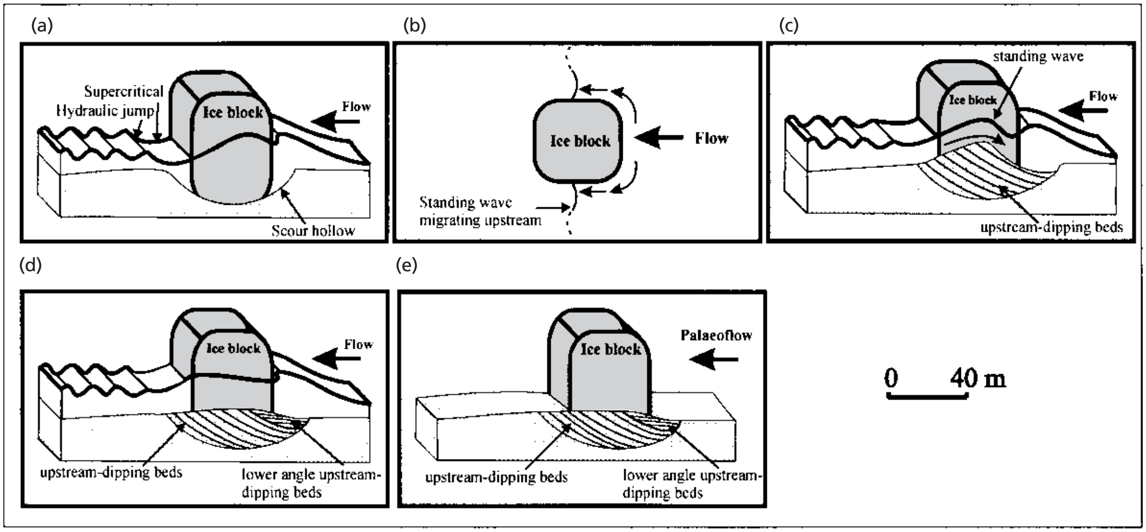

Fig. 9. Schematic model of the formation of antidune stoss-side strata around an ice block. (a) Flow becomes supercritical just down-flow of the ice block, generating an upstream-migrating standing wave. (b) Plan view of the upstream-migrating standing wave. (c) Antidune stoss beds are deposited from the upstream-migrating surface wave. (d) 'Washout': with increasing bedform height, flow on the upstream side slows and deepens, increasing the rate of sedimentation until the antidune is no longer stable and collapses. Associated with collapse, water stored upstream of the antidune is released, eroding the antidune strata and filling the antidune trough with low angle backset beds. (e) Resultant section after the flood has receded.

subglacial jökulhlaup channel migrated to the west to feed the main flood outlet. This westward diversion of flow would cause a reduction in flood power at field site A. This was accompanied by a removal of back-water effects as a result of major downstream channel widening.

In section 3 deposits of fluidal flow (Gs), which are conformable with the stream bed, truncate the upstream-dipping beds. This suggests that erosion took place before the deposition of the lens of Gs. The truncation of the steeper upstream-dipping beds by the stream bed in sections 4 and 6 (Figs 6 & 8) also indicates erosion has occurred in these locations after deposition of these beds. The lower angle backset beds in these sections have infilled the upstream antidune trough after the truncation of the more steeply dipping beds, suggesting that truncation of antidune stoss strata in obstacle marks 3, 4 and 6 is the result of 'wash out'. As bedform height increases, flow on the upstream side deepens and slows, increasing the rate of sedimentation on the top and upstream side of the antidune (Langford & Bracken, 1987). Eventually flow over the antidune slows and deepens until the antidune is no longer stable and collapses. The water stored upstream of the antidune is released, causing erosion of the antidune strata and filling of the adjacent antidune trough with lower angle backset beds (Langford & Bracken, 1987) (Fig. 9). Truncation of antidune strata by the stream bed at location B indicates that rapid deposition took place at this location followed by antidune washout on the waning stage of the flood, with little erosion on the late waning stage. According to the flood hydrograph for the Gígjukvísl (Snorrason *et al.*, 1997) flood flow did not suddenly wane at field site B. Russell & Knudsen (1999) suggest that sedimentation at this location continued into the late waning stage. A high sedimentation rate during the flood at field site B is confirmed by large numbers of buried ice blocks, which are forming new kettle holes. At field site C flow was of shorter duration than flow at the main outlet owing to the migration of flow to the west (Russell *et al.*, 2001). At this location, antidune strata are preserved as a result of both rapid deposition during the rising stage and reduced discharge on the late rising and waning stages of the flood.

CONCLUSIONS AND IMPLICATIONS

1 Newly identified obstacle marks interpreted as 'kettle-scours' are formed by flood flow and *in situ* melting of ice blocks after the flood recedes.
2 Flow around ice-block obstacles during both the rising and waning stages of the jökulhlaup resulted in

the deposition of 4-m-thick sets of upstream-dipping strata, including traction-carpet deposits, which are interpreted as the stoss-side beds of antidunes.

3 The 1996 jökulhlaup flow was predominantly subcritical, but flow was locally supercritical around ice blocks, as indicated by a change to planar bedding away from ice-block obstacles.

4 Preservation of stoss-side bedding on the rising stage fan and at the western Skeiðará indicates rapid sediment accumulation and little reworking owing to waning discharge. On the waning stage fan, stoss-side strata, deposited by rapid sediment accumulation and truncated by antidune washout, were preserved owing to a high sedimentation rate that continued late into the waning stage.

5 Large, coarse-grained, anticlinal-shaped bedforms found in the lee of (subsequently melted) ice blocks are interpreted as obstacle shadows and were formed by rapid aggradation on the rising stage of the jökulhlaup.

This study has important implications for the palaeohydraulic reconstruction of jökulhlaups in modern and ancient proglacial areas. The depth of kettle-scours provides a minimum thickness of sediment deposition in jökulhlaups. Given that upstream-moving antidunes develop under specific hydraulic conditions, $0.844 < Fr < 1.24$ (Allen, 1984), it is possible to bracket the Froude number and so have a clearer idea of velocity and depth of floods. As antidunes may be deposited around ice blocks during jökulhlaups, caution must be exercised when interpreting palaeoflow direction from jökulhlaup deposits in the sedimentary record of former proglacial areas, where direction of bed dip may be used. Likewise caution must be exercised when interpreting scour features in areas where ice blocks may have played a role. Although several models of obstacle-mark morphology and sedimentology have been proposed (Karcz, 1968; Allen, 1984; Russell, 1993), obstacle scours of large scale, their associated coarse-grained, anticlinal-shaped obstacle shadows and kettle-scours have not been represented. It is clear that the models of obstacle-mark morphology and sedimentology need revising to include the types of obstacle marks described in this study.

The characteristics of anticlinal-shaped obstacle shadows can be very similar to those of eskers viewed in cross-section. The obstacle shadows described in this study were composed of a mix of sandur material. As eskers also are composed of a wide variety of facies (Benn & Evans, 1998), care must be taken when interpreting anticlinal-shaped sedimentary structures in section. In contrast to eskers, ice-block obstacle shadows display marked differences in morphology and spatial variability in sedimentology down-shadow. Knowledge of associations between ice blocks and the bedforms described in this study will aid the identification of former jökulhlaup-dominated proglacial outwash and help predict the sedimentological and morphological impact of ice blocks during and following jökulhlaups.

ACKNOWLEDGEMENTS

This work was carried out while the author was in receipt of an NERC research studentship (award reference: GT04/97/114/FS) within the School of Earth Sciences and Geography at Keele University. I would like to thank Dr A.J. Russell, Dr Simon A. Lomas and Philip M. Marren for constructive comments on previous versions of this manuscript, and Thaiënne A.G.P. van Dijk, Mathew J. Roberts, Dr A.J. Russell, Óskar Knudsen and The Earthwatch Institute for assistance while in the field. I gratefully acknowledge the constructive criticism of my reviewers, Dr Richard Waitt, Professor Paul Carling, Dr I.P. Martini and Dr G. Plint.

REFERENCES

Acarlar, M.S. & Smith, C.R. (1987) A study of hairpin vortices in a laminar boundary layer. Part 1. Hairpin vortices generated by a hemisphere protuberance. *J. Fluid Mech.* **175**, 1–41.

Allen, J.R.L. (1966) On bedforms and palaeocurrents. *Sedimentology* **6**, 150–190.

Allen, J.R.L. (1984) *Sedimentary Structures, their Character and Physical Basis*, Vols 1 & 2, 611pp. & 679pp. Elsevier. Amsterdam.

Allen, J.R.L. (1985) *Principles of Physical Sedimentology*. Allen and Unwin, London.

Baker, V.R. (1973a) Erosional forms and processes for the catastrophic Pleistocene Missoula floods in eastern Washington. In: *Fluvial Geomorphology* (Ed. Morisawa, M.), pp. 123–148. Allen and Unwin, London.

Baker, V.R. (1973b) Palaeohydrology and sedimentology of Lake Missoula flooding in eastern Washington. *Geol. Soc. Am. Spec. Pap.* **144**, 1–79.

Baker, V.R. (1978a) Large-scale erosional and depositional features of the Channelled Scabland. In: *The Channelled Scabland: Comparative Planetary Geology Field Conference Guidebook, Columbia Basin* (Eds Baker, V.R. & Nummedal, D.), pp. 17–35. National Aeronautics Space Administration, Washington, DC.

Baker, V.R. (1978b) Palaeohydraulics and hydrodynamics of scabland floods. In: *The Channelled Scabland: Comparative Planetary Geology Field Conference Guidebook, Columbia Basin* (Eds Baker, V.R. & Nummedal, D.), pp. 59–79. National Aeronautics Space Administration, Washington, DC.

Barwis, J.H. & Hayes, M.O. (1985) Antidunes on modern and ancient washover fans. *J. sediment. Petrol.* **55**, 907–916.

Benediktsson, P. & Axelsson, A.L. (1996) *Eruption at the Ice Cap* (Video). Sjónvarpi, Reykjavík.

Benn, D.I. & Evans, D.J.A. (1998) *Glaciers and Glaciation*. Arnold, London.

Best, J.L. (1993) On the interactions between turbulent flow structure, sediment transport and bedform development: some considerations from recent experimental research. In: *Turbulence: Perspectives on Flow and Sediment Transport* (Eds Clifford, N.J., French, J.R. & Hardisty, J.), pp. 61–92. John Wiley & Sons, Chichester.

Björnsson, H. (1997) Grímsvatnahlaup Fyrr og Nú. In: *Vatnajökull: Gos og Hlaup* (Ed. Haraldson, H.), pp. 61–77. Vegagerðin, Reykjavík.

Bluck, B.J. (1979) Structure of coarse grained braided stream alluvium. *Trans. R. Soc. Edinburgh* **70**, 181–221.

Bogacki, M. (1973) Geomorphological and geological analysis of the proglacial area of Skeiðarájökull. Central western and eastern sections. *Geogr. Pol.* **26**, 57–88.

Bradley, J.B. & McCutcheon, S.C. (1987) Influence of large suspended sediment concentrations in rivers. In: *Sediment Transport in Gravel Bed Rivers* (Eds Thorne, C.R., Bathurst, J.D. & Hey, R.D.), 995pp. John Wiley & Sons, Chichester.

Breusers, H.N.C. (1991a) Scour around spur dikes and abutments. In: *Scouring Hydraulic Structures Design Manual 2* (Eds Breusers, H.N.C. & Raudkivi, A.J.), Bull. int. Assoc. Hydraul. Res., pp. 51–59. A.A. Balkema, Rotterdam.

Breusers, H.N.C. (1991b) Scour in rivers and river constrictions. In: *Scouring Hydraulic Structures Design Manual 2* (Eds Breusers, H.N.C. & Raudkivi, A.J.), Bull. int. Assoc. Hydraul. Res., pp. 37–50. A.A. Balkema, Rotterdam.

Broome, R. & Komar, P.D. (1979) Undular hydraulic jumps and the formation of backwash ripples on beaches. *Sedimentology* **26**, 543–559.

Carling, P.A. (1999) Subaqueous gravel dunes. *J. sediment. Res.* **69**, 534–545.

Carstens, T. & Sharma, H.R. (1975) Local scour around large objects. In: *Proc. int. Assoc. Hydraul. Res.*, pp. 251–262. A. A. Balkema, Rotterdam.

Caston, G.F. (1979) Wreck marks: indicators of net sand transport. *Mar. Geol.* **33**, 193–204.

Churski, Z. (1973) Hydrographic features of the proglacial area of the Skeiðarárjökull. *Geogr. Pol.* **26**, 208–254.

Costa, J.E. (1988) Rheologic, geomorphic, and sedimentological differentiation of water floods, hyperconcentrated flows, and debris flows. In: *Flood Geomorphology* (Eds Baker, V.R., Kochel, R.C. & Patton, R.C.), pp. 113–122. John Wiley & Sons, New York.

Elfström, A. (1987) Large catastrophic boulder deposits and catastrophic floods. *Geogr. Ann.* **69A**, 101–121.

Fahnestock, R.K. & Bradley, W.C. (1973) Knik and Matanuska rivers, Alaska: a contrast in braiding. In: *Fluvial Geomorphology* (Ed. Morisawa, M.), pp. 220–250. Allen and Unwin, London.

Fraser, G.S. & Bleuer, N.K. (1988) Sedimentological consequences of two floods of extreme magnitude in late Wisconsinan Wabash Valley. *Geol. Soc. Am. Spec. Pap.* **229**, 111–125.

Galon, R. (1973a) A synthetic description of deposits and landforms observed on the proglacial area of Skeiðarárjökull. Conclusions with regard to the age of the deposits and the way in which deglaciation is proceeding. *Geogr. Pol.* **26**, 141–150.

Galon, R. (1973b) Geomorphological and geological analysis of the proglacial area of Skeiðarárjökull. *Geogr. Pol.* **26**, 15–56.

Gudmundsson, M.T., Sigmundsson, F. & Björnsson, H. (1997) Ice–volcano interaction of the 1996 Gjálp subglacial eruption, Vatnajökull, Iceland. *Nature* **389**, 954–957.

Karcz, I. (1968) Fluviatile obstacle marks from the wadis of the Negev (southern Israel). *J. sediment. Petrol.* **38**, 1000–1012.

Karcz, I. (1973) Reflections on the origins of small scale longitudinal stream-bed scours. In: *Fluvial Geomorphology* (Ed. Morisawa, M.), pp. 149–173. Allen and Unwin, London.

Kehew, A.E. (1993) Glacial lake outburst erosion of the Grand Valley, Michigan, and impacts on glacial lakes in the Lake Michigan Basin. *Quat. Res.* **39**, 36–44.

Kehew, A.E. & Lord, M.L. (1986) Origin of large-scale erosional features of glacial-lake spillways in the northern Great Plains. *Geol. Soc. Am. Bull.* **97**, 162–177.

Kehew, A.E. & Lord, M.L. (1987) Glacial lake outbursts along the mid-continent margins of the Laurentide icesheet. In: *Catastrophic Flooding* (Eds Mayer, L. & Nash, D.), pp. 95–121. Allen and Unwin, Boston.

Klimek, K. (1972) Present-day fluvial processes and relief of the Skeiðarársandur plain (Iceland). *Geogr. Stud.*, *Polish Acad. Sci., Inst. Geogr.* **94**, 119 pp. (In Polish with English summary.)

Klimek, K. (1973) Geomorphological and geological analysis of the proglacial area of the Skeiðarárjökull. *Geogr. Pol.* **26**, 89–113.

Komar, P.D. (1983) Shapes of streamlined islands on Earth and Mars: experiments and analyses of the minimum-drag form. *Geology* **11**, 651–654.

Krigström, A. (1962) Geomorphological studies of sandur plains and their braided rivers in Iceland. *Geogr. Ann.* **3–4**, 328–346.

Langford, R. & Bracken, B. (1987) Medano Creek, Colorado, a model for upper-flow-regime fluvial deposition. *J. sediment. Petrol.* **57**, 863–870.

Maizels, J.K. (1977) Experiments on the origin of kettleholes. *J. Glaciol.* **18**, 291–303.

Maizels, J.K. (1989a) Sedimentology, palaeoflow dynamics and flood history of jökulhlaup deposits: palaeohydrology of Holocene sediment sequences in southern Iceland sandur deposits. *J. sediment. Petrol.* **59**, 204–223.

Maizels, J.K. (1989b) Sedimentology and palaeohydrology of Holocene flood deposits in front of a jökulhlaup glacier, south Iceland. In: *Floods: Hydrological, Sedimentological and Geomorphological Implications: an Overview* (Eds Beven, K. & Carling, P.), pp. 239–251. John Wiley & Sons, London.

Maizels, J.K. (1992) Boulder ring structures produced during jökulhlaup flows—origin and hydraulic significance. *Geogr. Ann.* **74A**, 21–33.

Maizels, J.K. (1995) Sediments and landforms of modern proglacial terrestrial environments. In: *Modern Glacial Environments, Processes, Dynamics and Sediments*, Vol. 1 (Ed. Menzies, J.), pp. 65–416. Butterworth-Heinemann, Oxford.

Maizels, J.K. (1997) Jökulhlaup deposits in proglacial areas. *Quat. Sci. Rev.* **16**, 793–819.

Martini, I.P. (1977) Gravelly flood deposits of Irvine Creek, Ontario, Canada. *Sedimentology* **24**, 603–622.

MIALL, A.D. (1978) Lithofacies types and vertical profile models in braided river deposits: a summery. In: *Fluvial Sedimentology* (Ed. Miall, A.D.), Mem. Can. Soc. petrol. Geol., Calgary, **5**, 597–604.

MIDDLETON, G.V. (1965) Antidune cross-bedding in a large flume. *J. sediment. Petrol.* **35**, 922–927.

NUMMEDAL, D., HINE, A.C. & BOOTHROYD, J.C. (1987) Holocene evolution of the south-central coast of Iceland. In: *Glaciated Coasts* (Eds Fitzgerald, D. & Rosen, P.S.), pp. 115–150. Academic Press, San Diego.

O'CONNOR, J.E. (1993) Hydrology, hydraulics, and geomorphology of the Bonneville Flood. *Geol. Soc. Am. Spec. Pap.* **274**, 83 pp.

PATTON, P.C. & BAKER, V.R. (1978) Origin of the Cheney–Palouse Scabland tract. In: *The Channelled Scabland: Comparative Planetary Geology Field Conference Guidebook, Columbia Basin* (Eds Baker, V.R. & Nummedal, D.), pp. 117–128. National Aeronautics Space Administration, Washington, DC.

PEABODY, F.E. (1947) Current crescents in the Triassic Moenkopi Formation. *J. sediment. Petrol.* **17**, 73–76.

PICKERING, K.T. & HISCOTT, R.N. (1985) Contained (reflected) turbidity currents from the Middle Ordovician Cloridorme Formation, Quebec, Canada: an alternative to the antidune hypothesis. *Sedimentology* **32**, 373–394.

PRAVE, A.R. & DUKE, W.L. (1990) Small-scale hummocky cross-stratification in turbidites: a form of antidune stratification? *Sedimentology* **37**, 531–539.

RAUDKIVI, A.J. (1991) Scour at bridge piers. In: *Scouring Hydraulic Structures Design Manual 2* (Eds Breusers, H.N.C. & Raudkivi, A.J.), Bull. int. Assoc. Hydraul. Res., pp. 61–98. A.A. Balkema, Rotterdam.

RICHARDSON, P.D. (1968) The generation of scour marks near obstacles. *J. sediment. Petrol.* **38**, 965–970.

RUSSELL, A.J. (1993) Obstacle marks produced by flow around stranded ice blocks during a glacier outburst flood (jökulhlaup) in west Greenland. *Sedimentology* **40**, 1091–1111.

RUSSELL, A.J. & KNUDSEN, Ó. (1999) Controls on the sedimentology of the November 1996 jökulhlaup deposits, Skeiðarársandur, Iceland. In: *Fluvial Sedimentology VI* (Eds Smith, N.D. & Rogers, J.), Spec. Publs int. Ass. Sediment., No. 28, pp. 315–329. Blackwell Science, Oxford.

RUSSELL, A.J. & MARREN, P. (1999) Proglacial fluvial sedimentary sequences in Greenland and Iceland: a case study from active proglacial environments subject to jökulhlaups. In: *The Description and Analysis of Quaternary Stratigraphic Field Sections* (Eds Jones, A.P., Tucker, M.E. & Hart, J.K.), pp. 171–208. Technical Guide Number 7, Quaternary Research Association, London.

RUSSELL, A.J., KNUDSEN, Ó., FAY, H.J.K., MARREN, P.M., HEINZ, J. & TRONICKE, J. (2001) Morphology and sedimentology of a giant, ice-walled jökulhlaup channel, Skeiðarárjökull, Iceland: implications for esker genesis. *Global planet. Change* **28**, 193–216.

SCHOLZ, H., SCHEIBER, B. & FUNK, H. (1988) Der einfluss von Gletscherlaufen auf die schmelzwasserablagerungen des Russell-Gletschers bei Søndre Strømfjord (WestGrönland). *Z. Gletscherk. Glazialgeol.* **24**, 55–74.

SENGUPTA, S. (1966) Studies on the orientation and imbrication of pebbles with respect to cross-stratification. *J. sediment. Petrol.* **36**, 362–369.

SNORRASON, Á., JÓNSSON, P., PÁLSSON, S., *et al.* (1997) Hlaupið Á Skeiðarásandi Haustið 1996 Útbreiðsla, rennsli og aurburður. In: *Vatnajökull: Gos og Hlaup* (Ed. Haraldson, R.H.), pp. 79–137. Vegagerðin, Reykjavík.

SOHN, Y.K. (1997) On traction-carpet sedimentation. *J. sediment. Res.* **67**, 502–509.

TODD, S.P. (1989) Stream-driven, high-density gravelly traction carpets: possible deposits in the Trabeg Conglomerate Formation, SW Ireland and some theoretical considerations of their origin. *Sedimentology* **36**, 513–530.

WERNER, F. & NEWTON, R.S. (1975) The pattern of large-scale bedforms in the Langeland Belt (Baltic Sea). *Mar. Geol.* **19**, 29–59.

YAGISHITA, K. (1994) Antidunes and traction-carpet deposits in deep-water channel sandstones, Cretaceous, British Columbia, Canada. *J. sediment. Petrol.* **A64**, 34–41.

YAGISHITA, K. & TAIRA, A. (1989) Grain fabric of a laboratory antidune. *Sedimentology* **36**, 1001–1005.

Spec. Publs int. Ass. Sediment. (2002) **32**, 99–109

A large-scale flood event in 1994 from the mid-Canterbury Plains, New Zealand, and implications for ancient fluvial deposits

G. H. BROWNE

Institute of Geological and Nuclear Sciences, PO Box 30368, Lower Hutt, New Zealand (Email: g.browne@gns.cri.nz)

ABSTRACT

Major flooding occurred in mid-Canterbury rivers of the South Island of New Zealand on 9 January 1994. Maximum flood discharges of 5594 cumecs were recorded in the Rakaia River, the highest in this river in over 40 yr of recordings. Flooding in the large braided rivers of mid-Canterbury is related to heavy orographic rainfall in the west, in alpine catchments of the Southern Alps. Over a three-day period immediately preceding and subsequent to the flooding, areas on the west coast of the South Island received 80–85% of their average January rainfall. On one of those days (8 January 1994, the day prior to the flooding event in the Canterbury rivers), the daily precipitation exceeded 190 mm for one of these west coast sites, some 40% of the average total monthly rainfall for January.

At the height of the flood, a 400-m-wide flood channel was created at the mouths of the Rakaia and Rangitata rivers, with flood discharge eroding the gravel beach normally fronting the rivers to the Pacific Ocean. This flood channel was subsequently modified and eventually was plugged by littoral sediment transported northward by longshore drift. Extensive chipping, scratching, and pitting of large boulders in the rivers indicates that mechanical abrasion of fluvial clasts is an important agent in downstream clast-size reduction.

Analogue strata of last glacial to latest Pleistocene age exposed in coastal cliffs adjacent to the Canterbury Plains show little evidence of fine-grained (silt- and clay-size) sediment. Where present, fine-grained sediment is confined to discrete permeability-controlled layers or clay bands (such as along foreset stratification). Based on observations of flood deposits in the modern deposits, these ancient sediments were probably deposited with considerable fine-grained sediment. It is inferred that fines are removed from the fluvial deposit, aeither by aeolian transport, or by interstitial water movement, some being concentrated in the distinct clay-bands.

INTRODUCTION

Floods in coarse-grained braided rivers are frequent events, closely related to major rainstorms, and/or snowmelt cycles (Miall, 1985). Like other large, coarse-grained braided rivers, those of the Canterbury Plains, South Island, New Zealand flood frequently, in this case, during the summer months of October to April (Griffiths, 1979; Griffiths & McSaveney, 1983; Waugh, 1983). In Canterbury, such high precipitation events are confined to the mountainous catchments in the Southern Alps (to elevations > 3700 m), many tens of kilometres west of the Canterbury Plains.

The Canterbury Plains along the eastern margin of the South Island are up to 70 km wide and 185 km long, and comprise an expansive braidplain (Fig. 1), underlain by > 500 m of Plio-Pleistocene fluvial and shallow marine gravel, sand, siltstone and lignite. In mid-Canterbury, the larger rivers are the Rakaia and Rangitata, with mean annual discharges of 190 and 90 cumecs, respectively. Each river has a source area in glaciated catchments of the Southern Alps, and enters the plains through a gorge incised into Mesozoic greywacke basement rocks. Smaller rivers in mid-Canterbury such as the Ashburton and Hinds rivers have considerably smaller catchments that are confined to the foothills of the Southern Alps. All rivers crossing the plains display an upstream and a downstream incised portion, separated by a zone of minimal erosion, an area that is prone to channel avulsion (Leckie,

Flood and Megaflood Processes and Deposits: Recent and Ancient Examples. Edited by I. Peter Martini, Victor R. Baker and Guillermina Garzón © 2002 International Association of Sedimentologists. ISBN: 978-0-632-06404-5

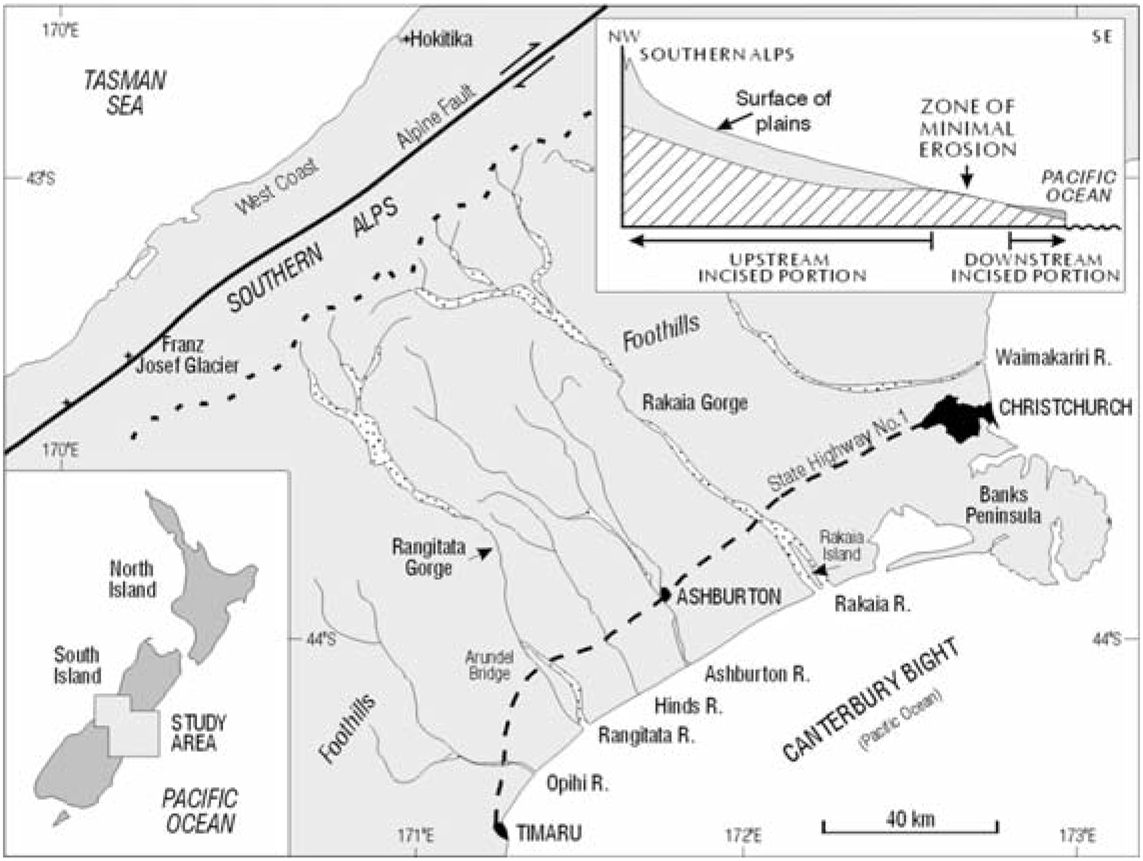

Fig. 1. Location map of the Canterbury Plains, and the rivers that cross it. Inset map shows study area location. Inset cross-section (from Leckie, 1994) shows a representative NW–SE profile through the Canterbury Plains, with zones of upstream and downstream incision, separated by a zone of minimal erosion.

1994). The vast majority of clasts in the rivers, and those making up the surface of the plains, comprise greywacke sandstone derived from the Carboniferous to earliest Cretaceous Torlesse Terrane, which makes up the bulk of the Southern Alps (MacKinnon, 1983; Bradshaw, 1989; Mortimer, 1995). Minor clast types include Cretaceous rhyolite, and a range of Late Cretaceous and Tertiary sandstone, siltstone, limestone and sub-bituminous coal to lignite lithologies (Field & Browne, 1989; Oliver & Keene, 1989).

All rivers show a meandering thalweg pattern immediately downstream of their respective gorges (Carson, 1984, 1986), which evolves into braided channels that persist to the river mouths, where they enter the Pacific Ocean along the Canterbury Bight (Figs 1 & 2).

Sediment yields from specific South Island catchments average 1856 ± 261 t km^{-2} yr^{-1} compared with the world average of 182 t km^{-2} yr^{-1}, and are among the highest known sediment yields (Griffiths & Glasby, 1985). Suspended load comprises 93% of the total sediment load transported during floods, whereas bedload in South Island rivers is minimal, and comprises only about 3% of the total load (Adams, 1980). Studies by Adams (1980) indicate that the bedload transport rates are highest in the headwaters of the Southern Alps, and decrease toward the coast. In this study it is shown that it is the bedload component that tends to be evident after the flood event, although Adams (1980) showed that this was a minor proportion of the total sediment load when the river was in flood. The suspended load sediment (sand and mud) is quickly lost from the resultant deposit, and is poorly preserved in the geological record.

The purpose of this paper is to document a large flood event that occurred in the mid-Canterbury rivers

Fig. 2. Photograph of the braided Rakaia River (looking downstream). The river is incised into older (loess mantled) floodplain deposits (on right). Total width of area of active channels in foreground is approximately 500 m.

during January 1994. In the case of the Rakaia River, this flood was the largest in over 40 yr of river gauging history. The preceding meteorological conditions of the flood event are described, as are observations made during and subsequent to the flood event. Implications for ancient fluvial deposits are also described, and some possible implications for petroleum reservoir equivalents indicated.

METEOROLOGICAL CONDITIONS RELATED TO FLOODING

Flood events in the large rivers of mid-Canterbury occur during late spring and summer (October–April) in association with major orographic rainfall in the Southern Alps, augmented by snowmelt (Kirk *et al.*, 1977; Griffiths, 1979; Griffiths & McSaveney, 1983; Waugh, 1983; Leckie, 1994). Flooding in these rivers is associated with strong frontal westerly wind conditions that result in excessive precipitation (> 200 mm day^{-1}) in the catchments of the Southern Alps. Flooding in the large rivers of Canterbury takes place when precipitation has an intensity of 0.2–0.3 m in a 24-h period (Griffiths, 1979). In contrast, flooding in the smaller rivers of mid-Canterbury (the Ashburton and Hinds rivers) occurs during winter months when easterly and south-easterly wind conditions prevail and produce excessive precipitation (up to 100 mm day^{-1}) in foothill catchments (Soons, 1968; Griffiths, 1979). The timing of flooding in the large rivers (summer) versus the smaller rivers (winter) therefore is quite distinct.

A significant flood event occurred in the large rivers of mid-Canterbury on 9 January 1994. Discharge measured at the Rakaia Gorge (Fig. 1) gauging station (instantaneous recording) peaked at 5594 cumecs at 2330 hours on 9 January 1994 (G. Davenport, personal communication, 1994). The Gumbel plot shown in Fig. 3 shows the largest flood events in the Rakaia River since records were established in 1957. The 1994 flood event has a calculated return probability of 0.04 or approximately a 40-yr return period (G. Davenport, personal communication, 1994). Similar, and equally dramatic flooding occurred in the Rangitata River

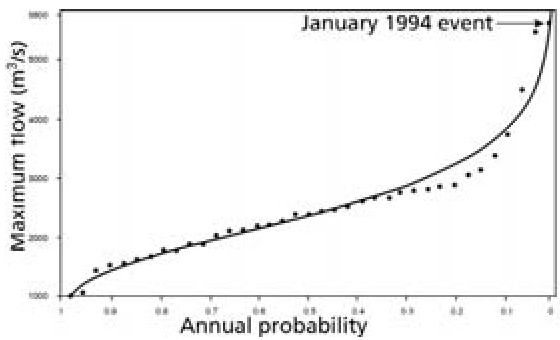

Fig. 3. Gumbel distribution for the Rakaia River for flood data recorded between 1957 and 1994. The plot shows maximum flow data collected at the gorge gauging station of the Rakaia River over the past 40 yr. The maximum flow (cumecs) is plotted against an annual probability scale of 0–1. Major flood events over this 40-yr period are plotted as discrete data points. Three flood events have maximum flows > 4000 cumecs. The January 1994 event was the highest discharge recorded in the river (5594 cumecs) with a calculated return probability of 0.04, or approximately a 40-yr return period. Data from the National Institute of Water and Atmospheric Research (NIWA), Christchurch.

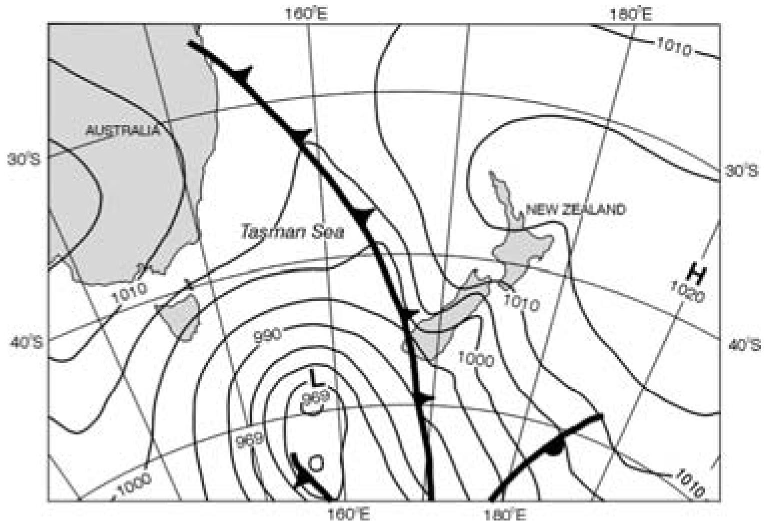

Fig. 4. Meteorological map for New Zealand and Tasman Sea area at 0000 hours (NZST), 9 January 1994 (courtesy of Meteorological Service of New Zealand Ltd). The map shows a large cold front in the Tasman Sea, about to cross the western side of the South Island, New Zealand. Isobaric pressure and isobars in hPa.

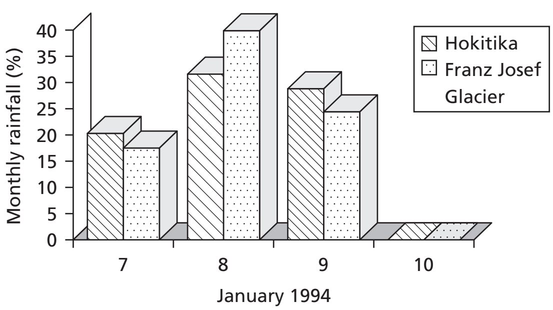

Fig. 5. Percentage of mean monthly rainfall recorded between 7 and 10 January 1994 at the two sites Hokitika and Franz Josef Glacier on the west coast of South Island (see Fig. 1).

during the same period (approximate peak discharge of 2640 cumecs: J. Young, personal communication, 1994), although two other flood events in this river (in 1957, 3460 cumecs and in 1979, 3440 cumecs) were larger. A flood of the 1994 magnitude in the Rangitata River has a return period of approximately 20 yr (G. Davenport, personal communication, 1994).

Although the westerly winds that accompany flooding are dominant throughout the year (Fig. 4; Hessell, 1982), during winter the resultant precipitation is represented by snow and is effectively 'locked' into the mountain catchments. Annual precipitation up to 13 000 mm has been recorded in some mountain areas (Griffiths & McSaveney, 1983), and daily rainfall up to 250 mm is common in summer months (Tomlinson, 1976). Over a three-day period from 7 to 9 January 1994, 80% of the mean monthly rainfall fell at both Franz Josef Glacier and Hokitika (Fig. 5). This rainfall peaked on 8 January, when 190 mm was recorded at Franz Josef Glacier (some 40% of the average total rainfall for the month of January fell on this day), and 80 mm at Hokitika (32% of the monthly average; Fig. 5). Note that these precipitation data are for catchments west of the main divide, and precipitation rates at the divide would have been considerably higher, although there are no rainfall data available at these altitudes. Flooding of the large rivers of mid-Canterbury does not relate to weather conditions on the Canterbury Plains but rather to precipitation occurring many tens of kilometres to the west in the Southern Alps (Griffiths, 1979; Waugh, 1983).

The consequences were considerable in the large rivers of mid-Canterbury. Extensive surface flooding occurred around State Highway 1 adjacent to both the Rakaia and Rangitata rivers (Fig. 1). Considerable threat was also created to road and rail bridges, farmland and rural communities. Plate 1 (facing p.104) shows the before and after situations at the Arundel Bridge, Rangitata River. At the coast, discharge from the rivers developed a large sediment plume that extended several kilometres offshore (Plate 2, facing p.104).

OBSERVATIONS MADE FROM THE JANUARY 1994 FLOOD

The interplay of rivers and the sea

Under normal fluvial flow conditions, the mid-Canterbury rivers enter the sea through a freshwater

Fig. 6. Flood channel of the Rakaia River on 10 January 1994. The photograph was taken on the south side of the flood channel, and shows a 400-m-wide flood channel cut through the former gravel beach (north margin of flood channel to left). Two-metre-high standing waves in the flood channel can be seen adjacent to the south channel margin, and a series of breaking waves can be seen offshore (cf. Rangitata River in Plate 2, facing p.104). These waves are breaking over a cone-shaped flood delta comprising coarse-grained fluvial gravels.

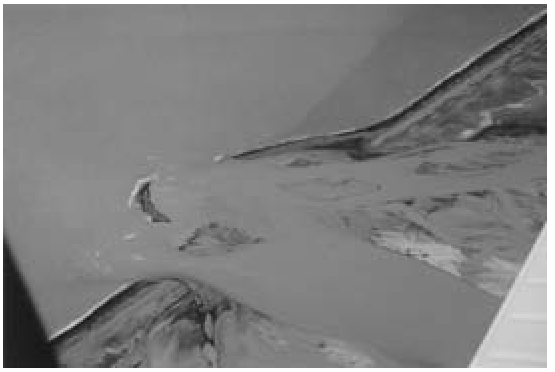

Fig. 7. Aerial view of Rakaia River mouth, taken on 12 January 1994. Figure 6 was taken two days earlier on the south bank of the flood channel (to right), looking toward the flood delta. The flood delta is clearly visible approximately 200 m offshore, and is accreted to the gravel beachface on its south side. The flood channel is at the apex of the flood delta, but during falling stage, a new channel has formed on the northern side of the flood delta (lower foreground). This subsidiary channel has in part destroyed the northern portion of the flood delta. Total channel width is approximately 500 m.

lagoon (Kelk, 1974; Kirk *et al.*, 1977; Todd, 1983; Kirk, 1991; Goring & Valentine, 1995). The rivers are fronted by a gravel barrier, and river flow is directed northward behind the barrier, for several hundred metres, before entering the sea (Plate 3, facing p.104). During major flooding, however, both the Rakaia and Rangitata rivers discharge directly to the sea by breaching the gravel beach, and cutting off the formerly occupied north-directed channel (Plate 2 and Fig. 6; Kelk, 1974; Todd, 1983; Kirk, 1991). In the January 1994 event, both the Rakaia and Rangitata rivers eroded the barrier, and in each case the flood channel that developed was approximately 400 m wide (Plate 2 and Fig. 6). The flood channel was closely associated with an arcuate-shaped subtidal flood delta (Plate 2 and Figs 6 & 7; Kirk, 1991). This flood delta comprised a cone of gravel (this feature was exposed above sea-level several days after the flood), which extended approximately 200 m seaward of the pre-existing gravel beachface. In Plate 2 and Figs 6 & 7, waves can be seen breaking over this flood delta. Observations made by the author on 10 January 1994 indicate that standing waves as much as 2 m high occur in the flood channel, and a visual estimate of flow velocity between 5 and 6 m s^{-1} (Fig. 6).

During falling stage, however, sediment supply through the flood channel was unable to keep up with the strong north-directed longshore drift in the littoral zone, and the mouth of the flood channel became increasingly modified by wave attack and longshore drift marine processes (Fig. 8). Longshore drift is particularly strong in the Canterbury Bight area, and studies have indicated that gravel up to cobble size, along with sand, is transported at rates of 400 000–700 000 m^3 yr^{-1} by longshore drift (Kirk & Hewson, 1978; Kirk & Tierney, 1978). The former flood channel in a matter of a few days became filled by falling stage fluvial sediment, and more significantly by gravel deposited by wave attack and north-directed longshore drift (Fig. 8C). Over the course of several months these two processes developed a new north-directed gravel spit similar to the original steady-state gravel spit, but slightly seaward of the former spit (Fig. 8D & E; Kelk, 1974; Kirk *et al.*, 1977; Todd, 1983; Kirk, 1991).

The return to 'equilibrium state' conditions that develop several months after the flood event are well illustrated in the smaller but comparable Ashburton River (Fig. 9). A freshwater lagoon area behind the beach marks a former fluvial discharge channel that once was directed north behind a gravel barrier (Plate 3, facing p.104). Flooding in the Ashburton River cut a flood channel directly into the Pacific Ocean (narrow beachface area in Fig. 9A labelled 'FC'). Subsequent to that event, beach gravel accreted from the south by longshore drift, such that a new beachface formed across the former fluvial discharge channel, to form a

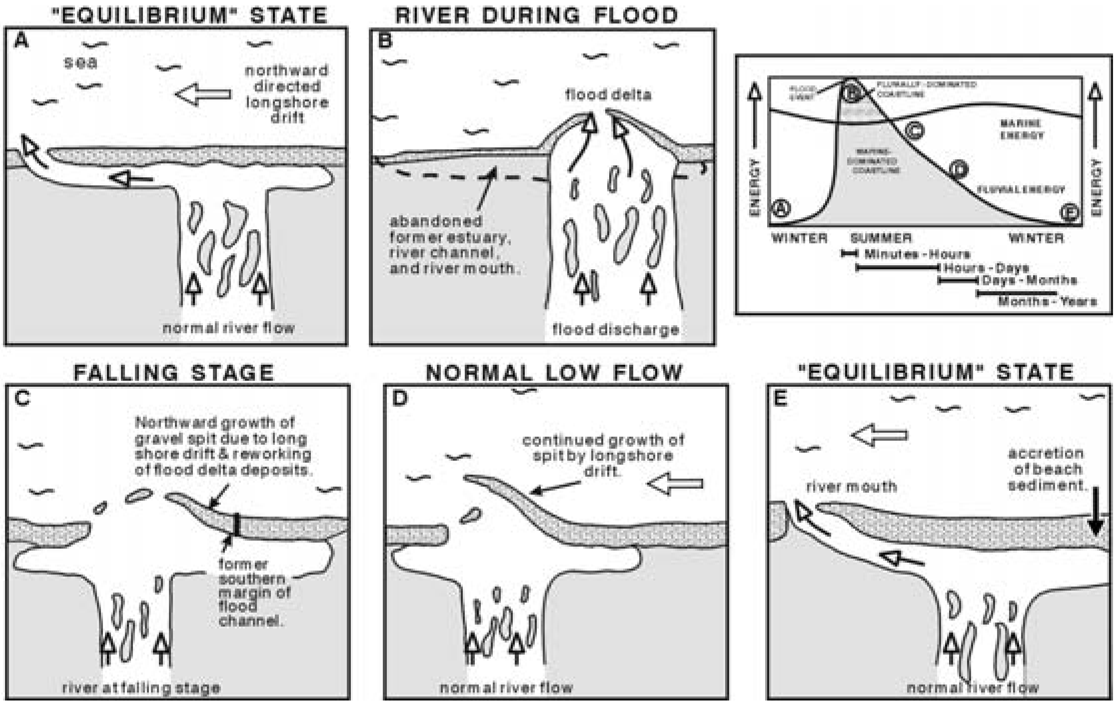

Fig. 8. Cartoon showing the evolution of river mouth development, from equilibrium state (A), through a major flood event (B–C), and the restoration to the equilibrium state (D–E). This process may take months to years. The model is based on observations of the 1994 flood and post-flood events (cf. Kelk, 1974; Todd, 1983; Kirk, 1991). Inset diagram is a schematic plot showing relative changes in fluvial and marine energy through time. River mouth developmental stages A–E are shown.

new gravel spit seaward of the former beach. Figure 9B shows these relationships at ground level. Similar scenarios for river flood and coastal interactions have been described in California by Hicks & Inman (1987), and in eastern Australia by Wright *et al.* (1980).

Sediment deposited during the 1994 flood

During the 1994 event, flood discharge extended from bank to bank in both the Rakaia and Rangitata rivers. In the case of the Rakaia River near the State Highway 1 bridge, the maximum width from bank to bank was 1.9 km. In the case of the Rangitata River, the bank to bank width was < 1 km. This, together with the different flood discharges in the two rivers, not surprisingly produced differences in flood deposit thickness, grain size and distribution in each of the rivers. In the Rakaia River, the flood deposit was relatively thin (< 0.5 m thick) but was extensive across the entire width of the river. Flood deposits in the Rangitata River were coarser grained, generally thicker (up to 1 m thick), but were more localized, and were confined largely to braid channel areas.

In both rivers, the flood deposit was typically a sandy gravel, with abundant log and other vegetation debris, with less abundant blocks of < 50 cm diameter, and bank-derived silt. The flood deposit was little different in grain size or sorting characteristics from the remainder of the sediment within the rivers, although this was not quantified in a rigorous manner. In the Rakaia River, both flood-deposited and pre-flood gravel has a mean *b*-axis dimension of 76 mm at the gorge (31 clasts), fining to 40 mm (31 clasts) at the coast. In the Rangitata River the mean *b*-axis clast size change is 80 mm at the gorge to 38 mm at the coast (measurements from 31 clasts at each site; G. Browne, unpublished data). After a few months, flood deposits were unrecognizable from the remainder of the braided river sediment. The inference therefore is that flood deposits are probably difficult to differentiate from the other, 'normal state' deposits, in such coarse-grained deposits. This appears to be true of last glacial fluvial gravels exposed in the coastal section adjacent to the Canterbury Bight (Browne & Thrasher, 1996; Ashworth *et al.*, 1999).

During the 1994 flood event, considerable flood

Fig. 9. (A) Aerial view of the Ashburton River mouth looking north showing geomorphological features of late-stage river mouth restoration to the equilibrium state (see text and Fig. 8D–E): AR, Ashburton River; FC, site of former flood channel; L, lagoon; S, newly accreted gravel spit; DC, new discharge channel; Po, Pacific Ocean (Canterbury Bight). Scale is indicated by houses on north bank. (B) Ground view of Ashburton River mouth taken from the south side of the new discharge channel (DC) looking north. Abbreviations used are the same as in (A). The new discharge channel is approximately 10 m wide.

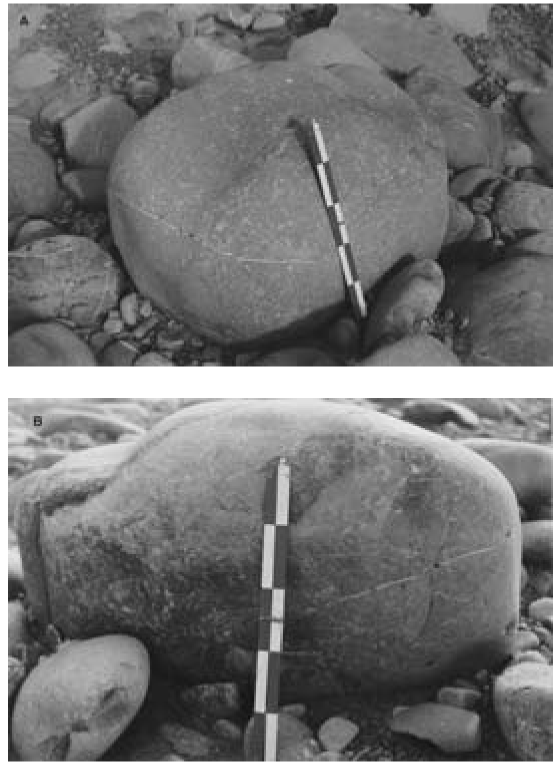

Fig. 10. A large boulder from the Rangitata River photographed from (A) an upstream (stoss) and (B) a downstream view, after the January 1994 flood. In the upstream view the boulder shows numerous scratch, percussion and grinding markings, whereas the downstream side is less marked, and retains abundant limonite staining. Scale is 50 cm with 10 cm divisions.

damage was reported throughout the zone of minimal erosion (*Christchurch Press*, 11 January 1994). Surficial flooding occurred immediately north of the Rakaia River along State Highway 1, and the road was closed for several hours while waters receded. Further downstream, the river breached the right bank, and caused considerable localized bank erosion over a 500-m reach. Considerable surface flooding occurred on the south side of the Rangitata River and for several kilometres downstream of State Highway 1. As a consequence considerable bank stabilization works subsequently have been undertaken in both rivers.

Downstream changes in clast size

Downstream clast size reduction is commonly observed in modern graded-bed rivers (Bradley, 1970; Griffiths, 1979; Knighton, 1982; Shaw & Kellerhals, 1982; Parker, 1991a,b; Kodama, 1994), although there is considerable debate regarding whether this is caused by hydraulic sorting or abrasion processes (Kodama, 1994).

From this study, it is not clear which of these processes is more significant, or if indeed both sorting and abrasion processes operate. Following the flood event, however, abrasion is evident in clasts from both rivers (Fig. 10). The upstream (stoss) side of large boulders (> 50 cm diameter) are lighter in colour, and show various surface markings, such as chips broken away from boulder margins, scratch-marks and scours, and various forms of pitting. The downstream side of the same boulders are often iron-stained, and lack the same degree of surface markings. Preservation of iron-staining suggests that these boulders were not rolled downstream or rotated during flooding, and were pitted and marked *in situ* during flooding. Although not all the surface markings can be related to the 1994 flood, they do attest to significant mechanical abrasion processes during flooding.

Engineering concerns

In the zone of minimal erosion (Leckie, 1994), a considerable threat is posed by flooding. This zone stretches over a distance of 10–15 km in both the Rakaia and Rangitata rivers, where the height of the river terrace is only 1–2 m above the gravel bed. On the south bank of the Rangitata River, groynes have been constructed to deflect flood discharge into the main river channel, and prevent it flowing down the South Branch, an abandoned former channel of the river. Blocking the South Branch in this manner effectively eliminates a natural escape route for flood waters, and places farmland, road and rail bridges, and the small community of Rangitata at greater risk of flooding than if the South Branch had remained open.

IMPLICATIONS FOR ANCIENT FLUVIAL DEPOSITS

Post-depositional loss of fines

During floods a large amount of suspended sediment is transported to the sea (Plate 2, facing p.104). Gibb & Adams (1982) calculated suspended loads in the Rakaia and Rangitata rivers of 8.56 and 2.61 Mt yr^{-1}, respectively. Observations made by the author indicate that fine-grained material, deposited along with sand and gravel-size sediment during the flood, is quickly removed from the resulting bedform. Fine-grained material is taken to include clay, silt and sand. The process of fines-depletion starts during falling stage. The bedform loses interstitial water during falling stage, by infiltration downward through, and horizontally along, abandoned bedforms. Small sand and mud sediment deltas developed during falling stage and channel abandonment attest to the volume of such fine-grained material moving interstitially through such bedforms (Fig. 11). In addition, observations made here indicate that rainfall washes fines through gravel bars and abandoned channel deposits where it accumulates in underlying layers.

Fig. 11. Small deltas built into a former pond during falling stage (strandlines indicate the former margin of the pond), Rakaia River, January 1994. These deltas were deposited from fine-grained sediment that had passed through the bar behind. The photograph illustrates that considerable fines are removed from former flood deposits by interstitial water movement through abandoned bedforms. Scale is 50 cm long with 10 cm divisions.

Once the flood deposits have dried out, sand and mud at the surface is subjected to removal by wind. The Canterbury 'nor-wester' is a common occurrence on the Canterbury Plains (Tomlinson, 1976), which is capable of carrying silt- and clay-sized sediment tens of metres into the air. Wind also moves coarser, sand-size sediment by saltation, often developing metre-scale climbing ripple laminated bedforms on the lee side of surface obstacles such as trees, roots and large rocks (Fig. 12).

Interstitial water and aeolian processes are therefore efficient mechanisms for the downward flushing and/or removal of fines, especially from the top of the bed. Within the fluvial deposits, fines appear to move by interstitial flow (not from direct observation but evident from Fig. 11). Over time, fines will continue to be lost from the deposit and the resultant fluvial deposit is very much biased toward coarser clast sizes. Fines depletion has implications for ancient deposits as described below.

Post-depositional introduction of clay bands

Ancient lowstand fluvial deposits equivalent to those described above (Burnham Formation of Suggate, 1963) are exposed in an impressive 60-km-long coastal section along the Canterbury Bight (Fig. 1). In these analogue strata of last glacial age, there is an abundance of sandy matrix-supported massive gravel (often with a long-axis pebble alignment), trough cross-

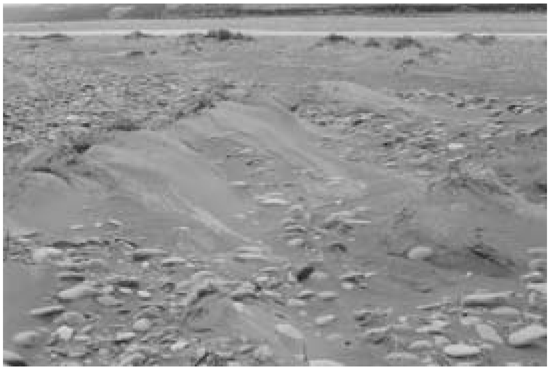

Fig. 12. Photograph of the bed of the Rakaia River, two months after the flood event showing extensive aeolian sand deposits on the lee side of shrubs and flood debris. Under strong summer prevailing north-west wind conditions, sand and finer grained sediments can be transported tens of kilometres downwind. This is an important process in removing fines (in this case fines include sediment up to medium-grained sand) from flood deposits. Wind direction is from top left to bottom right (towards observer).

Fig. 13. Centimetre-thick clay bands within late Pleistocene (Burnham Formation) gravels, Canterbury coastal section. Clay layers are concentrated along bounding sets and foreset stratification in planar tabular cross-bedded gravels. Clay bands like this were deposited by interstitial fluids moving through the deposit, a continuation of the processes happening in near-surface settings (cf. Fig. 11). Scale is 50 cm with 10 cm divisions.

bedded gravel and planar tabular gravel (Browne & Thrasher, 1996; Ashworth *et al.*, 1999). Most gravels are mixtures of sand and gravel (closed framework), with less common, thin (< 1 m thick) but discrete intervals of open framework gravels. Gravels of the Burnham Formation form stratal sets 1–3 m thick, intercalated with minor lenticular sand and loess-silt layers.

Various mechanisms have been invoked to explain coarse fluvial deposits with intercalated open and closed framework textures. Smith (1974) recognized as many as four alternating open and closed framework couplets within a single bar deposit, and interpreted them to be deposited from alternating fluvial discharge events. Open framework gravels were thought to represent high flow when fines were carried in suspension, while closed framework gravels were considered to represent low discharge. Changes between open and closed framework gravels have been attributed to other factors such as winnowing on foresets, periodic arrival of smaller bedforms on large gravel bars, and avalanching of gravel at bar crests (Rust, 1984). The evidence from this study suggests an alternative explanation for intercalations of open and closed framework gravel in which interstitial or ground water moves through the deposit, removing fines in open framework situations, and redepositing fines as closed framework gravels.

Mud-size sediment is in general lacking within the matrix and, where present, is confined to distinct, centimetre-thick layers such as the base of palaeochannels or along foresets (Fig. 13). These layers are referred to as clay bands, and clays within the strata appear to be confined to zones of contrasting permeability. Such clay bands represent sedimentation from ground water at zones of contrasting permeability, and appear to represent the end products of the immediately post-depositional process of fines remobilization (that is removal and redeposition) occurring within deposits of the modern rivers (Fig. 11).

Ancient braided river sediments described elsewhere show many similar characteristics. Rust (1984), for example, described an abundance of horizontally bedded and massive conglomerate from the Devonian Malbaie Formation, Quebec, and speculated that the matrix (coarse sand and granules) accumulated by subsequent infiltration at a lower flow stage. Similar mechanisms have been suggested by Eynon & Walker (1974) for Pleistocene gravels.

Implications for fluvial petroleum reservoirs

Ancient fluvial deposits are significant petroleum reservoir facies in many parts of the world (such as Prudhoe Bay, Alaska, the North Sea; Martin, 1993; Parkinson & Hines, 1995). Developing models that adequately predict their subsurface attributes are difficult because of their inherent heterogeneity of facies types, stratal architecture, and the range of spatial dimensions of channel systems (Miall, 1988; Martin, 1993; Webb, 1994; Olsen, 1995).

The post-depositional loss or redeposition of fine-grained sediment (as described above) suggests that the grain-size distribution of the resultant deposit is quite different from the fluvial sediment that was deposited originally. Over a relatively short time period, fines depletion will considerably favour permeability in certain zones and probably also enhance porosity characteristics of the deposit. The abundance of stacked fluvial channel systems observed in ancient equivalents will enhance vertical communication within a petroleum reservoir setting, provided that the bounding surfaces are not lined with silt. Clay layers, however, might act as internal baffles to communication in the reservoir, and hence reduce the flow of fluids. However, based on stratal geometries observed in the coastal cliff section, such clay layers occur over a lateral extent of only a few metres, and therefore would not be a major concern in a hydrocarbon reservoir context.

CONCLUSIONS

Flooding in the major rivers of mid-Canterbury is related to heavy orographic rainfall in the Southern Alps rather than to rainfall falling on the Canterbury Plains themselves. These meteorological conditions typically occur during summer months (October–April). The present study demonstrates that in large braided rivers, flooding may not be related to local meteorological conditions, and that the effects of flooding are confined largely to the fluvial channels themselves, except in a relatively narrow zone, where the rivers are not greatly incised into the floodplain. Major changes occur at the river mouths, where the gravel beach is breached by a flood channel.

In terms of recognition of similar ancient deposits, observations made from late Pleistocene outcrop equivalent strata suggest the recognition of flood deposits versus normal braided river deposits is not obvious. Fines will tend to be under represented in ancient deposits, although they were a major component of the total sediment load during flood conditions. In the Canterbury case, fines depletion and redeposition occurs by a variety of processes, including aeolian winnowing, and by the migration of water through the deposits.

ACKNOWLEDGEMENTS

Discussions were held with various colleagues, and in particular I would like to thank Adriaan Bal and Bob Kirk (University of Canterbury), Derek Todd (Tonkin & Taylor, Christchurch), Dale Leckie (Canadian Occidental Petroleum Ltd), Tim Naish (GNS), Phil Ashworth, Jim Best and Merren Jones (University of Leeds). Data were obtained from John Young (Rangitata Diversion Race Management Ltd) and Graeme Davenport, National Institute of Water and Atmospheric Sciences (NIWA), Christchurch. Permission to publish photographs by John Bisset (The Timaru Herald) and Lloyd Homer (Landscape Photographer—Lloyd Homer Ltd) is greatly appreciated. Meteorological Service of New Zealand Ltd allowed publication of climatic data (Fig. 4). Reviews by Peter Ashmore (University of Western Ontario), Martin Gibling (Dalhousie University), and Dale Leckie (Canadian Occidental Petroleum Ltd) are much appreciated. Figures were drafted by Sue Shaw, Jeremy Smith and Sarah Thornton (GNS). Funding for this work was received from the Foundation for Science and Research (FRST), contract CO5806. This contribution is GNS publication 1654.

REFERENCES

Adams, J. (1980) Contemporary uplift and erosion of the Southern Alps, New Zealand. *Geol. Soc. Am. Bull.* **91**, 1–114.

Ashworth, P.J., Best, J.L., Peakall, J. & Lorsong, J.A. (1999) The influence of aggradation rate on braided alluvial architecture: field study and physical scale modelling of the Ashburton River gravels, Canterbury Plains, New Zealand. In: *Fluvial Sedimentology VI* (Eds Smith, N.D. & Rogers, J.), Spec. Publs int. Ass. Sediment., No. 28, pp. 333–346. Blackwell Science, Oxford.

Bradley, W.C. (1970) Effect of weathering on abrasion of granitic gravel, Colorado River (Texas). *Geol. Soc. Am. Bull.* **81**, 61–80.

Bradshaw, J.D. (1989) Cretaceous geotectonics patterns in the New Zealand region. *Tectonics* **8**, 803–820.

Browne, G.H. & Thrasher, G.P. (1996) *Stratal Patterns and Sedimentology of Lowstand Deposits of Mid-Canterbury, New Zealand.* Science Report 96/13, Institute of Geological and Nuclear Sciences, Lower Hutt.

Carson, M.A. (1984) Observations on the meandering–braided river transition, the Canterbury Plains, New Zealand: Part 1. *N. Z. Geogr.* **40**, 12–17.

Carson, M.A. (1986) Characteristics of high-energy 'meandering' rivers: the Canterbury Plains, New Zealand. *Geol. Soc. Am. Bull.* **97**, 886–895.

Eynon, G. & Walker, R.G. (1974) Facies relationships in Pleistocene outwash gravels, southern Ontario: a model for bar growth in braided rivers. *Sedimentology* **21**, 43–70.

Field, B.D. & Browne, G.H. (1989) Cretaceous and Cenozoic sedimentary basins and geological evolution of the Canterbury region, South Island, New Zealand. *N. Z. geol. Surv. Basin Stud.* **2**, 94 pp.

GIBB, J.G. & ADAMS, J. (1982) A sediment budget for the east coast between Oamaru and Banks Peninsula, South Island, New Zealand. *N. Z. Geol. Geophys.* **25**, 335–352.

GORING, D. & VALENTINE, E. (1995) Gravel-bed river mouths. *New Zealand Meteorological and Hydrological Symposium*, University of Canterbury, Christchurch. Programme and Abstracts.

GRIFFITHS, G.A. (1979) Recent sedimentation history of the Waimakariri River, New Zealand. *J. Hydrol. (NZ)* **18**, 6–28.

GRIFFITHS, G.A. & GLASBY, G.P. (1985) Input of river derived sediments to the New Zealand continental shelf: I. Mass. *Estuar. coast. Shelf Sci.* **21**, 773–787.

GRIFFITHS, G.A. & MCSAVENEY, M.J. (1983) Distribution of mean annual precipitation across steepland regions of New Zealand. *N. Z. J. Sci.* **26**, 197–209.

HESSELL, J.W.D. (1982) *The Climate and Weather of Westland*. Miscellaneous Publication 115, New Zealand Meteorological Service, Wellington.

HICKS, D.M. & INMAN, D.L. (1987) Sand dispersion from an ephemeral river delta on the central California coast. *Mar. Geol.* **77**, 305–318.

KELK, J.G. (1974) *A morphological approach to process interaction on the mid-Canterbury coastline*. Unpublished MA Thesis, University of Canterbury, Christchurch.

KIRK, R.M. (1991) River–beach interaction on mixed sand and gravel coasts: a geomorphic model for water resource planning. *Appl. Geogr.* **11**, 267–287.

KIRK, R.M. & HEWSON, P.A. (1978) A coastal sediment budget for south Canterbury–north Otago. *Proceedings of the Conference on Erosion Control and Assessment in New Zealand*, pp. 93–120. New Zealand Association of Soil Conservators, Wellington.

KIRK, R.M. & TIERNEY, B.W. (1978) Nearshore sediment movement around the Port of Timaru. *New Zealand Harbour Engineers Association, Proceedings of the 7th Biennial Conference, Dunedin*, pp. 80–140.

KIRK, R.M., OWENS, I.F. & KELK, J.G. (1977) Coastal dynamics, East Coast of New Zealand, South Island. *3rd Australian Conference on Coastal and Ocean Engineering, Melbourne*, 18–21 April, pp. 240–244.

KNIGHTON, A.D. (1982) Longitudinal changes in the size and shape of stream bed material: evidence of variable transport conditions. *Catena* **9**, 25–34.

KODAMA, Y. (1994) Downstream changes in lithology and grain size of fluvial gravels, the Watarase River, Japan: evidence of the role of abrasion in downstream fining. *J. sediment. Res.* **A64**, 68–75.

LECKIE, D.A. (1994) Canterbury Plains, New Zealand—implications for sequence stratigraphic models. *Bull. Am. Assoc. petrol. Geol.* **78**, 1240–1256.

MACKINNON, T.C. (1983) Origin of the Torlesse terrane and coeval rocks, South Island, New Zealand. *Geol. Soc. Am. Bull.* **94**, 967–985.

MARTIN, J.H. (1993) A review of braided fluvial hydrocarbon reservoirs: the petroleum engineer's perspective. In: *Braided Rivers* (Eds Best, J.L. & Bristow, C.S.), Spec. Publ. geol. Soc. London, No. 75, pp. 333–367. Geological Society Publishing House, Bath.

MIALL, A.D. (1985) Architectural-element analyis: a new method of facies analysis applied to fluvial deposits. *Earth Sci. Rev.* **22**, 261–308.

MIALL, A.D. (1988) Resevoir heterogeneities in fluvial sandstones: lessons from outcrop studies. *Bull. Am. Assoc. petrol. Geol.* **72**, 682–697.

MORTIMER, N. (1995) Triassic to Early Cretaceous tectonic evolution of New Zealand terranes: a summary of recent data and an integrated model. In: *Proceedings of the 1995 PACRIM Congress* (Eds Mauk, J.L. & St George, J.D.), pp. 401–406. Australasian Institute of Mining and Metallurgy, Carlton, Victoria.

OLIVER, P.J. & KEENE, H.W. (1989) *Sheet K36AC & part sheet K35. Mount Somers.* Geological Map of New Zealand 1 : 50 000, Department of Scientific and Industrial Research, Wellington.

OLSEN, T. (1995) Sequence stratigraphy, alluvial architecture and potential reservoir heterogeneities of fluvial deposits: evidence from outcrop studies in Price Canyon, Utah (Upper Cretaceous and Lower Tertiary). In: *Sequence Stratigraphy on the Northwest European Margin* (Eds Steel, R.J., Felt, V.L., Johannessen, E.P. & Mathieu, C.), pp. 75–96. Elsevier, Amsterdam.

PARKER, G. (1991a) Selective sorting and abrasion of river gravel, I: theory. *J. Hydraul. Eng.* **117**, 131–149.

PARKER, G. (1991b) Selective sorting and abrasion of river gravel, II: application. *J. Hydraul. Eng.* **117**, 150–171.

PARKINSON, D.N. & HINES, F.M. (1995) The Lower Jurassic of the North Viking Graben in the context of Western European Lower Jurassic stratigraphy. In: *Sequence Stratigraphy on the Northwest European Margin* (Eds Steel, R.J., Felt, V.L., Johannessen, E.P. & Mathieu, C.), pp. 97–107. Elsevier, Amsterdam.

RUST, B.R. (1984) Proximal braidplain deposits in the Middle Devonian Malbaie Formation of eastern Gaspe, Quebec, Canada. *Sedimentology* **31**, 675–695.

SHAW, J. & KELLERHALS, R. (1982) The composition of recent alluvial gravels in Alberta river beds. *Alberta Res. Counc. Bull.* **41**, 151 pp.

SMITH, N.D. (1974) Sedimentology and bar formation in the upper Kicking Horse River, a braided outwash stream. *J. Geol.* **82**, 205–223.

SOONS, J.M. (1968) Canterbury landscapes: a study in contrasts. *N. Z. Geogr.* **24**, 115–132.

SUGGATE, R.P. (1963) The fan surfaces of the Central Canterbury Plain. *N.Z. J. Geol. Geophys.* **6**, 281–287.

TODD, D.J. (1983) *Effect of low flows on river mouth closure in the Opihi River*. Unpublished MSc Thesis, University of Canterbury, Christchurch.

TOMLINSON, A.I. (1976) Climate. In: *New Zealand Atlas* (Ed. Woods, I.), pp. 82–89. Government Printer, Wellington.

WAUGH, J.R. (1983) *Sedimentation and the Rangitata Diversion Race Sandtrap*. Publication 35, South Canterbury Catchment Board and Regional Water Board, 25 pp.

WEBB, E.K. (1994) Simulating the three-dimensional distribution of sediment units in braided-stream deposits. *J. sediment. Res.* **B64**, 219–231.

WRIGHT, L.D., THOM, B.G. & HIGGINS, R.J. (1980) Wave influences on river-mouth depositional process: examples from Australia and Papua New Guinea. *Estuar. coast. Mar. Sci.* **11**, 263–277.

Alluvial-fan floods

Flood and Megaflood Processes and Deposits: Recent and Ancient Examples. Edited by I. Peter Martini, Victor R. Baker and Guillermina Garzón ISBN: 978-0-632-06404-5

Spec. Publs int. Ass. Sediment. (2002) **32**, 113–40

Alluvial-fan sedimentation from a glacial-outburst flood, Lone Pine, California, and contrasts with meteorological flood deposits

T. C. BLAIR

Blair & Associates, 1949 Hardscrabble Place, Boulder, CO 80305, USA (Email: tcblair@aol.com)

ABSTRACT

Surficial deposits of the Lone Pine alluvial fan, Owens Valley, California, mostly accumulated during a catastrophic outburst flood. Sedimentation probably resulted from failure of a glacial moraine-dammed lake in the steep (15°), high relief (2.4 km), and high elevation (to 4417 m a.s.l.) Sierra Nevada catchment. Glacial moraines (facies A) consist of unsorted sand through boulders and blocks. The principal flood facies (B) is texturally similar to the moraine, consisting of unsorted, mostly matrix-supported, sandy, pebbly, cobbly, blocky, fine to very coarse boulder gravel in a unit 2–11 m thick distributed across the 13.6-km-long fan. Facies B was deposited during the initial phase of the outburst flood as a high-volume, noncohesive sediment gravity flow (NCSGF) probably initiated by water rapidly descending over moraine sediment. The NCSGF deposits differ from the moraine by their planar bed geometry, slope-transverse long-axis alignment of coarse clasts, and by shadow zones formed from flow separation around boulders deposited early in the flood. Deposition of the NCSGF was directly followed by a water flood phase caused by drainage of the breached lake after removal of sediment in the flood path. This discharge eroded channels 3–40 m deep and 6–100 m wide around the margins and across the fan from various departure points along the main flood channel (Lone Pine Creek). Laminated pebbly sand (facies D) accumulated on the channel beds. This discharge expanded on the distal fan into a sheetflood that deposited 4+ m of cobbly and sandy pebble gravel in planar couplet beds 5–20 cm thick (facies E). The final flood phase entailed downcutting of Lone Pine Creek, concentrating there a thick unit of boulder–cobble gravel (facies C), and stranding the other channels high on the fan surface. Minor modification of these facies and channels since the flood result from aeolian deposition (facies F), clast weathering, bioturbation and soil development.

Instigation of outburst floods in Owens Valley requires the glacial repositioning of colluvium from the steep catchment slopes to moraines on the valley floor, which dam drainage and form lakes. Outburst floods differ from meteorological floods in the valley by the high volume of water and sediment discharge, by deposition of massive NCSGF beds, and by large and rapid changes to the landscape such as the carving of channels. These differences produce fans with distinctive facies and potential hazards, the former providing diagnostic criteria for their recognition in both modern and ancient settings.

INTRODUCTION

Alluvial fans derived from non-glaciated upland catchments of the southwestern USA dominantly aggrade during infrequent floods generated by rapid spring snowmelt, intense thunderstorms, or prolonged rainfall from slow-moving, moist air masses (McGee, 1897; Pack, 1923; Woolley, 1946; Beaty, 1963, 1970). Flash floods are promoted by the introduction of this meteoric water into the typically high relief (1–3 km) and short contributary drainage net of the catchments. These floods commonly have high sediment load derived from colluvium mantling the steep catchment slopes, and incorporated through slope failures caused by saturation and undercutting (Campbell, 1974, 1975). Wet colluvial slips readily transform during initial motion into either water floods or debris flows that transport sediment to the fan, where aggradation occurs as a result of flow expansion. The fan deposits typically are poorly sorted, stratified in beds 5–150 cm thick, and have particle-size modes varying from cobbles to fine boulders (clast intermediate axes, d_I, of 5–50 cm; Hubert & Filipov, 1989; Blair & McPherson, 1994a,b,

Flood and Megaflood Processes and Deposits: Recent and Ancient Examples. Edited by I. Peter Martini, Victor R. Baker and Guillermina Garzón ISBN: 978-0-632-06404-5

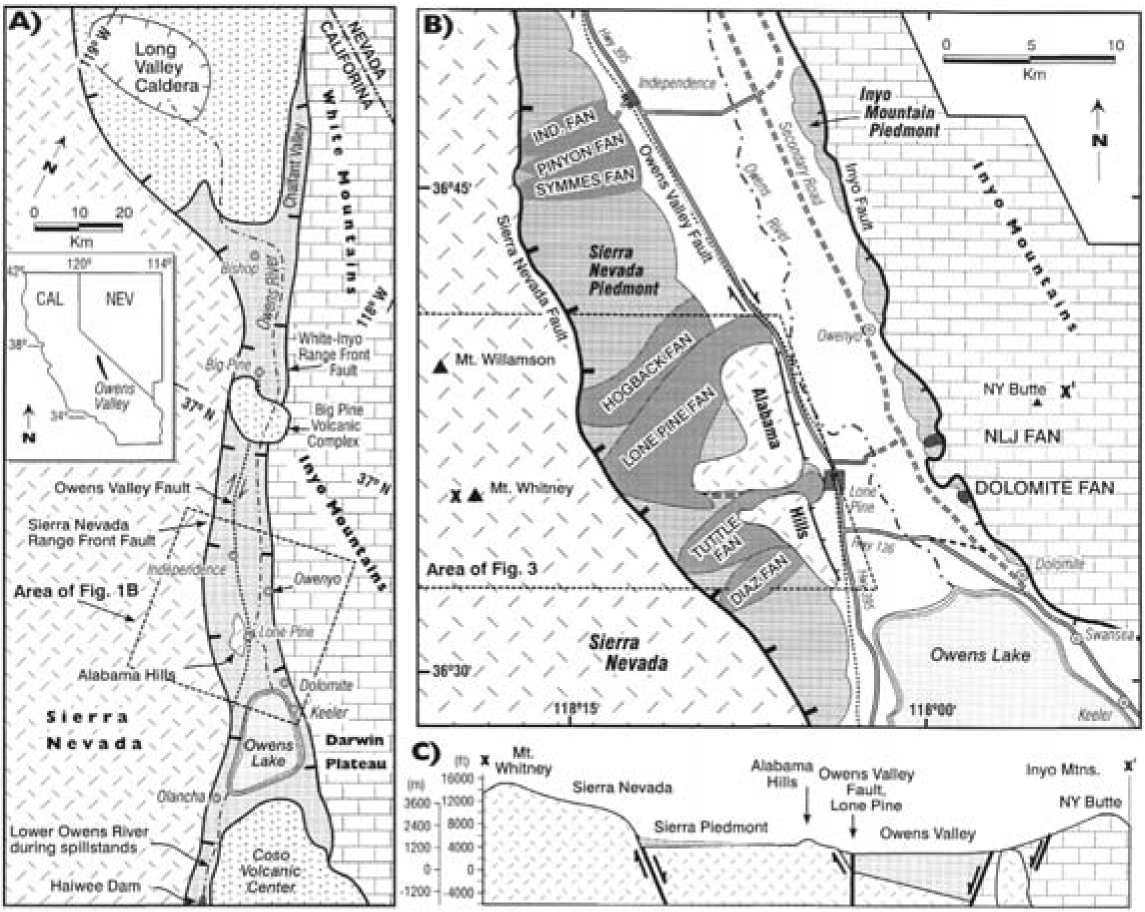

Fig. 1. (A) Location and geological features of Owens Valley, California (shaded). (B) Geological map of southern Owens Valley. Referenced fans of the Sierra Nevada piedmont are identified, as are the ends of cross-section *x–x′* of Fig. 1C, and the area covered in Fig. 3. (C) Structural section *x–x′* across the study area from the Sierra Nevada to the Inyo Mountains (after Pakiser *et al*., 1964).

1998). Coarser boulders (d_I of 50–200 cm) usually are dispersed as outsized clasts.

Large alluvial fans (radii 5–14 km) of the Sierra Nevada piedmont in Owens Valley, California (Fig. 1), differ from other fans of the southwestern USA by possessing thicker bedding and a fan-wide abundance of coarse boulders to medium blocks ($d_I = 100–1500$ cm). The size, distribution, and concentration of such coarse clasts on these Sierra Nevada fans have long been deemed atypical (Trowbridge, 1911; Knopf, 1918). Two sedimentary processes have been proposed for their origin. Trowbridge (1911) suggested that the fans accumulated from water flows in shifting distributary channels linked to catchment glaciation. On the basis of geomorphological studies, several of these fans alternatively were interpreted to have aggraded as debris-flow levees and lobes not related to glaciation (Whipple & Dunne, 1992; Bierman *et al*., 1995; Schumm *et al*., 1996), similar to fans lining eastern Owens Valley. Neither of these two process hypotheses, however, were supported by sedimentological analyses.

The objective of this paper is to provide a sedimentological case study of one of the large Sierra Nevada piedmont fans, and to reconstruct the depositional processes. This study is of the Lone Pine Canyon fan located immediately west of the town of Lone Pine (Figs 1 & 2). The methods of study included:

1 describing the facies as exposed at 29 stations;

2 determining maximum clast size (d_I) and clast orientations;

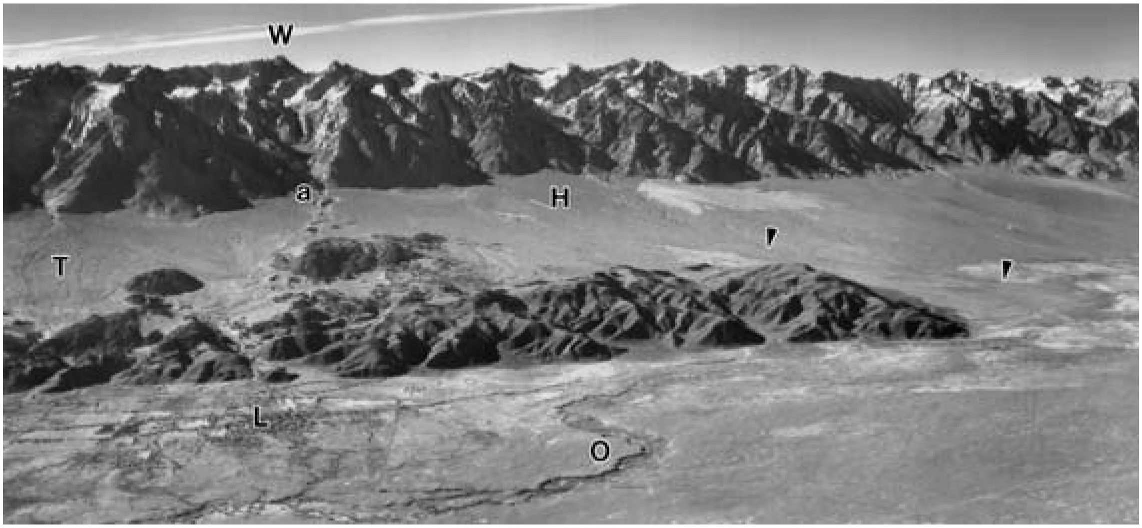

Fig. 2. Oblique aerial photograph of the Sierra Nevada (background), coalesced piedmont, Alabama Hills (bedrock uplift, middle ground), town of Lone Pine (L), Owens River (O) on the valley floor, and the Lone Pine ('a' at apex), Tuttle Canyon (T), and Hogback Canyon (H) fans. Arrows mark the distal north Lone Pine fan margin, and the incised Lone Pine Creek (right of 'a') approximates the south margin. Mount Whitney (W), at an elevation of 4417 m, defines the back wall of the Lone Pine fan catchment. Glaciers, cirques, and glacially carved U-shaped valleys dominate the catchments.

3 analysing the grain size of eight representative samples;
4 measuring slopes using a clinometer;
5 constructing topographic profiles and channel maps from field measurements, aerial photographs and U.S. Geological Survey 7.5′ quadrangles (scale = 1 : 24 000; contour interval = 10 m);
6 using the facies data to reconstruct their origin, and to develop an actualistic process–product model.
Textural terminology follows Folk (1974) as modified for gravel by Blair & McPherson (1999).

SETTING

Owens Valley is a modern continental rift located near the margin of the Basin and Range province in eastern California (Fig. 1). The valley floor has an elevation of about 1200 m a.s.l., is 15–25 km wide, and extends for 150 km along a N25°W trend. It is enclosed at both ends by Quaternary volcanoes, including Long Valley in the north and the Coso complex in the south. The precipitous Sierra Nevada towers with 3200 m of relief along western Owens Valley, and the 2200 m high White and Inyo mountains define the eastern margin. A lower relief (440 m) bedrock outlier 18.5 km long, called the Alabama Hills, is exposed within the basin immediately west of Lone Pine, elongated parallel to, and 7 km from, the Sierra Nevada front (Figs 1 & 2). A massive Cretaceous granitic batholith with Jurassic volcanic country rock comprise the Sierra Nevada and Alabama Hills, whereas Proterozoic to Permian sedimentary rocks dominate the White and Inyo mountains (Matthews & Burnett, 1965; Streitz & Stinson, 1977; Moore, 1981; Dunne & Walker, 1993). Owens Valley has a high desert climate resulting from its position in the rain shadow of the Sierra Nevada. Annual precipitation varies with elevation from 10 to 20 cm, falling as rain or snow during the cooler months, or as summer thunderstorms (Hollett *et al.*, 1991). Typical vegetation on the valley floor is desert grass and scrub, whereas juniper and pinyon pine are common at higher elevations.

The margins of Owens Valley are delineated by active, high-angle normal faults that include the Sierra Nevada fault on the west, with > 3500 m of throw, and an equally prominent high-angle normal fault on the east at the Inyo Mountains (Fig. 1; Pakiser *et al.*, 1964; Matthews & Burnett, 1965). Scarps 1–5 m high are common in the fans near these faults (Fig. 3). Additionally, the dextral strike-slip Owens Valley fault cuts axially down the basin along the eastern side

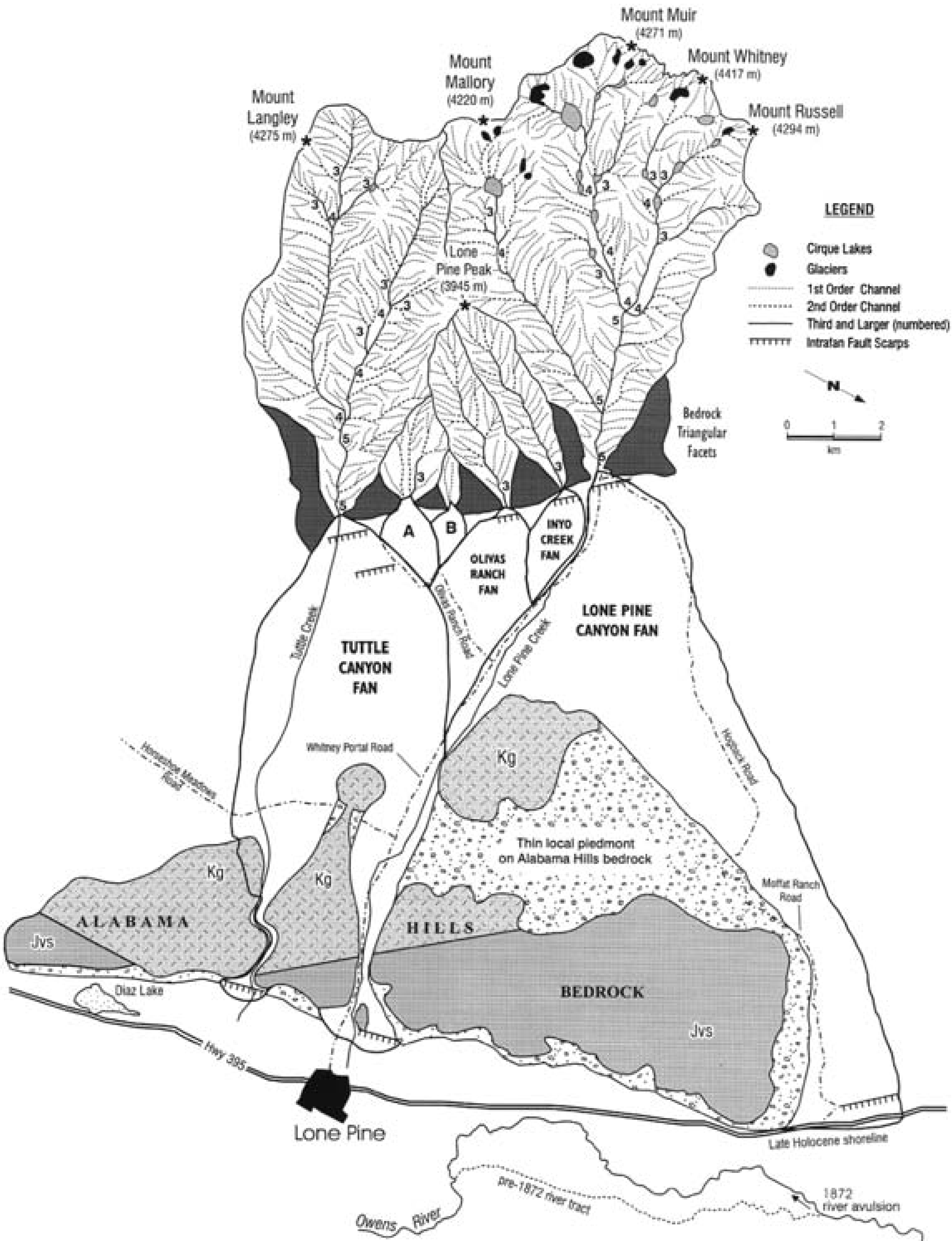

Fig. 3. Drainage net and other features of the Lone Pine and Tuttle fans and catchments constructed from 1 : 24 000 U.S. Geological Survey quadrangles (contour interval = 10 m). Channels are delineated using the stream ordering method of Horton (1945) as slightly modified by Strahler (1964). Bedrock types are Cretaceous granite (Kg) and Jurassic volcanic and volcaniclastic strata (Jvs).

of the Alabama Hills, straddling Highway 395 near Lone Pine. Both strike-slip (11 m) and dip-slip (2 m) motion occurred along this fault on 26 March 1872 during one of the largest historical earthquakes in the USA (Bateman, 1961; Lubetkin & Clark, 1988). Fault offset, surface tilting and subsidence during this earthquake formed Diaz Lake, offset fan deposits and caused Owens River to avulse westward toward the Owens Valley fault near Lone Pine (Fig. 3; Bateman, 1961). Rupture patterns indicate that the Alabama Hills are a bedrock fault ridge formed by transpressional motion along the Owens Valley fault. Geophysical data reveal that the Sierra Nevada piedmont behind this ridge constitutes a thin (100 m) cap on the bedrock, and that basin development near Lone Pine is from half-graben subsidence between the Owens Valley fault and the Inyo range front, where an eastward-thickening sediment wedge attains 2500 m (Fig. 1C; Pakiser *et al.*, 1964).

Sedimentologically, southern Owens Valley is characterized by basin-marginal alluvial fans of the Sierra Nevada and Inyo mountains piedmonts, and by Owens River and Owens Lake on the basin floor. The basin floor is drained by Owens River, which flows southward about 100 km from its headwaters to its present terminus in Owens Lake. Owens Lake is now a flat playa formed by the damming of Owens River at the south end of the valley by the Coso volcano. Historically, this lake was a perennial body about 10 m deep and 280 km^2 in area maintained by river inflow, but was desiccated during the early 1900s by river diversion into the Los Angeles Aqueduct (Hollett *et al.*, 1991). Owens Lake frequently spilled over the south margin of the valley during wetter Quaternary phases (Benson *et al.*, 1996). At its spill point, the lake had a depth of 65 m and an area of 700 km^2, extending northward to Independence, and straddling the eastern Alabama Hills (Fig. 1). The Owens River and Lake system is bordered on both sides of the valley by alluvial fans. The fans have longer radii (5–14 km) in the Sierra Nevada piedmont, coincident with where the basin fill is thin, and shorter radii (1–3 km) in the Inyo piedmont, near the basin depocentre. Many of the Sierra Nevada fans have associated perennial streams fed by rainfall, snowmelt or glacial icemelt in the catchments. In contrast, water discharge from the Inyo Mountains catchments is rare, mostly following thunderstorms (Beaty, 1963; Hubert & Filopov, 1989; Blair & McPherson, 1998). A unique feature of most of the perennial channels of the Sierra Nevada piedmont, such as Lone Pine and Tuttle creeks (Fig. 3), is that they flow near or around one of the fan margins, rather than directly across them (Trowbridge, 1911). These channels naturally continued either into Owens River or Owens Lake.

OVERVIEW OF THE LONE PINE CANYON FAN AND CATCHMENT

Overview of catchment

The Lone Pine fan catchment extends 2437 m in relief from the base of the range front to the eastern Sierra Nevada crest in the John Muir Wilderness (Figs 2 & 3). It is underlain by the porphyritic Whitney granodiorite, a pluton intruded into Jurassic metavolcanic rocks during Late Cretaceous time (Evernden & Kistler, 1970; Moore, 1981). Several of the highest peaks in the USA comprise the catchment rim, including Mount Whitney at 4417 m and Mount Russell at 4294 m. The catchment has an area of 30.7 km^2, a maximum length of 8.9 km, a maximum width of 6.5 km, and an average slope of 15.3°. It contains three compartments, each drained by perennial fourth-order channels that combine to form the main fifth-order feeder, Lone Pine Creek, leading to the fan (Fig. 3). The middle and northern compartments are drained by the South Fork and North Fork of Lone Pine Creek, and the southern one by Meysan Creek (Fig. 4). Above its confluence with the fan feeder, the Meysan compartment has an area of 9.6 km^2, the South Fork 9.7 km^2 and the North Fork 7.8 km^2. All three have broad U-shaped cross-sections that collectively contain 16 cirque lakes and 12 alpine glaciers, the latter in the headwalls at elevations above 3675 m (Fig. 4). The main channels are deeply incised in narrow zones below the U-shaped valley bottoms. The long profile of each compartment channel has a stepped pattern, with the Meysan Creek profile the smoothest (Fig. 5A–C). Cirque or moraine-dammed lakes exist on the flat profile segments, and hanging valleys with V-shaped channel incisions the steep segments (Fig. 6A & B).

Glacial moraines are numerous in the Lone Pine fan catchment. Large, sparsely vegetated young moraines are present near the margin of the active glaciers (Fig. 4; Moore, 1981). Older tree-covered, but morphologically pristine, terminal and lateral moraines dominate the lower catchment. These moraines are of straight-crested to slightly convex walls 500–2000 m long, 50 m wide, and 50–300 m high (Fig. 6B). The most prominent moraines are found near the lower compartment limits, all of which are breached by present channels (Fig. 4). The moraines consist of an unsorted

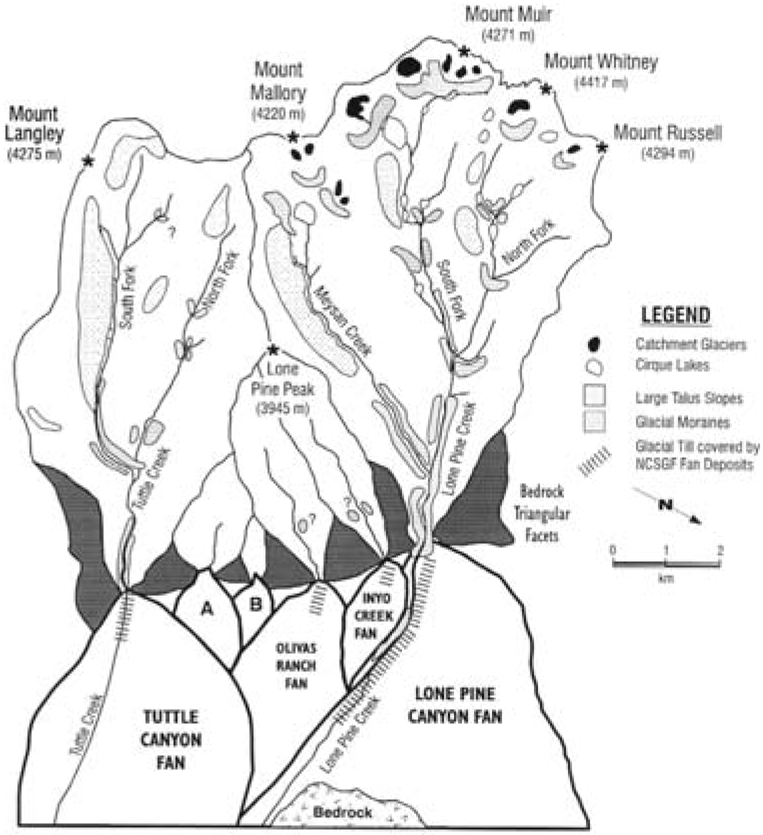

Fig. 4. Distribution of glaciers, moraines, large talus slopes and lakes in the Lone Pine and Tuttle fan catchments. Also shown are the known locations of glacial till on the fans.

and unstratified mixture of sand, granules, pebbles, cobbles, boulders and blocks with d_I as large as 15 m (Fig. 6C). A major effect of glaciation has been the stripping of colluvium from the steep granitic catchment slopes, and redeposition of this sediment along and across the bottoms of the higher order channels. Many of the cirque lakes are at least partly dammed by moraines. Post-glacial rockfall sedimentation also has occurred along the base of some of the upper catchment slopes, especially those facing north (Fig. 4).

Although not well studied in the Lone Pine area, late Quaternary moraines are documented in other Sierra Nevada catchments and directly on some of the fans (Knopf, 1918; Blackwelder, 1931; Sharp & Birman, 1963). Radiocarbon, cation-ratio, soil and boulder-weathering data from the Sierra Nevada moraines indicate that the two most expansive stages of glaciation occurred about 13–50 ka (Tioga stage) and 140–180 ka (Tahoe stage; Sharp & Birman, 1963; Dorn *et al.*, 1987; Berry, 1994; Benson *et al.*, 1996; Phillips *et al.*, 1996; Pohl *et al.*, 1996). During these periods the large Mount Whitney ice-cap probably covered nearly all but the upper spires of the Lone Pine catchment, as indicated by bedrock morphology (Fig. 2). Holocene glaciation in the Sierra Nevada has been much less extensive (Clark & Gillespie, 1997).

Overview of Lone Pine fan

The Lone Pine fan is laterally coalesced with the Tuttle Canyon, Olivas Ranch and Inyo Creek fans on the south, and Hogback Canyon fan on the north (Figs 1 & 3). The fan toe, at an elevation of 1144 m, is demarcated by the sandy Holocene shoreline bench of Owens Lake. The fan planview pattern is irregular owing to topographic interference from the Alabama Hills bedrock and fringing piedmont deposits (Figs 2 & 7A). The Alabama Hills piedmont is easily differentiated from the arkosic Lone Pine fan by its slope away from the hills, and by volcanic clast types reflecting the Jurassic bedrock. Lone Pine fan has an area of 25.4 km^2, total relief of 836 m, maximum width of 5.6 km, and a maximum length of 13.6 km. The Alabama Hills limit the south side of the fan to a radial length of

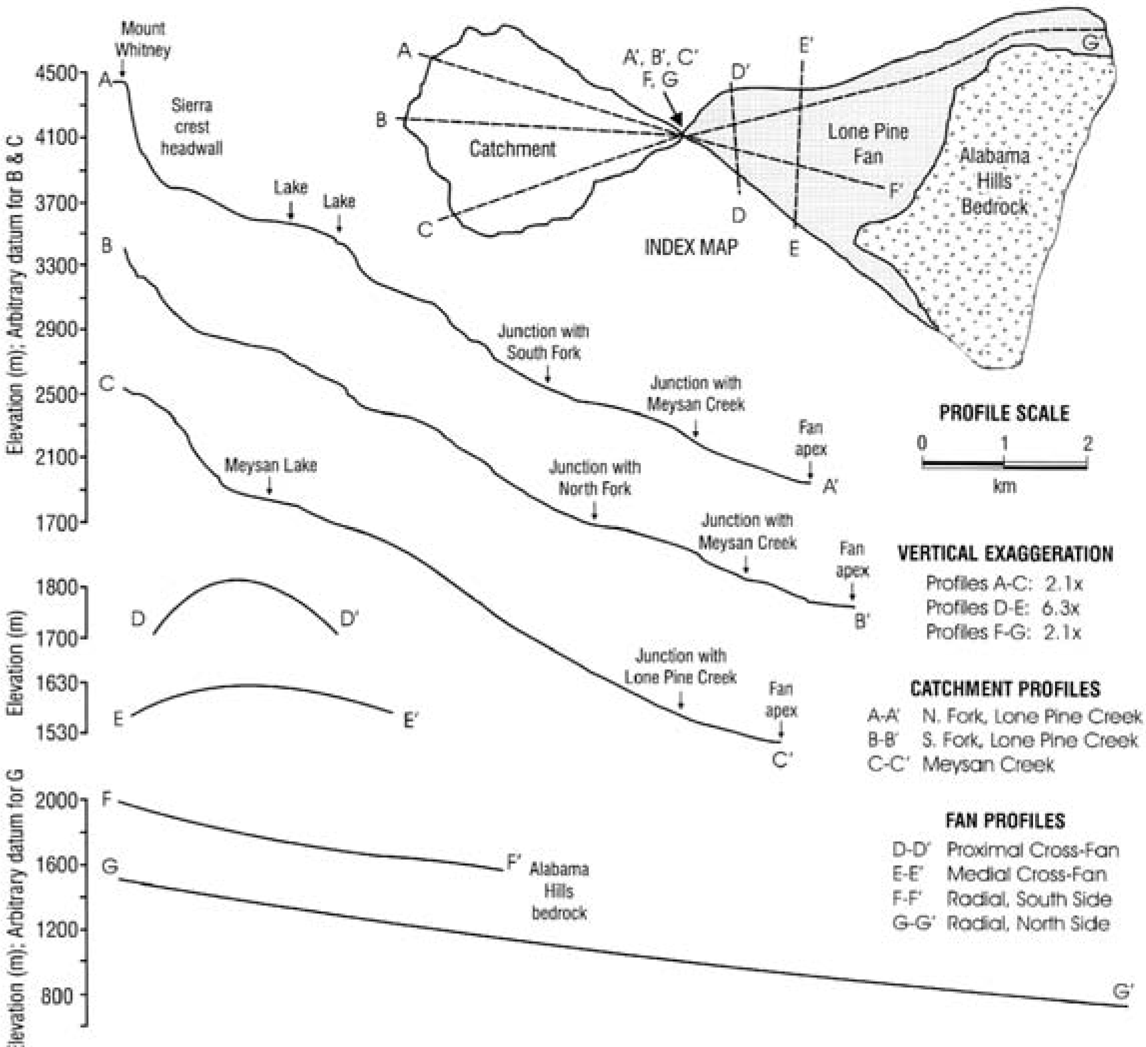

Fig. 5. (A–C) Topographic profiles of the north (A–A′), middle (B–B′), and south (C–C′) compartments of the Lone Pine fan catchment (see index for locations). (D and E) Cross-profiles of the proximal (D–D′) and medial (E–E′) Lone Pine fan. (F and G) Radial profiles of the south (F–F′) and north (G–G′) Lone Pine fan.

about 6 km. Field measurements show that the surface slope of the fan decreases from 5.5° near the apex to 3.5° distally (Fig. 7B). The proximal zone is covered by boulders and blocks, and the less steep distal zone by finer sediment amid dispersed boulders (Fig. 6D–F). Radial fan profiles are smooth, with the measured basinward decrease in slope perceived with difficulty (Fig. 5). Typical of alluvial fans, cross-profiles are bowed upwards, although the Lone Pine fan profiles are slightly asymmetric, with the steepest side along the restricted south margin.

Numerous channels radially traverse the Lone Pine fan, all of which have steep margins and flat-floored bottoms (Figs 6D–F & 8A). Lone Pine Creek is the largest and only channel with perennial discharge, with base flow maintained by catchment snowmelt, icemelt and rainfall. This channel is 50–100 m wide and is incised 5–40 m deep on the upper fan. Rather than bisecting the fan, it skirts the southern margin, and at 7.2 km from the apex it crosses on to the northern part of the adjoining Tuttle Canyon fan. Lone Pine Creek continues across the Tuttle fan through the

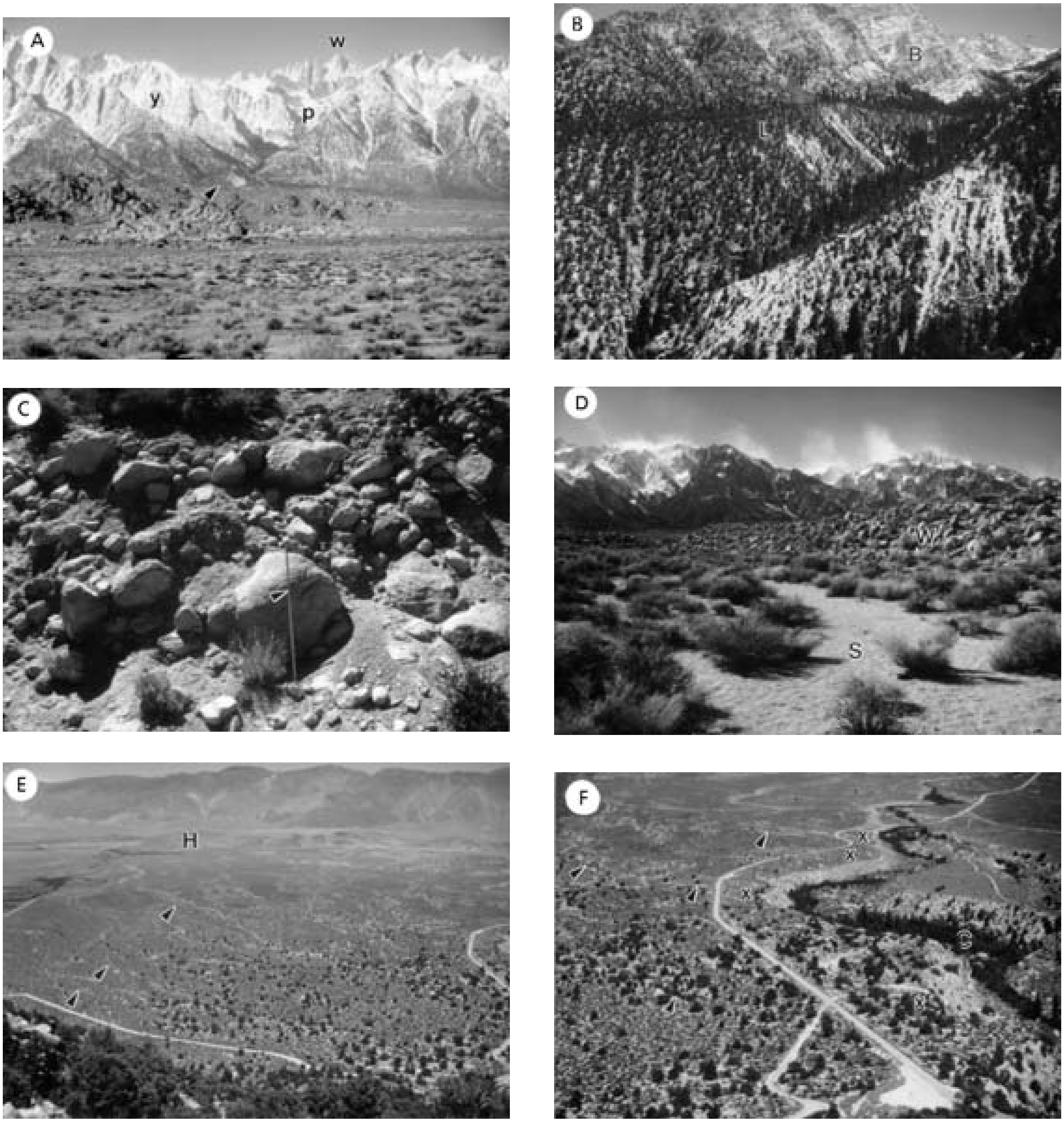

Fig. 6. (A) View of Lone Pine fan catchment, including Mount Whitney (w), Meysan Creek compartment (y), and the south and north Lone Pine Creek compartments ('p' above their confluence). Moraines are common, including near the fan apex (arrow). (B) View up Meysan Creek compartment from its confluence with Lone Pine Creek. Prominent lateral moraines (L) are 300 m high. Bedrock (B) underlies the highest slopes. (C) Exposure of catchment moraine consisting of unsorted, clast- to matrix-supported, pebbly to blocky boulder gravel. Jacob's staff (arrow) is 1.5 m long. (D) View near station 17 of a channel with a pebbly granular sand bed (S) of facies D, and steep walls (W) 2 m high of NCSGF deposits. (E) View downslope of the north and central Lone Pine fan from the apex to the Alabama Hills (H). Note the boulder-lined channels (arrows), the treed and boulder-rich surface of the proximal fan, and the sandy scrub-vegetated surface of the distal fan. (F) Down-fan view of the Lone Pine apex (lower right) illustrating the incised 15–80 m wide and 10–40 m deep tract of Lone Pine Creek (C). Now-abandoned splays depart from this channel at various points 0–2.8 km below the apex ('x' marks examples). Note the boulder-rich margins of the channels (arrows), and that they are perched 10–35 m above the Lone Pine Creek bed.

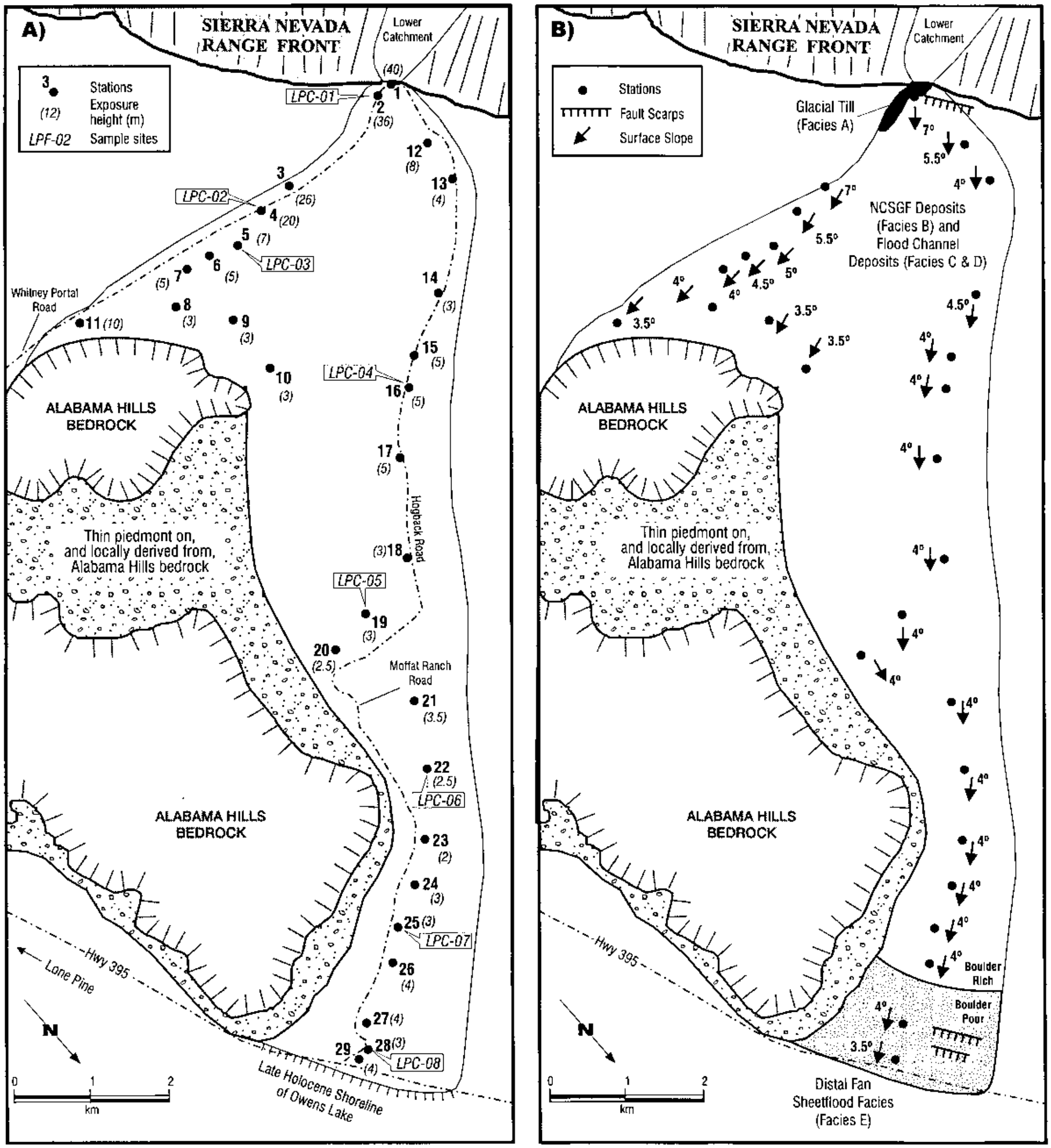

Fig. 7. (A) Map of the Lone Pine fan depicting study stations, exposure height, sample sites and other features. (B) Distribution of facies and fault scarps, and the measured surface slope at the fan stations.

Alabama Hills and beyond until reaching its terminus at Lone Pine (Fig. 3). This abnormal pattern of Lone Pine Creek has led to the erroneous mapping of the northern Tuttle fan as a part of the Lone Pine fan (Lubetkin & Clark, 1988; Bierman *et al.*, 1995). A similar situation exists on the northern side of the Lone Pine fan, where Hogback Creek of the adjoining Hogback fan crosses on to the Lone Pine fan about 2.8 km from the Sierra Range front, and then traverses the Lone Pine fan near its northern boundary.

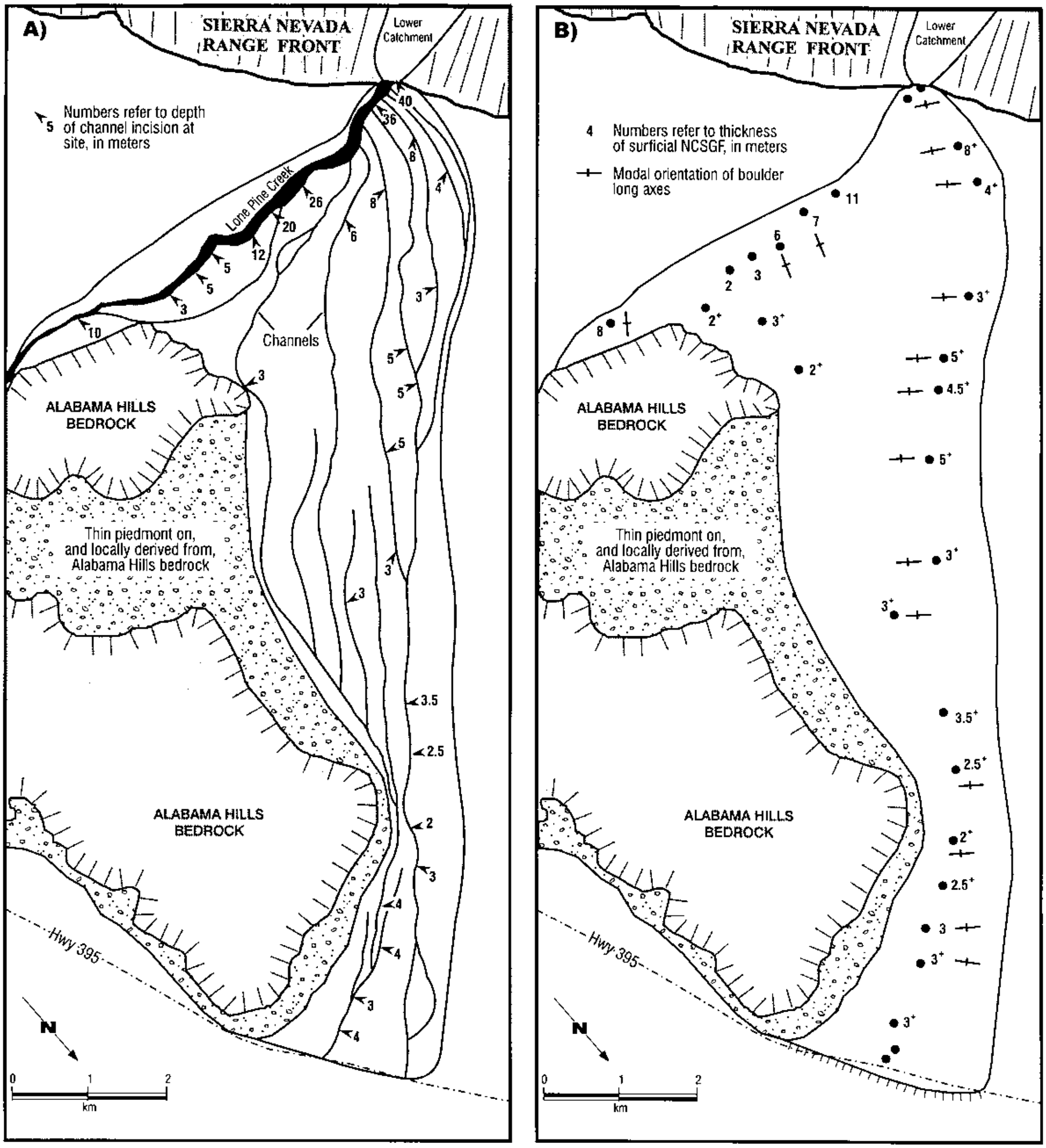

Fig. 8. (A) Distribution and measured depth of major channels on the Lone Pine fan. The channels splay from various points along Lone Pine Creek rather than emanating from the apex. (B) Map depicting the modal orientation of boulder long axes, and the thickness of the surficial NCSGF unit at the stations ('+' values indicate that the NCSGF base is not exposed).

Two other channel types, both non-perennial, are found on the Lone Pine fan. Several radially aligned channels are present upslope from the Alabama Hills, with the most prevalent ones mapped on Fig. 8A. Instead of emanating from the apex in a distributary pattern, these channels depart from the north margin of Lone Pine Creek at different points ranging from 20 to 2800 m below the apex. The channels typically are 5–20 m wide and 3–8 m deep, with depth generally increasing up-fan (Fig. 8A). At their points of origin,

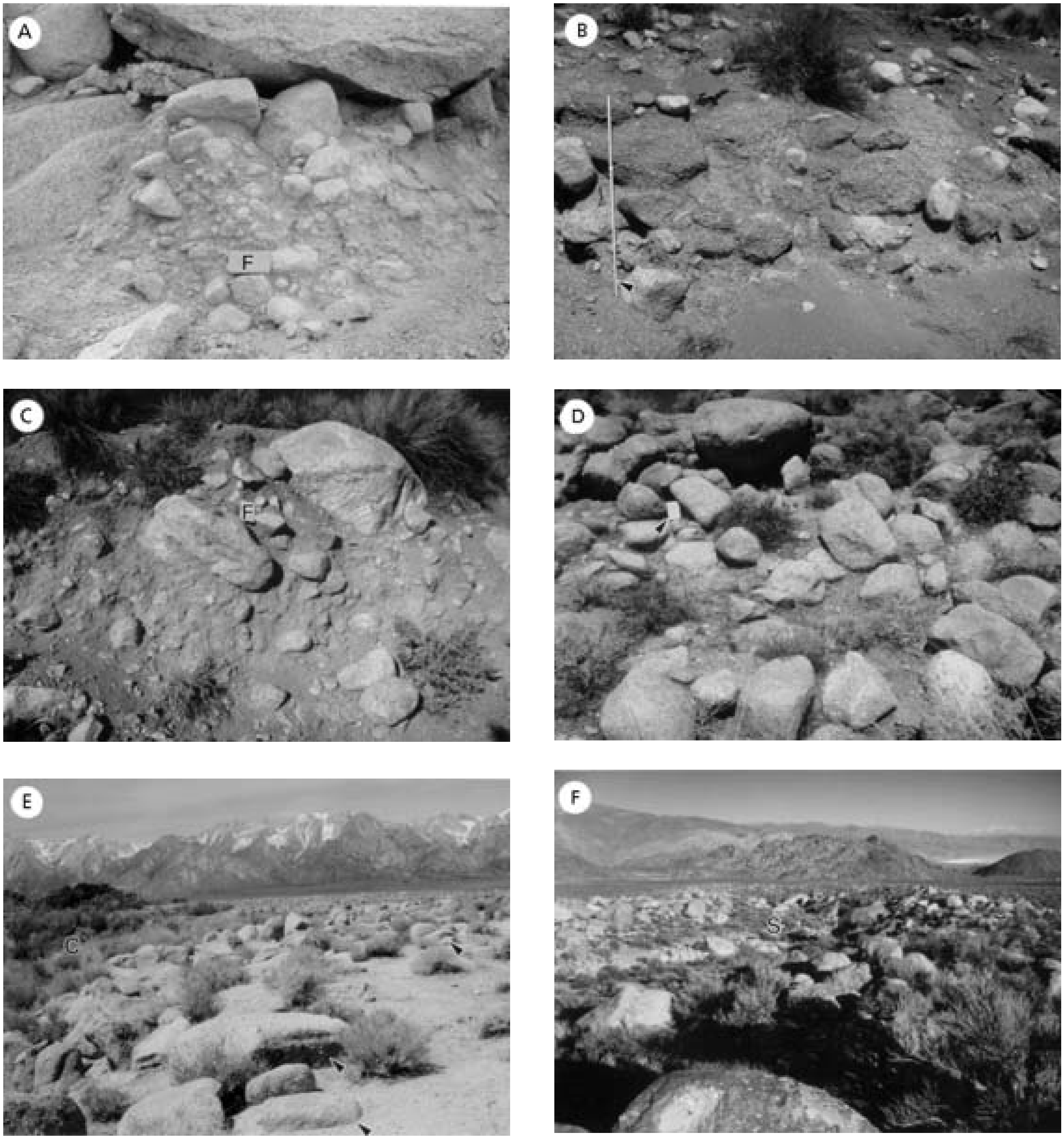

Fig. 9. (A) Unsorted, clast- to matrix-supported, sandy to blocky boulder gravel of facies A glacial till at station 2; fieldbook (F) is 20 cm long. (B) Reddened and unsorted facies A till at station 5; Jacob's staff is 1.5 m long (arrow). (C) Cut of facies B at station 9 consisting of matrix-supported, sandy pebbly cobbly coarse to fine boulder gravel; fieldbook (F) for scale. (D) Facies B cut 2 m tall at station 17 of unsorted, sandy to cobbly, fine to coarse boulder gravel; fieldbook (arrowed) for scale. (E) Facies B sandy to cobbly boulder gravel at station 24. Note the transverse long axis alignment of elongated boulders (arrows), and the lack of interclast matrix at the channel (C) margin. (F) Boulder-lined shadow channel (S) 1.5 m deep and 8 m wide extending downslope from a jam of blocks and boulders; station 10.

the floors of these channels are perched 10–35 m above the Lone Pine Creek bed (Fig. 6F), indicating that they are no longer active, except possibly from rainfall directly on the fan or on the Alabama Hills. The channel beds are sparsely vegetated and covered by pebbly granular sand, in contrast to the thickly vegetated, fine boulder and cobble gravel of the Lone Pine Creek bed. The second type of non-perennial channel is similar to the first, except that it heads directly on the fan. These channels are more abundant and smaller, with widths of 5–10 m and depths of 2–4 m.

SEDIMENTARY FACIES AND RECONSTRUCTED DEPOSITIONAL PROCESSES OF THE LONE PINE CANYON FAN

Sedimentary facies exposed along channel walls, fault scarps and gravel pits were documented at 29 stations on the Lone Pine fan (Fig. 7A). The unconsolidated exposures range in height from 2.5 to 40 m, with most between 3 and 10 m. Six facies, labelled A to F, were differentiated (Table 1).

Facies A

Description

Facies A consists of an unsorted but clast-rich mixture of sand, granules, pebbles, cobbles, blocks and fine to very coarse boulders (Fig. 9A & B). It occurs on the Lone Pine fan as a partially dissected moraine 40+ m thick near the apex, and as an unstratified unit 3+ to 26+ m thick beneath facies B along the proximal south fan margin (Figs 10A & B & 11). Clasts mainly are subangular to subrounded, and consist of fine to coarsely crystalline granite containing mafic xenoliths and 2–8 cm phenocrysts of potassium feldspar. About 20% of the clasts are extensively grusified and oxidized in the cuts near the fan apex, as are about 70% of the clasts at the other stations. The largest clasts range in size from fine to medium blocks (d_I = 450–750 cm). Long axes of boulders and blocks generally are disorganized, differing widely in orientation from vertical to horizontal, and having either a random planview mode or a weak slope-transverse trend. Facies A exposures vary from clast-supported to matrix-supported, with matrix consisting of sand to cobbles. Grain-size analysis of the finer than coarse pebble (< 1.6 cm) matrix of one sample (LPC-01) reveals a very poorly sorted texture (S_I = 2.97 ϕ) rich in fine and medium pebbles (37%), granules (14%), and medium to very coarse sand (32%) (Table 2; Fig. 12A & B). Although unstratified, local discontinuous shear zones within facies A impart a pseudobedding most apparent in pockets of finer sediment (discontinuous horizontal lines in Fig. 10A). These sheared zones are more compacted than other exposures of this facies. Variations in the degree of compaction, reddening and clast weathering define units within facies A, such as at station 2, where a sheared and compacted basal unit is sharply overlain by a more loose and fresh-appearing unit. Facies A is capped by a reddish brown Bt/Btk soil horizon 50–70 cm thick in the buried exposures at stations 3–11 (Fig. 10B).

Interpretation

The unsorted, unstratified, and disorganized character of facies A, and its presence near the fan apex in a

Table 1. Sedimentary facies and depositional processes.

Facies	Characteristics	Depositional process
A	Unsorted, unstratified, disorganized, sandy pebbly cobbly blocky boulder gravel	Glacial moraine
B	Massively bedded, unsorted, sandy pebbly cobbly blocky cobbly boulder gravel	Non-cohesive sediment gravity flow (NCSGF)
C	Channel-confined, clast-supported, thickly bedded cobbly boulder gravel	Flood and post-flood coarse gravel channel fill
D	Channel-confined, laminated, sandy pebbly granule gravel	Recessional flood ephemeral channel fill
E	Distal-fan planar couplets of sandy pebble gravel and cobbly pebble gravel	Outburst flood sheetflood couplets
F	Finely laminated, bioturbated, medium to very fine sand, rooted	Aeolian sandsheet, local coppice dunes

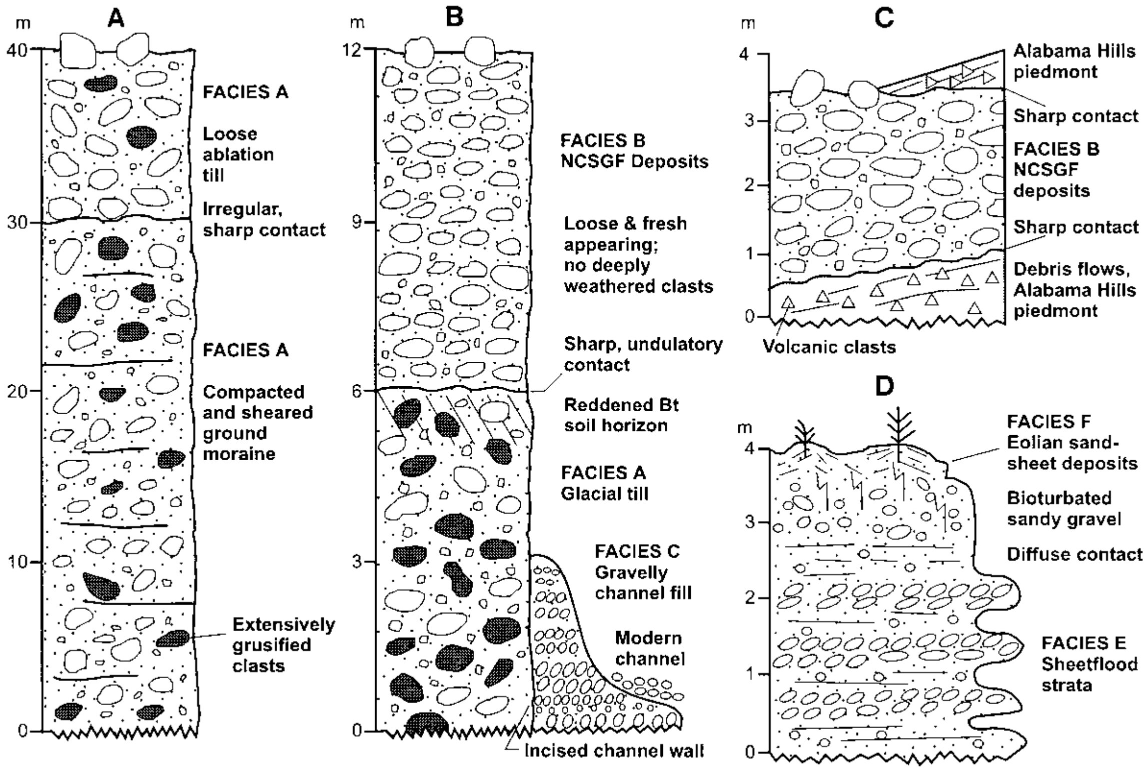

Fig. 10. Stratigraphical columns of the Lone Pine fan. (A) Glacial till (facies A) at station 2 consisting of a lower compacted unit overlain by a loose unit. (B) Glacial till (facies A) overlain by NCSGF deposits (facies B), and sidelapped by channel-fill gravel (facies C) at station 5. (C) NCSGF deposits (facies B) bounded by debris-flow deposits shed from the Alabama Hills; station 24. (D) Sheetflood couplets (facies E) capped by aeolian sand (facies F) at station 28. The upper 50 cm is homogenized by plant rooting.

landform diagnostic of moraine, indicate that it was deposited as glacial till. The lack of stratification or sorting, and the disorganized boulder fabric, differentiate these deposits from those of sediment gravity flows or water flows. Other evidence supporting a till origin are the textural match between this facies and the catchment moraines, and the presence of compacted and sheared intervals, the latter of which are typical of ground moraine deposited under the weight of the advancing glacier (Shaw, 1985). The presence of uncompacted ablation till upon ground moraine near the fan apex (Fig. 10A) records the retreat of a glacier that previously extended on to the Lone Pine fan. Approximate ages of the Lone Pine till can be assigned by comparative clast weathering indices, following Sharp & Birman (1963). The high percentage (*c.* 70%) of weathered clasts in the till at stations 3–11 matches that of the 140–180 ka Tahoe stage. The reddened Bt/Btk soil horizon capping the till at these stations (Fig. 10B) supports this age. The overlying fresher till near the fan apex (stations 1 and 2), wherein about 20% of the clasts are weathered, matches features of the 13–50 ka Tioga stage, as supported by more limited soil development. The two-stage stratigraphy exhibited near the apex of ground moraine capped by ablation till (Fig. 10A) thus records the last advance and retreat of a glacier on to the fan during latest Pleistocene time.

Facies B

Description

Facies B consists of an unsorted but boulder-rich mixture of clay to blocks, with the most common texture a sandy, granular, pebbly, cobbly, blocky, fine to very coarse boulder gravel (Figs 9C–F & 10B & C). This facies dominates the fan, comprising most (70–100%) of the exposures except south of the apex where till is present, and near the fan toe where facies E and F prevail (Fig. 11). Clasts consist of granite, which have

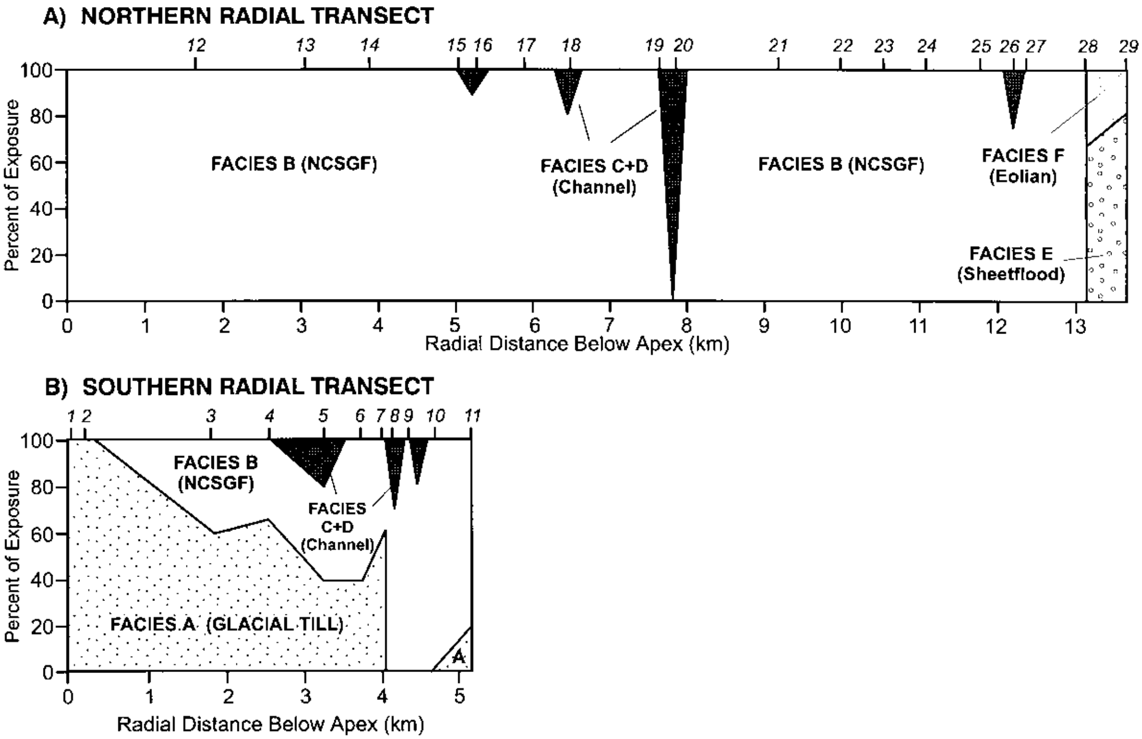

Fig. 11. Percentage of Lone Pine fan facies at the study stations plotted for a northern (A) and southern (B) radial transect. Numbers at top of panels refer to stations.

Table 2. Summary of grain-size data*.

Feature†	LPC-01	LPC-02	LPC-03	LPC-04	LPC-05	LPC-06	LPC-07	LPC-08
Facies	Till	NCSGF	NCSGF	NCSGF	NCSGF	NCSGF	NCSGF	SFLD
Mode (ϕ)	–3.88	–0.63	–0.63	–0.63	–0.63	–0.63	–0.63	–0.63
Sort (ϕ)	2.97	3.58	3.43	3.89	3.83	3.62	3.51	1.92
G–S–M	51–39–10	36–45–19	37–46–17	29–43–28	29–45–26	23–53–24	23–54–23	45–50–5
Nm S–Z–C	79–15–6	70–21–9	73–21–6	60–34–6	64–25–11	68–23–9	70–22–8	91–5–4
Distance (m)	260	2470	3250	5230	7530	8970	11 580	13 350
Grade‡	Weight per cent of total sample							
m pebble	20.7	8.9	12.2	2.8	6.0	5.7	4.8	6.7
f pebble	15.7	13.4	12.6	9.3	11.4	5.8	7.6	15.8
granule	14.4	14.2	11.8	16.9	11.9	11.3	10.7	23.0
vc sand	13.1	14.0	11.6	15.4	10.7	15.7	14.3	22.6
c sand	10.9	12.5	11.3	11.3	11.1	13.8	16.3	15.7
m sand	8.3	10.5	10.7	8.0	10.1	11.9	14.1	8.4
f sand	3.6	3.8	6.9	2.1	7.4	5.7	3.9	2.0
vf sand	3.0	3.8	5.6	5.7	5.9	5.5	4.9	0.8
c silt	2.3	3.4	4.5	6.8	4.8	4.7	5.2	0.5
m silt	1.9	3.5	3.8	6.8	4.4	4.7	4.5	0.5
f silt	1.7	3.4	2.8	6.0	4.4	4.3	3.9	0.9
vf silt	1.5	3.2	2.3	4.8	4.3	3.8	3.5	1.0
Clay	2.9	5.4	3.9	4.1	7.6	7.1	6.3	2.1

*Data are summaries of standard 1/4 ϕ split sieve and laser particle analyses of the < 1.6 cm (< –4 ϕ) fraction of representative samples (see Fig. 7A for sample locations).
†Sort: sorting is inclusive graphic standard deviation (S_I) of Folk (1974). G–S–M: gravel–sand–mud weight per cent. Nm S–Z–C: normalized sand–silt–clay weight per cent. Distance is from the fan apex. Facies: till = glacial till, NCSGF = non-cohesive sediment gravity flow deposits, SFLD = sheetflood couplet deposits.
‡Size abbreviations: vc = very coarse, c = coarse, m = medium, f = fine, vf = very fine.

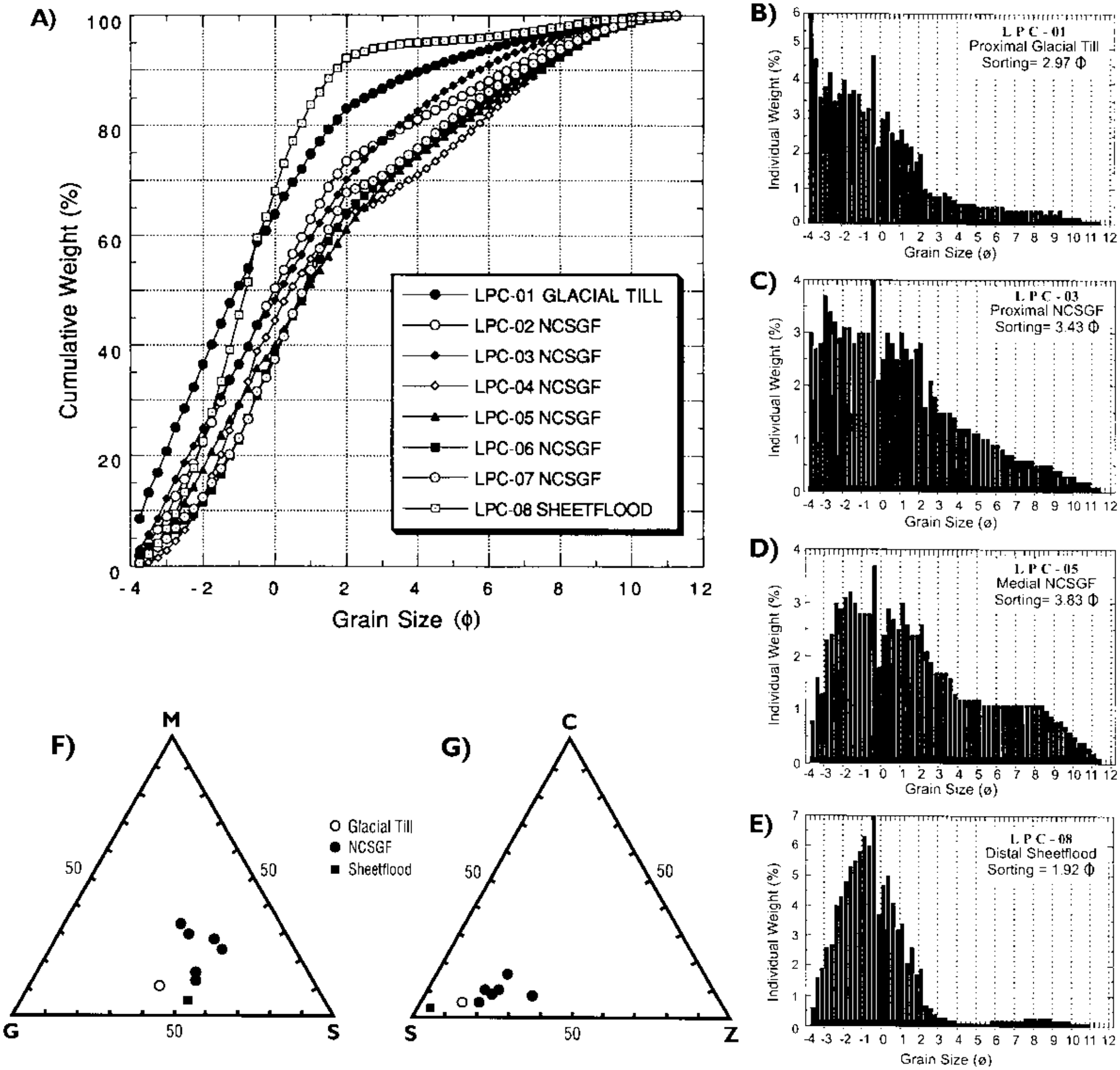

Fig. 12. Plots of grain-size data from the analysed Lone Pine fan samples (see Table 2 for data and Fig. 7A for sites). (A) Cumulative curves of the finer than -4 ϕ (< 1.6 cm) fraction of a glacial till sample (facies A), six NCSGF samples (facies B), and one sheetflood sample (facies E). (B–E) Histograms of representative samples. (F–G) Gravel–sand–mud (F) and normalized sand–silt–clay (G) ternary plots of the samples.

a subangular to subrounded outline locally interrupted by pockmarks. The intermediate diameters (d_I) of the largest clasts in facies B at each station range from 140 to 1290 cm (coarse boulders to medium blocks), with most between 200 and 600 cm. As shown by plots against distance from the apex, maximum clast size generally is consistent, rather than changing as a function of radial distance (Fig. 13A). The largest clast on the fan is in facies B at station 11, 5 km from the apex. It has dimensions of 840 × 1290 × 1680 cm, and an estimated weight of 4000 t. Facies B principally is matrix-supported, with matrix including sediment finer than coarse cobbles. Size analysis of the < 1.6 cm fraction of six samples collected from stations spanning the fan reveal that the matrix is extremely poorly sorted (S_I = 3.43–3.89 ϕ), and contains a full array of clay to medium pebbles (Table 2; Fig. 12A–D). They are enriched in the coarser grades, averaging 30%

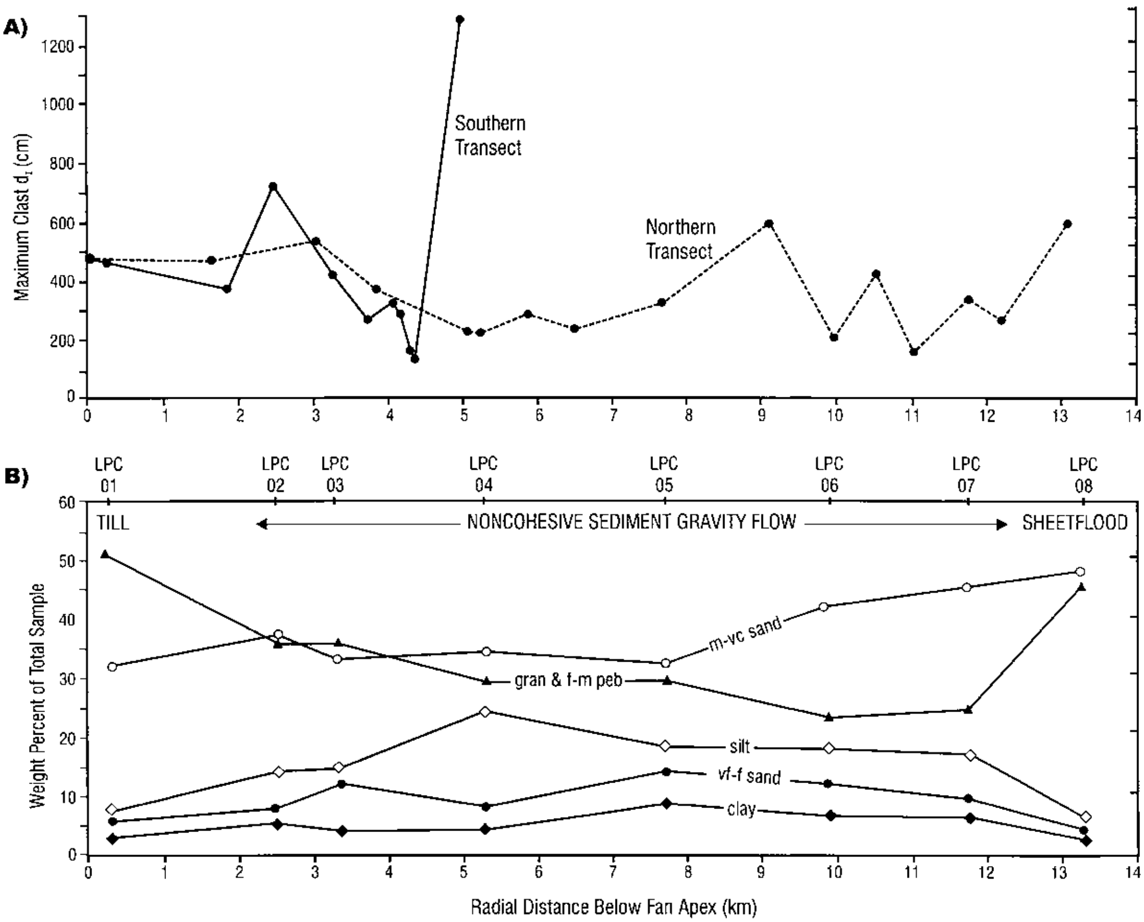

Fig. 13. (A) Plot of maximum clast size (d_I) versus radial position on the north and south Lone Pine fan transects. (B) Weight per cent versus radial position of the medium to fine pebble + granule (–4 to –1 ϕ), sand (–1 to 4 ϕ), silt (4–8 ϕ), and clay (8–12 ϕ) fractions of the size-analysed samples (Table 2).

granules to medium pebbles, 37% medium to very coarse sand, 10% very fine to fine sand, 17% silt and 6% clay. The gravel–sand–mud ratios are similar at an average of 30–48–22, as are the normalized sand–silt–clay ratios at an average of 68–24–8 (Fig. 12F & G). Like the maximum clast trend, a plot versus distance from the fan apex shows that grade abundance in the matrix samples is relatively consistent, lacking changes that correspond to radial position (Fig. 13B).

Another common aspect of facies B is a coarse-clast fabric. Fan-wide, the long axes of elongate boulders and blocks have a preferred horizontal alignment and a slope-transverse arrangement (Figs 8B & 9E). At a given site, most clasts are orientated within ±25° of the strike of the fan surface, with the few exceptions appearing to have been pivoted about an adjoining clast. This slope-perpendicular long-axis fabric exists whether the clasts are in contact or separated by matrix, although it is best developed in the clast-rich zones. In contrast, no preferred orientation of *a-b* planes, such as an imbricated fabric, exists, even in the boulder clusters. Another facies B feature is the presence of radially aligned troughs 2–4 m deep and 5–10 m wide located directly down-fan from clusters of very large boulders or blocks (Figs 9F & 14A). These ‘shadow channels’ extend radially downslope for hundreds of metres from their points of origin at the clusters. They typically have matrix-free boulder-rich margins and pebbly sand beds.

The base of the surficial facies B unit is not exposed at most stations despite cut heights of 2–8 m, indicating a minimum unit thickness of this amount (Fig. 8B).

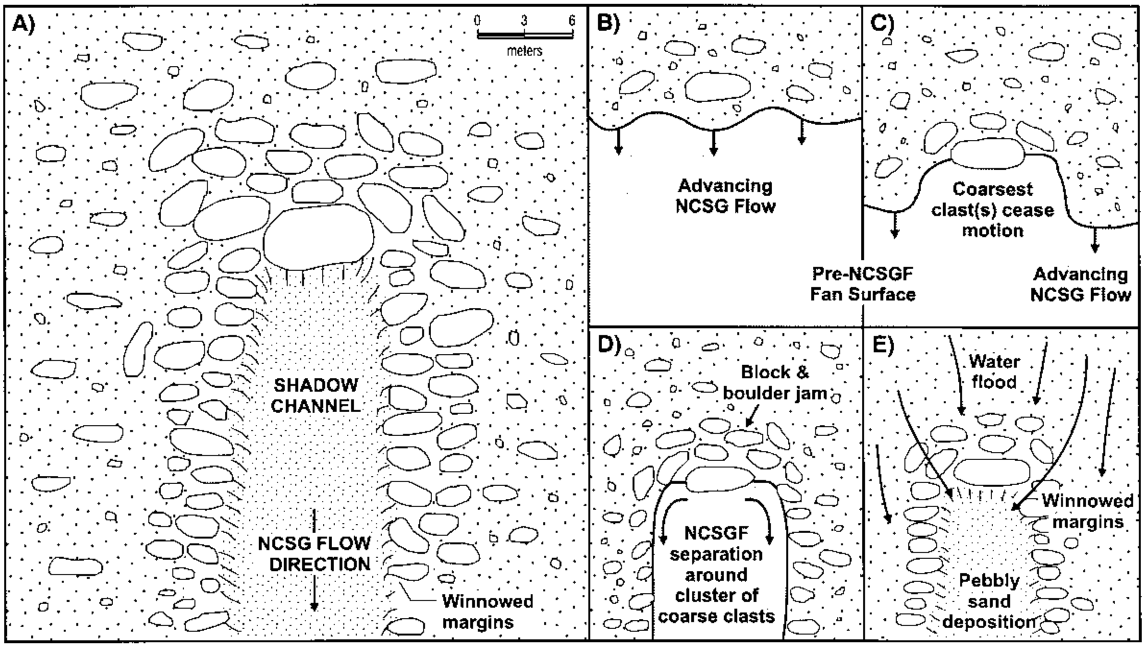

Fig. 14. (A) Fabric and form of a shadow channel. (B–E) Schematic origin of a shadow channel within a NCSGF. (B) The coarsest clasts in the advancing NCSGF are partly supported by matrix and are partly rolling. (C) As the flow thins, the coarsest clasts cease motion, locally jamming the flow. (D) The enlarging jam forces the NCSGF to separate around the cluster. (E) Subsequent water flow over the NCSGF facies winnows sand, granules and pebbles, and deposits this sediment on the channel bed.

The base is exposed at stations 3–11 and 24 and 25, revealing that this surface unit is 2–11 m thick in the proximal fan, and 2.5–3 m thick at the distal sites. Where seen, this base is sharp and slightly undulatory but not erosional, and overall is orientated with a 4–5° slope that is about parallel to the fan surface. This contact separates facies B from underlying glacial till near the fan apex, and from Alabama Hills piedmont deposits in the distal fan (Fig. 10B & C). Alabama Hills piedmont deposits also locally overlie facies B at the distal sites to define a lateral pinch-out geometry. Absolute and minimum thickness data show that the surficial facies B unit is at least 2 m thick on the south side of the fan, 3–5 m thick at the medial and distal north side of the fan, and up to 11 m thick near the fan apex (Fig. 8B). Using an average thickness of 4.5 m for the 89% (22.5 km^2) of the fan area underlain by facies B, the volume of this unit is estimated at 101.3 million cubic metres (101×10^6 m^3).

Interpretation

Textural similarities with moraines of the Lone Pine fan catchment indicate that facies B was deposited by a process that eroded sediment from the catchment till, and transported it to the fan with little modification. A fan-wide consistent light-grey desert varnish, and the consistent moderate cover of lichens on exposed boulders, further suggest that the fan-wide surficial facies B unit was deposited contemporaneously. The high volume (*c.* 101×10^6 m^3), massive (2–11+ m) bedding, non-erosional base, abundance of blocks and boulders, matrix-support, and lack of sorting collectively indicate that facies B accumulated as a highly competent sediment gravity flow of catastrophic proportion (Fig. 15). The friability of the deposits and the relatively low clay-to-sand ratio of the matrix denote low cohesive strength, suggesting that transport was as a noncohesive sediment gravity flow (NCSGF). Deposition by rainfall-induced debris flows is ruled out as an origin of facies B because these deposits have contrasting features such as thinner bedding (5–150 cm), separation of debris-flow units by water-washed zones, finer clast size, smaller volume, constituent levees and lobes, and the presence of the coarsest clasts in levees with a radial long-axis fabric (Beaty, 1963, 1970; Hubert & Filopov, 1989; Blair & McPherson, 1998).

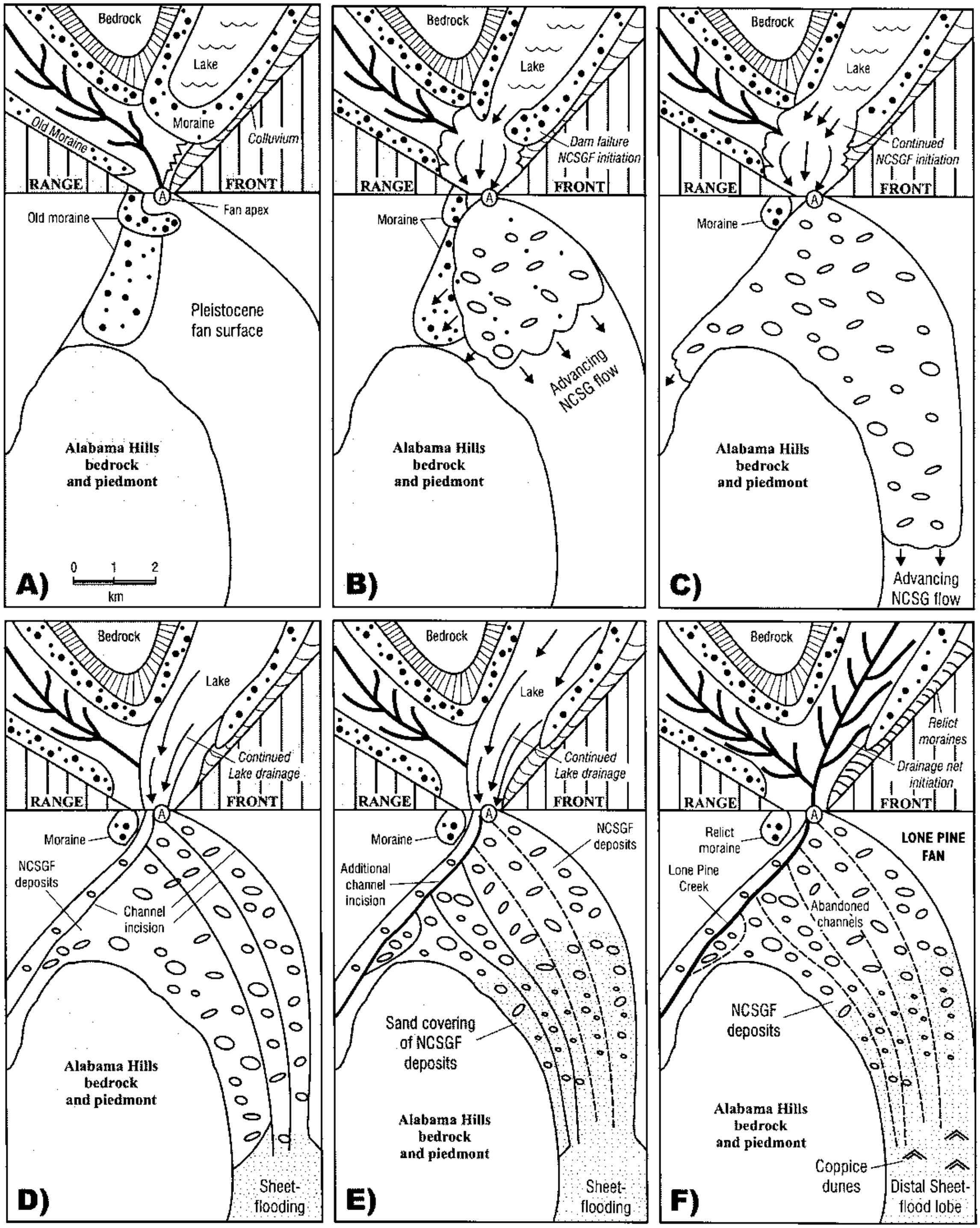
Bedrock
Lake
Moraine
Old Moraine
Colluvium
RANGE
FRONT
A
Old moraine
Fan apex
Pleistocene
fan surface
Alabama Hills
bedrock
and piedmont
A)
0 1 2
km
Dam failure
NCSGF initiation
Advancing
NCSG flow
B)
Continued
NCSGF initiation
C)
Continued
Lake drainage
NCSGF
deposits
Channel
incision
Sheet-
flooding
D)
Additional
channel
incision
Sand covering
of NCSGF
deposits
E)
Relict
moraines
Drainage net
initiation
Relict
moraine
Lone Pine
Creek
LONE PINE
FAN
Abandoned
channels
Coppice
dunes
Distal Sheet-
flood lobe
F)

Deposition by water flows is ruled out by thickness, lack of basal erosion, lack of sorting or imbrication and clast coarseness (Blair & McPherson, 1994b). The planar form, massive bedding, distribution, long-axis fabric and the presence of boulder clusters heading radially aligned shadow channels differentiate facies B from the glacial till.

The preferred slope-transverse alignment of the long axes of boulders and blocks suggests that these clasts were transported in the NCSGF mainly by rolling. The presence of pockmarks, and the matrix-rich fabric, additionally imply that the clasts were supported during flow both by matrix strength and by dispersive forces from clast collisions. The variable concentration of boulders to blocks in facies B denotes either weak particle segregation during flow, or differential motion perhaps related to surging. The lack of greater coarse-clast segregation in facies B when compared with more cohesive debris flows (Johnson, 1984; Blair & McPherson, 1998) probably reflects the low matrix strength of the NCSGF. Another variation of clast concentration in facies B is displayed by the shadow channels present downslope from many of the coarsest clasts, or from boulder clusters. The texture and form of these features suggest that local pockets of the flow ceased motion earlier than the rest due to the inability of the NCSGF to maintain in motion the heaviest clasts or the interlocked coarse clast clusters. Deposition of these clusters forced the NCSGF to separate around them, as indicated by the pivoted orientation of elongate boulders along their sides (Fig. 14). Local jamming of the flow from deposition of the coarsest clasts trapped other clasts up-flow, forming larger clusters with a slope-transverse long axis alignment. The selective deposition of some of the coarsest clasts from the NCSGF implies a loss of competence probably related to thinning as the flow expanded. At a distance of 5 km from the fan apex, for example, the flow was three times wider than at a point 1 km from the apex. The consistency in maximum clast size across the fan radius (Fig. 13A), however, shows that clast interlocking, rather than size, played the key role in the local loss of competency that produced the shadow channels. The presence of interlocked boulder clusters at the heads of shadow channels widely across the fan further implies that such clusters developed with time during flow as a result of variable interaction between abundant clasts of this size.

Large-volume NCSGF deposits such as facies B of the Lone Pine fan are poorly understood. A comparison with the historical NCSGF on a fan in Colorado (Blair, 1987) provides further insight to their origin. A large NCSGF unit texturally similar to that of the Lone Pine fan was deposited 15 July 1982 on the Roaring River fan in response to failure of a moraine dam in the fan catchment that maintained a cirque lake (Jarrett & Costa, 1986). The dam and sediment from other cross-valley moraines downstream were the source of this NCSGF. As in the Lone Pine case, late Pleistocene glaciation in the Roaring River catchment stripped colluvium from the side slopes, and repositioned this sediment as moraines crossing the floor of the higher order channels of the drainage net. The NCSGF instigation in the Roaring River catchment resulted from erosion of loose moraine material by the strongly turbulent and rapidly descending flood water released from the breached lake. The steep profile of the flood path probably aided flow transformation by promoting turbulence. The ensuing multiphase NCSGF moved a large volume of moraine sediment to the fan. Like the Lone Pine case, glacial till in the Roaring River catchment was derived from granitic rocks, and is dominated by blocks, cobbles and boulders, with a matrix of pebbles, granules and sand, but little clay (Fig. 16A). The clay-poor nature of the till promoted the development of an NCSGF when encountered by the descending water owing to the ease of sediment erosion.

By analogy with the Roaring River case, NCSGF deposition on the Lone Pine fan is interpreted to have been instigated by the rapid failure of one or more natural ice or moraine dams containing one or more lakes in the higher order channels of the catchment (Fig. 15A–C). Moraines present downslope from the failed dam probably provided additional sediment to the catastrophic flow. The specific dam(s) in the Lone

Fig. 15. (*opposite*) Schematic reconstruction of outburst flood sedimentation on the Lone Pine fan. (A) Glacial retreat strands moraines, creating moraine-dammed lakes in the catchment. (B) Initial failure of a natural dam rapidly releases lake water, which interacts with moraine sediment to form a NCSGF. Moraine near the fan apex diverts the NCSGF northward. (C) NCSGF initiation continues, moving to the fan in surges extending nearly to the fan toe. (D) NCSGF initiation in the catchment ceases owing to loss of flow-path sediment. Lake drainage continues, sending a clear-water flood to the fan that carves channels through and around previous NCSGF deposits. (E) Drainage of the breached lake ensues, with the flood water carving additional channels, and depositing eroded sediment at the fan toe by sheetflooding. (F) A major channel (now Lone Pine Creek) is incised along the south fan margin as the flood recedes, stranding the other channels. Upon cessation, the surface of the flood deposits is reworked by secondary processes, especially wind. Subsequent perennial catchment discharge flows solely through Lone Pine Creek.

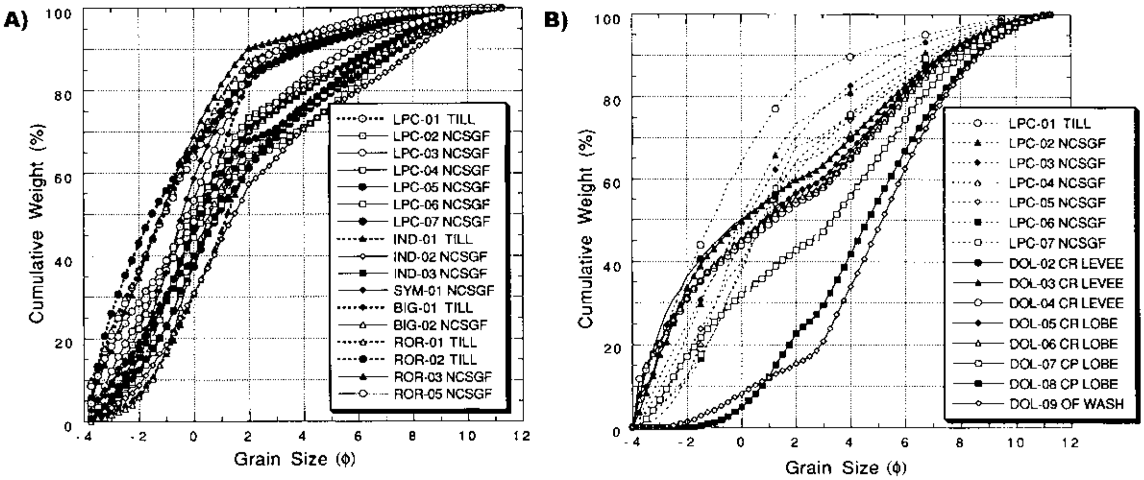

Fig. 16. (A) Cumulative curves of grain-size data of the < 1.6 cm fraction of till and NCSGF samples from the Lone Pine fan (LPC), other Sierra Nevada fans (IND, SYM and BIG), and the 1982 Roaring River fan outburst flood deposits (ROR; Blair, 1987). (B) Cumulative curves of grain-size data of the < 1.6 cm fraction of glacial till and NCSGF samples from the Lone Pine fan (LPC), and 1984 debris-flow deposits of the Dolomite fan (DOL) of the Inyo Mountains piedmont across the valley (Fig. 1; Blair & McPherson, 1998).

Pine catchment that failed remains unknown, although numerous lateral moraines with breached snouts (Fig. 4) provide several possibilities. The cause of the dam failure, too, is unknown. Historical failures of naturally dammed lakes are caused by mechanisms such as:

1 overtopping of the dam from anomalously high water input or by water displacement waves created from avalanches;

2 collapse of the dam as a result of weakening of the material by weathering or melting of contained ice;

3 settlement of the dam in response to earthquakes (Jackson, 1979; Clague *et al.*, 1985; Costa, 1985; Costa & Schuster, 1988).

All of these mechanisms are possible in the Lone Pine catchment. The low clay content of the sediment causes dams to be poorly consolidated and relatively permeable, making them susceptible to failure and readily eroded during flooding. Deep incision, high moraines (to 300 m), and steep slopes of the Lone Pine catchment promote the development of lakes with large volume, adding to instability. Destabilization of the Lone Pine catchment dams by earthquake-triggered ground motion also is probable given the seismically active nature of the faults in Owens Valley (Bateman, 1961; Lubetkin & Clark, 1988).

Differences between NCSGF deposits on the Lone Pine and Roaring River fans provide further insight to this flow phenomenon. One difference is that the volume of the surficial NCSGF unit on the Lone Pine fan is about 400 times larger than the Roaring River NCSGF unit. Also, the 12.5-km-long runout distance of the Lone Pine NCSGF is 20 times that of the Roaring River fan NCSGF. Several factors can account for these variations. The Lone Pine fan catchment area is only 24% larger than that of the Roaring River fan (30.7 km^2 versus 23.3 km^2), but it has 2.3 times greater relief (2437 m versus 1045 m), and an average slope nearly twice as steep (15.3° versus 8.3°). As a result, the Lone Pine catchment channels are more narrow and chute-like, allowing deeper lakes to be maintained on steeper slopes, and the more expeditious transfer of material to the fan (Fig. 2). Additionally, moraines are more abundant in the Lone Pine catchment (Fig. 6B). The more limited NCSGF runout on the Roaring River fan also was affected by tree cover of the fan site, which promoted jams between boulders, logs and upright trees (Blair, 1987).

Several lines of evidence allow an estimate of the age of the outburst flood that produced the facies B unit on the Lone Pine fan. The NCSGF in the proximal fan overlies glacial till deposited during the late Pleistocene Tioga stage. The degree of surface clast weathering and varnish, and the presence of soils that include carbonate coatings on the undersides of clasts, suggest that the NCSGF deposits accumulated before the Holocene. Recent cation-ratio dating of the surfaces of boulders on the part of the Lone Pine fan underlain by facies B indicates an age of about 25 000 ka, and a window of 21–29 ka (Bierman *et al*., 1995). Although the number of points (six) is limited, this age for NCSGF deposition is consistent with other information. The 25 ka time-frame post-dates the main stage (40–52.5 ka) of Tioga glaciation (Benson *et al*., 1996), and is near the time of the second Tioga stage (Phillips *et al*., 1996).

Facies C and D

Descriptions

Both facies C and D constitute sediment found in, and restricted to the fill of channels cut into glacial till or NCSGF deposits. They account for only a small part of the fan exposures, but prevail in channel cuts (Fig. 11). Facies C is the least common of the two, present as 1–3+ m units on the active bed and terraces of Lone Pine Creek. It consists of clast-supported, fine to coarse cobble gravel with scattered fine boulders (Fig. 17A & B). Pebble gravel and laminated pebbly granular sand constitute minor beds, and sand is common in interclast pores. Clasts are subangular to rounded, and display an imbricate fabric with long axes aligned transversely to slope, and with *a-b* planes dipping upslope. Individual beds, discernible from modal size changes, are 10–120 cm thick. Terraces of this facies commonly are capped by an organic-rich A soil horizon 10–20 cm thick. Similar soil horizons locally are buried by 20–50 cm of additional gravel. Facies D is finer than facies C, consisting of sandy granular fine to medium pebble gravel, or pebbly granular sand in planar-stratified sets 20–100 cm thick (Fig. 17C). Pebble beds are imbricated. Less common are low-angle (5–12°) cross-bed sets with bidirectional dip. Stratification is well developed in facies D except in the upper 30–60 cm, where it is diffuse or absent, and where it instead displays a mottled texture with calcite-lined plant roots. A 10–20 cm thick, organic-rich A soil horizon caps many of the sites, as do desert bushes and grass. Facies D is limited to, but dominates, all channels on the Lone Pine fan except for the Lone Pine Creek bed, where facies C is found.

Interpretation

The planar to low-angle bedding of facies D, gravel imbrication and the restriction of this facies to the bed of the non-perennial fan channels all indicate that it accumulated from water flows through these channels. Planar stratification denotes deposition as bedload under plane bed conditions, and the bidirectional low-angle bedding is a record of antidunes (Simons & Richardson, 1966). In contrast, the crudely stratified, imbricated bouldery cobble gravel of facies C is typical of bedload deposition in high-energy channels (Williams & Rust, 1969; Blair *et al*., 1991). The restriction of this facies to the bed of Lone Pine Creek indicates that it is a product of perennial discharge through this creek. The limited amount of sediment finer than cobbles on this creek bed, despite high availability, implies that flows competently move finer sediment downslope. The presence of both buried and surficial soil horizons in dissected terrace deposits denotes dynamic changes on the channel bed through time between erosion and deposition.

The restriction of facies D to the non-perennial channels carved into the NCSGF unit indicates that its deposition is linked to, and occurred after, channel cutting. The lack of buried soils, in contrast to facies C, further suggests that a single period of channel deposition was followed by channel inactivity. An energy mismatch exists between the extremely turbulent and competent flow needed for carving channels through the bouldery NCSGF deposits, and the comparatively quieter conditions required to deposit laminated pebbly granular sand on the beds of these channels. This relationship suggests that either channel cutting and filling were separate events, or that filling occurred during the recessional stage of a flood that cut the channels. The position of the heads of these channels at, but presently perched 10–35 m above the bed of Lone Pine Creek also indicates that the carving and partial filling of the non-perennial channels took place either when discharge was large enough to overtop the creek or, more likely, prior to incision of Lone Pine Creek. The emanation of these channels from various points along Lone Pine Creek, including the apex, also indicates that the flood was derived from the catchment, and was focused in the Lone Pine channel before deviating through the NCSGF deposits.

The high discharge that carved channels across the Lone Pine fan is interpreted to represent the second phase of the same outburst flood that produced the NCSGF unit. Initiation of NCSGFs during the initial phase of an outburst flood would cease when erodible sediment in the flood path is removed. As in the 1982 Roaring River flood case, continued drainage of the breached lake after the flood path was cleared caused sediment-deficient flood water to be discharged to the fan, where it eroded channels into the NCSGF deposits (Fig. 15D & E). The presence of channels carved through even the highest part of the NCSGF facies on the Lone Pine fan implies that the discharge was large enough to overtop the whole fan. The

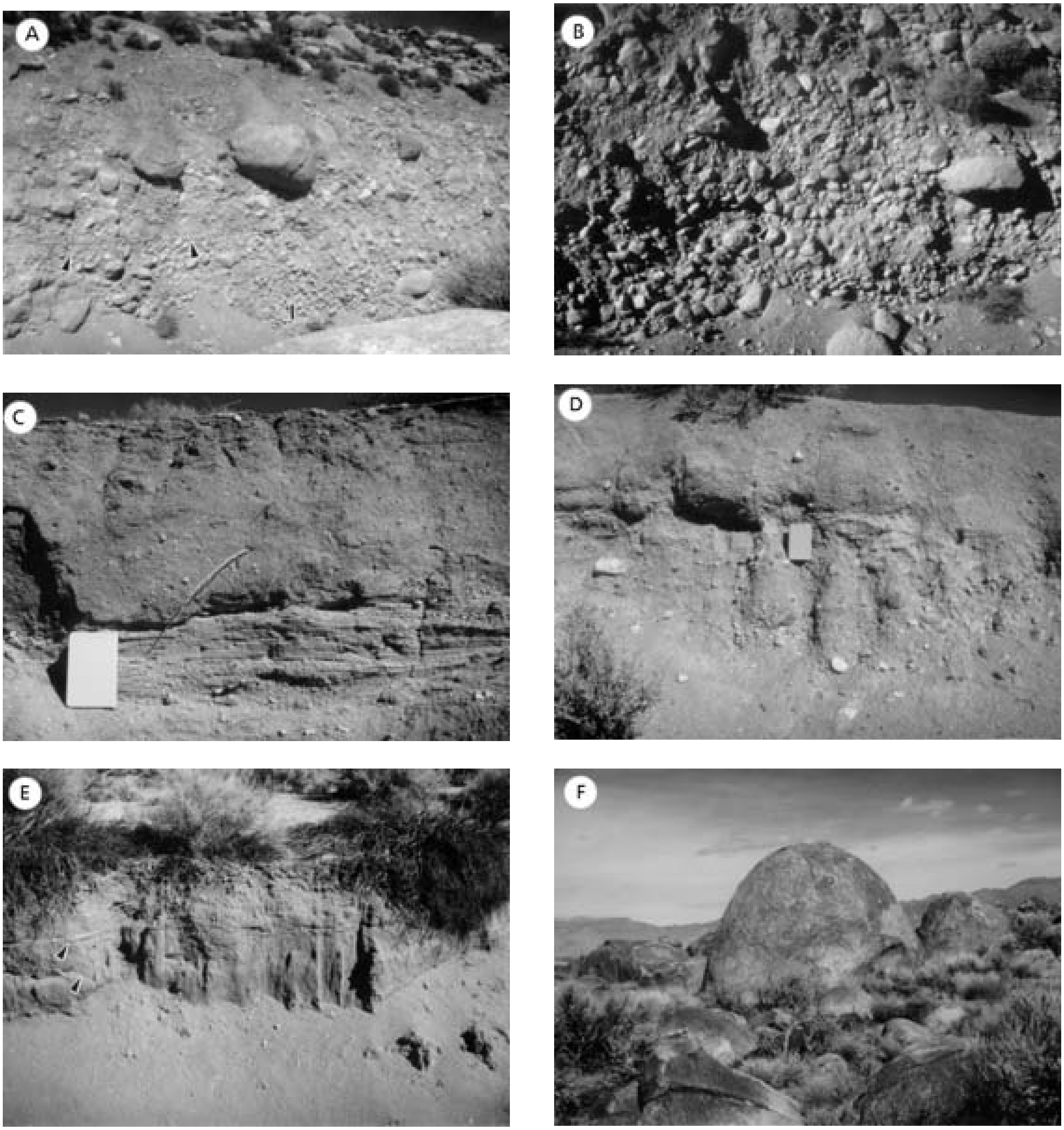

Fig. 17. (A) Four-m-high exposure along Lone Pine Creek at station 6 showing crudely stratified, clast-supported, boulder–cobble gravel (facies C). Note the sand interbeds (arrows) and imbricate fabric (I). (B) Cut 3 m tall at station 7 of crudely stratified, imbricated boulder–cobble gravel of facies C (fieldbook, arrowed, for scale). (C) Facies D exposure at station 23 of horizontally to low-angle stratified, sandy granular pebble gravel; fieldbook for scale. Bedding in the upper 50 cm was destroyed by rooting. (D) Cut 1.5 m tall at station 29 of sandy granule gravel and fine to coarse pebble gravel of facies E in evenly interstratified beds. The upper 40 cm lack stratification as a result of rooting. (E) Aeolian sandsheet deposits (facies F) near station 28 of finely laminated sand in sets 20–40 cm thick (arrows mark set boundaries). (F) Facies B boulders on the fan surface weathered in place by cracking, oxidation, exfoliation and grusification.

existence of channels around both fan margins also implies that the NCSGF deposits eventually became a topographic barrier to flow either from lessening of discharge, or from diversion of the flood into the deepening circum-fan channels, especially Lone Pine Creek. Incision of Lone Pine Creek to 10–40 m below the fan surface probably caused the eventual confinement of the flood within this channel. This third phase of the flood left previously eroded channels stranded above the Lone Pine Creek bed (Fig. 15F).

Deposition of facies D within the stranded flood channels probably occurred immediately before the cessation of outburst flooding across the fan. This interpretation explains how relatively tranquil sedimentation could occur after channel cutting, but prior to channel cut-off. Facies D deposition in the shadow channels also coincided with receding discharge across the fan, when winnowed fine sediment accumulated on the protected beds (Fig. 14E). Deposition of facies C, in contrast, commenced no earlier than the waning stage of the outburst flood, after Lone Pine Creek incision, and continues to the present.

Facies E

Description

Facies E consists of planar-interstratified beds of sandy medium to very coarse pebble gravel, and pebbly granular sand in a sequence 3–4+ m thick along the distal fan (Figs 7B & 11). These textures typically alternate in couplets 10–20 cm thick that are aligned with a 3–4° slope parallel to the fan surface (Fig. 17D). The bed boundaries are sharp and planar, but bedding is destroyed in the upper 80 cm by root-mottling. Cobbles and fine boulders are present as dispersed clasts. Gravel beds are clast-supported, and clast clusters are imbricated. Finer beds display planar lamination visible as a result of alternations in grain size from sand to granules. Size analysis of one sample (LPC-08) from a finer unit of this facies shows it is poorly sorted ($S_I = 1.92\ \phi$), and composed mostly of medium to fine pebbles (22%), granules (23%), very coarse sand (23%) and medium to coarse sand (24%; Fig. 12). The gravel–sand–mud ratio of this sample is 45–50–5, and the normalized sand–silt–clay ratio is 91–5–4 (Fig. 12F & G).

Interpretation

Bedforms and gravel imbrication indicate that facies E accumulated from water flows. The lack of evidence for channelling, and the alternating couplet motif and bedslope are typical of the deposits of alluvial-fan sheetfloods (Blair, 1987, 1999b, 2000; Blair & McPherson, 1994a,b). The prevalence of planar strata with a 3–4° slope indicates that aggradation occurred mainly as plane beds on the fan surface. Outsized boulders denote that the flow was competent to move such clasts, but the dominance of sand to pebbles suggests those grades were most available. By analogy to sheetflood case studies, the couplets formed by aggradation during a single large discharge event wherein supercritical standing wave trains were autocyclically developed and destroyed. The known flood conditions needed for depositing couplets, and the restriction of facies E to the distal Lone Pine fan directly downslope from where the outburst flood carved channels into NCSGF deposits, imply that the sheetflood facies accumulated during the same flood that produced the NCSGF facies and channels. Facies E probably consists of sediment eroded from the NCSGF unit as the channels were carved during the second flood phase (Fig. 15D & E). The presence of some volcanic clasts in this facies also indicates that the flood locally eroded the Alabama Hills piedmont. Facies E accumulated downslope from the NCSGF tract where the sheetflood lost competency as it expanded. The presence of 4+ m of stacked couplet deposits indicates that a sustained phase of sheetflooding took place; the accumulation of a similar thickness of couplets on the Roaring River fan required about 2 h of sheetflooding (Blair, 1987). Deposition of facies E on the Lone Pine fan probably ceased when flood discharge fell to the level at which it was no longer cresting the proximal fan, a time coincident with the start of the third phase of the outburst flood.

Facies F

Description

Facies F consists of moderately sorted, bimodal, very fine to fine and medium sand displaying even, pin-stripe lamination (Fig. 17E). Coarse sand to fine pebbles have a scattered distribution. Stratification is visible owing to the alternation of the finer sand and medium sand. Facies F beds slope in a variety of directions, commonly forming low-angle (3–15°) ramps that fringe desert bushes or flank the sides of gullies. Amalgamated sets 5–20 cm thick are differentiated by changes in the bedding attitude (Fig. 17E). Recent facies F deposits are slightly rooted, and older units are moderately rooted. These units are laterally discontinuous, varying in thickness from 0 to 100 cm over short (3 m) distances. This facies has a patchy distribution on the fan, occurring most abundantly upon the distal sheetflood deposits.

Interpretation

Facies F has depositional forms and textures typical of an aeolian sandsheet. The bush-fringing low-angle deposits are coppice dunes built where vegetation interfered with wind-blown sand (Blair *et al*., 1990). Planar, pin-stripe lamination forms from migrating, low-relief wind ripples (Fryberger & Schenk, 1988). The varying directions of dip of the low-angle beds reflect the changing morphology of these deposits. More open fan areas are deflated of fine sediment by the wind, with deposition of this material occurring nearby. Aeolian sandsheet deposits are common in the southwestern USA where sand is available, as is the case for the distal Lone Pine fan where the sand-rich sheetflood facies is exposed. The presence of facies F upon the sheetflood sequences indicates that it accumulated after the outburst flood.

Wind erosion and deposition are common processes that widely modify the fan surface, but result in little sediment aggradation. For this reason, they are differentiated as secondary fan processes (Blair & McPherson, 1994a,b). Another common secondary process on the Lone Pine fan is plant rooting, which has widely disturbed the upper 30–80 cm of the channel and sheetflood deposits (Fig. 17D). Rodent and insect burrows also modify these facies. Other secondary processes include soil development, formation of desert pavement and the weathering of surface clasts by oxidation, cracking, exfoliation, grusification and lichen growth (Fig. 17F). Flood deposits on the Lone Pine fan also are disrupted along fault scarps.

OUTBURST FLOODS VERSUS METEOROLOGICAL FLOODS ON FANS

The Lone Pine study exemplifies a fan type built of the deposits of rare outburst floods caused by the failure of naturally dammed catchment lakes. This poorly understood fan type probably is common where catchments are steep, of high relief and elevation, and glaciated. The main features and facies, including massive NCSGF deposits, channels incised into bouldery NCSGF deposits and lined with pebbly sand, and distal sheetflood deposits, all are related as the phases of a single, catastrophic outburst flood. As in the 1982 Roaring River case, outburst-flood deposition on the Lone Pine fan occurred in three phases linked to catchment changes as the flood progressed. In both cases the catchments were preconditioned by the glacial transfer of colluvial sediment from the steep slopes into cross-valley moraines, followed by glacial recession to form unstable moraine-dammed lakes. The first phase of outburst flooding entailed NCSGF deposition, indicating that initial flooding generated NCSGFs as the rapidly released lake water crossed loose catchment sediment in the flow path. The large volume of NCSGF deposits resulted from high sediment availability. The second phase of outburst flooding constituted a large volume of clear-water discharge that carved channels through and around the coarse NCSGF fan deposits, transporting the eroded sediment to distal sheetflood lobes. Finer sediment accumulated on the carved channels as the flood receded. This flood phase is linked to a change in the catchment caused by the removal of loose sediment in the flood path, resulting in the cessation of NCSGFs, and the onset of sediment-deficient water discharge to the fan as catchment drainage continued. The final outburst-flood phase on the Lone Pine fan involved the abandonment of all flood channels except Lone Pine Creek. Notable incision of the latter left the other channels perched 10–35 m above the Lone Pine Creek bed.

Besides a glaciated chute-like catchment with abundant sediment, another factor important to generating large outburst-flood NCSGF deposits such as those of the Lone Pine and Roaring River fans is the size suite of the colluvium. In both cases, catchment colluvium is dominated by medium sand to blocks, and little finer sediment (Fig. 16A). This suite is a product of the sediment yielded through the weathering of granitic bedrock, particularly by fracturing, jointing, oxidation and grusification. The low abundance of clay in the colluvium reflects a short residence time in the catchment, given that hydrolysis of abundant feldspar crystals in the detritus could otherwise yield much fine sediment. The low content of coarse silt to fine sand is explained by the crystal size of the Sierra Nevada plutons. The sandy gravel texture of the colluvium allows it to be easily eroded and transformed into large-volume NCSGFs when intersected by turbulent flood water. It also produces fan deposits with low cohesion, making them susceptible to erosion during the subsequent clear-water flood phase. As exemplified by the Dolomite fan across Owens Valley, more clay-rich catchment colluvium yielded from weathering of sedimentary bedrock is less erodible, and ensuing flows are of lower volume (Fig. 16B; Blair & McPherson, 1998).

The processes and facies of fans built by outburst floods contrast with those of meteorological floods, which encompass catchment discharge from rainfall, snowmelt or icemelt. As a result of water storage, outburst floods from natural dam failures have total and peak discharge values much larger (commonly 2–20 times) than those achieved in the same catchment from meteorological events (Jackson, 1979; Costa, 1985; Evans, 1986; Costa & Schuster, 1988; Desloges & Church, 1992; Walder & Costa, 1996). As illustrated by these authors, outburst floods also differ by more rapidly reaching peak discharge, and by attenuating rather than increasing in volume downslope. Because of the high volume and velocity of the water released, outburst floods also are more erosive in the catchment, causing greater and more widespread fan aggradation than is achieved by storm floods. Case studies in the southwestern USA show that alluvial fans built mainly from meteorological floods also have facies assemblages that differ from the outburst-flood deposits of the Lone Pine fan (Beaty, 1963, 1970; Hubert & Filopov, 1989; Blair & McPherson, 1994b, 1998; Blair, 1999a,b,c, 2000). Meteorological floods produce either sheetflood or debris-flow sequences across active depositional lobes, with the lobe position shifting with time. Whether dominated by sheetfloods or debris flows, deposits from an individual flood differ from the Lone Pine fan sequence by having a more limited areal extent and bed thickness (usually 5–150 cm), and by the common capping of the flood deposits with recessional stage winnowed lags. Aggradation of flood sequences with time creates a diagnostic stratigraphy that differs from that of outburst-flood sequences (Blair & McPherson, 1994b; Blair, 1999b,c, 2000). More thickly bedded rock-avalanche facies found on fans also can be differentiated from outburst flood facies by the diagnostic brecciated texture and form, and by association with sheetflood or debris-flow sequences (Blair & McPherson, 1994b; Blair, 1999a). Another contrasting feature of the fans in the southwest USA built by meteorological floods is the existence on the surface of sectors with variable intensities of rock varnish, which reflects different ages of aggradation as the active depositional lobe shifts with time. This pattern does not exist on the Lone Pine or Roaring River fans because of the fan-wide extent of the deposits of a single outburst flood.

RELEVANCE

Knowledge of the contrasting processes and facies of fans built mainly by outburst floods versus those built by meteorological floods has several applications. The form and facies of the Lone Pine fan system can be used to recognize other fans prone to, or that have experienced, outburst floods. The potential hazards on a fan built by outburst flooding differ from those prone to meteorological flooding by significantly higher discharge, by the breadth of the fan that is catastrophically inundated, by the lack of weather warnings now possible for storm flooding, and because outburst floods can occur on sunny days when the flood potential is not perceived. Systematic facies and catchment mapping thus can provide data useful for decisions on flood zoning and hazards remediation. The value of this knowledge is underscored by the fact that outburst floods are not yet recognized as a distinctive hazard type in the U.S. Federal Emergency Management Agency's guide to alluvial-fan flooding (Schumm *et al.*, 1996).

An example of how the Lone Pine fan model can be used for piedmont characterization is given by evaluating other fans of the Sierra Nevada piedmont that are reported to consist of debris-flow levee and lobe facies typical of meteorological floods, including the Pinyon, Symmes and Independence fans (Fig. 1; Whipple & Dunne, 1992; Schumm *et al.*, 1996). The high relief, elevation, slope and chute-like form of the catchments of these fans, their recent deglaciation, and an abundance of moraines are the same conditions of the Lone Pine fan catchment that promoted outburst flooding. Moraine-dammed cirque lakes are common in these other catchments (Blackwelder, 1931; Clark & Gillespie, 1997), as are cross-drainage moraines (Fig. 18A & B). Like the Lone Pine system, these catchments also are underlain by granitic rock that has yielded a sandy to blocky colluvial suite deficient in clay (Fig. 16A). Reconnaissance of these fans reveals that they are dominated by outburst-flood features such as a surface unit of matrix-rich blocky and bouldery NCSGF deposits with a slope-transverse long-axis fabric (Fig. 18A), carved flood channels, shadow channels with recessional pebbly sand beds, circum-fan channels, distal sheetflood lobes and a consistent surface varnish. Features offered to support a meteorological debris-flow origin, such as constituent levees, lobes or channel plugs (Whipple & Dunne, 1992; Schumm *et al.*, 1996), were not found on these fans, nor were other debris-flow features such as stacked matrix-rich beds 10–150 cm thick divided by washed gravel beds. Bioturbated distal-fan deposits appear to have been misidentified as debris-flow units, and winnowed margins of the flood channels as levees. The former are a part of a rooted surface widespread in Owens Valley, whereas the winnowed boulder

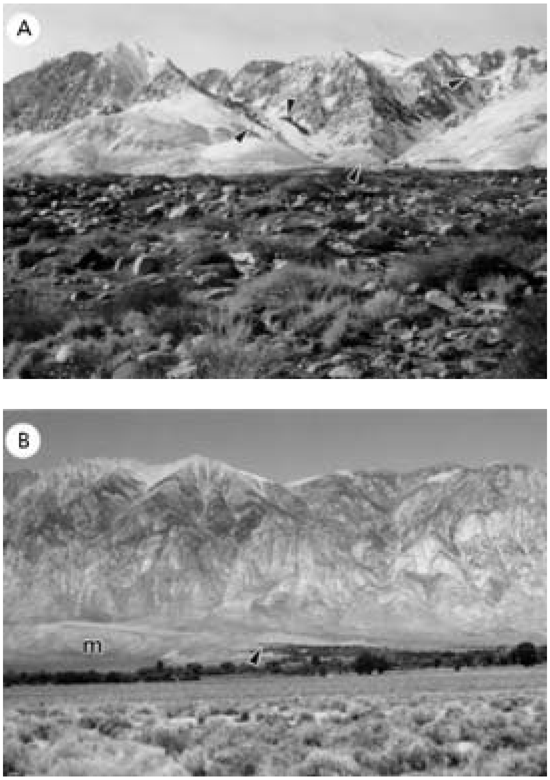

Fig. 18. (A) Overview of the Sawmill Canyon fan of the Sierra Nevada piedmont 30 km north of the Lone Pine fan. Surficial fan sediment is texturally similar to the Lone Pine NCSGF deposits, and moraines are common in the catchment (arrows). (B) View of the Big Pine fan of the Sierra Nevada piedmont 55 km north of Lone Pine. Prominent Pleistocene moraines (m) 250 m high and 1.1 km across extend 2.5 km on to the piedmont. The fan is prograding eastward from the breached snout of the moraine (arrow).

trains can easily be differentiated from debris-flow levees by their channel-margin shoulder form and their transverse boulder long-axis fabric, features that contrast with the ridge-like positive form and radial long-axis fabric of boulders typical of debris-flow levees. Thus, like the Lone Pine fan, these fans bear critical evidence for outburst flooding, suggesting that such floods have been common on the Sierra Nevada piedmont.

Another application of the Lone Pine fan model is to aid the identification of alluvial-fan sequences in the rock record that were deposited by outburst floods. Such realizations provide clues helpful to understanding processes and evolution of ancient piedmonts. Knowledge of the catchment conditions that produce outburst floods on fans further allows reconstruction of the palaeoconditions of catchments that no longer exist, such as localities where alpine glaciation previously took place.

CONCLUSIONS

Exposures of the surficial 2–40 m of the Lone Pine fan reveal that it was deposited mainly by a late Pleistocene catastrophic outburst flood probably triggered from the failure of a glacial moraine-dammed lake in the catchment. Over 100×10^6 m^3 of boulder-rich sediment accumulated in a 2–11 m thick fan unit during this event. The outburst flood occurred in three phases beginning with a large NCSGF generated where the rapidly released lake water intersected sandy to bouldery moraine in the flood path. Continued lake drainage subsequent to removal of the loose flood-path sediment sent clear-water discharge to the fan, which carved channels through and around the NCSGF deposits, and moved this sediment to the fan toe where it accumulated in sheetflood lobes. The final flood phase entailed deep incision of Lone Pine Creek, producing a fan-bypass channel that funnelled recessional flood discharge off the piedmont. Differentiating fan deposits of outburst floods from meteorological floods is critical for delineating hazards and resources, and for developing sound stratigraphical models useful for deciphering the rock record.

ACKNOWLEDGEMENTS

This research commenced in 1982 as part of the Roaring River flood studies, when the relationships between outburst flooding and fan sedimentation were first examined. Dr J.E. Costa is thanked for that collaboration. Drs R. Raynolds, J.G. McPherson, and A. Moscariello are thanked for fruitful discussions in the field. The manuscript benefited from the comments of Dr J. Hubert and an anonymous reviewer, and from editors I.P. Martini and G. Plint. Blair & Associates provided support for this study.

REFERENCES

Bateman, P.C. (1961) Willard D. Johnson and the strike-slip component of fault movement in Owens Valley, California, earthquake of 1872. *Bull. seismol. Soc. Am.* **51**, 483–493.

Beaty, C.B. (1963) Origin of alluvial fans, White Mountains, California and Nevada. *Assoc. Am. Geogr. Ann.* **53**, 516–535.

Beaty, C.B. (1970) Age and estimated rate of accumulation of an alluvial fan, White Mountains, California. *Am. J. Sci.* **268**, 50–77.

Benson, L.V., Burdett, J.W., Kashgarian, M., Lund, S.P., Phillips, F.M. & Rye, R.O. (1996) Climatic and hydrologic oscillations in the Owens Lake basin and adjacent Sierra Nevada, California. *Science* **274**, 746–749.

Berry, M.E. (1994) Soil–geomorphic analysis of late Pleistocene glacial sequences in the McGee, Pine, and Bishop Creek drainages, east-central Sierra Nevada, California. *Quat. Res.* **41**, 160–175.

Bierman, P., Gillespie, A. & Caffee, M.W. (1995) Cosmogenic ages for earthquake recurrence intervals and debris flow fan deposition, Owens Valley, California. *Science* **270**, 447–450.

Blackwelder, E. (1931) Pleistocene glaciation in the Sierra Nevada and Basin Ranges. *Geol. Soc. Am. Bull.* **42**, 865–922.

Blair, T.C. (1987) Sedimentary processes, vertical stratification sequences, and geomorphology of the Roaring River alluvial fan, Rocky Mountain National Park, Colorado. *J. sediment. Petrol.* **57**, 1–18.

Blair, T.C. (1999a) Form, facies, and depositional history of the North Long John rock avalanche, Owens Valley, California. *Can. J. Earth Sci.* **36**, 855–870.

Blair, T.C. (1999b) Sedimentary processes and facies of the waterlaid Anvil Spring Canyon alluvial fan, Death Valley, California. *Sedimentology* **46**, 913–940.

Blair, T.C. (1999c) Sedimentology of the debris-flow-dominated Warm Spring Canyon alluvial fan, Death Valley, California. *Sedimentology* **46**, 941–965.

Blair, T.C. (2000) Sedimentology and progressive tectonic unconformities of the sheetflood-dominated Hell's Gate alluvial fan, Death Valley, California. *Sediment. Geol.* **132**, 233–262.

Blair, T.C. & McPherson, J.G. (1994a) Alluvial fan processes and forms. In: *Geomorphology of Desert Environments* (Eds Abrahams, A.D. & Parsons, A.), pp. 354–402. Chapman & Hall, London.

Blair, T.C. & McPherson, J.G. (1994b) Alluvial fans and their natural distinction from rivers based on morphology, hydraulic processes, sedimentary processes, and facies. *J. sediment. Res.* **64**, 451–490.

Blair, T.C. & McPherson, J.G. (1998) Recent debris-flow processes and resultant form and facies of the Dolomite alluvial fan, Owens Valley, California. *J. sediment. Res.* **68**, 800–818.

Blair, T.C. & McPherson, J.G. (1999) Grain-size and textural classification of coarse sedimentary particles. *J. sediment. Res.* **69**, 6–19.

Blair, T.C., Clark, J. & Wells, S.G. (1990) Quaternary stratigraphy, landscape evolution, and application to archeology: Jarilla piedmont and basin floor, White Sands Missile Range, New Mexico. *Geol. Soc. Am. Bull.* **102**, 749–759.

Blair, T.C., Baker, F. & Turner, J. (1991) Cenozoic fluvial facies architecture and aquifer heterogeneity, Oroville, California, Superfund Site and vicinity. In: *Three Dimensional Facies Architecture of Terrigenous Clastic Sediments and its Implications for Hydrocarbon Discovery and Recovery* (Eds Tyler, N. & Miall, A.D.), pp. 147–159. Concepts in Sedimentology and Paleontology, 3, Society of Economic Paleontologists and Sedimentologists, Tulsa.

Campbell, R.H. (1974) Debris flows originating from soil slips during rainstorms in southern California. *Q. J. eng. Geol.* **7**, 339–349.

Campbell, R.H. (1975) Soil slips, debris flows, and rainstorms in the Santa Monica Mountains and vicinity, southern California. *U.S. geol. Surv. Prof. Pap.* **851**, 51 pp.

Clague, J.J., Evans, S.G. & Blown, I.G. (1985) A debris flow triggered by the breaching of a moraine-dammed lake, Klattasine Creek, British Columbia. *Can. J. Earth Sci.* **22**, 1492–1502.

Clark, D.H. & Gillespie, A.R. (1997) Timing and significance of late-glacial and Holocene cirque glaciation in the Sierra Nevada, California. *Quat. Int.* **38/39**, 21–38.

Costa, J.E. (1985) Floods from dam failure. *U.S. geol. Surv. Open File Rep.* **85–560**, 54 pp.

Costa, J.E. & Schuster, R.L. (1988) The formation and failure of natural dams. *Geol. Soc. Am. Bull.* **100**, 1054–1068.

Desloges, J.R. & Church, M. (1992) Geomorphic implications of glacier outburst flooding: Noeick River valley, British Columbia. *Can. J. Earth Sci.* **29**, 551–564.

Dorn, R.I., Turrin, B.D., Jull, A.J.T., Linick, T.W. & Donahue, D.J. (1987) Radiocarbon and cation-ratio ages for rock varnish on Tioga and Tahoe morainal boulders of Pine Creek, eastern Sierra Nevada, California, and their paleoclimatic implications. *Quat. Res.* **28**, 38–49.

Dunne, G.C. & Walker, J.D. (1993) Age of Jurassic volcanism and tectonism, southern Owens Valley region, east-central California. *Geol. Soc. Am. Bull.* **105**, 1223–1230.

Evans, S.G. (1986) The maximum discharge of outburst floods. *Can. geotech. J.* **23**, 385–387.

Evernden, J.F. & Kistler, R.W. (1970) Chronology of emplacement of Mesozoic batholithic complexes in California and western Nevada. *U.S. geol. Surv. Prof. Pap.* **623**, 42 pp

Folk, R.L. (1974) *Petrology of Sedimentary Rocks*. Hemphill's Publishers Co., Austin, Texas.

Fryberger, S.G. & Schenk, C.J. (1988) Pin-stripe lamination: a distinctive feature of modern and ancient eolian sediments. *Sediment. Geol.* **55**, 1–15.

Hollett, K.J., Danskin, W.R., McCaffrey, W.H. & Walti, C.L. (1991) Geology and water resources of Owens Valley, California. *U.S. geol. Surv. Water Supply Pap.* **2370**, 77 pp.

Horton, R.E. (1945) Erosional development of streams and their drainage basins: hydrophysical approach to quantitative morphology. *Geol. Soc. Am. Bull.* **56**, 275–370.

Hubert, J.F. & Filipov, A.J. (1989) Debris-flow deposits in alluvial fans on the west flank of the White Mountains, Owens Valley, California. *Sediment. Geol.* **61**, 177–205.

Jackson, L.E. Jr (1979) A catastrophic glacial outburst flood (jökulhlaup) mechanism for debris flow generation at the Spiral Tunnels, Kicking Horse River basin, British Columbia. *Can. geotech. J.* **16**, 806–813.

Jarrett, R.D. & Costa, J.E. (1986) Hydrology, geomorphology, and dam-break modelling of the July 15, 1982 Lawn Lake and Cascade Lake dam failures, Larimer County, Colorado. *U.S. geol. Surv. Prof. Pap.* **1369**, 78 pp.

Johnson, A.M. (1984) Debris flow. In: *Slope Instability* (Eds Brunsden, D. & Prior, D.B.), pp. 257–361. Wiley, New York.

Knopf, A. (1918) A geologic reconnaissance of the Inyo Range and the eastern slope of the southern Sierra Nevada, California. *U.S. geol. Surv. Prof. Pap.* **110**, 130 pp.

LUBETKIN, L.K.C. & CLARK, K.M. (1988) Late Quaternary activity along the Lone Pine fault, eastern California. *Geol. Soc. Am. Bull.* **100**, 755–766.

MATTHEWS, R.A. & BURNETT, J.L. (1965) *Geologic Map of California, the Fresno Sheet, Scale 1: 250 000*. California Division of Mines and Geology, Sacramento, CA.

MCGEE, W.J. (1897) Sheetflood erosion. *Geol. Soc. Am. Bull.* **8**, 87–112.

MOORE, J.G. (1981) *Geologic Map of the Mount Whitney Quadrangle, Inyo and Tulare Counties, California, Scale 1: 62, 500*. U.S. Geological Survey Map GQ-1545, Reston, VA.

PACK, F.J. (1923) Torrential potential of desert waters. *Pan Am. Geol.* **40**, 349–356.

PAKISER, L.C., KANE, M.F. & JACKSON, W.H. (1964) Structural geology and volcanism of Owens Valley region, California—a geophysical study. *U.S. geol. Surv. Prof. Pap.* **438**, 65 pp.

PHILLIPS, F.M., ZREDA, M.G., BENSON, L.V., PLUMMER, M.A., ELMORE, D. & SHARMA, P. (1996) Chronology for fluctuations in Late Pleistocene Sierra Nevada glaciers and lakes. *Science* **274**, 749–751.

POHL, M.M., HAJDAS, I. & BONANI, G. (1996) Assessing AMS ^{14}C ages of detrital organics from Holocene and late Pleistocene moraines, east-central Sierra Nevada, USA. *Holocene* **6**, 463–467.

SCHUMM, S.A., BAKER, V.R., BOWKER, M.F. *et al.* (1996) *Alluvial Fan Flooding*. National Academy Press, Washington, DC.

SHARP, R.P. & BIRMAN, J.H. (1963) Additions to the classical sequence of Pleistocene glaciations, Sierra Nevada, California. *Geol. Soc. Am. Bull.* **74**, 1079–1086.

SHAW, J. (1985) Subglacial and ice marginal environments. In: *Glacial Sedimentary Environments* (Eds Ashley, G.A., Shaw, J. & Smith, N.D.), Short Course Notes Soc. econ. Paleont. Miner., Tulsa, **16**, 7–84.

SIMONS, D.B. & RICHARDSON, E.V. (1966) Resistance to flow in alluvial channels. *U.S. geol. Surv. Prof. Pap.* **422-J**, 61 pp.

STRAHLER, A.N. (1964) Quantitative geomorphology of drainage basins and channel networks. In: *Handbook of Applied Hydrology* (Ed. Chen, V.T.), pp. 40–74. McGraw-Hill, New York.

STREITZ, R. & STINSON, M.C. (1977) *Geologic Map of the Death Valley Sheet, California, Scale 1: 250 000*. California Division of Mines and Geology, Sacramento, CA.

TROWBRIDGE, A.C. (1911) The terrestrial deposits of Owens Valley, California. *J. Geol.* **19**, 706–747.

WALDER, J.S. & COSTA, J.E. (1996) Outburst floods from glacier-dammed lakes: the effect of mode of the lake drainage on flood magnitude. *Earth Surf. Process.* **21**, 701–723.

WHIPPLE, K.X. & DUNNE, T. (1992) The influence of debris-flow rheology on fan morphology, Owens Valley, California. *Geol. Soc. Am. Bull.* **104**, 887–900.

WILLIAMS, P.F. & RUST, B.R. (1969) The sedimentology of a braided river. *J. sediment. Petrol.* **39**, 649–679.

WOOLLEY, R.R. (1946) Cloudburst floods in Utah 1850–1938. *U.S. geol. Surv. Water Supply Pap.* **994**, 159 pp.

Spec. Publs int. Ass. Sediment. (2002) **32**, 141–66

Alluvial fans in the Italian Alps: sedimentary facies and processes

A. MOSCARIELLO*, L. MARCHI†, F. MARAGA‡ *and* G. MORTARA‡

**Godwin Institute of Quaternary Research, University of Cambridge;*
†Research Institute for Prevention of Geological and Hydrological Hazard, Italian National Research Council, Padua; and
‡Research Institute for Prevention of Geological and Hydrological Hazard, Italian National Research Council, Turin

ABSTRACT

Sediment gravity flows are very common sedimentary processes in the Alpine region and are often characterized by rapid deposition of large amounts of material. Hazard evaluation in such mountainous areas depends on proper identification of the dominant sedimentary processes, interpreted both from modern and ancient sedimentary facies and their distribution. Three main groups of alluvial fans, characterized by different dominant sedimentary processes, have been distinguished on the basis of lithological characteristics of the catchment area. The dominant catchment lithologies are:

1 massive and/or crudely stratified carbonate rocks (dolomite and massive limestones);
2 fine-grained sedimentary and metamorphic rocks (schists, calc-schists, mica schists, slate, phyllites and quartzites);
3 massive crystalline rocks (granites, granodiorites).

Their main characteristics are illustrated by three case studies concerning large debris-flow events that occurred in the recent past. The comparison of sediment texture and grain-size distribution indicates that important differences in the sedimentological features of debris flows are generated by the three different rock types in the catchments. Colluvium lithology strongly controls the grain-size distribution of the debris available on the catchment that is mobilized, transported and accumulated on the fan during catastrophic flood events. The proportion of fine-grained particles (clay and fine silt) within the colluvium plays a key role in controlling the dominant primary sedimentary processes. The study of 23 flood events over the past 30 yr indicates that the catchments of group 1 and 2 fans produce large amounts of clay and fine silt, which typically can lead to the generation of cohesive sediment gravity flows. Group 3 fan catchments produce colluvium free of clay and fine silt that can be mobilized and transported by water flow processes, and which in extreme flood events usually are associated with non-cohesive sediment gravity flows.

INTRODUCTION

Alluvial fan formation and aggradation in Alpine regions is related to catastrophic sedimentary processes associated with extreme flood events. Generally, such events lead to the accumulation of exceptionally coarse and heterogeneous materials, which are often interpreted as debris-flow deposits. However, alluvial fans can be characterized by different sedimentary processes, which broadly can be distinguished as sediment gravity flows and sedimentary fluid flows (Blair & McPherson, 1994).

The rheologic characteristics of sedimentary flows can vary depending on lithology, grain-size distribution and sediment concentration (Pierson, 1980; Pierson & Costa, 1987; Hutchinson, 1988; Whipple, 1993). On the basis of these parameters several authors have described different processes, which range from water floods with limited amount of bedload and suspended load, to debris flows characterized by a highly concentrated load (Aulitzky, 1982; Pierson & Costa, 1987; Costa, 1988a; Meunier, 1991; Blair & McPherson, 1994).

* Present address: Shell U.K. Exploration and Production, Commercial Road, PO Box 4, Lowestoft, Suffolk, NR32 2TH, UK. Email: andrea.moscariello@expro.shell.co.uk

Flood and Megaflood Processes and Deposits: Recent and Ancient Examples. Edited by I. Peter Martini, Victor R. Baker and Guillermina Garzón © 2002 International Association of Sedimentologists. ISBN: 978-0-632-06404-5

Despite a wide interest in alluvial fan processes in the scientific community, mostly because of the associated geological hazards, few studies have analysed the sedimentary features, stratigraphy and related sedimentary processes (Beaty, 1963; Johnson & Rodine, 1984; Blair, 1987; Wells & Harvey, 1987; Hubert & Filipov, 1989; Blair & McPherson, 1998; Moscariello & Blair, 1998; Moscariello, 1998; Moscariello & Deganutti 2000). This results mostly from the difficulty in directly observing and describing sedimentary processes that often are associated with instantaneous, dangerous and unpredictable events.

Alluvial fan processes constitute a common geological hazard in the Italian Alps. A proper understanding of fan behaviour determined from the sedimentary record therefore is required to fully evaluate fan evolution, predict the dominant sedimentary processes and eventually assess the potential hazards (Maraga *et al.*, 1998).

This paper presents a contribution to the sedimentological study of modern Alpine alluvial fans by:

1 providing an overview of the sedimentary facies of selected alluvial fans that are considered to be representative of the most common sedimentary processes in the Italian Alps;

2 discussing the sedimentary processes interpreted from facies analysis and the stratigraphy of the alluvial fan deposits, with emphasis on the grain-size distribution and lithological characteristics of the drainage basin;

3 discussing the natural hazards related to alluvial fan processes and their impact on inhabited areas.

GEOLOGY, GEOMORPHOLOGY AND CLIMATE

The Alps form a large part of northern Italy. They extend east–west for about 720 km and reach almost 160 km in width. Geologically, the Alps are composed of a heterogeneous Mesozoic–Cenozoic sedimentary and volcanic sequence that overlies the Palaeozoic metamorphic basement. Complex structures have developed as a result of several phases of tectonic deformation over the past 15 million years (Dal Piaz, 1992; Hunziker *et al.*, 1992). The resulting geographical distribution of lithotypes are as follows:

1 Basement rocks consisting of magmatic (granites, gabbros and ophiolites) and Prealpine/Alpine metamorphic rocks with associated meta-sedimentary and sedimentary rocks prevail on the western side of the Alps.

2 The central and eastern calcareous Alps (the latter encompassing the Dolomites, Fig. 1) are characterized mostly by sedimentary and volcanic rocks. Local exceptions are represented by Tertiary plutonic massifs occurring in the central Alps, and by volcanic rocks and heavily tectonized and metamorphosed rocks cropping out in the eastern Alps.

The rock deformation style (type and density of fracture network) is variable throughout the Alps, depending mostly on the proximity of the major fault zones developed during the last Alpine tectonic phase. Intense deformation also is related to gravity processes (such as lateral spreading and rock flow), which can affect a large portion of slopes (Mortara & Sorzana, 1987; Pasuto & Soldati, 1996).

Quaternary glacial and fluvioglacial deposits are widespread throughout the Alpine valleys. Typically, these deposits have moderate to poor lateral continuity, but they can be relatively thick (up to 30–60 m) and cover large areas within the catchment basins.

Alluvial fans form prominent landforms throughout the Alpine region where tributary streams enter the main valleys. Many alluvial fans have been entrenched by streams as a result of tectonic uplift of the Alps over the past 15 000 yr, together with the lowering of base level during the Holocene (Carraro, 1992). The alluvial fans are characterized by perennial or ephemeral streams. Flow discharges display maxima during summer–autumn rainfalls and spring snow melting.

Complex orography influences the climate of the Italian Alps, causing high variability in the spatial distribution of precipitation and temperature even at a local scale. Valleys parallel to the Alpine structure are relatively dry, with annual precipitation of about 500–600 mm, whereas transverse-orientated valleys have a higher precipitation (1500–2000 mm). Annual amounts of precipitation exceed 3000 mm in some Prealpine areas. Seasonal distribution of precipitation is continental, with a summer maximum in the inner part of the Alpine range, whereas spring and autumn maxima are observed in the Prealpine belt.

METHODS

Institutes of the Italian National Research Council (CNR-IRPI) for prevention of geological and hydrological hazards in northern Italy have been studying and monitoring alluvial fan activity in the Alpine area since the mid-1970s. Field surveys often are carried out a few hours after the flood events and they have provided an extensive collection of data on flood dynamics, sedimentary processes and damage to inhabited areas. Detailed mapping and sedimentological description of the deposits accompanied by collection of samples

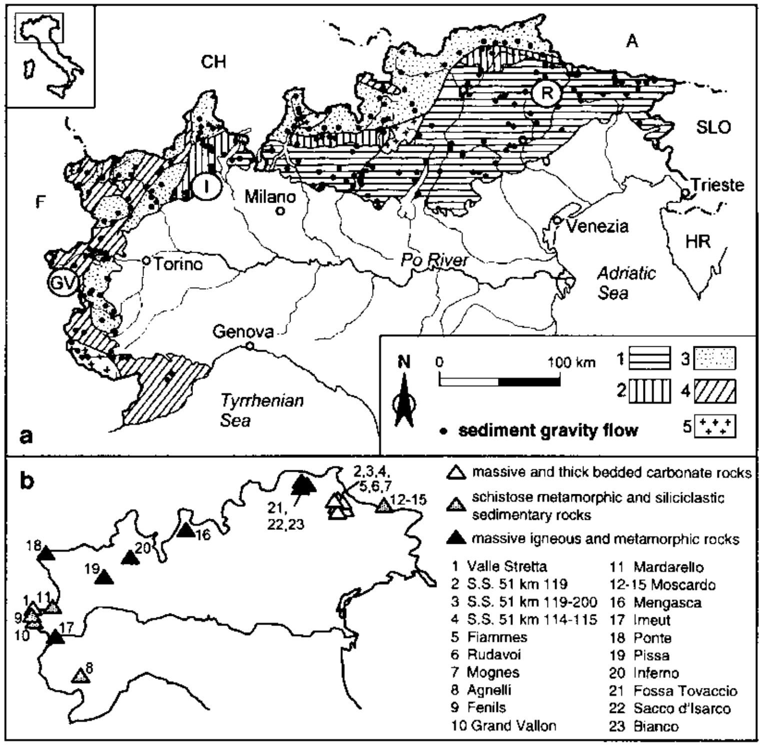

Fig. 1. Maps of the Italian Alps. (a) Geological map with location of catastrophic sediment gravity flows that have caused damage to inhabited areas since the fourteenth century (modified and updated after Govi *et al.* (1985a) and Maraga *et al.* (1998)). Case studies examined in this paper are indicated with letters: GV (Grand Vallon), I (Inferno) and R (Rudavoi). The lithological units include: 1—porphyry, sandstone, limestone, dolomite and flysch (Insubric Zone and southern calcareous Alps); 2—gneiss, kinzigites, micaschists, phyllites (Insubric Zone); 3—gneiss, mica schist, kinzigite, marble (Pennidic and Austroalpine Zone); 4—schist, vulcanite, quartzite, neritic fine-grained siliciclastic rocks, flysch, calc-schist, ophiolite (Pennidic, Austroalpine and Helvetic Zone); 5—massive crystalline rocks (granites, granodiorites of Palaeozoic and Tertiary plutonic complexes). (b) Location and lithological groups of alluvial fans sampled for this study.

from each facies also have been carried out. However, in many instances a thorough examination of fresh fan deposits (in particular those located at the fan toe) has been hindered by prompt reclamation work.

Monitoring of debris flows on the alluvial fan of the Moscardo torrent (eastern Italian Alps, Fig. 1b) was initiated about 10 yr ago (Arattano *et al.*, 1997). This study area was chosen because of the high frequency of debris flows (the Moscardo Torrent produces at least one debris flow per year). Instrumentation consisted of rain gauges, ultrasonic sensors to measure flow stage, and seismic sensors that record ground vibrations caused by debris flows. Monitoring also included analysis of sedimentary facies and processes at sites where quantitative parameters associated with seldom-observed debris-flow waves (hydrograph pattern, velocity, discharge and flowing volumes) were recorded (Moscariello & Deganutti, 2000).

The average time between floods in the same basin as well as the sediment gravity-flow frequency has been established from historical information (public and private archives, and libraries). Climatic conditions prior to and during the events have been inferred from historical records and, for recent events, measured instrumentally.

Textural analyses of fan deposits have been carried out with standard sieve and counting techniques. Wet-sieve analyses were performed on bulk samples. Clay and fine silt content was measured by hydrometer. Cumulative curves at the < 32 mm fraction better represent the distribution of the debris-flow sediment matrix. Grain-size analyses were performed on the < 32 mm fraction (matrix). This fraction contains the cohesive particles (clay and fine silt) that are considered to play a key role in sediment gravity-flow processes (Blackwelder, 1928; Sharp & Nobles, 1953; Johnson, 1970; Campbell, 1975; Pierson & Costa, 1987; Whipple, 1993; Blair & McPherson, 1994, 1998). The D_{75} and D_{25} are listed in Table 1, together with the Trask's sorting parameter (Folk, 1974).

Coarse deposits (boulder and block size) were measured using the Quadrillage technique (Cailleux & Tricart, 1959). This consists of measuring the intermediate diameter of 100 clasts occurring at the grid nodes of a squared net that has a side dimension similar to the intermediate diameter of the largest clast occurring in the survey area. The results from the Quadrillage technique have then been integrated into the sieve analysis results where fine-grained sediments represented more than 10% of the whole measured sediment.

Table 1. List of grain-size parameters for the matrix (<32 mm) of sediment gravity flow deposits sampled from alluvial fans of the Italian Alps. The results are grouped in three main categories based on the dominating lithological characteristic of the catchment basin.

No.	Torrent locality† (Province)	Hydrographic basin	Dominant lithology	Group	Grain-size parameters		
					D_{75}	D_{25}	$(D_{75}/D_{25})^{1/2}$
1	Valle Stretta–Pian del Colle (TO)	Dora Riparia	Dolomite and limestones	1	20	0.65	5.55
2	S.S.N. 51 km 199 (BZ)	Adige	Dolomite	1	8.45	1.83	2.15
3	S.S.N. 51 km 119+200 (BZ)	Adige	Dolomite	1	12.65	1.9	2.58
4	S.S.N. 51 km 113–114 (BL)	Piave	Dolomite	1	8.54	2.04	2.05
5	Fiammes (BL)	Piave	Dolomite	1	12.86	0.76	4.11
6	Rudavoi–S.S.N. 48 km 132 (BL)	Piave	Dolomite and limestones	1	15.31	1.7	3
7	Mognes (BL)	Piave	Dolomites	1	15.17	2.5	2.46
8	Agnelli —Tetto Canet (CN)	Gesso (Tanaro)	Quartzite	2	0.9	0.004	15
9	Fenils—Fenils (TO)	Dora Riparia	Calc-schist	2	3.5	0.018	13.94
10	Gran Vallon—Cesana (TO)	Dora Riparia	Calc-schist and phyllite	2	9	0.04	15
11	Mardarello—Novalesa (TO)	Dora Riparia	Calc-schist	2	5.5	0.065	9.2
12	Moscardo—Muse (UD)	Tagliamento	Phyllite	2	6.88	0.085	9
13	Moscardo—Muse (UD)	Tagliamento	Phyllite	2	8.3	0.12	8.32
14	Moscardo—Muse (UD)	Tagliamento	Phyllite	2	9.36	0.102	9.58
15	Moscardo—Muse (UD)	Tagliamento	Phyllite	2	6.79	0.089	8.73
16	Mengasca—S. Pietro (SO)	Adda	Gneiss	3	*	*	*
17	Imeut—Rostagni (TO)	Pellice	Mica schist with garnets	3	2.2	0.38	2.41
18	Ponte Planpincieux (AO)	Dora Baltea	Granite	3	3.9	0.7	2.36
19	Pissa Rif. del Mucrone (BI)	Sesia	Eclogitic mica schist	3	3	0.55	2.33
20	Inferno–Brughiere (NO)	Toce	Granite	3	2.4	0.45	2.31
21	Fossa Tovaccio–Mezzaselva (BZ)	Adige	Biotitic granite	3	2.7	0.6	2.12
22	Sacco d'Isarco (BZ)	Adige	Biotitic granite	3	3.7	0.25	3.85
23	Bianco–S.S.N. 12 km 491 (BZ)	Adige	Biotitic granite	3	2.4	0.48	2.24

*Quadrillage measurement only.
†S.S.N. = State road number.

Grain-size terminology follows the classification proposed by Folk (1974) and Blair & McPherson (1999).

In this text, 'sediment gravity flow' includes all varieties of debris flows plus their antecedent colluvial slides (Blair & McPherson, 1994). It indicates a sedimentary process where material is transported downslope by the force of gravity, with a variable amount of entrained water and air (Johnson, 1984). The term 'sediment gravity flow' does not imply cohesiveness and general rheologic properties of the flow. These are defined by the attributes 'cohesive' or 'non-cohesive', which depend on the amount of the very fine silt and clay fraction in the sediment. For the cases studied, a cut-off of 5% was used to separate cohesive and non-cohesive sediment gravity flows.

CASE STUDIES

Three types (groups) of alluvial fans generated in three different lithological areas (Fig. 1) are presented. The latter consist of the following:

1 massive and/or crudely stratified carbonate bedrock;

2 fine-grained sedimentary and metamorphic bedrock (schists, calc-schists, mica schists, slate, phyllites and quartzite);

3 massive crystalline bedrock (granites and gneiss).

The data presented derive from 23 floods events that have occurred since the early 1970s in the Alps (Fig. 1). For each group, a field case study that is considered to be representative of the various cases observed

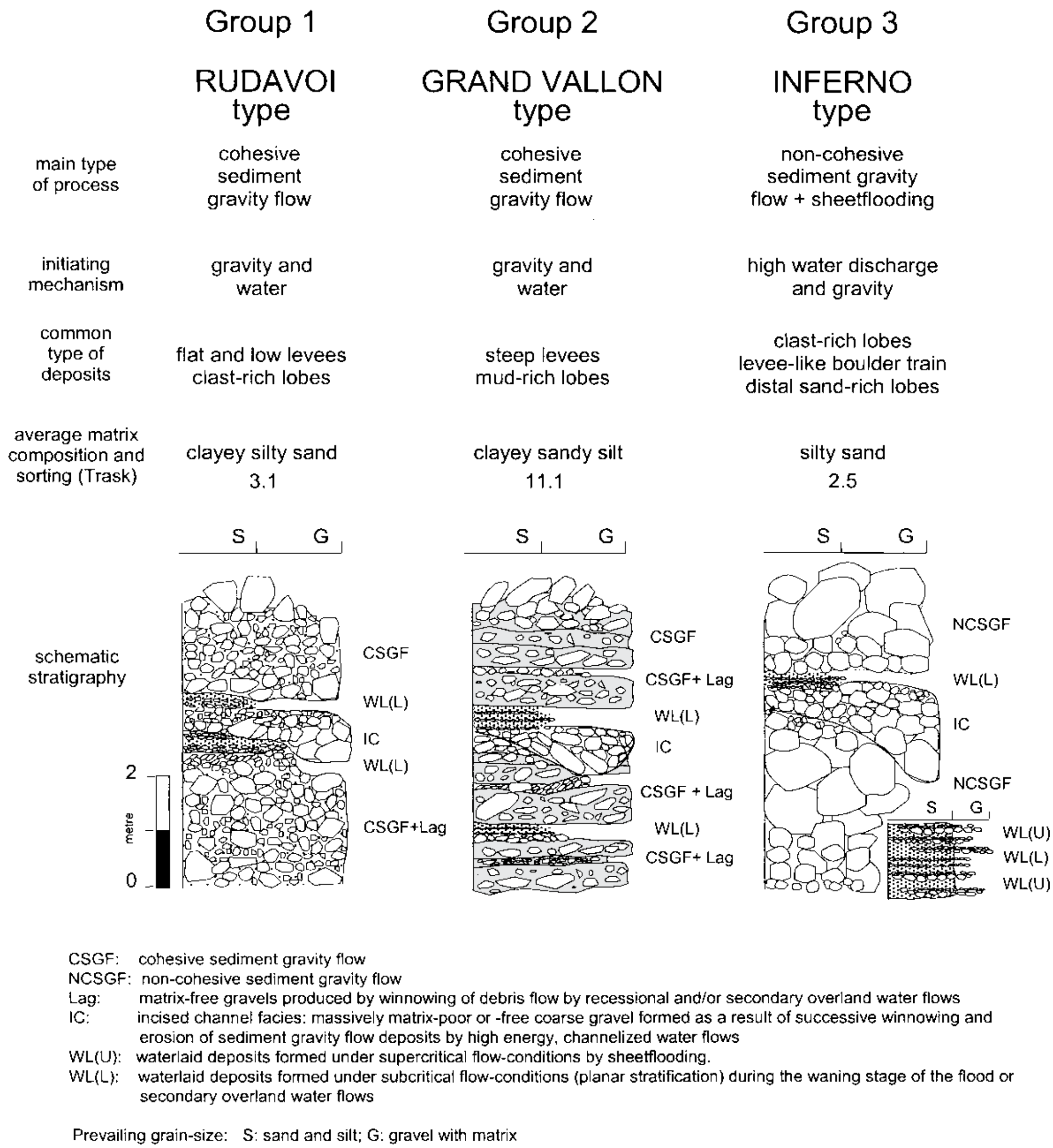

Fig. 2. Summary of the main sedimentary and geomorphological characteristics of the three groups of alluvial fans as defined in this study.

throughout the Italian Alps will be presented. Moreover, for each case, the geomorphology and lithology of the catchment, the flood characteristics and the related deposits will be presented, and sedimentary processes will be discussed (Table 2). A summary of the main sedimentary features and processes characteristic of the three case-study alluvial fans and related groups is shown in Fig. 2.

Table 2. Summary table of the morphometric and lithological parameters of the Rudavoi, Grand Vallon and Inferno alluvial fans and related catchment basins (Italian Alps).

Landform	Characteristics	Rudavoi	Grand Vallon	Inferno
Alluvial fan	Size (km^2)	0.6	0.23	0.14
	Radius (km)	1.25	0.5	0.33
	Dh toe/apex (m)*	135	70	65
	Average slope (°)	6.1	9	10
	Expansion angle (°)	65	145	130
	Main type of deposits†	CSGF	CSGF	N-CSGF
Catchment basin	Size (km^2)	3.32	2.81	1.64
	Length (km)	4.1	2.91	2.05
	Width (km)	1.3	1.17	1.28
	Average slope (°)	37.6	28	25
	Maximum channel order	3	4	3
	Lithology‡	D	S	G

*Height difference between fan toe and fan apex.
†CSGF, cohesive sediment gravity flow; N-CSGF, non-cohesive sediment gravity flow.
‡D = massive and thick bedded carbonate rocks (dolomite); G = massive crystalline rocks (granites); S = schistose metamorphic and siliciclastic sedimentary rocks.

Group 1

This group develops mainly in catchments underlain by massive and/or poorly stratified carbonate bedrock. The primary sediment gravity processes are dominated by cohesive debris flows. Commonly, in the Dolomite region, these processes occur both on large, steep (15–35°) talus cones and on alluvial fans characterized by a perennial or seasonal stream. Talus cones often mantle the bases of the vertical dolomitic cliffs and usually are fed by a small catchment basin (< 0.5 km^2), drained by a first-order feeder channel with a very steep slope (45–60°). Within the drainage basin, bedrock is exposed and colluvial deposits are rare. This allows immediate drainage of runoff into the talus cone debris located down-valley.

Debris flows typically are initiated at the transition between the bedrock wall and the talus accumulation, where there is the highest concentration of water flows during flood events (Fig. 3a). Debris flows often end on the talus cone. In some cases they generate elongate lobes, which form coalescent alluvial fans at the base of the talus. The fans usually extend for several hundreds of metres, forming large, planar and gently inclined (10–12°) sedimentary bodies (Fig. 3b). Both talus cones and alluvial fans can display either a poorly or well-developed incised channel that is connected directly with the drainage-basin feeder channel.

Alluvial fans with well-developed incised channels usually are associated with large catchments drained by a second- or third-order feeder channel. Catchments with areas ranging between 2 and 5 km^2 are very common in the eastern calcareous Alps and also are commonly associated with catastrophic, channelized debris-flow processes (Fig. 3c). Historical data indicate that catastrophic events generated from catchments of this size can result in deposition of up to 50 000–70 000 m^3 of debris per square kilometre of catchment (Marchi & Tecca, 1996).

The case study presented here relates to the sediment gravity flows that occurred recently during two successive flood events in the Rudavoi Torrent (eastern Dolomites—southern calcareous Alps; Fig. 1a). The floods caused repeated serious damage to an important communication route.

Geomorphology

The Rudavoi Torrent is a small stream situated in the eastern Dolomites. It originates from the southern slope of the Monte Cristallo group and flows south-eastward (Fig. 4). The drainage basin covers an area of 3.32 km^2 and ranges in elevation from 1435 to 3216 m a.s.l. (Table 2). Downstream of the outlet of the drainage basin, the Rudavoi Torrent reaches the main stream (Ansiei River) flowing through a low-gradient area where the fan is formed.

Lithologically, the drainage basin is characterized by Triassic dolomites (37% in planar area), and subordinately by marls and sandstones (22%). Quaternary deposits, consisting of talus debris, mostly derived from the dolomites, and old alluvial fan deposits (debris flow) are widespread throughout the basin

(41% of the catchment) and form the prevailing material cut by the Rudavoi Torrent.

The fan studied (Fig. 4 & Table 2) has a slope of about 6° and is confined laterally by other Quaternary deposits (landslide accumulations and fluvial deposits).

Flood events

Historical data of sediment gravity flows along the Rudavoi Torrent have been documented since the beginning of the 20th century, and transport of large blocks of some 400 m^3 has been reported (Istituto di Ricerca per la Protezione Idrogeologica Archive, unpublished).

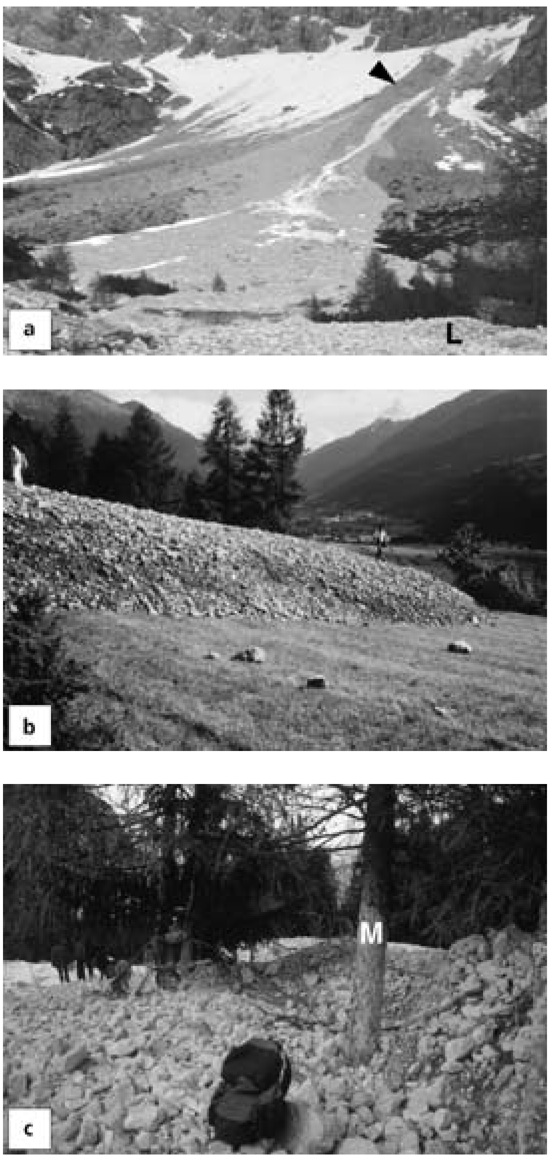

Fig. 3. Examples of sediment gravity flows generated from group 1 alluvial fans. (a) Talus cone (Mount Pelmo, Dolomites) merging downslope with a debris-flow dominated alluvial fan. The source area of the debris flow that occurred in September 1994 is indicated by the arrow. A distinct levee (L) formed at the margin of the trees. (b) A 3-m-thick frontal lobe consisting of moderately sorted, clast- to matrix-supported silty and clayey gravel containing cobbles, pebbles granules and sand. These sediments were generated from dolomitic rocks, transported as cohesive debris flow and deposited a few tens of metres from the fan apex (Valtellina, July 1992). Note the sharp boundary between the fresh deposit and the older fan surface, and the steepness of the lobe, which indicates high sediment cohesion. Isolated small boulders outside the lobe margin suggest that clast rolling and bouncing occurred during the transport, probably associated with grain-to-grain collision. (c) Depth of the debris-flow can be inferred by pebbles and cobbles and mud coating (M) on the trees (Mount Pelmo, Dolomites).

Over the last 10 yr, two main debris-flow events were observed in the Rudavoi basin. The first occurred in August 1992 and the second, far larger in volume, mobilized debris in September 1997.

The August 1992 debris flow was triggered by a local, intense rainstorm that was not recorded by the nearby raingauge station located only 4 km from the Rudavoi catchment basin. The debris flow deposited about 5000 m^3 of sediment ranging from silt to boulders as large as 15 m^3. Most of the deposition occurred where the channel slope decreased from 13° to 8°. The state road bridge, which crosses the torrent at about 1710 m a.s.l., partly dammed the flow and acted as a nodal point for debris deposition.

The debris flow of 4–5 September 1997 was generated by an intense rainstorm that lasted only about 3 h (Marchi & Pasuto, 1999). The volume of deposits was estimated at about 100 000 m^3. Variations in deposit distribution were associated with changes in channel slope, check dams and channel widening. The total channel length affected by debris-flow deposition was about 4.5 km, with an average slope of 7.4°. This debris flow destroyed the state road bridge (Fig. 4).

Sedimentary facies

Deposits were laid down mainly within the channel bed, on the channel banks (Fig. 5a) and in a few lateral clast-rich lobes (Fig. 5b).

The deposits, forming broad flat levees, are up to 4–5 m thick and commonly present isolated clusters of fine to coarse boulders up to 5–10 m^3 in volume. A very coarse boulder, with a volume exceeding 100 m^3,

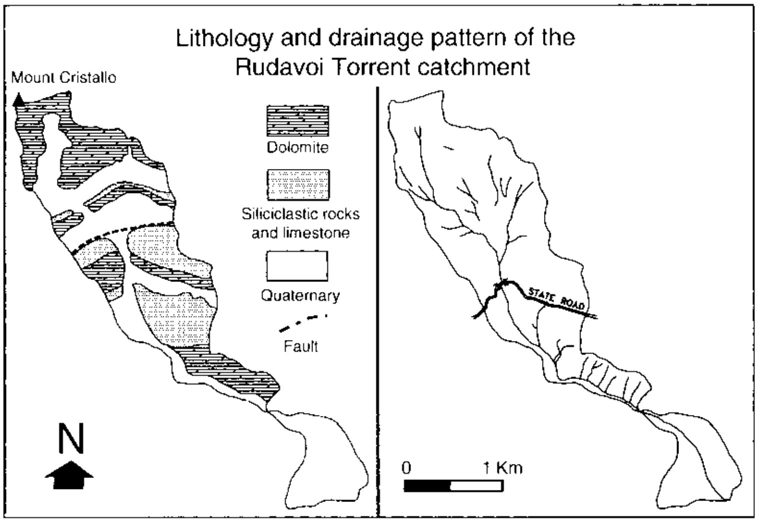

Fig. 4. Lithological map and drainage net of the Rudavoi Torrent catchment area. Quaternary deposits consist of colluvium, talus cone debris and debris-flow/alluvial deposits.

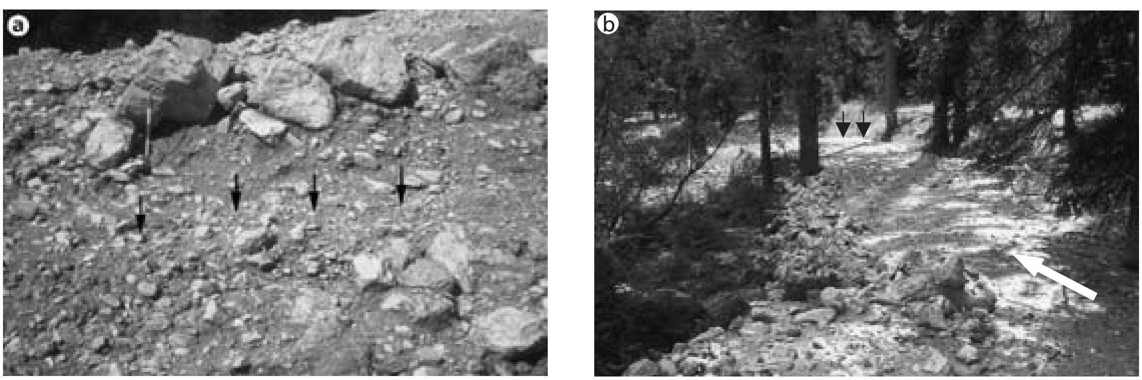

Fig. 5. (a) Close-up of the clast- to matrix-supported pebble, cobble, granular silty sandy gravels cropping out along the Rudavoi Torrent. Elongated clasts generally are orientated with long axes parallel to the slope and slightly dipping in the upslope direction. An angular boulder train is formed behind a block jam. The arrows indicate the base of the 1996 debris-flow deposits, which overlies older clast-rich debris-flow deposits. (b) Clast-rich lobe front deposited during the 1996 flood event on the right-hand side of the Rudavoi Torrent incised channel. Note the fabric of elongated clasts with their long axis orientated parallel to the lobe margin. White arrow = flow direction; black arrows = lobe front.

stopped at the site of the road bridge (Fig. 4). Debris-flow matrix consists of granules and coarse to fine silty sand. The grain-size distribution (Fig. 6a) is consistent with the distribution found in other similar deposits generated in this geolithological setting (Maraga *et al.*, 1998).

Typically, levee and lobe deposits are unsorted to poorly sorted, angular to subangular, matrix- to clast-supported gravels (Fig. 2). The deposits consist of muddy sand, granules, pebbles, cobbles and scattered medium to fine boulders. The rare boulders show long (*a*) axes with preferred orientation parallel to the flow. When associated with fixed obstacles (such as upright trees or pre-existing very large blocks or boulder jams), boulders form trains 4–6 m long orientated in an upfan direction (Fig. 5a).

The lobes usually show a well-defined fabric (Parise & Moscariello, 1997; Blair & McPherson, 1998; Major, 1998). Elongated clasts, show their long (*a*) axis preferentially orientated parallel to the lobe margin, being parallel to the fan slope at the lobe side, and having a transverse orientation at the lobe snout.

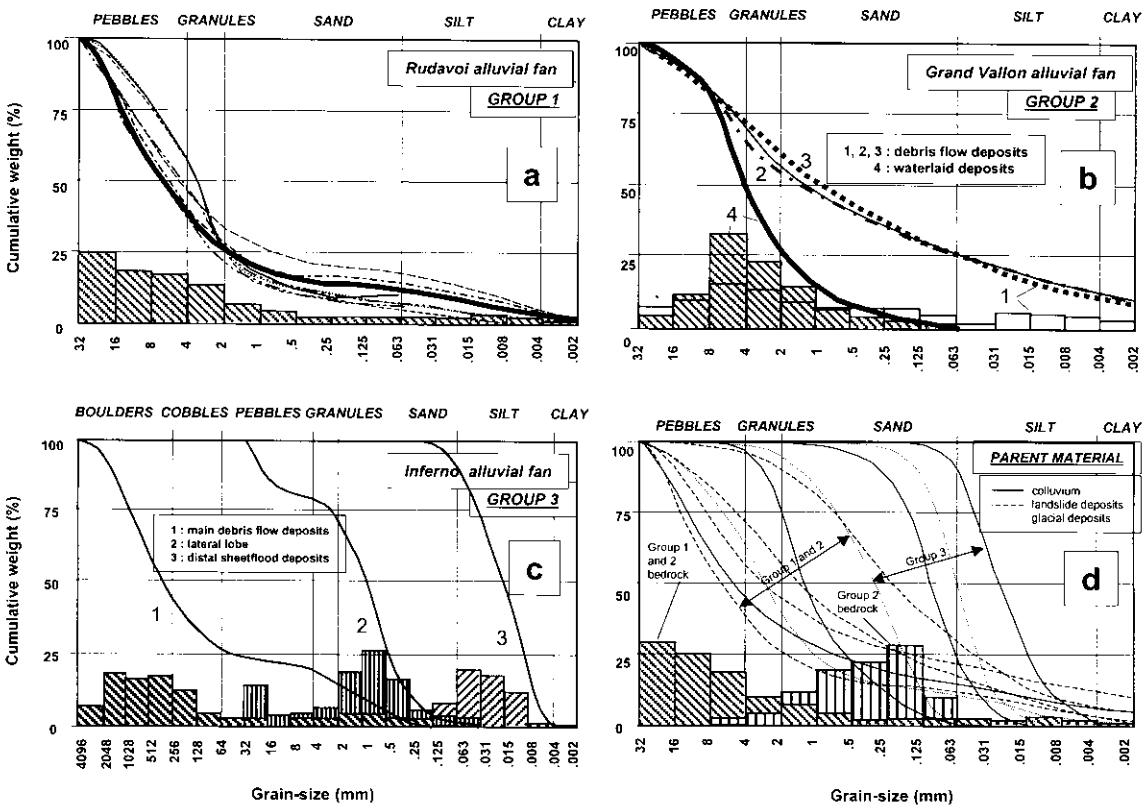

Fig. 6. Grain-size distribution of alluvial fan deposits from the three case studies presented in this paper. (a) Group 1 alluvial fan deposits from different localities in the Dolomites (eastern Italian Alps, see Fig. 1). Overall, cumulative curves show a homogeneous distribution and a typical flexure at the gravel–sand boundary. Bold solid curve and histogram refer to the Rudavoi torrent samples (modified after Maraga *et al.*, 1998). (b) Group 2 alluvial fan deposits from the Grand Vallon fan accumulated during the 1992 flood event. Curves 1, 2 and 3 correspond to samples from a lateral overbank debris-flow lobe (see Fig. 10a) collected at the edge, middle and frontal margin position, respectively. Curve 4 corresponds to waterlaid deposits accumulated within the incised channel during the recessional flood (see Fig. 10b). (c) Group 3 alluvial fan deposits accumulated during the 1996 flood event on the Inferno fan. (d) Grain-size distribution of different types of parent material from which sediment gravity flows originated in the Italian Alps. Note the clear difference in composition between deposits associated with group 1 and 2 and group 3 bedrock types.

Intense erosion persisted for a few days within the river bed and the freshly accumulated debris-flow deposits were incised, supplying fine gravel, sand, silt and clay to the stream.

Sedimentary process

The sediment gravity flow that affected the Rudavoi alluvial fan can be described as a cohesive debris flow (Sharp, 1942; Sharp & Nobles, 1953; Johnson, 1970, 1984; Blair & McPherson, 1994). The material entrained by the debris flow was generated from failure of talus slope deposits and erosion and collapse of channel banks incised in older matrix-rich fan deposits.

The roughness of the incised channel, and the erosional features recognized along the debris-flow path, suggest that the sediment gravity flow moved in a turbulent manner within the main channel. On the other hand, the non-erosional base and sides of the clast-rich lobes that formed outside the incised channel, together with the steepness of the lobe margins, attest to laminar flow conditions (Johnson, 1970; Rodine & Johnson, 1976; Blair & McPherson, 1998). Although fine to coarse boulders are present in the colluvium, their availability is insufficient to cause the formation of well-defined, clast-rich levees in debris-flow deposits.

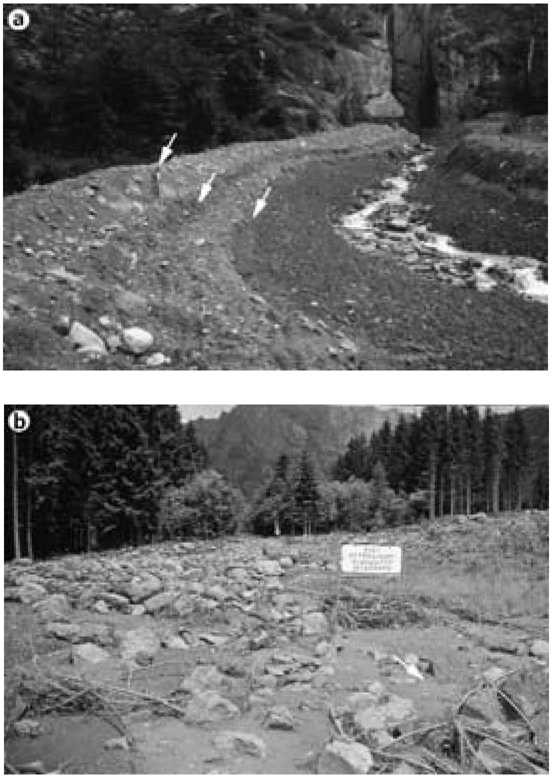

Fig. 7. Examples of sediment gravity flows generated from group 2 alluvial fans. (a) Debris-flow deposits accumulated at the apex of the Mardarello alluvial fan. A flat crested, curved levee formed during the 1992 flood event. This consists of poorly sorted, silt and clay-rich, matrix-supported cobbly, pebbly, sandy gravels. The waning stage of the flood induced the progressive erosion of the deposits with the formation of three different terraces (arrows). (b) Frontal margin of a lobe formed during a recent debris-flow event on the Moscardo alluvial fan. The elongated clasts show longest axis preferentially orientated perpendicular to the flow direction (indicated by the arrow). Note the effect of recessional debris-free water flow that concentrated vegetal debris on top of debris-flow deposits. The oil pipeline signpost located at the margin of the lobe was not damaged by the debris-flow indicating relatively low shear strength at the lobe margin during deposition.

Group 2

The alluvial fans of this group develop from catchments underlain by fine-grained siliciclastic and carbonate sedimentary and metamorphic rocks. These drainage basins are typically characterized by large amounts of clay/silt-rich material available in the feeder channels and the catchment slopes. These conditions favour the formation of cohesive debris flows. These types of debris flow have been studied in the Mardarello Torrent and Moscardo Torrent (Figs 1 & 7) drainage basins (Tropeano *et al.*, 1996; Arattano *et al.*, 1997), both of which are characterized by a high frequency of debris-flow events. These are ideal cases in which to study triggering mechanisms, hydraulic characteristics of the flow and sedimentary processes (Govi *et al.*, 1994; Moscariello & Mortara, 1994; Arattano *et al.*, 1997; Moscariello & Deganutti, 2000).

This case study is of the Grand Vallon Torrent alluvial fan (Fig. 1), which has experienced five major flood events over the past 8 yr (Tropeano & Turconi, 1998). The Grand Vallon catchment is characterized by geomorphic and sedimentary features that can be considered representative of many drainage basins throughout the Alps.

Geomorphology

The Grand Vallon Torrent alluvial fan is located in the upper Susa Valley (western Alps, Fig. 1), on the left bank of the Dora Riparia River (Fig. 8). The fan has a triangular, semi-conical shape, with an average slope of 7° and expansion angle of 70°. The fan is cut by a 4–8 m deep and 10–25 m wide incised channel. The channel joins the receiving river Dora Riparia after displaying a large bend on the fan. The Dora Riparia River incises the fan toe transversally.

Across the surface there are several abandoned channels, often delimited on both sides by old clast-rich levees covered by lichens and moss. They cross-cut each other, indicating intense fan activity prior to the strong base-level lowering that generated the incised channel. A dense coniferous forest occupies the fan surface and the escarpment at the toe.

The drainage basin has an area of 2.81 km^2 and ranges from 3130 m a.s.l. (Mount Chaberton) to 1450 m a.s.l. at the fan apex. The bedrock is mostly of calc-schists with phyllite intercalations and stratified limestones and dolomites. Widespread fracture networks control the high-density drainage pattern, which led to the formation of a fourth-order feeder channel. Quaternary deposits here consist of talus debris and a discontinuous colluvial cover, which tends to accumulate at the junction of high-order feeder channels within the catchment. Substantial accumulations of unconsolidated deposits also are represented by widespread artificial talus that formed across the slope during the construction of a military fort and its access road on the summit of Mount Chaberton.

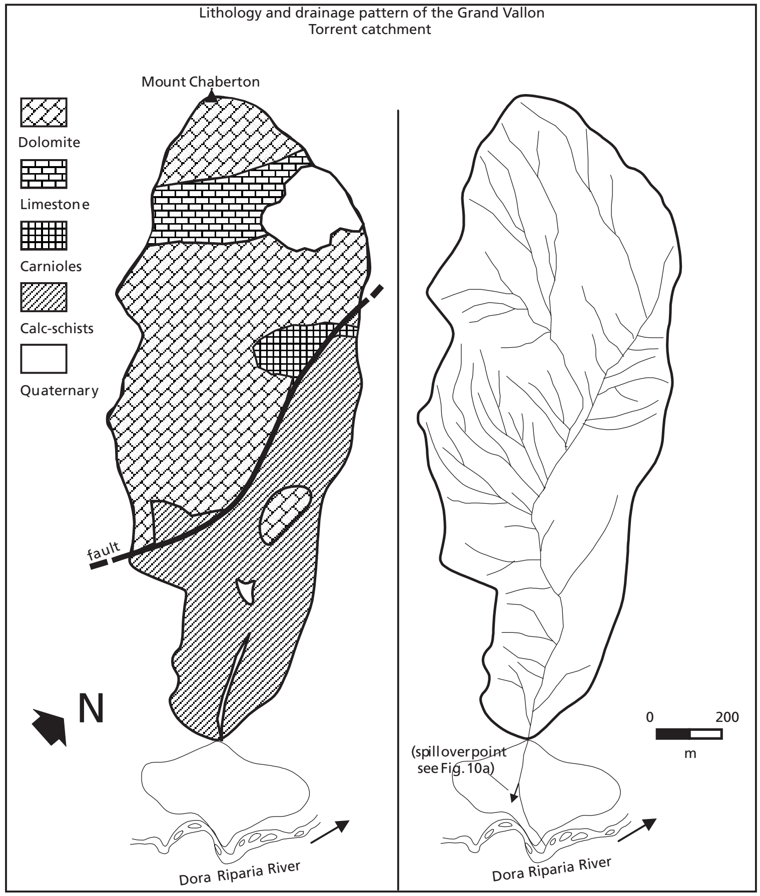

Fig. 8. Lithological map and drainage net of the Grand Vallon catchment area. Quaternary deposits consist of colluvium and talus cone debris, and debris-flow/alluvial deposits.

Flood event

The flood event on 21 July 1992 was triggered by a very localized, intense rainstorm, which affected the upper Grand Vallon catchment. Rain gauges in the nearby villages (*c.* 2 km away) recorded only 8 mm of rainfall for that day. Eyewitness accounts indicate that the flood was characterized by several surges that filled the entire incised channel (Fig. 9). An overbank lobe (Fig. 10a) stopped only a few hundred metres from an occupied holiday house.

Sedimentary facies

Several types of deposits have been recognized (Fig. 2). Cumulative grain-size curves of different deposits collected within the incised channel and on the fan surface are shown in Fig. 6b. A clear difference in grain-distribution is displayed between poorly sorted sediments of the mud-rich debris flow, and the fairly well sorted, bedded, pebbly, sandy waterlaid deposits.

Channel deposits form elongated and discontinuous bodies. They consist of matrix-supported, extremely poorly to poorly sorted muddy gravel containing angular pebbles, cobbles and rare fine boulders. The fine to medium pebble and granule content forms about 40–50% of the bulk, the sands 25–30%, silt 10–15% and clay 10–15%. Cobbles and boulders comprise up to 5% of the bulk (Fig. 6b). Planar bedded, downslope dipping, fining upward, medium to fine pebble, granular, coarse to fine sand deposits form patchy accumulations within the incised channel. These deposits are degraded and show 8–15-cm-high steps, which separate surfaces dipping 3–5° down-valley and displaying at the top a lag deposit made up by matrix-free, small to medium pebbles (Fig. 10b).

Along the channel, at the junction between the Grand Vallon Torrent and the receiving river, a widespread 0.5-m-thick silt and clay-rich fan deposit containing pebbles, granules and sand has been observed lying lateral to the present watercourse (Fig. 10c). On the other hand, matrix-free, coarse-grained, clast-supported sediments with typical imbricate transverse fabrics were deposited close to the present watercourse (Fig. 10c). Mud-rich deposits also have been observed on the opposite slope on the right bank of the Dora Riparia River. There, up to 2-m-high mud coatings at the base of the standing trees were found for about 100 m downstream. Elongated levees 0.8–1.6 m high, 0.6–2.5 m wide and 40–100 m long form the dominant deposit. Levees are distributed along the incised-channel banks (Fig. 10a) and often are laterally bounded by standing trees.

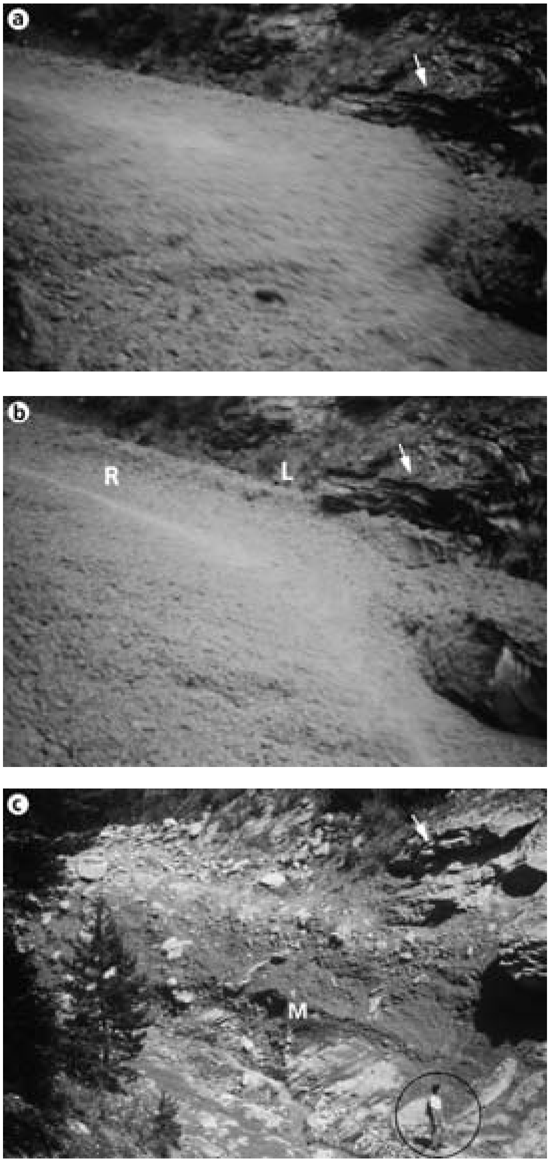

Fig. 9. Channelized cohesive debris flow photographed during the 1992 flood event on the Grand Vallon alluvial fan. The arrows indicate the same reference point in all three photographs. (a) Image during the flood event of a frontal lobe generated by a secondary debris-flow surge. Deposits have entirely filled the incised channel. (b) Image taken during the falling stage of the flood. Note the lateral levee formed on the left-hand side of the channel (L) and the shear zone defined by the rill occupied by running water (R) on top of the high-density debris flow. (c) Photograph taken at the same location after the event. Note the mud coating along the incised channel sides (M). Levee remnants can still be seen on the incised channel bank and are indicated by boulder texture typically orientated parallel to the channel. Erosional processes during the debris flow and recessional flood exhumed the bedrock on the river bed. Person in the circle for scale.

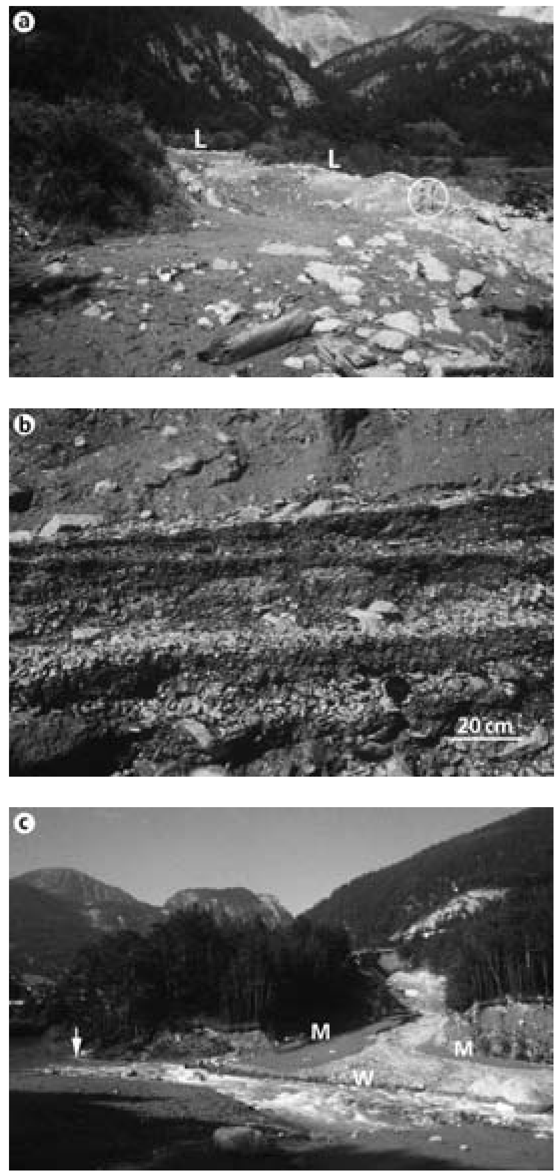

Texturally, the levee deposits consist of unsorted to poorly sorted, matrix- to clast-supported muddy and sandy gravels containing pebbles, cobbles and medium to small boulders (Fig. 2). Clasts are angular to subangular and often tabular and elongated in shape, preferentially orientated along the fan slope. Typically, levees display a coarsening upwards texture.

Overbank sediments (mud-rich lobes) have been deposited adjacent to the channel bend in the lower fan (Fig. 8). They are 0.3–0.6 m thick and 5–25 m wide, 15–50 m long and consist of pebbly, granular, sandy, silty clay-rich gravel (Fig. 10a). Large clasts (cobbles and boulders) are rare and concentrated at the lobe head. Similar to the other lobes described for group 1 alluvial fans, the clast orientation shows a typical fabric with longest axes parallel to the lobe margin. The largest tree logs display a similar orientation, whereas smaller branches are orientated parallel to the flow direction, having been reorientated by recessional water flows (Fig. 10a).

On the fan surface, on both sides of the incised channel, almost 1-m-high mud coatings are present at the base of standing trees.

Sedimentary processes

The sediment gravity flow of 21 July 1992 is interpreted as a cohesive debris flow originating from multiple sources in the upper part of the basin. Numerous shallow landslide scars that occurred on the catchment slopes and channel banks document this. According to eyewitness accounts, the Grand Vallon debris flow was characterized by multiple pulses (surges), which probably formed as a consequence of diachronous colluvium failures (Fig. 9a & b).

The main sediment gravity flow was confined to the incised channel. A survey carried out before and after the July 1992 event showed that several large blocks (20 m^3) within the drainage basin were displaced down-valley. Some of them moved for several tens of metres and were reorientated with their longest axis parallel to the channel slope.

Torrent bed deepening, with exhumation of older debris-flow deposits (2800 ^{14}C yr BP; Tropeano & Olive, 1993), occurred. At the fan apex, the gravity flow expanded and spilled over the incised-channel walls. Contrary to what has been observed for the Rudavoi Torrent fan, the large availability of fine to coarse boulders in the Grand Vallon catchment allowed the formation of well-defined levees.

Considerable amounts of overbank material did not stop on the fan surface (forming levees or lobes) but flowed beyond the incised-channel walls for hundreds of metres and re-entered the channel further down-valley.

Most of the material mobilized during the debris-flow process actually bypassed the fan and joined the receiving stream, producing a temporary dam that caused the formation of an ephemeral lake within the Dora Riparia valley (Fig. 10c).

The effects and sedimentary products of the recessional flood of the Grand Vallon Torrent were clearly visible after the events. Stratified sandy gravels deposited within the incised channel represent the results of high-velocity tractive currents that mobilized and evacuated the mud fraction down-valley, and redeposited the sorted coarser fraction. The typical small-pebble-rich, step-like surfaces that characterize these deposits formed during the waning stage of the flood (Fig. 10c). The matrix-free (openwork), coarse gravel concentrated at the fan toe formed as a result of the winnowing process of mud-rich lobes during the recessional water flood stage that followed the main debris-flow surge.

Fig. 10. (*opposite*) Grand Vallon alluvial fan after the 1992 flood event. (a) Overbank mud-rich lateral lobe accumulated on the fan surface on the right-hand side of the incised channel during the 1992 flood event. Note the concentration of larger clasts at the lobe head. Clasts and larger logs display the longest axis orientated parallel to the lobe margin, whereas smaller branches are orientated parallel to the flow direction having been reoriented by recessional water flows. Persons in the circle are standing on the left bank of the channel. Boulder rich levees (L) can be seen up-fan on both sides of the incised channel. (b) Planar bedded, downslope dipping, fining upward deposits of medium to small pebble, granular, coarse to fine sand accumulated during the recessional water flow within the incised channel. (c) Junction of the Grand Vallon Torrent with the receiving Dora River. Note remnants of mud-rich debris-flow deposits preserved laterally to the watercourse (M). Matrix-free, coarse-grained, clast-supported deposits (W) with typical imbricate transverse fabric represent the results of winnowing process of mud-rich lobes during the recessional water flood stage of the 1992 event following the main debris-flow surge. An ephemeral lake formed upstream from the junction between the fan stream and the receiving river (white arrow).

Group 3

This group develops from catchments underlain by massive crystalline rocks (granites, gneiss and granodiorites) and is often characterized by catastrophic sediment gravity flows (Venzo & Largaiolli, 1968; Mortara *et al.*, 1986; Luino *et al.*, 1994; Chiarle & Luino, 1998; Maraga *et al.*, 1998). Historical documents and field observations highlight three main characteristics that distinguish these deposits from the others discussed in this paper:

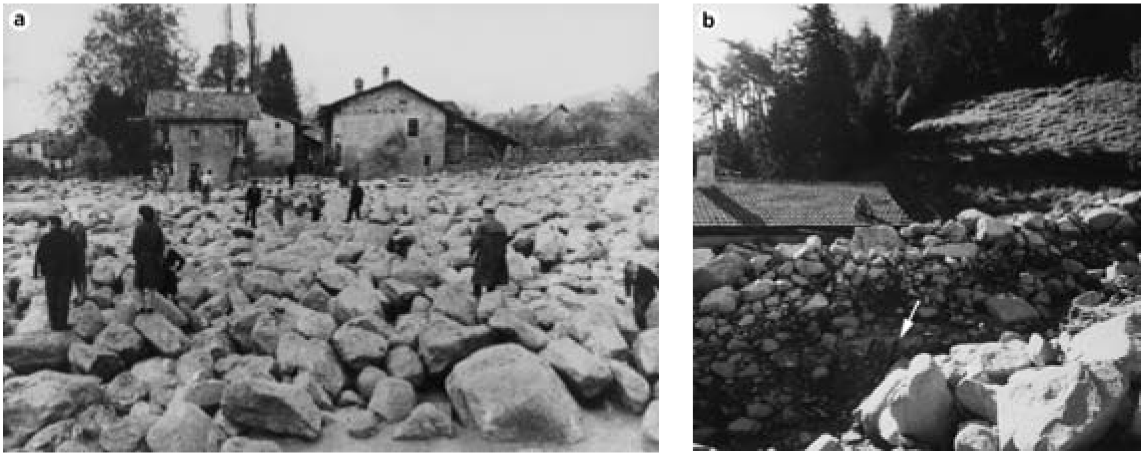

Fig. 11. Examples of sediment gravity flows generated from group 3 alluvial fans. (a) Moderately to well-sorted, subangular to well-rounded matrix-free, boulder-rich, cobble and pebbly gravel, accumulated during the 1966 flood event on the Chieppena Torrent alluvial fan. Clast lithology consists of granites. These deposits are interpreted to have been generated as a non-cohesive sediment gravity flow. (Photograph by Farganello, used by permission.) (b) Fossa di Tovaccio alluvial fan (Isarco valley). Well-developed, coarsening upward texture on the levee formed during the 1985 flood event. Note the clast-supported texture in most of the levees and the elongated clast orientation with *a*-axes parallel to the fan slope. The incision of the deposits down to the bedrock (arrow) occurred during the recessional flow associated with the waning stage of the flood event. A levee formed against the obstacle represented by a house (built in 1867), which laterally confined and slowed down the flow (from Mortara *et al*., 1986).

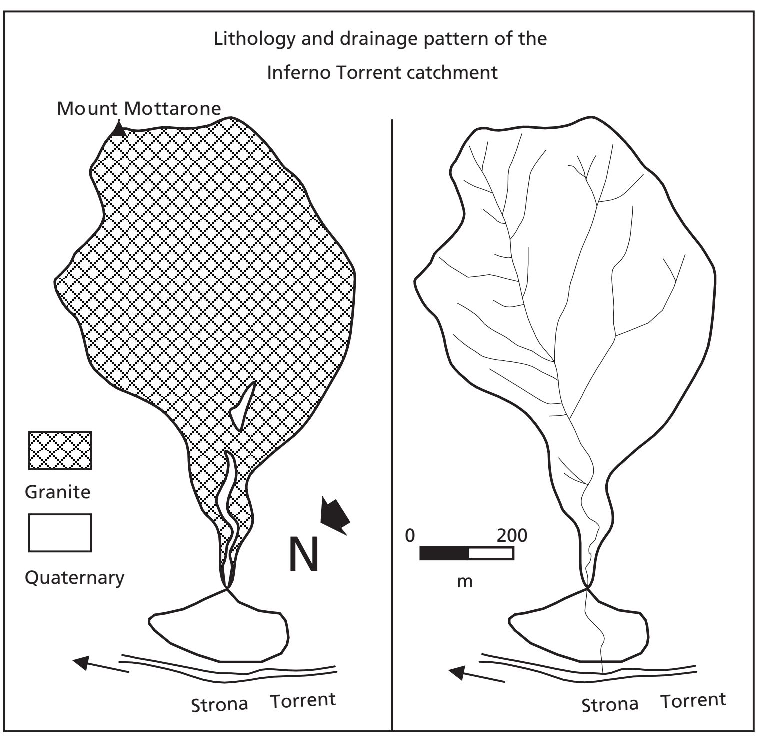

Fig. 12. Lithological map and drainage net of the Inferno Torrent catchment area. Quaternary deposits consist of colluvium, talus cone debris and debris-flow/alluvial deposits.

1 generally, grain size is coarser and abundance of medium to small boulders and blocks is greater than in deposits generated from other lithotypes (Fig. 2);
2 clasts ranging from cobbles to small blocks generally show higher degrees of roundness than similar sizes generated from different lithotypes;
3 the fine-grained matrix of the deposits has a sandy modal distribution that reaches 26% within the 1–0.5 mm class.

The catastrophic floods that affected the Chieppena Torrent alluvial fan (Fig. 11a) in 1851, 1882 and 1966 provide an example of exceptional accumulations of matrix-free, rounded boulders and blocks in the Italian Alps (Venzo & Largaiolli, 1968; Cerato, 1999). These flood events resulted in deposition of up to 1×10^6 m^3 of debris.

The case study presented here concerns the basin of the Inferno Torrent (Figs 1 & 12). This basin recently experienced a catastrophic flood event, which produced a large debris accumulation on the fan (Fig. 13) and considerable damage to houses and infrastructure (bridge, road and defence walls).

Geomorphology

The catchment has an area of 1.76 km^2 and an average slope of 42°, with a difference in height of about 1000 m (Table 2). The feeder channel, which collects three main secondary tributaries, is about 800 m in length with an average slope of 25°. The drainage basin lies on the western slope of the Mottarone Mountain (1491 m a.s.l.), which comprises granites and granodiorites (Fig. 12). Poorly consolidated glacial deposits, talus deposits and ancient debris-flow deposits are mostly preserved at the junction of secondary feeder channels within the catchment. These deposits form the main source of material within the drainage basin.

The alluvial fan has a semi-conical shape with a radius of 330 m and a slope of 10°. The axial part of the fan is aligned with the direction of the main feeder channel and displays a pronounced positive morphology.

Flood events

The flood event on 8 July 1996 occurred during an exceptionally heavy rainstorm, which produced 139.8 mm of precipitation in 2 h. These values have a return period close to 200 yr (Chiarle and Luino, 1998). The sediment volume deposited on the fan reached 30 000 m^3. An indirect post-event estimate of peak discharge, using the method described in Johnson and Rodine (1984), indicates a value of about 750 m^3 s^{-1} and a velocity of about 7.5 m s^{-1} (Chiarle & Luino, 1998).

The flood event caused disruption of the communication routes crossing the fan and serious damage to the Omegna village situated at the fan toe.

Historically, only a few events have been recorded from this fan; the most recent prior to this one occurred in 1968 (Maraga *et al*., 1998).

Sedimentary facies

Rapid deposition of very coarse material, mostly forming large lobes, occurred on a large portion of the alluvial fan surface from the apex to the toe. The different sedimentary bodies observed from the aerial photographs (Fig. 13) taken after the event clearly indicate that they formed during successive surges of the flood.

Clast-rich lobes are the most common type of deposits. They consist of unsorted to poorly sorted, poorly to moderately rounded, clast-supported sandy, granular gravel containing pebbles, cobbles and fine to large boulders (Fig. 2). Grain-size measurements on clast-rich lobes (Fig. 6c) indicate that 25% of the deposits are formed by coarse to very coarse boulders (intermediate axis > 1 m). Usually, elongated boulders and blocks show long axes orientated perpendicular to the flow direction (Fig. 14a) both at the front and within the lobe.

Distinct boulder trains ('levees') also formed along the feeder channel walls within the drainage basin in proximity to the fan apex and on the upper fan at the side of the main channel. In vertical section, they typically show upward coarsening and a clast-supported texture. Elongated boulders tend to have intermediate (*b*) axes orientated parallel to the flow direction (Fig. 14b & c); locally, at the northern margin of the fan, boulders show long axes orientated parallel to the flow direction. Broken edges and pressure marks on large clasts also were observed. Normally graded fine-grained sediments showing crude horizontal bedding (Fig. 14b) often overlie boulder-rich deposits.

Finer-grained lobes accumulated down-fan, outside the fan boundaries and lateral to the main, coarse-grained depositional area. They consist mostly of moderately to well-sorted, coarse gravel formed by clast-supported cobbles, pebbles mixed with granules and very coarse sand. Coarse clasts display imbricate transverse fabric. The gravels are interstratified with granular, fine to medium silty sand, with rare scattered small to medium pebbles. Typically, gravel and sand interstratification is regular, showing horizontal bedding and bimodal, normal gradation.

Fig. 13. Low-altitude aerial photograph of the Inferno alluvial fan after the 1996 flood event. Variation in grain-size and texture distribution of the deposits throughout the fan reflect differences in competency, intensity of turbulence of successive surges combined with relative degrees of confinement (i.e. varying vegetation effects) and fan topography. Boulder and block trains formed against tree lines and the defence wall (W) that protect the village. Fine-grained deposits were mostly accumulated in a distal position down-valley from the state road. Buildings indicated by (a) and (b) were invaded by gravels up to the second floor. Arrow indicates the frontal lobe margin depicted in Fig. 9(a).

Grain-size analyses of selected samples from the main debris-flow accumulation zone, a lateral lobe and a distal sand-skirt lobe are shown in Fig. 6c.

Sedimentary processes

The sedimentary processes related to the 8 July 1996 flood event of the Inferno Torrent can be described as non-cohesive sediment gravity flows. These processes are known to be generated by high water discharge down a steep channel containing abundant unconsolidated sediment that can be readily mobilized. The genesis of these processes has been discussed extensively by Church & Desloges (1984), Jarrett & Costa (1985) and Blair (1987). The virtual absence of clay and fine silt in the source materials suggests that the non-cohesive sediment gravity flow was triggered by the avalanching motion of sediment-rich water flowing down the steep feeder channel of the Inferno basin.

The drag force operated by high water discharge thus overcame the shear strength of coarse material lying within the initiation area (slope and feeder channel). In the case of the Inferno flood event this probably can be related to rapid transfer of water generated from high magnitude (total cumulative) and very intense rainfall, from the catchment to the fan. This process, in turn, could have been facilitated by the sudden and catastrophic release of water from breaching of natural temporary dams formed during the event (Ives, 1986; Costa, 1988b; Costa & Schuster, 1988; Dutto & Mortara, 1992; Walder & Costa, 1996). The turbulence and dispersive pressure indicated by pressure marks on large clasts would have allowed their dispersion throughout the fan.

Clast imbrication and long-axis orientation perpendicular to the flow, which mimics fabric developed during fluvial deposition, indicate that clasts were transported by tractive forces and that rolling and bouncing occurred during the transport. Large clasts were lifted mostly by grain-to-grain collision (Rodine & Johnson, 1976), turbulence (Enos, 1977; Lowe, 1979) and differential buoyancy to the top of the flow. Because of the greater velocity of the top of the flow, caused by frictional bedload along the base (Johnson & Rodine, 1984), larger clasts were conveyed to the front head of the flow. This process caused the largest clasts to be concentrated preferentially at the outer part of the lobe head (Figs 2 & 13). A similar sorting process is described for downslope transfer of bedload material under the influence of gravity (Bagnold, 1954; Brush, 1965). Surge flows confined within the incised channel, both in the catchment and on the fan, formed well-defined levee-like boulder trains. In this case, clasts were pushed laterally by the front of the flow and, because of the resistance along the flow margins (owing to incised-channel walls, trees and man-made defence walls), they reorientated their long axes parallel to the channel and fan slope. Levee-like block and boulder trains also formed behind boulder jams against obstacles such as standing trees (Blair, 1987) or previously deposited blocks. These features formed irregularity in the flow bed, which enhanced the scouring of pools where fine-grained, crudely normally graded deposits were rapidly formed (Fig. 14b).

Fig. 14. (a) Frontal lobe margin accumulated during the 1996 flood event on the Inferno alluvial fan. Note the clear orientation of elongated boulders and blocks perpendicular to the flow direction. The matrix consists of cobbly, pebbly granular coarse to fine sand and is still visible between the clast. (b) Fine-grained sediments (arrow) consisting of silty coarse sand, granules with scattered pebbles and cobbles showing a rough horizontal bedding and normal gradation are present on top of the boulder-rich deposit (from Chiarle & Luino, 1998). (c) Longitudinal exposure within the main Inferno catchment feeder channel. Note fresh, coarse deposits (arrow) accumulated over the left channel bank forming a levee-like boulder train. Overall, sediment texture shows very coarse grain-size formed by moderately to well-rounded cobbles, boulders and small blocks within a sandy matrix. Matrix-free gravels lying on the channel bed were formed by winnowing processes during recessional stage of the flood (from Chiarle & Luino, 1998).

The few elongated boulders orientated with the longest axes parallel to the fan surface observed on the northern side of the fan also suggest strong water discharge after the main debris-rich surges, which partially remobilized and reorientated the larger clasts parallel to the flow. The reorientation of clasts could have been induced by obstacles (such as trees or earlier deposited boulders) that acted as fulcrum points.

The fine-grained stratified sediments deposited down-fan were transported as bedload and deposited by sheetflooding (Hogg, 1982). Similar facies have been described by Blair (1987), Wells & Harvey (1987), Moscariello (1998) and Moscariello & Blair (1998) and interpreted to result from violent breaking and shooting downslope of standing waves associated with antidune development and dissipation. The sheetflood expanded at several points along the fan during successive surges. Flow characteristics determined from field observations would indicate supercritical conditions that commonly occur in low-sloping alluvial fans (Blair & McPherson, 1994).

Overland flow caused by post-event rainfall reworked the sediments accumulated during the peak flood event. This occurred during the waning-flood stage and was responsible for winnowing fine sediments from the fan surface to the receiving stream.

TEXTURE OF ALLUVIAL FAN DEPOSITS

The grain-size data indicate that sediment generated by group 1 lithologies (dolomites) have on average a coarser matrix than those generated by group 2 and 3 lithologies (Fig. 15). The median is approximately 4 mm and the sorting index ranges between 2 and 5, with an average value of 3.13 (Table 1).

The matrix of debris-flow sediments associated with the group 3 fans has a median grain-size of about 2 mm. It shows the best particle sorting, with values ranging between 2 and 3 (average of 2.25). The sediments associated with the group 2 fans (fed by fine-grained schistose rocks) show smaller median grain-sizes (*c.* 0.5 mm) with a sorting index always larger than 8 (average of 10.54).

The geomechanical characteristics of the bedrock favour the action of disaggregation processes and weathering, which are controlled both by physical processes (freeze and thaw) and biological activity (roots and burrows) and ultimately are related to climatic characteristics. Moreover, the splitting properties of the bedrock produce fine-grained material that, with time, readily transforms into silt and clay. Under continental climatic conditions these processes can produce abundant colluvial material and relatively thick soils (0.3–1 m), which can be remobilized easily on steep slopes by heavy rainfall (Govi *et al.*, 1985b). Thus, discrepancies can be found between different geographical areas. This would explain the difference between the values presented by Costa (1984) for 43 recent deposits of debris (mud) flow from the USA. There, the sorting index for deposits generated from dolomite rocks (group 1) ranges between 3.9 and 12.3, which in the Alps correspond to values measured for the sediments generated from group 2 lithologies.

The clay and very fine silt content (< 8 μm) is considered a discriminant factor, which changes considerably over the three groups. The clay fraction in the colluvium, which is needed to initiate a debris-flow process (Blair & McPherson, 1994), is generated both by *in situ* weathering (by freeze–thaw process) and subordinately by intense biological activity (lichen and blue algae corrosion). Secondary enrichment in fine particles mainly results from infiltration of melting snow-related runoff and rainwater percolation. The maximum measured very fine silt and clay content for sediment gravity flow deposits of group 1 alluvial fans is 11%, whereas it reaches 25% for the group 2 fans (Fig. 15). On the other hand, sediment gravity flow deposits generated from group 3 lithologies do not contain any fine silt and clay, medium silt being the smallest particle size range present in the sediments (Fig. 15). The finest sediments sampled from group 3 alluvial fans are associated with waterlaid deposits and consist mostly of silt (mode 0.031–0.08 mm) with a very fine silt content of 5% (Fig. 6c). Field data indicate (Maraga *et al.*, 1998) that the range of particle distribution of waterlaid deposits is very similar for all the three types of fan deposits studied.

The various alluvial fan deposits also can be clearly distinguished (Fig. 15) by using a 40-μm (coarse silt) cut-off, often used in rheological studies (Coussot &

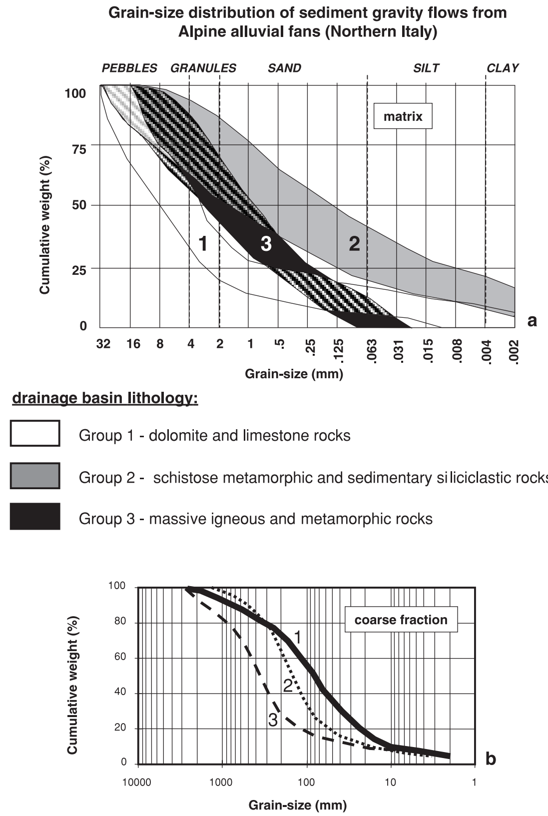

Fig. 15. (a) Cumulative curves of the < 32 mm fraction based on grain-size analysis of 23 samples from sediment gravity flow deposits collected throughout the Alps. The results are grouped in three main categories that reflect different dominating drainage basin lithology. On the whole, the results indicate that the average diameter is larger for dolomite rocks; heterogeneity is greater for schistose rocks and sorting is higher for crystalline lithologies. (b) Cumulative curve of the coarser grain-size measured in the field using the Quadrillage technique.

Meunier, 1996) to discriminate between fine and coarser sediment components. Thus, group 2 deposits have up to 43% fine sediments, group 1 deposits have a maximum of 17% and group 3 deposits have the lowest amount at less than 7%. However, these values do not differentiate between clay and very fine silt, which is the key discriminating factor that ultimately controls the cohesiveness of the sediment gravity flow.

Deposits with the largest grain size (up to medium block size) and thickness (up to 5 m) formed during a single flood event typically are generated from massive lithologies (group 3 and subordinately group 1; Fig. 15b). Boulders and blocks are relatively rare in the group 1 fan deposits, where usually they are isolated within a fine-grained cohesive matrix.

Generally, sediment gravity flows generated from group 2 lithologies produce finer and thinner deposits when compared with group 3 alluvial fans. Mud-rich lobes are a common feature and they present a typical tongue shape even when they are only a few centimetres thick. However, boulder-rich lobes also can be formed, and levees can reach 1–3 m in height.

Overall, this suggests a higher aggradation rate per single event for the group 3 fans in comparison with those of groups 1 and 2. On the other hand, primary sedimentary events for group 2 are on average more frequent than for the group 3 fans.

DISCUSSION

Fan deposits

Overall, field observations suggest that deposition produced by cohesive sediment gravity flows (groups 1 and 2) commonly generate levees orientated parallel to the direction of flow propagation. However, the occurrence of well-defined and sharp, clast-rich levees depends on availability and abundance of fine to coarse boulders forming the colluvium, which in turn is related to the splitting properties of the bed-rock. In the case of group 1, selective coarse-fraction sorting—which normally occurs during levee formation (Blackwelder, 1928; Sharp & Nobles, 1953; Johnson, 1970; Blair & McPherson, 1998)—is often ineffective and only large flat lobe-like levees are deposited. Lobes typically diverge from the direction of flow propagation (5–15°) and can reach distances of tens of metres from the main flow path. In the fans studied, the flow commonly reaches the toe and the receiving stream, where debris is evacuated down-valley.

On the other hand, non-cohesive sediment gravity flows (group 3) mostly generate extensive boulder-rich lobes. Levee-like boulder trains form where natural flow expansion is obstructed laterally or downstream.

The grain-size distribution of coarser components also controls the shape and texture of debris-flow deposits (levees and lobes) and, in turn, the possibility of constraining successive sediment gravity flow pulses. This controls the expansion potential of the sedimentary flow from the incised channel.

Deposits accumulated by recessional flood processes are texturally very different from those accumulated by sediment gravity flows. They clearly suggest the action of tractive currents and dominating bed-load transport, and high-velocity unconfined sheet-floods, associated with non-cohesive sedimentary flows, develop under supercritical conditions, which typically produce horizontally bedded gravels and sands generated from the development and dissipation of antidunes.

In the Alps, different types of sediment gravity flows are widely recognized. The widespread occurrence has allowed physical and mathematical modelling of debris flows by researchers from different Alpine countries. French studies deal mainly with muddy, clay-rich debris flows (Meunier, 1994; Coussot, 1996). Debris flows that occurred in 1987 in Switzerland have been interpreted as granular, non-cohesive debris flows (Rickenmann, 1999). The data presented in this paper suggest that somewhat different processes reflect the lithological composition and grain-size distribution of the parent material in the catchment (colluvium and other types of Quaternary sediments; Fig. 16).

Lithological control on fan processes and sediments

Comparison of source area materials and debris-flow deposits (Fig. 6d) indicate that the catchment lithology controls the clay and fine-silt content of the parent deposits (colluvial, landslide and glacial deposits), which in turn influence the type of sedimentary processes on the fan. During the various types of sediment gravity flow that exhibit either a cohesive or non-cohesive behaviour, in fact, no significant grain-size sorting occurs between the source and the deposit areas (Johnson & Rodine, 1984; Cojean *et al.*, 1999). Very fine silt and clay are the key components that allow discrimination between groups 1 and 2 cohesive sediment gravity flows, and group 3 non-cohesive sediment gravity flows. Cohesive debris flows commonly are generated from lithologies that can produce clay and/or fine silt size particles. They are associated with

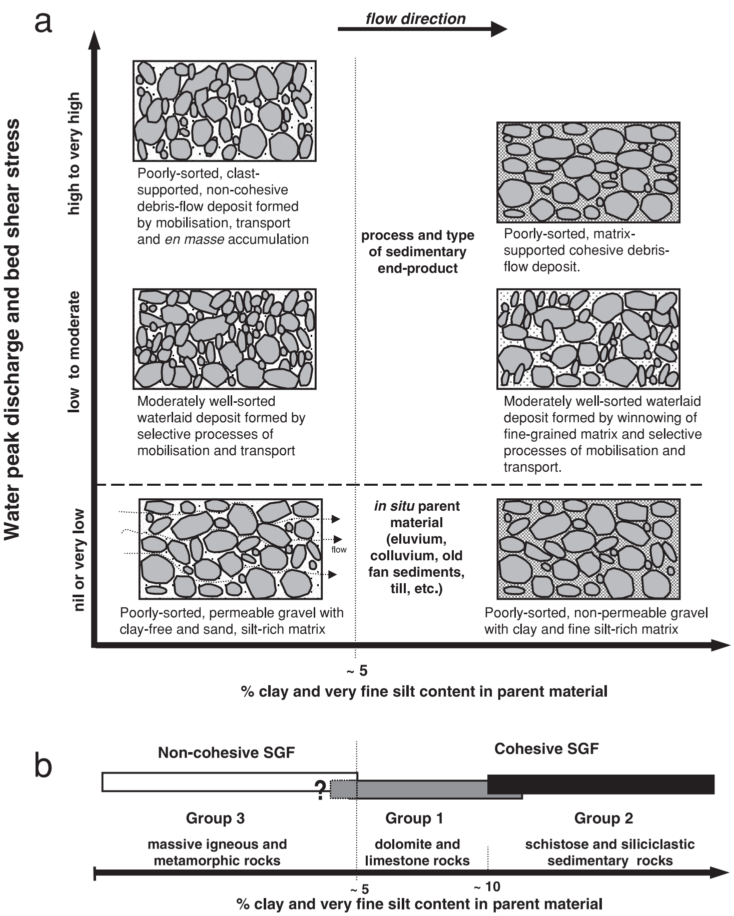

Fig. 16. (a) Schematic summary of changes in sedimentary processes and textural characteristics of alluvial fan deposits in response to variations in intensity of water discharge and bed shear stress. Different fan processes depend upon textural characteristics of the parent material in the catchment, which broadly can be distinguished on the basis of its fine-silt and clay content. A cut-off of 5% between fine-rich and fine-poor parent material is based on grain-size analyses throughout the alluvial fan deposits of the Italian Alps and is here proposed as a boundary between cohesive and non-cohesive debris-flow processes. The sketches depict different types of sediment textures (seen in plan view) resulting from different sedimentary processes. (b) Summary of types of sediment gravity flows (SGF) occurring for the three groups of alluvial fans distinguished on the basis of the dominant catchment lithology, as has been observed in the Italian Alpine region, and composition of the parent material. Note that fan deposits generated from carbonate lithologies also could lead to a non-cohesive type of SGF, depending on the local lithological characteristics.

both group 1 (massive and/or roughly stratified carbonate bedrock) and group 2 (calc-schists, mica schists, phyllites and limestone bedrock) fans, despite the considerable differences in matrix grain-size distribution. Cohesive debris flows can develop even if clay and very fine silt make up a small percentage of the bulk matrix (5–15% for group 1 fans). On the other hand, non-cohesive sediment gravity flows typically are produced from quartz-rich, coarse-grained lithologies such as granites and granodiorites (group 3), which yield virtually clay-free colluvial deposits. This influences the rheological properties of the matrix, which in turn control the fan sedimentary processes.

As described earlier, group 2 and 3 deposits display a rather different texture that ultimately is the result of different sedimentary processes and the composition of parent material involved. On the other hand, group 1 deposits show distinct characteristics that compositionally can be described as intermediate between groups 2 and 3. Depending on mineralogical and lithological composition (pure versus marly limestone), splitting properties (tectonic and weathering history), the occurrence of heterogeneous intercalations (interbedded shales) and type of cementation, carbonate rocks also can produce clay- and fine-silt-free colluvium. This leads to the development of alluvial fans dominated by water gravity flow processes (sheetfloods) as described in the Death Valley region (Moscariello & Blair, 1998).

Fan processes

Sediment gravity flows are the most important sedimentary processes with respect to the amount of material delivered to the fan from the catchment (Blair & McPherson, 1994). They can be initiated either by failure of colluvium, which is conveyed down-valley and transforms into a debris flow by entrainment of air and water (Costa, 1988a), or when sediments lying in the drainage basin are intersected by a fast-moving, high-discharge water flow. The difference in matrix permeability between groups 1, 2 and 3 fans controls the hydraulic conditions necessary to generate a sediment gravity flow. Indeed, the generation of a debris flow depends on the shear strength necessary to initiate the movement of coarse sediments (Blair & McPherson, 1994), which in turn can be related to the matrix permeability properties. Highly permeable, clay-poor material will allow water to pass between the clasts (Fig. 16) and will have higher shear strength than clay-rich materials. Boulder-rich, coarse-grained, clay-free sediments subjected to low and moderate energy water flow will experience a dispersed horizontal stress enabling the mobilization of selected particle sizes. Very high water discharge and bed shear stress, on the other hand, will trigger non-cohesive sediment gravity flows.

In contrast, a non-permeable, clay-rich material will experience an overall higher horizontal stress because of the high pressure exerted over a large surface by the water flow. Therefore, the transformation of clay-rich parent material into a cohesive sediment gravity flow usually requires less bed shear stress and lower peak discharge than is required for the generation of a non-cohesive sediment gravity flow, provided a comparable total volume of debris is involved.

Hence, for a given slope, clay-free, coarse-grained sediments, if compared with fine-grained, clay-rich sediments, will require more water to be mobilized and generate sediment gravity flows (Jarrett & Costa, 1985). The latter are often associated with exceptional floods that are characterized by very high peak water discharge caused by low-frequency–high-intensity rainfall events (Chiarle & Luino, 1998) or, for instance, by catastrophic dam failure (Costa, 1983). Similar observations come from a large number of field case studies in other regions of the world (Japan, China and Canada), where cohesive sediment gravity flows usually show less strength and are associated with more frequent flood events and lower peak discharges than the non-cohesive sediment gravity flows (Mizuyama *et al.*, 1992; Bovis & Jakob, 1999).

Alluvial fan sedimentary facies, together with information provided by eyewitness accounts of flood events, and indications from monitoring systems, suggest that alluvial fan reactivation typically can be subdivided into two main phases. These two phases are common to all cases studied. They are independent of the type of sedimentary process (which depends on lithological properties of the colluvium), the geomorphological characteristics of the fan, and the magnitude and chronological distribution of rainfall.

The first phase is characterized by the triggering of the sediment gravity flow by sudden colluvium failure (Wieczorek, 1996). The sediment flow moves rapidly down-valley and is conveyed within the main drainage-basin feeder channel. At the fan site, the incised channel is in many cases undersized relative to the volumes of liquid/solid discharge. Therefore, the debris overspills the incised channel and forms levees and lobes in different positions on the fan, depending on rheology of the sediment mobilized, lateral constraint to the flow, sinuosity of the channel, slope morphology and gradient of the channel bed and/or obstacles. Generally, these processes occur over a time interval spanning a few minutes to a few hours.

The second phase is typified by a considerable decrease in solid discharge because the debris produced by slope failure is no longer available in the catchment. During this phase the catchment continues to drain the waning rainfall. This is the recessional water-flood stage (Blair & McPherson, 1994, 1998) where erosional and water flow processes characterized by formation of lower flow-regime sedimentary structures take place. Typically, these processes last for a few hours. However, erosional processes associated with overland flow and rainsplash (secondary processes *sensu* Blair & McPherson, 1994) can rework and redistribute the fan deposits during successive minor flood events. Erosion and transport (bedload and suspended load) occur primarily by water flow processes.

The heterogeneity of fan deposits, coupled with observations during flood events, also indicate that sediment gravity flow processes are characterized by extremely variable flow conditions. Clear indication of torrent bed deepening associated with debris-flow events would in fact indicate turbulent flow conditions. In contrast, the non-erosional base of the mud-rich lobes together with the steepness of the lobe margins would suggest non-erosional, laminar flow conditions (Johnson, 1970; Rodine & Johnson, 1976; Blair & McPherson, 1998).

This difference can be explained by changes in the lateral flow boundary conditions (confined flow versus unconfined flow), which in turn depend on channel and fan morphology and surficial distribution of sediments. They actually control the lateral shear and differential movement of the flow components, the difference in roughness of the flow-bed (irregular surface of the channel versus planar surface of the fan) and the velocity and shear stress (high velocity for channelized flow versus low velocity for overbank deposits).

Fan-related hazards

Catastrophic floods affecting alluvial fans throughout the Italian Alps occur on average once every 1.7 yr; they often produce casualties and serious damage to dwellings and other human structures (Govi *et al*., 1985a; Fig. 1). Historical data and accurate description of past events, together with geomorphological observations after flood events within the past 40 yr (Govi *et al*., 1994), indicate that hazards associated with alluvial fan processes mostly are related to:

1 the magnitude (volume and duration) and recurrence of the flood event;

2 the amount of mobilized debris exceeding the capacity of transport within the incised channel;

3 the velocity of transport of the debris that is accumulated on the fan surface;

4 local topographic conditions such as the height of the apex incision, which corresponds to the point of maximum expansion potential of the flow, with the latter, in turn, controlling the spread of a sediment gravity flow over the fan surface and thus the severity of damage associated with debris deposition.

Fan activity and climate

The discontinuous activity of alluvial fans in inhabited Alpine valleys is typically shown by historical records of catastrophic events, which significantly affected villages, infrastructure and people.

These indications, together with past instrumental records of exceptional rainfall or water discharge in the main receiving streams, help in tracing the average frequency of major catastrophic floods. Further information also can be obtained through dendrochronological investigations (Strunk, 1992). Information on debris-flow occurrence then can be used to build stochastic prediction models and understand the relationship between climate and fan activity. In particular, historical research on alluvial fan activity over the past 190 yr (Govi *et al*., 1994) indicates that 66% of the devastating events occurred during the summer (July, August and September). These basins are mostly located in areas characterized by a continental climatic regime. However, sedimentological evidence from fan deposits in the Italian Alps indicates that alluvial fans dominated by cohesive sediment gravity flows occur in similar climatic settings as alluvial fans dominated by waterlaid sediment. This clearly indicates that climatic conditions do not affect the type of primary fan processes. However, in the past, different climatic conditions (glaciations, Holocene warm and humid periods; Magny, 1995) could have favoured intense chemical and physical weathering processes, causing the formation of large amounts of colluvium and hence creating favourable conditions for the generation of sediment gravity flows. On the other hand, the present-day climatic conditions control the frequency and magnitude of processes on alluvial fans (Nilsen, 1982; Dunne, 1988; Rachocki & Church, 1990; Blair & McPherson, 1994) and the production rate of movable sediment in the catchment. This, in turn, controls the *sediment recharge time* (Moscariello & Mortara, 1994). The frequency of debris-flow events, in fact, depends on the availability of material that can be transported down-valley and the sensitivity of the catchment to rainfall. The rainfall threshold necessary to trigger debris flows and shallow landslides depends again on a combination of the catchment morphology (slope steepness), the geomechanical properties of the bedrock and/or colluvium material and antecedent moisture conditions (Moser & Hohensinn, 1983; Cancelli & Nova, 1985; Wieczorek, 1987; Johnson & Sitar, 1990; Deganutti *et al.*, 2000).

Climatic characteristics also control the frequency and effectiveness of secondary processes (runoff, soil and vegetation development, and burrowing activity) and the rate of reworking and redistribution of sediment on the fan surface.

The results of several studies on palaeoclimatic proxies contained in natural sedimentary archives (lacustrine or bog sediments) clearly indicate that global climate modifications over the past 15 000 yr induced important changes in the Alpine natural environment (Ammann *et al*., 1994; Wohlfarth *et al*., 1994; Moscariello, 1996). Substantial environmental modifications particularly affected the mountain regions, where the sensitive ecosystems were impacted by occurrences of extreme weather events and natural catastrophes (floods, landslides and debris flows, i.e. Burri, 1974; Jorda, 1992; Rosique, 1993). Multidisciplinary studies of the long interglacial lacustrine succession from Piànico-Sèllere (Moscariello *et al.*, 2000) suggest that increased debris-flow activity occurred as a consequence of major climate-driven changes in vegetation cover on the slopes surrounding the lake. Alluvial fan deposits intercalated with continuous sedimentary records thus represent a useful tool for reconstructing the evolution of climate-controlled erosional processes and slope activity throughout the past.

In the case of ongoing global warming, as indicated by the atmospheric general circulation models (Houghton *et al*., 1995), an increase in Alpine alluvial fan activity in fact can be predicted: the increased melting of the glacial and permafrost cover will produce higher slope instability in the highest Alpine areas (Dramis *et al*., 1995). This, in turn, could lead to an increase in the river sediment load (Zimmerman & Haeberli, 1989). Such a scenario seems to be supported both by an average temperature increase of 1°C measured between 1961 and 1990 in the Swiss Alps and the increased frequency and magnitude of flood events observed in the same region (Gees, 1997).

CONCLUSIONS

This paper highlights the key role of catchment lithology in determining the dominant alluvial fan sedimentary processes. The study presented here emphasizes the importance of the lithological control on the textural characteristics of alluvial fan deposits and related processes and provides guidance for distinguishing between the different dominant sedimentary processes throughout the Alpine region. Other factors such as the tectonic setting (intensity of fracturing), weathering history and modern climatic conditions (intensity and frequency of precipitation) control the rate of colluvium production and the average frequency of flood events.

The study of several modern alluvial fans throughout the Italian Alps enabled the recognition of three different groups of fan deposits, which reflect the dominant catchment lithology and, in turn, the grain-size distribution of the parent material held in the catchment.

Primary sedimentary processes occurring on a fan sourced from massive crystalline rocks (group 3) are regarded as potentially less frequent than for alluvial fans generated from massive and/or crudely stratified carbonate rocks (group 1) and fine-grained sedimentary and metamorphic rocks (group 2). However, the transport and depositional mechanisms (dispersive pressure, turbulence and large water discharge) that typify the fans generated from group 3 lithologies suggest a higher geological hazard potential. This mostly is because of the catastrophic character (low-frequency–high-intensity rainfall) of the flood events, which enables the mobilization of larger average clast sizes and their distribution over large areas. Conversely, cohesive debris flows usually are generated from less intense flood events.

The prediction of future evolutionary trends and morphological modifications of Alpine alluvial fans also can be based on a detailed understanding of the mechanisms and processes that controlled the accumulation of past sedimentary records.

Debris-flow hazard assessment and reduction are complex tasks that require the synergy of research covering geomorphology, rheology, hydraulic and hydrological modelling, land-use planning and management. However, sedimentological investigations of modern fan deposits can provide unique information to define areas prone to debris flows and predict depositional processes. The improved understanding of modern alluvial fan deposits also provides a valuable tool for the correct interpretation of the stratigraphical record and sedimentary environment of ancient deposits.

ACKNOWLEDGEMENTS

This work was supported financially by the Italian National Research Council and the National Group for Prevention of Hydrogeological Hazards and the publication partly supported by GNDCI (Publication no. 2217). This study was also partly supported by CNR Grant no. 201.05.24 (A.M.). The authors wish to thank M. Chiarle, A.M. Deganutti, F. Luino, A. Pasuto and D. Tropeano for their helpful and constructive comments during the preparation of the paper. A.M. is indebted to T.C. Blair and J.G. McPherson for constructive and stimulating discussions. The authors also are very grateful to G. Garzón, I.P. Martini, M. Marzo and M. Parise for criticisms and comments which improved an early version of this paper. Assistance during morphometric study of the catchment basins was provided by G. Rivelli. Grain-size analyses were performed by R. Massobrio, E. Viola and G. Peruzzo. Photographs and figures were prepared with the contribution of P.G. Trebò, E. Viola and G. Peruzzo. We also thank P. Gibbard and M. Sarginson for improving the English version of the manuscript.

REFERENCES

Ammann, B., Eicher, U., Gaillard, M.-J., *et al.* (1994) The Wurmian Late-glacial in lowland Switzerland. *J. Quat. Sci.* **9**, 119–125.

Arattano, M., Deganutti, A.M. & Marchi, L. (1997) Debris flow monitoring activity in an instrumented watershed on the Italian Alps. In: *Debris-Flow Hazards and Mitigation: Mechanics, Prediction and Assessment* (Ed. Chen, C.), *Proceedings of First International Conference of Water Resources Engineering Division/ASCE*, 7–9 August, San Francisco, CA, pp. 506–515.

Aulitzky, H. (1982) Preliminary two-fold classification of torrents. *Mitt. Forstl. Bundes-Versuchsanst. Wien* **144**, 243–256.

Bagnold, R.A. (1954) Experiments on a gravity-free dispersion of large solid spheres in a Newtonian fluid under shear. *Proc. R. Soc. London, Ser. A* **225**, 49–63.

Beaty, C.B. (1963) Origin of alluvial fans, White Mountains, California and Nevada. *Assoc. Am Geogr. Ann.* **53**, 516–535.

Blackwelder, E. (1928) Mudflow as a geologic agent in semi-arid mountains. *Geol. Soc. Am. Bull.* **39**, 465–484.

Blair, T.C. (1987) Sedimentary processes, vertical stratification sequences, and geomorphology of the Roaring river alluvial fan, Rocky Mountain National Park, Colorado. *J. sediment. Petrol.* **57** (1), 1–18.

Blair, T.C. & McPherson, J.G. (1994) Alluvial fans and their natural distinction from rivers based on morphology, hydraulic processes, sedimentary processes, and facies assemblages. *J. sediment. Res.* **A64** (3), 450–489.

Blair, T.C. & McPherson, J.G. (1998) Recent debris-flow processes and resultant form and facies of the Dolomite alluvial fan, southern Owens valley, California. *J. sediment. Res.* **68** (5), 800–818.

Blair, T.C. & McPherson, J.G. (1999) Grain-size distribution and textural classification of coarse sedimentary particles. *J. sediment. Res.* **69** (1), 6–19.

Bovis, M.J. & Jakob, M. (1999) The role of debris supply conditions in predicting debris flow activity. *Earth Surf. Process. Landf.* **24**, 1039–1054.

Brush, L.M. (1965) Sediment sorting in alluvial channels. In: *Primary Sedimentary Structures and their Hydrodynamic Interpretation* (Ed. Middleton, G.V.), Spec. Publ. Soc. econ. Paleont. Miner., Tulsa, **12**, 25–33.

Burri, M. (1974) Histoire et préhistoire glaciaires des vallées des Drances (Valais). *Eclogae geol. Helv.* **67**(1), 135–154. [In French.]

Cailleux, A. & Tricart, L. (1959) *Initiation à l'étude des sables et des galets*, Tome 1. Centre Documentation Universitaire, Paris. [In French.]

Campbell, R.H. (1975) Soil slips, debris flows and rainstorms in the Santa Monica Mountains and vicinity, Southern California. *U.S. geol. Surv. Prof. Pap.* **851**, 51 pp.

Cancelli, A. & Nova, R. (1985) Landslides in soil debris cover triggered by rainstorms in Valtellina (Central Alps—Italy). *Proceedings IV International Conference and Field Workshop on Landslides, Tokyo, August*, pp. 267–272.

Carraro, F. (1992) Evoluzione Plio-Quaternaria. In: *Le Alpi dal M. Bianco al Lago Maggiore* (Ed. Dal Piaz, G.V.), Guide Geologiche Regionali, Societá Geologica Italiana, Vol. 3, pp. 82–90. BE-MA Editrice. [In Italian.]

Cerato, M. (1999) Contributi per una storia delle sistemazioni idrauliche e forestali in Valsugana. *Provincia Autonoma di Trento, -Azienda Speciale di Sistemazione Montana*. [In Italian.]

Chiarle, M. & Luino, F. (1998) Colate detritiche torrentizie sul Monte Mottarone innescate dal nubifragio dell'8 luglio 1996 (Lago D'Orta—Piemonte). *Proceedings of the Conference on Prevention of Hydrogeological Hazards: The Role of Scientific Research, Alba, 5–7 November, 1996*, pp. 231–245. [In Italian.]

Church, M. & Desloges, J.R. (1984) Debris torrents and natural hazards of steep mountain channels—east shore of Howe Sound. In: *Canadian Association of Geography, Field Trip Guidebook no. 7*. Department of Geography, University of British Columbia, Vancouver, 83 pp.

Cojean, R., Sorgi, C., Bland, S., *et al.* (1999) *Contribution of Armines-CGI.* E.U. contract ENV4 CT96 0253 'Debris Flow Risk', European Union, Brussels.

Costa, J.E. (1983) Paleohydraulic reconstruction of flash-flood peaks from boulder deposits in the Colorado Front Range. *Geol. Soc. Am. Bull.* **94**, 986–1004.

Costa, J.E. (1984) Physical geomorphology of debris flows. In: *Developments and Applications of Geomorphology* (Eds Costa, J.E. & Fleisher, P.L.), pp. 268–317. Springer-Verlag, Berlin.

Costa, J.E. (1988a) Rheologic, geomorphic, and sedimentologic differentiation of water floods, hyperconcentrated flows, and debris flows. In: *Flood Geomorphology* (Eds Baker, V.R., Kochel, R.C. & Patton, R.C.), pp. 113–122. John Wiley & Sons, New York.

Costa, J.E. (1988b) Floods from dam failure. In: *Flood Geomorphology* (Eds Baker, V.R., Kochel, R.C. & Patton, R.C), pp. 439–463. John Wiley & Sons, New York.

Costa, J.E. & Schuster, R.L. (1988) The formation and failure of natural dams. *Geol. Soc. Am. Bull.* **100**, 1054–1068.

Coussot, Ph. (1996) Les laves torrentielles. Connaissances à l'usage du praticien. *Collection Etudes: Equipements pour l'eau et l'environnement*, 23, Cemagref Editions, Lyon. [In French.]

Coussot, Ph. & Meunier, M. (1996) Recognition, classification and mechanical description of debris flows. *Earth Sci. Rev.* **40**, 209–227.

Dal Piaz, G.V. (1992) *Le Alpi dal M. Bianco al Lago Maggiore. Guide Geologiche Regionali*. Vol. 3, Società Geologica Italiana, BE-MA Editrice, 311 pp. [In Italian.]

Deganutti, A.M., Marchi, L. & Arattano, M. (2000) Rainfall and debris flow occurrence in the Moscardo basin (Italian Alps). In: *Debris-flow Hazards Mitigation: Mechanics, Prediction and Assessment* (Eds Wieczorek, G.F. & Naeser, N.D.), pp. 67–72. Proceedings of the 2nd International Conference on Debris-flow Hazards Mitigation, Taipei, Taiwan, 16–18 August 2000. Balkema, Rotterdam,

Dramis, F., Govi, M., Guglielmin, M. & Mortara, G. (1995) Mountain permafrost and slope instability in the Italian Alps: the Val Pola landslide. *Permafrost and Periglacial Process.* **6**, 73–82.

Dunne, L.A. (1988) Discussion on fan deltas and braid-deltas: varieties of coarse-grained deltas. *Geol. Soc. Am. Bull.* **100**, 1308–1309.

Dutto, F. & Mortara, G. (1992) Rischi connessi con la dinamica glaciale nelle Alpi italiane. *Geogr. Fis. Din. Quat.* **15**, 85–99. [In Italian.]

Enos, P. (1977) Flow regimes in debris flow. *Sedimentology* **24**, 133–142.

Folk, R.L. (1974) *Petrology of Sedimentary Rocks*. Hemphill Publishing Company, Austin, TX, 182 pp.

Gees, A. (1997) Analyse historischer und seltener Hochwasser in der Schweiz. Bedeutung für das Bemessungshochwasser. *Geogr. Bernensis* **G53**, 1–156. [In German.]

Govi, M., Mortara, G. & Sorzana, P.F. (1985a) Crues et laves torrentielles avec des conséquences graves ou catastrophiques dans les Alpes italiennes. *Comptes Rendus 25° Congrès Inernational Géographie 'les Alpes', Parigi, August 1984*, pp. 36–37. [In French.]

Govi, M., Mortara, G. & Sorzana, P.F. (1985b) Eventi idrologici e frane. *Geol. Appl. Idrogeol.* **20**(II), 359–375. [In Italian.]

Govi, M., Marchi, L., Mortara, G. & Turitto, O. (1994) Ricerche sulle colate detritiche torrentizie (debris flow) in ambiente alpino. *GNDCI-CNR Linea 1, Report 1990–91*, pp. 405–420. Presidenza del Consiglio dei Ministri, Dipartmento della Protezione Civile, Rome. [In Italian.]

Hogg, S.E. (1982) Sheetfloods, sheetwash, sheetflow, or…? *Earth Sci. Rev.* **18**, 59–76.

Houghton, J.T., Meira Filho, L.G., Bruce, J., *et al.* (1995) *Climate Change 1994*. Cambridge University Press, Cambridge, 339 pp.

Hubert, J.F. & Filipov, A.J. (1989) Debris flow deposits in alluvial fans on the west flank of the White Mountains, Owens Valley, California. *Sediment. Geol.* **61**, 177–205.

Hunziker, J.C., Desmons, J. & Hurford, A.J. (1992) *Thirty-two years of geochronological work in the Central and Western Alps: a review on seven maps*. Memoire de Géologie 13, Université de Lausanne, Lausanne, 59 pp.

Hutchinson, J.N. (1988) Morphological and geotechnical parameters of landslides in relation to geology and hydrogeology. In: *Proceedings of the Fifth International Symposium on Landslides* (Ed. Bonnard, C.) *Lausanne, 10–15 July 1988*, Vol. 1, pp. 3–35. Balkema, Rotterdam.

Ives, J.D. (1986) *Glacial lake outburst floods and risk engineering in the Himalaya*. Occasional Paper 5, International Centre for Integrated Mountain Development, Kathmandu.

Jarrett, R.D. & Costa, J.E. (1985) Hydrology, geomorphology, and dam-break modeling of the July 15, 1982 Lawn Lake Dam and Cascade Lake Dam failures, Larimer County, Colorado. *U.S. geol. Surv. Open File Rep.* **84–612**, 109 pp.

Johnson, A.M. (1970) Formation of debris flow deposits. In: *Physical Processes in Geology*, pp. 433–448. Freeman Cooper & Company, San Francisco, 577pp.

Johnson, A.M. & Rodine, J.R. (1984) Debris flow. In: *Slope Instability* (Eds Brunsden, D. & Prior, D.B.), pp. 257–361. John Wiley & Sons, New York.

Johnson, K.A. & Sitar, N. (1990) Hydrologic conditions leading to debris-flow initiations. *Can. Geotech. J.* **27**, 789–801.

Jorda, M. (1992) Morphogenèse et fluctuation climatiques dans les Alpes Françaises du sud de l'Age du Bronze au Haut Moyen Age. *Les Nouvelles L'archéologie* **50**, 14–20. [In French.]

Lowe, D.R. (1979) Sediment gravity flow: their classification and some problems of its application to natural flows and deposits. In: *Geology of Continental Slopes* (Eds Doyle, L.J. & Pilkey, O.H., Jr), Spec. Publ. Soc. econ. Paleont. Miner., Tulsa, **27**, 75–82.

Luino, F., Chiarle, M., Moscariello, A. & Arattano, M. (1994) Un fenomeno di mobilizzazione in massa presso Oropa (VC). *GEAM—Geoingegneria Ambientale e Mineraria* **83**(2/3), 149–156. [In Italian.]

Magny, M. (1995) *Une histoire du climat*. Editions Errance, Paris, 176 pp. [In French.]

Major, J.J. (1998) Pebble orientation on large scale, experimental debris-flow deposits *Sediment. Geol.* **117**, 151–164.

Maraga, F., Marchi, L., Mortara, G. & Moscariello, A. (1998) Colate detritiche torrentizie: aspetti granulometrici e influenza sul territorio. *Mem. Soc. geol. Ital.* **53**, 75–96. [In Italian.]

Marchi, L. & Pasuto, A. (1999) A debris flow in the Dolomites, Northeastern Italy. *Landslide News* **12**, 9–12.

Marchi, L. & Tecca, P.R. (1996) Magnitudo delle colate detritiche nelle Alpi Orientali Italiane. *GEAM—Geoingegneria Ambientale e Mineraria* **33**(2/3), 79–86. [In Italian.]

Meunier, M. (1991) Eléments d'hydraulique torrentielle. *CEMAGREF, Etud. Sér. Montagne* **1**, 1–278. [In French.]

Meunier, M. (1994) Les progrès de la connaissance et les méthodes d'étude des phénomènes torrentiels. *La Houille Blanche* **3**, 25–31. [In French.]

Mizuyama, T., Kobashi, S. & Ou, G. (1992) Prediction of debris flow peak discharge. *Interpaevent, International Symposium, Bern, Switzerland. Tagespublikation* **4**, 99–108.

Mortara, G. & Sorzana, P.F. (1987) Fenomeni di deformazione gravitativa profonda nell'arco Alpino Occidentale italiano. Considerazioni lito-strutturali e morfologiche. *Boll. Soc. Geol. Ital.* **106**, 303–314. [In Italian.]

Mortara, G., Sorzana, P.F. & Villi, V. (1986) L'evento alluvionale del 6 agosto 1985 nella vallata del fiume Isarco tra Fortezza ed il Passo del Brennero (Alto Adige). *Mem. Sc. Geol., Univ. Padova* **38**, 427–457. [In Italian.]

Moscariello, A. (1996) *Quaternary Geology of the Geneva Bay (Lake Geneva, Switzerland). Sedimentary Record, Palaeoclimate and Palaeoenvironmental Reconstruction since the Last Glacial Cycle*. Terre et Environnement, 4, University of Geneva, Geneva.

Moscariello, A. (1998) *Continental sedimentary record of climate change and catastrophic flood events: processes, forms and facies of alluvial fans in the Western U.S.A.* Post-doctoral Research Report, Fellowship of the Swiss National Science Foundation No. 81GE-048184, Bern, 30 pp.

Moscariello, A. & Blair, T.C. (1998) Sedimentary processes and reservoir properties of alluvial fans: Examples from Death Valley, California, U.S.A. In: *Abstracts of the AAPG Hedberg Conference, Integrated Structural and Sequence Stratigraphic Analysis in Rift Settings*, 20–23 *October, Cairo*.

Moscariello, A. & Deganutti, A.M. (2000) Sedimentary and hydrologic processes of a debris-flow dominated alluvial fan (Moscardo Fan, Italy). In: *Debris-flow Hazards Mitigation*: *Mechanics, Prediction and Assessment* (Eds Wieczorek, G.F. & Naeser, N.D.), pp. 301–309. Proceedings of the 2nd International Conference on Debris-flow Hazards Mitigation, Taipei, Taiwan, 16–18 August 2000, Balkema, Rotterdam.

Moscariello, A. & Mortara, G. (1994) *Fotointerpretazione applicata a problemi di dinamica fluviale e torrentizia*. Internal Report M.I. 94/9, Consiglio Nazionale delle Ricerche—Istituto di Ricerca per la Protezione Idrogeologica del Bacino Padano, Turin, 16 pp. [In Italian.]

Moscariello, A., Ravazzi, C., Brauer, A., *et al.* (2000) A long lacustrine record from the Pianico-Sellere Basin (Middle–Late Pleistocene, Northern Italy). *Quat. Int.* **73–74**, 47–78.

Moser, M. & Hohensinn, F. (1983) Geotechnical aspects of soil slips in Alpine regions. *Eng. Geol.* **19**, 185–211.

Nilsen, T.H. (1982) Alluvial fan deposits. In: *Sandstone Depositional Environments* (Eds Scholle, P.A. & Spearing, D.), Mem. Am. Assoc. petrol. Geol., Tulsa, **31**, 49–86.

Parise, M. & Moscariello, A. (1997) Geologic hazards and relative slope stability on the inactive Slumgullion landslide, Southwestern Colorado. *U.S. geol. Surv. Open File Rep.* **97–706**, 1–16.

Pasuto, A. & Soldati, M. (1996) Rock spreading. In: *Landslide Recognition: Identification, Movement and Causes* (Eds Dikau, R., Brunsden, D., Schrott, L. & Ibsen, M.-L.), pp. 122–136. John Wiley & Sons, New York.

Pierson, T.C. (1980) Erosion and deposition by debris flows at Mt. Thomas, North Canterbury, New Zealand. *Earth Surf. Process. Landf.* **5**, 227–247.

Pierson, T.C. & Costa, J.E. (1987) A rheologic classification of subaerial sediment–water flows. *Geol. Soc. Am. Rev. eng. Geol.* **7**, 1–12.

Rachocki, A.H. & Church, M. (1990) *Alluvial Fans: a Field Approach*. John Wiley & Sons, New York, 391pp.

Rickenmann, D. (1999) Empirical relationships for debris flows. *Natural Hazards* **19**(1), 47–77.

Rodine, J.D. & Johnson, A.M. (1976) The ability of debris, heavily freighted with coarse clastic materials, to flow on gentle slopes. *Sedimentology* **23**, 21–234.

Rosique, T. (1993) Détritisme torrentiel et activité érosive post-würmiens dans les Alpes méridionales françaises: l'exemple de la région de Gap (Hautes-Alpes). *Trav. Unite Rech. Assoc. Cen. Nat. Rech. Sci.* **22**, 53–61. [In French.]

Sharp, R.P. (1942) Mudflow levees. *J. Geomorphol.* **5**, 222–227.

Sharp, R.P. & Nobles, L.H. (1953) Mudflow of 1941 at Wrightwood, Southern California. *Geol. Soc. Am. Bull.* **64**, 547–560.

Strunk, H. (1992) *Reconstructing Debris Flow Frequency in the Southern Alps Back to AD 1500 using Dendromorphological Analysis*. Publication 209, International Association of Hydrological Sciences, Wallingford, pp. 299–306.

Tropeano, D. & Olive, P. (1993) Eventi geomorfologici nelle Alpi italiane e nella pianura occidentale del Po: inquadramento cronologico in base a radiodatazioni 14C. *Il Quaternario* **6**(2), 189–204. [In Italian.]

Tropeano, D. & Turconi, L. (1998) Colate detritiche del 12, 15 e 16 agosto 1998 in alta Valle di Susa (Piemonte). *GEAM—Geoingegneria Ambientale e Mineraria* **35**(2–3), 177–188. [In Italian.]

Tropeano, D., Casagrande, A., Luino, F. & Cescon, F. (1996) Processi di mud-debris flow in Val Cenischia (Alpi Graie). Quaderni di Studi e Documentazione, 20 (Suppl.) *GEAM—Geoingegneria Ambientale e Mineraria* **33**(2–3), 5–31. [In Italian.]

Venzo, G.A. & Largaiolli, T. (1968) Il bacino del torrente Chieppena (Trentino). *Mem. Mus. Trent. Sci. Nat.* **17**(2), 1–190. [In Italian.]

Walder, J.S. & Costa, J.E. (1996) Outburst floods from glaciers-dammed lakes: the effect of mode of lake drainage on flood magnitude. *Earth Surf. Process. Landf.* **21**, 701–723.

Wells, S.G. & Harvey, A.M. (1987) Sedimentologic and geomorphic variations in storm-generated alluvial fans, Howgill Fells, Northwest England. *Geol. Soc. Am. Bull.* **98**, 182–190.

Whipple, K.X. (1993) Interpreting debris-flow hazard from study of fan morphology. *Proceedings of Hydraulic Engineering '93, San Francisco, 25–30 June* (Eds Hsieh Wen Shen, Su, St. & Fen Wen), Vol. 2, pp. 1302–1307.

Wieczorek, G.F. (1987) Effect of rainfall intensity and duration on debris flows in central Santa Cruz Mountains, California. *Geol. Soc. Am., Rev. eng. Geol.* **7**, 93–104.

Wieczorek, G.F. (1996) Landslide triggering mechanisms. In: *Landslides: Investigation and Mitigation* (Eds Turner, A.K. & Schuster, R.L.), pp. 76–90. Special Report 247, Transportation Research Board, National Research Council. National Academy Press, Washington, DC.

Wohlfarth, B., Gaillard, M.-J., Haeberli, W. & Kelts, K. (1994) Environment and climate in southwestern Switzerland during the last termination 10–15 ka BP. *Quat. Sci. Rev.* **13**, 361–394.

Zimmermann, M. & Haeberli, W. (1989) Climatic change and debris flow activity in high mountain areas. In: *Landscape Ecological Impact of Climate Change on Alpine Regions* (Eds Rupke, C. & Boer, M.M.), pp. 34–45. Lunteren, The Netherlands.

Spec. Publs int. Ass. Sediment. (2002) **32**, 167–93

Analysis of terrestrial hyperconcentrated flows and their deposits

M. BENVENUTI* *and* I.P. MARTINI†

**Dipartimento di Scienze della Terra, Università di Firenze, Italy (Email: marcob@geo.unifi.it); and*
†Department of Land Resource Science, University of Guelph, Ontario, Canada

ABSTRACT

The term *hyperconcentrated flow* refers to intermediate states between debris flows and fluid flows, where fluid turbulence remains an important dispersal mechanism of clastic particles. Whereas the end-member flows are fairly well understood, unanimous agreement has not been reached on the subdivision and boundary definition of hyperconcentrated flows, both in meaningful rheological terms and, more so, in terms of the characteristics of their deposits. This paper briefly reviews the main characteristics of hyperconcentrated flows resulting from either suspended-load hyperconcentration or bedload hyperconcentration (traction carpet), and focuses on the analysis of three deposits possibly associated with these flows. The first two deposits formed in ancient, temperate alluvial fans of Pliocene–Pleistocene post-collision basins of the Northern Apennines, Italy, and the third in Upper Pleistocene glacial outwash of Ontario, Canada. The main finding is that geomorphological setting, climate and substrate geology are the prime control for hyperconcentrated flows in terms of frequency, magnitude and rheological properties of the flow. Recognition of hyperconcentrated-flow deposits through facies analysis leads to a better understanding of the developmental dynamics of alluvial sediment succession, and provides powerful information for risk assessment of localities possibly affected by hydrogeological hazards.

INTRODUCTION

The objectives of this paper are to review concepts and deposits of the so-called ‘hyperconcentrated flows’ formed in terrestrial settings, and analyse three cases from alluvial and outwash fan settings to establish whether diagnostic characteristics can be detected.

In sediment transport and deposition processes it is well known that a continuum exists between sediment-gravity flows and fluid-gravity flows, affected by matrix strength, dispersive pressure and turbulence (Middleton & Hampton, 1973; Lowe, 1982; Nemec & Steel, 1984). Lately, considerable interest has been shown in sedimentary deposits produced by intermediate flows. This has led to a proliferation of terms, with similar terms used for different processes and deposits, or different terms for the same feature. This has also led sedimentary geologists to the indiscriminate application of few well-described models to many settings. Hydraulic engineers, engineering geologists and fluvial geomorphologists have treated the problem of sediment hyperconcentration in subaerial flows. Several classifications have been proposed, based mainly on the suspended sediment concentration and on rheological properties of flows in open channels (Beverage & Culbertsone, 1964; Bradley & McCutcheon, 1987; Pierson & Costa, 1987; Costa, 1988). As a consequence, a major difficulty exists in comparing different perspectives on the same topic, such as the rock record on one side and the properties of present-day water–sediment flows on the other side.

This paper is based on the premise that the sedimentary characteristics allow identification of the relative importance of the various types of flow and sediment-support mechanism active at the time of deposition. First, a review is made of the various types of flow and of the sediment-support mechanisms. Second, selected examples of deposits formed in different environmental settings (volcanic, alluvial fan and fluvial) are reported from the literature in order to identify diagnostic facies and facies associations. To this purpose, the importance of the recognition of the sedimentation unit (the ‘bed’ of Campbell, 1967) is stressed, which is not always a trivial problem in amalgamated

Flood and Megaflood Processes and Deposits: Recent and Ancient Examples. Edited by I. Peter Martini, Victor R. Baker and Guillermina Garzón ISBN: 978-0-632-06404-5

sequences. Third, descriptive–genetic models are derived from the various examples. Fourth, applicable models are tested in a few new cases, two dealing with alluvial-fan deposits and the other with glaciofluvial deposits.

THE END-MEMBER FLOWS AND RELATED DEPOSITS

The debris-flow and stream-flow end-members

Renewed interest on processes of mass and sudden flow transport events has been prompted by the increasing necessity of evaluating debris-flow and flood hazards in populated areas. The various classifications of subaerial water–sediment flows that have been proposed (see reviews in Bradley & McCutcheon, 1986; Mainali & Rajaratnam, 1991; Coussot & Meunier, 1996) are difficult to compare because of the inherent gradual changes in the physical properties and processes of subaerial flows, and the different diagnostic criteria utilized (Bradley & McCutcheon, 1986; Pierson & Costa, 1987). Thus, although criteria such as triggering mechanisms and rheological–kinematic behaviour of flows have been used, the sediment concentration has been considered the main parameter in most of the classifications proposed by engineers and geomorphologists working on recent settings. On the other hand, geologists (sedimentologists) have subdivided the subaerial flow *continuum* mainly on clast-support mechanisms (Middleton & Hampton, 1973) and rheology of the flows (Lowe, 1982; Nemec & Steel, 1984), because sediment concentration cannot be easily assessed from deposits. Furthermore, as pointed out by Shanmugan (1996), little agreement exists on the sediment concentration at which a sediment-laden water flow becomes a hyperconcentrated flow. Although the distinguishing threshold between them cannot be established uniquely, there is overall agreement among scientists on the existence of the two flow end-members—debris flows (cohesive and non-cohesive) and stream flow (fluid flow)—and an intermediate flow, the hyperconcentrated flow. First we present a selective review of the debris-flow and stream-flow end-members as viewed primarily by sedimentary geologists, and later we analyse the concept of hyperconcentrated flow and show examples of its deposits.

Debris flow

Debris flows have been long known (Blackwelder, 1928) to be an efficient process for sediment transport and deposition in alluvial (Blair & McPherson, 1994) and slope (Blikra & Nemec, 1998) settings. In their classification of sediment gravity flows, Middleton & Hampton (1973) defined the debris flow as a one-phase flow represented by a mixture of sediment particles, clay matrix and water moving along a slope in response to gravity. Sediment particles (from sands to boulders) are sustained in the flow mainly by matrix strength and by buoyancy. The rheology of this flow has been described by the Coulomb viscous model simplified in the following equation (Johnson, 1970):

$$\tau = c + \sigma_n \tan\phi + \eta\varepsilon$$

where τ is the internal shear stress, c is the cohesion, σ_n is the internal normal stress, ϕ is the angle of internal friction, η is the viscosity and finally ε is the rate of shear strain. The $(c + \sigma_n \tan\phi)$ factor is the yield strength, an intrinsic and variable property of the flow given by the combination of cohesion and intergranular friction. The motion is prevented when applied shear stress is lower than the yield strength. The 'debris flows' of Middleton & Hampton (1973) are dominated by the cohesion and density of the clay–water matrix.

Lowe (1982) provided a further contribution to the discussion. He modified the classification of Middleton & Hampton (1973), adding to the sediment-support mechanism a new distinctive criterion: the flow behaviour. Sediment flows can behave as plastic or fluid substances according to their rheology. In Lowe's classification, debris flows are plastic flows that can be subdivided into *cohesive debris flows* (mudflows) if the dominant sustaining mechanisms are the matrix strength and matrix density, or *grain flows* if the sediment particles are supported fully by dispersive pressure. These two types of debris flow differ also in their modes of deposition. Cohesive freezing dominates in the deposition of mudflows and frictional freezing controls the deposition of grain flows. Within the cohesive debris-flow class, Lowe distinguishes subtypes of flow, characterized by the variable degree of sediment support provided by cohesive matrix and turbulence. Clasts in cohesive debris flows can be fully or partially sustained by matrix strength or partly sustained by turbulence.

Nemec & Steel (1984), although in a general agreement with Lowe's classification, modify slightly the terms distinguishing *cohesive debris flows* (mudflows) from *cohesionless debris flows* (grain flows). These terms refer to a rheological view of debris flows, where 'cohesive' refers specifically to the dominant grain-support mechanism provided by matrix strength and density, whereas the term 'cohesionless' refers to a system where the mechanism of dispersive pressure prevails. The rheological difference between the two types is given by the presence or absence of the cohesive-strength component, the factor *c* in the Coulomb viscous model.

Postma (1986) provided a different perspective on the geologically orientated classification of sediment gravity flows. Postma suggests that only the conditions existing at the moment of sedimentation can be inferred from deposits, and that considerations of the flow behaviour and grain-support mechanisms during transport are speculative. Postma distinguishes a cohesive debris flow from a cohesionless debris flow. These are characterized during deposition by high sediment concentration, laminar flow and presence/absence of cohesion. Postma's debris flows differ from those of Lowe (1982) and Nemec & Steel (1984) because the cohesionless debris flows are considered to have formed by deposition from fluid, rather than plastic, bodies.

In the last decades new and significant contributions to the physical understanding of debris-flow processes have been provided, mainly through process-oriented studies by engineers and hydraulic geologists (Chen, 1997; Iverson, 1997). Iverson (1997) attempted to describe the complex behaviour of debris flows, from flow initiation to transport to deposition. His contribution is based on the general assumption that the rheological and hydraulic models (the Bingham viscoplastic and the Bagnold grain-flow models) commonly used to predict the behaviour of a debris flow fail to explain some important observed features related both to the flow and depositional stages. Experiments in large flumes have confirmed the occurrence of many of the features described in natural debris flows (Pierson, 1980, 1981), such as surge flows and the distinction of a slow-moving granular head of the flow from a more watery body and tail zones. A new and significant implication of the experimental studies was the discovery that debris flows are normally unsteady flows in which a strong non-uniform interaction between the fluid and the solid exists. The flow initiation (mainly from rocky, water-saturated masses undergoing landsliding) and the motion are related to fluid pore pressure and to its non-uniform interaction in space and time with the granular temperature; that is, the conversion of flow translational energy into a grain vibration kinetic energy. A major implication of the new view of debris flow for sedimentary geologists is the lateral rheological differentiation of the flow (Iverson, 1997). The 'head' of the flow has the maximum flow depth, a low pore pressure and is characterized by a densely packed granular material forming the typical snout and levees of a debris flow. This feature may be related to a contraction (consolidation) of the material in the head with consequent fluid expulsion toward the 'body' region. So the body and the 'tail' display high pore pressure determining the occurrence of a quasi-liquefied flow. Although this study on debris flow relies mostly on the physics of processes, it has implications for any depositional model inferred by geologists analysing debris-flow deposits. One such analysis is provided by the work of Sohn *et al.* (1999) on the possible depositional transformation of ancient debris flows inferred to have had physical features similar to those predicted by Iverson's model (see below).

Debris-flow deposits. Debris-flow deposits have been reported from alluvial fans and alluvial valleys under every climatic condition (Blackwelder, 1928; Blissenbach, 1954; Bull, 1964; Denny, 1965; Hooke, 1967; Fisher, 1971; Kochel & Johnson, 1984; Wells & Harvey, 1987; Blair & McPherson, 1994). Debris-flow deposits normally have been described as massive, poorly bedded mixtures of unsorted sediments ranging in size from boulders to clays, where larger clasts float in a fine-grained matrix (Fisher, 1971; Middleton & Hampton, 1973). Lowe (1982) described three types of debris flow deposits:

1 ungraded, matrix-supported with clasts fully suspended in the matrix;
2 ungraded, clast-supported;
3 stratified, with a clast-supported lower division overlain by a matrix-supported upper division.

The first type is referred to as a 'true' cohesive debris flow, the second type as a not fully cohesive debris flow where clast interactions play a significant role, and the third type as a density-stratified debris flow. In the latter case, the lower division is deposited from the turbulent cohesive portion of the flow and the upper division by cohesive freezing. This deposit reflects the modification of the flow during the depositional phase when turbulence is damped by flow deceleration and larger clasts are deposited directly from suspension.

Shultz (1984) recognized four distinct lithofacies in the upper Palaeozoic alluvial-fan deposits of the Cutler Formation, Western Colorado: (1) matrix-supported, massive; (2) matrix-supported, inversely to normally graded; (3) clast-supported, inversely graded; (4) clast-supported, massive. These lithofacies are considered to represent flow conditions varying from plastic debris flow dominated by matrix strength (lithofacies 1), to clast-rich debris flow where dispersive stress cooperates with matrix strength to sustain the particles (lithofacies 3), to pseudoplastic debris flow dominated by low strength and turbulent flow (lithofacies 2 and 4), to pseudoplastic debris flow with inertial bedload (lithofacies 3). The variations in flow conditions are related to variable amounts of floodwater mixing with debris flows initiated by slumping.

Stream flow

Stream flows, also named water flows (Bull, 1964), 'normal' stream flows (Pierson & Costa, 1987) and water floods (Costa, 1988), are of Newtonian fluids. Their behaviour is described by the equation:

$$\tau = \mu\varepsilon$$

where τ is the shear stress applied, μ is the dynamic viscosity and ε is the rate of shear strain. As a Newtonian fluid, stream flow has a linear relationship between shear stress and rate of shear strain; that is, a stream flow is characterized by absence of any strength, and the deformation is directly proportional to the shear stress applied. The lack of strength dictates the low sediment concentration (1–40% by weight, Costa, 1988) of stream flows in which sediment and water are two distinct phases. Sediments are transported in fluvial channels mainly as suspended load and bedload. In the latter, sediment particles roll and saltate grain-by-grain along the bed, driven by the shear stress transferred from the fluid to the sediment. Turbulence is the dominant mechanism sustaining the clast in motion and clast interaction on the bed becomes important only when sediment concentration increases. Bedload transport primarily is related to the ratio between inertial and gravitational forces, expressed by the Froude number:

$$F = u/(gd)^{1/2}$$

where u is the flow velocity, g is the gravity force and d is the diameter of sediment particles. Increasing flow velocity causes increase of F with progressive morphological modification of the bed owing to development of different types of bedforms, from dune bed ($F < 1$, subcritical flow) to plane bed ($F \approx 1$) to antidune and standing wave bed ($F > 1$, supercritical flow).

Stream-flow deposits. Fluvial deposits have been long studied and their facies analysis honed over the last few decades (Miall, 1978, 1996; Rust and Koster, 1984; Collinson, 1984; Hickin, 1993). Facies analysis allows, among other things, reconstruction of changes in fluvial style (meandering, braided, low sinuosity and anastomosed) in the stratigraphical record. Stream-flow deposits are, in general, characterized by relatively good sorting, preferred orientation of clasts, and, for sandy materials, cross-bedding and cross-lamination.

Hyperconcentrated flows

In natural conditions, some factors normally disrupt the end-member cases discussed above, making transitional flows (such as hyperconcentrated flows) the norm rather than the exception. As a consequence, the particles in a sediment–water mixture can be kept separated by a combination of dispersal mechanisms and eventually a flow may gradually change into another type. When matrix strength and/or dispersive pressure contribute, to approximately the same extent as fluid turbulence, to the separation of particles, hyperconcentration is achieved.

Most studies on hyperconcentration of subaerial flows are by hydraulic engineers, engineering geologists and fluvial geomorphologists. Sedimentary geologists have paid less attention to subaerial hyperconcentrated flows than to subaqueous hyperconcentration, such as turbidites (Middleton & Hampton, 1973; Walker, 1978; Lowe, 1982; Pickering *et al.*, 1989; Mutti, 1992; Kneller, 1995; Shanmugan, 1996; Mutti *et al.*, 1999).

Hyperconcentrated suspension was proposed originally by Beverage & Culbertsone (1964) for stream flows characterized by sediment concentration between 40 and 80% by weight. Successive classifications considering hyperconcentrated flows were based on their rheological, geomorphological and sedimentological features. *Hyperconcentrated stream flows* (Pierson & Costa, 1987) and *hyperconcentrated flows* (Costa, 1988) are defined as plastic, non-Newtonian flows (yield strength about 100–400 dynes cm^{-2}) that still flow like a fluid, in which solids and water are separate phases (Coussot & Meunier, 1996). Accordingly, buoyancy, dispersive stress and turbulence can variably interact in supporting the clasts in suspension. Hyperconcentrated flow also is used by Chinese authors to mean both Newtonian and non-Newtonian (Bingham) fluids (Qian *et al.*, 1980; Bradley & McCutcheon, 1987) as debris flow also is considered a particular type of hyperconcentrated flow.

In addition to the sediment concentration, particle size and shape, and mineralogy (density) of clasts and matrix, the changes that occur in a water–sediment flow are highly dependent on downcurrent flow transformations. In subaerial settings the following can occur.

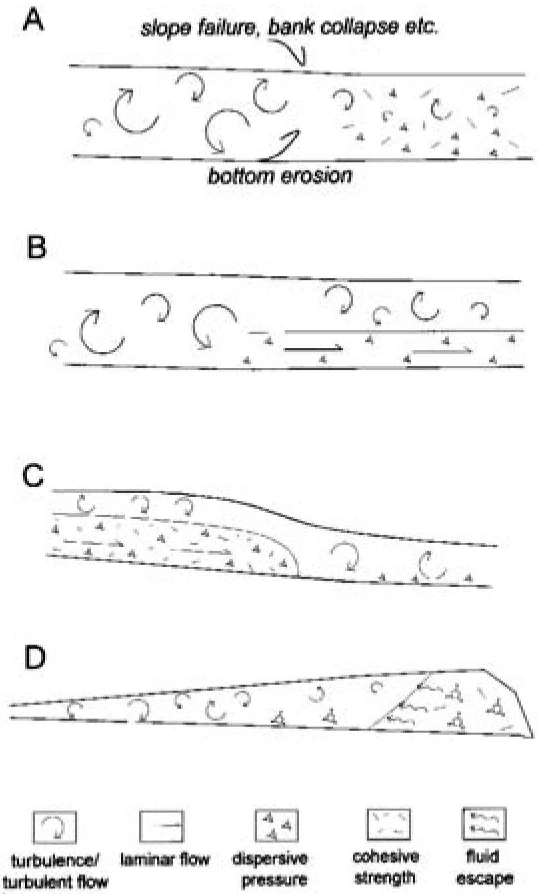

Fig. 1. Diagram illustrating the main flow transformations that characterize the subaerial sediment–water flows spanning the mass-flow–fluidal-flow *continuum*: (A) sediment bulking; (B) gravity transformation (after Fisher, 1983); (C) surface transformation (after Fisher, 1983); (D) fluidization of the body and tail regions of a debris flow owing to fluid migration from an overpressured head region (after the *elutriation transformation* of Fisher, 1983; see also Iverson (1997), Mutti *et al.* (1999) and Sohn *et al.* (1999) for similar transformation hypotheses in, respectively, turbidites, and recent and ancient subaerial debris flows).

1 When a polymodal sediment mixture is added in quantity to a fluid-gravity flow, the turbulence is progressively dampened and the whole flow may be transformed into a 'suspended-load hyperconcentrated flow' and, later, eventually, into a cohesive debris flow (Fig. 1A). In fluvial systems, the sediment addition to turbulent floodwater can be sudden (from slope failure) or gradual (from runoff merging in the main channel) leading to a flow transformation known as sediment bulking (Smith & Lowe, 1991; Meyer & Wells, 1997).

2 When a turbulent fluidal flow expands over a surface, a two-phase flow may develop owing to the large particle-density/fluid-density ratio, whereby a more concentrated, coarser grained bottom flow-layer (bedload) moves more slowly than the upper turbulent flow-layer carrying washload and other suspended load (Fig. 1B). Such a flow transformation is termed a gravity transformation (Fisher, 1983).

The concept of density-stratified turbulent flow is rather old (see review in Sohn, 1997) and it has been popularized by the work of Lowe (1982), who, utilizing Bagnold's theory for transport and deposition of granular dispersions, predicted the depositional behaviour of a dissipating, sediment-laden, turbulent flow termed a high-density turbidity current. In this type of subaqueous flow, the progressive increase in sediment concentration toward the bed generates a hyperconcentrated lower portion (*traction carpet*) dominated by granular interaction, hence dispersive pressure, whereas the upper portion is a low-concentration turbulent dispersion. Deposition from the basal portion is characterized by *en masse* frictional freezing and the development of a diagnostic inverse grading due to (i) the uplifting effect of dispersive and pore pressure on coarser grains and (ii) the downward freezing related to the occurrence of a rigid plug on top of the traction carpet. In this model, the traction carpet is closely related to the turbulent upper portion of the flow because the shear stress exerted by the turbulent portion allows a prolonged and efficient motion of the basal granular portion. The traction carpet concept also has been applied to alluvial deposits characterized by bipartite gravelly sandy beds (Todd, 1989). The gravelly portion records the deposition in a coarse-grained traction carpet; that is, in the basal part of the flow transformed into a bedload hyperconcentrated flow.

The concept of traction carpet being applied to deep-marine sand deposition has some support from experimental results (Postma *et al.*, 1988), but it also has been criticized (Hiscott, 1994; Shanmugan, 1996). A reassessment is provided by Sohn (1997), who is in general agreement with the Lowe model (that is, a traction carpet is related genetically to a dissipating turbulent flow) but discusses an alternative rheological and depositional model. His innovative approach is to assume that the velocity profile in flows with a traction carpet is concave–convex up rather than concave up as in the Lowe model. Accordingly, Sohn's model lacks a rigid plug on top. This has important consequences for the depositional pattern of sediments. In the Sohn model, the traction carpet is characterized by two distinct rheological regions, being therefore a density-stratified flow itself. The lower 'frictional region' and the upper 'collisional region' are characterized by different particle concentrations (more than 80% of the packed bed in the frictional region, 15–80% in the collisional region). There is a different degree of interaction between particles, being least in the 'locked' frictional region, and most in the collisional region. The frictional region is characterized by low strain rate and possibly null dispersive pressure. The collisional region has a high strain rate, a consequence of the high stress exerted by the overlying turbulent flow, and dispersive pressure owing to particle collision. The deposition of the traction carpet reflects: (i) a continuously aggrading bed owing to deposition from the base to the top (opposite to the rigid plug of Lowe), with upward migration of the rheological boundaries in the traction carpet allowing the development of thick traction carpet deposits; and (ii) the rheological difference of the two regions, the thicknesses (a function of grain size, fall-out rate and shear stress) of which influence the type of traction carpet deposit. As a consequence, a great variety of traction carpet deposits can occur, characterized by different bedding and textural features. The inverse grading, often considered a diagnostic feature of a traction carpet, can be present when the collisional region is well developed, but it may be absent when a frictional region dominates. Inverse grading is discussed by Sohn (1997) as a feature possibly produced by concurrent phenomena occurring in the collisional region, such as dispersive pressure generated by grain collision, kinetic sieving and other grain-size filtering mechanisms, and the lifting force exerted by high shear on large clasts in the boundary zone between the collisional region and the overlying turbulent flow.

3 When both cohesive and noncohesive debris flows enter a fluvial channel and undergo dilution ('surface transformation', Fisher, 1983), there is a progressive downcurrent increase in the contribution of turbulence to sustaining the clasts. The initial mass flows can be progressively transformed into hyperconcentrated flows and eventually into fully turbulent flows (Fig. 1C). A further ('gravity') transformation can occur when the progressive sediment load dilution allows the larger clasts to settle to the lower part of the flow, generating a highly concentrated bedload and, eventually, a basal traction carpet (Smith, 1986; Todd, 1989).

A possible further type of flow transformation of subaerial debris flows into hyperconcentrated flows is related to longitudinal (downslope) rheological differentiation existing in the parent flow (Fig. 1D). Significant water escape owing to the excess pore pressure in the densely packed head of the flow, where strong grain interaction determines an overpressurized fluid phase, makes the body and tail region of the flow progressively more fluidal (Iverson, 1997; Sohn *et al.*, 1999). The body region therefore can represent a hyperconcentrated-flow stage in the downslope evolution of the debris flow. Similar transformations in sediment gravity flows (Fisher, 1983) considered to have great significance in turbidites (Mutti *et al.*, 1999) have been grouped under the term *elutriation transformation*.

HYPERCONCENTRATED-FLOW DEPOSITS: CASE HISTORIES FROM THE LITERATURE

Deposits from hyperconcentrated flows have been described from volcanic (Pierson & Scott, 1985; Smith, 1986; Scott, 1988), alluvial-fan (Nemec & Steel, 1984; Blair, 1987; Todd, 1989; Meyer & Wells, 1997) and fluvial (Martin & Turner, 1998) settings, and from glaciofluvial environments (Lawson, 1982; Maizels, 1993; Brennand, 1994; Brennand & Shaw, 1996; Shaw, 1998)—see Table 1.

Volcanic setting

Pierson & Scott (1985) and Scott (1988) analysed the volcaniclastic deposits of the 1980 and 1982 eruptions of Mount St Helens. These catastrophic events caused the generation of large debris flows (*lahars*) through the fluvial valleys below the volcano. Their path and changing flow characteristics were recorded in the deposits along the valleys. The deposits show the following characteristics:

1 proximal (up-valley) massive to slightly inverse- and normal-graded gravelly deposits of lahars (debris-flow deposits);

2 bipartite layers in the middle portion of the valley, characterized by a basal, crudely laminated sandy-pebbly division, and an upper, massive, inverse- to normal-graded gravelly division;

3 distal, crudely laminated sands and fine gravels with internal inverse grading;

4 distal cross-stratified pebbly sands (stream-flow deposits).

Thus, the deposits show a gradational downstream transformation from a debris flow (their deposit 1) to a stream flow (*'lahar-runout' stage*; their deposit 4), through a hyperconcentrated-flow stage (*'transitional* *facies'*; their deposit 3; Pierson & Scott, 1985; Scott, 1988). The common occurrence of inverse grading in the transitional and distal deposits indicates that dispersive pressure is an important grain-support mechanism in this kind of flow.

Smith (1986) utilized Pierson & Scott's (1985) finding that debris flows undergo downcurrent surface transformation by dilution, to interpret Tertiary to Recent volcaniclastic deposits of the western United States. He recognized three main types of deposits showing sedimentological features intermediate between those of debris flows and stream flows:

1 a gravelly, poorly sorted, clast-supported deposit with common normal grading and bimodal clast orientation, with the coarser clasts orientated perpendicular to the flow;

2 a graded, gravelly sandy deposit characterized by a massive to normally graded, basal gravelly division grading up into a horizontally laminated, poorly sorted, sandy division;

3 a sandy deposit characterized by horizontally laminated, poorly to well-sorted sand with weak internal grading.

These deposits can occur as isolated entities or, commonly, in vertical successions with the gravelly or gravelly sandy type at the base, grading up into the sandy type. Smith (1986) grouped these deposits under the general term of *hyperconcentrated flood-flow deposits*. Like the transitional facies of Pierson & Scott (1985), he found that hyperconcentrated flood-flow deposits commonly are overlain by cogenetic debris-flow deposits within the same sedimentation unit. Unlike Pierson & Scott (1985), Smith (1986) interpreted turbulence to be a persistent, major, grain-supporting mechanism. Therefore, Smith's cases represent conditions of greater dilution (greater transformation) or higher water/sediment ratio of the flow than those of Pierson & Scott (Smith & Lowe, 1991).

Other hyperconcentrated-flow deposits have been described in volcaniclastic successions ranging in age

Table 1. Sedimentological features of selected hyperconcentrated-flow deposits from ancient and recent terrestrial settings.

(a) Volcanic setting

Characteristics of the deposits	Ancient: Smith (1986) *Hyperconcentrated flood flow*			Recent: Scott (1988) *Hyperconcentrated stream flow*	
	Gravelly type	Graded type	Sandy type	Transition	Lahar-runout
Lithology*	sg	ps, g/s + g	s		s + pumice
Matrix composition†	vcs, p	?	?		
Grain size†	Polymodal	Polymodal/mcs	mcs		mcs
Sorting‡	Very poor	Very poor/poor			1.1–1.6 ϕ
Orientation:					
a(t)	Boulder	Boulder/			
a(p)	Pebble	Pebble/			
imbrication	Poor	Poor/			
Framework§:					
matrix-supported					
clast-supported	+++	+++/			
openwork					+++
Grading§:					
normal	++	++/		/++	
inverse				/+++	+
ungraded			+++		
Sedimentary structures§:					
low-angle inclined lamination				+++?	
planar/horizontal lamination			/+++	+++	+/
inclined layer					
ripple cross-lamination					
massive		+++/			++
Bedding§:					
horizontal			+++		
lenticular					
bed thickness (m)		1–15	1–30		

(*cont'd on p. 174*)

Table 1. (*cont'd*)

(b) Fluvial and alluvial setting

Characteristics of the deposits	Ancient: Martin & Turner (1998) *Sheet-like, massive-type sandstone*	Ancient: Todd (1989) *Stream-driven high-density traction carpet*	Ancient: Shultz (1984) *Pseudoplastic debris flow* (PPDF)		PPDF *with inertial bedload*	Recent: Meyer & Wells (1997) *Hyperconcentrated flow*		Recent: Blair (1997) *Non-cohesive sediment gravity flow*
			Dmg	Dcm	Dci	Gravelly splay	Sandy splay	Boulder levee
Lithology*	s	sg/s	g	g	g	g	s	g
Matrix composition†		s–p/				s	Muddy s	p, gr, s
Grain size†	fs (ϕmed 2.7–3.15)	p–b/m–vcs	p–c	c–b	B	c–b		Polymodal
Sorting‡		Poor–moderate/				Poor ($\sigma_G = 1.9$–$2.9\ \phi$)	Poor ($\sigma_G \approx 2\ \phi$)	Poor
Orientation§:								
a(t)		++/						Boulder
a(p)		++/						
imbrication								Boulder
Framework§:								
matrix-supported			+++					++
clast-supported		+++/		+++	+++	+++		++
openwork						/+		
Grading§:								
normal		+ (11%)	+++	++		+		++
inverse		++ (17%)	+/		+++			++
ungraded		+++ (82%)		++				
Sedimentary structures§:								
low-angle inclined lamination	+							
planar/horizontal lamination		/++						
inclined layer		/+						
ripple cross-lamination								
massive	+++	++/++					++	
Bedding§:								
horizontal	+++					+++	++?	
lenticular								
bed thickness (m)	< 8	< 0.4/< 0.5	< 1			0.3–1	0.03–0.3	1.5

(*cont'd*)

Table 1. (*cont'd*)
(c) Glacial setting

Characteristics of the deposits	Recent: Lawson (1982) *Flow type III*	Recent: Maizel (1993) *Lithofacies GRm in sequence B3 of volcano-glacial jökulhlaup* hyperconcentrated grain flow	Ancient: Brennand (1994) *Imbricate, polymodal matrix-rich gravel*	Ancient: Brennand & Shaw (1996) *Imbricate, polymodal gravel and sandy in-phase wave structure*
Lithology*	g–s	gr	g	g–s
Matrix composition†			s	
Grain size		D_{50} 0.26–3.1 mm	Maximum clast –6.5 ϕ	
Sorting‡	Mean –2.5 to 2.5 ϕ SD 3.5 to 2 ϕ		Polymodal	Polymodal
Orientation:				
a(t)				48–63% (cobble)
a(p)				34–51% (pebble)
imbrication				
Framework§:				
matrix-supported	++		+++	++
clast-supported	++			
openwork				
Grading§:				
normal			+	+
inverse			+	+
ungraded		+++	++	+
Sedimentary structures§:				
low-angle inclined lamination				+++
planar/horizontal lamination				
inclined layer				
ripple-cross lamination				
massive	+++	+++		
Bedding§:				
horizontal		+++		++
lenticular				++
bed thickness (m)	0.5–3.5	Up to 3–4	> 1.5	

*g = gravel; s = sand; ps = pebbly sand; gr = granulae; the notation '/', such as in g/s, refers to bipartition of beds with g in the lower and s in the upper parts.
†p = pebble; s = sand; gr = granule; b = boulder; c = cobble; p = pebble; fs = fine sand; mcs = medium-coarse sand; vcs = very coarse sand.
‡Sorting can be expressed by qualitative (i.e. 'very poor') and quantitative (i.e. SD: standard deviation, ϕ, σ, σ_G, D_{50}) values.
§+ = occasional feature; ++ = common feature; +++ = very common feature; in some cases quantitative assessment (in %) is provided.

from Mesozoic (Bahk & Chough, 1996) to Tertiary and Quaternary (Waresback & Turberville, 1990; Cole & Ridgway, 1993), but their interpretation of depositional mechanisms does not differ substantially from the models of *hyperconcentrated stream flow* of Pierson & Scott (1985) and *hyperconcentrated flood flow* of Smith (1986). The paper by Nemec & Muszynski (1982) on the interaction between active volcanism and alluvial sedimentation in the Tertiary of Bulgaria is a seminal work on hyperconcentrated-flow deposits. The authors describe both normally graded gravelly units and bipartite gravelly sandy units, interpreted to be deposited from flows transitional between debris flow and stream flow, which in most of their features resemble the different types of hyperconcentrated flood-flow deposits described by Smith (1986). Nemec & Muszynski (1982) link, in a conceptual scheme, these transitional deposits with debris-flow and stream-flow end-members, and suggest that flow transformations, including a transitional stage (hyperconcentrated flow), can occur starting from a debris flow as well as from a stream flow. This paper therefore represents an early contribution toward the conceptual view of the sediment-gravity–fluidal-flow *continuum* in volcano-alluvial settings (Smith & Fritz, 1989; Smith & Lowe, 1991).

Alluvial-fan setting

Hyperconcentrated-flow deposits also have been reported from non-volcanic alluvial settings where there are large amounts of readily available sediment (Ballance, 1984; Nemec and Steel 1984; Shultz, 1984; Wells, 1984; Schmitt & Olson, 1986; Wells & Harvey, 1987; Todd, 1989; Webb *et al*., 1989; Whipple & Dunne, 1992; Brierley *et al*., 1993; Horton & Schmitt, 1996; Melis *et al*., 1997; Meyer & Wells, 1997; Sohn *et al*., 1999). In most cases, hyperconcentration was achieved by addition of sediment (bulking) to the floodwaters from failure of colluvial aprons caused by impact of runoff at the base of cliffs in high elevation catchments (the *firehose effect* of Griffith *et al*., 1996), overland sheet flows, rill erosion and bank failure.

Meyer & Wells (1997) described this process as it occurs on recent alluvial fans laid bare by forest and brush fires in Yellowstone Park. They reported formation of boulder and cobble splays, sandy splays and sandy sheets. Internally, these deposits are poorly sorted, generally with abundant matrix, in some places normally graded, locally massive with crude surface-parallel laminations. The authors interpreted these as hyperconcentrated-flow deposits.

Surface transformation (Shultz, 1984; Melis *et al*., 1997) and gravity transformation (Todd, 1989) have been mentioned as alternative ways of generating hyperconcentrated flows in alluvial settings. Some of the debris-flow (although not so named) deposits analysed by Shultz (1984) show characteristics similar to those of hyperconcentrated flows. An example of this is illustrated by deposits containing much matrix (his subfacies Dmg) with well-developed normal grading shown by concentration of large clasts toward the base. Locally, these deposits also show basal inverse grading, which could indicate the effect of dispersive pressure. The author refers these deposits to 'pseudoplastic' debris flows dominated by low matrix strength and turbulent flow, which are rheologically consistent with the definition of hyperconcentrated flow (Pierson & Costa, 1987; Costa, 1988). If considered in terms of flow transformation, Shultz's (1984) interpretation implies that the flow underwent a surface transformation such that the matrix strength was not the only supporting mechanism for the coarse particles. Shultz reported that in other deposits the coarser grained, clast-supported basal part (his subfacies Dcm) was thick enough to become an entity of a bipartite unit, the upper part of which comprises the normally graded subfacies Dmg.

Todd (1989) suggested that a transitional stage between sediment gravity and fluidal flow conditions could be achieved in the basal part of flood flows through settling (gravity transformation) of suspended material. He described Palaeozoic alluvial deposits of southwest Ireland consisting of gravelly and sandy sheet-like depositional units. These are bipartite with (i) a basal division composed of clast-supported, poorly sorted, sandy gravel, with diagnostic basal inverse grading and *a*(p) *a*(i) fabric; and (ii) an upper division composed primarily of plane- to cross-laminated sand. The author proposed the following interpretation for the depositional processes during a sedimentation event:

1 a confined turbulent flood flow suddenly expands on the alluvial-fan surface giving rise to a bipartite flow;

2 the basal part of the flow moves as a hyperconcentrated bedload or traction carpet where the dispersive pressure is a significant to predominant grain-support mechanism;

3 this mode of transport can be sustained for considerable distances even on gentle slopes, owing to the shear effect and energy transfer exerted by the overriding turbulent flow.

Sohn *et al*. (1999) proposed a new depositional model for the debris-flow–hyperconcentrated-flow transformation from the analysis of Cretaceous alluvial-fan deposits of central Korea. These authors suggest that a debris flow moving downslope precedes a transitional (hyperconcentrated flow) and a fully fluidal flow, and all these generate a graded depositional unit with vertical and lateral transition from debris-flow gravels to bipartite gravelly sandy units marking the hyperconcentrated-flow to stream-flow sandy deposits. The differentiation of the flow in this case is not related to dilution with floodwater but to the longitudinal change in the rheology of the flow. The frontal portion of the flow is a dense slurry with snout and levees that act as a 'dam' confining more dilute portions of the flow behind it. The watery body and tail of the flow is considered to be derived from fluid migration from the head because of frontal consolidation of the flow (Iverson, 1997). In the intermediate part, a density-stratified flow represents the hyperconcentrated-flow phase followed up-flow by a fully fluidal stream-flow phase. Owing to their mobility, the latter flows can bypass the debris-flow front, explaining the vertically and laterally graded depositional units documented by the authors.

A peculiar condition in alluvial settings for the development of sediment–water flows intermediate between mass flow and fluidal flow is represented by catastrophic floods derived from the breaching and collapse of artificial dams (Scott & Gravlee, 1968; Jarret & Costa, 1986; Blair, 1987). A good example, both in terms of hydrological and sedimentological consequences, is the 15 July 1982 dam-break of Lawn Lake in Colorado (Jarret & Costa, 1986; Blair, 1987). The flood wave generated erosion and depositional features. In particular, an alluvial fan developed during the 6-h flood event at the confluence of the Roaring River, subtended by the dammed lake, and the Fall River (Blair, 1987). The fan consisted of three lobes formed at peak discharge (lobe I) and during waning stages of the flood (lobes II and III). The three lobes were deposited primarily by a turbulent sheetflood carrying the gravelly fraction as bedload. In the case of lobe I, the early deposits consist of paired, 1.5 m high and 60–70 m long levees composed of a poorly sorted, matrix- to clast-supported mixture of trees and wood fragments, sand, granule and pebbly to bouldery gravels. The levee deposits were characterized by crude normal and inverse grading with elongated boulders showing well-developed *a*(t) imbrication. The boulder levees, similar to other high-magnitude flood-flow deposits (*boulder berms*, Scott & Gravlee, 1968; *debris torrent*, Carling, 1987), were interpreted to have been deposited by a non-cohesive sediment-gravity flow in which the sediment mixture was dispersed by both turbulence and dispersive pressure. Cohesion was virtually absent owing to the lack of the silty–clayey fraction. Turbulence allowed rolling and imbrication of larger clasts and high dispersive pressure developed through the frequent clast collisions indicated by percussion marks. Deposition occurred because of rapid flow expansion and frictional freezing giving rise to a hyperconcentrated flow at the sedimentation stage.

Fluvial setting

Structureless or poorly organized gravelly and sandy units have commonly been described in braided-river successions (Miall, 1978, 1996; Steel & Thompson, 1983; Todd, 1989; Martin & Turner, 1998). They are variously interpreted as resulting from rapid sedimentation of bedload and suspended load from fluidal flows, or to *en masse* deposition (freezing) of sediment gravity flows.

Steel & Thompson (1983) describing braided river conglomerates of the Triassic ‘Bunter’ Pebble Beds, England, provide an explanation for the recurrent massive gravelly units (the *Gm lithofacies* of Miall, 1978) visible in ancient and recent coarse-grained river deposits. Among horizontally stratified conglomeratic units the authors describe a recurring subtype made of polymodal, disorganized clast- or matrix- (poorly sorted sand-sized) supported conglomerates in centimetre to decimetre thick subhorizontal beds. Other horizontal stratified units alternate with the previous one and show a better textural organization, with bimodal (sandy–gravelly) and openwork levels. Both the disorganized and the organized conglomerates are interpreted by the authors as the product of longitudinal, diagonal or median bar migration in braided rivers. The textural differences are explained in terms of relative position within the bars. The disorganized deposits are interpreted to have been deposited from high water discharge and highly concentrated flows at the head of the bars during high-flow stages, whereas the organized units possibly formed at low-flow stages. We suggest here that the disorganized conglomerates may be reinterpreted as hyperconcentrated-flow deposits derived in large part by a sudden bulk deposition from turbulent flows possibly through a gravity transformation as a result of flow expansion.

Martin & Turner (1998) described the occurrence of massive sandstone layers interbedded with cross-stratified units in braided-river successions of the Late Carboniferous–Triassic of England, eastern USA and Australia. They recognized both channel-like and sheet-like sandstone types. A further subdivision was made depending on whether the contacts between beds were erosive or not, and on the relationship between the local palaeocurrent direction of the sands and the overall palaeoflow direction of the main river channel. Both the channel-like and the sheet-like bodies are characterized by fine to very fine, moderately well-sorted sandstone, locally displaying diffuse laminae, solitary cross-beds, water-escape structures and isolated mud clasts. Channel-like bodies have width/thickness ratios between 12 and 20 and are characterized by palaeocurrents parallel or transverse to the overall palaeoflow of the unit in a ‘non-erosive subtype’, and only transverse in an ‘erosive subtype’. Sheet-like bodies are up to 8 m thick and more than 250 m wide and show palaeocurrents parallel to the overall palaeoflow of the unit in an ‘undulose-base subtype’, and parallel or transverse palaeocurrents in a ‘highly erosive subtype’ (terminology of Martin & Turner, 1998). The sheet-like sandstones are interpreted as deposits of hyperconcentrated stream flows related to high-magnitude floods, and the channel-like sandstone as deposits of mass flows (slide, slump, sandy debris flow) generated by bar or bank collapse.

Glacial setting

Various types of flows and deposits spanning the mass-flow–fluidal-flow *continuum* occur in different glacial environments. Several diamict types, for example, are formed at the terminus of the Matanuska Glacier, Alaska (Lawson, 1982). Four main deposits have been described:

1 lobate bodies, 0.1–2 m thick, made of matrix-supported, polymodal gravels with boulder-size clasts;
2 lobate to channelled bodies, 0.1–1.6 m thick, consisting of graded, clast- to matrix-supported, polymodal gravels;
3 channelled bodies, 0.3–0.6 m thick, made of graded to homogeneous matrix-rich gravels;
4 channelled bodies, 0.02–0.15 m thick, made of ungraded sandy clayey material with few pebbles and granules at the base.

The four deposits record a downslope transition from a fully 'plastic flow' (mass flow) (deposit 1), initiated by slumping of sediments off the ice, to progressively more fluidal flows (deposits 2, 3 and 4) as the water content of the mixture increases. As the flows become more fluid, their erosion power increases, and the textural characteristics of their deposits changes from deposit 2 to 4, with a progressive separation of suspended load from bedload and release of coarse clasts.

The glacial outwash plains of Iceland (sandur) experience both high-frequency floods related to seasonal rainfall and glaciers melting, and occasional catastrophic floods (*jökulhlaup*) produced by rapid ice melting as a result of subglacial volcanic eruptions and sudden draining of ice-dammed lakes. Maizels (1993), among others, described sandur deposits ranging from muds to boulder gravels, characterized by various structures and stacked in characteristic vertical successions. Such successions characterize, on the whole, different sandur types:

1 a sandur not experiencing large floods (non-jökulhlaups sandur);
2 a sandur experiencing large sudden floods from breaching of ice dams of lakes (limno-glacial jökulhlaups sandur);
3 volcano-glacial jökulhlaups sandur directly associated with melting by subglacial eruptions.

In type 1 sandur, horizontally bedded, imbricated gravels and cross-stratified sands alternate with subordinate fines in thin vertically stacked units. In type 2 sandur, the sedimentary succession is composed of massive clast-supported, crudely bedded, coarsening upward gravels up to 7 m thick, overlain by progressively finer grained gravel, and finally capped by horizontally bedded sands. The type 2 sandur shows more variable deposition. A representative succession is up to 10 m thick and is characterized by the following four, stacked lithofacies, from the base upward: (i) coarse-grained, crudely bedded, clast-supported polymodal gravel; (ii) massive, granule gravel with scattered outsized clasts showing at the bottom and top subhorizontal laminations; (iii) trough cross-bedded granule gravel resting erosively on the previous unit; and (iv) horizontally bedded, granule gravel and sand.

Maizels (1993) interpreted the complex facies architecture of the Iceland sandar (singular: sandur) in terms of type, magnitude, duration and frequency of the floods, and transport mechanisms. Accordingly, a type 1 sandur is dominated by high-frequency, low-magnitude, short-duration floods during which coarse clasts and sand are transported prevalently as bedload in fluidal turbulent flows. Less frequent, higher magnitude, longer lasting floods during which the sediments are transported in highly concentrated fluidal flows, both as bedload and in suspension, dominate type 2 sandur. The coarsening upward central facies of the most characteristic sedimentary successions are interpreted to record rising flood stages, whereas the fining upward facies at the top indicates waning flood stages. Finally, the type 3 sandur shows in its variety of lithofacies different flow types, ranging from debris flow to hyperconcentrated flow, in which, owing to the granular nature of the material, dispersive pressure dominates ('hyperconcentrated grain flows' of Maizels, 1993), to fluidal flow. The volcano-glacial jökulhlaups of type 3 sandur are low-frequency, high-magnitude floods with a brief peak stage, normally combining a pulsating water discharge with a large amount of volcanic sediment. The characteristic four-unit lithofacies succession that is formed is interpreted to record a volcano-glacial jökulhlaup during which the main flood flow became hyperconcentrated, depositing massive granule gravel.

Structureless gravelly and sandy units also have been described in subglacial deposits of Late Wisconsinan eskers of Southern Ontario, Canada (Saunderson, 1977; Brennand, 1994; Brennand & Shaw, 1996; Shaw, 1998). Saunderson (1977) described massive, poorly sorted, polymodal matrix-supported gravels with poorly developed orientation and with matrix consisting of fine pebbles and granules. By analogy with flows in pipelines, Saunderson (1977) considered such deposits formed from a *sliding bed*, defined as a highly concentrated particle–fluid mixture moving *en masse* under supercritical regime within a full pipe. In such a situation, the sliding of the highly concentrated, lower portion of the flow is caused by the overall pressure gradient in the system and the shear stress generated by the faster moving overlying flow.

Brennand (1994) and Brennand & Shaw (1996) have described poorly sorted gravels in eskers in Ontario and Quebec, Canada.

1 One succession consists of boulder to pebble gravels that show well-developed imbrication, are polymodal and matrix-rich, with the matrix composed of a poorly sorted mixture of small pebbles, granules and sand. The gravels occur as tabular to lenticular units grading into other subhorizontal gravels characterized by similar textural features but with less abundant matrix (*heterogeneous unstratified gravels* and *massive imbricate, clast-supported gravels*, Brennand, 1994).

2 A second succession has gravels texturally similar to the previous one but has more pronounced lenticular bedding and is arranged in wavy bedforms. This gravel type is often associated with well-sorted, graded, coarse- to medium-grained sand with low-angle swaley cross-lamination.

The gradation observed among the first hyperconcentrated-flow gravelly deposit and gravelly units with less matrix ('heterogeneous unstratified gravels' and 'massive imbricate, clast-supported gravels') is interpreted by Brennand (1994) to indicate a transition between hyperconcentrated flows and fully turbulent fluidal flows. Brennand & Shaw (1996) considered the second wavy gravelly sandy deposit to be derived from hyperconcentrated flows (*sensu* Smith, 1986; Costa, 1988), where deposition occurred from traction load plus fallout. Gravelly sandy in-phase wave structures were formed by a high rate of sedimentation from fluid flow moving under critical to supercritical flow regime. Similar structures have been reported to form both during river floods and sediment gravity flows such as turbidity currents and volcaniclastic surge flows (Shaw, 1998).

Hyperconcentrated flows as geohazard

Hyperconcentrated flows present major environmental hazards in certain regions, such as areas of continental volcanism, and have been analysed extensively by geoscientists (Chen, 1997). Their high velocities, long run-out distances, and high sediment concentration make these flows highly destructive. Several recent cases attest to this, such as the catastrophic floods in the Mediterranean basin (Poesen & Hooke, 1997; Benito *et al*., 1998), recurrent landslides and floods in the western USA, or those triggered by extreme events such as Hurricane Mitch in Central America (Sheridan *et al*., 1999). In the Mediterranean area, the Sarno case in Campania and the Versilia case in Tuscany (Italy) demonstrate such a hazard.

1 The Sarno area is located near Naples in a mountainous region affected throughout the Quaternary up to historical times by the explosive activity of Vesuvius (Eventi idrogeologici in Campania; web page HTTP://www.protezionecivile.it/). The slopes had been tampered with, being laid barren by forest fires and indiscriminate human clearing of vegetation, and many isolated houses and some villages were built in hazardous areas. A strong rainfall on 4 and 5 May 1998 (up to 100 mm in 48 h), preceded by intense precipitation in April, which saturated the soils of this area, caused a flood wave in the catchments, triggering widespread shallow landslides (up to 150 in a few hours) of the thin (few metres thick) Quaternary pyroclastic cover mantling Mesozoic limestones. The landslides rapidly transformed downslope into cohesive debris flows. These underwent further transformation in the main river channels, being progressively diluted into fast-moving hyperconcentrated flows, which destroyed several villages in the Sarno River alluvial plain causing 160 casualties and damages of about 16.5 billion Italian lira (Fig. 2).

2 The 16 June 1996 catastrophic Versilia flood (northern Tuscany, Italy; Rosso & Serva, 1998) was triggered by torrential rainfall (up to 475 mm in about 12 h). Floodwaters in the drainage system were rapidly bulked with large amounts of debris supplied by widespread soil slips and shallow landslides. Although some landslides possibly were transformed into cohesive debris flows and eventually diluted into hyperconcentrated flows in the river channel, much of the sediment bulked a turbulent flood flow. The deposits at a major enlargement of the valley record the pulsating flood flow, characterized at the depositional stage by high clast interactions responsible for dispersive pressure producing inverse grading (Fig. 3). A possible alternatative interpretation of the inversely graded units is that they record the rising stage of several surges during the flood event. In either case, the consequence of this event was the almost complete destruction of a village and some casualties.

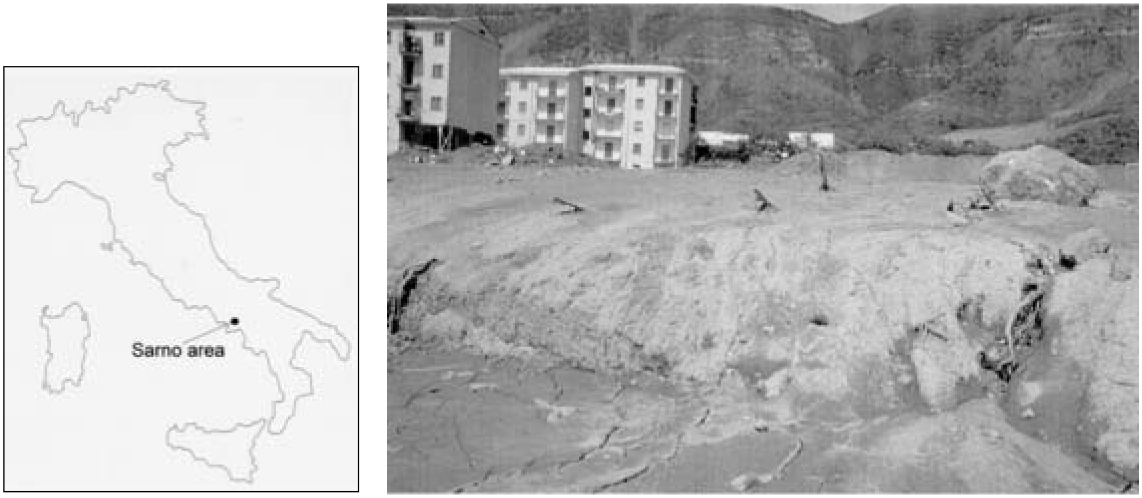

Fig. 2. Photograph showing the effect of the catastrophic flood in the Sarno area, southern Italy: the mudflow/hyperconcentrated-flow deposits buried an urbanized area close to the hill slopes (in the background) from which several shallow landslides were generated during the 5 May 1998 high rainfall event. (Photograph by A. Jolti.)

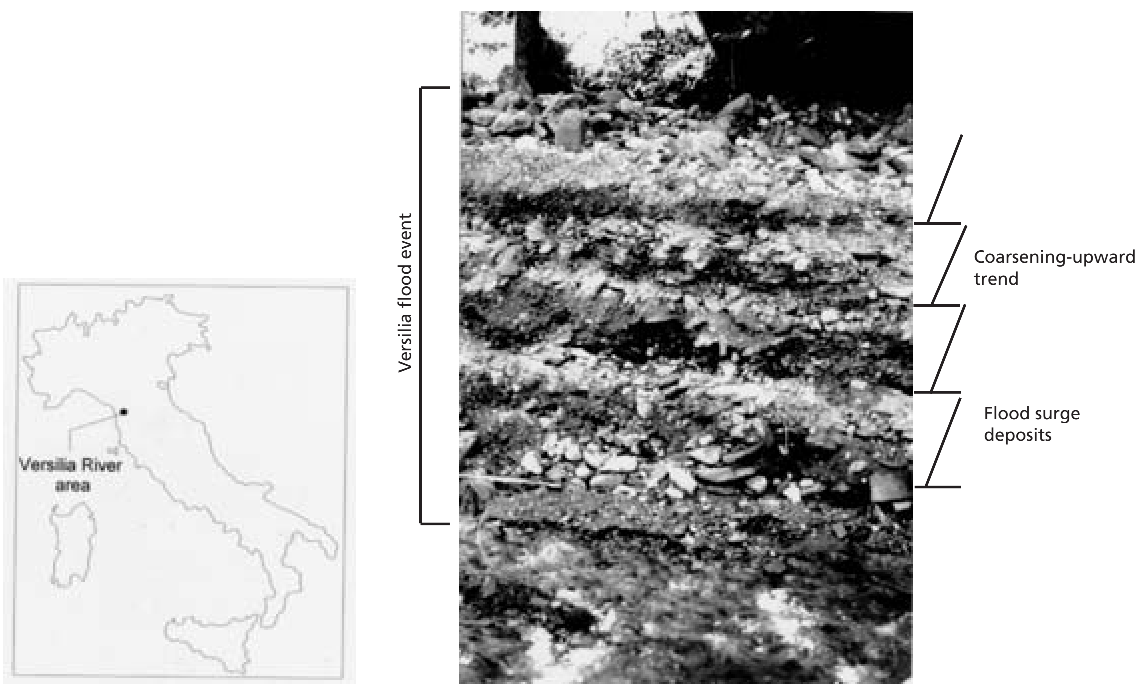

Fig. 3. Photograph showing clast-supported, imbricated gravels with poorly sorted matrix arranged in five subhorizontal layers, each showing inverse grading, deposited during the Versilia (north-western Tuscany, Italy) flood event in a major valley enlargement. The outcrop is about 1 m high. (Photograph by U. Tarchiani.)

HYPERCONCENTRATED-FLOW DEPOSITS: NEW CASES SHOWING LINGERING DIFFICULTY IN THEIR RECOGNITION

Deposits of Pliocene–Pleistocene alluvial fans from a tectonically active area and of glacial outwash from a cratonic location have been analysed specifically to establish whether:

1 gravelly and sandy deposits showing features intermediate between mass-flow and fluidal-flow deposits could be considered the product of hyperconcentrated flows;

2 the depositional setting influences the type of hyperconcentrated flows;

3 some general criteria can be extracted from facies analysis in order to distinguish different types of hyperconcentrated-flow deposits.

Alluvial fan deposits of the Neogene–Quaternary basins of the Northern Apennines (Italy)

In Tuscany (Italy), the Northern Apennines are characterized by a series of NW–SE elongated half-grabens (20–40 km long and 10–15 km wide; Fig. 4a), which have developed over pre-existing thrust-imbricated zones of the chain (Sestini, 1970; Martini & Sagri, 1993). These basins contain fluvial, lacustrine (such as the Mugello Basin; Benvenuti, 1997) and/or shallow marine (such as the Elsa Basin; Dominici *et al*., 1995) clay and sand at the centre (500–2000 m thick) and well-developed, generally coarse-grained alluvial fans on their steep, high flanks with coarse clasts derived from not-too-distant weathering bedrock. During the Quaternary, these basins experienced dry and wet conditions, in part associated with glacial and interglacial periods. As at Present, the rainfall distribution within the narrow, deep basins may have been influenced by orographic effects.

The Mugello Basin upper fan-delta deposits

Description. The Mugello is an intermontane basin filled with more than 500 m of upper Pliocene to Quaternary fluviolacustrine and fluvial terrace deposits (Fig. 4b & c). The fluviolacustrine sediments record the development of two fan deltas (upper and lower fan deltas, UFD and LFD) in response to the syndepositional uplift of the north-east shoulder of the basin. Major uplift stages are recorded by angular unconformities, one of which separates the gravels and sands of LFD from those of UFD (Benvenuti, 1997). Possible hyperconcentrated-flow deposits occur in the UFD (Fig. 4d). Typical occurrences are characterized primarily by clast-supported, imbricated, cobbly to pebbly gravels (facies 1), or sandy–gravelly, ungraded foresets (facies 2) (Figs 4d & 5).

Facies 1 is composed of clast-supported, boulder to pebble gravels with interstices filled with sandy–silty matrix. The clasts are subangular to well rounded and show poorly to moderately well-developed imbrication. Boulders generally are orientated transverse to the palaeoflow direction [a(t) a(i)] as indicated by the overall exposed geometry of the alluvial fans, and cobbles and pebbles lie parallel to the palaeoflow [a(p) a(i)]. This deposit consists of ungraded to crudely normally graded beds up to 5 m thick with erosional bounding surfaces.

Facies 2 generally is composed of cobbly pebbly gravels in downflow inclined planar layers 10–50 cm thick, resting on gravels of facies 1. Internally, each inclined layer has texture similar to facies 1; that is, the inclined layers are apparently massive, clast-supported with sandy–silty matrix. Clasts show no or weakly developed a(p) orientation. Similarly stratified deposits also are common in middle Pliocene fluvial sediments of the Elsa Basin (Fig. 6).

Facies 1 and 2 generally are amalgamated in thick (tens of metres) bodies in proximal alluvial fan areas, or capped by pedogenically modified massive to locally thinly laminated, fossiliferous (land molluscs and plant remains), greyish clayey silts, in distal areas.

Interpretation. Sediments of facies 1 are interpreted to have been deposited within channels from a flood flow carrying a high sediment bedload and suspended load, sufficient for the particles to interact with each other and develop an a(p) orientation. Sedimentation by massive freezing of the load is inferred by both the preservation of the a(p) fabric and the abundant, poorly sorted matrix present in the gravels. The matrixrich inclined beds of facies 2 indicate poor downcurrent segregation of sediment particles during transport and massive deposition in alluvial lobes formed by flow expansion at the mouth of the channels filled up-flow by facies 1.

Flood-generated coarse-grained bars similar to those of the Mugello and Elsa basins have been reported from several geological settings and interpreted as typical of catastrophic flood-dominated river systems (Mutti *et al*., 1996). Such bars (also termed 'flood-generated sigmoidal bars', Mutti *et al*., 1996) are characterized by concave up, lensoid sedimentary bodies 0.5–2 m high and 5–10 m long, laterally (downcurrent) and vertically graded, from coarse gravels to

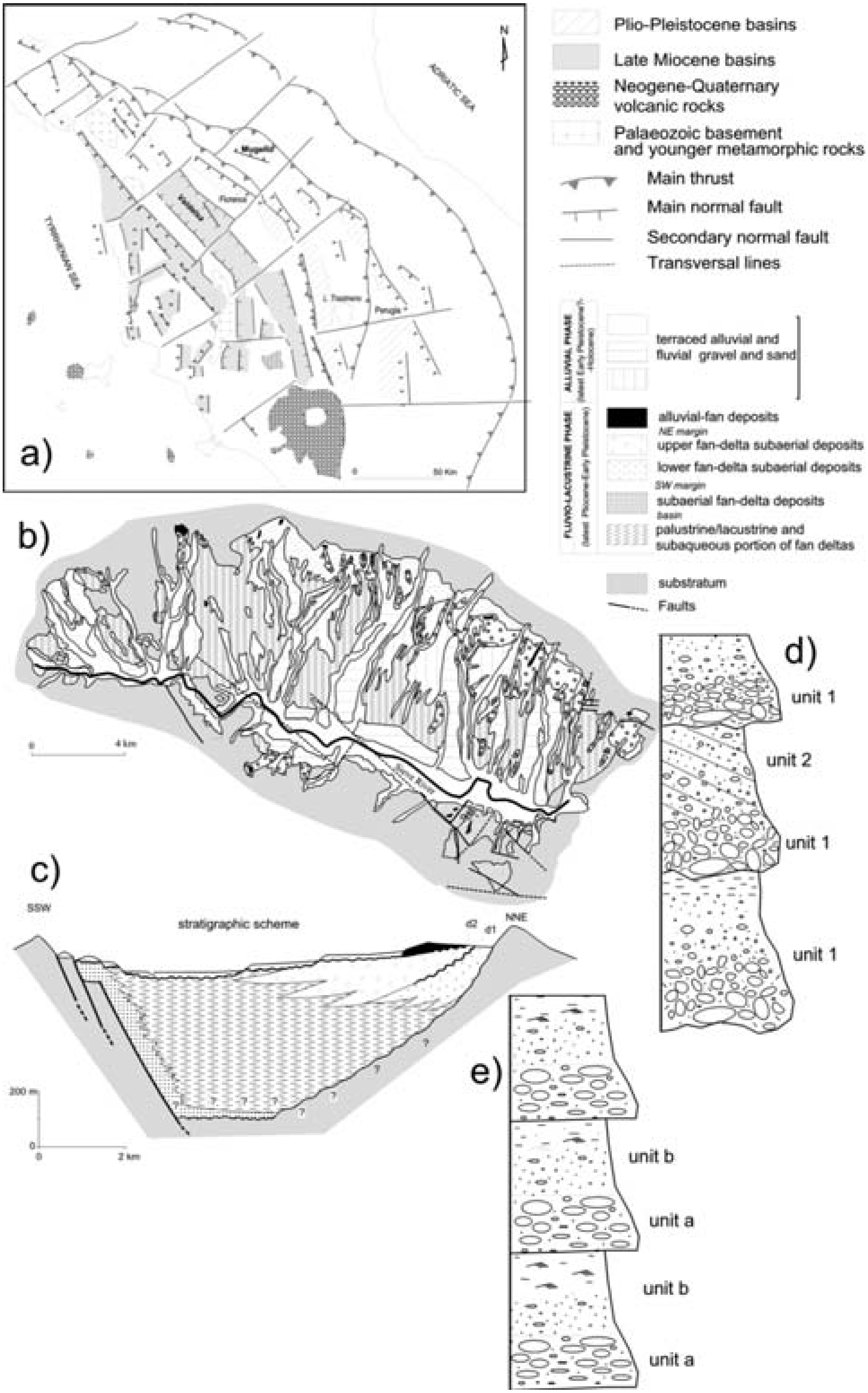
a)
N
ADRIATIC SEA
TYRRHENIAN SEA
Florence
Perugia
50 Km
Plio-Pleistocene basins
Late Miocene basins
Neogene-Quaternary volcanic rocks
Palaeozoic basement and younger metamorphic rocks
Main thrust
Main normal fault
Secondary normal fault
Transversal lines
ALLUVIAL PHASE
FLUVIO-LACUSTRINE PHASE
terraced alluvial and fluvial gravel and sand
alluvial-fan deposits
NE margin
upper fan-delta subaerial deposits
lower fan-delta subaerial deposits
SW margin
subaerial fan-delta deposits
basin
palustrine/lacustrine and subaqueous portion of fan deltas
substratum
Faults
b)
4 km
c)
SSW
stratigraphic scheme
NNE
d2
d1
200 m
0
2 km
d)
unit 1
unit 2
unit 1
unit 1
e)
unit b
unit a
unit b
unit a

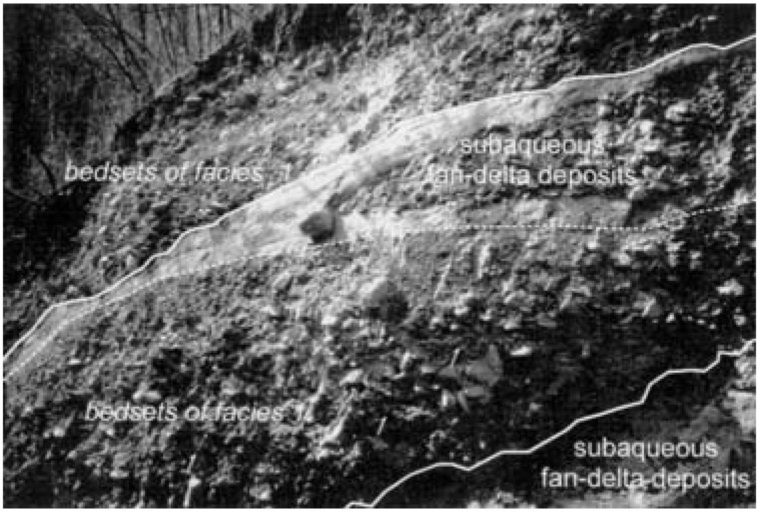

Fig. 5. Photograph showing bedsets of facies 1 encased within subaqueous fan-delta deposits in the Mugello Basin: the half-arrows indicate fining upward trends inside the basal channel-fill. The outcrop is about 5 m high.

Fig. 6. Panoramic photographic view of the stratigraphical relationships between facies 1 and facies 2 in middle Pliocene fluvial deposits of the Elsa Basin: note the lateral transition between horizontal bedded facies 1 gravels and inclined gravels and sands of facies 2. Floodplain muds cap these deposits. The outcrop is 3 m high.

silt and mud, and internally displaying different bedding and sedimentary structures. At least six main facies have been described by Mutti *et al.* (1996) for the ideal complete bar development. Facies 1 and 2 are coarse grained, varying from coarse-grained conglomerate to coarse sandstone, and are clast-supported massive (facies 1) or have high- to low-angle cross-stratification (facies 2). Facies 3–5 are composed of coarse to fine sandstone, crudely graded and unstratified (facies 3), wavy to horizontally stratified (facies 4) or cross-laminated (facies 5), interpreted to result from down-flow migration of hummocky bedforms. Fine-grained sediments (mudstone, facies 6) drape the previous deposits. These deposits are interpreted to be associated with frictional freezing of a hyperconcentrated flow forced by a hydraulic jump (flow expansion), giving rise to facies 1, followed by traction plus fallout of the pebbly sandy populations in the flow generating facies 3–5, and finally facies 6 marks the settlement of fines at the end of the flood. Variations occur in the bars, some lacking the finer facies owing to a more effective fine sediment bypass. The flood bars observed in the UFD deposits of the Mugello Basin, as well as in other basins of Tuscany (such as the Elsa Basin), fit the general depositional model of Mutti

Fig. 4. (*opposite*) Maps and vertical sections of Neogene–Quaternary basins of Tuscany, Northern Apennines, Italy: (a) Map of the post-collisional basins; (b) schematic geological map of the Mugello Basin; (c) stratigraphical scheme of the Mugello Basin fill; (d) schematic log of characteristic deposits of the upper fan (UFD) of the Mugello Basin; (e) schematic log of characteristic deposits of the lower fan (LFD) of the Mugello Basin.

Fig. 7. Photograph of typical facies of the LFD deposits of the Mugello Basin: note the slightly erosive boundary between facies a and the underlying facies b in the lower part of the picture.

et al. (1996). They lack, however, the wavy stratified downcurrent portions of the complete bars (that is, facies 4 and 5) of Mutti *et al.* (1996), so they may record floods having high flow momentum causing an efficient sediment bypass.

On the whole the features of the UFD deposits record both bedload and suspended-load sediment hyperconcentration during floods. The high sediment concentrations were probably caused by sediment bulking during transport and, for facies 2 at least, by rapid reduction of capacity as a result of flow expansion.

The Mugello Basin lower fan-delta deposits

Description. A different deposit possibly produced by hyperconcentrated flows occurs in the LFD of

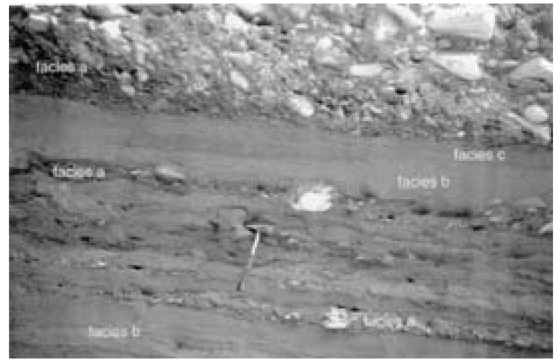

Fig. 8. Detailed view of facies a and its relationship with other facies. Note basal inverse grading of the topmost gravelly deposits.

the Mugello Basin and rarely in other basins of the Northern Apennines (Fig. 4b & c). This layered deposit is characterized by the following gradationally superimposed facies (Figs 4e & 7).

1 A lower facies (a) of clast-supported gravel, up to 2 m thick. The gravel consists of moderately to well-sorted cobbles and pebbles with interstitial sandy–silty matrix. Locally it shows basal inverse grading a few centimetres thick (Fig. 8) and generally good clast *a*(p) imbrication.

2 An intermediate, 1–4 m thick facies (b) of sand, medium grained with disseminated, floating pebbles, generally laminated.

3 A top facies (c) of cross-laminated medium- to fine-grained sand, 0.2–1 m thick.

On the whole, the layers (facies) are bounded by low-angle erosion surfaces and have internal horizontal, apparently continuous, sheet-like laminations.

Interpretation. Applying the Todd (1989) model, these deposits can be interpreted to record deposition from (a) hyperconcentrated flow at the base (facies a), where inverse grading has developed and, thus, dispersive pressure was an important mechanism for sustaining clasts; (b) fluidal, possibly supercritical flow in the middle (facies b); and (c) diluted subcritical conditions at the top (facies c). If the Sohn (1997) concept of traction carpet as a progressively aggrading lower portion of a dissipating density-stratified turbulent flow is applied instead, then the graded units of the LFD succession can be interpreted differently. In this case the inversely graded to massive facies (a) could represent the deposition of a thin traction carpet continuously fed with sediment from above (see fig. 4B in Sohn, 1997). In the Sohn model, in fact, the thickness of the traction carpet deposit does not express the original thickness of the traction carpet region in the flow; the development of thick traction carpet deposits results from a continuous aggradation and consequent upward migration of the rheological interface between the traction carpet and the dilute flow, if enough sediment is supplied from the overlying turbulent portion of the flow. Facies b and facies c record the 'normal' traction developed when the downward flux of sediment is diminished and the traction carpet is coming to an end.

Upper Pleistocene Guelph outwash

Modern and ancient glacial outwash deposits have been described from every continent. They are characterized by rapid variations in textures and structures reflecting the strongly variable water and sediment discharges they experienced, associated with ice melting and rainstorms. Because much sediment of great variety of sizes is readily available, a variety of sediment-transport mechanisms operate, ranging from debris flows to fully developed turbulent fluid flows, and thus hyperconcentrated flows are to be expected as well. The deposits of hyperconcentrated flows, however, are not readily recognized because robust diagnostic criteria have not yet been established. The definition of these criteria in such an environment would help in understanding other similarly variable settings of tectonically active areas or areas experiencing strong climatic variations and ephemeral floods.

The Guelph outwash is located west of Toronto in southwestern Ontario, Canada, on a cratonic area stable since the late Palaeozoic (Fig. 9a). During the last deglaciation (about 14–12 ka), extensive outwash deposits formed in front of various ice lobes retreating from the land into the Great Lakes basins (Karrow, 1989). The deposits are well, albeit temporarily, exposed in numerous sand and gravel pits. Their sedimentary architecture is dominated by the alternation of gravelly and sandy lithofacies (Fig. 9b).

Description. The Guelph outwash deposits, such as those exposed in the Erin pit (Fig. 9), are composed primarily of gravel, sand and minor silt. They lack clay. They are characterized mostly by three major facies (Fig. 9c).

1 Facies 1 has clast-supported, bouldery to pebbly, imbricated (both *a*(p) and *a*(t)) gravel with a poorly sorted, sandy matrix (Fig. 10). It occurs in sub-horizontal, ungraded to crudely vertically graded, ill-defined beds 0.1–0.5 m thick, amalgamated in bedsets up to 5 m thick. Internally, individual gravel beds show (i) a few-clasts-thick basal layer in which interstitial matrix can contain some silt, (ii) few-centimetres-thick basal lenses with inverse grading, and (iii) pebble clusters, few clasts thick, generally dispersed in the bed.

2 Facies 2 is characterized by graded pebble gravels occurring in foresetted units 20 cm to 1 m high (Fig. 11). The foresets show quasi-regular reoccurrence of three layers: (i) gravel with polymodal distribution of pebbles, granules and poorly sorted sand; overlain by (ii) sandy gravel to gravelly sand showing marked bimodality, one mode representing fairly well-sorted pebble to cobble size clasts, and the other medium to coarse sand; overlain by (iii) openwork pebble to fine cobble gravel. Facies 1 and 2 commonly are stacked in vertical sequences bounded by erosional surfaces; in a few places it is possible to observe the former grading downflow into the latter facies.

3 Facies 3 is represented by cross-bedded to plane bedded, fairly well-sorted medium to coarse sand, which most commonly is found in erosional lenses 0.5–2 m thick within gravels of facies 1, or, in places, as more continuous beds separating the gravelly deposits into two or three bedsets.

Interpretation. During deposition of facies 1 various mechanisms may have been active, ranging from local matrix support exerted by temporary slightly higher concentration of fines, to dispersive pressure responsible for the formation of the inverted graded lenses, to contemporaneous mass freezing of mixtures of large clasts and poorly sorted matrix. These alternated irregularly with partial reworking of the upper part of the deposits by fluidal flows, and particle-by-particle deposition from a turbulent flow with development of imbricated pebble clusters and *a*(t) fabrics. Hyperconcentration probably was achieved in this case at the depositional stage through a granular freezing of the poorly sorted bedload carpet. The cross-stratified facies 2 records progradation of macroforms into pools. The internal rhythmic foreset deposition has been described and discussed for some time (Smith, 1972, 1974; Eynon & Walker, 1974; Steel & Thompson, 1983; Rust, 1984; Anketell & Rust, 1990; Shaw & Gorrel, 1990). The formation of the three, or in many cases two, layers (the openwork layer is not present in some cases) is a complex phenomenon related to a combination of various processes and events as follows.

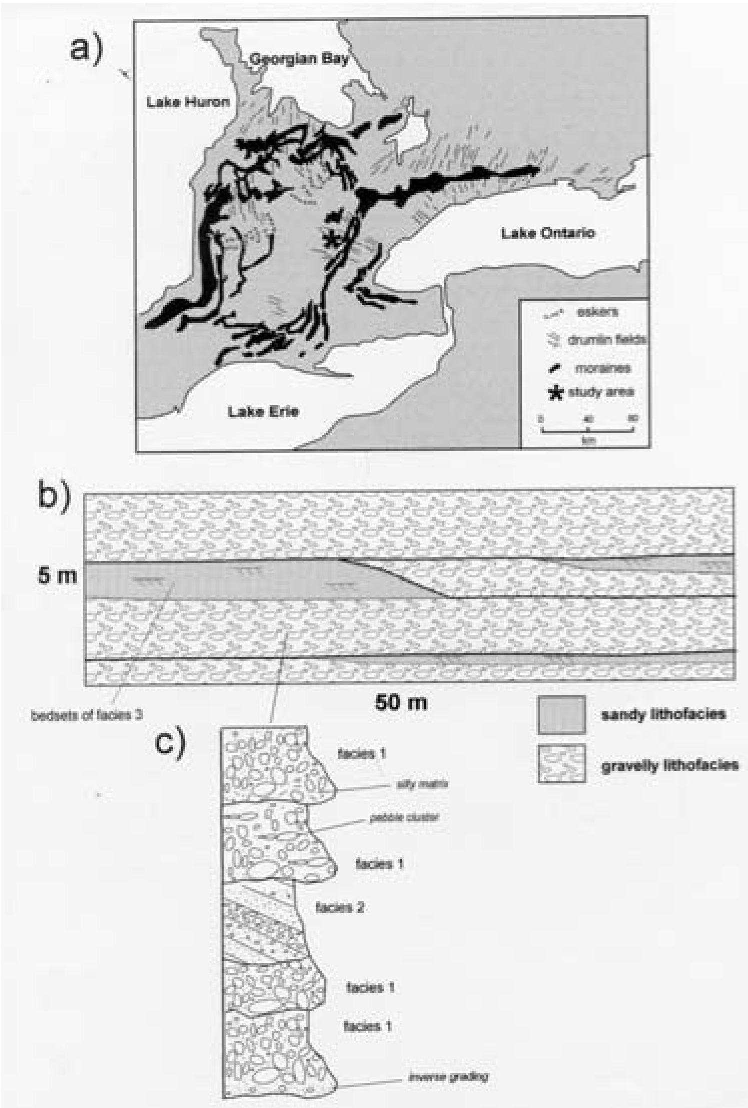

Fig. 9. Maps and stratigraphical diagrams of south-western Ontario, Canada: (a) map showing the main glacigenic features (after Karrow, 1989); (b) sketch of outwash gravels and sands exposed in the Erin Pit, in the Guelph outwash(*); (c) schematic log of the deposits characterizing the gravelly lithofacies in the Erin Pit.

1 Gravity flows (local debris flows along foresets) with perhaps some turbulent-flow drag prevailing during the formation of the polymodal, large clast-matrix mixture of some foresets. This mixture records the continuous input of unsorted material moved along the streambed as a hyperconcentrated traction carpet and injected *en masse* on to the inclined foresets.

2 The openwork layers may be related to differential sorting of particles on the stream bottom with the pulsed arrival of different particle populations at the brink of the sloping bedform. The material is then moved and deposited along the slope by gravity (grain flows), forming open framework gravel lenses, commonly with the coarser clasts closer to the toes of the slope.

3 The bimodal deposit layers probably are formed by settling of suspended sand into part of the coarse foreset-toe openwork gravel deposits and/or by larger particles rolling on to sandy beds in the low-pressure flow separation bubble downstream from the bedform. Essentially these foresets record the effect of two quite distinct processes, grain flows and turbulent flows.

Whereas facies 1 may represent processes occurring during peak flows, perhaps associated with meltwater

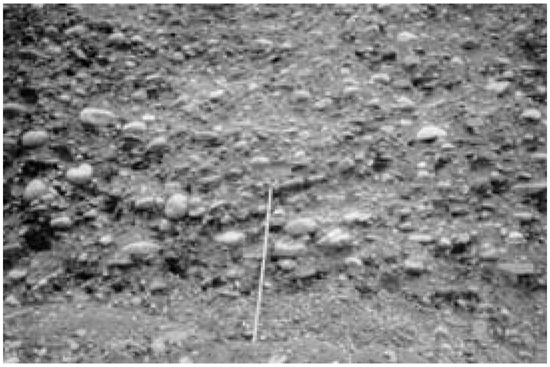

Fig. 10. Photograph showing the typical feature of facies 1 in the Erin Pit. Note the well-developed imbrication of cobbles and pebbles. The rod is 1 m long.

outbursts, the cross-stratified facies 2 represents waning flow stages with variable transport and deposition modes; finally, the well-structured sands of facies 3 record lower turbulent flood stages or flows marginal to the main channels.

DISCUSSION

It is the contention of this paper that in certain terrestrial environments variation in sediment–water flows is the norm, and steady state conditions in water discharge, sediment transport and deposition are not achieved or are short lived. Where much sediment is available, hyperconcentration can be achieved throughout the flow when a high proportion of fine particles is present, or at the bottom of the flow when coarse particles prevail. Variation in sediment input or in flow conditions, in part associated with the morphology of the flow pathway, may lead to local hyperconcentration and sedimentation. Hyperconcentration commonly develops in volcanic and tectonically or climatically variable settings, such as alluvial fans, glacial environments or any location where sudden movement of large masses of water and materials is triggered. Whereas the various modes of hyperconcentration may occur everywhere, some are favoured by certain conditions.

Volcanic settings are prone to low-frequency, high-magnitude mass movements of large amounts of sediment derived directly from the eruption or reworked from the volcanic slopes, and moved into the fluvial drainage system downvalley. So, in many recent (Scott, 1988) and ancient (Smith, 1986) volcanic systems the dominant mode of hyperconcentration is by surface transformation of debris flows, although sediment bulking may occur as well. The recent case of Sarno, southern Italy, demonstrates that what is typical of volcanic terrains also can occur in alluvial settings not directly affected by active volcanic eruptions (Smith, 1986).

Non-volcanic, alluvial-fan settings, especially in the temperate mid-latitude areas, are characterized by variable magnitude floods and local slumping resulting from cloudbursts or other discontinuous high-magnitude meteoric events (seasonal, annual). Sediment production may be high owing to tectonic rejuvenation of the slopes and intense weathering. Although some local large landslides can occur that can be transformed into debris flows and hyperconcentrated flows, the most common mode of achieving hyperconcentration is through areally widespread sediment bulking of floodwaters, with sediments derived from numerous but relatively small landslides, overland and rill erosion, and bank slumping along the main streams. A

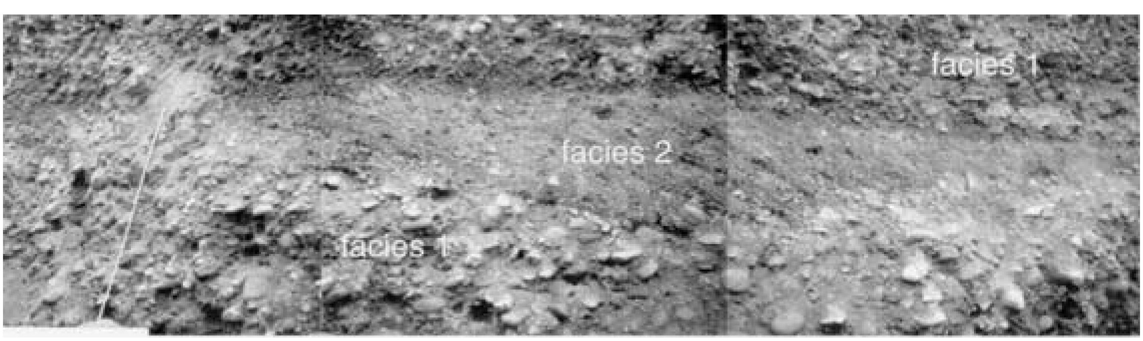

Fig. 11. Photographs showing cross-stratified and graded gravelly deposits of facies 2 resting erosively on facies 1, in the Erin Pit. The rod is 1 m long.

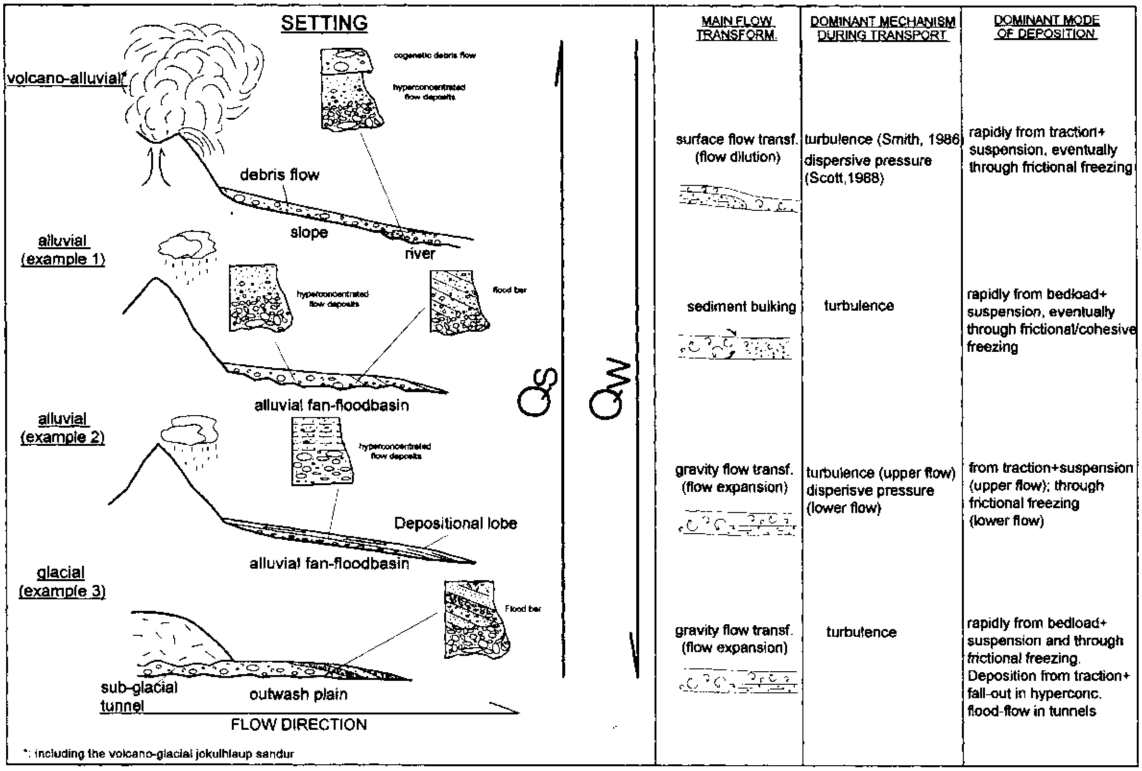

Fig. 12. Synoptic diagram showing the more common conditions for the development of hyperconcentrated flows in continental settings.

recent example in the Mediterranean area is provided by the Versilia flood, illustrating the importance of rainfall in triggering major floods at mid-latitudes. High-magnitude, flood-triggering storms occur mostly in the tropics and are related to monsoon circulation and, at higher latitude, to frontal circulation (Hayden, 1988). Mid-latitude zones, such as the Mediterranean area, are seasonally affected by both storm types, and hence they are prone to floods. Furthermore, when this climatic factor is acting on a tectonically active landscape, where fans are crossed by steep and narrow channels, erosion and transport of large quantities of sediment occur and hyperconcentration of flows is common if not the norm.

The glacial systems are regulated by seasonal large volumes of meltwater, generating floods of various dimensions, including occasional megafloods as a result of outburst of ice- or moraine-dammed lakes or owing to subglacial volcanic eruptions (Bretz, 1969; Baker, 1973; Rudoy & Baker, 1994; Guðmundsson *et al.*, 1997). Recent temperate glaciers of Alaska and parts of Greenland may be used as a partial analogue for ancient Pleistocene glacial settings. The Icelandic jokulhlaup-dominated sandar can be considered good analogues for Pleistocene outwash processes, although their floods most commonly are triggered by subglacial volcanism and carry volcanic debris having low density (pumice). The meltwater floods become laden with much sediment, repeatedly achieving hyperconcentration throughout the flow within and at the mouth of subglacial tunnels and in various parts of the outwash plain. During large floods, hyperconcentration probably is achieved in the lower part of the flood mostly everywhere during the main depositional stage in the outwash; that is, many sediments are not deposited particle by particle, but they are in part released *en masse*, with partial penecontemporaneous reworking owing to fluctuations in flow and sediment load.

This study has produced two major results.

1 A first result indicates that hyperconcentration can be achieved in different ways in different settings (Fig. 12). Hyperconcentrated flows broadly can be expressed in terms of the relationship of sediment discharge (Q_s) and water discharge (Q_w).

(a) When $Q_s > Q_w$, hyperconcentrated flows can develop from surface transformation of mass flows

and this is the dominant mode in volcano-glacial settings, being possible also in alluvial (the Sarno case; Shultz, 1984), fluvial (Martin & Turner, 1998) and glacial (Lawson, 1982) settings. The hypothesis of Sohn *et al*. (1999) provides an alternative view of debris-flow–hyperconcentrated-flow transformation, in cases where, as predicted by this hypothesis, the debris-flow deposits prevail over those of more diluted (hyperconcentrated flow and stream flow) flows, and where their top surface shows evidence of erosion and reworking.
(b) When $Q_s < Q_w$, hyperconcentrated flows can develop only during the deposition stage, generally through flow expansion and frictional freezing of bedload and rapid settling of suspended load. This is the dominant development mode of hyperconcentration in both subaerial (the Guelph outwash case) and subglacial (Brennand, 1994; Brennand & Shaw, 1996) streams, in dam-break floods (non-cohesive sediment-gravity flow; Blair, 1987) and in high-gradient mountain rivers (debris torrent; Carling, 1987).
(c) When Q_s and Q_w are equal, hyperconcentrated flows develop during transport as a result of sediment bulking and/or at the transport–deposition transition through gravity transformation. This is the typical alluvial realm where the Mugello Basin UFD deposits and Todd's model apply.

Thick alluvial successions made of normally graded or bipartite, hyperconcentrated flow units therefore are considered evidence of subaerial depositional systems dominated by macroturbulent flood flows bulked with sediment in the first case or suddenly expanded on the depositional surfaces in the second case. The Sohn *et al*. (1999) model, linking normal graded and bipartite units to the deposition from differently mobile rheological portions of debris flows, can be an alternative explanation. A conceptual linkage of these different modes to achieve hyperconcentration therefore can be entertained, starting from the surface transformation extreme (Q_s maximum), passing into the sediment bulking, then into the gravity flow transformation, and finally into the frictional freezing extreme (Q_w maximum).

Facies analysis at the sedimentation unit scale (units formed during a depositional event, see Fig. 12) allows discrimination between the various ways to achieve hyperconcentrated flows (Mutti, 1992; Mutti *et al*., 1994).
(a) It is suggested here that hyperconcentrated flows derived from surface transformation of debris flows generate during a single event a typical suite of facies characterized, from proximal to distal locations, by matrix-supported gravels gradually passing into crudely graded, clast-supported gravels and eventually into horizontally laminated coarse sands (that is, hyperconcentrated-flow deposits). A vertical profile of the sedimentation unit should show the hyperconcentrated-flow deposits overlain by the cogenetic debris-flow deposits progressively thinning down-flow.
(b) In the case of hyperconcentrated flows developed at the depositional stage from macroturbulent flood flows, the characteristic facies succession should be the one described herein for the glacial outwash settings (outwash); that is, a proximal to distal transition from massive, clast-supported, matrix (sand)-rich, imbricated gravels, to inclined, rhythmically layered gravelly units. The latter reflect the development of a frontally accreted macroform possibly during the waning stages of floods. Such deposits also may occur in high-gradient mountain rivers (Carling, 1987) or in rivers affected by natural or artificial dam-break floods as gravelly macroforms ('boulder berms'). These, however, may have a low preservation potential.
(c) In the case of alluvial hyperconcentrated-flow deposits produced from sediment bulking and gravity transformation, the facies tracts can show, respectively: (i) a proximal to distal transition from massive, clast-supported, matrix (sand to clay)-rich, imbricated gravels to crudely inclined massive gravelly sandy units representing depositional lobes (flood bars; Mutti *et al*., 1996); (ii) a proximal to distal transition from a massive, clast-supported, matrix (sand to clay)-rich, imbricated gravelly unit to a bipartite gravelly sandy unit showing a pervasive planar fabric evidenced by *a*(p) orientation of gravels and horizontal lamination in sands.

2 A second general result of this study is the recognition of the great variation in frequency and magnitude of the hyperconcentrated-flow depositional events in different settings.

Low-frequency and high-magnitude depositional events characterize the volcanic settings, the present-day Iceland sandar and the late Quaternary subglacial and proglacial systems. The alluvial setting on the contrary is characterized by higher frequency depositional events. A recent analysis of flood-dominated alluvial and fluviodeltaic systems in tectonically active basins where a great variety of hyperconcentrated-flow deposits can be found suggests that the flood dynamic is controlled mostly by the interplay of tectonic uplift, relief denudation and climate (Mutti *et al*., 1996). During an uplift–denudation cycle, the sediment eroded in the catchments is supplied to the ultimate depositional basin by high-magnitude floods, which may bypass the alluvial, fluvial and paralic systems, depositing, through flood-driven hyperpycnal flows, sediment lobes in the terminal marine or lacustrine basins. During the late stages of each cycle, progressively lower magnitude, smaller volume floods distribute sediment in the coastal, fluvial and, finally, in the alluvial systems developed on the tectonically active shoulder of the basin. The basin dynamic therefore plays a major control on the sediment production through relief rejuvenation. The sediment reworking, however, is controlled in great part by water discharge and this mostly is related to climate, specifically to the modes of rainfall generation (Hayden, 1988). This recurrent way to provide water for floods seems the most suitable mechanism to explain the thick alluvial successions bearing hyperconcentrated-flow deposits in the geological record. Very high-magnitude floods, such as those produced from large glacial-lake outbursts, represent specific-setting, low-frequency events that cannot explain the wide temporal and spatial occurrence of hyperconcentrated-flow deposits. Although rainfall is the most probable candidate to trigger hyperconcentrated-flow floods, its relationship with climate is not easily assessed in the geological past. How the atmospheric circulation controlling the rainfall pattern, and hence flood generation, has responded to past climatic change is in fact poorly described in general models (Perlmutter & Matthews, 1990). What is now known for the Quaternary (Adams *et al.*, 1999) suggests that this response could have been very complex, rendering recognition of the connections between climate (rainfall pattern) and hyperconcentrated flows a non-trivial problem.

The documented occurrence of inferred hyperconcentrated-flow deposits in Precambrian clastic successions (Eriksson *et al.*, 1998) suggests a further non-actualistic scenario for hyperconcentrated flow, making it an important process for the redistribution of continental sediments throughout the ages. Precambrian and early Palaeozoic periods lacking terrestrial vegetation may have represented times when (i) large amounts of sediment were available for the sedimentary systems, and (ii) rapid release of rainwater may have occurred generating flows frequently bulked with sediment.

CONCLUSIONS

1 Hyperconcentrated flows are common in recent terrestrial settings and may have been responsible for a significant part of the geological fluvial and alluvial-fan record.

2 Hyperconcentration is reached in various ways, the necessary conditions being availability of sediments and the appropriate transport mechanism, either mass gravity flows or fluid flood flows.

3 Hyperconcentration can be reached during transport by flow surface transformation and sediment bulking, at the transport–deposition transition by gravity transformation, and at the deposition stage by non-cohesive freezing of granular sedimentary load. Flow transformations occur either through progressive sediment bulking of a turbulent fluid flow or as dilution of debris flows.

4 Hyperconcentration of floodwater is fostered by different events in different settings:

(a) by catastrophic sediment and water discharge to the basin in the case of volcano-glacial settings where eruptions, melting glaciers and/or heavy rainstorms occur;

(b) by the interplay of tectonism, relief denudation and climate in the alluvial systems of tectonically active areas.

These different modes have important implications for interpreting the stratigraphical record. The volcano-glacial events, in fact, can affect instantaneously the whole basin, leaving a legacy of widespread but punctuated assemblages of erosional and depositional features. The events in the alluvial settings responding to the interplay of tectonism and climate leave a cyclic imprint, in terms of sedimentary sequences of different thickness, of depositional and erosional processes.

5 Facies analysis is the principal tool to decipher ancient hyperconcentrated-flow deposits. For best results, the analysis should be applied wherever possible at the depositional event scale through lateral tracing of proximal facies into distal facies. This approach allows recognition of different types of hyperconcentrated-flow deposits with respect to tectonic, volcanic and climatic controls on their formation.

6 Deciphering hyperconcentrated-flow deposits not only allows a better understanding of ancient alluvial systems, but contributes to the risk assessment of disaster-prone areas, such as the volcanic Sarno area in southern Italy and the flood-prone Versilia area in western Tuscany.

ACKNOWLEDGEMENTS

We thank M. Sagri and P. Ghetti for discussions and support during this research and S. Sadura for reading and helping to make early drafts of the manuscript easier to read and understand. We also are grateful for the criticisms by L. Rudd and G.A. Smith (reviewers), which forced us to revise and sharpen our analysis, and for the final review by V. Baker. Financial support was provided by CNR (Programma Short-term Fellowship 1996) and Canadian Government (Canadian Studies Program, 1998) to M.B., and by the National Science and Engineering Research Council (NSERC Canada; Grant A7371) to I.P.M.

REFERENCES

Adams, J., Maslin, M. & Thomas, E. (1999) Sudden climatic transitions during the Quaternary. *Prog. phys. Geogr.* **23**, 1–36.

Anketell, J.M. & Rust, B.R. (1990) Origin of cross-stratal layering in fluvial conglomerates, Devonian Malbaie Formation, Gaspé, Quebec. *Can. J. Earth Sci.* **27**, 1773–1782.

Bahk, J.J. & Chough, S.K. (1996) An interplay of syn- and interruption depositional processes: the lower part of the Jangki Group (Miocene), SE Korea. *Sedimentology* **43**, 421–438.

Baker, V.R. (1973) Palaeohydrology and sedimentology of Lake Missoula flooding in eastern Washington. *Geol. Soc. Am. Spec. Pap.* **144**, 1–79.

Ballance, P.F. (1984) Sheet-flow-dominated gravel fans of the non-marine middle Cenozoic Simmler Formation, Central California. *Sediment. Geol.* **38**, 337–359.

Benito, G., Grodek, T. & Enzel, Y. (1998) The geomorphic and hydrologic impacts of the catastrophic failure of flood-control-dams during the 1996 Biescas flood (Central Pyrenees, Spain). *Z. Geomorphol.* **42**, 417–437.

Benvenuti, M. (1997) Physical stratigraphy of the fluvial–lacustrine Mugello Basin (Pleistocene, Northern Apennines, Italy). *Giorn. Geol.* **59**, 91–111.

Beverage, J.P. & Culbertsone, J.H. (1964) Hyperconcentrations of suspended sediment. *Hydraul. Div. Am. Soc. Civ. Eng. J.* **90**, 117–128.

Blackwelder, E. (1928) Mudflow as a geologic agent in semi-arid mountains. *Geol. Soc. Am. Bull.* **39**, 465–484.

Blair, T.C. (1987) Sedimentary processes, vertical stratification sequences, and geomorphology of the Roaring River alluvial fan, Rocky Mountain National Park, Colorado. *J sediment. Petrol.* **57**, 1–18.

Blair, T.C. & McPherson, J.G. (1994) Alluvial fans and their natural distinction from rivers based on morphology, hydraulic processes, sedimentary processes, and facies assemblages. *J sediment. Res.* **A64**, 450–469.

Blikra, L.H. & Nemec, W. (1998) Postglacial colluvium in western Norway: depositional processes, facies and palaeoclimatic record. *Sedimentology* **45**, 909–959.

Blissenbach, E. (1954) Geology of alluvial fan in Southern Nevada. *Geol. Soc. Am. Bull.* **65**, 175–190.

Bradley, J.B. & McCutcheon, S.C. (1987) Influence of large suspended-sediment concentrations in rivers. In: *Sediment Transport in Gravel-bed Rivers* (Eds Thorne, C.R., Bathurst, J.C. & Hey, R.D.), pp. 645–689. J. Wiley & Sons, Chichester.

Brennand, T.A. (1994) Macroforms, large bedforms and rhythmic sedimentary sequences in subglacial eskers, south-central Ontario: implications for esker genesis and melt-water regime. *Sediment. Geol.* **91**, 9–55.

Brennand, T.A. & Shaw, J. (1996) The Harricana glaciofluvial complex, Abitibi region, Quebec: its genesis and implications for meltwater regime and ice-sheet dynamics. *Sediment. Geol.* **102**, 221–262.

Bretz, J.H. (1969) The Lake Missoula floods and the Channeled Scabland. *J. Geol.* **77**, 505–543.

Brierley, G.J., Liu, K. & Crook, K.A.W. (1993) Sedimentology of coarse-grained alluvial fans in the Markham Valley, Papua New Guinea. *Sediment. Geol.* **86**, 297–324.

Bull, W.B. (1964) Geomorphology of segmented alluvial fans in western Fresno County, California. *U.S. geol. Surv. Prof. Pap.* **352E**, 128 pp.

Campbell, C.V. (1967) Lamina, laminaset, bed and bedset. *Sedimentology* **8**, 7–26.

Carling, P.A. (1987) Hydrodynamic interpretation of a boulder berm and associated debris-torrent deposits. *Geomorphology* **1**, 53–67.

Chen, Chen-lung (Ed.) (1997) *Debris-flow Hazards Mitigation: Mechanics, Prediction and Assessment*. American Society of Civil Engineers, New York.

Cole, R.B. & Ridgway, K.D. (1993) The influence of volcanism on fluvial depositional systems in a Cenozoic strike-slip basin, Denali fault system, Yukon Territory, Canada. *J sediment. Petrol.* **63**, 152–166.

Collinson, J.D. (1984) Alluvial sediments. In: *Sedimentary Environment and Facies*, 2nd edn (Ed. Reading, H.G.), pp. 21–62. Blackwell Scientific Publications, Oxford.

Costa, J.E. (1988) Rheologic, geomorphic, and sedimentologic differentiation of water floods, hyperconcentrated flows and debris flows. In: *Flood Geomorphology* (Eds Baker, V.R., Kochel, R.C. & Patton, R.C.), pp. 113–122. J. Wiley & Sons, Chichester.

Coussot, P. & Meunier, M. (1996) Recognition, classification and mechanical description of debris flows. *Earth Sci. Rev.* **40**, 209–227.

Denny, C.S. (1965) Fans and pediments. *Am. J. Sci.* **265**, 81–105.

Dominici, S., Mazzanti, S., & Nencini, I.C. (1965) Geologia dei dintorni di S. Miniato tra l'Arno, l'Elsa e l'Era. *Suppl. Quad. Mus. St. Nat. Livorno* **14**, 1–35.

Eriksson, P.G., Condie, K.C., Tirsgaard, H., *et al.* (1998) Precambrian clastic sedimentation systems. *Sediment. Geol.* **120**, 5–53.

Eynon, G. & Walker, R.G. (1974) Facies relationships in Pleistocene outwash gravels, southern Ontario: a model for bar growth in braided rivers. *Sedimentology* **21**, 43–70.

Fisher, R.V. (1971) Features of coarse-grained, high-concentration fluids and their deposits. *J sediment. Petrol.* **41**, 916–927.

Fisher, R.V. (1983) Flow transformation in sediment gravity flows. *Geology* **11**, 273–274.

Griffiths, P.G., Webb, R.H. & Melis, T.S. (1996) Initiation and frequency of debris flows in Grand Canyon, Arizona. *U.S. geol. Surv. Open File Rep.* **96–491**, 35 pp.

Guðmundsson, M.T., Sigmundsson, F. & Björnsson, H. (1997) Ice–volcano interaction on the 1996 Gjálp subglacial eruption, Vatnajökull, Iceland. *Nature* **389**, 954–957.

Hayden, B.P. (1988) Flood climates. In: *Flood Geomorphology* (Eds Baker, V.R., Kochel, R.C. & Patton, R.C.), pp. 13–26. J. Wiley & Sons, Chichester.

HICKIN, E.J. (1993) Fluvial facies models: a review of Canadian research. *Progr. phys Geogr.* **17**, 205–222.
HISCOTT, R.N. (1994) Traction-carpet in turbidites: fact or fiction? *J sediment. Petrol.* **A64**, 204–208.
HOOKE, R. LEB. (1967) Processes on arid-region alluvial fans. *J. Geol.* **75**, 438–460.
HORTON, B.K. & SCHMITT, J.G. (1996) Sedimentology of a lacustrine fan-delta system, Miocene Horse Camp Formation, Nevada, USA. *Sedimentology* **43**, 133–155.
IVERSON, R.M. (1997) The physics of debris flows. *Rev. Geophys.* **35**, 245–296.
JARRETT, R.D. & COSTA, J.E. (1986) Hydrology, geomorphology, and dam-break modelling of the July 15, 1982 Lawn Lake Dam and Cascade Lake Dam failures, Larimer County, Colorado. *U.S. geol. Surv. Prof. Pap.* **1369**, 78 pp.
JOHNSON, A.M. (1970) *Physical Processes in Geology*. W.H. Freeman, New York.
KARROW, P.F. (1989) Quaternary Geology of the Great Lakes subregion. In: *Quaternary Geology of Canada and Greenland* (Ed. Fulton, R.J.), pp. 326–350. *Geology of North America*, K1, Geological Survey of Canada, Ottawa.
KNELLER, B. (1995) Beyond the turbidite paradigm: physical models for deposition and their implications for reservoir prediction. In: *Characterization of Deep Marine Clastic Systems* (Eds Hartlett, A.J. & Prosser, D.J.), Spec. Publ. geol. Soc. London, No. 94, pp. 31–49. Geological Society Publishing House, Bath.
KOCHEL, R.C. & JOHNSON, R.A. (1984) Geomorphology and sedimentology of humid-temperate alluvial fans, Central Virginia. In: *Sedimentology of Gravels and Conglomerates* (Eds Koster, E.H. & Steel, R.J.), Mem. Can. Soc. petrol. Geol., Calgary **10**, 109–122.
LAWSON, D.E. (1982) Mobilization, movement and deposition of active subaerial sediment flows, Matanuska Glacier, Alaska. *J. Geol.* **90**, 279–300.
LOWE, D.R. (1982) Sediment gravity flows: II. Depositional models with special reference to the deposits of high-density turbidity currents. *J sediment. Petrol.* **52**, 279–297.
MAINALI, A.P. & RAJARATNAM, N. (1991) *Hydraulics of Debris Flows, a Review*. Department of Civil Engineering Report, WRE 91–2, University of Alberta, Edmonton.
MAIZELS, J. (1993) Lithofacies variations within sandur deposits: the role of runoff regime, flow dynamics and sediment supply characteristics. *Sediment. Geol.* **85**, 299–325.
MARTIN, C.A.L. & TURNER, B.R. (1998) Origins of massive-type sandstones in braided river systems. *Earth Sci. Rev.* **44**, 15–38.
MARTINI, I.P. & SAGRI, M. (1993) Tectono-sedimentary characteristics of Late Miocene–Quaternary extensional basins of the Northern Apennines, Italy. *Earth Sci. Rev.* **34**, 197–233.
MELIS, T.S., WEBB, R.H. & GRIFFITHS, P.G. (1997) Debris flows in Grand Canyon National Park: peak discharges, flow transformations, and hydrographs. In: *Debris-flow Hazards Mitigation: Mechanics, Prediction and Assessment* (Ed. Chen-Lung Chen), pp. 727–736. American Society of Civil Engineers, New York.
MEYER, G.A. & WELLS, S.G. (1997) Fire-related sedimentation events on alluvial fans, Yellowstone National Park, U.S.A. *J sediment. Res.* **67A**, 776–791.
MIALL, A.D. (1978) Facies types and vertical profile models in braided river deposits: a summary. In: *Fluvial Sedimentology* (Ed. Miall, A.D.), Mem. Can. Soc. petrol. Geol., Calgary **5**, 597–604.
MIALL, A.D. (1996) *The Geology of Fluvial Deposits*. Springer-Verlag, New York.
MIDDLETON, G.V. & HAMPTON, M.A. (1973) *Sediment Gravity Flows: Mechanics of Flow and Deposition*. Society of Economic Paleontologists and Mineralogists, Pacific Section, Los Angeles, CA, pp. 1–37.
MUTTI, E. (1992) Turbidite Sandstones. Azienda Generale Italiana Petroli, Milan, and Parma University.
MUTTI, E., DAVOLI, G., MORA, S. & SGAVETTI, M. (Eds) (1994) The eastern sector of the south-central folded Pyrenean foreland: criteria for stratigraphic analysis and excursion notes. *Second International Conference on High-Resolution Sequence Stratigraphy, Guidebook*, Istituto Di Geologia, University of Parma.
MUTTI, E., DAVOLI, G., TINTERRI, R. & ZAVALA, C. (1996) The importance of ancient fluvio-deltaic systems dominated by catastrophic flooding in tectonically active basins. *Mem. Sci. Geol. Padova* **48**, 233–291.
MUTTI, E., TINTERRI, R., REMACHA, E., MAVILLA, N., ANGELLA, S. & FAVA, L. (1999) *An Introduction to the Analysis of Ancient Turbidite Basins from an Outcrop Perspective*. American Association of Petroleum Geologists, Tulsa, Continuing Education Course Note Series, 39.
NEMEC, W. & MUSZYNSKI, A. (1982) Volcaniclastic alluvial aprons in the Tertiary of the Sofia district (Bulgaria). *Ann. Soc. Geol. Pol.* **52**, 239–303.
NEMEC, W. & STEEL, R.J. (1984) Alluvial and coastal conglomerates: their significant features and some comments on gravelly mass-flow deposits. In: *Sedimentology of Gravels and Conglomerates* (Eds Koster, E.H. & Steel, R.J.), Mem. Can. Soc. petrol. Geol., Calgary **10**, 1–31.
PERLMUTTER, M.A. & MATTHEWS, M.D. (1990) Global Cyclostratigraphy—a model. In: *Quantitative Dynamic Stratigraphy* (Ed. Cross, T.A.), pp. 233–260. Prentice Hall, New Jersey.
PICKERING, K.T., HISCOTT, R.N. & HEIN, F.J. (1989) *Deep Marine Environments. Clastic Sedimentation and Tectonics*. Unwin Hyman, London.
PIERSON, T.C. (1980) Erosion and deposition by debris flows at Mt Thomas, North Canterbury, New Zealand. *Earth Surf. Process.* **5**, 227–247.
PIERSON, T.C. (1981) Dominant particle support mechanisms in debris flows at Mt Thomas, New Zealand, and implications for flow mobility. *Sedimentology* **28**, 49–60.
PIERSON, T.C. & COSTA, J.E. (1987) A rheologic classification of subaerial sediment–water flows. *Geol. Soc. Am. Rev. eng. Geol.* **7**, 1–12.
PIERSON, T.C. & SCOTT, K.M. (1985) Downstream dilution of a lahar: transition from debris flow to hyperconcentrated streamflow. *Water Resour. Res.* **21**, 1511–1524.
POESEN, J.W.A. & HOOKE, J.M. (1997) Erosion, flooding and channel management in Mediterranean environments of southern Europe. *Progr. phys. Geogr.* **21**, 157–199.
POSTMA, G. (1986) Classification for sediment gravity-flow deposits based on flow conditions during sedimentation. *Geology* **14**, 291–294.
POSTMA, G., NEMEC, W. & KLEINSPHEN, K.L. (1988) Large floating clasts in turbidites: a mechanism for their emplacement. *Sediment. Geol.* **58**, 47–61.
QIAN, Y., YANG, W., ZHAO, W., CHENG, X., ZHANG, L. & XU, W. (1980) Basic characteristics of flow with

hyperconcentration of sediment. *Proceedings of International Symposium on River Sediments, Bejing*.

Rosso, R. & Serva, L. (1998) 16 Giugno 1996: alluvione in Versilia e Garfagnana. Un caso di studio. Agenzia Nazionale Protezione Ambientale—Agenzia Regionale Protezione Ambientale e Territoriale, Toscana.

Rudoy, A.N. & Baker, V.R. (1993) Sedimentary effects of cataclysmic late Pleistocene glacial outburst flooding, Altay Mountains, Siberia. *Sediment. Geol.* **85**, 53–62.

Rust, B.R. (1984) Proximal braidplain deposits in the Middle Devonian Malbaie Formation of Eastern Gaspé, Quebec, Canada. *Sedimentology* **31**, 675–695.

Rust, B.R. & Koster, E.H. (1984) Coarse alluvial deposits. In: *Facies Models*, 2nd edn (Ed. Walker, R.G.), Geosci. Can. Reprint Ser. **1**, 53–69.

Saunderson, H.C. (1977) The sliding bed facies in esker sands and gravels: a criterion for full-pipe (tunnel) flow? *Sedimentology* **24**, 623–638.

Schmitt, J.G. & Olson, T.J. (1986) Hyperconcentrated flood-flow deposition of coarse-grained sediment on temperate, semi-arid to humid alluvial fans. *Geological Society of America 99th Annual Meeting*, San Antonio, TX, Abstract 741.

Scott, K.M. (1988) Origins, behavior, and sedimentology of lahars and lahar-runout flows in the Toutle–Cowlitz river system. *U.S. geol. Surv. Prof. Pap.* **1447-A**, 74 pp.

Scott, K.M. & Gravlee, G.C. (1968) Flood surge on the Rubicon River, California—hydrology, hydraulics and boulder transport. *U.S. geol. Surv. Prof. Pap.* **422-M**, 40 pp.

Sestini, G. (1970) Postgeosynclinal deposition. In: *Development of the Northern Apennines Geosyncline* (Ed. Sestini, G.). *Sediment. Geol.* **4**, 481–520.

Shanmugan, G. (1996) High-density turbidity currents: are they sandy debris flows? *J sediment. Res.* **66**, 2–10.

Shaw, J. (1998) Sedimentary evidence favouring the formation of Rogen landscapes by outburst flood. http://www.sentex.net/~tcc/rogen/main.html.

Shaw, J. & Gorrel, G. (1991) Subglacially formed dunes with bimodal and graded gravel in the Trenton drumlin field, Ontario. *Geogr. phys. Quat.* **45**, 21–34.

Sheridan, M.F., Bonnard, C., Carreno, R., *et al.* (1999) 30 October 1998 Rock fall/avalanche and breakout flow of Casita Volcano, Nicaragua, triggered by Hurricane Mitch. *Landslide News* **12**, 2–4.

Shultz, A.W. (1984) Subaerial debris-flow deposition in the Upper Palaeozoic Cutler Formation, Western Colorado. *J sediment. Petrol.* **54**, 759–772.

Smith, G.A. (1986) Coarse-grained nonmarine volcaniclastic sediment: terminology and depositional process. *Geol. Soc. Am. Bull.* **97**, 1–10.

Smith, G.A. & Fritz, W.J. (1989) Volcanic influence on terrestrial sedimentation. *Geology* **17**, 375–376.

Smith, G.A. & Lowe, D.R. (1991) Lahars: volcano-hydrologic events and deposition in the debris flow–hyperconcentrated flow continuum. Spec. Publ. Soc. econ. Paleont. Miner., Tulsa **45**, 59–70.

Smith, N.D. (1972) Some sedimentological aspects of planar cross-stratification in a sandy braided river. *J sediment. Petrol.* **42**, 624–634.

Smith, N.D. (1974) Sedimentology and bar formation in the Upper Kicking Horse River, a braided outwash stream. *J. Geol.* **82**, 205–223.

Sohn, Y.K. (1997) On traction-carpet sedimentation. *J sediment. Res.* **67**, 502–509.

Sohn, Y.K., Rhee, C.W. & Kim, B.C. (1999) Debris flow and hyperconcentrated flood-flow deposits in an alluvial fan, northwestern part of the Cretaceous Yongdong Basin, Central Korea. *J. Geol.* **107**, 111–132.

Steel, R.J. & Thompson, D.B. (1983) Structures and textures in Triassic braided stream conglomerates ('Bunter' Pebble Beds) in the Sherwood Sandstone Group, North Staffordshire, England. *Sedimentology* **30**, 341–367.

Todd, S.P. (1989) Stream-driven, high-density gravelly traction carpets: possible deposits in the Trabeg Conglomerate Formation, SW Ireland and some theoretical considerations of their origin. *Sedimentology* **36**, 513–530.

Walker, R.G. (1978) Deep-water sandstones facies and ancient submarine fans: models for exploration for stratigraphic traps. *Mem. Am. Ass. petrol. Geol.* **62**, 932–966.

Waresback, D.B. & Turberville, B.N. (1990) Evolution of a Plio-Pleistocene volcanogenic-alluvial fan: the Puye Formation, Jemez Mountains, New Mexico. *Geol. Soc. Am. Bull.* **102**, 298–314.

Webb, R.H., Pringle, P.T. & Rink, G.R. (1989) Debris flows from tributaries of the Colorado River, Grand Canyon National Park, Arizona. *U.S. geol. Surv. Prof. Pap.* **1492**, 39 pp.

Wells, N.A. (1984) Sheet debris flow and sheetflood conglomerates in Cretaceous cool-maritime alluvial fans, south Orkney Islands, Antartica. In: *Sedimentology of Gravels and Conglomerates* (Eds Koster, E.H. & Steel, R.J.), Mem. Can. Soc. petrol. Geol., Calgary **10**, 133–145.

Wells, S.G. & Harvey, A.M. (1987) Sedimentologic and geomorphic variations in storm-generated alluvial fans, Howgill Fells, northwest England. *Geol. Soc. Am. Bull.* **92**, 182–198.

Whipple, K.X. & Dunne, T. (1992) The influence of debris-flow rheology on fan morphology, Owens valley, California. *Geol. Soc. Am. Bull.* **104**, 887–900.

Spec. Publs int. Ass. Sediment. (2002) **32**, 195–209

Catastrophic debris-flow deposits from an inferred landslide-dam failure, Eocene Berga Formation, eastern Pyrenees, Spain

E. SAULA*, E. EMILI MATO* *and* C. PUIGDEFABREGAS†

**Institut Cartogràfic de Catalunya, Parc de Montjuic, E-08038 Barcelona; and*
†Institut de Ciències de la Terra (CSIC), Carrer Lluis Solé Sabarís, E-0828 Barcelona/Norsk Hydro Research Centre, N-5020 Bergen, Norway (Email: cai@ceab.csic.es)

ABSTRACT

The Berga Alluvial Fan System (Upper Eocene to Oligocene) has developed at the northern active margin of the South Pyrenean Foreland Basin. A number of individual debris-flow conglomerate beds have been identified within the otherwise stream-flood-dominated fan system. One of these, the Pedret Bed, has been mapped throughout the area. It is characterized by a monomictic Mesozoic limestone clast composition that contrasts with the polymictic composition of the host alluvial fan sequence, by a remarkable clast angularity, and by its great lateral extent of about 146 km^2. A well-defined pattern of sediment distribution within the Pedret Bed mirrors the inner, mid and outer fan facies belts of the host alluvial fan sequence. The Pedret Bed, 8 m thick at most, includes four distinctly mappable successive units, which seem to correspond to different flow events.

The bulk of the Pedret Bed was deposited mainly from debris-flow processes. The resulting sequences show some of the characteristics of subaqueous debris flows, although as inferred from regional evidence, subaqueous deposition of the Pedret Bed seems highly unlikely. The breccia-like texture, the contrasting locally derived clast composition, the great lateral extent, and the mass-flow origin suggest that the flows depositing the estimated 266×10^6 m^3 of sediment of the Pedret Bed originated from a landslide-dam failure within the drainage basin. Such a process, involving large amounts of sediment but also large amounts of water, would account for the similarities of these deposits with those resulting from subaqueous debris flows.

Debris flows generated from landslide-dam failure may constitute an ordinary process in alluvial-fan systems at the geological scale, and may be an important process accounting for the deposition of large volumes of sediment in alluvial fans.

INTRODUCTION

Debris-flow deposits have been widely reported from ancient alluvial fans, but the actual mechanisms of the generation of debris flows in these sedimentary systems have drawn relatively little interest. Debris flows traditionally have been attributed to events of heavy rainfall in the catchment valley. However, recent reports on the generation of large debris flows by dam failures, by glacial-lake outburst, or by lahars entering river channels (Scott & Gravlee, 1968; Pierson & Scott, 1985; Costa, 1988; Lord, 1991; Baker *et al.*, 1993) point to the possibility that at least some of the ancient catastrophic debris flows within alluvial-fan sequences might owe their origin to the formation and failure of landslide dams in fan-feeding valleys. Rock avalanches and related mass movements are common in subaerial high-relief terrains (Mudge, 1965; Hsü, 1975; Melosh, 1979; Yarnold, 1993), and the voluminous products of these processes can block the feeder valley of an alluvial fan, and result in a catastrophic debris flow owing to the accumulation of water and its outburst. Such debris flows would be associated with widespread floods, have a considerable lateral extent, and possibly serve as useful markers within an alluvial-fan succession.

The present study from the South Pyrenean Foreland Basin focuses on conglomerate beds of monomictic clast composition associated with flash floods interbedded in alluvial-fan sequences of contrasting

Flood and Megaflood Processes and Deposits: Recent and Ancient Examples. Edited by I. Peter Martini, Victor R. Baker and Guillermina Garzón ISBN: 978-0-632-06404-5

polymictic composition. The monomictic deposits usually are interpreted as rock avalanches, with their origin related to new thrust-generated rock exposures, or to the process of capture of an adjacent drainage basin. When mapping the Eocene alluvial-fan formations in the Berga area, at the active northern margin of the basin, we have identified a number of such extensive monomictic beds and used them as stratigraphical markers in the regional 1 : 25 000-scale mapping project of the Geological Survey of Catalonia. In this paper, we describe and discuss the Pedret Bed, one of these beds with a monomictic clast composition and remarkable clast angularity, which are in contrast to the rest of the hosting alluvial-fan sequence. We conclude that the monomictic debris was derived from the failure of a landslide dam that temporarily blocked the main feeder valley of the alluvial-fan system. To the best of our knowledge, few ancient examples of such catastrophic debris-flow deposits have ever been reported in the literature, and we thus hope that the following detailed description of the deposit, its component facies and geometry may help in the recognition of analogous flash-flood products in the ancient alluvial-fan sequences.

REGIONAL SETTING AND GENERAL CHARACTERISTICS OF THE BERGA FORMATION

The Berga Formation (Solé-Sugrañes, 1970), or Berga alluvial system (Mató & Saula, 1991), is a conglomeratic succession, more than 2000 m thick, located at the northern margin of the Ebro Foreland Basin (Fig. 1). The Ebro Basin formed between two orogenic belts: the E–W trending Pyrenees at the northern margin, and the NE–SW trending Catalan Coastal Ranges at the southern margin. The Berga alluvial system developed as the basin-margin syntectonic conglomerate wedge, associated with the southward propagation of the thrust system in the eastern Pyrenees (Riba, 1976; Puigdefàbregas *et al.*, 1986, 1992; Martinez *et al.*, 1988; Vergés & Muñoz, 1990; Mató & Saula, 1991; Millán *et al.*, 1995; Vergés *et al.*, 1995). West of Berga, the coeval alluvial system of Sant Llorenç de Morunys affords a classic example of a syntectonic progressive unconformity, first described by Riba (1967, 1976) and more recently studied by Ford *et al.* (1997).

The syntectonic character of the Berga alluvial system is shown by its growth wedge geometry related to the marginal progressive unconformity (Mató & Saula, 1991). The deposition occurred during Upper Eocene and Oligocene times, when shallow lacustrine and evaporitic systems occupied the central part of the Ebro Basin, and an alluvial-fan belt prograded from the tectonically active basin margins. The Vallfogona thrust constitutes the emergent floor thrust of the South Pyrenean fold-and-thrust system in this area (Vergés *et al.*, 1992), which gradually separated, as sedimentation went on, the present-day outcrop area of the Berga alluvium in the footwall from its former catchment in the hanging wall. During sedimentation of the Berga alluvial system, the area therefore must have been tectonically active. Later folding and thrusting also affected the area (Fig. 1).

The Berga alluvial system includes three main units (Figs 1c & 2) showing a southward progradation, and a distinct internal zonation. The inner, medial and outer fan zones are defined as areas of prevailing conglomerates, sandy conglomerates, and finer grained deposits, respectively, with no particular palaeohydraulic implications. The zone boundaries are gradational and have been subject to southward as well as northward shifting during the evolution of the system. The alluvial system grades southward into distal finer grained facies, linking the conglomeratic basin-margin wedge with the deposits of the fluvial systems that drained towards the lacustrine areas of the central Ebro Basin.

The conglomerates of the Berga alluvial system are of polymictic composition, with *c*. 30% of the clasts derived from igneous rocks and quartz veins, *c*. 40% derived from older sedimentary rocks, mainly Mesozoic, and *c*. 30% derived from Palaeozoic metamorphic rocks. The proportion of these components shows little significant variation. Clast roundness generally is good, but the sphericity varies and is strongly dependent on lithology. The conglomerate beds show planar and cross stratification. The associated sandstone lenses are parallel or cross-stratified, and also there are intercalations of sandy and silty mudstones of variable thickness. The conglomerates are interpreted to be stream-flood deposits, often with distinct stacked bars and related channel-fill deposits of gravel-bed braided streams (Mató *et al.*, 1993). Debris-flow deposits are also present but generally uncommon. Within the upper 250 m of the second progradational unit, four distinct debris-flow beds have been recognized (Fig. 2), differing from the stream-flow alluvium by their extensive sheet-like geometry, internal features and a monomictic clast composition. Carbonate rock-debris predominates, whereby these beds stand out in the outcrops as better cemented and of lighter, whitish colour (Fig. 3). The uppermost of the four debris-flow beds, referred to as the Pedret Bed, is the

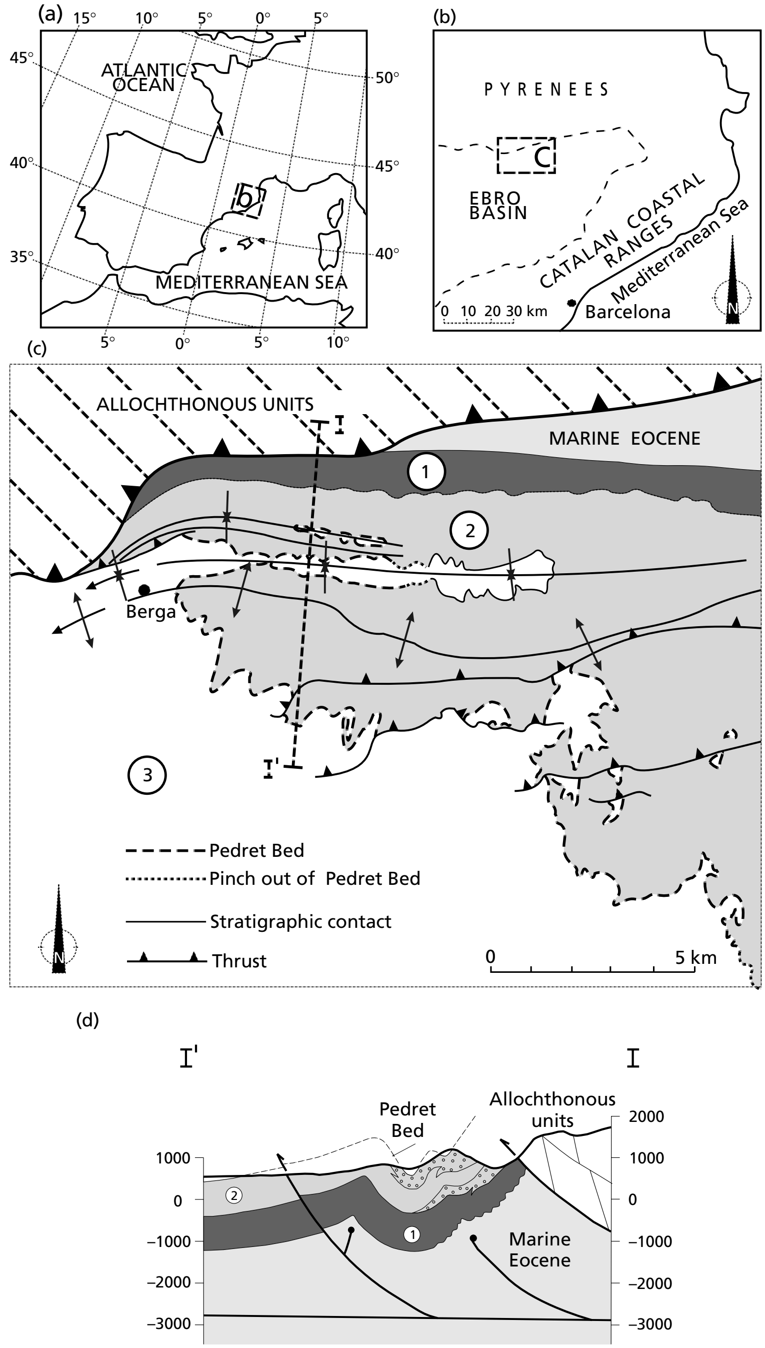

Fig. 1. Location maps and geological setting of the study area on the northern margin of the Ebro Basin around Berga. The Palaeogene Berga Alluvial System, or Berga Formation, includes three alluvial fan progradational members (1, 2 and 3 in Fig. 1c). At a mapping scale, the Pedret Bed constitutes the boundary between members 2 and 3.

thickest and laterally most extensive. It occurs within the uppermost 50-m portion of the second progradational unit, where a slight retrogradational trend of the alluvial system marks the transition to the third progradational unit (Fig. 2). Similar beds of monomictic composition also have been reported by López-Blanco (1991) and López-Blanco *et al.* (1994) in the south-eastern margin of the same Eocene Ebro Basin.

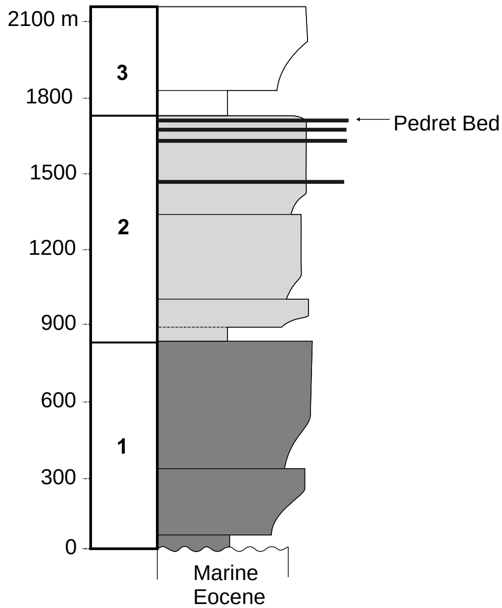

Fig. 2. Vertical succession of the Berga Alluvial System (or Berga Formation) in inner fan reaches, with the three progradational members (1, 2 and 3) represented. The position of four debris-flow beds within the second member is indicated by thick solid lines. The Pedret Bed is the uppermost of the intercalated debris-flow beds.

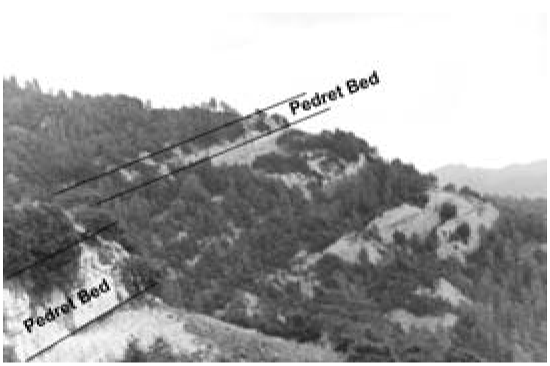

Fig. 3. Debris-flow beds intercalated within the braided stream deposits of the Berga Alluvial System. The Pedret Bed (labelled) is the last of them. The debris-flow beds are easy to recognize in the field because of the extended outcrop continuity, the sharp basal and top surfaces, and the light grey colour resulting from the monomictic limestone clast composition.

GENERAL FEATURES OF THE PEDRET BED

Lateral extent

The Pedret Bed occurs in a gently folded sedimentary succession, but is mappable over an area of about 100 km^2 (Fig. 1c). The outcrop area is cut in the central part by a 5-km long thrust, separating two subareas where the bed is continuously exposed with little problem of lateral correlation (Figs 1 & 4). In the north-western area (zone 1), E–W trending folds with westward dipping axes provide numerous large exposures, whereas minor thrusting in the south-eastern area (zone 2) conveniently increases the outcrop length. Mapping has shown that the Pedret Bed pinches out to both the east and the south (Fig. 1), and disappears under the younger deposits towards the south-west, where the pinch-out thus is not observable.

Thickness and volume

An isopach map of the Pedret Bed has been constructed based on the outcrop measurements (Fig. 4). Maximum bed thickness is 12 m in the northernmost outcrops and decreases gradually, or locally quite rapidly, away from this area of maximum thickness. Based on the isopach map, the volume of the Pedret Bed is estimated at 266×10^6 m^3.

Clast composition

Up to 80% of gravel clasts in the Pedret Bed represent limestones of one particular Mesozoic formation, comprising partly or completely dolomitized wackestones and bioclastic echinoid-rich packestones. The remaining debris represent metamorphic rocks (8%), granitoids (6%), vein quartz (2%) and other Mesozoic limestones and sandstones (4%). This remarkably monomictic composition of the Pedret Bed is clearly in contrast to the polymictic composition of the surrounding alluvium.

Clast size and shape

The Pedret Bed is characterized by the angular shape of the component limestone clasts, which gives a distinct breccia-like texture, in contrast with the rounded limestone clasts in the host alluvial sequence (Fig. 5). The coarser limestone clasts in the Pedret Bed are somewhat rounded, and roundness of the granite and

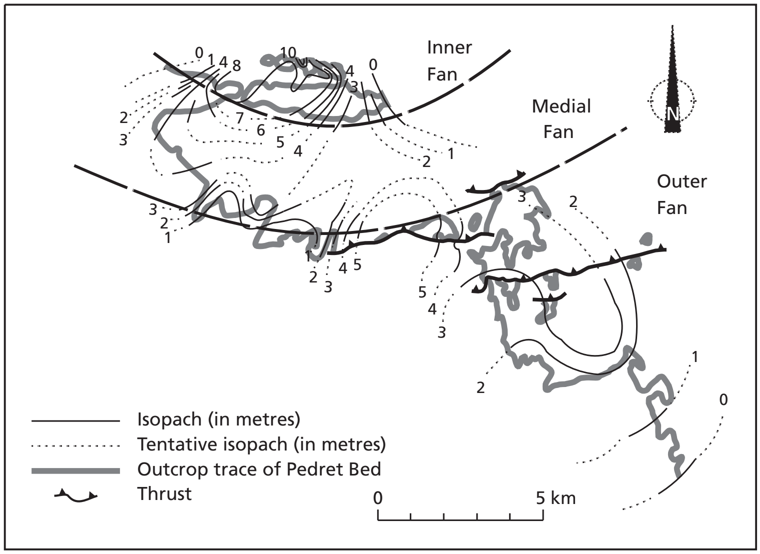

Fig. 4. Restored isopach map of the Pedret Bed, with the outcrop trace also restored. Dotted lines interpolate isopach lines in non-outcropping areas of the Pedret Bed. The reconstruction has been used to evaluate the areal extension and the volume of the Pedret Bed. Inner, medial and outer fan zones are defined as areas dominated by conglomerates, sandy conglomerates and finer grained deposits, respectively.

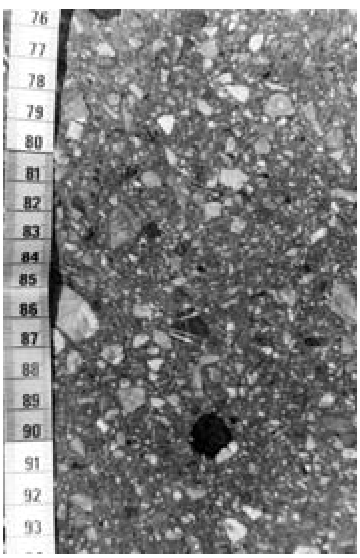

Fig. 5. Detail of fine conglomerates (granules and small pebbles up to 16 mm), with sand-sized matrix. Clast roundness is very low. The scale is in centimetres.

metamorphic rock clasts approaches the normal values observed in the host sequence. The limestone and granite clasts tend to be more spherical, whereas those of metamorphic rocks are mainly rod and blade shaped. Down-flow variation of clast roundness and sphericity has not been studied, but no significant lateral changes are apparent.

The conglomerates of the Pedret Bed have a polymodal texture. Finer grained conglomerate includes granules to small pebbles, 2–16 mm in size, whereas the coarser conglomerate is up to boulder in size. Sand predominates as matrix (Fig. 5), but gravel finer than 10 mm is arbitrarily considered as matrix in the coarser conglomerate varieties. Most of the sand-sized sediments (*c*. 70 vol.%) is derived from the same Mesozoic wackestone–packstone formation, and the rest comprises quartz (25%), feldspar and other rock detritus (5%). In sandstone beds, the relative amount of carbonate grains decreases significantly to less than 50 vol.%. The roundness of the carbonate sand grains is generally very low.

There is a recognizable areal distribution of grain sizes in the Pedret Bed, from coarse to finer grained conglomerates and to sandstones, which roughly coincides with the inner, medial and outer reaches of the host alluvial-fan sequence.

FACIES AND ARCHITECTURE OF THE PEDRET BED

The internal structure of the Pedret Bed includes five units (A, B, C, D and E), recognizable in outcrop as sediment layers defined by distinct bounding surfaces, and differing by their own internal characteristics. In the inner fan zone, units A to D are stacked directly upon one another, but unit E is absent (Fig. 6a). In the western mid-fan zone, the succession consists of units

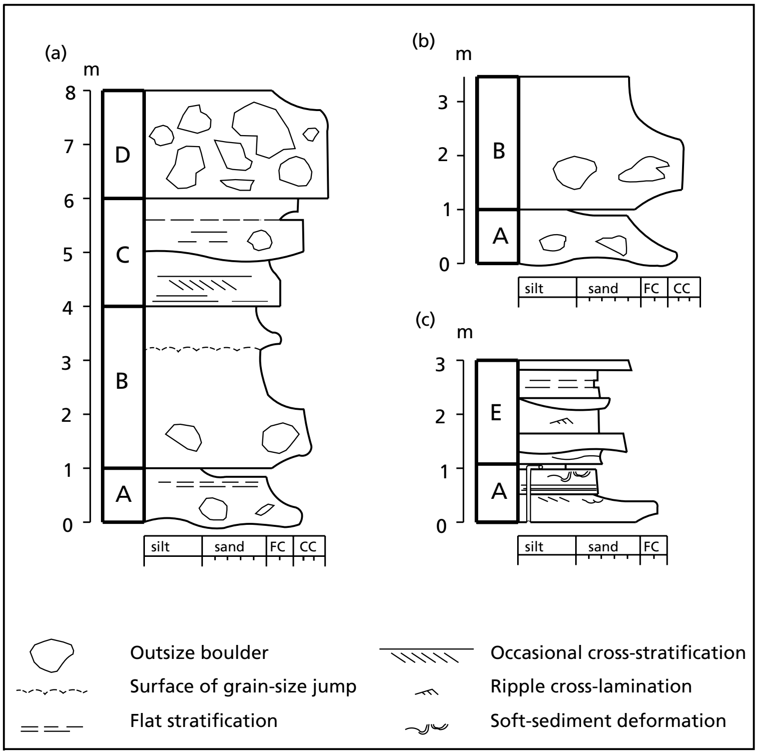

Fig. 6. Type sections of the Pedret Bed: (a) in the inner fan zone; (b) in the medial fan zone; (c) in the outer fan zone. FC: fine-grained conglomerate. CC: coarse-grained conglomerate.

A and B only (Fig. 6b). In the rest of the area, unit A is directly overlain by unit E (Fig. 6c).

Unit A

This is the basal and most extensive architectural unit within the Pedret Bed (Fig. 7a). Unit A is 1–2 m thick in most of its extent, with a maximum thickness of 2.5 m, but experiences a gradual down-flow change of the internal characteristics. The content of limestone clasts is 50–70%, lower than in the rest of the Pedret Bed, particularly at the inner fan reaches, where granite clasts locally constitute up to 30% of the gravel fraction. In the inner and mid-fan zones, unit A consists of coarse pebble gravel. The unit occurs irregularly, with occasional erosive basal scours up to 1 m in relief, but locally it may be absent. Unit A in these inner and mid-fan zones overlies polymictic braided-stream conglomerates, and is overlain by unit B. In the outer fan zone, unit A consists of a granule conglomerate overlain by a graded sandstone, and its basal surface is very flat. The unit overlies mudstones and fine-grained sandstones, and is overlain by unit E in this outer fan zone.

The internal structure of unit A in the inner and mid-fan zones is normally or inverse-to-normally graded (Fig. 8a). The texture is fully clast-supported, with occasional development of horizontal fabric. Imbricate clasts are rare, and outsize clasts are up to 40 cm. The top part of unit A may show better developed upward-fining and occasional wedge-shaped lenses of parallel laminated or ripple cross-laminated sandstone. Unit A generally is draped with a 1–2-cm-thick layer of carbonate siltstone distinctly burrowed and with occasional desiccation cracks (Fig. 9). This layer is very persistent throughout the areal extent of unit A, but may be locally eroded by the base of unit B.

In the outer fan reaches, unit A is only 1 m thick and its profile shows three distinct intervals (Fig. 10). The lower interval is an inversely graded granule sandstone to fine pebble conglomerate. The middle interval is a normally graded coarse sandstone with evidence of depositional pulses (grain-size fluctuations), and with the occurrence of reddish mud, both as matrix and as isolated, slightly contorted lenses. The two lower and middle intervals are separated by a sharp, undulating surface with a pronounced grain-size jump. The

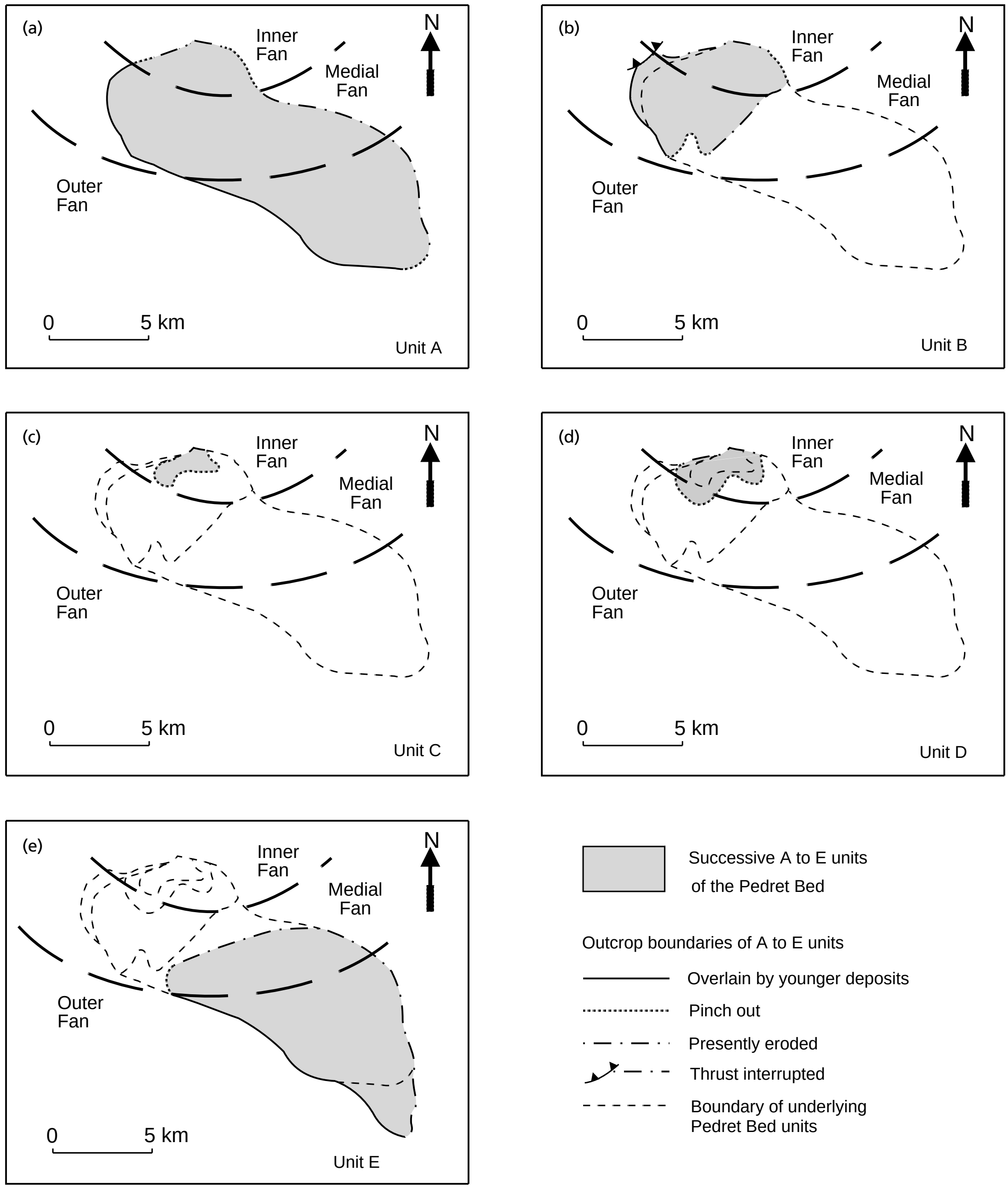

Fig. 7. Distribution map of units A, B, C, D and E within the Pedret Bed.

upper interval is mud-free, parallel laminated to cross-laminated fine-grained sandstone with common soft-sediment deformation. Vertical burrows penetrate through all the three intervals, and horizontal burrows occur at the top surface. Unit A in the outer fan reaches shows a number of features generally typical of the deposits of high-density turbidity currents, such as an inversely graded lower division, an overall

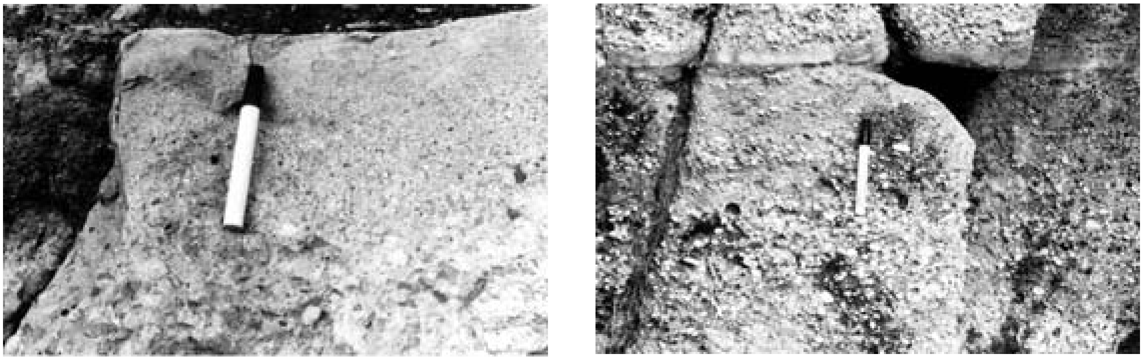
(a) (b)

Fig. 8. The normally graded interval in unit A. Distribution grading in a grain-supported texture is shown in (a), and normal grading with horizontal stratification in (b).

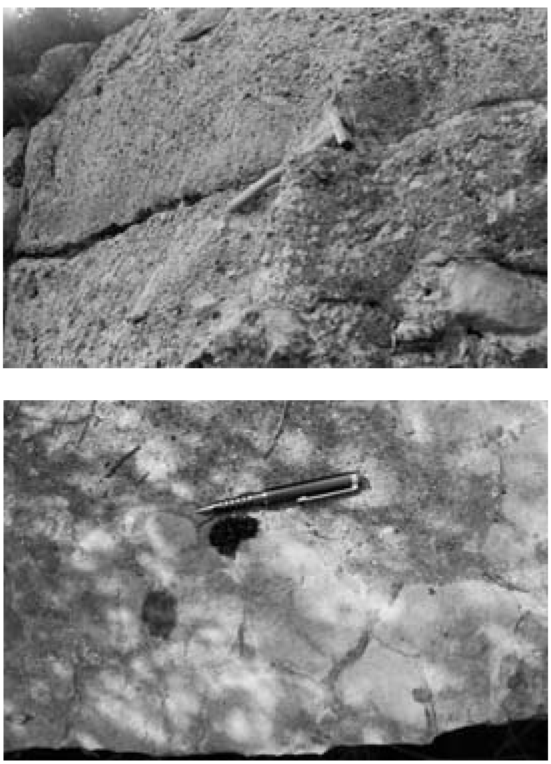
(a) (b)

Fig. 9. (a) Thin, laterally persistent layer of carbonate siltstone between units A and B. (b) Desiccation cracks associated with the same layer.

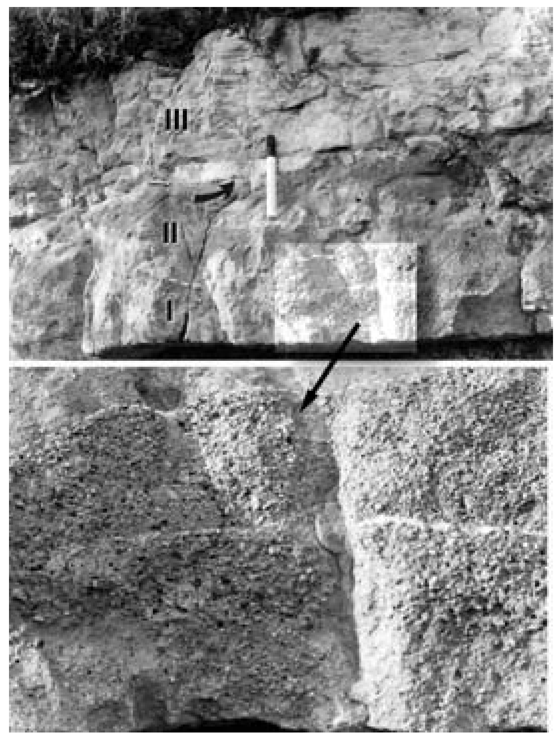

(a) (b)

Fig. 10. The unit A in the outer fan zone, with three distinct intervals separated by sharp contacts (a). The basal interval of fine conglomerate (I) shows inverse to disorganized grading. The intermediate interval (II) is composed of medium to coarse granule sand. The dashed white line is at the undulating contact between I and II (b). The upper sandy interval (III) shows flat, or water-escape-deformed lamination. Arrow indicates a reddish mud lens at the sharp contact between intervals II and III in Fig. 10a.

upward change from graded massive to stratified sediment, and a down-flow change into a thinner, finer grained and more stratified deposit. There are also some differences, such as the sharp transitions between the three intervals, and the frequent grain-size fluctuations in the normally graded middle interval, all of which indicate marked flow unsteadiness with pronounced heterogeneities in the grain-size distribution of the sediment load carried by the flow (Kneller & Branney, 1995). Although remarkably unsteady and pulsatory, the deposition was probably rapid and led quickly to the traction conditions reflected in the upper division.

Unit A may be interpreted in terms of deposition from a high-concentration flash flow that spread laterally, with the water column thinning faster than the rate of sediment flux, the turbulence in the basal part being suppressed by the sediment fallout and depositional shearing, and the traction transport being limited to the dilute final phase. The burrowed and desiccated top surface of unit A indicates a significant time gap, at least of a few days, between this flood event and the following event responsible for the deposition of unit B.

Unit B

Unit B is present only in the inner and mid-fan zone (Fig. 7b), where it overlies unit A or, locally, the substratum of braided-stream polymictic conglomerates (Fig. 6). Unit B has a maximum thickness of 9 m in the inner fan reaches and pinches out to the east and west (Fig. 7b), but shows rapid lateral variation in thickness and internal characteristics. In the mid-fan zone, unit B is exposed over a distance of 5 km without significant internal changes, but becomes thinner and finer grained before pinching out eastwards. The southward and south-westward pinch-out is buried under younger deposits.

Internally, unit B is typically inverse-to-normally graded. The base is flat and sharp, but non-erosive, except for local low-relief scour cutting into the siltstone layer capping unit A. Three intervals with gradational contacts can be distinguished in the vertical profile of unit B.

1 A lower interval of inverse grading, averaging 16% of the total thickness of unit B, and comprising very coarse sandstone passing upwards into granule or fine pebble conglomerate. The texture changes upwards from grain-supported to matrix-supported. Depositional shear imbrication with steepening-upward clast fabric (Massari, 1984; Nemec, 1990) often is observed in the inversely graded interval (Fig. 11a).

2 A middle interval of non-graded coarse pebble conglomerate with a matrix-supported texture and outsized cobbles and boulders (up to 80 cm).

3 An upper interval with normal grading, showing an irregular contact (Fig. 11b) with the underlying disorganized interval, involving a jump to finer grain-sizes. The grading is not uniform, but comprises several graded layers (depositional pulses), around a decimetre thick, which are laterally impersistent and have

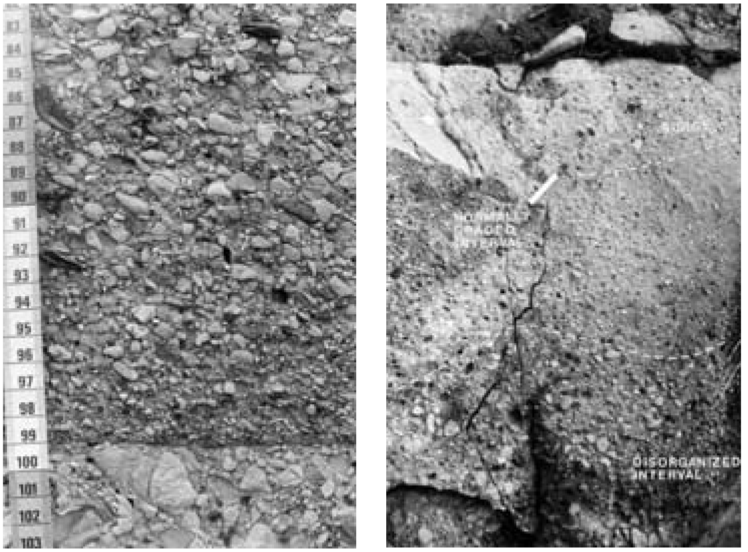

Fig. 11. (a) Inversely graded interval with associated imbrication due to depositional shearing, at the lower part of unit B (scale in cm). (b) Disorganized and normally graded intervals at the upper part of unit B. Contacts are irregular and gradational (lower dashed line). Two successive normally graded intervals are observed, separated by the upper dashed line.

(a) (b)

diffuse to sharp, but non-erosive boundaries. In the western area, the unit is capped by a stratified sandy to granule, decimetre-thick traction interval.

The three intervals suggest a flow with depositional conditions changing progressively from an intensely sheared cohesionless debris flow dominated by particle collisions (Nemec & Steel, 1984), to a moderately sheared debris flow composed of coarsest gravel, to pulsatory rapid dumping of fine gravel and successively sand from high-concentration turbulent suspension. It is uncertain if the three intervals represent successive phases of an evolving flow, or basically coexisting storeys of a tripartite flow. In the latter scenario, the intense shearing at the base of the flow would result in inverse grading, the expelled matrix would be entrapped in the poorly sheared higher part of the flow, and the turbulent uppermost part of the flow would be decoupled, dragging outsize clasts along the base (Postma *et al.*, 1988) and dumping sediment in depletive pulses. The recurrent pulses of rapid sediment fallout from turbulent suspension, reported from ancient megaturbidites (Rupke, 1976), can be attributed to surges occurring within the flow itself (Lowe, 1982) and caused by the flow unsteadiness, possibly related to heterogeneities in sediment concentrations (Kneller & Branney, 1995). The surging phase would be indicative of flow dilution, leading eventually to traction flow conditions (Nemec & Steel, 1984), as observed at the top of the unit in the inner fan zone.

The thickness of unit B changes locally by a few metres within a distance of a few hundred metres. This lateral variation may be explained either by the channelled character of the overlying unit C, or by the depositional topography of unit B involving large bar reliefs, such as those reported by Baker *et al.* (1993), with lengths of up to 100 m, produced by a catastrophic flood jökulhlaup generated by the outburst of an ice-dammed lake.

Unit C

Unit C is recognizable at some localities in the inner fan zone (Fig. 7c), where it occurs above unit B (Fig. 6a), is a few centimetres to 3 m thick, has a sharp and flat or broadly channelized base, and is typically characterized by crude parallel stratification (Fig. 12). The deposit is conglomeratic, with clast sizes ranging from granule to coarse pebble gravel rich in small cobbles and scattered outsize clasts, including 1-m boulders. The conglomerate is polymodal, showing alternating crude strata of markedly different clast sizes. Texture ranges from fully matrix-supported

Fig. 12. Polymodal, horizontally stratified conglomerates in unit C.

to clast-supported, with random or horizontal and imbricate clast fabric. The crudely defined strata have diffuse to sharp contacts, and are between 1 and 60 cm thick, but laterally impersistent. The individual strata are non-graded, or inverse-to-normally graded. Interlayers of sandy granule conglomerate occasionally show parallel stratification or trough cross-stratification, the latter observed only in the coarser sandy granule conglomerate varieties.

Unit C is interpreted to have resulted from a surging, dense sand–gravel flow that deposited a number of successive layers. Laminar shear during the waxing phases resulted in inversely graded intervals, whereas the fluctuating waning flow conditions produced heterogeneities in the sediment load and led to the alternation of massive and stratified intervals (Kneller & Branney, 1995). The flow probably was channelized in the inner fan zone and probably did not spread much over the fan surface, and possibly graded downslope into normal traction deposits difficult to identify in medial and outer fan reaches.

Unit D

This is the uppermost unit of the Pedret Bed (Fig. 6a) in the inner fan zone (Fig. 7d), where it is overlain erosively by the polymictic conglomerates of the host alluvium of the Berga Formation. Internally, unit D is generally massive, composed of polymodal coarse gravel, with a matrix-supported or less often clast-supported texture. The maximum thickness is about 6 m and the clasts are up to cobble size, but outsized boulders are common, some up to 2.5 m in length. The uppermost 10–60-cm interval of the unit in some of the outcrop sections is a normally graded, matrix-supported fine conglomerate (Fig. 13) with a sharp

Fig. 13. Top-only graded section of unit D. The normally graded interval is sometimes confined between protruding boulders (upper left in the picture). The upper contact with the overlying polymictic conglomerates is indicated by the arrow.

base. This interval is laterally impersistent, perhaps owing to erosion by the overlying braided stream alluvium, and recognizable in the most proximal (northern) outcrops only. The thickness and clast size of unit D generally decrease down-fan, as the unit grades laterally into a massive fine pebble conglomerate, a few decimetres thick, that pinches out at the transition to the mid-fan zone. Unit D is interpreted to be a deposit of a cohesionless debris flow (Nemec & Steel, 1984), or density-modified grain flow (Lowe, 1976, 1982) with a watery, turbulent top in some areas.

Unit E

A unit of very fine- to coarse-grained sandstone and siltstone, up to 10 m thick, overlies unit A in the outer fan zone (Figs 6c & 7e). This unit consists of decimetre-thick layers that also are monomictic in clast composition, being locally slightly more polymictic than the underlying unit A. Unit E is finer grained in the down-flow direction, where fine sandstone and siltstone predominate. The component layers have flat bases and show horizontal stratification and ripple cross-lamination, abundant bioturbation and common desiccation cracks. The layers of medium to coarse sandstone have irregular bases, locally with a significant scour relief. These thicker layers may be normally graded, or more often planar stratified or trough cross-stratified.

Unit E is thought to consist of waterlain deposits formed by surges of sediment-laden sheetflood that probably spread down-fan from the turbulent flows that ended the deposition of units B to D, and later by the initial renewed activity of the alluvial fan after the main body of the Pedret Bed had been deposited.

FLOW CHARACTERISTICS

The Pedret Bed is a composite depositional unit. Three successive sediment gravity-flow events responsible for the deposition of units A, B and D are estimated to have carried minimum sediment volumes of 69×10^6 m^3, 55×10^6 m^3 and 6×10^6 m^3, respectively. The internal sedimentary features of these units, such as clast-size grading, clast sorting and fabric, and the upward increase in sand content and traction features, all indicate that the mobility of the first flow was very high, slightly lower in the case of the second flow, and markedly lower in the third flow, probably reflecting the amount of water involved, which correlates with the estimated sediment volume involved in each flow.

The deposition of the Pedret Bed was subaerial on the surface of the alluvial fan, but some of the features of the successive depositional units, such as the well-developed grading and the marked upward increase in matrix content within the graded-bed intervals, are reminiscent of subaqueous sediment gravity-flow deposits (Lowe, 1982; Nemec & Steel, 1984). These characteristics can be attributed to the watery nature of the catastrophic mass-flow events. It was probably water from the outburst of a landslide-dammed stream that entrained the sediment and made it spread as mobile mass flows. In the normal cases of debris flows derived by mountain slope failures, the amount of water is limited and it is the sediment that entrains its pore water, rather than vice versa. When the amount of water is high and the sediment is polymodal, the flow will have little strength and high capability to segregate sediment fractions into different behaving phases, as reflected in the component intervals of units A to D.

The interpreted down-flow evolution of the depositing mass flows is shown in Fig. 14, based on the outcrop sections of the Pedret Bed. The principal down-flow changes include a decrease in the flow competence (grain size) and an increase in turbulence and traction transport (normal grading and stratification), which is shown particularly well by unit A.

Walker (1975) and Lowe (1982) suggested that a subaqueous debris-flow deposit would show, in the down-flow direction, a change from ungraded to inversely graded, to inverse-to-normally graded, to normally graded and finally to normally graded and stratified internal pattern. The characteristics of the

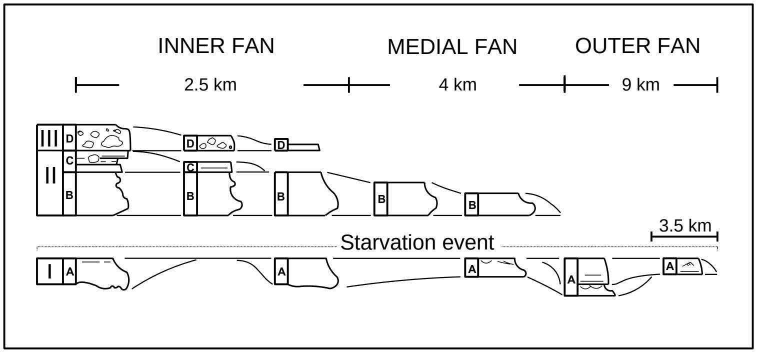

Fig. 14. The down-flow evolution of units A to D across the alluvial fan zones as shown by the correlation of the outcrop sections. I, II and III are the outburst events from the inferred dam failures.

depositional units of the Pedret Bed are roughly consistent with this model, but some significant differences are worth noticing. For example, unit D does not seem to change down-flow from a massive to a normally graded deposit. Stratified intervals occur in the uppermost parts of units A and B virtually everywhere, particularly in the inner fan reaches in the case of unit B. The basal inversely graded intervals are laterally impersistent, but can be identified even in the outer fan reaches. The model for submarine debris-flow evolution is not necessarily a norm (Nemec & Steel, 1984; Surlyk, 1984), but the differences in the present case can be attributed partly to the subaerial depositional conditions.

FLOW GENERATION

Each of the individual flows that deposited the Pedret Bed apparently needed a huge amount of water to form, particularly in the case of units A and B. The nearly monomictic composition of the Pedret Bed is clearly in contrast to the polymictic composition of the rest of the Berga alluvium and implies a localized source of debris. The sediment must have been derived chiefly from one point in the valley, rather than by a flow sweeping the fan catchment area. The remarkable clast angularity suggests a previous short, probably mass-flow transport and temporary storage. Accordingly, we suggest that the catastrophic flash flows have been generated by the failure of a landslide dam that temporarily blocked the fan's feeder valley. There are a number of recent and subrecent examples of landslides that have blocked valleys and resulted in large lakes (see review by Costa, 1988). The Tortum Lake between Artvin and Erzurum in eastern Turkey was created by a Quaternary landslide that formed a dam 80 m high. In the winter of 1840, a landslide in the upper Indus valley (Nanga Parbat region) formed a lake 305 m deep and 64 km long. The dam collapsed in June 1841 and the lake outburst devastated the Indus valley over hundreds of kilometres (Mason, 1929). In the Paute river valley (Ecuador) on 29 March 1993, a huge landslide blocked the Paute and Jadan rivers by forming a natural dam 100 m high, resulting in a lake 20 km long, which completely filled the valley (from press information). Numerous examples of landslides that were triggered by heavy rainfall and partly or completely blocked mountain valleys have been reported from the Pyrenees (1982 flood at the localities of Pont de Bar and Oix; information from the Geological Survey of Catalonia). In short, valley obstruction by landslides is fairly common in mountain areas and is a recurrent phenomenon. There are good reasons to believe that this phenomenon also occurred in the feeder valleys of many alluvial fans in the geological past, with the landslides ranging from rockslides and rockfalls to debris flows.

The break-up of a landslide dam and the outburst of the accumulated water is a violent event, generating discharges of several tens of thousands of cubic metres per second and capable of remobilizing most of the dam debris volume (Scott & Gravlee, 1968; Costa, 1988). Landslides may be multiple and become piled up in a valley (Costa, 1988), whereby the volume of the resulting natural dam may be considerably greater than that of an artificial rockfill dam designed by an engineer. The estimated volumes of debris in the various modern cases of landslide dams are in the order of several hundred million cubic metres (Costa, 1988).

The deposition of the Pedret Bed involved two major surges of a flashy, watery sediment gravity-flow, separated by a phase of waning and desiccation recorded by the fine-grained capping of unit A. This bipartition suggests that the failure of the inferred landslide dam occurred in two successive stages, recorded by units A and B, with the dam probably restored by the recurrence of the valley-side landslide. A renewed landslide mobilization on the valley-side could have resulted from undercutting by the first outburst event.

The first outburst was the largest, as it flushed at least 69×10^6 m^3 of sediment from the valley and produced the most extensive deposit (unit A). The flow itself was bipartite, apparently involving a debris flow and a turbulent high-concentration flow reminiscent of a high-density turbidity current (cf. Lowe, 1982). The admixture of granite clasts and other non-limestone debris in unit A suggests that the flash flood also swept some sediment from the lower valley and fan apex zone, mixing it with the limestone debris of the inferred landslide dam. A similar interpretation is suggested by Scott & Gravlee (1968) to explain the resedimented composition of the otherwise monomictic sediments related to the dam failure in the Rubicon River. The evidence of fully turbulent and largely traction flow behaviour in some of the outcrop sections of unit A suggest that the flow developed highly watery (fluidal) thalwegs when spreading on the fan surface. Alternatively, these may be the earliest deposits of the flood, recording the initial spill of water through the breaking dam. In any case, the final phase of the flow was watery enough to smooth out the fan surface and deposit sediment from traction.

The second episode of the inferred dam failure originated a debris flow with at least 55×10^6 m^3 of sediment. The amount of water involved was smaller and the flow was thus less prone to become turbulent. The deposits of unit B show characteristics of a density-modified grain flow (Lowe, 1976, 1982), or a cohesionless debris flow (Nemec & Steel, 1984) with some role of grain collisions and dispersive pressure. Units C and D can be attributed to minor outbursts related to the second failure of the inferred landslide dam, probably caused by the collapse of the debris barrier undercut by the second major outburst. The joint volume of units C and D is estimated at 9×10^6 m^3.

The waterlain sandstones of unit E probably were derived by stream flows that swept the valley after the destruction of the dam, because the polymictic sediment indicates supply from the fan's 'normal' feeder system. The volume of unit E is at least 133×10^6 m^3, which equals *c.* 50% of the estimated sediment volume of the Pedret Bed. Unit E is never found overlying unit B or D, and occurs laterally adjacent to B in the lower mid-fan zone (Fig. 7e). The deposition of unit E thus is thought to have been accommodated by fan surface irregularities related to the positive depositional relief of units B, C and D.

CONCLUDING REMARKS

Large landslides blocking mountain valleys are a common phenomenon in the catchment areas of many alluvial fans, and the catastrophic flows generated by outburst of the associated dam lakes may be an important episodic process in the formation of alluvial fans. The resulting deposits are sheets that extend over a large portion of the alluvial-fan surface, in the order of several hundreds of square kilometres. The volume of redeposited sediment may reach several million cubic metres depending on the size of the landslide dam and on the amount of water and sediment involved on the lake outburst event. Because of the highly watery and flashy character of the sediment-laden flood flow, the resulting conglomeratic deposits may show some similarity to the products of subaqueous sediment gravity-flows, such as the typical sequence of inverse-to-normal grading, the upwards migration of matrix and the fluctuating grain-size jumps within the normally graded interval. The deposits of alluvial fans are typically very polymictic, swept from a broader catchment, whereas a landslide dam is likely to involve one type of rock and render the resulting flood deposit monomictic. The products of catastrophic floods thus tend to stand out by their great lateral extent and 'unusual' clast composition and shape, which render these deposits very useful marker beds in the stratigraphical succession of basin-margin alluvium.

Landslide dams can form in a range of physiographic settings (Costa, 1988), but their occurrence generally is favoured in tectonically active zones (Adams, 1981; Keefer, 1984). Active thrust-and-fold belts with high mountainous relief, such as in the Pyrenees in Eocene and Oligocene times, are considered to be some of the most favourable settings for the formation of landslide dams in fan-feeding valleys.

The other three beds of chiefly monomictic sediment recognized in the upper part of member 2 of the Berga Formation (Fig. 2) have depositional characteristics similar to those of the Pedret Bed and are interpreted to be the product of analogous catastrophic events. The stratigraphical position of all these beds, at the upper part of a progradational fan succession just where the retrogradational trend initiates, suggests that the formation of landslide dams and the occurrence of catastrophic lake-outburst floods may occur at any stage of an alluvial fan, but the preservation potential of the flood products increases with the decreasing fan activity.

ACKNOWLEDGEMENTS

The manuscript benefited from a thorough revision by W. Nemec. His dedication, including evening discussions in Side, are deeply appreciated by the authors. Thanks are also due to R. Walker and M. López-Blanco for their pertinent review and useful comments.

REFERENCES

Adams, J. (1981) Eathquake-dammed lakes in New Zealand. *Geology* **9**, 215–219.

Baker, V.R., Benito, B. & Rudoy, A.N. (1993) Paleohydrology of late Pleistocene superflooding, Altay Mountains, Siberia. *Science* **259**, 348–350.

Costa, J.E. (1988) Floods from dam failures. In: *Flood Geomorphology* (Eds Baker, V.R., Kochel, R.C. & Patton, R.C.), pp. 439–463. J. Wiley & Sons, Chichester.

Ford, M., Williams, E.A., Artoni, A., Vergés, J. & Hardy, S. (1997) Progressive evolution of a fault-related fold pair from growth strata geometries, Sant Llorenç de Morunys, SE Pyrenees. *J. struct. Geol.* **19**, 413–441.

Hsü, K.J. (1975) Catastrophic debris streams (Sturzstroms) generated by rockfalls. *Geol. Soc. Am. Bull.* **86**, 129–140.

Keefer, D.K. (1984) Landslides caused by earthquakes. *Geol. Soc. Am. Bull.* **95**, 406–421.

Kneller, B.C. & Branney, M.J. (1995) Sustained high-density turbidity currents and the deposition of thick massive sands. *Sedimentology* **42**, 607–616.

López-Blanco, M. (1991) *Estratigrafía y sedimentología del sector occidental del abanico costero de Sant Llorenç del Munt al Este de Sant Vicenç de Castellet (Eoceno, cuenca de antepaís surpirenaica)*. Unpublished PhD thesis, University of Barcelona, Barcelona.

López-Blanco, M., Piña, J. & Marzo, M. (1994) Diferentes estilos de organización secuencial en depósitos de abanico aluvial y abanico costero lateralmente relacionados (Sant Llorenç del Munt, Eoceno, cuenca de antepaís surpirenaica). *Geogaceta* **15**, 49–51.

Lord, M.L. (1991) Depositional record of a glacial-lake outburst. Glacial Lake Souris, North Dakota. *Geol. Soc. Am. Bull.* **103**, 290–299.

Lowe, D.R. (1976) Grain flow and grain flow deposits. *J. sedim Petrol.* **46**, 188–199.

Lowe, D.R. (1982) Sediment gravity flows, II. Depositional models with special reference to the deposits of high density turbidity currents. *J. sedim Petrol.* **52**, 279–297.

Martinez, A., Vergés, J. & Muñoz, J.A. (1988) Secuencias de propagaciôn del sistema de cabalgamientos de la terminaciôn oriental del manto del Pedraforca y relaciûn con los conglomerados sinorogènicos. *Acta Geol. Hisp.* **23**, 119–127.

Mason, K. (1929) Indus floods and Shyok glaciers. *Himalayan J.* **1**, 10–29.

Massari, F. (1984) Resedimented conglomerates of a Miocene fan-delta complex. Southern Alps, Italy. In: *Sedimentology of Gravels and Conglomerates* (Eds Koster, E.H. & Steel, R.J.), Mem. Can. Soc. petrol. Geol., Calgary **10**, 259–278.

Mató, E. & Saula, E. (1991) Los ciclos sedimentarios del Eoceno medio y superior en el sector NE de la Depresión del Ebro (zona de Berga-Vic). Caracterizaciôn de sus lìmites. *Geogaceta* **10**, 45–48.

Mató, E., Saula, E., Martinez, A., Muñoz, J.A., Vergés, J. & Escuer, J. (1993) *Mapa Geológico de España. E. 1: 50.000. Hoja 293 (Berga)*. Instituto Tecnologica y Geominero de España, Madrid.

Melosh, H.J. (1979) Acoustic fluidization: a new geologic process? *J. geophys. Res.* **84** (B13), 7513–7520.

Millán, H., Den bezemer, T., Vergés, J., *et al*. (1995) Palaeo-elevation and effective elastic thickness evolution at mountain ranges: inferences from flexural modeling in the Eastern Pyrenees and Ebro Basin. *Mar. petrol. Geol.* **12**(8), 917–928.

Mudge, M.R. (1965) Rockfall-avalanche and rockslide-avalanche deposits at Sawtooth Ridge, Montana. *Geol. Soc. Am. Bull.* **76**, 1003–1014.

Nemec, W. (1990) Aspects of sediment movement on steep delta slopes. In: *Coarse-grained Deltas* (Eds Colella, A. & Prior, D.B.), Spec. Publs int. Ass. Sediment., No. 10, pp. 29–73. Blackwell Scientific Publications, Oxford.

Nemec, W. & Steel, R.J. (1984) Alluvial and coastal conglomerates: their significant features and some comments on gravelly mass-flow deposits. In: *Sedimentology of Gravels and Conglomerates* (Eds Koster, E.H. & Steel, R.J.), Mem. Can. Soc. petrol. Geol., Calgary **10**, 1–31.

Pierson, T.C. & Scott, K.M. (1985) Downstream dilution of a lahar: transition from debris flow to hyperconcentrated streamflow. *Water Resour. Res.* **21**, 1511–1524.

Postma, G., Nemec, W. & Kleinspehn, K.L. (1988) Large floating clasts in turbidites: a mechanism for their emplacement. *Sediment. Geol.* **58**, 47–61.

Puigdefàbregas, C., Muñoz, J.A. & Marzo, M. (1986) Thrust belt development in the eastern Pyrenees and related depositional sequences in the southern foreland basin. In: *Foreland Basins* (Eds Allen, P.A. & Homewood, P.), Spec. Publs int. Ass. Sediment., No. 8, pp. 229–246. Blackwell Scientific Publications, Oxford.

Puigdefàbregas, C., Muñoz, J.A. & Vergés, J. (1992) Thrusting and foreland basin evolution in the southern Pyrenees. In: *Thrust Tectonics* (Ed. McKlay, K.), pp. 247–254. Chapman & Hall, London.

Riba, O. (1967) Resultados de un estudio sobre el Terciario continental de la parte este de la depresión central catalana. *Acta Geol. Hisp.* **2** (1), 1–6.

Riba, O. (1976) Syntectonic unconformities of the Alto Cardener, Spanish Pyrenees: a genetic interpretation. *Sediment. Geol.* **15**, 213–233.

Rupke, N.A. (1976) Sedimentology of very thick calcarenite–marlstone beds in a flysch succession, southwestern Pyrenees. *Sedimentology* **23**, 43–65.

Scott, K.M. & Gravlee, G.C. (1968) Flood surge on the Rubicon River, California—hydrology, hydraulics and boulder transport. *U.S. geol. Surv. Prof. Pap.* **422-M**, 1–40.

Solé-Sugrañes, L. (1970) *Estudio geológico del Prepirineo entre los rìos Segre y Llobregat*. Unpublished PhD thesis, Universitat de Barcelona.

Surlyk, F. (1984) Fan-delta to submarine fan conglomerates of the Volgian-Valanginian Wollaston Foreland Group, East Greenland. In: *Sedimentology of Gravels and Conglomerates* (Eds Koster, E.H. & Steel, R.J.), Mem. Can. Soc. petrol. Geol., Calgary **10**, 359–382.

Vergés, J. & Muñoz, J.A. (1990) Thrust sequences in the Southern Central Pyrenees. *Bull. Soc. Gèol. France* **8** VI(2), 265–271.

Vergés, J., Muñoz, J.A. & Martinez, A. (1992) South Pyrenean fold-and-thrust belt: role of foreland evaporitic levels in thrust geometry. In: *Thrust Tectonics* (Ed. McKlay, K.), pp. 255–264. Chapman & Hall, London.

Vergés, J., Millán, H., Roca, E., *et al*. (1995) Eastern Pyrenees and related foreland basins: pre-, syn- and post-collisional crustal-scale cross-sections. *Mar. petrol. Geol.* **12**(8), 893–915.

Walker, R.G. (1975) Upper Cretaceous resedimented conglomerates at Wheeler Gorge, California: description and field guide. *J. sedim. Petrol.* **45**, 105–112.

Yarnold, J.C. (1993) Rock-avalanche characteristics in dry climates and the effect of flow into lakes: insights from mid-Tertiary sedimentary breccias near Artillery Peak, Arizona. *Geol. Soc. Am. Bull.* **105**, 345–360.

Alluvial valley floods

Flood and Megaflood Processes and Deposits: Recent and Ancient Examples. Edited by I. Peter Martini, Victor R. Baker and Guillermina Garzón ISBN: 978-0-632-06404-5

Spec. Publs int. Ass. Sediment. (2002) **32**, 213–31

Coarse-grained flood bars formed at the confluence of two subarctic rivers affected by hydroelectric dams, Ontario, Canada

S.-J. MOSHER *and* I. P. MARTINI*

Department of Land Resource Science, University of Guelph, Guelph, Ontario, Canada
*(*Email: pmartini@uoguelph.ca)*

ABSTRACT

This paper illustrates the morphological changes produced in subarctic streams by regulated floods released from hydroelectric dams, and analyses sedimentologically the gravelly flood bars formed at the confluence of two streams in northern Ontario. Subarctic rivers have nival regimes, where strong floods occur during spring snow-melting and low flows for the rest of the year. Northern Ontario is a relatively flat region, and artificial reservoirs are not sufficiently large to retain the spring floodwaters nor, in most cases, can the waters be released through the turbines into the main stream. Instead, spillways are built, through which floodwaters bypass the hydroelectric stations, rejoining the main river downstream. In 1963, excess water in the headpond of the Mattagami River hydroelectric complex was spilled for the first time along the small (25 m wide and a few metres deep), meandering Adam Creek. Since then, regulated spring-flood discharges through the creek have averaged approximately 2100 $m^3 s^{-1}$, with a few floods exceeding 4000 $m^3 s^{-1}$. Adam Creek has experienced severe erosion along its lower reaches, which are underlain by Quaternary glacial deposits and poorly cemented, Mesozoic, clastic rocks. Approximately 52×10^6 m^3 of sediment have been eroded and a canyon about 200 m wide and up to 30 m deep has developed. Approximately 2.5×10^6 m^3 of this eroded material, predominantly the coarse fraction (boulders to coarse sand), have been retained in a junction bar and in three alternating side bars that have developed along a 5-km reach of the main stream (Mattagami River) at and immediately downstream from the confluence with the Adam Creek spillway. The erosion of the spillway, the formation of the coarse-grained bars and the related local narrowing and deepening of the main river may have developed rapidly during the first few floods; subsequent floods have modified the surface structures (chutes, secondary channels, terraces) of the bars.

INTRODUCTION

In the early 1960s, four small run-of-the-mill hydroelectric stations were constructed along a section of the Mattagami River, a tributary of the Moose River that empties into the subarctic, mesotidal James Bay, northern Ontario, Canada (Fig. 1). The dams were constructed on the hard, resistant rocks of the Precambrian Shield, near the boundary with Mesozoic sedimentary rocks and Quaternary sediments of the Hudson Bay Lowland (HBL). Owing to the low relief of the land, a headpond was built at the southernmost hydroelectric station (Little Long, Fig. 1B) to store water used by all generating stations. The headpond has insufficient capacity to hold the spring meltwater floods (freshets). The excess water cannot be funnelled along the main river through the turbines, so it is re-routed through a spillway, Adam Creek, which rejoins the Mattagami River 35 km downstream, 17 km north of the northernmost hydroelectric station (Kipling, Fig. 1B). Adam Creek runs for about 22 km on Precambrian rocks and for the remainder through thick Pleistocene glacial deposits and lignite-bearing, poorly cemented Mesozoic sedimentary rocks of the HBL. Severe erosion has occurred along the banks and floor of the lower reaches. The coarser material (boulders to coarse sand) is redeposited on newly formed bars at the confluence of Adam Creek and the Mattagami River; most of the sand and finer material is, instead, carried farther downstream.

The southern part (latitudes 52° to 50°N) of the HBL has a modified subarctic to boreal, cold continental

Flood and Megaflood Processes and Deposits: Recent and Ancient Examples. Edited by I. Peter Martini, Victor R. Baker and Guillermina Garzón ISBN: 978-0-632-06404-5

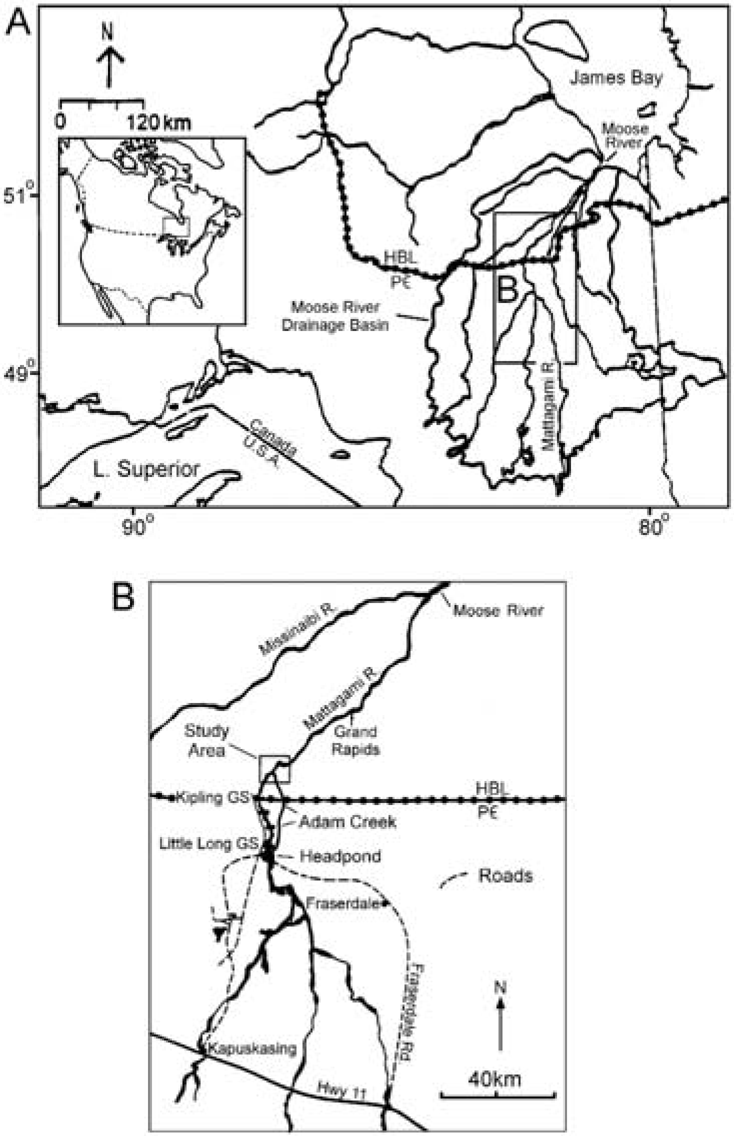

Fig. 1. Location maps and generalized geological setting (P€ = Precambrian; HBL = Hudson Bay Lowland).

climate with a mean annual temperature of 3.9°C; a mean daily July temperature of 22.8°C; a mean daily January temperature of –15.6°C; a mean daily January minimum temperature of –26.7°C; a mean annual precipitation of 66 cm; and a mean annual snowfall of 241 cm (Chapman & Thomas, 1968; Hutton & Black, 1975). The waterways are covered with ice from November to late April/early May, when spring freshets develop. The HBL rivers generally have low gradients, except at the boundary of the Precambrian and Mesozoic–Palaeozoic areas, and, except during spring freshets, they are generally shallow and slow moving.

The principal objectives of this paper are to:

1 report on the morphological changes that have occurred along reaches of a subarctic stream as a result of the diversion of floodwaters and the regulation of flow by hydroelectric dams;

2 analyse flood sediments of a gravelly junction bar and three alternating side bars formed at the confluence of Adam Creek and the Mattagami River (Fig. 2).

METHODS

The study area encompasses a 2-km stretch along the lowermost reaches of Adam Creek, and a 5-km stretch of the Mattagami River. This remote area is accessible only by boat and helicopter. The principal fieldwork was done during the summer of 1995, and modifications to the bars were noted by overflights during the summer of 1996 after an exceptionally strong spring flood.

Fieldwork included the following:

1 the changing geometry of the channels and bars was analysed using aerial photographs taken in 1961, 1965, 1977, 1983, 1991 and 1995 (Ontario Hydro photograph library);

2 a survey of the morphology of the channel (echo-sounding) and of the bars (transects) was performed;

3 the texture, fabric of sediments and sedimentary structures were mapped in detail on the exposed surface of the bars and measured in shallow pits (approximately 1 m deep) and natural exposures (2–3 m high);

4 detailed measurements were made of eight representative Pleistocene sections exposed along the eroded banks of Adam Creek, where the concentrations of boulders, cobbles and pebbles were estimated in the field, and the grain size of sandy deposits and matrix were measured by sieving and pipetting in the laboratory;

5 a mini-shipek was used to sample stream-bottom sediments;

6 current velocity of the Mattagami River was measured using a hand-held Gurley Cup current-meter; however, these measurements were conducted during low summer flow and have limited value. Ontario Hydro routinely measures the maximum water discharge through Adam Creek at the gates of the headpond. Given the discharge, the surveyed cross-sections and

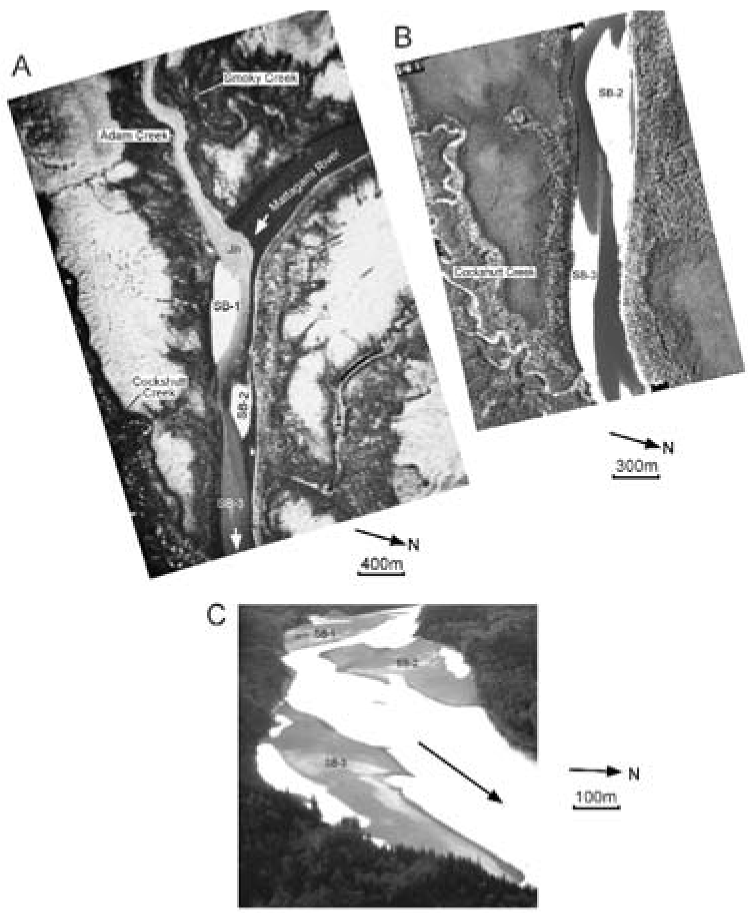

Fig. 2. Photographs of the confluence of the Mattagami River and Adam Creek. (A) Junction bar (Jn) and three side bars (SB-1, -2 and -3) (1995). (B) Downstream reach from the confluence showing side bars SB-2 and SB-3 (1995). (C) Oblique photograph of the study area, looking upstream (south) along the Mattagami River (1996). The Adam Creek junction is in the background to the left. Arrows in the Mattagami River indicate water flow direction.

the maximum floodwater height marked during spring boat trips, the approximate flood-flow velocity could be calculated in the lower reaches of the spillway.

PHYSIOGRAPHY

The Hudson Bay Lowland where Adam Creek joins the Mattagami River is covered by peatlands, mainly fens and bogs, cut by entrenched rivers flowing through thick Pleistocene glacial sediments. A spruce-dominant forest has developed along the better-drained channel banks (Fig. 2).

The Mattagami River has a regular, low-sinuosity, meandering course with long, straight crossover reaches. It has an average width of 300 m and a maximum depth of about 4 m at low flow stages, with the exception of the reach at and just downstream of the Adam Creek confluence. There, the Mattagami River is narrow (approximately 130 m), deep (maximum depth of approximately 7 m), and has a sinuous meandering pattern owing to newly formed, alternating gravelly side bars. Most banks are vegetated to the water edge, except along the bank opposite (north) the mouth of Adam Creek and along the outer bends of the newly formed meanders, where they are erosional and expose Pleistocene sediments. The bank height varies from about 5–6 m to locally more than 20 m, the latter being associated with glacial landforms.

Adam Creek is now an intermittent river (spillway) entrenched into a slightly meandering canyon as much as 200 m wide and 30 m deep in the lower reaches (Fig. 2A). Prior to 1964, Adam Creek had a narrow (20–40 m), tortuous channel (Fig. 3A & B), which underwent dramatic changes when large floods (greater than 3000 $m^3 s^{-1}$) were funnelled into it. Rapid erosion occurred and steep banks developed (Fig. 3C). The channel widened, deepened and became increasingly straight especially along the last kilometre of the creek (Fig. 3B). Traces of old meander loops occur perched high on the canyon flanks.

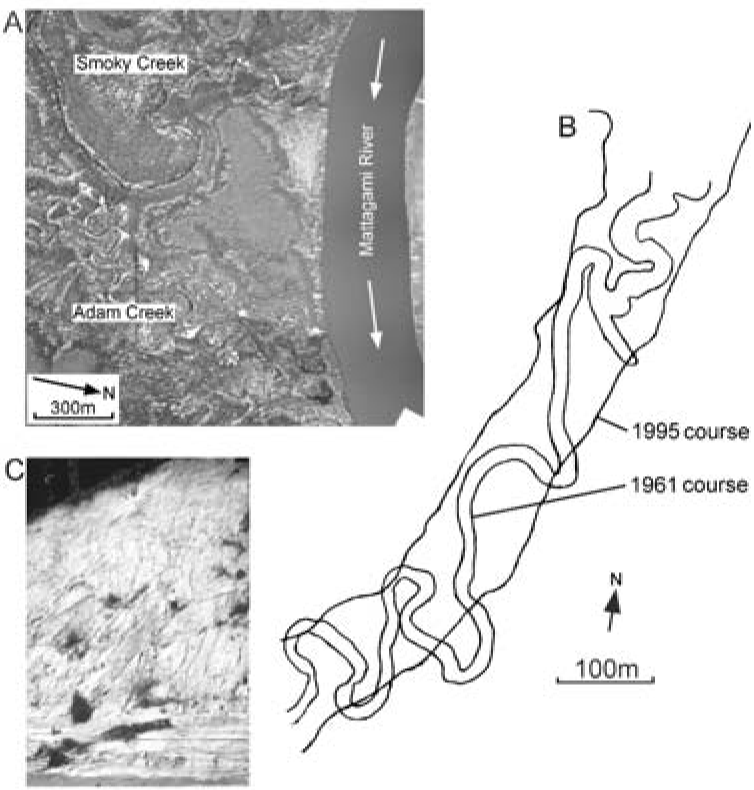

Fig. 3. Features of lower reaches of Adam Creek. (A) Aerial photograph of the Mattagami River–Adam Creek confluence area before use of Adam Creek as a spillway (1961). (B) Variation in channel width and linearity between pre- (1961) and post-dam (1995) construction. (C) Steep, erosive bank of canyon.

RESULTS

Hydrology and sediment transport

The hydrograph of the Mattagami River upstream from the hydroelectric complex has a nival regime with relatively low flow for most of the year and high flows during the spring melt. For most of the year, the daily inflow to the headpond is below turbine capacity (approximately 420 $m^3 s^{-1}$) and is passed through the generating stations. During spring floods (freshets), the inflow into the headpond exceeds maximum turbine capacity and thus most of the flow is diverted through the Adam Creek spillway, drastically changing the hydrographs of both the creek and some reaches of the Mattagami River (Fig. 4A). During spring, the average peak discharge of Adam Creek is approximately 2100 $m^3 s^{-1}$, with two maximum peak flows of 4535 $m^3 s^{-1}$ in 1979 and 4391 $m^3 s^{-1}$ in 1996. It has been calculated that the speeds of these flows through the surveyed cross-section near the mouth of Adam Creek were approximately 4.0 m s^{-1} and 3.9 m s^{-1}, respectively (Mosher, 1997). Furthermore, the average intermediate diameter of the 10 largest boulders on the Mattagami River bars at the confluence with Adam Creek exceeds 1 m. Based on the least-squares regression curve method (Costa, 1983) ($v = 0.20d_I^{0.455}$; where v is velocity and d_I is intermediate diameter of clast), the velocity required to move these boulders would be 4.7 m s^{-1} in a stream with a maximum depth of 7 m (Table 1). The estimated competence of the floods and the required velocities necessary for movement of the large particles are sufficiently close to indicate that such boulders can be moved only during the major floods (Fig. 4B). The transport velocity for the cobbles and pebbles of the bars ranges between 1.7 and 2.5 m s^{-1}. All large spring floods of Adam Creek averaging 2100 $m^3 s^{-1}$ can readily transport such particles (Mosher, 1997).

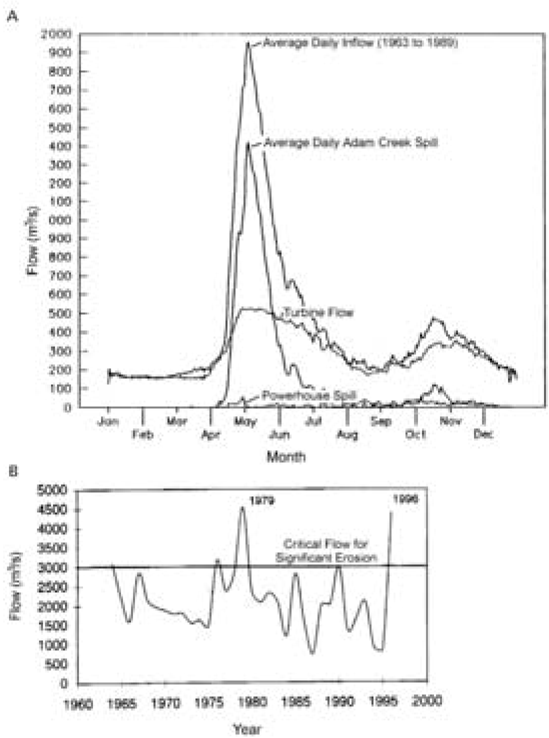

Fig. 4. Diagrams showing discharge through the Mattagami River and Adam Creek. (A) Average daily discharges in various parts of the system between 1963 and 1989 (from Ontario Hydro, 1993). Note nival regime of stream upstream of headpond (average daily inflow into headpond), regulated nival regime in Adam Creek spillway, and regulated regime in the Mattagami River (turbine flow). (B) Plot of annual maximum daily discharge through Adam Creek (from Ontario Hydro, 1993).

Table 1. Flow strength required to move variously sized particles through the mouth of Adam Creek (with flood stage depth of 7 m and cross-sectional area of 1139 m^2) into the bars. Costa (1983) equation ($v = 0.20d_I^{0.455}$) was used.

Particle size (d_I in mm)	Facies	Velocity (v in m s^{-1})
1030	G_{BB}	4.7
265	G_{BC}	2.5
145	G_{CB}	1.9
108	G_{Ci}	1.7

Flow dynamics at the confluence

Summer flow is practically nil in Adam Creek. Summer flow in the Mattagami River is variable, as evidenced by the 1-m fluctuation in water level of the river in response to the use of hydroelectric turbines. Velocities of both the daily high and low flows were recorded at a quarter of the water depth at the centre and one-quarter distance points of transects of the Mattagami River (Fig. 5A, Table 2). The speed is slow in the wide, straight reach upstream from the confluence with Adam Creek. Acceleration is recorded as a function of width in the channel bounded by newly formed gravelly bars downstream.

During spring freshets, the flow pattern at and downstream from the rivers confluence is altered. The

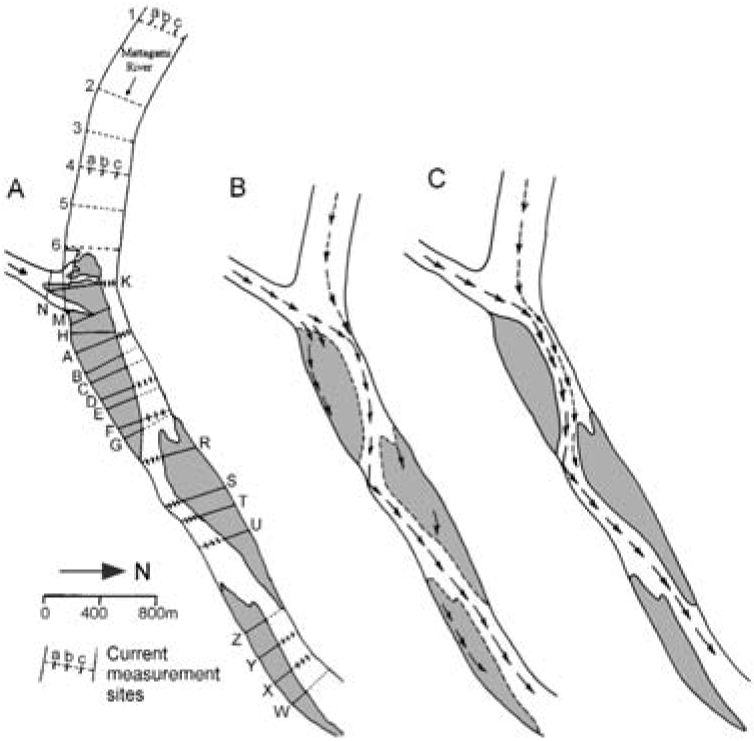

Fig. 5. Maps of study area showing location of bars (shaded). (A) Location map of inland (solid lines) and water (dashed lines) transects measured, and of sites where current meter measurements were made (small barbs in water transects). (B) Map showing current paths (arrows) during extreme high floods when most parts of the bars are submerged. (C) Map showing current paths (arrows) during normal spring floods; the flows of the Mattagami River and of Adam Creek are restricted to the deep narrow channel meandering around the bars.

Table 2. Measured speed (m s^{-1}) of flow along transects of the Mattagami River during 1995 summer, at a quarter water depth. Values in parentheses indicate speed measured at low daily flow, the others at high daily flow.

Transect	a	b	c
1	(0.11)	(0.18)	(0.16)
	0.40	0.35	0.29
4	(0.18)	(0.13)	(0.10)
	0.36	0.27	0.17
K	(0.09)	(0.22)	(0.20)
	0.26	1.31	1.29
A	(0.03)	(0.13)	(0.17)
	0.08	1.03	0.53
D	(0.08)	(0.17)	(0.09)
	0.22	0.94	0.13
F	(0.17)	(0.15)	(0.03)
	0.89	0.58	0.09
R	(0.09)	(0.23)	(0.13)
	0.29	1.04	0.50
S	0.55	0.55	0.10
T	(0.11)	(0.15)	(0.05)
U	0.53	0.64	0.64
Y	(0.75)	(0.83)	(0.65)
	10.9	1.30	0.66
X	(0.25)	(0.22)	(0.06)
	0.76	0.56	0.47

flow from Adam Creek enters into the Mattagami River at an angle of 70° and impinges on the Mattagami River flow, pushing it toward the left bank (Fig. 5B). High flows (greater than 3000 $m^3 s^{-1}$) funnelling through Adam Creek can extend across the entire width of the Mattagami River, thus developing a steep hydraulic gradient. The flow from both rivers converges along the left bank of the main river and accelerates downstream across and around the gravel bars. Smaller spring floods (less than 3000 $m^3 s^{-1}$) of Adam Creek do not extend across the entire width of the channel, but the discharge is still concentrated along the left bank of the Mattagami River, thus increasing local erosion and transport power (Fig. 5C).

Bar morphology

The junction (Jn) bar is located at the mouth of Adam Creek and protrudes into the Mattagami River (Figs 2A & C & 6). It is a fan-shaped feature consisting of three chutes separated by interchute areas. Some chutes terminate into chute bars (cb) locally dissected by smaller channels and chutes.

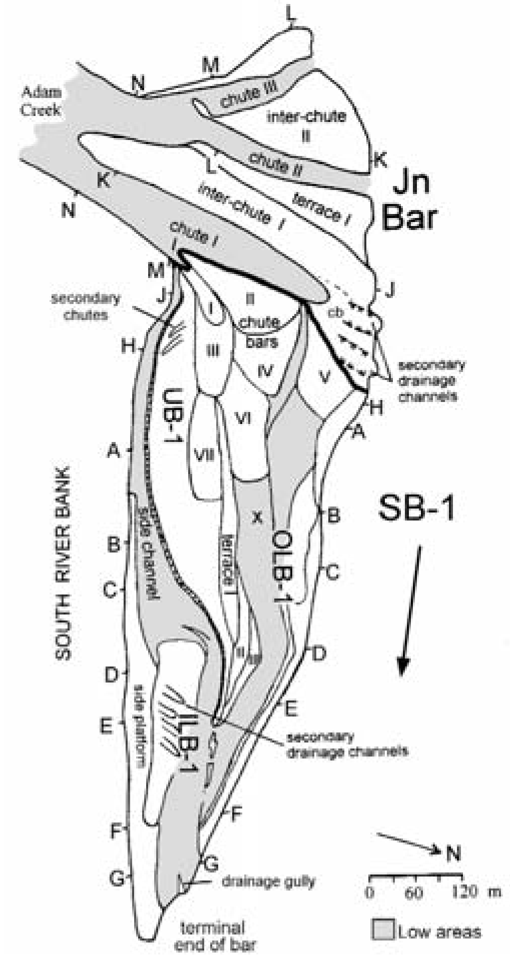

Fig. 6. Map showing morphological features of Jn and SB-1 bars and location of survey transects (A–N). Arrow indicates low-water flow in the Mattagami River.

Side bar 1 (SB-1) is characterized by several surficial features (Figs 2 & 6): (a) upper bar area (UB-1), (b) inner (ILB-1) and outer (OLB-1) lower bar areas, (c) numerous chute bars, (d) a well-defined side channel, (e) a side platform and (f) a downstream terminal area. The UB-1 surface generally is featureless except at the upstream end, where there are small chute bars (I, III and VII: numbering is in order of inferred time of formation from young to old) and drainage channels emptying into the side channel. Flat, wide channels and chutes funnelling floodwaters from the side channel toward the main river channel characterize ILB-1. The OLB-1 zone also contains numerous chute bars (II, IV, V and VI), a long, flat-bottom channel (X), and is bounded along the main stream by a steep slope and a narrow, top-slope-edge berm of coarse gravel. The downstream terminal area of SB-1 has a flat, sandy, silty surface, and is structureless except for small ripple marks. A deep drainage gully is eroded into the downstream terminal avalanche slope of the bar.

The second side bar (SB-2) has similar morphological features to SB-1; that is, a well-defined upstream chute and chute bars (I, II and III) system, an upper (UB-2) and a lower bar (LB-2) surface, and a side channel (Figs 2 & 7A). The floodwater covering the UB-2 zone is returned to the main stream through several drainage channels. The floodwater of the side channel is returned to the main channels through several chutes and secondary drainage channels. Several depositional and erosional terraces mark the water level during various growth stages of the bar.

The third side bar (SB-3) is the smallest, lowest and simplest bar. However, it still maintains an upstream chute, albeit not well developed, a side channel and secondary drainage channels and chutes (Figs 2 & 7B).

Bar deposits

The junction (Jn) bar and the three coarse-grained, alternating side bars (SB-1, -2 and -3) that formed immediately downstream from the confluence with Adam Creek are composed of varying amounts of gravel (G), sand (S) and rarely silt (F). Nine common lithological facies have been recognized and mapped on the surface of the bars on the basis of texture (Table 3; Figs 8–11). The lithofacies are characterized by large boulders (G_{BB}), boulders and cobbles (G_{BC}), cobbles and boulders (G_{CB}), cobbles (G_C) and pebbles (G_P). In most cases, the clasts show preferred upstream imbrication (i), and the gravels generally are massive to plane bedded. The sand and silt facies are characterized by coarse-grained sand (S_E), locally with much granules (S_N), medium-grained well-sorted sand (S_M) and fine-grained sand and silt (S_F). The sand occurs locally on the surface in small-scale ripple marks (S_R). In cross-section, the coarse to medium sand occurs in massive, cross-bedded and cross-laminated units. (In this nomenclature, B = boulders (BB = boulder coarser than 50 cm, up to 2 m in diameter), C = cobbles, P = pebbles, E = coarse, M = medium well-sorted, R = ripples, i = preferred imbrication of *a*/*b* planes of the clasts. This nomenclature has been found useful in this study, but is not proposed for general use.) The clast composition varies from place to place, but on the whole the large boulders are primarily of

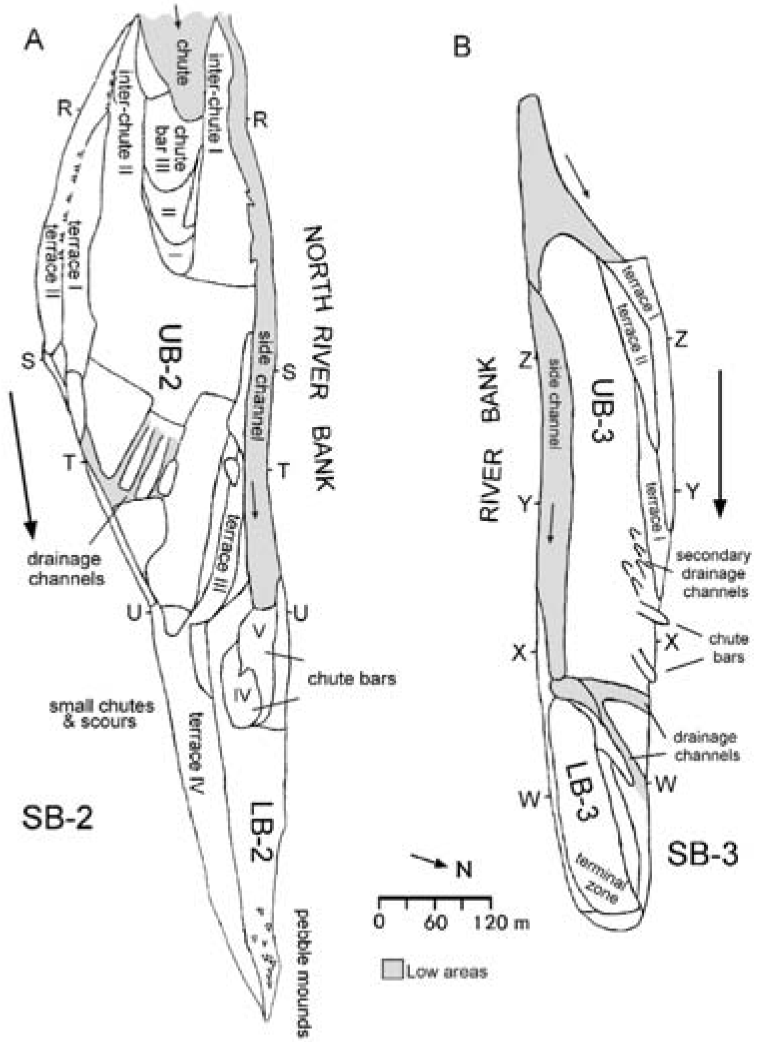

Fig. 7. Maps showing morphological features of SB-2 (A) and SB-3 (B) bars and location of survey transects (R–Z). Arrows indicate low-water flow in the Mattagami River.

granitoid and gneiss, while the smaller boulders consist mainly of granitoid, gneiss and mafic rocks, with some carbonate and few quartzite. The cobbles and pebbles are approximately one-third carbonates, one-third gneiss and granitoid, one-quarter mafic rocks and the remainder are composed of siltstone, sandstone, conglomerate and quartzite.

Subsurface bar facies associations were observed in shallow (*c.* 1 m deep) pits dug in sandy gravel to gravelly sand areas and in natural cuts (*c.* 2.5 m high) elsewhere. Most of the gravelly facies are deflated at the surface, but in the subsurface consist mostly of massive, grain-supported gravel (granules to boulders) with a coarse- to medium-grained sandy matrix, as well as few openwork units of small pebbles and granules. The sandy facies are cross-laminated, cross-bedded, plane bedded or massive, with some units containing disseminated granules and pebbles (Figs 12 & 13). The sandy successions occur predominantly at the downstream ends of the bars.

Other surficial features

Numerous flow and ice features have been mapped on the bars (Figs 14 & 15). Flow features include imbricated pebble clusters, transverse ribs, shadow deposits, tree-drag scours (Fig. 15A) and orientated

Table 3. Major sedimentary facies and their characteristics.

Facies symbol	Description
G_{BB} Fig. 10A	Large (50–190 cm), rounded boulder gravel partially filled with smaller, subrounded boulders, cobbles and pebbles. Average 10 largest clasts = 133 cm. No preferred particle orientation. Fluted tree trunks present. This facies occurs only on the junction bar (Jn)
G_{BC} Fig. 10B & C	Boulders and cobbles, with largest size measuring 148 cm; the average of 10 coarsest clasts is 89 cm. Clasts are rounded to subrounded, generally imbricated (i). The clasts occur either in open framework units or, generally, with pebbly and sandy matrix (G_{BCS})
G_{CB} Fig. 10D	Rounded cobble (predominant) and boulder gravel, varying from open framework with very small amount of granules and sandy matrix (G_{CB}), to gravel with abundant (about 30%) sandy matrix (G_{CBS}). This facies is common in small chutes and drainage channels of the upper parts of the bars
G_C Fig. 11A	Cobble gravel with minor amounts of boulders and pebbles. Subfacies are recognizable in pebbly cobble gravel without (G_{CP}) or with abundant sandy matrix (G_{CPS}). Coarsest clast *c.* 82 cm, average of ten coarsest clasts *c.* 48 cm. Coarser clasts are rounded; pebbles vary from subrounded to subangular
G_P Fig. 11B	Pebble gravel with minor cobbles. It occurs as open framework (G_P) or with a sandy matrix (G_{PS})
S Fig. 11C & D	Various types of sand have been identified on the basis of particle size: coarse sand with small pebbles and granules (S_N) on deflated areas; coarse sand (S_E) with small pebbles and granules mixed throughout is found in various parts of the bar, at the surface particularly toward their downstream ends, and as matrix in the subsurface gravelly units; fine sand to sandy silt (S_F) occurs in local patches; moderately well-sorted, medium-grained sand (S_M) generally of aeolian origin found mainly in local patches. Locally ripple marks are present (S_R)

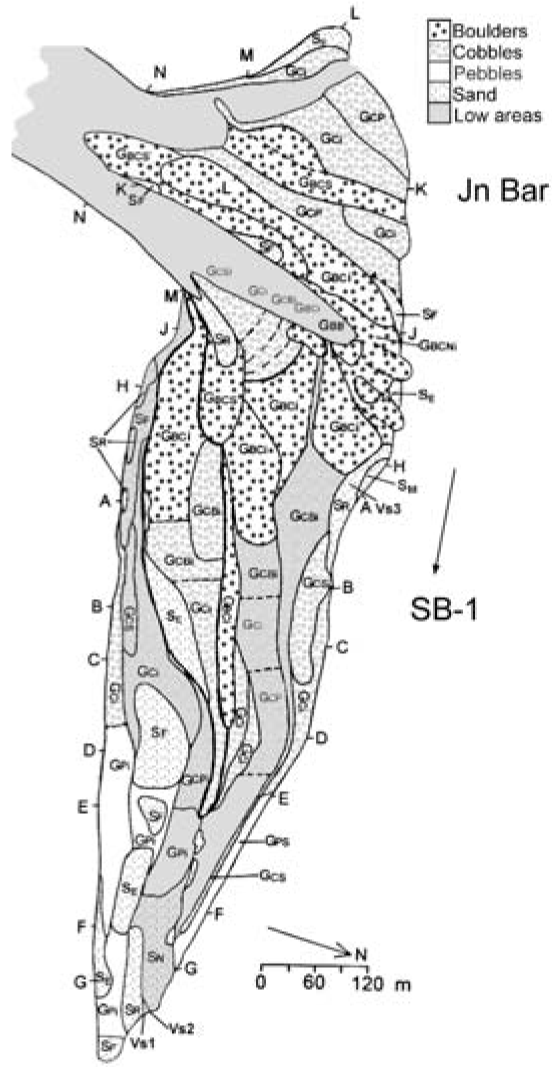

Fig. 8. Map showing distribution of surficial deposits on Jn and SB-1, and locations of survey transects. Arrow indicates direction of low-water flow of the Mattagami River.

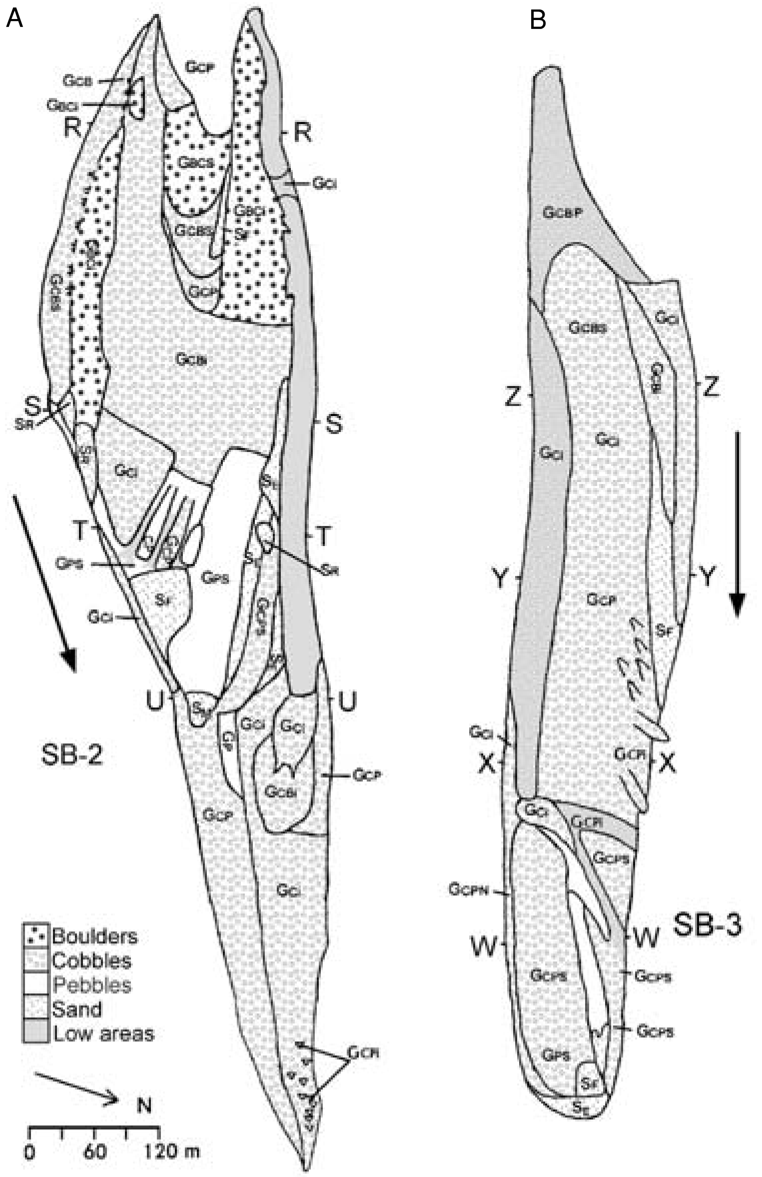

Fig. 9. Maps showing distribution of surficial sediments on SB-2 (A) and SB-3 (B), and location of survey transects. Arrows indicate direction of low-water flow of the Mattagami River.


(A) (B)

Fig. 10. Features of selected sedimentary facies: (A) G_{BB} on Jn, looking upstream toward the mouth of Adam Creek (in the background); (B) G_{BCi} on Jn. (*cont'd*)

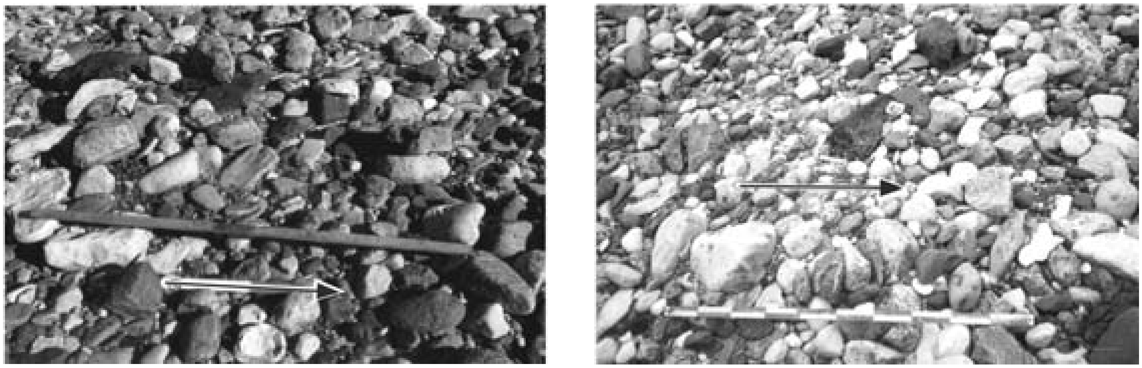

(C) (D)

Fig. 10. (*cont'd*) (C) G_{BCNi} on SB-1; (D) G_{CBi} on SB-1. Arrows indicate direction of depositing flow.

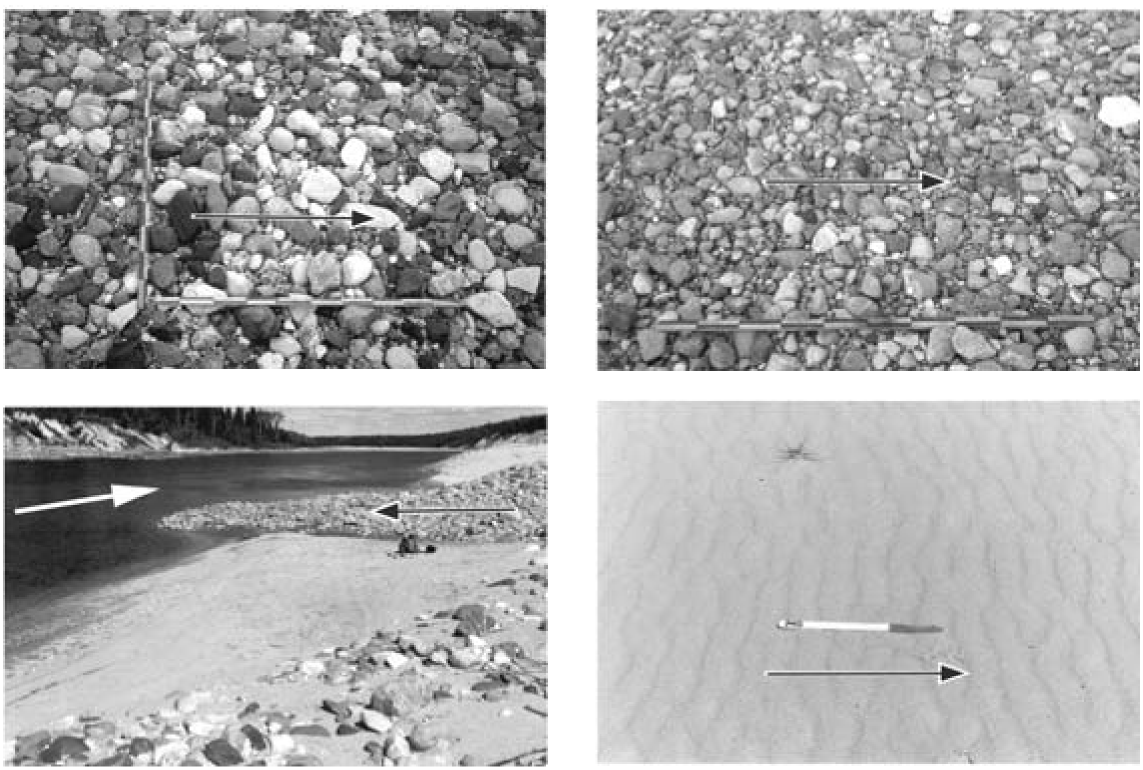

(A) (B) (C) (D)

Fig. 11. Features of selected sedimentary facies on SB-1: (A) G_{Ci}; (B) G_P; (C) S_E sand cover just upstream and downstream of a gravelly chute-bar tongue of Jn, looking downstream along the Mattagami River; (D) S_M with aeolian ripple marks (black arrows indicate direction of depositional current; white arrow indicates flow direction of river).

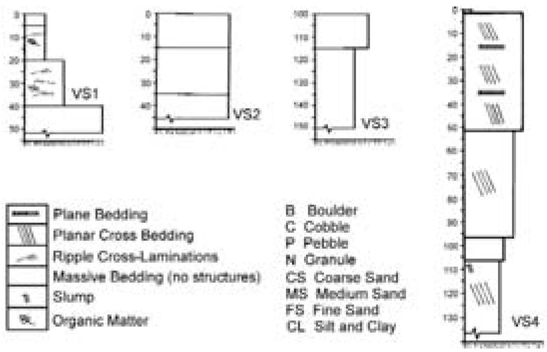

Fig. 12. Representative stratigraphical sections of SB-1: VS1 from upstream chute bar showing basal massive G_B gravel overlain by cross-laminated sand of Fig. 11(D); VS2 from highest area of bar showing homogenized beds of massive sandy gravel; VS3 from sandy gravel terminal part of the bar showing a crude vertical fining upward succession of fine to medium size gravel; VS4 from sandy downstream end of bar showing superimposed cross-bedded units, some with cross-laminated sand cap (Fig. 13B).

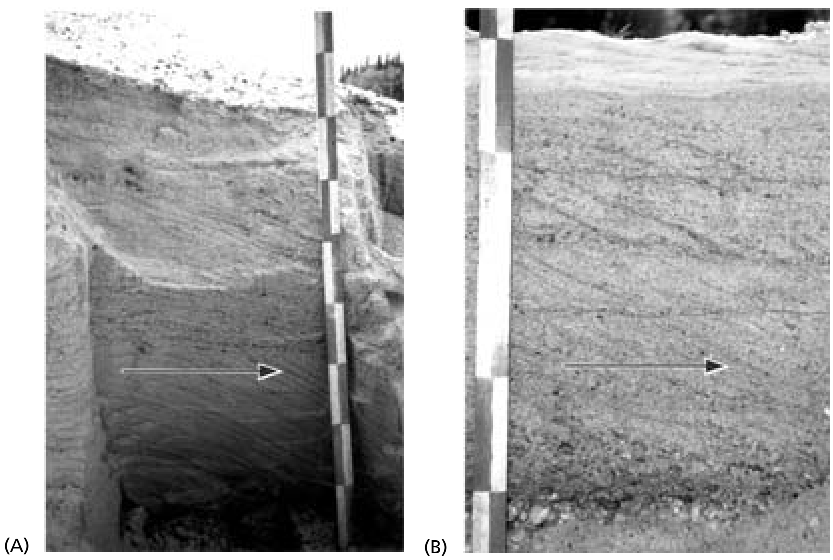

Fig. 13. (A) Superimposed sandy cross-beds from the downstream terminal area of SB-1 bar. Some (B) have well-developed cross-laminated, water-laid, fine sands. These cross-beds are not associated with migrating train of sand dunes; rather they are related to the downstream terminal avalanche slope of the bar.

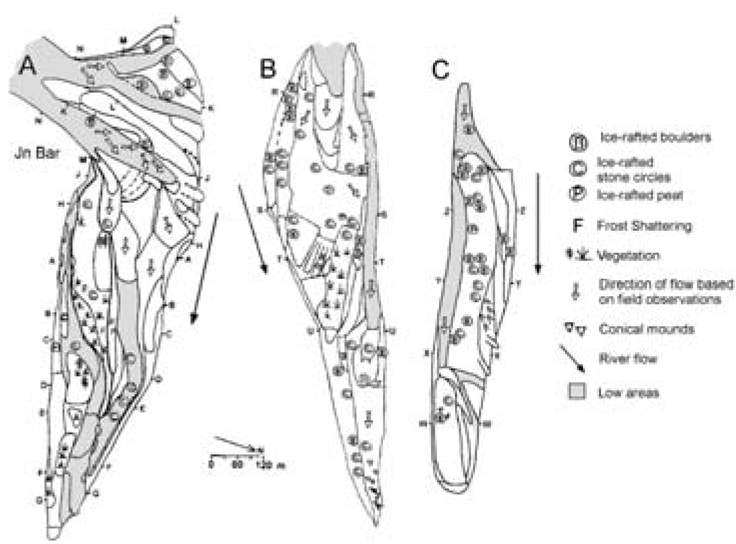

Fig. 14. Maps showing surficial features of the bars: (A) Jn and SB-1, (B) SB-2 and (C) SB-3.

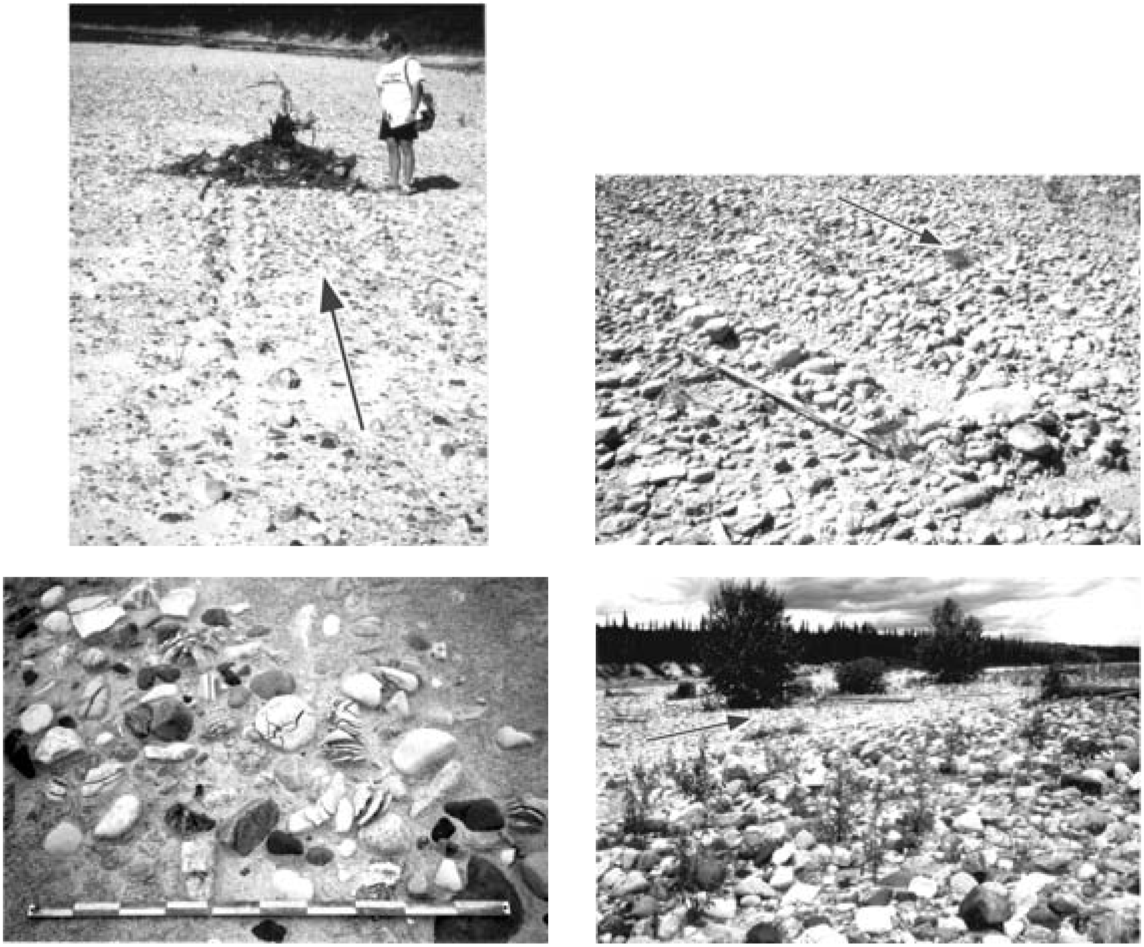

(A) (B) (C) (D)

Fig. 15. Surficial features of side bars. (A) Scours generated by roots of dragged tree. (B) Scour generated by ice-pushed boulder. (C) Frost-shattered clasts on highest surface (UB-1) of SB-1. (D) Incipient vegetation growth (shrubs and young spruce) on SB-1 (along transect D). Arrows indicate direction of depositing flow.

logs. Ice features include ice-push scours (Fig. 15B), erratic boulders, stone circles, ice-rafted materials and conical-shaped mounds (Fig. 16). Other features found on the bar surfaces are frost-shattered clasts (Fig. 15C) and vegetation (Fig. 15D). The latter two are located preferentially in older parts of the bars (UB-1 and UB-2) unaffected by normal annual spring floods.

Sediment dispersal

Considering the well-known materials in the source area, here an estimate is made of the type and relative amount of sediment trapped in the bars of the study area in relation to what is transported farther downstream. Although highly approximate, such information is of interest both for a sedimentological understanding of the system, and for assessing the environmental impact of human interference of this type.

The total amount of sediment deposited and the volume of each size fraction trapped in the bars has been estimated using broad assumptions in order to compare them with the quantity and type of sediment exiting Adam Creek. The assumptions and procedure are as follows.

1 The volume of the bars was estimated using their surface area and a thickness calculated in the following manner.

(a) The bars were subdivided into two portions, the section exposed above the low-flow water level and the submerged part.

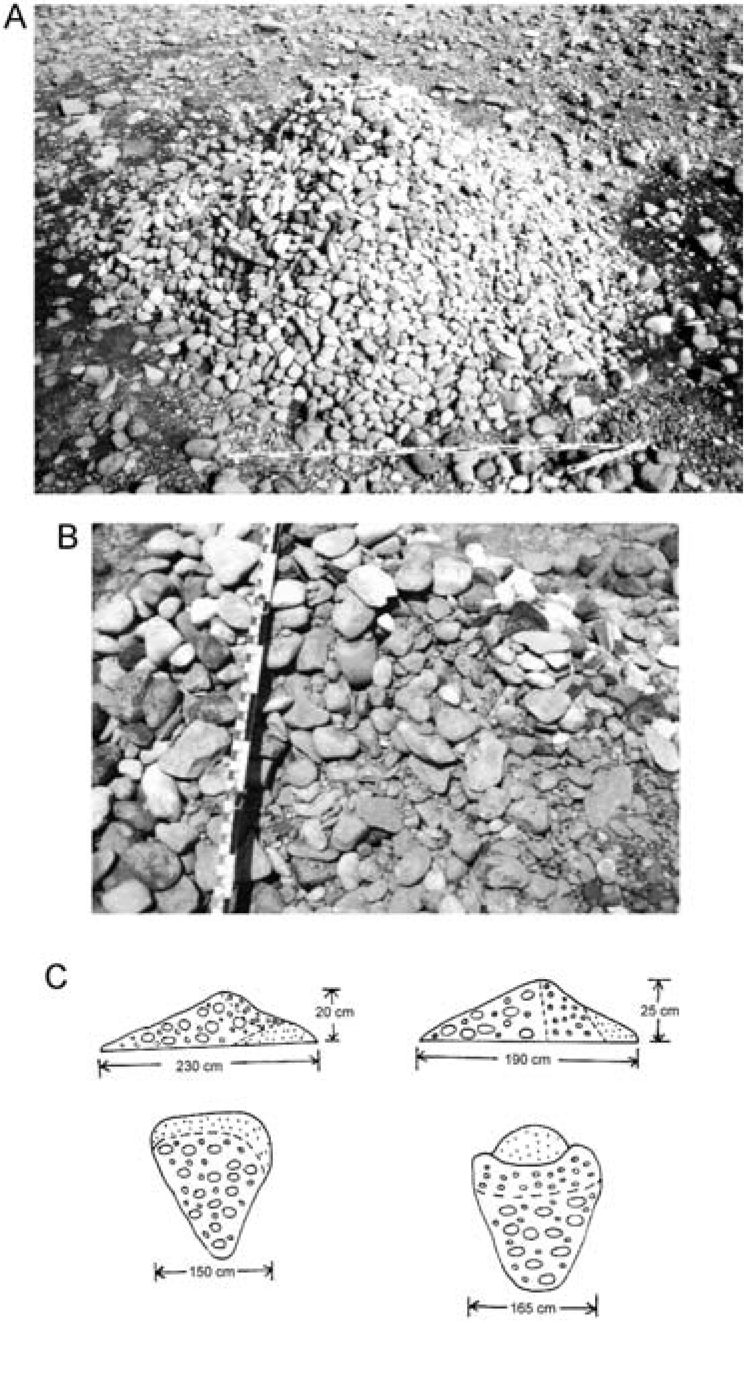

Fig. 16. Conical pebble mounds found on SB-2 (see Fig. 14 for location). (A) Surficial view (arrow indicates direction of depositing flow). (B) Vertical cut showing pebbles with granules as matrix. (C) Schematic diagrams of two mounds, showing some secondary reworking and streamlining by water current.

(b) The thickness of the emerged part was determined by surveyed transects.
(c) The submerged thickness of the bar was estimated by assuming that no bar was present at that location prior to 1963 as is the case for other present, small, undisturbed distributaries in the area (Figs 2 & 3), and that the depth of the channel at this location was similar to that of the present channel of the Mattagami River just upstream from the confluence with Adam Creek. This upstream reach of

the river has remained essentially unchanged since dam construction. The average depth from each of the echo-sounding transects in this upstream reach was determined and assumed to represent the vertical thickness of the bars below water level. This value was added to the emerged thickness for each bar and an average estimated total thickness was determined for each bar (Mosher, 1997).

2 The volume of the various sediment facies in the bars was estimated assuming that the facies observed at or near the surface persist for the total thickness of the bar at those locations. This is only a first approximation because, in reality, the sediment composition may vary with depth and the various facies probably are time-transgressive in a downstream direction. Furthermore, coarse-grained bars such as those studied may have undergone numerous erosion and deposition events, rendering an orderly facies architecture improbable.

3 The volume occupied by the various sediment class sizes in the bars was estimated in the following way (Mosher, 1997). The gravel facies were estimated to contain, on average, approximately 15% sandy matrix. For sandy facies and for interstitial sand in gravelly deposits, the percentage of coarse, medium to fine, and very fine sand to silt fractions was estimated using sieve analyses. The previously calculated volume of each facies was partitioned into its different particle-size components, thus providing the volume occupied by each particle size class (Table 4).

4 The type and amount of sediment produced by erosion from the banks of Adam Creek has been estimated by measuring representative sections along the canyon walls and extrapolating the values through the lower reaches of the creek (Skinner, 1973; Mosher, 1997). The relative amounts of each size class in each exposed stratigraphical unit were expressed as percentages of the sections measured (gravel = 9.5%, sand = 22.8%, fines (silt and clay) = 67.7%). On first approximation, these fractions were assumed representative of the material eroded from the HBL part of Adam Creek (Mosher, 1997). Ontario Hydro has estimated that 52 million m^3 of material has been eroded from Adam Creek between 1963 and 1993. Based on the stratigraphical data, it therefore can be estimated that over 35 million m^3 of the eroded material was fine sand, silt and clay, 6.5 million m^3 was medium sand, 5.3 million m^3 was coarse sand, 3.5 million m^3 was pebbles, and less than 1 million m^3 was cobbles and boulders. The boulders and cobbles combined thus represent less than 5% of the total material eroded from Adam Creek.

DISCUSSION

Managed river floods

Along a regulated stream, most of the sedimentary load generally gets trapped in the artificial reservoir and the water released from the dam is essentially sediment-free; thus it has great erosional power causing bed degradation downstream near the dam (Taylor, 1978; Petts, 1979, 1984; Williams & Wolman, 1984). The situation in the Mattagami River is somewhat different in that the river water was almost sediment-free prior to impoundment, so that its power of erosion has not changed significantly as a result of regulation. Upstream from the dams, the Mattagami River flows over resistant bedrock covered by a thin layer of overburden, so there is not much sediment to be eroded. Downstream from the last hydroelectric station, the river eventually crosses the soft, sedimentary rocks of the Hudson Bay Lowland, which are overlain by thick layers of glacial and post-glacial sediments. With the exception of a pool just below the last (northernmost) hydroelectric generating station and the section of the channel at or just below the confluence with Adam Creek, no significant channel modification has occurred along the Mattagami River since impoundment because: (a) the channel was already at quasi-equilibrium with the original stream flow, (b) the river bed was already partially armoured by numerous large boulders (a legacy of reworked underlying tills) and (c) the magnitude of the erosive spring floods has been reduced by diversion of meltwater through the Adam Creek spillway.

The large quantity of floodwater diverted along the spillway has, instead, drastically modified parts of the channel of Adam Creek creating a deep wide canyon and a 5-km stretch of the Mattagami River where gravelly bars have developed. In Adam Creek there are two types of flow: (a) occasional, large, flash spring

Table 4. Volumetric amount of the variously sized particle in the bars.

Grain size	Boulders	Cobbles	Pebbles	Coarse sand	Medium sand	Fines (fine sand to clay)
Volume (m^3)	285 726	927 157	556 218	502 454	100 566	40 859

floods with discharges greater than 3000 $m^3 s^{-1}$, and (b) regular, spring floods with average discharge of 1200 $m^3 s^{-1}$ (Ontario Hydro, 1987, 1993). The original, small, tortuous, meandering creek (about 25 m wide) was much too small to accommodate such discharges, and massive erosion occurred, mostly during the first few floods. Strong erosion has continued since then, but at a decreasing rate, because the channel had enlarged significantly and adjusted to the floods, and the channel profile has adjusted to a more gradual slope. There is still an erosional feedback between the secondary floods and the large floods: the secondary floods gradually erode the banks by undermining and fostering slumping, thus continually congesting the channel; and the large floods clear the channel out by reworking the slumped deposits, so that the entrenched channel of Adam Creek gradually widens.

The maximum flow speed through the mouth of Adam Creek was estimated to be 4.0 m s^{-1} and 3.9 m s^{-1} for the largest floods of 1979 (4535 $m^3 s^{-1}$) and 1996 (4391 $m^3 s^{-1}$), respectively. These values are slightly smaller than the critical speed of 4.7 m s^{-1} calculated for transport of the largest boulders observed on the bars (Table 1). However, the calculations of the speeds involved assume that the discharge at the mouth of Adam Creek is the same as the discharge at the gates of the headpond approximately 36 km upstream. Any increase in water discharge resulting from basin drainage would increase the water speed at the mouth and most likely account for the apparent difference (0.7 m s^{-1}) between the calculated flow speed and the speed required for movement of the boulders. In any case, the largest boulders observed on the Jn bar were probably moved through Adam Creek during a few extreme floods when the channel slope was steeper than the present.

Flow and sediment dynamics at the confluence

Flow at the confluence of Adam Creek and the Mattagami River is similar to that described by Best (1986, 1987, 1988); that is, it consists of zones of relative flow stagnation, flow deflection, flow separation, maximum velocity, gradual flow recovery and several distinct shear layers associated with vortex generation (Fig. 17).

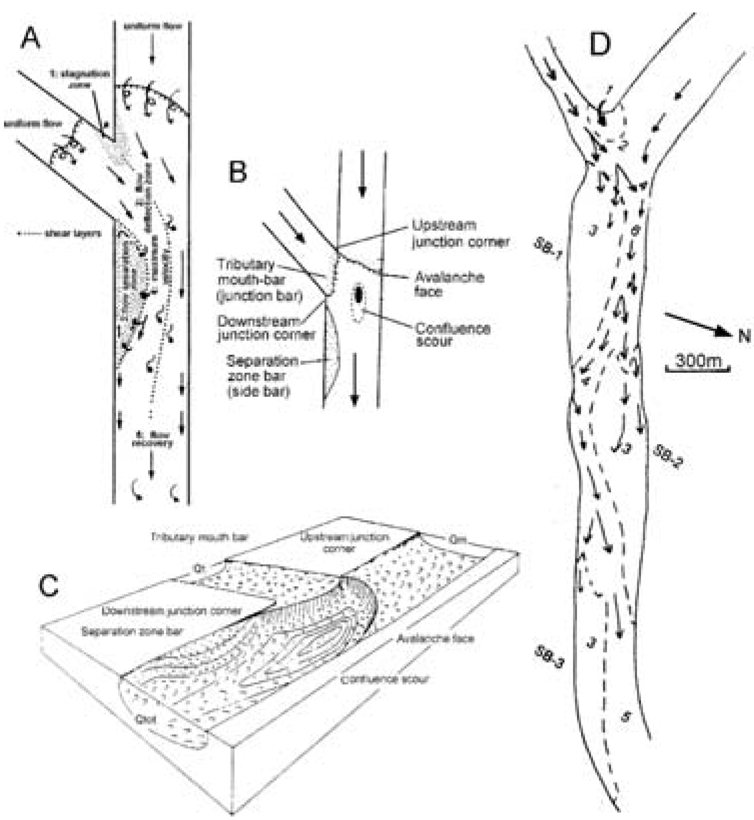

Fig. 17. Diagram showing schematic flow features at the confluence of two streams. (A) Plan-view model for an asymmetrical confluence (after Best, 1987). (B & C) Diagrams showing bed morphology and depositional features developed at asymmetric confluences (B = plan view; C = three-dimensional illustration). (D) Inferred flow paths (arrows) during high floods at the confluence between Adam Creek and Mattagami River, showing zones of flow stagnation (1), flow deflection (2), flow separation (3), area of maximum velocity (4), area of gradual flow recovery (5) and area of distinct shear layers (6). Most parts of the bars are submerged during extremely high floods.

1 Stagnation of flow occurs at the upstream junction corner and a relatively low amount of fine-grained sediments is deposited there.
2 The zone of deflection occurs along the terminal end of the Jn bar along the narrow channel of the Mattagami River.
3 This zone of flow separation that occurs immediately downstream from the confluence is very distinct owing to the development of the large SB-1 bar. The zone at this confluence occupies more than half the width of the original channel. Its large size is a function of the high junction angle (70°) and the recurring high-magnitude floods of Adam Creek (Modi *et al*., 1981; Best & Reid, 1984; Best, 1986). Best (1986) and McGuirk & Rodi (1978) stated that a shear layer is created along the boundary between the separation zone and the zone of maximum velocity (Fig. 17A). These zones differ in that the separation zone has a low-speed, recirculating flow, and the zone of maximum velocity has a high-magnitude flow. Sandy deposits on downstream parts of SB-1 evidence the recirculating flow or back eddying.
4 The zone of maximum velocity occurs along the narrow channel between SB-1 and the left bank of the Mattagami River. Scouring has deepened the channel to 8 m.
5 The zone of flow recovery begins in the channel along SB-3 where there is a reduction of flow speed and mixing of the waters from Adam Creek and the Mattagami River.

The main flood events occurring in the study area are as follows.
1 Large floods exiting Adam Creek expand into the Mattagami River with an immediate decrease in flow speed and thus in competence, resulting in deposition of sediment at the confluence in the form of a junction bar (Jn) that is characterized by several chutes and chute bars, and a first side bar (SB-1).
2 During high floods, the combined flow of the Mattagami River and Adam Creek accelerates past bar SB-1 and part of it impinges on bar SB-2. A large upstream chute is generated and diverts flow on to bar SB-2, thus developing local chute bars and downstream drainage channels. Part of the flow is deviated downstream and, upon acceleration, forms a similar chute system, albeit smaller, on bar SB-3. In addition, during some of the high flood stages, the side channels of the three side bars are reactivated.

Coarse-grained flood-bar deposits

Of the 52 million m^3 of sediment eroded from Adam Creek (Ontario Hydro, 1993), only 2.5 million m^3 (less than 5%: the coarsest fraction) is stored in the bars formed at the confluence along the Mattagami River (Mosher, 1997). The rest is carried farther downstream with the finer fractions, possibly all the way to James Bay more than 100 km to the north (Poehlman, 1996). The bars are mainly composed (approximately 1.8 million m^3) of cobbles, pebbles and boulders and a smaller amount (0.72 million m^3) of coarse sand.

McGowen & Garner (1970) have previously described coarse, sandy bars. Although similarity exists between the bars described by McGowen & Garner (1970) and those of the Mattagami River, the predominantly coarse-grained materials of the latter impede development of numerous structures, in particular cross-beds. Although the Mattagami River bars are abundantly ornamented by surficial erosional and depositional forms, the internal structures, where visible, are consistently massive in gravelly beds and plane to very locally cross-bedded sandy units toward the downstream tip of the bars. Possible inclined accretionary units can develop on the flank of the bars toward the main river channel at some flood stages, but most are removed during high flood stages when the discharge is funnelled into the narrowed main river channel (Fig. 17D). Channel-pool fillings with coarse cross-stratified units are expected to develop during receding flood stages and movement of pebbles continues to some extent during low flow from the upstream platform into the pool of maximum flow velocity near the stream junction. These deposits could not be observed directly as they are not exposed. Inclined units are expected to develop also in parts of chute bars (McGowen & Garner, 1970), but most of the chute deposits of the Mattagami River bars are too thin and coarse grained (boulders to coarse pebbles) to form distinctive cross-beds.

The strong fluctuation in discharge and the abundant variety of material available leads to significant variations in grain size in the deposits, with finer particles being deposited interstitially in coarse-grained frameworks and as drapes in pools. This leads to coarse-grained deposits irregularly alternating with isolated, thin lenses of finer gravels and/or sands. Well-developed sandy cross-beds represent filling of bar-top pools (part of secondary drainage chutes) or the downstream avalanche face of the bar itself.

The deposits of these bars are diagnostic of flood conditions, and the distribution of their facies is diagnostic of river-confluence settings. They therefore could be readily recognized in a geological record of valley fills, but they would not be easily distinguishable as channel-confluence features in more complex coarse-grained, aggradational fluvial deposits where numerous erosional events alternate with depositional ones. Only the stratigraphical relationships between various distinctive channel and interchannel depositional units can ultimately reveal the palaeomorphological settings.

CONCLUSIONS

Adam Creek is a managed spillway that experiences short-lived, seasonal, high floods (up to 4535 $m^3\ s^{-1}$) causing major erosion. Its morphology has changed from a tortuous meandering, shallow (less than a few metres) and narrow (less than a few tens of metres) channel to a large, straighter canyon, approximately 200 m wide and 30 m deep in the lower 15-km-long reach where it crosses soft sediments and rocks of the Hudson Bay Lowland. Much of the erosion of this canyon probably was accomplished rapidly during the first few large floods, and continued by cutting into the bank composed of Pleistocene till, glaciolacustrine deposits, and poorly cemented Mesozoic lignite-bearing clastic rocks. Approximately $52 \times 10^6\ m^3$ of material has been eroded from the lower reaches of Adam Creek, the vast majority of which is silt to medium sand (approximately 70%). Approximately $2.5 \times 10^6\ m^3$ of gravelly to coarse sand has been trapped in bars at the confluence of Adam Creek and the Mattagami River. The remaining $49.5 \times 10^6\ m^3$ of finer sediment has been transported farther downstream, some to James Bay located more than 100 km to the north.

The original, wide meander of the Mattagami River at the confluence with Adam Creek has been modified along a 5-km stretch, with the formation of a junction bar and several alternating side bars. Along this reach, the Mattagami River channel has become narrower (from more than 300 m to less than 100 m approximately) and has been deepened from about 2 to 8 m (during low summer flows) where constricted by the bars, and the flow speed has increased enough to locally enable the transport of loose pebbles at low summer flows.

The bars have formed in the area of abating maximum flow velocity at the confluence (junction bar), and in the alternating zones of flow separation (side bars). Farther downstream, shoals have developed in the area of gradual flow recovery. The architecture (chutes and channels) of the junction bar is determined by boulders strewn during the maximum floods; however, its surface is modified by recurring annual floods. The deposits consist mostly of very coarse bouldery to pebble gravels. The clasts are generally imbricated upstream, but do not always show preferred orientation of the long axes.

Upstream erosional chutes characterize the side bars. Most chutes terminate into chute bars on top of the main bars, by a side channel, and by slightly inclined terraces. The floodwater funnelled on the bars and side channels eventually returns to the main stream through small drainage channels that develop secondary chutes and chute bars. The main bodies of the bars are formed by sandy (coarse sand) gravels (pebbles to small boulders). The coarse clasts show good upstream imbrication of the *a*/*b* plane, but generally multimodal orientation of the *a*-axis. Several features mark the surfaces of the bars, which are diagnostic of their origin when observed on the recent surface of the bar, some clearly related to ice rafting and pushing and therefore indicative of the cold-climate setting. However, several features may be difficult to recognize in cross-section in ancient deposits, especially those diagnostic of cold-climate setting. These features include linear scours by tree roots dragged by the water flow, coarse transversal ribs, numerous shadow deposits around boulders or tree-trunks, local thin aeolian sandy deposits, scours by ice-pushed boulders, and local, conical mounds of well-sorted medium-sized pebbles formed by ice-rafted clasts released in moulins within or among ice blocks. Frost-fractured clasts found on recent surfaces may instead be diagnostic albeit proportionally rare features for interpreting ancient cold-climate deposits.

Internally, the sandy gravels are generally massive, and the gravelly sands are massive to plane bedded. At the downstream tip of the bars, local cross-beds develop as the pebbly sand is moved from the bar top to the bar end. Ripple cross-laminated sand occurs in patchy areas on the bars. Numerous small-scale ripple marks are found on thin silty and sandy veneer deposited during receding floods on limited surfaces of downstream parts of the bars. These diagnostic bar deposits can be readily preserved in the geological record, and would provide good information on flood events and stages, but their river-confluence origin could only be recognized in the context of the associated stratigraphical units.

ACKNOWLEDGEMENTS

Numerous individuals and organizations helped to complete this research. We thank Kevin Buddell, Steve Sadura and Michelle Hawke for their help in the field. We are grateful to M. Peréz and other unknown reviewers who were very helpful in showing the shortcomings and solutions for the finalization of the manuscript. The following organizations graciously contributed equipment: Canada Centre for Inland Waters (CCIW), Department of Fisheries and Oceans, Environment Canada-Water Survey Division, Ontario Geological Survey and Ontario Hydro. Funds were provided by a NSERC Grant to I.P.M. (0GP0007371). S. Sadura helped in making an early version of the manuscript more readable, and in finalizing the figures.

REFERENCES

Best, J.L. (1986) The morphology of river channel confluences. *Prog. phys. Geogr.* **10**, 157–174.

Best, J.L. (1987) Flow dynamics at river channel confluences: implication for sediment transport and bed morphology. In: *Recent Developments in Fluvial Sedimentology* (Eds Ethridge, F.G., Flores, R.M. & Harvey, M.D.), Spec. Publ. Soc. econ. Paleont. Miner., Tulsa **39**, 27–35.

Best, J.L. (1988) Sediment transport and bed morphology at river channel confluences. *Sedimentology* **35**, 481–498.

Best, J.L. & Reid, I. (1984) Separation zone at open channel junctions. *J. hydraul. Eng.* **10**, 1588–1594.

Chapman, L.J. & Thomas, M.K. (1968) *The Climate of North Ontario*. Climatological Studies, no. 6, Meteorological Branch, Department of Transport Canada, Toronto.

Costa, J.E. (1983) Paleohydraulic reconstruction of flash-flood peaks from boulder deposits in the Colorado Front Range. *Geol. Soc. Am. Bull.* **99**, 986–1004.

Hutton, C.L.A. & Black, W.A. (1975) *Ontario's Arctic Watershed*. Map Folio, no. 2. Mutual Press, Ottawa.

McGowen, J.H. & Garner, L.E. (1970) Physiographic features and stratigraphic types of coarse-grained point bars: modern and ancient examples. *Sedimentology* **14**, 77–111.

McGuirk, J.J. & Rodi, W. (1978) A depth average mathematical model for the near field of side discharge into open channel flow. *J. Fluid Mech.* **86**, 761–781.

Modi, P.N., Ariel, P.D. & Dandekar, M.M. (1981) Conformal mapping for channel junction flow. *J. Hydraul. Div., Am. Soc. Civil Eng.* **107**, 1713–1733.

Mosher, S.-J.R. (1997) *Deposition of gravelly bars at the junction of two regulated streams in northern Ontario: Mattagami River and Adam Creek*. MSc thesis, University of Guelph, Canada.

Ontario Hydro (1987) *Mattagami River Hydroelectric Development Smoky Falls GS Extension and Bank Erosion Study 1986*. Geotechnical Investigation Results and Evaluation, Report no. 87049, Montreal.

Ontario Hydro (1993) *Preliminary Assessment of Adam Creek*. Hydroelectric Developments Department, Erosion Process Report no. 935028, Montreal.

Petts, G.E. (1979) Complex response of river channel morphology subsequent to reservoir construction. *Prog. phys. Geogr.* **3**, 329–362.

Petts, G.E. (1984) *Impounded Rivers: Perspective for Ecological Management*. J. Wiley & Sons, Chichester.

Poehlman, T.N. (1996) *Fluvial and sediment dynamics at the head of a subarctic estuary affected by human activity, Moose River, Moosonee*. MSc thesis, University of Guelph, Canada.

Skinner, R.G. (1973) Quaternary stratigraphy of the Moose River Basin, Ontario. *Geol. Soc. Can. Bull.* **225**, 77 pp.

Taylor, K.V. (1978) Erosion downstream of dams. In: *Environmental Effects of Large Dams*, pp. 165–179. International Commission on Large Dams, U.S. Commission, American Society of Civil Engineering.

Williams, G.P. & Wolman, M.G. (1984) Downstream effect of dams on alluvial rivers. *U.S. geol. Surv. Prof. Pap.* **1286**, 7–64.

Spec. Publs int. Ass. Sediment. (2002) **32**, 233–49

Comparison of the flood response of a braided and a meandering river, conditioned by anthropogenic and climatic changes

G. GARZÓN* *and* A. ALONSO†

**Dpto de Geodinámica, Fac. de Geología, Universidad of Complutense, 28040 Madrid, Spain (Email: minigar@geo.ucm.es); and*

†Sección de Ciencias de la Tierra, Fac. de Ciencias, 15071 La Coruña, Spain

ABSTRACT

The effects of floods in the last decade have been studied in two tributaries of the Tajo River in the Tertiary basin of Madrid (central Spain). Although the streams flow parallel to each other, one, the Jarama River, has a meandering pattern with gravel bedload, and the other, the Guadarrama, is braided with sandy bedload. In spite of their planform differences, the main effects of flooding on both rivers have been channel incision, widening and straightening, with meander cut-offs. Both rivers show similar recent behaviour, mainly because of the loss of discharge and bedload.

The decrease in the discharge is related to dam construction and water pumping for irrigation, whereas the bedload has been reduced as a result of gravel mining, either directly from the channel bed, or from areas on the floodplain connected to the channel. These effects have been identified in aerial photographs from 1956 onwards, although it is since the 1970s that these processes have become acute. The study of historical maps and older aerial photographs reveals that some of the effects may have started even before 1956. Furthermore, the sedimentary record of the floodplain shows intense aggradation since the beginning of last century, indicating that channel incision is not just a recent anthropogenic effect but a natural tendency of the rivers, which may be related to long-term adjustment to changing climate conditions. After a significant period of alluviation and aggradation, the rivers are now going through a new entrenchment stage, with the anthropogenic activity enhancing the natural trend.

INTRODUCTION

The Guadarrama and Jarama are two tributaries of the Tajo River, which drain an important intracratonic Tertiary basin in the Central Iberian Peninsula (Fig. 1). Although both streams flow parallel to each other and have very similar geological and environmental conditions, they have different planform patterns and bedload. Their sources are both in the Central Spanish Cordillera and they run across the clastic sediments of the Tajo depression. However, whereas the Guadarrama channel shows a braided pattern with sandy bedload, the Jarama is a medium-sinuosity meandering stream with gravel bedload.

In recent years, floods of these two rivers have led to major economic losses and have therefore aroused social alarm. The notable increase in damage is not the result of unusual natural events but of intensive human occupation of the floodplain, and even of some parts of the channel. The anthropogenic activity on the watershed in recent years has induced alterations in channel dynamics and local magnification of processes.

Despite the proximity of these river beds to the major city of Madrid, there are few detailed studies of their characteristics and behaviour in flood situations. The Jarama River is a gravelly meandering river of sedimentological interest, and its deposits are economically valuable. Although there has been a long history of morphological studies on the Jarama terraces (Hernández & Aranegui, 1927; Riba, 1957; Asensio & Vadour, 1967; Lopez & Pedraza, 1976; Cabra *et al*., 1983) and Pleistocene deposits (Pérez-González *et al*., 1974; Pérez-González, 1980; Arche, 1983; Silva *et al*., 1988; Alonso & Garzón, 1994), it is only since the recent floods that river variability and flood behaviour have been taken into account (Garzón

Flood and Megaflood Processes and Deposits: Recent and Ancient Examples. Edited by I. Peter Martini, Victor R. Baker and Guillermina Garzón ISBN: 978-0-632-06404-5

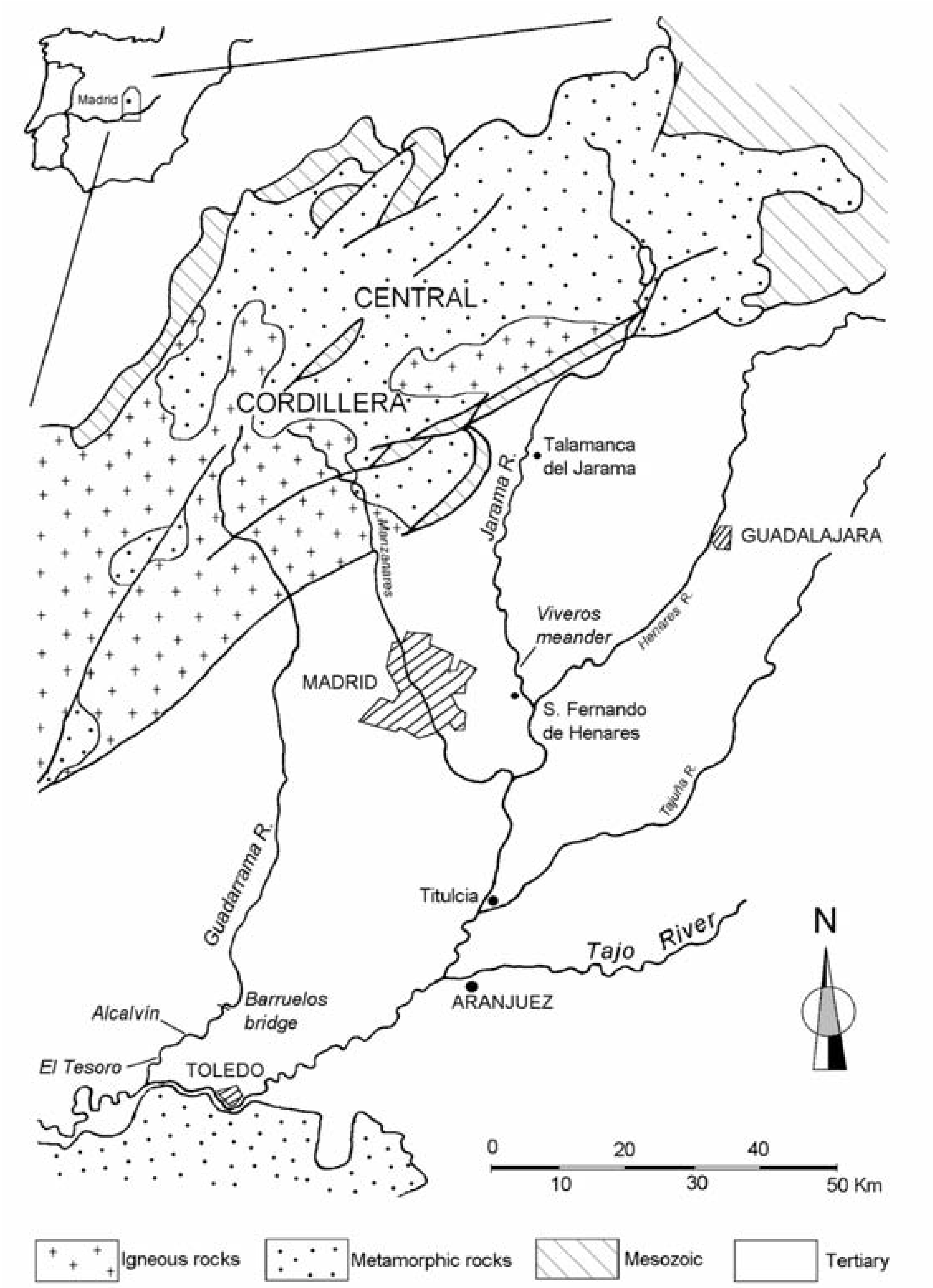
Madrid
CENTRAL
CORDILLERA
Talamanca
del Jarama
Jarama R.
Manzanares
GUADALAJARA
Viveros
meander
Henares R.
MADRID
S. Fernando
de Henares
Tajuña R.
Guadarrama R.
Titulcia
N
Tajo River
ARANJUEZ
Barruelos
bridge
Alcalvín
El Tesoro
TOLEDO
0
20
40
10
30
50 Km
Igneous rocks
Metamorphic rocks
Mesozoic
Tertiary

et al., 1990, 1992; Garzón & Alonso, 1995; Alonso & Garzón, 1997). With regard to the Guadarrama, there is only one report on channel morphology and sedimentology (Garzón & Alonso, 1996).

Although the two rivers present different characteristics, geological and physiographic conditions are very similar; therefore the first objective of this study is to interpret and compare their natural evolutionary trends. For this reason the study is designed as a comparative analysis of responses to floods, and of recent channel changes. In this way it is possible to distinguish between intrinsic or human-induced conditioning, and to derive climatic deductions.

Since the introduction of the concept of river pattern metamorphosis (Schumm, 1968) and its climatic and anthropogenic controls, much literature has been published on Holocene channel variability (Gregory, 1977; Petts *et al.*, 1989; Gurnell & Petts, 1995). As observed by Starkel (1995) and colleagues, channel changes have been especially intense in central and western Europe, where glacial periods drastically affected the fluviatile environment. Most studies therefore have dealt with these areas, where the extensive floodplains, rich in organic material, are suitable for dating and pollen analysis. Furthermore, there has been increasing interest in channel restoration in these countries.

Not much work has been done, however, on the Holocene and Recent evolution of Mediterranean areas, and more specifically on the Iberian Peninsula. In these regions, rivers are controlled mainly by channel incision, and changes in the water–sediment budget are more clearly reflected in aggradation/incision stages; channel patterns are controlled mostly by bedload type and slope. During the Pleistocene evolution of the Jarama River terraces, the present meandering trend of the river was preserved during the different incision stages, and only changes in discharge and in bedload size could be identified between them (Alonso & Garzón, 1994). In a first compilation of Mediterranean Quaternary river environments, Lewin *et al.* (1995) summarized the complex response of these alluvial systems and stated that there are several superimposed factors: tectonic activity, well-differentiated seasonality, and intense anthropogenic influence already apparent after 8000–5000 yr BP. Specific studies on the Iberian Peninsula confirm this complexity and the present difficulty in establishing a good correlation of events. Mather *et al.* (1995) and Harvey (1984) document the last important incision, which occurred during the Würm–Holocene period in south-east Spain. Macklin & Passmore (1995) recognized aggradation during the last dry-humid stage of the last glacial period in the Ebro Basin. The beginning of the Holocene Jarama terrace has been dated to at least around 6000 yr BP (Alonso & Garzón, 1994). Before that, a deep dissection of about 20 m had occurred in the late Pleistocene terrace.

The aim of this research therefore is to identify criteria with which to determine whether the present trends of entrenchment and straightening of both rivers are the result only of the direct or indirect action of man, or whether there is a pre-existing natural tendency as a response or adjustment of these systems to climatic changes.

Several methods have been used: analysis of the present morphology, sedimentological study of outcropping materials in terraces and in the floodplain, measurement and description of the morphology in the river bed as well as those deposited after a flood. Follow-up work has been carried out on channel evolution, control of erosion of river banks, migration of bars and large forms. In addition, the characteristics of fine layers, pedogenic levels and minor structures in the floodplains were analysed, with wood samples obtained for radiocarbon dating and characterization. At the same time, an extensive study was carried out on the principal human activities that could possibly have affected the system, particularly those concerning losses in discharge and load, artificial changes in the shape and characteristics of the channel, and activities on the floodplain such as construction and excavation. Recent river variability was studied by temporal comparison between historical maps and aerial photographs in order to establish the beginning of river changes.

The rivers studied flow across semi-arid areas and have great hydrological irregularity, with well-defined low-water seasons. Bedload is mobilized during flood stages. Rivers also have low suspended load owing to the low rate of chemical weathering in the basin. Existing general sedimentological models usually deal with aggrading systems, whereas these Spanish rivers are clearly in a state of degradation. The study of such rivers can provide sedimentological and morphological information about the response of this type of river during floods, which could be crucial for prevention of damage in such situations. In addition, analysis of the deposits and morphological changes of such rivers during the last two centuries provides some

Fig. 1. (*opposite*) Location of Jarama and Guadarrama rivers and geological map (Tajo Tertiary basin, central Spain).

information on climatic changes with respect to the displacement of climatic belts toward the north, and the increase in the incidence of catastrophic floods.

THE BRAIDING GUADARRAMA RIVER

The Guadarrama River (from the Arabic *Wadi-al-rambla*, meaning 'stream of sands') has medium-grained sand bedload derived from the Central Cordillera granitic piedmont. The middle reach of the river maintains a constant slope and a braided pattern. In the lower reaches, there is a change in regional slope from 0.2% to close to 0.3%, significant enough values for pattern changes. In fact, the morphology of the stream indicates a significant increase in sinuosity, but at the same time maintaining a braided pattern.

As in any braided system, the channel bars are complex and have high lateral mobility (Garzón & Alonso, 1996). Bars are located centrally in the channel or laterally attached to the banks, and are planar crested and migrate downstream. They have superimposed megaripples (three-dimensional dunes) and linguoid ripples, forming planar or trough cross-bedding on bar sections. This same channel pattern is reflected in the floodplain sections, which exhibit sandy sets with troughs and occasional cross-bedding, corresponding to the braid bars (Fig. 2). They are capped by silty sands with ripples and sandy lenses, representing sand wedges and ripple migration in less active areas. Overbank deposits consist of fan-shaped bodies built up by sandy wedges with high-energy planar bedding, and distal silts with ripples.

Flood effects and the modified channel response

After a 5-yr drought, rainfall was relatively intense throughout the Iberian Peninsula in the winters of 1996–1998. As a consequence, there have been recurrent major flood episodes in many parts of the country. Significant flooding occurred in the Guadarrama River during the winters mentioned above, which enabled sufficient field data to be collected to deduce that, although the dynamics of the Guadarrama River are consistent with the characteristics of a braided channel, its flood response has been somewhat unusual. Floods in a braided river normally are expected to occupy a wide active channel at the bottom of the valley, mobilize the bars, and perhaps reactivate some that are vegetated. In the Guadarrama River, instead, the flood led to incision of the channel, formation of erosive swales in the floodplain and widening of the pre-existing narrow chutes. These effects and their immediate consequences were analysed in detail on two river reaches, Barruelos Bridge and Tesoro meander. They represent two types of chute cut-offs at stream bends, one in an area with significant channel entrenchment, and the other with little entrenchment, although, in both cases, the river clearly shows an important bedload deficit.

Chute cut-off in a slightly entrenched lobe (Tesoro meander)

The site known as Tesoro meander is located on the lower stretch of the river in a sector of fairly high sinuosity (Fig. 1). The sinuous channel is narrow (30 m) and deep and may be incising into the substrate given that soft intraclasts have been found, and the thickness of the alluvial layer is not over 1 m (Fig. 3). This incised channel is the only functional one, and its entrenchment inhibits lateral migration because its banks are protected by dense riparian vegetation.

As shown in aerial photographs, this meander lobe had already been cut off before 1945 (Fig. 3a). After that, it gradually widened and shifted upstream, but

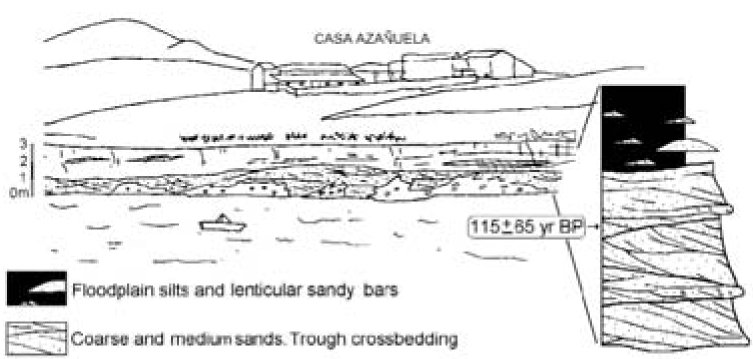

Fig. 2. Floodplain sedimentological section at Barruelos Bridge, on the Guadarrama River, showing braiding characteristics with a basal sandy unit and a silty unit on top (115 ± 65 ^{14}C yr BP).

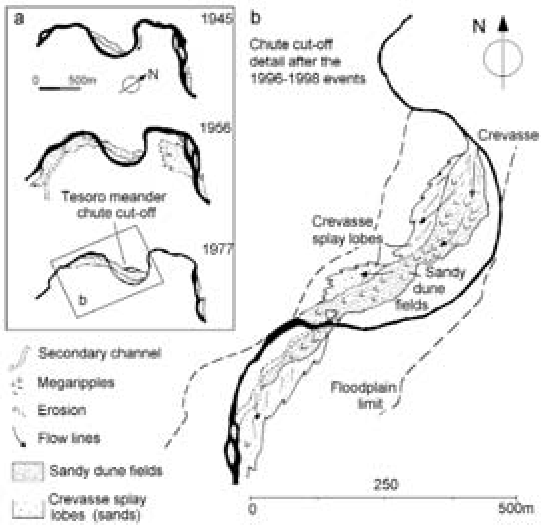

Fig. 3. Map showing chute cut-off on the Guadarrama River at the Tesoro meander. (a) Cut-off development and widening from 1945 to 1977 from aerial photographs. (b) Dune fields and crevasse splay features of the chute channel after the 1996 and 1997 floods.

the cut-off still remains active only during floods. More recent photographs show how the chute cut-off has widened, and exhibits considerable remobilization of sand within it. During the recent floods, studies reveal intense activity in the chute cut-off, as apparent in the formation of fields of straight-crested, medium- to coarse-grained sand dunes (Fig. 3b), with heights of up to 0.5 m and wavelengths of several metres. Laterally and between them silts and fine sands with linguoid ripples occur. Activity has been so great that, in the past few years, a depression artificially produced by a sand pit, visible in the 1987 photograph at the centre of the chute, has been filled and is no longer recognizable.

The general trend in the chute, then, is one of intensive downstream migration of sands: in 1996 the sandflat described previously was in the central part of the chute; in 1997 it has moved beyond the bank escarpment and splayed on the floodplain; and in 1998 it extended over the floodplain. Moreover, the last flooding episode, at the mouth of the cut-off and extending at least 100–200 m from this upper area, produced only erosion, mobilizing the sands of previous floods and transporting them downstream from the cut. It is deduced from this that there is a lack of bedload in the system; the river thus needs to reutilize its own sand, no longer entraining it from the channel but mobilizing that of previous floods to refill the new chute channel downstream.

On the inner margin of the chute, the flood deposits advanced over the plain, forming a wide crevasse-splay lobe that has grown considerably in the 3 yr of floods (Fig. 3b), as the infill material of the chute channel prograded downstream. On this margin a considerable accumulation of sand occurred, in part trapped by herbaceous vegetation on the riverbank. Beyond it, the splay lobe expanded over the plain with progressive down-flow fining. The sedimentary structures change from megaripples on the riverbank to linguoid ripples in distal muddy areas.

To summarize this river reach, floods have caused mobilization and local deposition of great amounts of material, which is consistent with the entrenchment trend inferred for the channel. Deposition can be abundant in areas of active adjustment, but there is an overall tendency to channel incision.

Chute cut-off in a lobe with significant entrenchment (Barruelos Bridge)

The Barruelos Bridge area (Fig. 4) is located at the upstream end of the sinuous stretch of the river. Here the valley forms a series of bends in which the river migrates. The tendency observed in the channel from 1945 to the present is for these bends to be cut off. Upstream of the Barruelos Bridge, the 1945 photograph shows the presence of a small incipient channel (Fig. 4a) that became a clearly defined chute channel in 1956. Later photographs taken between 1977 and 1987 show that the Barruelos cut-off was not very active and became obliterated by human activity after the building of a transverse dyke to prevent flooding. During the last floods, the old chute channel could not be reused and overbank flooding originated further downstream.

The floods carried small amounts of suspended load and therefore the effects of floods on the floodplain show up mainly as erosive grooves with deposition of small bars on the floodplain (Fig. 4b). Several water flow paths have been recognized, mapping the shape of bars left on the floodplain. The dominant flow led to the development of a main swale with long fringe-like bars deposited on either side of it, and a large fan at the end. Two other flows parallel to the principal one gave rise to another longitudinal bar and an arrow-like bar isolated on the floodplain.

Such sedimentary patterns represent flooding under conditions of major bed material deficit, owing to the channel being in an active phase of entrenchment

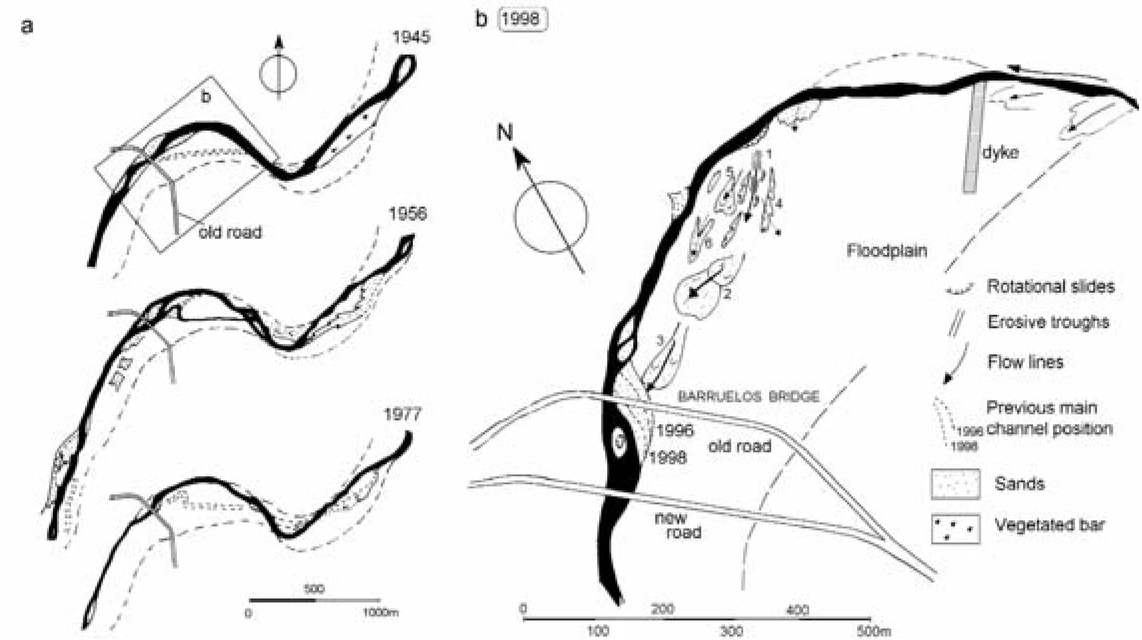

Fig. 4. Map showing flood features on the floodplain of Guadarrama River at Barruelos Bridge. (a) Evolution of the cut-off from aerial photographs after 1945. (b) Development of a chute after the 1996 and 1997 floods, with development of erosive troughs (1), fan-like deposits (2), elongated flow return bar (3), fringing bars (4), longitudinal bars (5) and arrow-like bar (6).

within a raised floodplain. In addition, the extraordinary incision occurring at this special area is exaggerated by the extraction of sands directly from the river bed a few kilometres farther downstream.

The channel responds to the entrenchment with enhanced sapping of banks, which leads to widening and migration of the bars within it. In fact, immediately downstream of the described cut-off, right on the Barruelos Bridge, the principal channel in 1996 flowed along the left margin of the bridge (Fig. 4b). Since the floods of 1997, it has been totally displaced to the right margin, eroding the bank and destroying a 30-m-wide lateral bar that was already vegetated. A new bar has been built up on the other margin, resting against the bank. It remains active as a diagonal bar only during floods, since at present the river has only one functional channel most of the time.

In summary, there is an overall entrenchment of the Guadarrama River, but its effects manifest themselves in different ways depending on local conditions. In straight stretches, and also where incision has been accelerated by human extractive activities, stream incision is followed by channel widening and bar migration. In incised curved stream reaches, where the principal channel continues to be dominant during floods, overbank flow is unable to consolidate its cut-offs and the result is only slight erosion, with the development of incipient floodplain troughs and shallow bars. The lowering of water level caused by present channel entrenchment possibly also hinders the formation of new cut-offs in the sinuous sections.

Alternatively, in the sinuous reaches where an authentic chute cut-off channel has already formed, there is headwater erosion and widening of the cut-off. There is considerable mobilization of material with the formation of dune fields that advance downstream alongside the chute. The sediment transport in these prograding areas is such that large crevasse splays have been able to spread on the floodplain. In spite of this activity during floods, the channel maintains the meandering course during low water stages.

The present incising situation of the Guadarrama River, with reduction in the width of the active channel and a net deficit of bedload supply, means that its braiding dynamics are limited to the straight stretches of the channel and to areas in which chute channel cut-off already exists. The rest of the valley bottom behaves as a raised floodplain, in which overbank flow is erosive, reactivating small troughs where mobilization and washing of older material occur.

Historical variability of the Guadarrama River

In order to evaluate the extent to which the deduced entrenchment of the river, the changes in morphology and the recent cuts are caused by recent or past human activity, a series of maps and aerial photographs have been analysed. The oldest maps available, a 1776 map of the Tajo River and a French military map of 1823, show the Guadarrama River in sufficient detail to accurately estimate changes that have occurred since then. However, its downstream section seems to be less sinuous than the present one, and the Tesoro meander is barely distinguishable. One outstanding feature is the change at the river mouth. In the 1823 map, the river is straight and does not show the meander that exists nowadays. It is possible that this new course developed through reutilization of an old meander of the Tajo River, as this area is part of the Tajo River floodplain that is characterized by meander scars. The recent activity of this last Guadarrama River meander is also shown by the undercutting of the valley slope, which has induced active landsliding.

The first detailed topographical map with contour lines, on a scale of 1 : 50 000, dates from 1882, which remained unmodified until 1944 when land-use changes were added. The 1944 map shows no meander cut-offs along the Guadarrama River. These cut-offs appear for the first time only in a 1987 map, where the Tesoro cut-off and a smaller one in the Alcalvin meander lobe were shown (Fig. 5).

The first aerial photographs in the region were taken in 1945. They show that the Guadarrama River was a sandy stream that occupied about 20–30% of the width of the valley. The channel was slightly incised, and there are some traces of recent flood deposits on the floodplain, but these are not very conspicuous because they are partially obliterated by intense land use. Some scouring activity seems to start on the floodplain, and there are incipient chute channels at some river bends. A first cut-off is shown in the Tesoro meander (Fig. 3a) and there are incipient chute channels in the Alcalvin (Fig. 5) and Barruelos (Fig. 4a) reaches.

Up to 1956 the floodplain had been very active, as indicated by the development of cut-offs and the evidence of flood deposits in numerous places. These photographs were taken in spring during high water stage; cultivation had been abandoned in those years and the maintenance and cleaning of the irrigation channels were discontinued. Even so, there is evidence that indicates river entrenchment, such as the active development of cut-offs and the mobilization of deposits along them, where the river could develop its braiding character without constraints. By that time a second cut-off had developed at the Tesoro meander (Fig. 3a), as well as the Alcavin chute cut-off (Fig. 5).

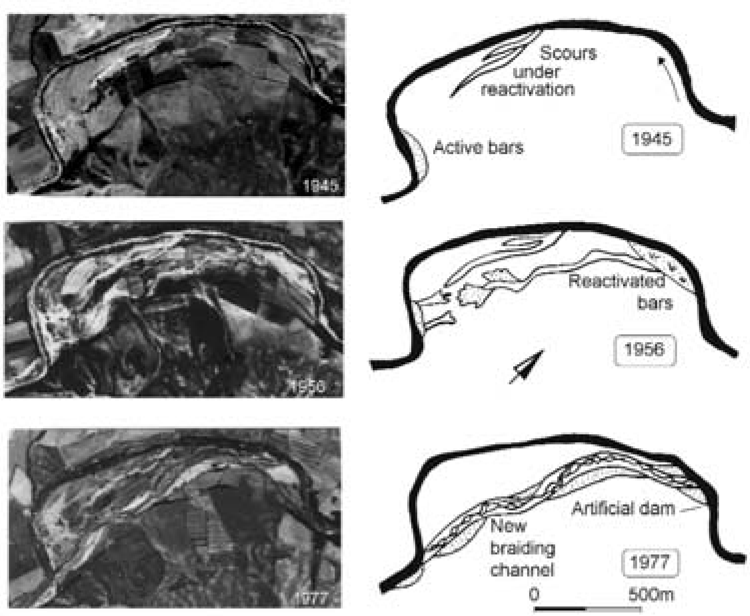

Fig. 5. Aerial photographs and map showing changes in the Alcalvin meander of the Guadarrama River. Incipient scours appear in 1945, by 1977 the chute cut-off is already formed and in 1956 a braided pattern is formed in the cut-off channel.

In the 1977 and 1987 aerial photographs, no major changes were observed from the situation of 1956; no large floods have been reported for those times. The river seems to have become less active, but the trend towards entrenchment is evident: the meander lobes remained functional but were becoming narrower and constricted by riparian vegetation and the cut-offs kept widening, In this new incised straight channel section, braiding activity is emphasized as would be expected from the increase in channel slope and high availability of mobilized material.

THE MEANDERING JARAMA RIVER

The Jarama River is a coarse bedload channel, with low sinuosity and well-developed lateral bars, corresponding to Miall's model for gravelly meandering rivers (Arche, 1983; Miall, 1985). It has developed a wide floodplain (Fig. 6a). A single fining upward sequence representing channel infill and abandonment (Fig. 6b) has been identified in this floodplain unit (Alonso & Garzón, 1994). It displays basal gravels that form a sheet-like body with an erosive base, well-developed clast imbrications and large-scale lateral accretion geometry. The basal gravel is overlain by sand and gravel, in turn capped by a slightly pedogenic silt and clay deposit of the recent river floodplain. Scroll bars are separated by sand levels with trough cross-stratification and linguoid ripples representing the last stages of channel abandonment.

Recent flooding behaviour under artificially modified conditions

The recent dynamics of the river have been studied using aerial photographs from 1956 and a survey of the 1989 and 1991 floods. Human modifications have considerably influenced the form and type of stream response, resulting in important sedimentary and erosive effects during floods (Garzón *et al*., 1990, 1992; Alonso & Garzón, 1997). The principal human interference is the result of gravel extraction from the channel and floodplain, and dam construction upstream. Reservoirs reduce the ordinary flood discharge but do not prevent large floods.

The studied middle–lower reach of the river is characterized by entrenchment, to a variable depth, from 2.5 to 4 m. In some sectors the channel runs over older gravel bars in a continuous process of washing out and destruction, but in others the incision has reached the arkosic rock substratum.

As a consequence of incision, there is accelerated bank erosion along the river. This especially is evident in the reaches where the stream is constricted by man-made structures, such as in the proximity of Madrid

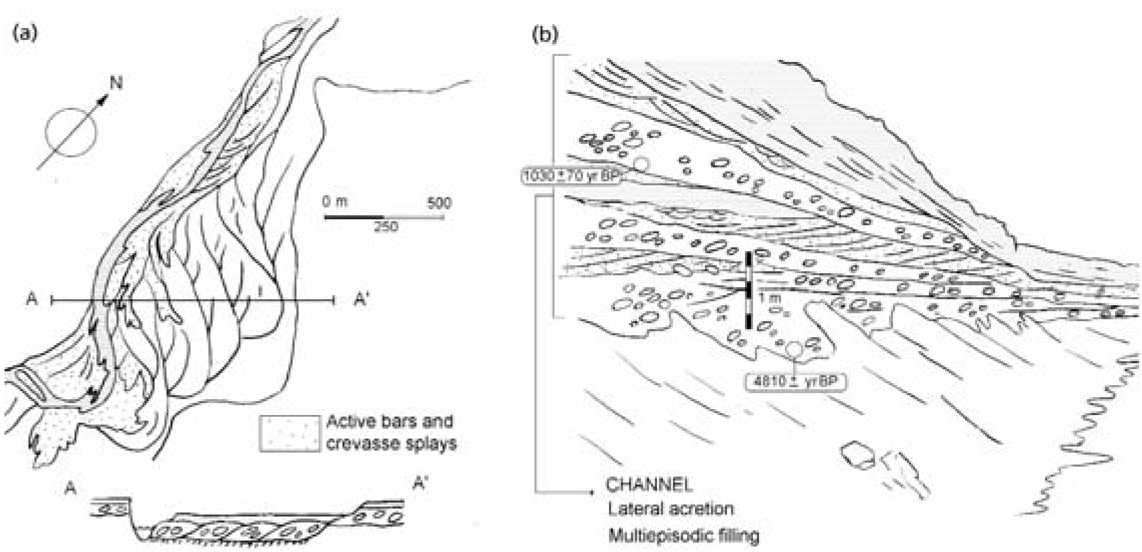

Fig. 6. Map and cross-sections of Jarama River floodplain and ^{14}C dates. (a) Map showing lateral accretion and downstream migration of meander. (b) Cross-section displaying a single fining upward succession from gravels with lateral accretion at the base, to silts and sands at top.

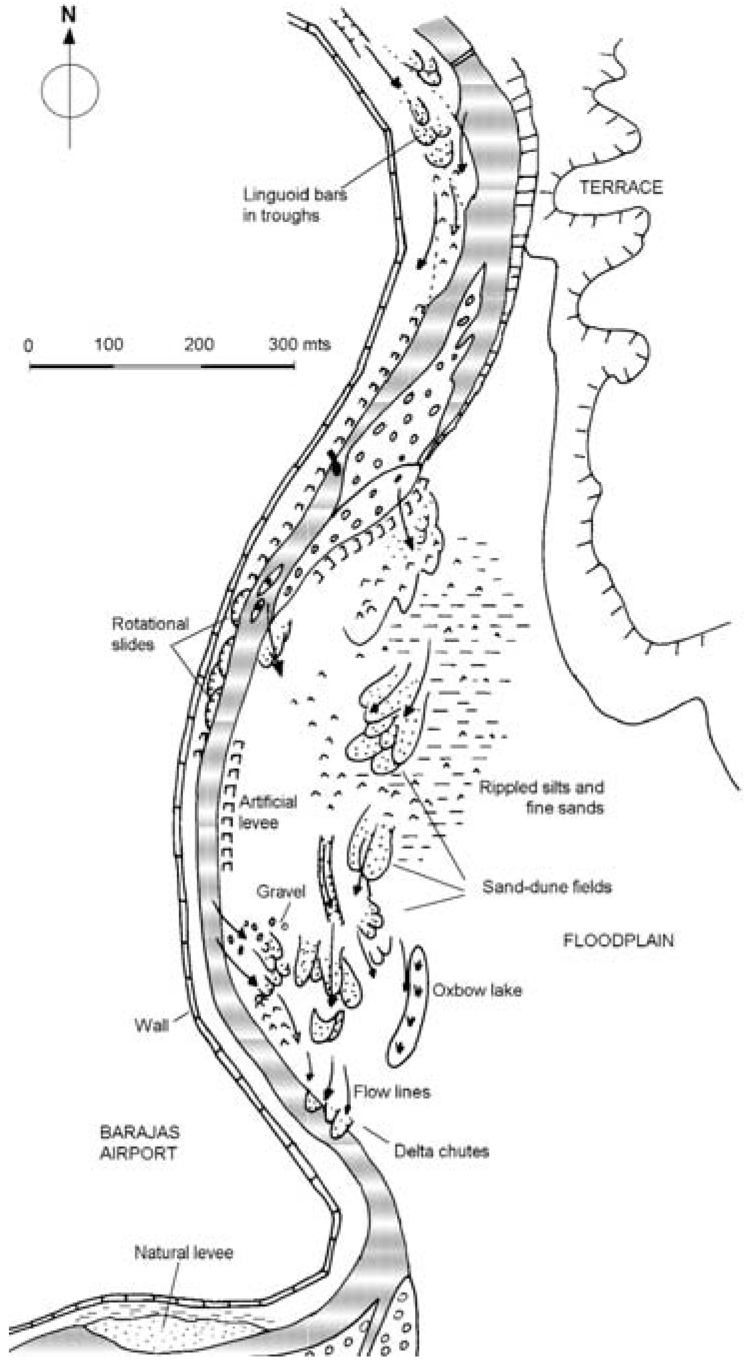

Fig. 7. Map showing features generated by 1989 flood in the Jarama River at the meander of Viveros. The flow constriction produced by the Barajas Airport wall on one bank induced the breaching of an artificial levee and overflooding on the opposite bank. The result is the building up of sand dune fields and extensive accumulation of rippled silts and fine sands.

Barajas Airport, at Viveros meander, where the existence of a wall near the river bank has caused slumps on the concave bank (Fig. 7). In the channel, some changes in the gravel bars can be seen, such as erosion, winnowing of finer clasts, concentration of coarser sizes and realignment and imbrication of pebbles.

Shallow erosion is observed in some areas on the floodplain, and, occasionally, shallow channels or depressions around obstacles are scoured following the flow lines. In nearly every situation, the erosional processes can be related to anomalous acceleration of the water flow, as a result of obstacles or previous excavations that interfere with normal expansion of the bankfull discharge.

Considering floodplain sedimentation, the former meandering trend of the river has been reduced considerably by lack of bedload on the channel as a result of gravel extraction. During flooding the river reactivates the swales and sandy linguoid chute bars are generated, up to 10 m in width and 1 m in height (Fig. 7). Chute-bar deltas were frequent in the past, according to older aerial photos and sedimentological evidence in the Pleistocene terraces (Arche, 1983), but owing to the present reduced bedload they are not common now. In the concave bank of some meanders, overbank flow has caused levee development, formed by coarse- to medium-size sand, with laminations gently sloping into the floodplain, passing laterally to fine sand and silt with linguoid ripples. The levees are about 25 cm high and 20 m wide, and are only partially preserved because of recurrent bank instability.

Floods also have broken some artificial levees, as at Viveros meander, inundating the floodplain with extensive crevasse splays of rippled silts, muds and clays (Fig. 7). At the same time, the scattered trenches excavated by anthropogenic activity on the floodplain, induced, owing to flow acceleration, the appearance of fields of lunate sand megarripples averaging 30 cm in height.

Spectacular sedimentary consequences of flooding have occurred in the numerous artificial pits excavated in the floodplain, even below the water level. These have been dug along the riverbank and usually are separated from the channel by a narrow man-made embankment, or a strip of original terrain. These quarries are responsible for the major accelerated loss of bedload, as they act as sediment traps when the levees are breached and most of the transported gravels and bars make their way into the depressions. One example studied in great detail is the reach of the river south of Talamanca del Jarama. This reach was subject to very intensive quarrying activity, which removed the gravels from the terraces, a large part of the floodplain, the lateral streams and from the channel itself (Fig. 8a). By 1989 the activity had ceased and an artificial levee running parallel to the eastern river bank was left to preserve the depressions and carry a road.

During the 1989 flood, the levee was breached in five sectors and the sedimentary effects were quite remarkable. The main breach (85 m wide) occurred at the point where a secondary channel was still functional in 1947, but completely abandoned in 1956. The gravels used to build the embankment were shifted in the process, creating spillover lobes of imbricated gravels approximately 50–110 m long and up to 1 m high (Fig. 8b). Diffuse erosion was conspicuous in the floodplain following the main flow path and, beyond the bypass zones, large fields of dunes extended on to the pit floor. A large amount of sediment was moved into the lowered floor of the pit, in part carried from the river channel and in part from the erosion of the floodplain. The sandy field is up to 150 m long and 100 m wide, with dunes up to 1 m high. The main breach was repaired soon after the episode but was again broken during the minor spring flooding of 1991, showing the instability of this reach. The river channel suffered enormous loss of bedload during this particular flood, and the river is actively downcutting, particularly in reaches immediately upstream of gravel extraction areas where the channel longitudinal profile needs to be readjusted upstream (Simons & Li, 1982).

Summarizing, the anthropogenic changes affecting the morphology of the meandering Jarama River have transformed its sedimentary dynamics, particularly during floods, owing to the loss of bedload and the concomitant increase in the erosive capacity of the water during floods. Furthermore, the straightening of the channel has increased the flow velocity and the disruptiveness of floods on the floodplain. As a consequence, floods are particularly destructive, with the breaching of artificial levees and the invasion of human-occupied areas. The main result is erosion, which is manifest in different ways, such as the cutoff meanders, rotational slides, scouring and diffuse erosion on the floodplain, and entrenchment of the river bed. The areas of sedimentation and the sedimentary forms have been modified too. Instead of meander growth and migration, the resulting sedimentary effects are limited to the reuse of swales for sand winnowing and bar migration, formation of small crevasse splays in pre-existing depressions on the floodplain and, above all, infilling of abandoned quarries, which have acted as sediment traps.

Historical Jarama River variability

Two stages have been identified in the evolution of the Jarama River (Garzón & Alonso, 1995; Alonso & Garzón, 1996): one from the beginning of the nineteenth century until the twentieth, and the other from then to now. During the first stage, the river shows a

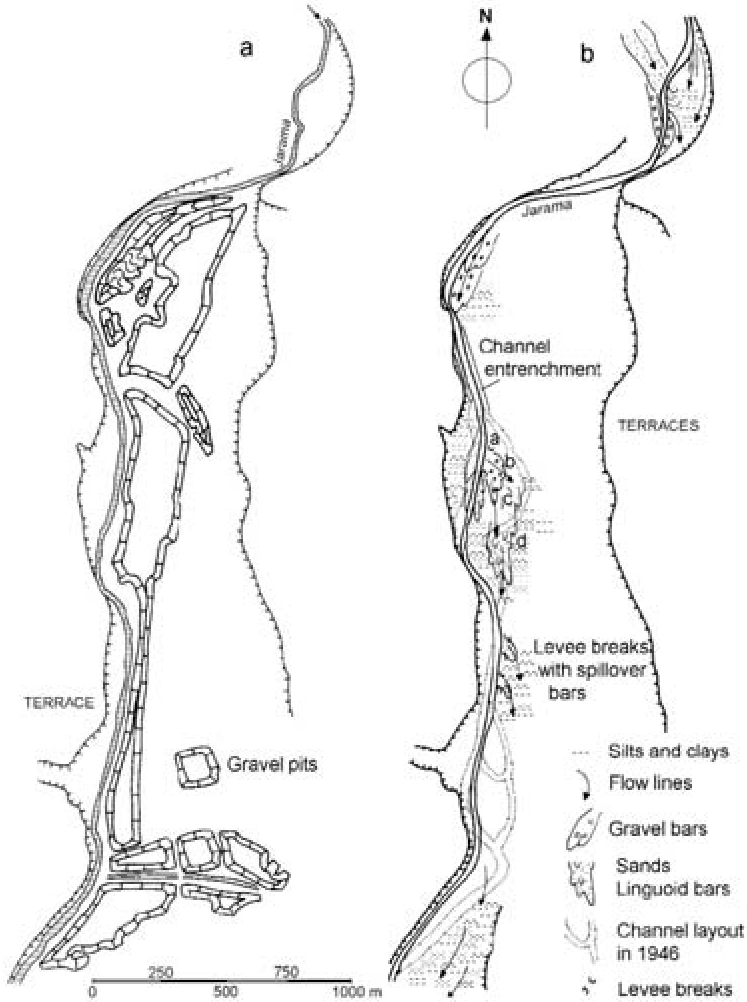

Fig. 8. Map showing effects of gravel pits on the floodplain south of Talamanca del Jarama. (a) Map of quarries excavated into the floodplain. (b) The breaching of artificial levees is followed by the building up of spillover lobes of imbricated gravels and fields of sandy dunes that develop inside the pits.

medium sinuosity, regularly shifting across the floodplain, and considerable aggradation (Fig. 9). In 100 yr, lateral accretion was probably in the order of three or four scroll bars.

The natural dynamics of the river during flooding are clearly appreciable from the 1947 aerial photographs and even more so from those of 1956, where the extensive sedimentary effects of a flood can be observed on the alluvial plain (Fig. 10). The natural evolution of the river shows how the meanders tend to migrate by rotating downstream. Meander cut-off occurs by chute channels in all cases, owing to the coarse nature of the bedload and reuse of former swales. The photographs clearly show how the overflows are the cause of meander cut-offs, reactivation of old channels and sedimentation of chute bars.

The more recent stage of evolution shows a radical change in the river dynamics. The channel has incised 2 or 3 m, has straightened, and many meanders have been cut off. In the lower 80 km, the sinuosity has been reduced to between 1.25 and 1.15. The blurring of the old channel and point-bar swales, however, has occurred in no more than 30 yr, owing to intense activity of crevasse splay infill and vertical accretion during floods.

COMPARATIVE ANALYSIS OF THE TWO RIVERS AND DISCUSSION

By analysing the response of both rivers to floods through time it is possible to establish changing environmental and climatic conditions in the study

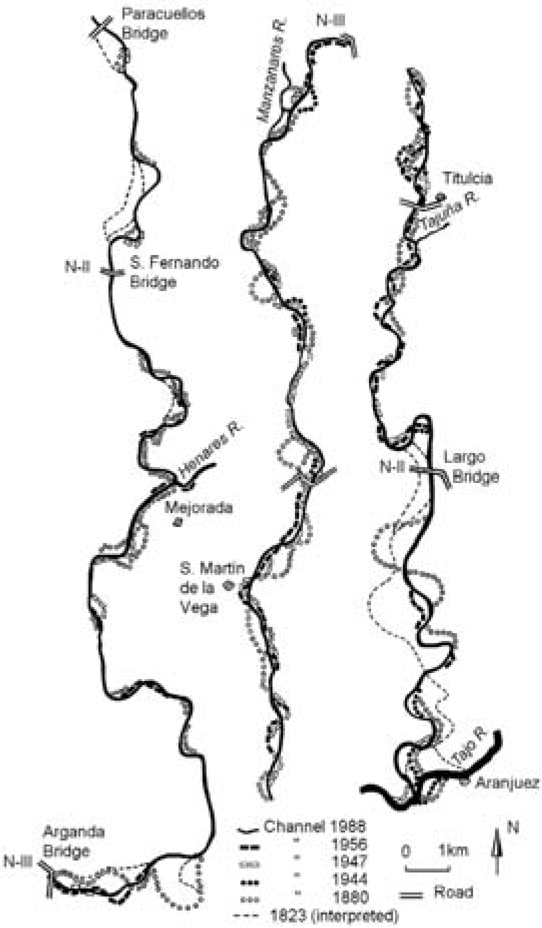

Fig. 9. Changes and channel straightening of the lower reach of the Jarama River since 1823, reconstructed from maps and aerial photographs.

area. It has been shown that the recent evolution of the two rivers has been similar, both experiencing active entrenchment and significant bedload deficit. Although their morphology differs somewhat, the response of the two rivers to floods is similar: little sedimentation and considerable erosion occurs now in the floodplain. This indicates more violent floods on the floodplain than would be expected, but with hardly any aggradation effects. Examples of important sedimentary effects and scouring occur on the floodplain, usually in areas where direct anthropogenic interference can be deduced. In both rivers these effects became significant subsequent to 1956, although in some cases prior destabilization is already evident on the 1946 photographs. The most notable difference observed between the two rivers is the mobility of the channel previous to the deduced incision stage. Whereas the planform of the Guadarrama River has remained fairly constant since the nineteenth century, the Jarama River manifested active meander migration until 1956. This difference relates mostly to the pattern characteristics of the rivers and therefore the modifications probably had similar causes, be they human activities or climate.

The entrenchment trend on both rivers can be explained by the decrease in water discharge and bedload owing to recent and accelerated anthropogenic interference. The decrease in discharge is the result of upstream dam construction and of water pumping for irrigation. The bedload has been reduced as a result of gravel extraction, either directly from the channel bed or from areas in the floodplain sporadically connected to the channel. The first consequence of this decrease has been channel incision, but other processes are triggered as well. These effects are evident especially at flood stages, when the effect of dams is reduced or eliminated, and the rivers behave naturally. Nevertheless, the lack of yearly or high-frequency floods because of impoundment induces reduction of channel flow capacity owing to vegetation colonization. The diminished channel draining capacity increases the damaging effects of floods.

These effects became acute after the 1950s, but modifications in the river systems had started even before then. Therefore the question arises whether these changes are the result only of recent intensification of human activity, or whether they represent a longer term natural trend. A fact that would support the second hypothesis is that both rivers have not been exposed to the same human-induced pressure. The Jarama River is a system in which dams were first built to supply water to Madrid in the last century, and the gravel extraction activity has been intensive in the last decades. The Guadarrama River instead, has been impounded only recently and has few dams, and the extraction activities are limited. Only the lowering of the groundwater level as a result of pumping for irrigation could be significant here. The responses of both rivers to floods are very similar, however, which implies that the causes could lie in more general or regional factors such as climate.

In order to elucidate the extent to which these results are not conditioned only by recent intensification of human activity, the historical evolution of both rivers must be interpreted from the morpho-sedimentary record of the floodplain. In the Jarama River, mobility through bar migration with important lateral accretion was still occurring in 1946. At that time,

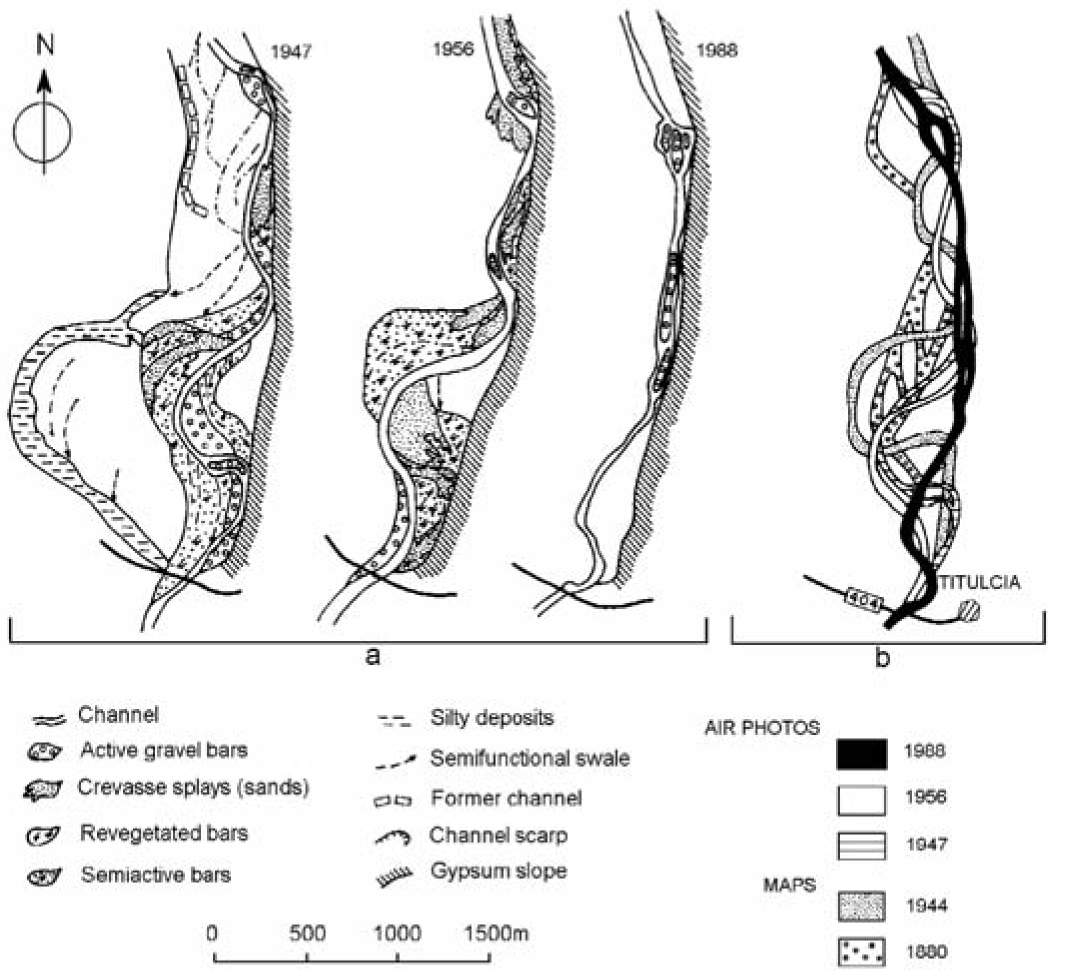

Fig. 10. Map showing morphological variations of the lower reach of the Jarama River. (a) The decreased meander migration is shown between the 1947 and 1988. (b) Composite map showing traces of the channel from maps and aerial photographs. The meanders were migrating downstream until 1956, but afterwards the river straightened its course.

new scroll bars were generated, showing active downstream and minor lateral progradation. The sedimentological record is consistent with the morphological one. Fining upward successions have developed showing basal conglomerate with well-defined lateral accretionary surfaces, overlain by silt with intercalated sandy lenses, which correspond to vertical accretion. The base of the silt has been dated at 390 ± 80 yr BP. This means that meander migration started a long time ago and continued up to 1956. By 1956 this activity had ceased and sinuosity decreased because of meander cut-offs, although considerable activity at the channel banks with remobilization of material and crevasse formation was observed. This feature can be explained by the fact that the stream entrenchment described results in channel straightening and the bank erosion produces much coarse bedload material.

In the Guadarrama River, unlike the Jarama River, no change in the general channel morphology can be identified from the maps available since 1883. There is no meander lobe migration either, only a slight increase in sinuosity. Starting in 1945, however, the beginnings of river destabilization and the formation of cut-off chutes can be observed in aerial photographs. The sedimentological record confirms the morphological one, as no point-bar bodies are detectable in the sections, indicating that meanders did not actively migrate. Sedimentation occurred mostly by vertical accretion on the floodplain and the sinuosity observed on the maps is not reflected in the development of point bars. It is possible, however, that the increased sinuosity and low channel mobility is recorded in the deposition of silts and lenticular sandy bars, corresponding to vertical accretion of floodplain sediments toward the top of the sedimentary sequence. This is confirmed by the ^{14}C dates of around 150 yr BP obtained at the intermediate level of the floodplain stratigraphical section, showing intense aggradation during that period.

Increased sinuosity and the trend toward dominant vertical accretion on the floodplain can be explained by a decrease in the bedload/discharge ratios in the channel, owing either to a relative increase in discharge or to a diminishing bedload. A discharge increase is suggested by the fact that the second half of the nineteenth century was the most important historical period of flooding in the Iberian Peninsula and the largest floods are recorded for most rivers (Benito *et al.*, 1996; Martinez & Garzón, 1996). Little information exists about the influence of these recent climatic changes in other Iberian streams. However, in the largest Spanish river, the Ebro, a major increase in sinuosity also has been described towards the end of the 1800s (Ollero, 1996). The reach of the Tajo River between the confluence of the Jarama and the Guadarrama rivers also appears to have been more sinuous at the beginning of the nineteenth century than later on, although cartography prior to contour line maps is not very reliable. This fact has also been referred to for the lower Jarama River and its confluence with the Tajo (Pinilla *et al.*, 1995).

Finally, during the past 50 yr, the Guadarrama River has experienced major erosion in the meander lobes and mobilization of great quantities of sand with development of the cut-offs. The 1956 aerial photographs show considerable activity in the channel with the development of new cut-offs. This activity could indicate the onset of channel destabilization and entrenchment.

Change from aggradation to incision occurred in this river previous to anthropogenic modification. This fact could be explained by a self-regulatory mechanism of incision of the river system after the actively aggrading period.

Evolution of the rivers

The evolution of the Guadarrama and Jarama rivers can be reconstructed as follows (Fig. 11 and Table 1).

Stage I—aggradation (Little Ice Age?)

Active bar accretion and point-bar migration occur on both the Guadarrama and the Jarama rivers.

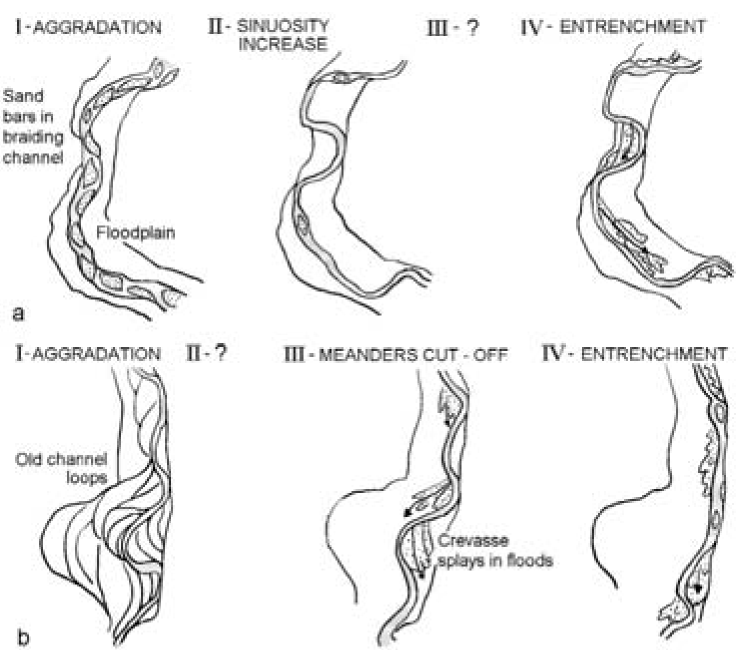

Fig. 11. Schematic maps showing the various stages of evolution of the Guadarrama (a) and Jarama (b) rivers during the past two centuries.

Table 1. Evolutionary stages of the Guadarrama and Jarama rivers since the beginning of the nineteenth century, showing a similar trend in both rivers, from aggradation to entrenchment.

Evolutionary stages	Guadarrama River	Jarama River
I. Aggradation (Little Ice Age?)	Active bar accretion	Point bar migration and floodplain aggradation
II. Accretion decay (1850?–1930)	Channel constriction Floodplain accretion	(Not recognizable)
III. Incipient instability (1930–1956)	Swales incision and intense flooding and crevassing	Meander cut-off and infilling
IV. Active incision (1956 to present)	Channel incision and bank erosion. Renewed braiding	Channel entrenchment and straightening

Aggradation of the floodplain occurs in both rivers as well, recorded in the Jarama River since 1600 and in the Guadarrama River since 1800. As this stage has been recorded since AD 1600 it tentatively could be related to the Little Ice Age, although this period is not well defined in the Iberian Peninsula.

Stage II—aggradation decay (1850?–1930)

By the end of the previous stage, channel aggradation would have diminished, resulting in increased channel constriction and sinuosity in the Guadarrama River. Significant floodplain accretion, however, would have continued, represented by the silt and sand deposits capping the successions. This stage is recorded in the Guadarrama River but not in the Jarama River.

Stage III—incipient instability (1930–1956)

Instability is marked by a renewed flooding period between l930 and 1956, which triggered the start of active channel entrenchment. The Guadarrama River exhibits numerous incision scours and the signs of intense flooding and crevassing. The Jarama River reacts with meander cut-offs and infilling of swales.

Stage IV—active incision (1956 to present)

From 1956 to the present, active entrenchment continues, with renewed braiding and widening in the Guadarrama River, and channel straightening in the Jarama River.

CONCLUSIONS

The Guadarrama and Jarama rivers flow through similar semi-arid environments and valley slopes, but present different stream patterns owing to bedload differences. The former is a sandy, mostly braided river that develops a braided–meandering character only in its lower reaches. The latter is a meandering gravelly river.

The two rivers respond to flooding in a similar way, and experience erosion of the river banks and occasionally of floodplains, and widening of cut-offs. In the Guadarrama River braiding occurs in the cut-off reaches where the initial straight reaches are modified by enlargement and migration of a few bars. Overbank flows supply little material from the channel to the floodplain. In the floodplain, diffuse erosion and concentrated flow in small troughs generate local sand-bar migration.

A similar response occurs in the meandering Jarama River, with the difference that considerable extraction of gravel has occurred in the floodplain, and the abandoned pits trap much of the flood sediments. Floods have no great effect on point bars any more, except for reworking some clasts. Both rivers experience incision under bedload-deficit conditions.

The present entrenchment is the most recent stage of an evolutionary sequence that can be reconstructed from the sedimentary record of the floodplain, from maps since 1800 and from aerial photographs since 1946. Four major evolutionary stages have been identified. The first aggrading stage was characterized by intense bar migration, point-bar progradation and minor vertical accretion in the floodplain. A second stage is evident only in the Guadarrama River, and reflects a decrease in the bedload/discharge ratios. The third stage represents the commencement of channel destabilization, with the onset of incision of cut-off channels. The fourth stage is characterized by an acceleration of entrenchment, 3–4 m in the Jarama River and 1–2 m in the Guadarrama River.

These changes probably have been caused by both climatic variations and human activities. In the

Guadarrama River the entrenchment of the river started before the intensification of human activity of the last half century, suggesting that climatic factors triggered the changes. The Jarama River, on the other hand, has undergone so many anthropogenic modifications that it is not possible to determine with certainty the effects of climatic variations, although indication exists that entrenchment also started before intense human interference.

The fact that both rivers flow under the same environmental conditions and present similar evolution suggests that they have responded to overall climatic change. Nevertheless, the superposed human activity has induced not only intense alterations in channel dynamics, but also local magnification of processes. It therefore is suggested that the triggering of incision-derived events during floods is the result of both climatic and anthropogenic factors. The latter are the ones that, in this case, accelerate the natural evolutionary trend of the rivers, and may localize floods.

ACKNOWLEDGEMENTS

This research has been supported by CICYT's Projects NO HID 96–1318/96 and PB94–0276-CO2–01. The authors are very grateful to J. Vanderbergen for his comments and helpful reflections, as well as to another anonymous reviewer. We would also like to thank the effort of I.P. Martini for improving the manuscript readability and to M. Leeder for his kind final corrections.

REFERENCES

Alonso, A. & Garzón, G. (1994) Quaternary evolution of a medium sinuosity gravel bed river, Jarama River, Central Spain. *Terra Nova* **6**, 465–475.

Alonso, A. & Garzón, G. (1996) The Jarama river. In: *Palaeohydrology in Spain* (Eds Benito, G., Perez-Gonzalez, A., Machado, M.J. & de Alba, S.), pp. 21–34. Field Excursion Guide, 2nd International Meeting on Global Continental Palaeohydrology, Toledo.

Alonso, A. & Garzón, G. (1997) Efectos sedimentarios de las inundaciones en un río fuertemente antropizado: El Jarama, Madrid. *Cuad. Geol. Ibérica* **22**, 265–282.

Arche, A. (1983) Coarse-grained meander lobe deposits in the Jarama river, Madrid (Spain). In: *Modern and Ancient Fluvial Systems* (Eds Collinson, J.D. & Lewin, J.), Spec. Publs int. Ass. Sediment., No. 6, pp. 313–321. Blackwell Scientific Publications, Oxford.

Asensio Amor, I. & Vadour, J. (1967) Depósitos cuaternarios en los alrededores de Mejorada del Campo (Valle del río Jarama). *Estud. Geol.* **23**, 237–256.

Benito, G., Machado, M.J. & Perez-Gonzalez, A. (1996) Climate change and flood sensitivity in Spain. In: *Global Continental Changes: the Context of Palaeohydrology* (Eds Branson, J., Brown, A.G. & Gregory, K.J.), Spec. Publ. geol. Soc. London, No. 155, pp. 85–98. Geological Society Publishing House, Bath.

Cabra, P., Goy, J.L., Hoyos, M. & Zazo, C. (1983) Estudio geomorfológico del Cuaternario y de las formaciones superficiales del sector meridional de la Sierra Cabrera. *Tecniterrae* **51**, 32–42.

Garzón, G. & Alonso, A. (1995) Variabilidad holocena y reciente de un río de gravas. El río Jarama. Madrid. In: *Reconstrucción de Paleoambientes y Cambios Climáticos Durante el Cuaternario* (Eds Aleixandre, T. & Pérez-González, A.), pp. 79–92. Monografías 3, CSIC, Centro de Ciencias Medioambientales, Madrid.

Garzón, G. & Alonso, A. (1996) El río Guadarrama, morfología y sedimentación actual en un río arenoso tipo braided. *Cuad. Geol. Ibérica* **21**, 369–393.

Garzón, G., Alonso, A., Lopez, J. & Arche, A. (1990) Desbordamientos en el río Jarama (Prov. de Madrid) e interferencia humana en la llanura de inundación. In: *VIII Reunión de Medio Ambiente y Ordenación Del Territorio*, pp. 259–271. Servicio Publicaciones Universidad de Oviedo.

Garzón, G., Martinez-Goytre, J. & Alonso, A. (1992) Los cambios antrópicos en la dinámica del río Jarama (Madrid) como modificadores del riesgo de inundaciones. In: *Cambio Climático y Riesgos Naturales*, pp. 628–638. Simposiums III Congreso Geológico de España, 3. Salamanca.

Gregory, K.J. (Ed.) (1977) *River Channel Changes*. J. Wiley & Sons, Chichester.

Gurnell, A. & Petts, G. (Eds) (1995) *Changing River Channels*. J. Wiley & Sons, Chichester.

Harvey, A.M. (1984) Aggradation and dissection sequences on Spanish alluvial fans: influence on morphological development. *Catena* **11**, 289–304.

Hernández-Pacheco, E. & Aranegui, P. (1927) Las terrazas cuaternarias en las inmediaciones de San Fernando de Jarama y de Torrelaguna. *Bol. R. Soc. Esp. Hist. Nat.* **27**, 310–316.

Lewin, J., Macklin, M.G. & Woodward, J.C. (Eds) (1995) *Mediterranean Quaternary River Environments.* Balkema, Rotterdam.

López Vera, F. & Pedraza, J. (1976) Síntesis geomorfológica de la cuenca del río Jarama en los alrededores de Madrid. *Estud. Geol.* **32**, 499–508.

Macklin, M.G. & Passmoore, D.G. (1995) Pleistocene environmental change in the Guadalope basin, northeast Spain: fluvial and archaeological records. In: *Mediterranean Quaternary River Environments* (Eds Lewin, J., Macklin, M.G. & Woodward, J.C.), pp. 103–113. Balkema, Rotterdam.

Martinez-Goytre, J. & Garzón, G. (1996) Análisis de las avenidas históricas del Río Jucar.-6th. In: *6th Spanish Congress and International Conference on Environmental Geology and Land-Use Planning, Granada* (Eds Chacon, J. & Irigaray, C.), Vol. 3, pp. 29–41.

Mather, A.E., Silva, P.G., Goy, J.L., Harvey, A.M. & Zazo, C. (1995) Tectonic versus climate: an example from late Quaternary aggradational and dissectional sequences of the Mula basin, southeast Spain. In: *Mediterranean Quaternary River Environments* (Eds Lewin, J., Macklin, M.G. & Woodward, J.C.), pp. 77–87. Balkema, Rotterdam.

MIALL, A.D. (1985) Architectural-element analysis: a method of facies analysis applied to fluvial deposits. *Earth Sci. Rev.* **22**, 261–308.

OLLERO, A. (1996) *El curso medio del Ebro*. Publications Consejo de la Protección de la naturaleza de Aragón, Zaragoza.

PÉREZ-GONZÁLEZ, A. (1980) Geología y estratigrafía de los yacimientos de áridos en la llanura aluvial de Arganda (Madrid). In: *Ocupaciones Achelenses En El Valle Del Jarama*, pp. 49–61. Publicaciones de la Excelentísima. Diputacíon Provincial de Madrid, Madrid.

PÉREZ-GONZÁLEZ, A., ALEIXANDRE, T., GALLARDO, S., PINILLA, A. & MEDINA, A. (1974) Guía de la excursión B. Valle del Henares-Jarama. In: *Trabajos Sobre Neógeno-Cuaternario*, pp. 223–230. Actas I Reunión Nacional Grupo Trabajo del Cuaternario, Consejo Superior de Investigaciones Científicas, Madrid.

PETTS, G.E., MOLLER, H. & ROUX, A.L (Eds) (1989) *Historical Changes of Large Alluvial Rivers: Western Europe*. John Wiley & Sons Ltd, Chichester.

PINILLA, L., PEREZ-GONZALEZ, A. & BENITO, G. (1995) Cambios históricos de los cauces de los ríos Tajo y Jarama en Aranjuez. *Geogaceta* **18**, 101–104.

RIBA, O. (1957) Terrasses du Manzanares et du Jarama aux environs de Madrid. *Livret Guide de L'Excursion V Congrés International*, International Union for Quaternary Research, Madrid.

SCHUMM, S.A. (1968) River adjustment to altered hydrologic regimen, Murrumbidgee River and palaeochannels, Australia. *U. S. geol. Surv. Prof. Pap.* **598**, 65 pp.

SILVA, P., GOY, J.L. & ZAZO, C. (1988) Neotectónica del sector centro-meridional de la cuenca de Madrid. *Estud. Geol.* **44**, 415–427.

SIMONS, D.R. & LI, R.M. (1982) Application of flow routing techniques to river regulation. In: *Gravel-bed Rivers* (Eds Hey, R.D., Bathurst, J.L. & Thorne, C.R.), pp. 583–599. John Wiley & Sons Ltd, Chichester.

STARKEL, L. (1995) Changes of river channels in Europe during the Holocene. In: *Changing River Channels* (Eds Gurnell, A. & Petts, G.), pp. 27–42. J. Wiley & Sons, Chichester.

Spec. Publs int. Ass. Sediment. (2002) **32**, 251–67

Effects of land-use and precipitation changes on floodplain sedimentation in the nineteenth and twentieth centuries (Geul River, The Netherlands)

M. H. STAM

Faculty of Earth Sciences, Vrije Universiteit, De Boelelaan 1085, 1081 HV Amsterdam, The Netherlands (Email: stam@geo.vu.nl)

ABSTRACT

The effects of land-use change and precipitation variability on the flow regime and sedimentation rates of floodplain deposits were studied in the Geul River in the southern part of The Netherlands. The catchment has a history of industrial mining, thus providing a means for dating the sediment. Several cut-bank sections were analysed for grain size, organic matter, Zn, Pb and ^{137}Cs, and sedimentation rates were calculated for the periods 1806–1845, 1845–1885, 1885–1955 and 1955–1996. Sedimentation rates were high between 1806 and 1885, very low between 1885 and 1955, and high again between 1955 and 1996. Rates of channel change derived from the analysis of aerial photographs show an increase after 1949 and 1981.

Comparison with precipitation and land-use data indicates that the high sedimentation rates in the nineteenth century were caused by mining activities and deforestation, resulting in more floods in the low-magnitude–high-frequency range. The termination of industrial mining around 1885, subsequent reforestation, and the agricultural crisis of 1878–1895 all contributed to the low river activity during the first half of the twentieth century. The modernization of agriculture and increased precipitation have contributed to an increase in sedimentation rate and channel-change rate during the second half of the twentieth century. Increased soil erosion associated with the modernization of agriculture is an important new source of sediment.

INTRODUCTION

In December 1993 and January 1995 the Meuse River (flowing through France, Belgium and The Netherlands; Fig. 1a) flooded severely, causing extensive damage and forcing massive evacuations. These events sparked an interest in land-use and climate change as possible causes of the recent, apparent increase in flood frequency. To separate the effects of land-use change and precipitation variability on the peak discharges of the Meuse, one would ideally need single cause–effect relationships for discrete time periods and a long discharge time-series. For a river basin such as the Meuse (33 000 km^2) there are no such undisturbed cause–effect relationships, because it is used for international commercial shipping and various other economic purposes, and therefore has been heavily engineered. Generally, peak discharges in the Meuse lead to flooding problems when peak discharges in subcatchments such as the Ourthe and the Sambre (Fig. 1a) coincide with those of the main channel (Berger, 1992; Dijkman & Pedroli, 1994). Thus, the effects of height and timing of peak discharges in subcatchments are of major importance. Unfortunately, discharge measurements in most of the subcatchments started as late as 1970 and consequently the time-series are not long enough to properly determine long-term effects of either land-use or precipitation change. Therefore, the effects of land-use and precipitation for the period before discharges were measured had to be determined another way. The quality of data available for land-use and precipitation limits this period to approximately two centuries.

Flooding history of a catchment is sometimes recorded in the floodplain sediments. If the flood sediment can be dated, different time periods can be compared in terms of sedimentation rate and sediment characteristics, providing information on flooding frequency and sediment deposition. Methods that have been used for dating floodplain sediment are

Flood and Megaflood Processes and Deposits: Recent and Ancient Examples. Edited by I. Peter Martini, Victor R. Baker and Guillermina Garzón ISBN: 978-0-632-06404-5

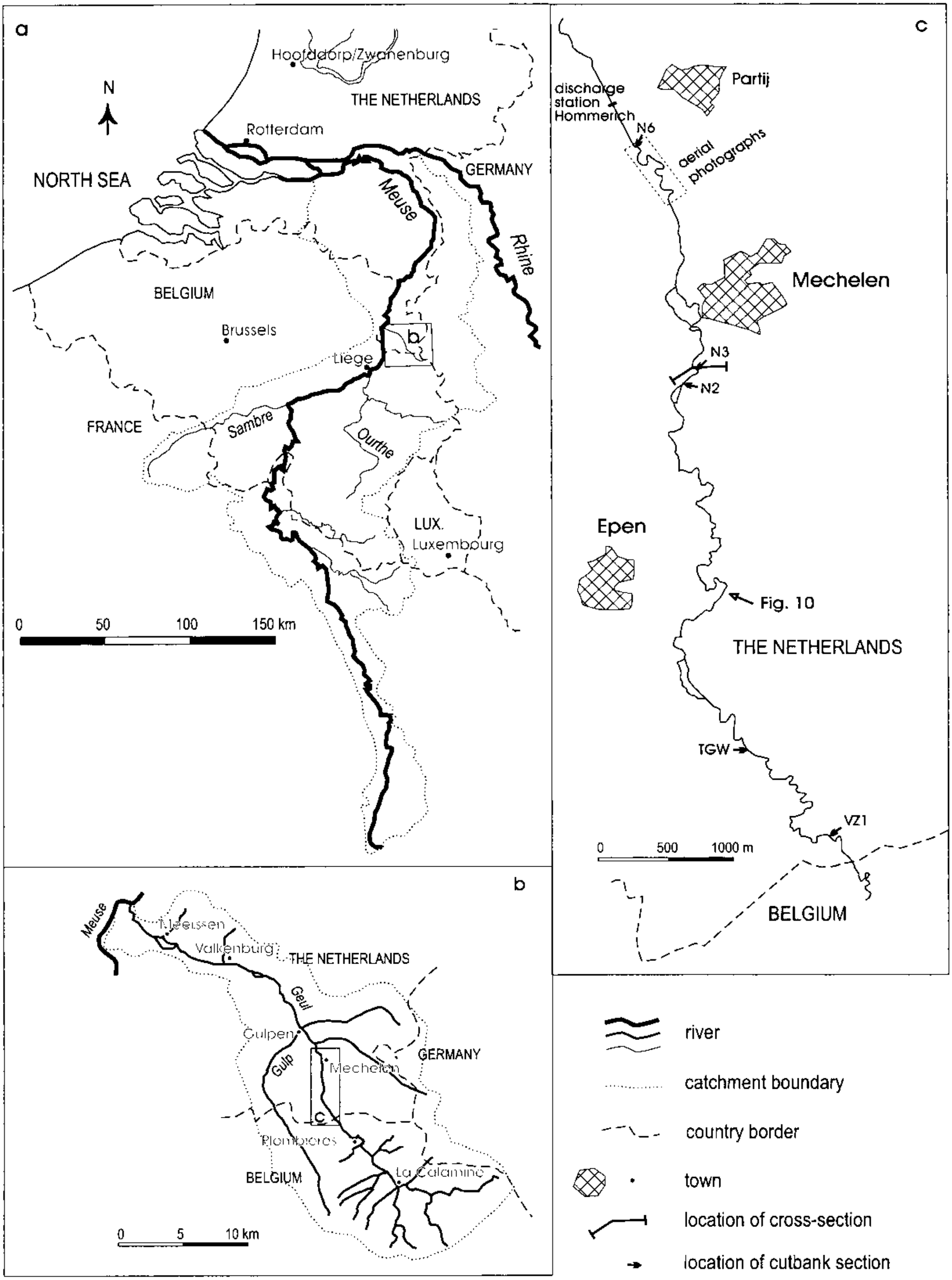

Fig. 1. The Meuse River and Geul River catchments and the study site.

^{210}Pb (Walling *et al*., 1996), ^{137}Cs (Walling & He, 1993, 1997; Walling *et al*., 1996), and heavy metal contamination in catchments with a history of industrial mining (Klimek & Zawilinska, 1985; Swennen *et al*., 1994; Macklin, 1996; Middelkoop, 1997).

The Geul River (Fig. 1b), a small tributary of the Meuse flowing through Belgium and the southernmost tip of The Netherlands, has good possibilities for sediment dating because it has a history of nineteenth century lead and zinc mining, which has caused elevated metal levels in the flood sediment (Leenaers, 1989; Swennen *et al*., 1994).

The aim of this research is to reconstruct the flood history in the Geul River catchment over the past two centuries by interpreting the sedimentation characteristics in terms of land-use and precipitation changes. This was done by studying the sediment characteristics of floodplain deposits and by dating the sediments using heavy metals and ^{137}Cs as tracers in order to calculate average sedimentation rates. In addition, the land-use history for the catchment has been derived from a literature search and combined with a reconstructed precipitation time-series for comparison with the sediment characteristics.

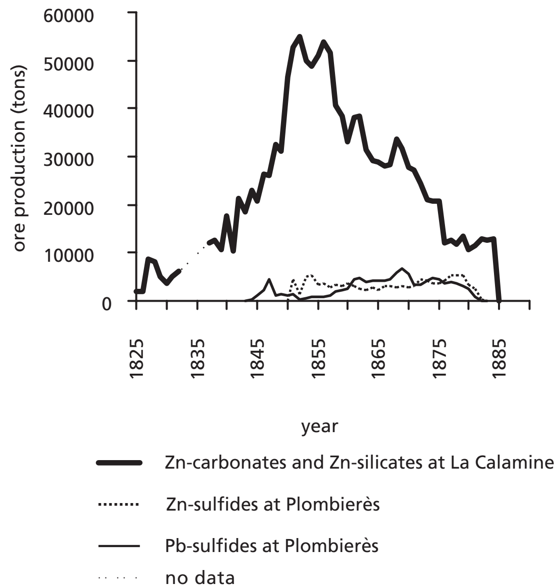

Fig. 2. Metal production and ore types in La Calamine and Plombières in the nineteenth century (after Dejonghe *et al*., 1993).

The Geul River catchment

The Geul River (also known as 'die Göhl' and 'la Gueule') is a meandering river originating in eastern Belgium and flowing into the Meuse at Meerssen (The Netherlands) after 56 km (Fig. 1b). Its catchment area is 350 km^2 and its gradient ranges from 0.02 m m^{-1} near the source to 0.005 m m^{-1} near the Belgian–Dutch border and 0.0015 m m^{-1} at its confluence with the Meuse. The Belgian part of the river valley is incised in Famennian sandstone, Tournaisian to Lower Visean dolomite, Visean limestone and Namurian shale (Swennen & Viaene, 1990). In The Netherlands, the river is asymmetrically incised in Cretaceous chalk and Tertiary sand. As a braided river it has deposited several metres of Pleistocene gravel, which is topped by several metres of finer Holocene sediments (Van de Westeringh, 1980). The present meandering river channel is 3–7 m wide and incised into the Holocene silts and partly into the Pleistocene gravel. Average discharge of the Geul River since 1969 is 3.4 m^3 s^{-1} at Meerssen, with a minimum of 0.8 m^3 s^{-1} and a maximum of 45 m^3 s^{-1}. Discharges at the Belgian–Dutch border are generally slightly less than half those at Meerssen.

Lead and zinc mining in the Geul River catchment started in the Middle Ages, but did not gain significance until 1806 when industrialized zinc mining started at La Calamine (Dejonghe *et al*., 1993) (Fig. 1b). Production figures for the first decades of exploitation are lacking but Fig. 2 shows that this mining location was most productive between 1848 and 1850. In 1879 La Calamine was exhausted although production continued until 1885 and some old waste piles were re-treated until 1887 and in the 1930s at one of the plants (Dejonghe *et al*., 1993). From 1845 until 1885, subsurface mining occurred at Plombières (Figs 1b & 2), producing lead and zinc (Dejonghe *et al*., 1993). Several smaller mines, all located further upstream than La Calamine, were active until the 1930s.

Leenaers (1989) has dated five sections in overbank sediment with ^{137}Cs in the Dutch part of the Geul River catchment and estimated deposition rates since 1963. He found a large spatial variability (0.43–1.41 cm yr^{-1} for 1963–1986) and increased values for the period April 1986 to June 1988. Swennen *et al*. (1994) estimated sedimentation rates since 1806 for three sections in the Belgian part of the catchment and found increased sedimentation in the period of active mining (0.8–1.06 cm yr^{-1} for 1806–1900).

A detailed description of the land-use history of this catchment in the nineteenth and twentieth centuries will be presented in a later section.

METHODS

Cut-bank sections were described along a 10-km stretch of the Geul River from the Dutch–Belgian border to Gulpen (Fig. 1c); surface levels were 1.5–3.5 m above water level during the time of the survey. Several cross-sectional profiles were cored across the valley floor. Twelve cut-bank profiles were selected and sampled in 5-cm intervals. Lacquer peels were made from a few typical cut-banks.

Trace metal analyses

Bulk samples were dried overnight (at 105°C), sieved to obtain the fraction smaller than 2 mm, and pulverized. They were mixed with one part wax (TM Ceridust 9615 A) to five parts sample (8 g) and ground again. This mixture was pressed into a tablet and each tablet was analysed for Pb and Zn by X-ray sequential spectrometer. Detection limits were 5 p.p.m. for Zn and 2 p.p.m. for Pb.

Cesium-137 analyses

Determination of ^{137}Cs activity was done by gamma counting of 40–60 g of dried sediment. Each sample was sealed by closing a Petri dish with tape and seal-plastic. The samples were stored for 1 month. The samples were counted for 3 days on a 1000-mm^2 germanium detector designed for low-energy gamma-ray spectrometry and a coaxial detector with a relative efficiency of 30%. The ^{137}Cs activity was determined by the 661.6 keV line.

Grain size and organic matter analyses

Samples were dried at 70°C, disaggregated and homogenized. They were treated with 30% H_2O_2, 10% HCl, and tetra-sodium diphosphate-10-hydrate. Grain sizes were analysed using the Fritsch laser particle sizer A22. Therefore, 8 μm was used as the upper limit of the clay fraction (Konert & Vandenberghe, 1997). Organic matter content was determined by loss on ignition at 550°C on dried, homogenized samples. The sediments contained little or no $CaCO_3$.

THE FLOODPLAIN DEPOSITS

The lowest unit in the cut-bank sections of the Geul River in the area studied is the Pleistocene gravel (Van de Westeringh, 1980). Recent floods bear evidence that these gravels are still being reworked at high discharges. Directly on top of the gravel unit, a few centimetres of coarse organic material, such as branches and leaves sometimes mixed with sand and gravel, are often present. Overlying the gravel and organic detritus three different fine-grained units can be recognized by different lithological and sedimentary features. Figure 3 is a cross-section of the Geul

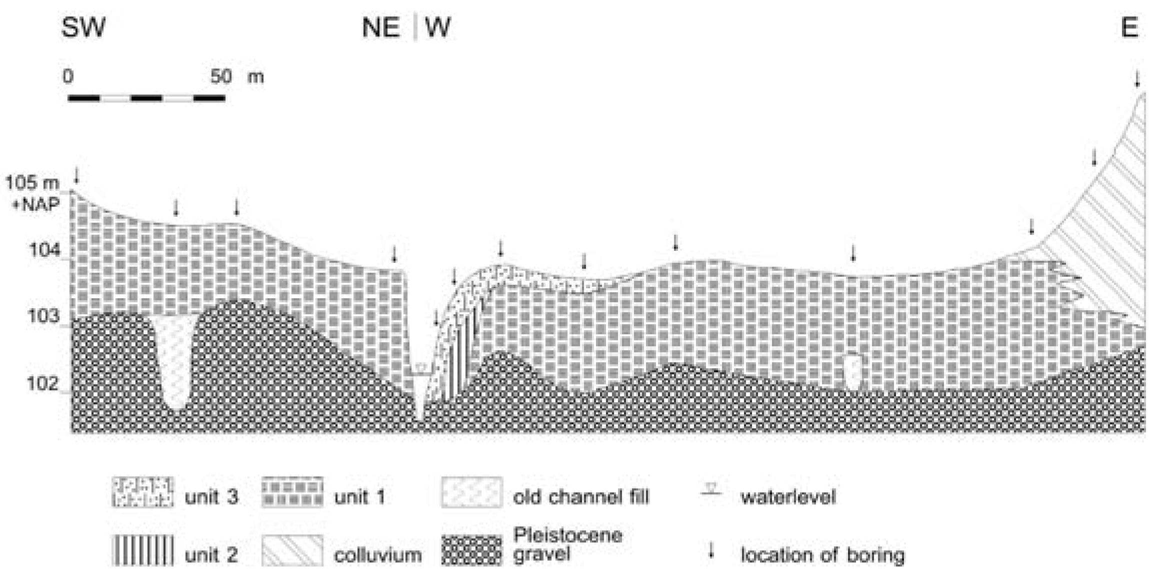

Fig. 3. Cross-section of the Geul River valley (location Fig. 1c) showing the lateral extent of units 1, 2 and 3.

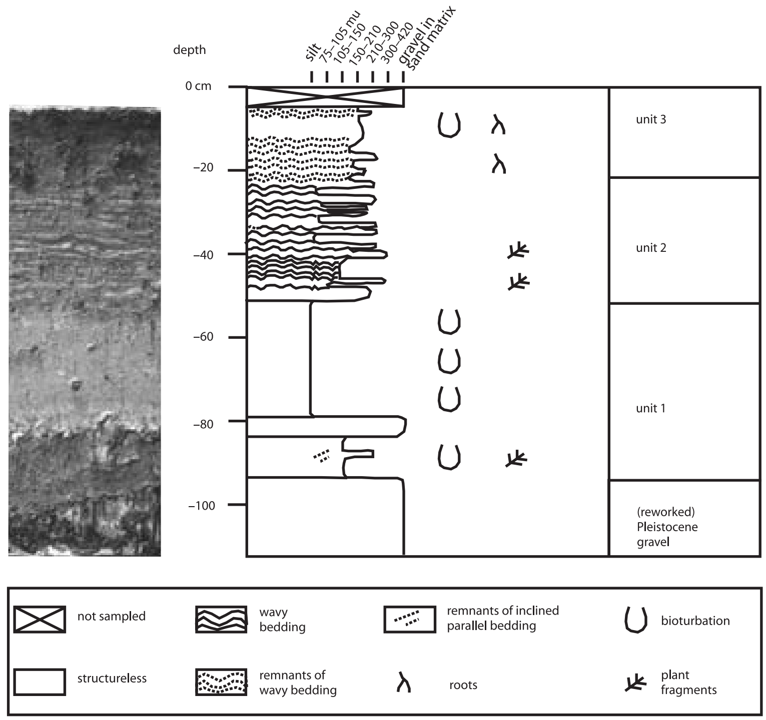

Fig. 4. Lacquer peel showing (in order of deposition): the Pleistocene gravel, homogeneous and bioturbated unit 1, laminated unit 2 and coarser unit 3 (section N6, Fig. 1c).

River valley showing the lateral extent of the three units in the valley fill. Units 2 and 3 lie close to the channel and the rest of the floodplain consists of unit 1 on top of the gravel with perhaps some traces of units 2 and 3 incorporated in the topsoil. Also, most cut-banks consist only of unit 1 topped by slightly coarser topsoil but some cut-banks display all three fine-grained units (cut-bank N6, Fig. 4).

Grain-size distribution, organic matter content, metal content and ^{137}Cs activity of five cut-bank sections are shown in Figs 5–9, and Table 1 summarizes some general characteristics of the three sedimentary units.

Sedimentary units

Unit 1 consists primarily of strongly bioturbated silts; sometimes a faint layering can be discerned. Some sections contain some coarser material in the form of sand or pebble lenses, or isolated pebbles lodged within the silts. The top of this unit often contains coal, brick and organic fragments up to 5 mm in diameter. Where this unit underlies unit 2, the top part contains more coarse sand than specified in Table 1 (up to 18%). The coarse sand content also can be higher than specified near the gravel unit (up to 22%). An example of unit 1 can be seen in cut-bank N6, positioned in a former point bar (Figs 4 & 9a).

Unit 1 is found in levees and flood basins of the Geul River (Fig. 3). Van de Westeringh (1980) characterizes the levee soils in the Geul River valley as coarse silt (clay content between 10 and 20%) and the basin deposits as fine silt (clay content 20% and more), both of which are found in unit 1. The Geul River catchment is located in the loess region of the southern Netherlands and north-eastern Belgium. The modal grain size of the silt fraction of unit 1 is comparable to that of the loess deposits of the region, but it contains both more sand and clay, indicating fluvial reworking (Vandenberghe *et al.*, 1985). This is further evidenced by the presence of former channel fills (Fig. 3) and the occasional sand or gravel lenses, which represent splay deposits.

Van de Westeringh (1980) estimates that the start of the fine-grained valley fill (unit 1, Fig. 3) dates back to the Roman era when large parts of South Limburg were cleared and used for farming. A strong increase in valley sedimentation at the beginning of the Subatlantic period has been found in many European rivers (De Smedt, 1973; Vandenberghe, 1977;

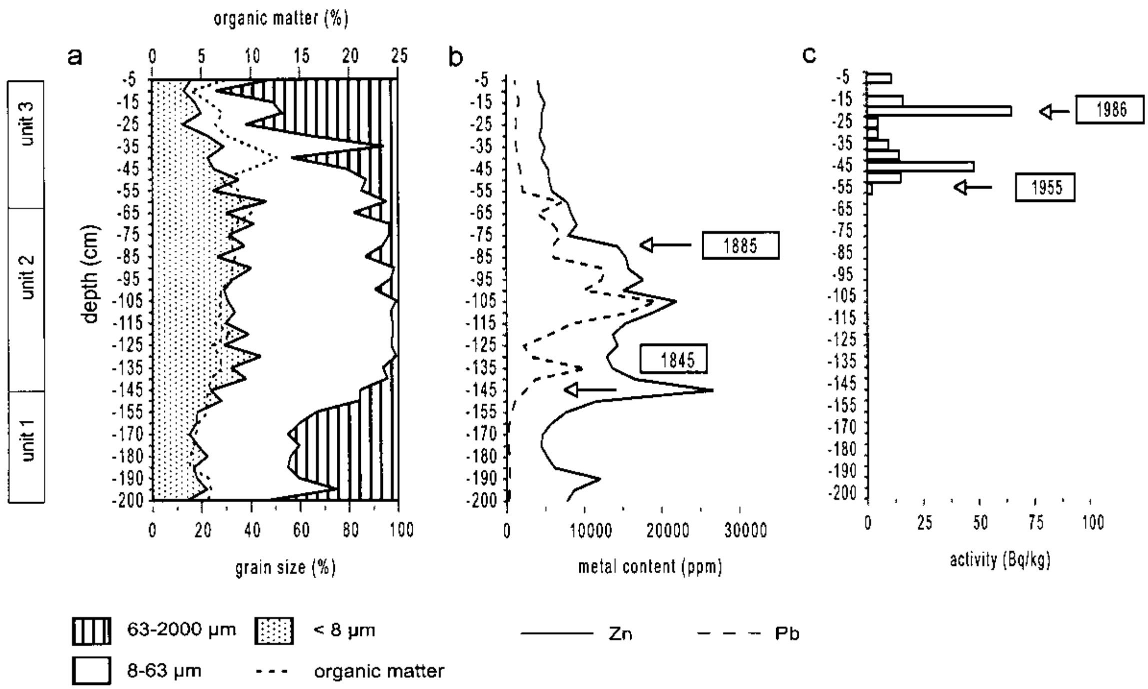

Fig. 5. (a) Grain size and organic matter content; (b) Zn and Pb content; (c) ^{137}Cs activity for cut-bank VZ1 (location in Fig. 1c).

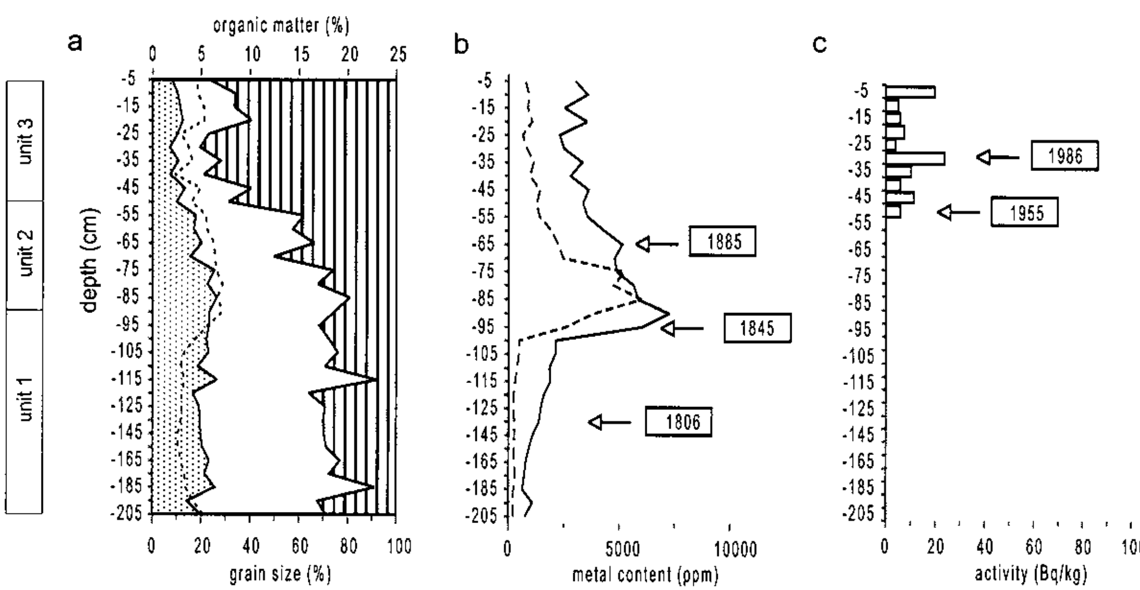

Fig. 6. (a) Grain size and organic matter content; (b) Zn and Pb content; (c) ^{137}Cs activity for cut-bank TGW (location in Fig. 1c). Legend in Fig. 5.

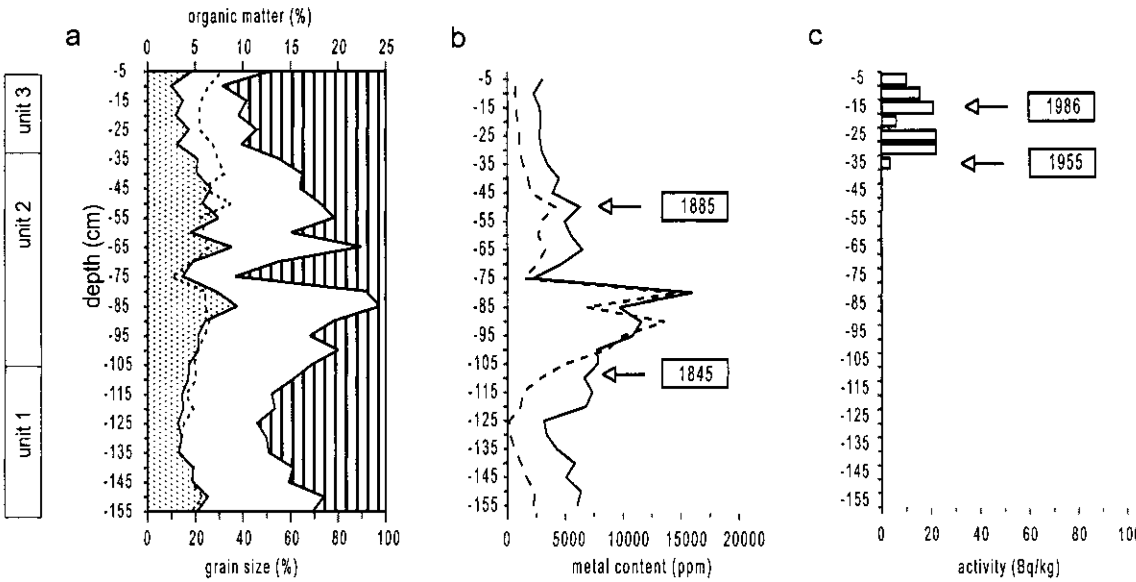

Fig. 7. (a) Grain size and organic matter content; (b) Zn and Pb content; (c) ^{137}Cs activity for cut-bank N2 (location in Fig. 1c). Legend in Fig. 5.

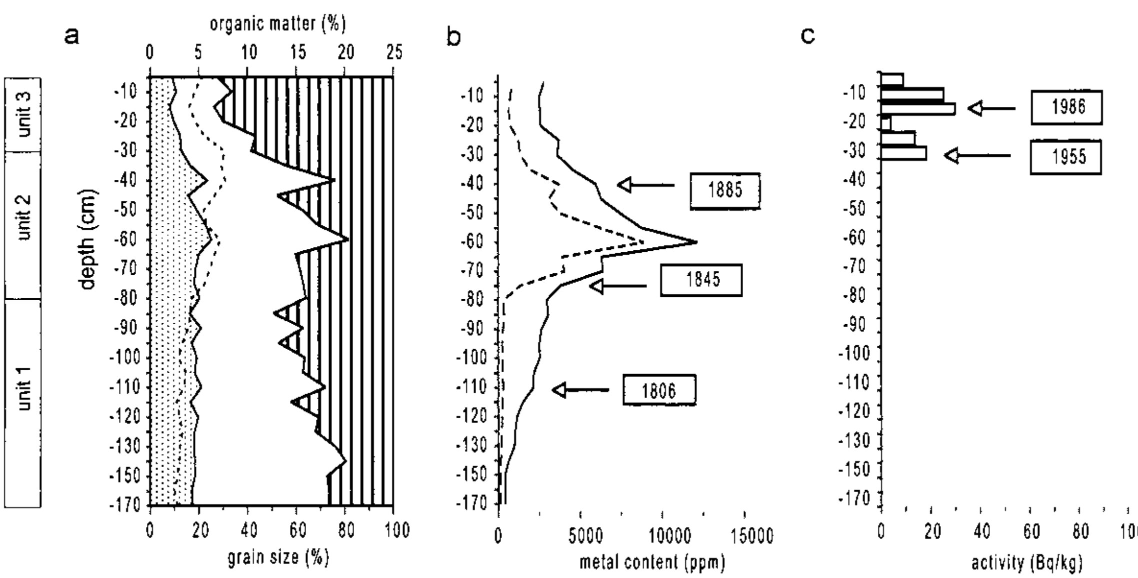

Fig. 8. (a) Grain size and organic matter content; (b) Zn and Pb content; (c) ^{137}Cs activity for cut-bank N3 (location in Fig. 1c). Legend in Fig. 5.

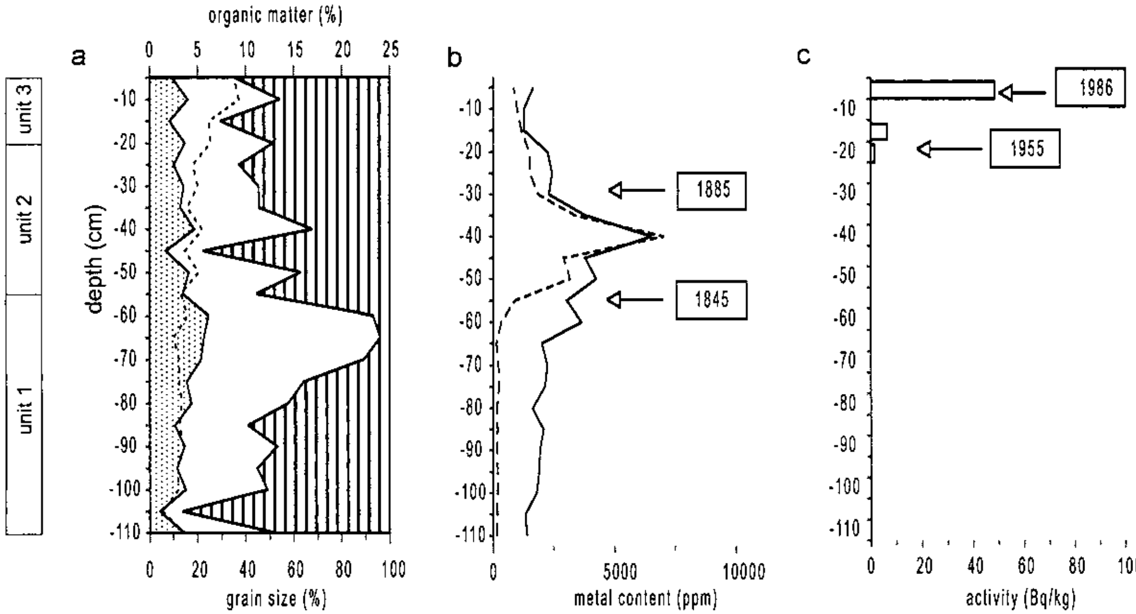

Fig. 9. (a) Grain size and organic matter content; (b) Zn and Pb content; (c) ^{137}Cs activity for cut-bank N6 (location in Fig. 1c). Legend in Fig. 5.

Table 1. Sediment characteristics of the three fine-grained sedimentary units in the Geul valley.

Characteristics	Unit 1			Unit 2			Unit 3		
	Minimum	Maximum	Modal (range)	Minimum	Maximum	Modal (range)	Minimum	Maximum	Modal (range)
Clay content (%)	10	40	20	7	45	15–25	7	30	10–15
Sand content > 63 μm (%)	2	65	15	1	80	35	6	80	50–70
Sand content > 420 μm (%)	0	10	0	0	40	–	3	38	15
Loss-on-ignition (%)	1	7	3.5	3	10	6	2	12	4–8
Munsell colour	Brown (10 YR 4/4)			Fine: brownish black (10 YR 3/1) Coarse: grey yellow brown (10 YR 5/2)			Dull yellowish brown (10 YR 5/3)		
Number of samples	136*			55			38		

*Samples with high sand contents near the lag deposit are not included.

Riezebos & Slotboom, 1978). The coarser grained top of unit 1 (not indicated in Fig. 3) is estimated to have been deposited after the Middle Ages, reflecting even more extensive reclamations (Havinga & Van den Berg van Saparoea, 1980; Van de Westeringh, 1980).

Unit 2 consists of alternating beds of clay-rich silts and sandy silts to sands (Fig. 4). The variety in grain sizes (Table 1; Figs 5a–9a) is dependent largely on the ratio of coarse-grained and fine-grained beds in the sample. Beds are up to 2 cm thick, show both normal and reverse grading and sometimes internal wavy lamination. Laminae of fine organic detritus can be incorporated in the beds as can brick, slag and coal fragments (more frequently towards the top of this

Fig. 10. Current example of local scour in the concave bank (location Fig. 1c) at high water, in which a bench may eventually develop.

unit). There is no sign of erosional surfaces between the beds and almost no bioturbation. The thickness of this unit varies greatly but measures up to 1 m.

Unit 2 is present only locally, in point bars (Fig. 3) and in former local scours of the channel bank. These former scours are positioned in the concave bank (VZ1, Fig. 1c) and sometimes along straight channel sections (N2, Fig. 1c). The widening of the channel through the development of scours causes flow expansion in the main channel and this leads to a local loss of stream power. As a result, a longitudinal-shaped bar of bed material is deposited between the scour hole and the main channel, on top of which a bench is formed, a process described in detail by Page & Nanson (1982). Benches are defined as flat-surfaced, often vegetated, depositional sediment bodies along the channel bank and have been described in Australia (Taylor & Woodyer, 1978; Woodyer *et al.*, 1979; Page & Nanson, 1982; Erskine & Livingstone, 1999), Canada (Page & Nanson, 1982), England (Macklin *et al.*, 1992) and the embanked floodplains of the Rhine in The Netherlands (Middelkoop, 1997). Figure 10 shows an example of a typical recent scour found along the Geul River; it is still active and hence not a sampling site. The development of scour holes along the Geul River is often limited by trees impeding bank erosion (Fig. 10) and thus the spatial extent of the bench also is limited. Deposition on the old benches, such as the ones sampled, has reached the floodplain level. Bench deposition is characterized by reverse flow conditions that result in relatively high percentages of clay, silt and organic debris, wavy lamination around vegetation, and a variety of grading types in sand and mud layers (normal, reverse and mud–sand–mud (waxing–waning)) (Taylor & Woodyer, 1978; Woodyer *et al.*, 1979; Page & Nanson, 1982). Woodyer *et al.* (1979) concluded that sand laminae must occur from within-channel flood waves and that more than one sand-depositional episode may be associated with one flood wave. The deposits of unit 2 have many characteristics of bench sediments as described above and they are deposited in narrow sedimentary bodies with a discontinuous longitudinal distribution, which is also a bench characteristic (Erskine & Livingstone, 1999).

Unit 3 consists of silts to coarse sands. It is more homogeneous than unit 2, but more heterogeneous than unit 1. It is coarser grained than the other two units. Where thin (10–30 cm, Figs 8a & 9a), this unit is poorly layered and fairly strongly bioturbated, especially in the root zone. Where thick (up to 90 cm, Figs 5a–7a), sandy layers of 5–15 cm thick are present, sometimes with internal cross-bedding, and the layers contain pebbles and small brick and slag fragments up to 0.5 cm; the unit as a whole coarsens upward. Organic matter is often present in thin debris layers. Various anthropogenic materials are incorporated, such as candy wraps, plastic and aluminium foil. Even a flashlight and a carpet have been found. Cut-bank N6 (Figs 4 & 9a) is an example of a thin unit 3.

Unit 3 is present in the same locations as unit 2, although its deposits sometimes can be traced farther from the channel bank than those of unit 2 (Fig. 3). As the surface of the bench approaches floodplain level, the deposits gradually take on the characteristics of overbank deposits immediately adjacent to the channel, such as levees. The depth below floodplain surface of the transition between units 2 and 3 is very variable and the transition itself is quite abrupt. Therefore it seems unlikely that the sole cause of the coarse character of unit 3 is the approach of the bench level to floodplain level. The transition of unit 2 to unit 3 seems to indicate a change in regime toward floods with higher sediment carrying capacities.

Sediment age determination

The age of the sediments of the Geul River valley was determined by analysis of the mining history within the catchment and ^{137}Cs dating. The five cut-bank sections were analysed for trace metals, grain size and ^{137}Cs. Results are shown in Figs 5–9.

It is customary to correct heavy metal content of soil samples for organic matter and clay content, for example by calculating correlation and regression parameters between clay fraction, organic matter

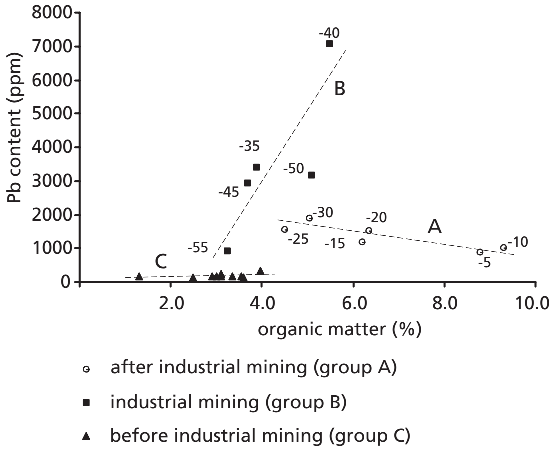

Fig. 11. Scatter plot of Pb content versus organic matter content, indicating the samples belonging to the different metal input intervals, with the samples of groups A and B labelled for depth (section N6, Fig. 1c).

content and the metal content (Leenaers, 1989; Middelkoop, 1997). Previous research claimed that correlations between metal content and either grain size or clay content can be neglected in the Geul River valley and corrections are not necessary (Leenaers, 1989; Swennen *et al.*, 1994). In order to check these claims scatter plots were made for metals versus organic matter and clay content (Fig. 11) making it clear that correlations for cut-bank sections as a whole are indeed low but that relationships between metals and soil characteristics change over time, resulting in the three groups that are marked in Fig. 11. The different intervals represent the lower part of the cut-bank section with low metal content (group C), the depth interval with maximum metal content (group B) and the upper part of the section with decreasing metal content (group A) (Stam, 1999). This author interpreted the different intervals as representing periods of varying metal inputs into the river system: the period before industrial mining, the industrial mining period, and afterwards. The scatter plots of each cut-bank section (only N6 is presented in this paper in Fig. 11) can be of use in pinpointing the end of mining in the cut-bank sections, by the separation of the samples of the mining period and the post-mining period. This transition is often not clear from metal levels alone, owing to the gradual decrease of metal production in both mines (Fig. 2), the erosion of the huge mine tailings that were left at La Calamine and Plombières, the metal input by more remote and smaller mines, and the reworking of previously deposited polluted flood sediments (Leenaers, 1989; Swennen *et al.*, 1994). Because the absolute metal levels were not important for this study, no correction of the metal content for grain size and organic matter content was deemed necessary.

The shape of the ^{137}Cs profile can be modelled in several ways, accounting for the percentage of cultivated soils and for the atmospheric input versus sediment input (Walling & He, 1992, 1993, 1997). As discussed by Stam (1999), the sampling methods used in this study result in considerable imprecision, and therefore the use of a sophisticated model would seem excessive. It is assumed that the time lag between atmospheric deposition over the catchment and deposition of the marked flood sediments has not been more than a few years owing to the widespread soil erosion in this area, the frequent floods, and the deposition of the dated sediments under or at bankfull discharge. Assuming that remobilization of ^{137}Cs has been smaller than the sampling interval, ^{137}Cs activity should give a fairly rough age estimate for the early to mid-1950s, the early 1960s (not used in this study), and the late 1980s (the Chernobyl accident) (Popp *et al.*, 1988; Leenaers, 1989; Ely *et al.*, 1992; Walling & He, 1992). The first appearance of ^{137}Cs in the sections is therefore marked as the year 1955 in Figs 5(c)–9(c). The top peak of ^{137}Cs activity in the sediment profiles has been marked as 1986.

The following dates could be defined in the sediment.

1806 In 1806 mining starts in La Calamine, leading to elevated zinc levels. Lead levels remain relatively low, because the ore body did not contain lead ores. Sedimentation at VZ1 (Fig. 5b), N2 (Fig. 7b) and N6 (Fig. 9b) started after 1806, judging by the zinc levels in the bottom of these sections, which are higher than background levels elsewhere. Visually the sediments deposited before and after 1806 are hardly distinguishable, although the grain-size analyses show an increase in coarse-grained sand content and there are more brick, slag and coal fragments. 1806 falls within unit 1.

1845 In 1845 lead mining starts in Plombières, causing elevated lead levels; zinc levels remain high. The transition from unit 1 to unit 2 occurs approximately at this date; in all cases it is within 5 cm (one sample distance) of the sample dated as 1845.

1885 Large-scale industrial mining (Fig. 2) ends in 1885 and this date has been determined by the shift in correlation between metals and organic matter from group A to group B (Fig. 11). 1885 falls within the deposits of unit 2.

1955 ^{137}Cs first appears in the atmosphere around 1955. The transition from unit 2 to unit 3 occurs near this date. Only in VZ1 (Fig. 2) does this transition occur slightly before 1955, indicating that the transition may have moved downstream with time.

1986 The explosion at Chernobyl causes a second peak in ^{137}Cs content. No change in sediment characteristics is observed in the deposits of unit 3 at this time.

Sedimentation rates

The combined results of heavy metal and ^{137}Cs dating for all five sections are presented in Fig. 12. Although the peak in ^{137}Cs associated with Chernobyl (1986) can be recognized in the sections, the time period since this accident is very short in comparison with the 5-cm spacing between subsequent samples and with the other time periods, and therefore not very accurate. As such, it has not been used for the calculations of sedimentation rates, and the most recent period for which sedimentation rates were calculated lasts from 1955 until 1996. Owing to variations in factors controlling sediment deposition between the five locations, such as local flow conditions, sedimentation rates deviate between the locations. Sections VZ1 and N2 (Fig. 1c), which are located in concave benches, show significantly higher sedimentation rates between 1845 and 1885 than the other locations, which are point bars (N3 and N6) and a former point bar in an artificially cut off meander belt (TGW). In addition to local variations, a more general trend is present: sedimentation rates are high between 1806 and 1845, and between 1845 and 1885 (Fig. 12). After 1885, sedimentation rates are much lower; from the 1950s onwards they are high again.

Even though the sections show no signs of erosion there must be many non-depositional surfaces, because flood sediments are deposited only during high discharges. It is to be expected that floods of a lower magnitude and higher frequency (including sub-bankfull floods) are registered at the bottom of the section (Woodyer *et al.*, 1979; Macklin *et al.*, 1992). Benches are formed in persistent periods of small floods, between periods of large floods in which the channel is excavated and benches are reworked (Erskine, 1992; Warner, 1994; Erskine & Livingstone, 1999). At the top of the section only larger (and thus fewer) floods can have deposited sediment owing to the elevated depositional surface. Currently scours can be seen to develop in every flood (Fig. 10), but there is no evidence that benches are presently being formed in the Geul River beyond the incipient stage of gravel bars, sometimes vegetated, just above the low-water level. Since the fieldwork was done in 1996, the deposits of bench VZ1 (Fig. 1c) have been almost completely removed by several metres of bank erosion. These observations indicate that a change in regime from smaller floods to larger floods has taken place, in addition to the natural tendency toward registering larger floods in the deposits. Therefore, the recent sedimentation rates represent larger floods than those of the nineteenth century. The regime change is most likely to have coincided with the transition between sedimentary units 2 and 3, which occurs around 1955.

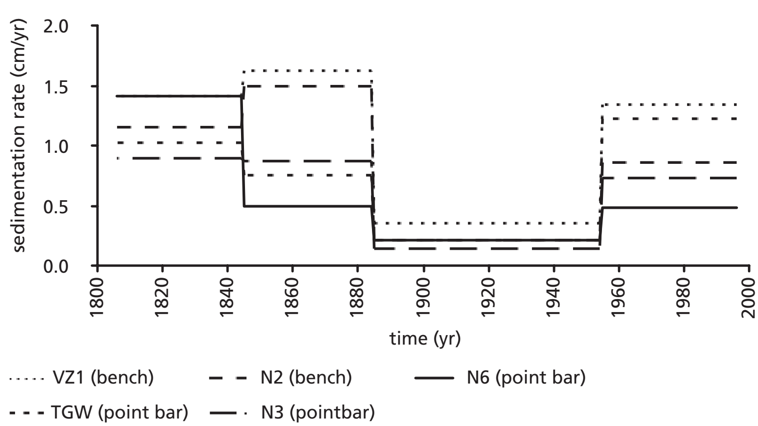

Fig. 12. Sedimentation rates in the nineteenth and twentieth centuries at five cut-bank sections.

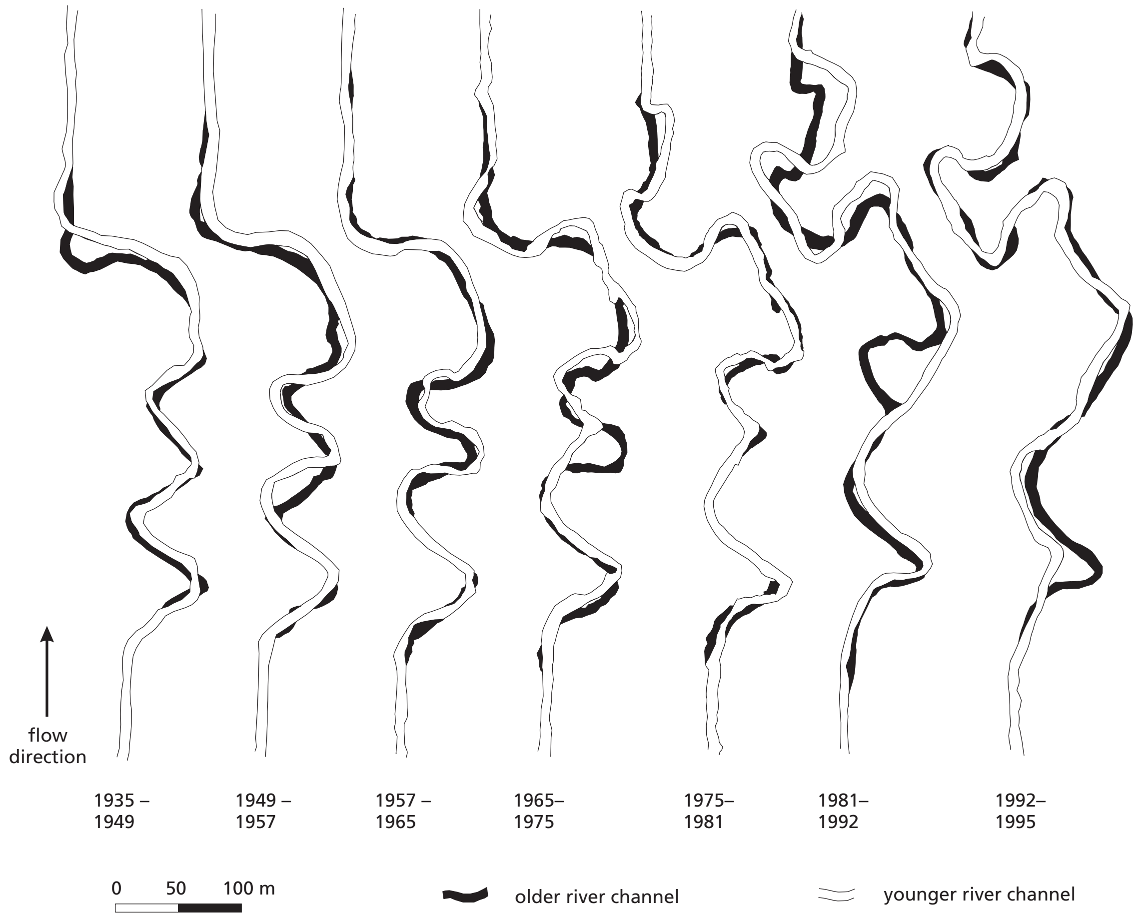

Fig. 13. Channel changes since 1935 for a river segment near Partij derived from aerial photographs (location Fig. 1c).

Channel-migration rates

When comparing the position of the Geul River channel on historic maps from the mid-nineteenth century onward with that on recent maps, the channel appears to have been immobile over practically the entire course between the border and its confluence with the Meuse. Overmars *et al*. (1996) accredit this to the active maintenance of the river channel in order to accommodate the large number of water mills in the valley. However, one segment of the channel near Partij (Fig. 1c), downstream from a mill and just upstream from a channel section that was straightened in the second part of the nineteenth century (Mols, 1939), has apparently been free to meander actively (Fig. 13). The channel-migration rate of this segment was quantified as the surface area between two river positions divided by the number of years between the two photographs (Fig. 14). The modest increase in

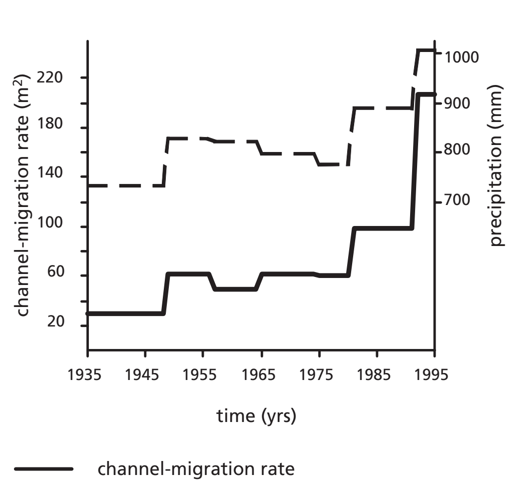

Fig. 14. Channel-migration rate of the river segment near Partij and average annual precipitation.

channel-migration rate that occurs after 1949 coincides with the increase in sedimentation rates around that time (Fig. 12). The channel-migration rate then remains quite stable until 1981, when it increases again, and after 1992 there is another sharp increase. The annual average precipitation data, which are included in Fig. 14, will be discussed in the next section.

FLOOD DEPOSITS IN RELATION TO PRECIPITATION AND LAND-USE

Precipitation

There are no precipitation time-series that go back 200 yr in The Netherlands, except the reconstructed Hoofddorp-Zwanenburg series located near Amsterdam (Figs 1a & 15) (Buishand & Velds, 1980). For this study it is assumed that even though the absolute yearly precipitation figures for Hoofddorp -Zwanenburg are not the same as in the Geul River catchment, wet and dry periods (on the level of years to decades) concur. The discharges of the Geul River at Hommerich are shown in Fig. 16. The discharges show infrequent floods between 1969 and 1974, and no floods between 1975 and 1978. From 1979 to 1987 the Geul River floods twice a year on average, and after 1987 it floods once a year. The average yearly precipitation at Hoofddorp for these periods is 721, 704, 899 and 839 mm, respectively. The average over the last 260 years is 758 mm. This indicates that the average annual precipitation can be used as a measure of flood activity. Alternatively, the number of years in each period with precipitation over a certain threshold (for instance 900 mm) could be used to determine relative wetness, but comparison of precipitation and flood occurrence in individual years does not give evidence of a simple relationship between height of annual precipitation and the flooding frequency in the same year. Therefore, average annual precipitation has been used for comparison with sedimentation rates.

Land-use history

At the start of the nineteenth century, roughly 80% of the surface area in South Limburg was cultivated (of which 10% was left fallow each year). The main crops were rye and winter wheat, and cattle fodder plants such as clover (Bieleman, 1992). During the first half of the nineteenth century there was an increase of the population in the mining areas in Belgium (256 people in 1816 versus 2572 people in 1858 for the city of La Calamine (Malvoz, personal communication, as quoted by Swennen *et al.* (1994)). The metal mining period also was characterized by deforestation and channelization of the Geul River in the mining area, with an increased discharge owing to groundwater pumping from the mines at Plombières (Engelen, 1976; Dejonghe *et al.*, 1993). The end of mining in the early 1880s practically coincided with the agricultural crisis (1878 until 1895). In this period many arable fields were converted into pastures and orchards, even more so after 1900 when the demand for manual labour in the Limburg coal mines made less labour-intensive farming practices necessary (Bieleman, 1992). In the community of Gulpen (Fig. 1b) the area of arable fields decreased, whereas the area of grassland and grazed orchards increased (Fig. 17; Renes, 1988). The population growth in the Geul River catchment is thought to have started after 1910, with an urbanized area of 0.54% of the total surface area in 1834, 3.97% in 1989, and 6.03% in 1992 (Dutoo, 1994). The evolution of the forest cover in the Lower Meuse region (which

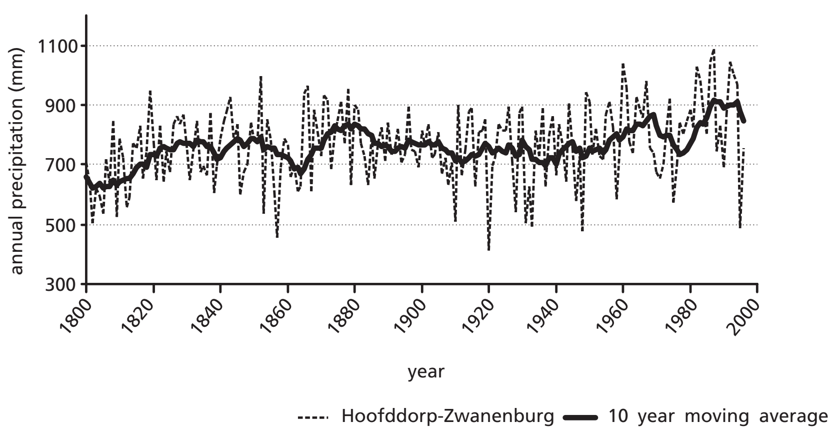

Fig. 15. Annual precipitation at Hoofddorp-Zwanenburg in the nineteenth and twentieth centuries and the 10-yr moving average.

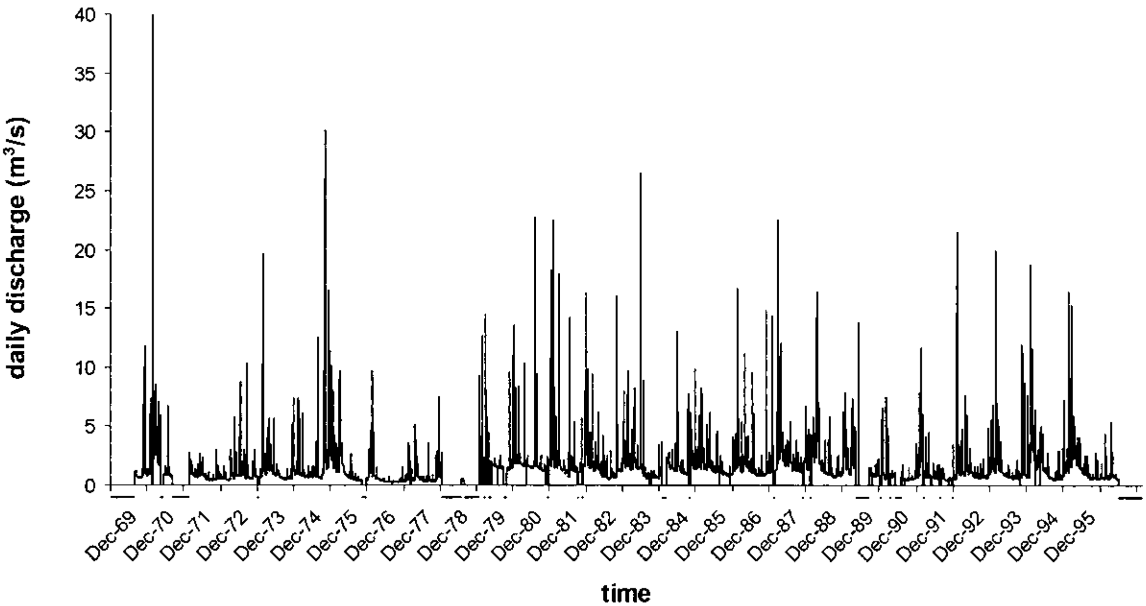

Fig. 16. Daily discharges at the Hommerich discharge gauge since 1969.

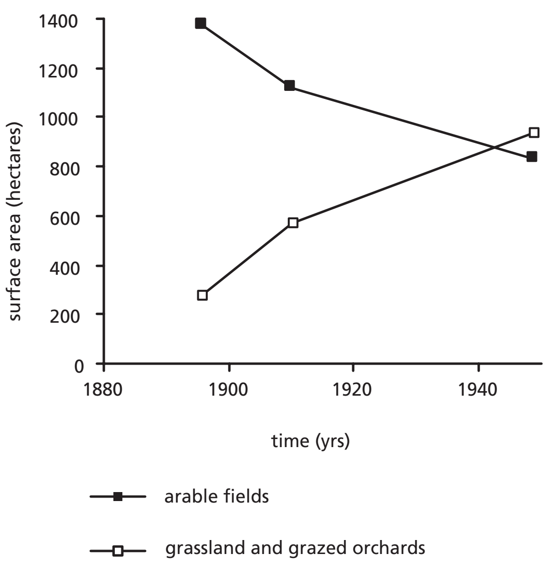

Fig. 17. Land-use changes in the community of Gulpen in the last century showing an increase in grassland at the expense of arable fields (after Renes, 1988).

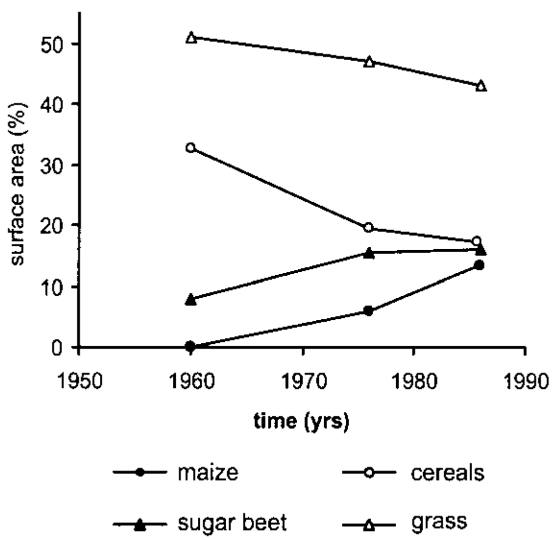

Fig. 18. Changes in crops in South Limburg in the last 30 yr showing an increase in crops causing soil erosion (maize and sugar beet) (after Renes, 1988).

includes the Geul River catchment) shows a decline until *c.* 1870, an increase between 1870 and 1920, and a small increase between 1960 and 1980 (Dutoo, 1994).

Since the 1950s, agricultural practices have been greatly altered in this area. The introduction of heavy machinery has resulted in upscaling, removal of 'graften' (linchets), changing of the plough direction from parallel to perpendicular to the contour lines, conversion of grassland into arable fields, improved drainage, and the introduction of crops such as maize and sugar beet that leave the fields fallow for 6 months of the year (Fig. 18; Schouten *et al.*, 1985;

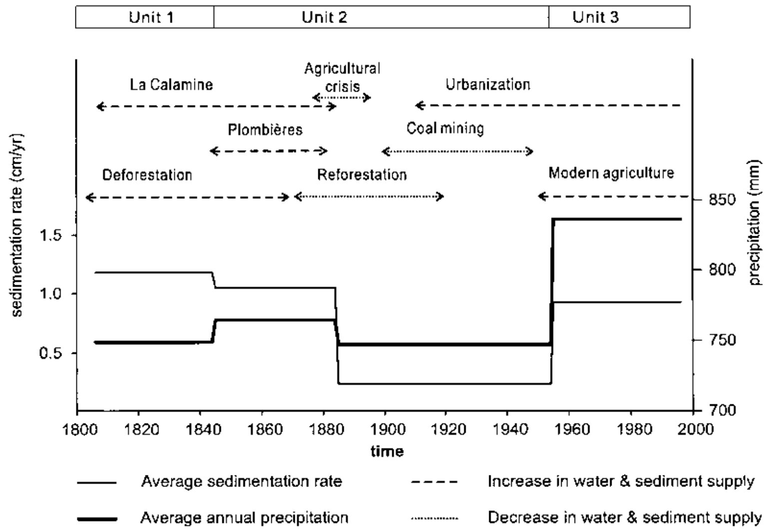

Fig. 19. Average sedimentation rates, average annual precipitation and land-use effects.

Van der Helm *et al.*, 1987; Leenaers, 1989; Leenaers *et al.*, 1990; De Roo, 1993). It has been estimated that crops like maize and sugar beet cause 92% of the total soil erosion in South Limburg (Van der Helm *et al.*, 1987). Total soil loss on cultivated slopes was estimated to be 15 t ha^{-1} yr^{-1} in 1985 (Bouten *et al.*, 1985).

Effects of land-use and precipitation on sedimentation

Between 1806 and 1885 annual precipitation was relatively low and sedimentation rates were relatively high (Fig. 19). Singh (1989) and Calder (1993) have given overviews of the effects of land-use changes on stream flow and sediment yield. In this period mine-water pumping and deforestation had a distinct effect on the water and sediment supply.

The start of mining in Plombières in 1845 did not lead to a further increase in sedimentation rate but it resulted in the transition from sedimentary unit 1 to unit 2, characterized by high metal content and a lack of bioturbation (perhaps caused by the metal content) (Figs 4 & 9b). Fieldwork conducted by Swennen *et al.* (1994) a few kilometres upstream from the study site revealed a rise in Zn in the sediment owing to the start of mining in Calamine in 1806 and subsequently a decline in Zn contamination that coincides with a rise in Pb content. This decline in Zn was associated with a new ore treatment plant in La Calamine, built in 1850. The increase in Pb content in our fieldwork area is accompanied (Figs 6b & 8b) or just preceded by a sharp increase in Zn (Figs 5b, 7b & 9b); evidently, most of the 'plume' of mining wastes from La Calamine (which is located further upstream than Plombières; Fig. 1b) did not reach the fieldwork area until well after 1806, although Zn contents are elevated before the mining in Plombières caused the transition to sedimentary unit 2 (Fig. 5b).

Between 1885 and 1955 average annual precipitation hardly decreased but land-use changed dramatically, with the closure of the metal mines, the agricultural crisis and reforestation, and this is reflected in the greatly decreased sedimentation rates (Fig. 19). The increasing urbanization after 1910 may have added to this effect by increasing storm runoff, but not the sediment supply, leading to bed and bank erosion and lower flood frequencies. The deposited sediment still bears the characteristics of the previous period even if the metal levels are lower, suggesting that bench-forming processes were still active and that there may still have been input of sediment into the system from the mining wastes and spoil heaps in the area (Swennen *et al.*, 1994).

The transition from sedimentary unit 2 to unit 3 in the 1950s (Figs 5–9) signals a change in flood regime as evidenced by the end of bench-type sedimentation and the increase of channel-migration rate. It is likely that the increased soil erosion from cultivated slopes, which was caused by the change in agricultural practices described in the previous section, is an important new source of sediment. Both the intensified agricultural practices and the increase in average annual precipitation could be the cause of the increased sedimentation rates since 1955 (Fig. 19) and the increased channel-migration rate after 1949 (Fig. 14). The importance of precipitation is suggested by the mostly similar pattern between channel-migration rate and the average annual precipitation since 1935 (Fig. 14). However, the period between 1975 and 1981 has relatively low average precipitation but the channel-migration rate is just as high as in the previous period (Fig. 14). The low precipitation average is the result of two consecutive dry years (1976 and 1977), followed by 4 years with precipitation slightly over 800 mm (which is still not high compared with the precipitation in the previous periods). The few floods during this period (Fig. 16) must have done significant geomorphological work, possibly as a result of the previous dry years, which may have decreased bank stability and enhanced sediment availability.

CONCLUSIONS

The floodplain deposits of the Geul River consist of Pleistocene and Holocene sand and gravel, topped by three fine-grained sedimentary units. The oldest unit is deposited as overbank fines over the entire floodplain, mostly before active Pb and Zn mining in the middle of the nineteenth century. Unit 2 consists of channel sediments deposited on point bars and benches, between the middle of the nineteenth century and the middle of the twentieth century. Unit 3 has been deposited as levee sediment since the 1950s. The sediments have been dated successfully by comparing the metal mining history with the heavy metal content of the sediment and by ^{137}Cs dating. Sedimentation rates for five cut-bank sections could be calculated for 1806–1845, 1845–1885, 1885–1955 and 1955–1996. A trend of high sedimentation rates between 1806 and 1885, low rates between 1885 and 1955, and higher rates after 1955 is evident. The higher sedimentation rates in the nineteenth century represent mostly high-frequency–low-magnitude flood events and are caused mainly by mining activities and deforestation. After the 1880s sedimentation rates dropped as a result of the end of mining activities, reforestation and the agricultural crisis, which, combined with the start of coal mining, resulted in arable fields being converted into meadows and orchards. Since the 1950s, the transition to sediment unit 3 is caused most likely by the increased soil erosion that accompanied the modernization of agriculture in the area. In addition, the flood regime shifted toward larger floods owing to a significant increase in precipitation. This is supported by the rates of channel migration, derived from aerial photographs since 1935, which correlate by and large with the average annual precipitation.

ACKNOWLEDGEMENTS

I am grateful to A. van Mierlo, H. Ludwig, A. van der Klis and S. Keesstra for doing the bulk of the fieldwork and a substantial part of the laboratory work. M. Konert has been very helpful in the sediment laboratory. M. Broekema analysed hundreds of samples with the X-ray sequential spectrometer. W. Boer of NIOZ analysed the ^{137}Cs activities and discussed them with me. A. van Mierlo did preliminary work on the channel-change rates. The time-series of discharge at Hommerich are courtesy of 'Waterschap Roer en Overmaas'. Several people have helped shape this paper by commenting on earlier drafts: J. Vandenberghe, C. Kasse, T. Hobma and D. Gibbs. I have greatly benefited from several discussions with R. Swennen of Leuven University and both he and M.C. Bourke have provided helpful reviews that allowed me to improve the manuscript.

REFERENCES

Berger, H.E.J. (1992) *Flow forecasting for the River Meuse*. PhD thesis, Delft Technical University, Delft.

Bieleman, J. (1992) *Geschiedenis Van de Landbouw in Nederland, 1500–1950*. Boom, Amsterdam.

Bouten, W., Van Eijsden, G., Imeson, A.C., Kwaad, F.J.P.M., Mücher, H.J. & Tiktak, A. (1985) Ontstaan en erosie van de loessleemgronden in Zuid Limburg. *K. Ned. Aardkund. Genootsch. Geogr. Tijdschr.* **XIX**, 192–207.

Buishand, T.A. & Velds, C.A. (1980) *Neerslag en verdamping*. Koninklijk Nederlands Meteorologisch Instituut (Royal Netherlands Meteorological Institute), De Bilt.

Calder, I.R. (1993) Hydrologic effects of land-use change. In: *Handbook of Hydrology* (Ed. Maidment, D.R.), pp. 13.1–13.50. McGraw-Hill, New York.

Dejonghe, L., Ladeuze, F. & Jans, D. (1993) *Atlas Des Gisements Plombo-Zincifères Du Synclinorium de Verviers (Est de la Belgique)*. Belgisch Geologische Dienst/Service Géologique de Belge, Brussel.

De Roo, A.P.J. (1993) *Modelling surface runoff and soil erosion in catchments using Geographical Information Systems.* PhD Thesis, Utrecht University.

De Smedt, P. (1973) *Paleogeografie En Kwartair-Geologie Van Het Confluentiegebied Dijle-Demer*. Geografisch Instituut Katholieke Universiteit Leuven/Institut de Géographie Université Catholique de Louvain, Leuven.

Dijkman, J. & Pedroli, B. (1994) Hydrologische aspecten. In: *Onderzoek Watersnood Maas*, Vol. 4. Waterloopkundig laboratorium/Delft Hydraulics, Delft.

Dutoo, D. (1994) Het Belgische Stroombekken. In: *Onderzoek Watersnood Maas, Achtergrondrapport 1.* Water-loopkundig Laboratorium Delft/Delft Hydraulics, Delft.

Ely, L.L., Webb, R.H. & Enzel, Y. (1992) Accuracy of post bomb ^{137}Cs and ^{14}C in dating fluvial deposits. *Quat. Res.* **38**, 196–204.

Engelen, F.H.G. (1976) Delfstoffen en hun invloed op politieke beslissingen. *Grondboor En Hamer* **1**, 20–31.

Erskine, W.D. (1992) Channel response to large-scale river training works: Hunter River, Australia. *Regulated Rivers Res Man.* **7**, 261–278.

Erskine, W.D. & Livingstone, E.A. (1999) In-channel benches: the role of floods in their formation and destruction on bedrock-confined rivers. In: *Varieties of Fluvial Form* (Eds Miller, A.J. & Gupta, A.), pp. 445–475. J. Wiley & Sons, New York.

Havinga, A.J. & Van den Berg van Saparoea, R.M. (1980) Former vegetation and sedimentation in the valley of the river Geul. *Meded. Landbouwhogesch. Wageningen* **80**, 47–59.

Klimek, K. & Zawilinska, L. (1985) Trace elements in alluvia of the Upper Vistula as indicators of palaeohydrology. *Earth Surf. Process. Landf.* **10**, 273–280.

Konert, M. & Vandenberghe, J. (1997) Comparison of laser grain size analysis with pipette and sieve analysis: a solution for the underestimation of the clay fraction. *Sedimentology* **44**, 523–535.

Leenaers, H. (1989) *The Dispersal of Metal Mining Wastes in the Catchment of the River Geul (Belgium–The Netherlands)*. Koninklijk Aardkundig Genootschap/Geografisch Instituut Rijksuniversiteit Utrecht, Amsterdam/Utrecht.

Leenaers, H., Rang, M.C. & Schouten, C.J. (1990) Integraal Waterbeheer of dweilen met de kraan open. *Publ. Natuurhist. Genoot. Limburg* **XXXVIII**, 102–108.

Macklin, M.G. (1996) Fluxes and storage of sediment-associated heavy metals in floodplain systems: assessment and river basin management issues at a time of rapid environmental change. In: *Floodplain Processes* (Eds Anderson, M.G., Walling, D.E. & Bates, P.D.), pp. 441–460. J. Wiley & Sons, New York.

Macklin, M.G., Rumsby, B.T. & Newson, M.D. (1992) Historic floods and vertical accretion of fine-grained alluvium in the lower Tyne valley, North East England. In: *Dynamics of Gravel-Bed Rivers: 3rd International Workshop on Gravel-Bed Rivers* (Eds Billi, P., Hey, R., Thorne, C. & Tacconi, P.), pp. 573–589. J. Wiley & Sons, New York.

Middelkoop, H. (1997) *Embanked floodplains in the Netherlands. Geomorphological evolution over various time scales.* PhD Thesis, Utrecht Universiteit.

Mols, W.M.J. (1939) *De Geul met Zijbeken*. Provinciale waterstaat Limburg, Maastricht, 195 pp.

Overmars, W., Helmer, W. & Litjens, G. (1996) *Beekdalontwikkeling Beneden-Geul. Deel 1 Hoofdrapport*. Bureau Stroming, Laag Keppel.

Page, K. & Nanson, G. (1982) Concave-bank benches and associated floodplain formation. *Earth Surf. Process. Landf.* **7**, 529–543.

Popp, C.J., Hawley, J.W., Love, D.W. & Dehn, M. (1988) Use of radiometric (Cs-137, Pb-210), geomorphic, and stratigraphic techniques to date recent oxbow sediments in the Rio Puerco drainage Grants uranium region, New Mexico. *Environ. Geol. Water Sci.* **11**, 253–269.

Renes, J. (1988) *De Geschiedenis Van Het Zuidlimburgse Cultuurlandschap*. Van Gorkum, Maastricht.

Riezebos, P.A. & Slotboom, R.T. (1978) Pollen analysis of the Husterbaach peat (Luxembourg): its significance for the study of subrecent geomorphological events. *Boreas* **7**, 75–82.

Schouten, C.J., Rang, M.C. & Huigen, P.M.J. (1985) Erosie en wateroverlast in Zuid-Limburg. *Landschap* **2**, 118–132.

Singh, V.P. (1989) Hydrologic effects of land use. In: *Watershed Modelling* (Ed. Singh, V.P.), pp. 260–276. Prentice Hall, New Jersey.

Stam, M.H. (1999) The dating of fluvial deposits with heavy metals, ^{210}Pb and ^{137}Cs in the Geul catchment (The Netherlands). *Phys. Chem Earth Part B Hydrol. Oceans Atmos.* **24**, 155–160.

Swennen, R. & Viaene, W. (1990) Lithogeochemical patterns around Pb–Zn mineralizations in Dinantian carbonate rocks of Eastern Belgium. *Miner. Deposita* **25**, 251–261.

Swennen, R., Van Keer, I. & De Vos, W. (1994) Heavy metal contamination in overbank sediments of the Geul river (East Belgium): Its relation to former Pb–Zn mining activities. *Environ. Geol.* **24**, 12–21.

Taylor, G. & Woodyer, K.D. (1978) Bank deposition in suspended-load streams. In: *Fluvial Sedimentology* (Ed. Miall, A.D.), Mem. Can. Soc. petrol. Geol., Calgary **5**, 257–275.

Vandenberghe, J. (1977) *Geomorfologie Van de Zuiderkempen*. Paleis der Academiën, Brussel.

Vandenberghe, J., Mücher, H.J., Roebroeks, W. & Gemke, D. (1985) Maastricht–Belvédère: stratigraphy, palaeoenvironment and archeology of the middle and late Pleistocene deposits. *Meded. Rijks geol. Dienst.* **39**, 8–18.

Van der Helm, P.P.M., De Roo, A.P.J. & Schouten, C.J. (1987) Milieu-effecten van het ruimtegebruik in streekplangebied Zuid Limburg. Deel 3: Bodemerosie en wateroverlast. MSc Thesis, Utrecht University.

Van de Westeringh, W. (1980) Soils and their geology in the Geul Valley. *Meded. Landbouwhogesch. Wageningen* **80**, 1–25.

Walling, D.E. & He, Q. (1992) Interpretation of caesium-137 profiles in lacustrine and other sediments: the role of catchment-derived inputs. *Hydrobiologia* **235/236**, 219–230.

Walling, D.E. & He, Q. (1993) Use of cesium-137 as a tracer in the study of rates and patterns of floodplain sedimentation. In: *Tracers in Hydrology (Proceedings of the Yokohama Symposium)* (Ed. Peters, N.E.), pp. 319–328. Publication 215, International Association of Hydrological Sciences, Wallingford.

Walling, D.E. & He, Q. (1997) Use of fallout ^{137}Cs in investigations of overbank sediment deposition on river floodplains. *Catena* **29**, 263–282.

Walling, D.E., He, Q. & Nicholas, A.P. (1996) Floodplains as suspended sediment sinks. In: *Floodplain Processes* (Eds Anderson, M.G., Walling, D.E. & Bates, P.D.), pp. 399–440. J. Wiley & Sons, New York.

Warner, R.F. (1994) Temporal and spatial variations in erosion and sedimentation in alternating hydrological regimens in southeastern Australian rivers. In: *Variability in Stream Erosion and Sediment Transport* (Eds Olive, L.J., Loughran, R.J. & Kesby, J.A.), pp. 211–219. Publication 224, International Association of Hydrological Sciences, Wallingford.

Woodyer, K.D., Taylor, G. & Crook, K.A.W. (1979) Depositional processes along a very low-gradient, suspended-load stream: the Barwon river, New South Wales. *Sediment. Geol.* **22**, 97–120.

Spec. Publs int. Ass. Sediment. (2002) **32**, 269–79

Use of remote sensing in monitoring river floods and their effects on the landscape

L. HALOUNOVÁ

MGE DATA, Vrchlického 60, Prague, Czech Republic (Email: Halounov@fsv.cvut.cz)

ABSTRACT

Intense rainfall caused extensive flooding in the eastern part of the Czech Republic in July 1997. On 4 July 1997, a low-pressure system originating in northern Italy tracked north-east to the Moravia region of the Czech Republic bringing intense rainfall as it moved to the south-east of Poland and Silesia on the morning of 6 July. Over a 5-day period, 500 mm of rain fell over one-third of Moravia (10 000 km^2). The average rainfall for the Czech Republic is 600 mm yr^{-1} (Halounová *et al.*, 1999). The region of South Moravia was imaged three times by the RADARSAT satellite: one image was taken at the flood peak, one image after the peak, and the last one at the end of the flood. These radar images allowed detailed monitoring of the flood and its effects. The flood-peak image was used for choosing flooded areas in an agricultural region. Each flooded 'area' was part of a larger 'field'; that is, of a parcel of land delimited by natural or manufactured features visually recognizable on available SPOT and Thematic Mapper images and on the peak-flood RADARSAT image. Flood-induced changes to the land surface could be detected by comparing the backscatter mean values of areas with those of their associated fields and by considering the fields and areas backscatter standard deviations measured on the peak-flood image and two subsequent RADARSAT images taken during flood recession. This could be done because of the peculiar characteristics of radar images. Radar backscatter values are influenced mainly by surface roughness (the higher the roughness the higher the backscatter) and by moisture (the higher the moisture the higher the backscatter). Depending on the backscatter mean values of areas and their respective fields in the various images, it was possible to reconstruct events during the flood in that region. For example, if the post-peak flood surface of a given area was smoother (lower mean backscatter) than its field, it was a zone of sedimentation. If the surface roughness (similar backscatter) was the same in an area as in its field, nothing had changed. If the surface was rougher in the area than in the field, it may be attributable to erosion or sedimentation of coarse material. These conclusions were validated by using the standard deviation values of the backscatters of the fields. This novel method of analysis is effective in studying open terrains, such as agricultural lands, but cannot be used in forested lands. There the flood delineation can be carried out only at the moment of imaging: flooded forest backscatter mean values are generally higher than non-flooded forest backscatter mean values.

INTRODUCTION

The objective of this study is to establish a procedure for estimating the effects of river floods in large areas utilizing remote sensing satellite data. Floods usually occur unexpectedly and generally last a short time. Satellite image data can show floods instantaneously over tens of thousands of square kilometres. Radar satellite data can be recorded at scales of 1 : 25 000, 1 : 50 000 and smaller, under any atmospheric situation. They thus can be obtained when needed during various floods stages, the only limiting factor being the satellite orbit position. There are several satellites equipped with radar sensors, such as ERS (Europe) and RADARSAT (Canada). RADARSAT offers different pixel resolution (from 9 m in Fine Mode to 30 m in Standard Mode or Wide Mode, to 50 m in ScanSAR Narrow Mode and 100 m in ScanSAR Wide Mode). Each mode can image Earth's surface under several different ranges of incidence angles (that is, the Fine Mode offers five incidence angle ranges, the Standard Mode seven incidence angle ranges, Wide Mode three incidence angles ranges). The RADARSAT time resolution (time period between two possible images of the same area by the same sensor) varies from one to ten days depending on the

Flood and Megaflood Processes and Deposits: Recent and Ancient Examples. Edited by I. Peter Martini, Victor R. Baker and Guillermina Garzón © 2002 International Association of Sedimentologists. ISBN: 978-0-632-06404-5

beam mode chosen and the latitude of the area of interest (RSI, 1995).

Three radar images obtained during the flood on 14, 24 and 27 July 1997 by the RADARSAT satellite with C-band wavelength were used in this study (Table 1). In addition, three scanner images with visible and infrared wavelength bands (two SPOT images (5 & 18 May 1997) prior to the flood, and one Thematic Mapper (25 August 1997) showing the study area after the flood) were used.

This study was based on two phenomena of radar: its sensitivity to roughness, and to moisture in relation to incidence angles. A radar image is a record of the interaction of energy and objects at the Earth's surface. Its appearance is dependent on such variables as geometric shape, surface roughness and moisture content of the target objects, as well as the sensor-target geometry and the 'look direction' of the radar sensor. Radar transmits microwave pulses towards a target, receives a returned portion of the transmitted signal (backscatter) after it has interacted with the target and observes the strength, temporal behaviour and the time delay of the returned signals. The radar image is a display of grey tones, which are proportional to the amount of backscatter that is received from a target. Targets that produce a large amount of backscatter appear as light grey tones on a radar image.

Radar images can be viewed as single-channel, black and white images, which have a characteristic 'salt and pepper' appearance. Pixel values (= backscatter values) represent the strength of the returned radar signal from Earth's surface. For each surface feature, there is a statistical distribution of the probable strength of the returned signal. Each pixel representing that surface is assigned a value selected randomly from the statistical distribution. Therefore, a seemingly homogeneous surface area has an irregular distribution of light and dark pixels, producing a granular effect. This effect is termed 'speckle' and is an inherent property of radar images (RSI, 1995). Several procedures were used to alleviate these effects. First, the original image data were compressed from 16 bit to 8 bit data and, second, the images were smoothed out utilizing a 5×5 pixel spatial filter. It should be noted that the same target may show different average backscatter values at different times owing to different states of all targets (moisture, temperature and so on).

Frequency and incidence angle of a radar beam are the two main parameters that determine its penetration capabilities through an agricultural or forested target. Higher frequency microwaves (X-band and C-band) primarily interact at the surface, whereas lower frequency microwaves (L-band and P-band) penetrate into the canopy and soil. The RADARSAT sensor operates at a single microwave frequency, known as C-band (5.3 GHz frequency and 5.6 cm wavelength). RADARSAT transmits and receives its microwave energy in a HH (horizontal transmit—horizontal receive) polarization of electric field. The spectral resolution of processed images is 16 bits per pixel. RADARSAT digital products can be delivered as six different data types. A Path Image product (used in this case) is aligned parallel to the satellite orbit path. Latitude and longitude position information were added to identify the positions of first, middle and last pixel. The product was delivered calibrated, primarily for electrical stability of the radar sensor and to assure repeatable measurements over time: the RADARSAT system has been designed to achieve high radiometric accuracy (within one scene < 1.0 dB, over 3 days < 2.0 dB with global dynamic range 30.0 dB). The accuracy is defined (Rignot & van Zyl, 1993) as

$$dB = 10 \log_{10}(\text{ratio of digital numbers}).$$

Steeper incidence angles result in greater signal penetration through a canopy because roughness effects from the vegetation are minimized. The radar sensitivity to moisture is higher at steeper incidence angles, whereas the radar sensitivity to the roughness is higher at shallower incidence angles. Ulaby (1974) suggested that steep incidence angles (10–20°) are optimal for soil moisture studies. The surface roughness cannot be distinguished on scanner data (such as those of Thematic Mapper from Landsat and SPOT images); the soil moisture can be partly detected from scanner data. Flooded forests cannot be determined from scanner data.

A radar beam obliquely hitting a smooth surface

Data type	Date	Image size (km^2)	Incidence angle (°)
Standard 7	14 July 1997	100×100	45–49
Standard 5	24 July 1997	100×100	36–42
Wide 1	27 July 1997	150×150	20–31

Table 1. RADARSAT images with descending orbit in South Moravia used in this study.

is reflected away and is not returned to the satellite sensor. That is why a smooth water surface is black (pixel values are zero) and easily recognizable on radar images and even scanner images. Surface water that is hidden in forests is not distinguishable on scanner images. Radar images allow us to see flooded parts of forests because double-bounce scattering (= corner reflector in forest stand) of the radar beam between tree trunks and the water surface can give a very strong return (Richards *et al.*, 1987; Ahern, 1995). It has been proven that images from synthetic aperture radar (RADARSAT is an SAR) can be interpreted to map flood inundation over large areas of forested wetlands (Krohn *et al.*, 1983; Ormsby & Blanchard, 1985; Place, 1985; Imhoff *et al.*, 1987; Hess *et al.*, 1990; Sippel *et al.*, 1994; Wang *et al.*, 1995). Wang *et al.* (1995) also compared the C- and L-bands with respect to the detection of flooding in Amazonian forests, and reported that L-band radar provided the best distinction of flooding in a forest. C-band of RADARSAT was not the most suitable for the flood detection in forest areas. However, C-band data may provide useful soil moisture information (Beaudoin *et al.*, 1990; Pietroniro *et al.*, 1993; Merot *et al.*, 1994; Wang *et al.*, 1994), and these being those provided by RADARSAT have been used in this study.

STUDY DESIGN AND METHODS

This study first analyses modifications of open agricultural land surfaces caused by flooding and, second, tries to determine the extent of flooding in forested lands. The study covers part of the lower reaches of the Moravia River, at the boundary between the Czech Massif and the Carpathians (Fig. 1; Krumpera *et al.*, 1988). The valley has a slope of 0.6–1.2%. Two localities were selected: an upstream one was several hundred metres wide and up to 22 km long; the downstream one was up to 4 km wide and 45 km long. Most of the inundated terrains studied had nearly mature crops (corn two or three weeks before harvest, maize about six weeks, and beets about two months), or were forested.

Flooding can be observed either directly or, as contended in this paper, can be determined even after the water has retreated from a locality and is no longer visible. This is because floods modify floodplains by smoothing them out either by bending vegetation or depositing sediments, or roughen them by eroding or depositing coarse sediments and/or temporarily changing soil moisture. These features are readily distinguishable on RADARSAT images and can be quantified through measurements of backscatter.

The testing procedure for agricultural lands was to select 28 fields (sites) seen partially flooded on the 14 July peak-flood RADARSAT image, and determine changes as detected on images of 24 and 27 July as the flood receded (Fig. 2). The fields were delimited by boundary features visible both on the RADARSAT images and on available SPOT and Thematic Mapper images. They contained areas that were flooded on the 14 July image (in this paper the terms ‘area’ or ‘flooded area’ are used exclusively to indicate ‘a terrain selected for study that was seen to be flooded on the 14 July RADARSAT image’; the term ‘field’ is used to indicate ‘a land parcel selected (site) for study that is defined by visibly distinguishable bounding features and was composed of flooded (area) and non-flooded terrains on the 14 July RADARSAT image’). Changes that occurred during flood recession were measured by the changing ratios of the average backscatter of the areas and of their associated fields. Average backscatter cannot, however, necessarily and uniquely characterize the features of land that may have a different internal distribution of pixel brightness. This characteristic was evaluated by examining the backscatter standard deviation of each area and its field, and by a visual estimate of the texture (uniform or clustered bright and dark pixel distributions) of the terrain. The latter information was used to establish whether similar average backscatter values derived from an area and its field represent similar textural characteristics. For example, a flooded area so defined on the 14 July image can in a subsequent image have the same average backscatter and standard deviation as the field it is associated with, but a very different texture because a part of it may still be under water and therefore be completely black (no backscatter) and another part can be very bright (high backscatter values) owing to the residual high soil moisture.

Flooded forests were distinguished from non-flooded forests because of their visibly higher backscatter. This was studied on 20 flooded forest sites and 15 adjacent non-flooded forest sites. Fields and areas cannot be defined in forested terrains, and the numbering of flooded and non-flooded sites studied indicates only geographical proximity and views on the same image. Figure 4, for example, shows an inundated forest site (land between flood delineation lines) and adjacent non-flooded forest site (the large zone adjacent to the inundated one). All three RADARSAT images (14, 24 and 27 July) combined were used for the selection of the forest sites.

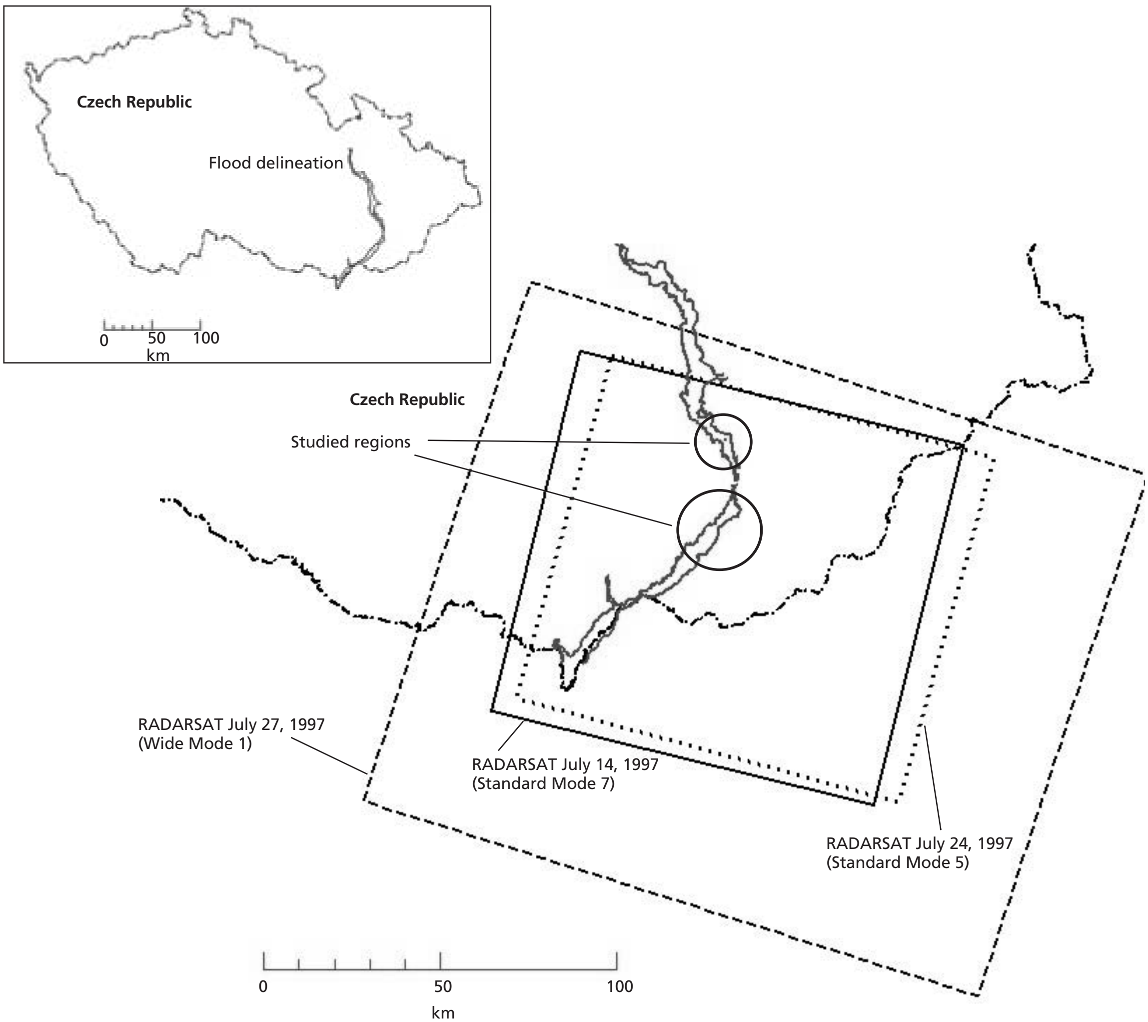

Fig. 1. Map of the Czech Republic with boundaries of the available RADARSAT images and studied regions (north is top of page).

RESULTS

Flood effects on agricultural areas

The mean backscatter values of the flooded areas (as defined on the 14 July peak-flood image) and associated fields for the 24 and 27 July images are shown in Fig. 3. Five terrain conditions (cases) were distinguished.

Case 1 (Table 2, Fig. 3a–d: sites 1, 2, 3 and 4) is characterized by areas that have low backscatter standard deviation and the same mean backscatter value of near zero as that of their associated fields on the 24 July RADARSAT image. Changes can be observed on the July 27 image: (i) areas 1 and 2 still have low standard deviation but the average mean backscatter value is lower than that of the fields; (ii) area 3 has high standard deviation and average backscatter of the area similar to that of the field; and (iii) area 4 has a very high standard deviation and an average backscatter value higher than that of the field. This has been interpreted to indicate that areas 1 and 2 have acquired a smooth surface, possibly owing to deposition of a thin sedimentary layer; area 3 has not experienced

Table 2. Relationships between backscatter parameters of areas and fields. The term 'not decided' relates to sites with high moisture where it is not possible to distinguish roughness and compare with conditions existing before the flood or in non-flooded terrains.

		24 July			27 July		Interpretation	
Case	Site	Mean backscatter of area and field	Area mean backscatter	Area standard deviation	Mean backscatter of area and field	Area mean backscatter	Changes on the land surface	Cause: sedimentation/ erosion
1	1	Equal to	Zero	Low	Lower than	Low	Yes	Yes
1	2	Equal to	Zero	Low	Lower than	Low	Yes	Yes
1	3	Equal to	Zero	High	Equal to	High	No	
1	4	Equal to	Zero	High	Greater than	Very high	Not decided	Potential erosion
2	5	Lower than	Low	Low	Lower than	Low	Yes	Yes
2	6	Lower than	Low	Low	Lower than	Low	Yes	Yes
2	7	Lower than	Zero	Low	Lower than	Low	Yes	Yes
2	8	Lower than	Zero	Low	Lower than	Low	Yes	Yes
2	9	Lower than	Zero	Low	Lower than	Low	Yes	Yes
2	10	Lower than	Low	Low	Lower than	Low	Yes	Yes
2	11	Lower than	Zero	High	Equal to	High	Not decided	Potential erosion
3	12	Lower than	High	High	Lower than	High	Yes	Yes
3	13	Lower than	High	High	Equal to	High	No	
3	14	Lower than	High	High	Lower than	High	Yes	Yes
3	15	Lower than	High	High	Lower than	High	Yes	Yes
3	16	Lower than	High	High	Lower than	High	Yes	Yes
4	17	Equal to	High	High	Greater than	High	Not decided	Potential erosion
4	18	Equal to	High	High	Greater than	High	Not decided	Potential erosion
4‘	19	Equal to	High	High	Lower than	High	No	
4‘	20	Equal to	High	High	Lower than	High	No	
4“	21	Equal to	High	High	Equal to	High	No	
4“	22	Equal to	High	High	Equal to	High	No	
5	23	Greater than	High	High	Equal to	High	No	
5	24	Greater than	High	High	Greater than	Very high	Not decided	Potential erosion
5	25	Greater than	High	High	Greater than	High	Not decided	Potential erosion
5	26	Greater than	High	High	Greater than	Very high	Not decided	Potential erosion
5	27	Greater than	High	High	Greater than	Very high	Not decided	Potential erosion
5	28	Greater than	High	High	Greater than	Very high	Not decided	Potential erosion

major changes; and area 4 had an increase in surface roughness possibly related to erosion or variation in soil moisture. Indeed, one of the limitations of this study for this and the other cases is the unavailability of ground-truthing during this event, nor the availability of an additional image taken during a subsequent drier period, which would have allowed evaluation of the effect of decreasing moisture and thus confirmed the validity of the erosional interpretation. Site (field and area) 2 is illustrated as Case 1 in Fig. 2.

Case 2 (Table 2, Fig. 3a–d: sites 5–11) is characterized by areas with backscatter standard deviations that are low and the mean backscatter values are lower than those of the associated fields, both on the 24 and 27 July images. The exception is site 11, which has high backscatter mean values both in the area and the associated field on the 27 July image. In the 27 July image, however, the areas have higher mean backscatter values than in the previous image, and their standard deviations are lower than those of their associated fields. All this is interpreted to indicate that the areas were probably still covered by water or smoothed out by a thin sediment layer on the 24 and 27 July images. The fact that the backscatter values of the areas are relatively low on 27 July further indicates that high moisture is not the main factor. If that was the case, much higher backscatter values should have been measured on the 27 July image because it was taken at a steeper incidence angle (Wide 1) and thus would have been more sensitive to moisture than the 24 July image taken at a shallower angle of incidence (Standard 5). Furthermore, because the difference in mean backscatter between the areas and their fields is not great, moisture is not considered to be a determinant variable. Therefore, the low backscatter mean

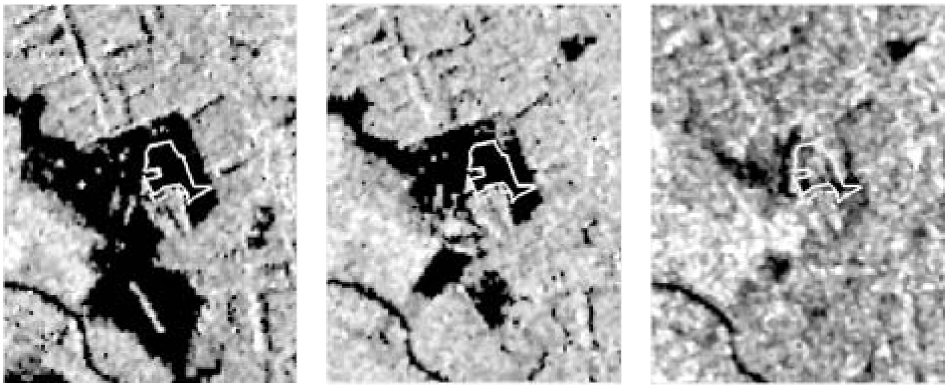

Case 1

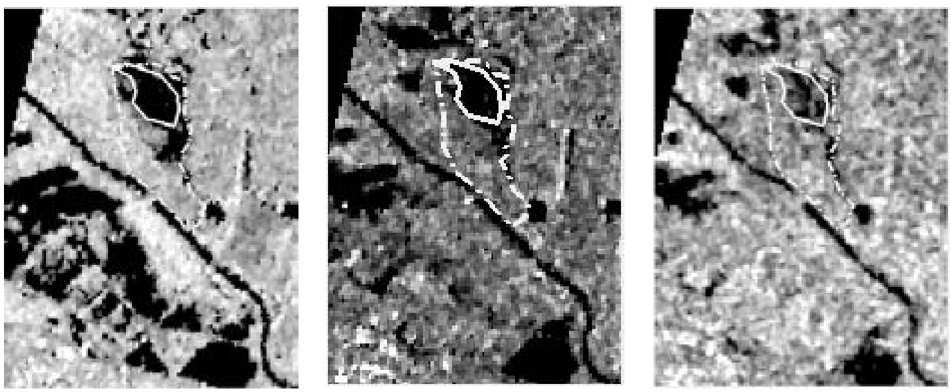

Case 2

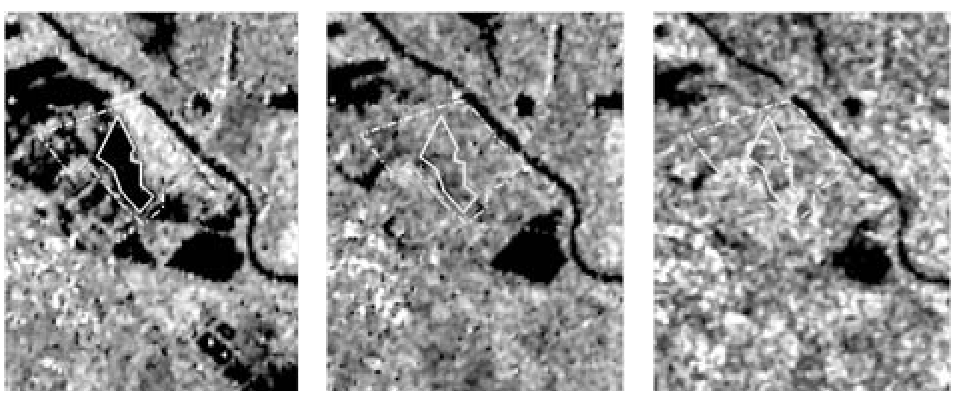

Case 3

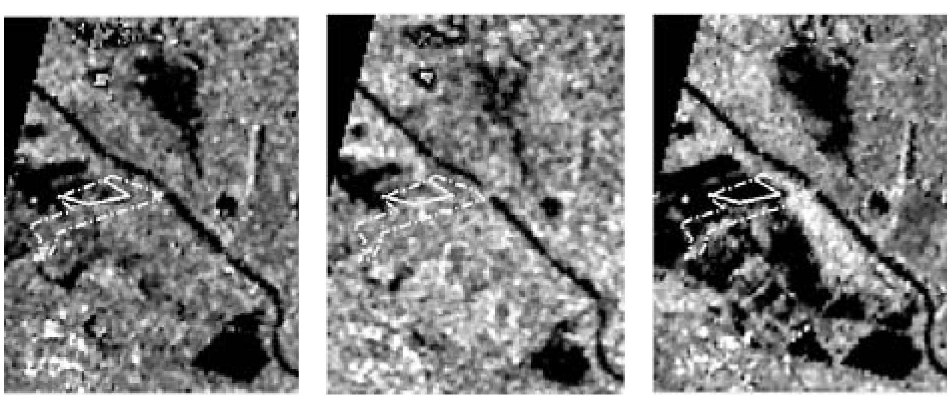

Case 4

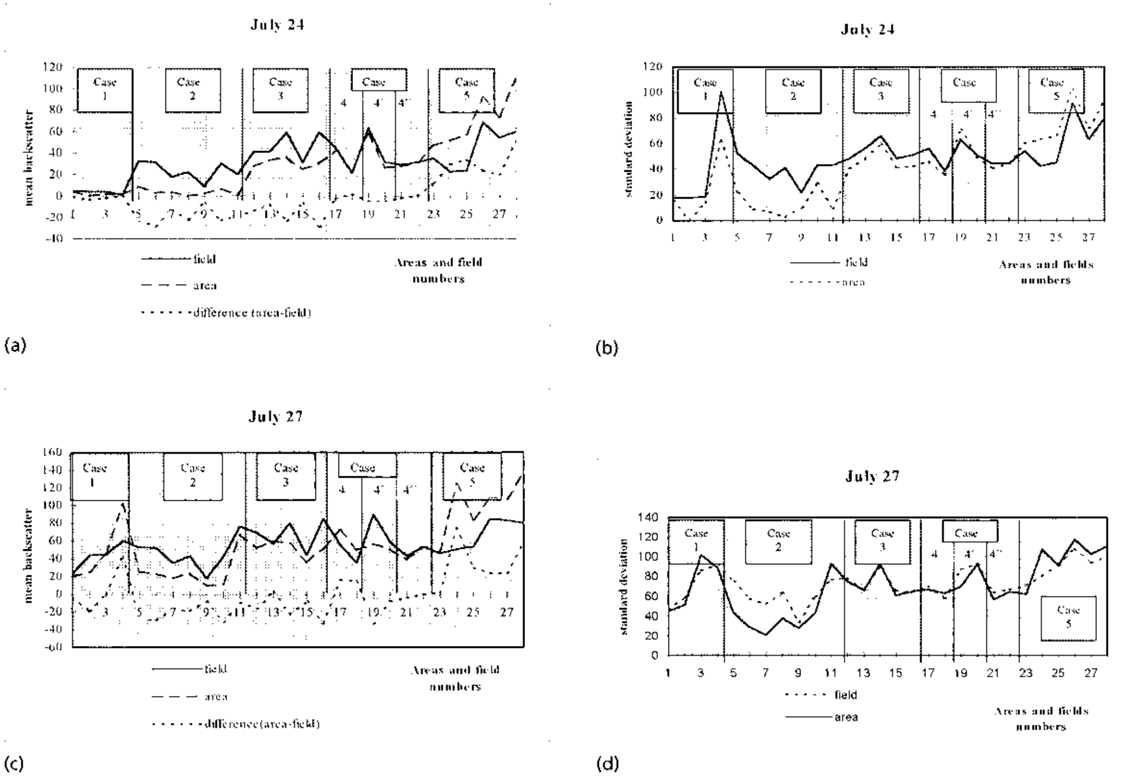

Fig. 3. Diagrams illustrating relationships between mean backscatter values and standard deviations of the various sites measured on different RADARSAT images. (a) Mean backscatter values of fields and areas of agricultural terrains measured on the 24 July image; (b) standard deviations of fields and areas of agricultural terrains measured on the 24 July image; (c) mean backscatter values of fields and areas of agricultural terrains measured on the 27 July image; (d) standard deviations of fields and areas of agricultural terrains measured on the 27 July image.

and standard deviation values of these areas and the difference that exists from their fields are interpreted to represent a smoothing out of the surface of the areas as a result of bending of the crops and of deposition of a sediment veneer. Area 11 has backscatter values similar to those of its associated field, indicating that major changes resulting from the flood have not occurred. It is not possible to determine whether its high mean backscatter and standard deviation values on the 27 July image are due to possible erosion and not only to moisture. An additional image taken during a later drier season would have been needed to properly evaluate the contribution of soil moisture to the backscatter measurements. Site (field and area) 6 is illustrated as Case 2 in Fig. 2.

Case 3 (Table 2, Fig. 3a–d: sites 12–16) is characterized on the 24 July image by areas with high backscatter standard deviations, slightly higher than those of their fields, and mean backscatter values lower than those of the fields. On the 27 July images, similar high standard deviations have been found in both the areas and associated fields, and the area mean backscatters are slightly lower than those of the fields. Site 13 is the exception as the means for the area and the field are the same. This is interpreted to indicate that the surfaces of the areas are slightly smoother than those of the associated fields (sites 12, 14, 15 and 16), but the backscatter value does not suggest major vegetation damage or sedimentation. Area 13 in

Fig. 2. (*opposite*) RADARSAT images illustrating changes that may occur during receding floods. Case 1 is illustrated by site 2; Case 2 by site 6; Case 3 by site 12; Case 4 by site 20. Fields are delimited by dashed lines; measured flooded areas by solid lines. First column to the left contains peak-flood images of 14 July, centre column contains images of 24 July, and third column contains images of 27 July. Black areas are flooded or smooth areas.

particular does not show any flood-related change, the value of the area being the same as that of the field on the 27 July image. Site (field and area) 12 is illustrated as Case 3 in Fig. 2.

Case 4 (Table 2, Fig. 3a–d: sites 17–22) is characterized by areas with high backscatter standard deviations, and mean backscatter values similar to those of the fields on the 24 July image and variable response on the steeper incidence angle image of 27 July. Two sites (17 and 18) show average backscatter values for areas greater than those of the fields, two lower (19 and 20), and two equal to those of the fields (21 and 22). Here, variation in moisture rather than damage to vegetation, erosion or sedimentation seems to be the dominant variable. In the first two sites the higher mean values are the expected response to higher soil moisture on the steeper incidence angle image, although some possible erosion cannot be discarded. The second two sites show the opposite, indicating that the areas are drier than the associated fields. If this effect was the result of smoother surfaces, that would have led to mean backscatter values of the areas being higher than the field ones for the shallower incidence angle image of 24 July. The two sites, which have the same area values as those of their associated field, indicate that the floods had low impact on their surfaces. Site 20 is shown as Case 4 in Fig. 2.

Case 5 (Table 2, Fig. 3a–d: sites 23–28) is characterized by areas with high backscatter standard deviations, and mean values, higher than those of the fields on both the 24 and 27 July images. In all fields but number 23, the absolute backscatter values are higher on the steeper incidence angle images of 27 July than on the shallower incidence angle images of 24 July. This indicates that although soil moisture was continuously high, surface roughness influenced the backscatter of the 24 July images more, and moisture those of 27 July. Therefore the results are not very conclusive owing to the combination of both parameter effects. The earlier images may suggest flood erosion, but the persistent moisture effect on the later images renders such interpretation dubious. Similarly, the backscatter values for field 23 suggest no major flood-related modification; however, similar values could be due either to similar moisture or a combination of moisture and roughness variations between the area and the correspondent field. This dilemma could be resolved only by analysing an additional image taken during subsequent drier times.

DETECTION OF FLOOD UNDER FOREST CANOPY

The flooded forest delineation was carried out visually considering the backscatter differences on the RGB image obtained by combining three available images, each assigned to a different channel: the 27 July (Fig. 4)

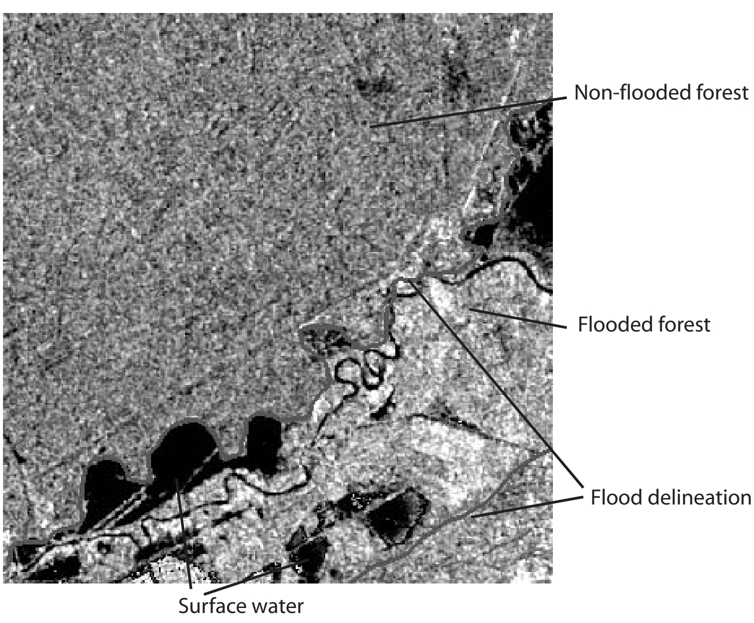

Fig. 4. Example of flooded and non-flooded forest sites seen on the 27 July RADARSAT image.

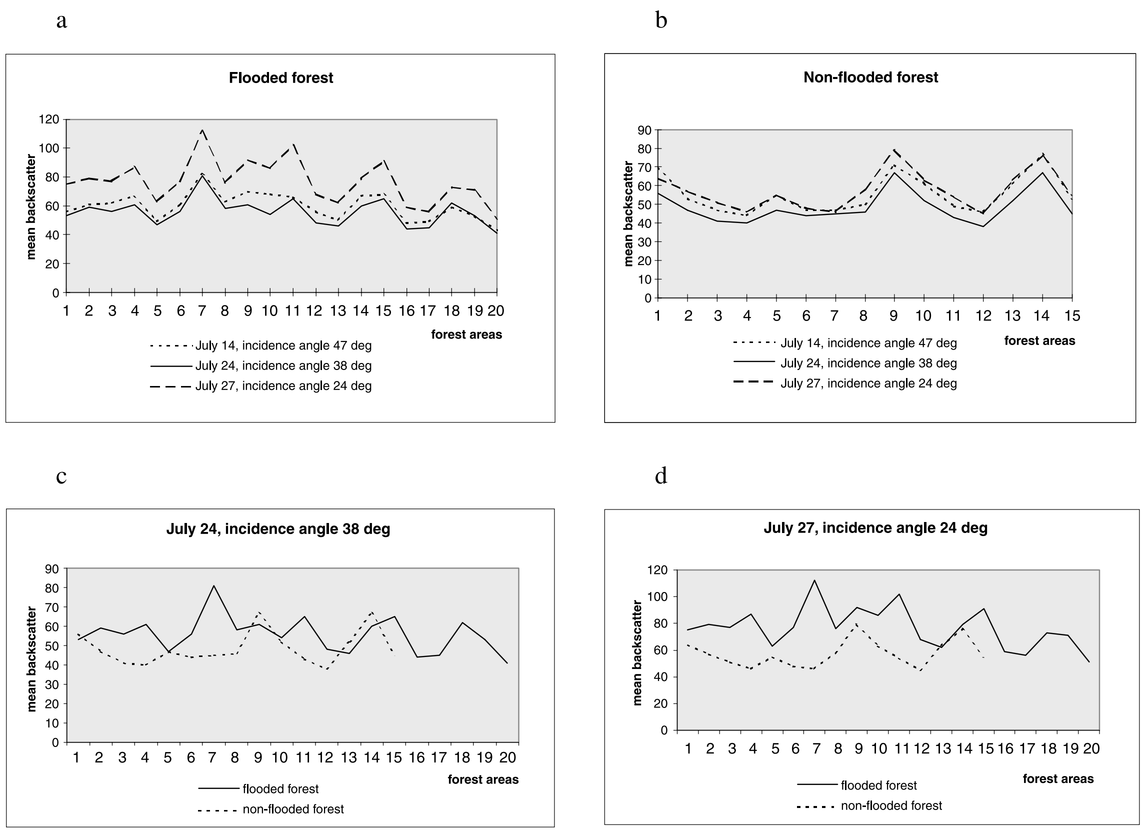

Fig. 5. Diagrams showing mean backscatter values of flooded and non-flooded forest sites. (a) Values for 20 flooded forest sites measured on the 14, 24 and 27 July images; (b) values for 15 non-flooded forest sites measured on the 14, 24 and 27 July images; (c) values for 20 flooded and 15 non-flooded sites measured on the 24 July image; (d) values for 20 flooded and 15 non-flooded sites measured on the 27 July image.

image was in RED channel, 24 July in GREEN channel, and 14 July in BLUE channel. Backscatter measurements were made of the delineated flooded and non-flooded forest sites and the results are presented in Fig. 5.

1 The effect of different incidence angles on mean backscatter values was analysed for flooded and non-flooded forest sites. The mean backscatter values of 20 flooded forest sites are shown on Fig. 5(a). The mean backscatter values for the non-flooded sites are graphed in Fig. 5(b). In every case, the image with the steepest incidence angle (24°) registers the highest backscatter values, attesting to a better penetration through the canopy.

2 The mean backscatter values obtained from two images with 38° and 24° incidence angle were compared in order to differentiate quantitatively between flooded and non-flooded forests. Twenty sites (1–20 solid line) were seen flooded on the 14 July RADARSAT, 15 sites (1–15 dotted line) were not flooded. When the backscatter values of flooded and non-flooded forest sites measured on the various images are analysed, it is evident that their flood status is very distinct on the image of 27 July with the steep (24°) incidence angle, whereas there is no distinct variation in values at most sites on the image of 24 July with shallower (38°) incidence angle.

DISCUSSION

The difference between backscatter values of two or more images usually is determined utilizing a pixel-by-pixel ratio method (Townsend & Walsh, 1998). In this research, the mean backscatter values were used in areas and fields of selected agricultural terrains and in selected forested sites. Furthermore the validity of the differentiation obtained through average backscatter measurements was validated considering the standard deviations of the various sites, and a visual observation to establish the textural pattern, for example whether brightness clustering existed or not.

The reason for using this hybrid method is that most important information obtained from radar images that present 'pepper/salt' (or 'granular') texture is not usually carried by the single pixel backscatter values but rather by the image texture as a whole. The unique mathematical definition of such textures, however, is not yet possible with existing software. The mono-colour RADARSAT images allow distinction of lighter from darker granular patches and also its texture (distribution of light and dark pixels or clusters of pixels). This effect was transformed in the method presented here into calculation of backscatter mean values of areas and fields in agricultural terrains (24 and 27 July images), and of forest sites (14, 24 and 27 July images). These values were accompanied by standard deviation calculation to take textures into account. The method can provide useful data on the effects (such as sedimentation and erosion) of floods on open terrains, such as agricultural lands, even if pre-flood images are not available, by comparing changes that occur in flooded areas within delimitable fields. For forested sites, the extent of the flood can be established if C-band radar data are available obtained at a steep (24°) incidence angle.

CONCLUSIONS

Multitemporal radar images make it possible to study flooded areas remotely. The study reported in this paper was performed using mean backscatter values of selected areas, fields and parts of forests, rather than single pixel values, for evaluating changes that have occurred on the land as a result of floods.

To study changes in open agricultural lands, the best information can be obtained from sets of images consisting of a pre-flood image, a peak-flood image and a post-flood image taken at shallow incidence angle (greater than 30° measured from normal to Earth). However, good results also can be obtained with a more limited set of images obtained during receding flood stages, considering sites (fields) that have been only partially flooded (areas). Changes resulting from the flood can be detected by comparing mean backscatter values of flooded areas and associated fields of the various images. The standard deviation of the various sites needs to be considered as well in order to make sure that compatible textures are examined The flood extent in forested terrains can be best determined at the moment of flood by utilizing C-band radar under steep incidence angle (24°).

ACKNOWLEDGEMENTS

The Ministry of Environment of the Czech Republic financed this project. The help of I.P. Martini and C. Duke in finalizing this paper is gratefully acknowledged.

REFERENCES

Ahern, F.J. (1995) *Fundamental Concepts of Imaging Radar: Basic Level*. Unpublished manual, Canada Centre for Remote Sensing, Ottawa, Ontario.

Beaudoin, A., Le Loan, T. & Gwyn, Q.H.V. (1990) SAR observations and modeling of the C-band backscatter variability due to multiscale geometry and soil moisture. *IEEE Trans. Geosci. Remote Sens.* **28**(5), 886–895.

Halounová, L., Dixon, R., Pokrant, H., *et al.* (1999) RADARSAT imaging of the 1997 Czech Republic flood. In: *Fluvial Sedimentology V* (Eds Smith, N.D. & Rogers, J.), Spec. Publs int. Ass. Sediment., No. 28, pp. 71–75. Blackwell Science, Oxford.

Hess, L.L., Melack, J.M. & Simonett, D.S. (1990) Radar detection of flooding beneath the forest canopy: a review. *Int. J. Remote Sens.* **11**(7), 1313–1325.

Imhoff, M.L., Vermillion, C., Story, M.H., Choudhury, A.M., Gafoor, A. & Polcyn, F. (1987) Monsoon flood boundary delineation and damage assessment using space borne imaging radar and Landsat data. *Photogram. Eng. Remote Sens.* **53** (4), 405–413.

Krohn, M.D., Milton, N.M. & Segal, D.B. (1983) SEASAT Synthetic Aperture Radar (SAR) response to lowland vegetation types in eastern Maryland and Virginia. *J. geophys. Res.* **88**(C3), 1837–1852.

Krumpera, O., Foldyna, J. & Zorkovský, V. (1988) *General Geology* (in Czech). Nakladatelství technické literatury, Praha.

Merot, P., Crave, A., Gascuel-Odoux, C. & Louhala, S. (1994) Effect on saturated area on backscattering coefficient of the ERS 1 synthetic aperture radar: first results. *Water Resour. Res.* **30**(2), 175–179.

Ormsby, J.B. & Blanchard, B.J. (1985) Detection of lowland flooding using active microwave systems. *Photogram. Eng. Remote Sens.* **51**(3), 317–328.

Pietroniro, A., Soulis, E.D., Kouwen, N., Rotunno, O. & Mullins, D.W. (1993) Extracting distributed soil moisture information from C-band wide swath SAR imagery. *Can. J. Remote. Sens.* **19**(1), 77–82.

Place, J.L. (1985) Mapping of forested wetland: use of radar images to complement conventional sources. *Prof. Geogr.* **37**(4), 463–469.

Richards, J.A., Woodgate, P.W. & Skidmore, A.K. (1987) An explanation of enhanced radar backscatter from flooded forest. *Int. J. Remote Sens.* **8**(7), 1093–1100.

Rignot, E.J.M. & van Zyl, J. (1993) Change detection techniques for ERS-1 SAR data. *IEEE Trans. Geosci. Remote Sens.* **31**(4), 896–906.

RSI (1995) *RADARSAT Illuminated*. Unpublished Guidebook, RADARSAT International Inc., Richmond, British Columbia.

Sippel, S.J., Hamilton, S.K., Melack, J.M. & Choudhury, B.J. (1994) Determination of inundation area in the Amazon River floodplain using the SMMR 37 GHz polarization difference. *Remote Sens. Environ.* **48**, 70–76.

Townsend, P.A. & Walsh, S.J. (1998) Modeling floodplain inundation using an integrated GIS with radar and optical remote sensing. *Geomorphology* **21**, 295–312.

Ulaby, F.T. (1974) Radar measurements of soil moisture content. *IEEE Trans. Anten. Propag.* **2**, 257–265.

Wang, Y., Kasischke, E.S., Melack, J.M., Davis, F.W. & Christensen, N.L. Jr (1994) The effects of changes in loblolly pine biomass and soil moisture on ERS-1 backscatter. *Remote Sens. Environ.* **49**, 25–31.

Wang, Y., Hess, L.L. & Melack, J.M. (1995) Understanding the radar backscattering from flooded and nonflooded Amazonian forests: results from canopy backscatter modeling. *Remote Sens. Environ.* **54**(3), 324–332.

Special cases

Flood and Megaflood Processes and Deposits: Recent and Ancient Examples. Edited by I. Peter Martini, Victor R. Baker and Guillermina Garzón © 2002 International Association of Sedimentologists. ISBN: 978-0-632-06404-5

Spec. Publs int. Ass. Sediment. (2002) **32**, 283–90

Sedimentary traces as indicator of temporary ice-marginal channels in the Westphalian Bight, Germany

J. HERGET

Institute of Geography, Ruhr-University Bochum, Universitaetsstr. 150, D-44801 Bochum, Germany
(Email: juergen.herget@ruhr-uni-bochum.de)

ABSTRACT

In the catchment of the Lippe River, Westphalian Bight of north-west Germany, traces of fluvial sediments and structures have been found at several locations that cannot be explained using palaeoriver reconstructions. The Scandinavian ice-sheet reached and crossed the Lippe River valley during the Saalian glaciation, and several temporary ice-marginal channels may have developed. These channels were fed by meltwater from the ice-sheet and followed several temporary courses. The important difference between these and other ice-marginal channels described in the literature is the temporary character of the Lippe valley channels, as they do not necessarily relate to a stable ice margin. Because of blocked river courses, the presence of temporary palaeolakes is hypothesized as well, although no clear evidence has been found of lacustrine sediments.

INTRODUCTION

To understand the development of the Lippe River valley, a tributary of the lower Rhine River in north-west Germany (Fig. 1), the influence of glaciation on the course of this river must be appreciated (Herget, 1997, 1998). The distribution of isolated fluvial sediments and features is analysed in this paper. The fluvial sediments typically consist of reworked gravel; many such deposits have been quarried since they were first described. Nevertheless such information and the analysis of the remaining deposits allow reconstruction of interesting, seldom-considered settings. The glaciofluvial dynamics at the margin of the glacier that once occupied the area is the key factor in explaining the isolated fluvial sediments and features of the area. After some background information about the Quaternary glaciations of the study area, four selected examples of temporary river and meltwater channels are presented here. A comparison with proglacial fluvial phenomena in other areas is included as well.

GLACIATIONS OF NORTHERN GERMANY

The extent of the Quaternary glaciations of northern Germany can be summarized as follows (Fig. 1). Further details can be found in Brunnacker (1986), Grube *et al.* (1986), Ehlers (1994), Skupin *et al.* (1993) and Skupin & Staude (1995).

The Saalian glaciation, which is equated with the marine oxygen isotope stages (OIS) 8–6 and lasted between 300 and 127 ka BP, had its maximum extension in the western parts of central Europe during OIS 8, which is traditionally called the Drenthe stadial. In eastern Germany and areas of Poland, the Elsterian glaciation of more than 330 ka BP represents the maximum extension of the Scandinavian ice-sheet. The last or Weichselian glaciation did not cross the Elbe valley anywhere. In the Westphalian Bight, the ice-sheet extended south of the recent Lippe valley to the northern rim of the central European hilly country. The Scandinavian ice-sheet carried clasts of granite, gneiss and quartzite of Nordic provenance (Smed & Ehlers, 1994) into north-western Germany, where those lithologies are not exposed at the surface. The

Flood and Megaflood Processes and Deposits: Recent and Ancient Examples. Edited by I. Peter Martini, Victor R. Baker and Guillermina Garzón ISBN: 978-0-632-06404-5

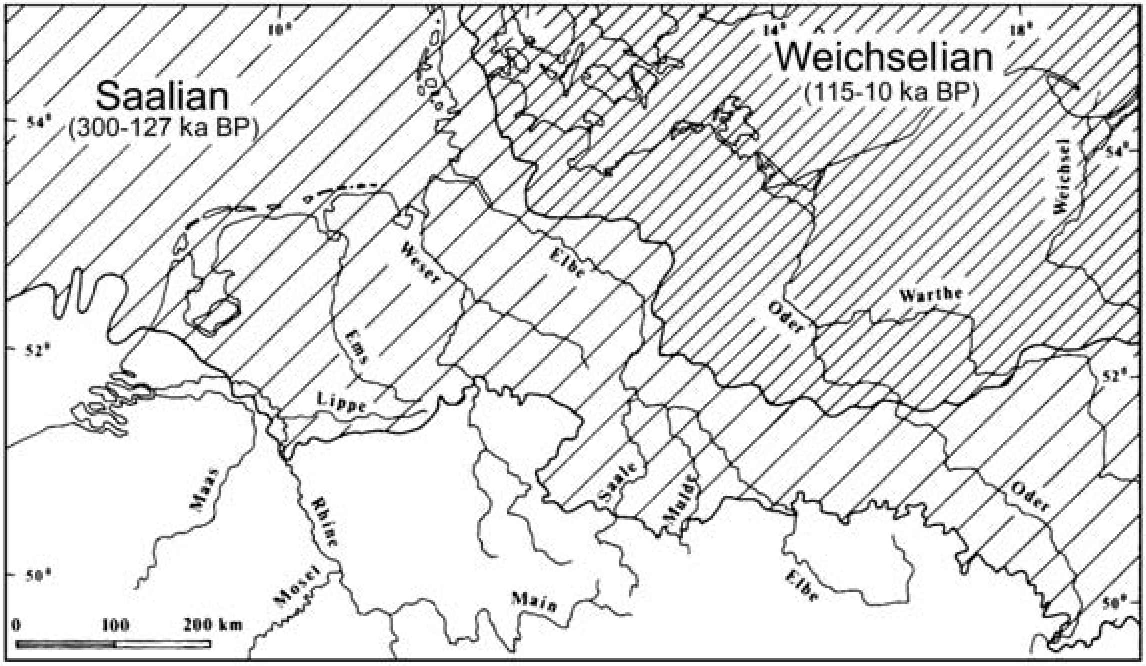

Fig. 1. Map showing the maximum extension of the Weichselian and Saalian (respectively Elsterian in eastern Germany and Poland) glaciations in central Europe (after Ehlers, 1994).

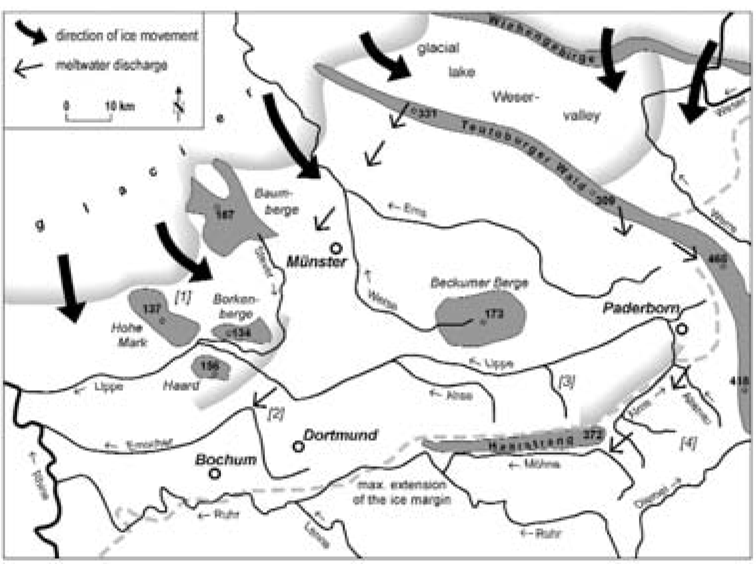

Fig. 2. Map showing the advancing Scandinavian ice-sheet during the Saalian glaciation in the Westphalian Bight. The four selected locations of temporary proglacial fluvial features are marked by numbers: [1] Hohe Mark, [2] divide between Emscher and Lippe valley, [3] Pöppelsche valley and [4] Eiler Berg. The named groups of hills in the lowland area of the Westphalian Bight are drawn in a shaded style and their maximum heights in metres are indicated.

Scandinavian ice-sheet is the only primary source for those rocks in the Westphalian Bight and therefore the occurrence of crystalline material indicates deposition during the Drenthe stadial of the Saalian glaciation in the area.

The Scandinavian ice-sheet reached the Westphalian Bight between the Teutoburger Wald and the Haarstrang from the north-west, and later crossed surrounding mountains of the Wiehengebirge and the Teutoburger Wald (Fig. 2). The ice blocked north-westward drainage and forced the rivers to flow westward towards the lower Rhine River because of the surrounding chains of mountains (Gibbard, 1988). Although the glacial lake in the Weser valley with its spillways into the Westphalian Bight (Thome, 1983) and several diversions of the Weser River (Rohde, 1994) are well known, the proglacial environment within the Westphalian Bight presented in this paper was unknown and its dynamics were unrevealed (Herget, 1997).

Thome (1983) summarizes many local studies about the spillways that are cut into the Teutoburger Wald and their deposits in the Westphalian Bight (Fig. 2). He characterizes the sediments as being mainly composed of sand and silt. Gravels occur locally as thin layers at the base of strata. Within the proglacial lake basins, glaciofluvial and glaciolacustrine silt, sand and gravel are found in close proximity. Variations in dominant grain size and the absence of clays and varves can be explained by constantly changing lake levels ahead of the advancing ice margin and continuous flow through the lakes, even in winter. Under these circumstances, no clays could have been deposited and varves could not develop.

The fluvial history of the Weser and Leine rivers is based mainly on geological mapping and on gravel provenance analyses of the 6.3–12.5 mm fraction (Rohde, 1994). According to the distribution and altitude of fluvial sediments, the Weser River was flowing northward in the area of the city of Hannover before the Saalian glaciation. At the beginning of the Saalian glaciation the course changed to the north-west along the northern rim of the Wiehengebirge for about 50 km and turned northward again at its western margin. Along this path several channels of the Weser River and its tributaries are distinguished. The recent northern course of the Weser River through the Porta Westfalica gap of the Wiehengebirge was caused by modification of the relief by subrosion (a general expression applied to karst processes influencing the course of a river (Rohde, 1994)) and Elsterian meltwater channels at low altitudes. Although Rohde (1994) does not mention the direct influence of the Saalian ice-sheet on the dynamics of the river courses, its influence is obvious because these changes occurred during the Saalian glaciation.

While the ice was moving south to its maximum extension, temporary ice margins occupied many different locations until the Saalian maximum extension was reached. These dynamic ice margins are not related to temporary hiatuses in ice advance or to an interstadial, but they allowed the formation of many short-lived, individual temporary ice-marginal channels.

EXAMPLES OF THE TEMPORARY ICE-MARGINAL CHANNELS

Examples showing the influence of the temporary ice margins on the fluvial environment in the Westphalian Bight are analysed in detail at four locations (Fig. 2) (Herget, 1997).

Nordic sediments at the Hohe Mark

At the northern and north-eastern rim of the Hohe Mark, Braun (1975) mentions fluvial sediments that are interpreted as being from an old Pleistocene terrace of the Lippe River (location [1], Fig. 2). He describes cross-bedded sands and gravels with pebbles of well-rounded quartz sandstone, quartz and diabase, which were correlated with outcrops in the valley of the Lenne River (Fig. 2). He interpreted the Lippe River to have taken a course along the northern rim of the Hohe Mark during this sedimentation. Supporting evidence for this is the altitude of the sediments at 60 m a.s.l., which is comparable to terrace sediments of the lower Rhine River of the same age. This is the only argument for his interpretation.

Recent mapping of the same area has shown, however, that Nordic gravels (granite and metamorphic pebbles) occur among the sediments of the suggested old Pleistocene river terrace (Herget, 1997). Therefore, the sediments cannot be older than the Drenthe stadial of the Saalian glaciation and the interpretation by Braun (1975) could be wrong. On the other hand, these sediments cannot be interpreted as a Drenthe stadial river terrace either because all other fluvial sediments of this age are found at lower altitudes of about 50 m a.s.l., which is an important difference in the lowland area of the Westphalian Bight.

The origin of the gravels is related to the advancing ice-sheet. As shown in Fig. 2, the valleys of the Weser and Ems rivers, among many others in central Europe, were blocked to the north by the ice-sheet, such that the combined discharge of the rivers and glacial meltwater was forced to flow to the west. The advancing ice-sheet was slightly influenced by the mountains but eventually reached the northern rim of the Hohe Mark. During this time the collected river water and meltwater had to pass between the ice margin and the mountains. This temporary river and meltwater channel was active until the ice-sheet reached the Hohe Mark and blocked it. Up to that time, water was flowing quasi-parallel to the northern slope of the Hohe Mark and might have left fluvial sediments that contain Nordic gravels carried by meltwater from the

Scandinavian ice-sheet. Even the few pebbles of diabase do not lead to any complications as they are also part of the Nordic gravels (Smed & Ehlers, 1994) and do not necessarily derive from outcrops in the catchment of the Lenne River. The altitude of these proglacial fluvial sediments is not a critical issue because the ice-sheet displaced the marginal channels as it moved southward. This displacement even continued up the northern slopes of the Hohe Mark until the water formed a submarginal channel or used a spillway south of the ice margin.

West of the city of Münster, Speetzen & Weber (1999) describe a small 0.8 m thick gravel deposit that consists mainly of coarse pebbles of local marlstone up to 25 cm in diameter together with a smaller portion of finer Nordic components. These coarse deposits commonly originate from creeks and rivers with considerable gradient and discharge; indeed, the hilly landscape of the Baumberge provides a sufficient gradient, but, owing to the limited catchment, not the necessary discharges. Therefore, the origin of this gravel deposit is explained by the influence of strong meltwater streams originating from the Saalian ice-sheet. These probably were temporary streams that flowed between the ice margin in the north and the hills of the Baumberge in the south, similar to those that flowed along the northern rim of the Hohe Mark.

Divide between the Emscher and Lippe valleys

In the lower Lippe valley south-east of the Haard and Borkenberge mountains, a suspected ice margin may have blocked the Lippe River (location [2], Fig. 2). A lake developed until the elevation of the recent divide between the Lippe and Emscher rivers was reached and lake water spilled into the Emscher valley. A channel with a width of 20–40 m and up to 2 m depth was formed at an altitude of 67 m a.s.l. The channel was filled with gravels containing Nordic sediments and was covered by till. The sediments have been described by Fricke *et al*. (1949), but have since been completely quarried. Fricke *et al*. (1949) found light brown medium sand with minor cross-bedded coarse gravels and local lenses of clay. According to their interpretation, the channel indicates a former course of the Lippe River leading into the valley of the Emscher River. This should have been the course of the river until the Saalian glaciation. The problem with this interpretation is the explanation of the process that forced the Lippe River to change course out of the Emscher valley toward a north-western direction. For example, an accumulation of sediments during the last glacial can be excluded because the Weichselian terrace does not reach the altitude of the channel in question. Therefore, the development of the course of the Lippe River has to be seen as leading in a north-western direction before the glaciation, a temporary blocking by the ice-sheet during the Saalian glaciation, a diversion into the Emscher valley and a return to the former course after the ice margin retreated.

For this argument, other fluvial sediments should be considered, which are located 6 km south-east of the location of the former temporary spillway channel at an altitude of 77 m a.s.l., 10 m higher in elevation than those of the palaeo-Lippe River. These sediments consist of medium to fine sand that cannot be connected with other fluvial sediments to reconstruct a palaeoriver course (Bode & Udluft, 1939; Herget, 1997). Although these isolated fluvial deposits do not contain Nordic clasts they probably can be explained by temporary proglacial streams similar to those at Hohe Mark.

Thome (1983) described an ice-marginal channel leading from the Westphalian Bight into the incised valley of the Ruhr River between the headwaters of the Emscher River and the Ruhr valley south-west of the city of Dortmund. In the absence of sediments, he argued, that a large valley at Witten-Annen, now occupied by a misfit creek, represents a temporary meltwater channel during the Saalian glaciation. It is, however, problematic to draw conclusions only from recent morphology, because details of the landscape development since glaciation cannot be quantified.

Exotic fluvial deposits

In the south-eastern part of the Westphalian Bight, exotic fluvial deposits are found among the sediments of the Pöppelsche, a small creek on the northern slope of the Haarstrang (location [3], Fig. 2). The whole catchment of the creek is incised into Upper Cretaceous limestones and the stream is ephemeral owing to karstification.

The fluvial deposits are composed mostly of well-rounded limestone clasts but also contain some lydite (black siliceous shale). The lydite originates from Palaeozoic deposits underlying the Upper Cretaceous limestones (Fig. 3) and is exposed only in the catchment of the Möhne and Alme rivers and in older sediments in the recent Ems River catchment north of the Lippe River. To reach the Pöppelsche, it must have been transported over the divide of other rivers. According to the scenario of temporary marginal

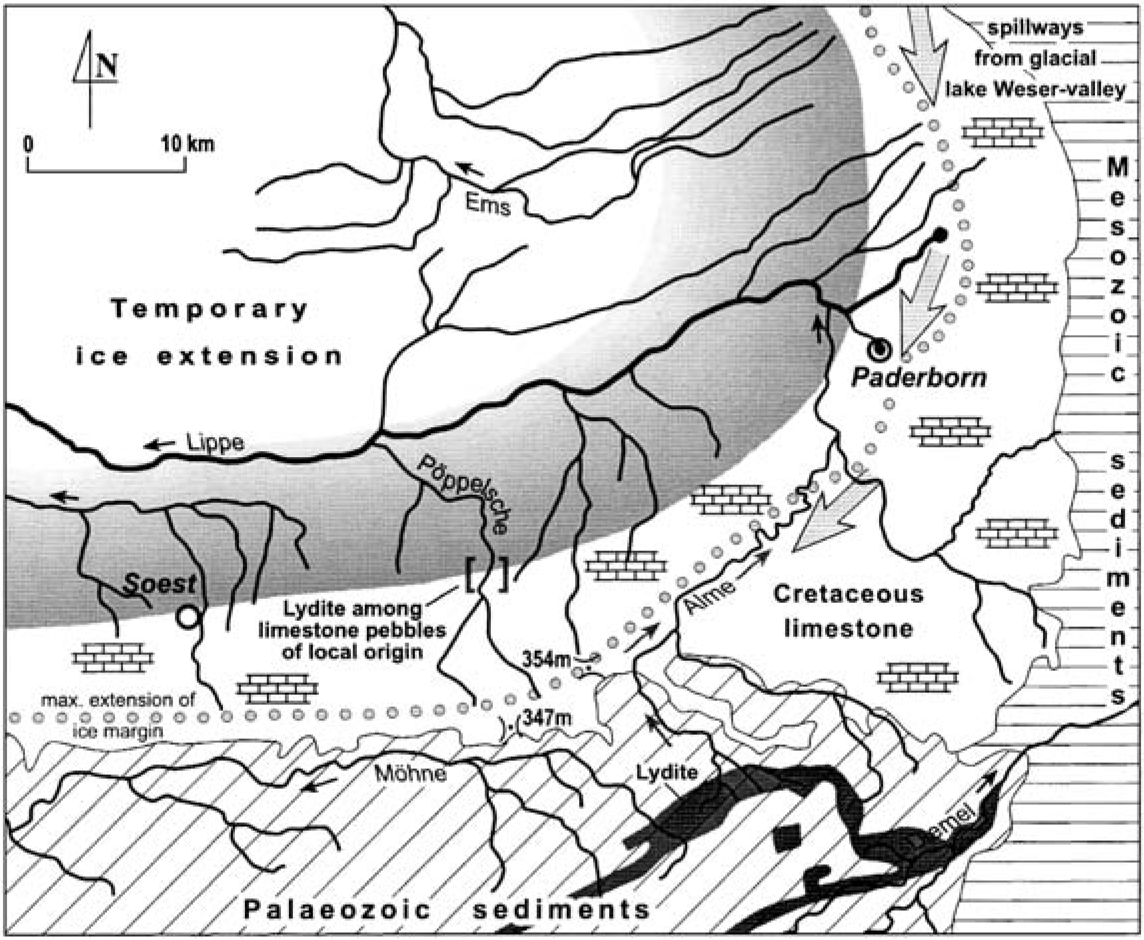

Fig. 3. Map showing exogenic fluvial deposits of lydite in the catchment of the Pöppelsche Creek (after Herget, 1997, with geology from various sources).

channels, the sediments of the Alme River may have been displaced by the ice-marginal drainage. In the ice-marginal channel there was also a contribution of water from the catchment of the River Weser, which was blocked by the ice and developed spillways that flowed into the Westphalian Bight. This water reworked older fluvial sediments that contain lydite and might have crossed the divide to the north, because it was running at a relatively high elevation above the valley floor. After the Scandinavian ice-sheet melted down, lydite pebbles were moved into the catchment of the Pöppelsche, and were redeposited together with locally derived limestone clasts.

K. Skupin (personal communication, 1996) has offered an alternative interpretation, in which the lydite pebbles may have derived from older glacial sediments of the Ems River. The lowest deposits in the valleys of the Ems and Lippe rivers contain a small amount of lydite pebbles (Lotze, 1953), indicating a connection between the Alme and Ems rivers. If this interpretation were true, Nordic sediments should have been found in the Pöppelsche catchment, too. However, Skupin (1995) did not report any Nordic gravel, even from the Drenthe stadial terrace of the Pöppelsche, which contains 5% Palaeozoic sediments.

Nordic sediments beyond the maximum ice extension

Nordic sediments are present at several localities in the south-eastern corner of the Westphalian Bight, such as on top of the Eiler Berg at an altitude of 364 m a.s.l. (location [4] in Fig. 2, and Fig. 4). The difficulty in

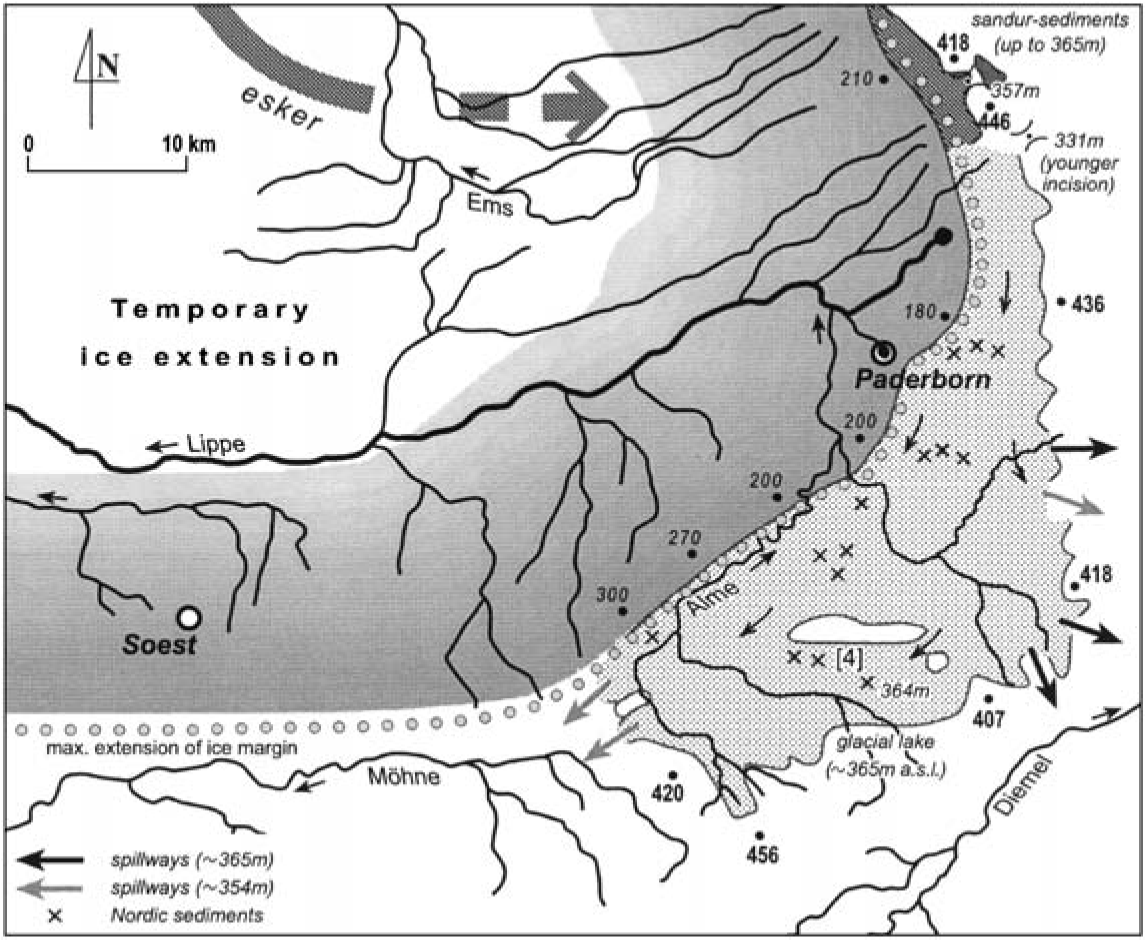

Fig. 4. Map of Nordic sediment distribution beyond the maximum ice extension south of Paderborn (distribution of Nordic sediments after Stille (1904, 1935a, b), Hiss (1989), Skupin (1989) and this investigation).

interpreting these coarse (clasts up to 10 cm in diameter) deposits stems from the fact that they are located more than 10 km beyond the maximum extension of the Scandinavian ice-sheet at an elevation about 100 m higher than the nearest recorded Saalian ice margin, the southernmost glacier to ever reach this area. An anthropogenic origin, such as agricultural or other activities, can be excluded because of the size of the sediments involved and the fact that they were reported at those localities prior to modern industrialization (Stille, 1904).

No satisfactory explanation exists for the distribution of the Nordic sediments of this region. These gravels have been used variously to argue for a more southerly ice maximum (Deutloff, 1976), a short-lived advance during the Saalian glaciation (Skupin, 1989) and for alternative interpretations of an Elsterian glaciation of the area (Skupin, 1989). The analysis of proglacial fluvial dynamics may provide an alternate hypothesis. A proglacial lake may have formed by blockage of ice-marginal channels in the area south of Paderborn (Fig. 4). It may have reached a level of 365 m a.s.l., allowing Nordic gravels to be deposited from melting icebergs stranded on the beach. The lake might have had several spillways now at elevations of 365 m a.s.l. The elevation of these spillways corresponds to the altitude of the Eiler Berg with the Nordic sediments on its top. Two main spillways at lower elevations (354 m today) might have been in use: a broad, poorly incised one to the east, and another with two parallel, south-west orientated channels. This second spillway drained into the Möhne valley, which is sharply incised and large compared with the valleys of the surrounding area. It is possible that the eastern spillway was formed by younger periglacial erosion, like the divide to the north-east at an altitude of 331 m a.s.l., north-east of Paderborn.

The temporary lake had one main influx from a subglacial meltwater stream recorded by an esker ('Münsterländer Kiessandzug'), which ran below the ice-sheet of the Westphalian Bight and shows a direction towards sandur sediments north of Paderborn (Skupin & Staude, 1995). The sandur sediments also reach an altitude up to 365 m a.s.l. (Farrenschon, 1990) and therefore locally cross the surrounding chain of mountains. More importantly, however, they have the same altitude as the suspected temporary proglacial lake, which was fed by the discharge of the Weser River flowing through the mentioned spillways in the Teutoburger Wald, too. No lacustrine sediments have yet been identified in the study area, but perhaps such probably thin deposits should not be expected to have persisted owing to intense post-glacial erosion.

DISCUSSION

The hypothesis of temporary river and meltwater channels in the proglacial environment of the Westphalian Bight during the Saalian glaciation may explain the otherwise unconnectable remnants of fluvial sediments of the area. Such short-lived meltwater streams flowed between the Scandinavian ice-sheet and the southern slopes of the Westphalian Bight.

Ice-marginal channels and proglacial lakes are described from nearly all areas of Pleistocene and recent glaciations (Baker & Bunker, 1985; Elson, 1992; Arkhipov *et al.*, 1995; Teller, 1995; Carling, 1996; Benn & Evans, 1998; Grosswald, 1998). Emphasis is placed on systems that develop in front of relatively stationary ice margins such as the 'Urstromtäler' (= pradolina) (Liedtke, 1981) or other systems reported in Benn & Evans (1998). However, temporary ice-marginal channels may develop in front of an unstable ice margin, which do not necessarily leave large structures but, as is argued in this paper, a cryptic record. The suspected temporary channels of the study area belong to the Drenthe stadial of the second last glaciation (Saalian). Their modification in the periglacial environment during the Warthe stadial of Saalian glaciation and during the last glaciation (Weichselian) is uncertain. Their original distribution, subsequent differential erosion, burial by more recent sediments and lack of exposures makes their systematic investigation difficult. However, if nothing else, this case study should serve as a warning for interpreting ancient deposits that may not necessarily conform with commonly presented sedimentation models.

ACKNOWLEDGEMENTS

I thank P. Carling, H. Liedtke, I.P. Martini, K. Skupin and K. Thome for important discussions and comments. Financial support for the studies was kindly provided by the 'Deutsche Forschungsgemeinschaft' (German Research Foundation) (Li 86/21–1). R. Wieland and S. Steinert have improved the maps and helped to give them a presentable style.

REFERENCES

Arkhipov, S.A., Ehlers, J., Johnson, R.G. & Wright, H.E. (1995) Glacial drainage towards the Mediterranean during the Middle and Late Pleistocene. *Boreas* **24**, 196–206.

Baker, V.R. & Bunker, R.C. (1985) Cataclysmic late Pleistocene flooding from glacial Lake Missoula, a review. *Quat. Sci. Rev.* **4**, 1–41.

Benn, D.I. & Evans, D.J.A. (1998) *Glaciers* and *Glaciation*. Arnold, London.

Bode, H. & Udluft, H. (1939) *Geologische Karte von Preussen und benachbarten deutschen Ländern—Erläuterungen zu Blatt Waltrop Nr. 2432* (= new no. 4310). Preussische Geologische Landesaufnahme, Berlin.

Braun, F.J. (1975) Quartär. In: *Geologische Karte von Nordrhein-Westfalen 1:100.000—Erläuterungen zu Blatt C 4306 Recklinghausen* (Eds Braun, F.J. & Thiermann, A.), pp. 94–122. Geologisches Landesamt NRW, Krefeld.

Brunnacker, K. (1986) Quaternary stratigraphy in the Lower Rhine area and northern Alpine foothills. *Quat. Sci. Rev.* **5**, 373–379.

Carling, P. (1996) Morphology, sedimentology and palaeohydraulic significance of large gravel dunes, Altai Mountains, Siberia. *Sedimentology* **43**, 647–664.

Deutloff, O. (1976) Geologie (map). In: *Deutscher Planungsatlas Bd. 1-NRW–Lieferung 8* (Eds Akademie für Raumforschung und Landesplanung & Ministerpräsident des Landes NRW). Schroedel, Hannover.

Ehlers, J. (1994) *Allgemeine und Historische Quartärgeologie*. Enke, Stuttgart.

Elson, J.A. (1992) Glacial lakes. In: *Encyclopedia of Earth System Science* (Ed. Nierenberg, W.A.), Vol. 2, pp. 347–360. Academic Press, San Diego.

Farrenschon, J. (1990) Geologische Karte von Nordrhein-Westfalen 1 : 25.000—Erläuterungen zu Blatt 4119 Horn—Bad Meinberg. Geologisches Landesamt NRW, Krefeld.

Fricke, K., Hesemann, J. & von der Wülbecke, J. (1949) Ein neuer Aufschluß mit Elster- und saalezeitlichen Bildungen im Lippe-Diluvium bei Waltrop. *Neues Jahrb. Mineral. Geol. Paläontol. Abh.* **181**, 325–363.

GIBBARD, P.L. (1988) The history of the great northwest European rivers through the past three million years. *Philos. Trans. R. Soc. London* **B318**, 559–602.

GROSSWALD, M.G. (1998) New approach to the ice age paleohydrology of Northern Eurasia. In: *Palaeohydrology and Environmental Change* (Eds Benito, G., Baker, V.R. & Gregory, K.J.), pp. 199–214. J. Wiley & Sons, Chichester.

GRUBE, F., CHRISTENSEN, S., VOLLMER, T., DUPHORN, K., KLOSTERMANN, J. & MENKE, B. (1986) Glaciations in north west Germany. *Quat. Sci. Rev.* **5**, 347–358.

HERGET, J. (1997) Die Flußentwicklung des Lippetals. *Bochumer Geogr. Arbeiten* **62**, 1–143.

HERGET, J. (1998) Temporäre Entwässerungsbahnen am Südrand der Westfälischen Tieflandsbucht—ein Szenario. In: *Physische Geographie und Landeskunde—Festschrift für Herbert Liedtke* (Eds Glatthaar, D. & Herget, J.), Bochumer Geogr. Arbeiten Sonderreihe **13**, 23–30.

HISS, M. (1989) *Geologische Karte von Nordrhein-Westfalen 1 : 25.000—Blatt 4417 Büren*. Geologisches Landesamt NRW, Krefeld.

LIEDTKE, H. (1981) Die nordischen Vereisungen in Mitteleuropa. *Forsch. Deutsch. Landeskunde* **204**, 1–307.

LOTZE, F. (1953) Zur Talgeschichte der Alme, oberen Lippe und Ems—Neue Ergebnisse der Quartärgeologie Westfalens XXI. *Neues Jahrb. Geol. Paläontol. Monatsh.* **1953**, 306–311.

ROHDE, P. (1994) Weser und Leine am Berglandrand zur Ober- und Mittelterrassen-Zeit. *Eiszeitalter Ggw.* **44**, 106–113.

SKUPIN, K. (1989) *Geologische Karte von Nordrhein-Westfalen 1 : 25.000—Blatt 4418 Wünnenberg*. Geologisches Landesamt NRW, Krefeld.

SKUPIN, K. (1995) *Geologische Karte von Nordrhein-Westfalen 1 : 25.000—Erläuterungen zu Blatt Lippstadt 4316*. Geologisches Landesamt NRW, Krefeld.

SKUPIN, K. & STAUDE, H. (1995) Quartär. In: *Geologie Im Münsterland* (Ed. Geologisches Landesamt NRW), pp. 71–95. Geologisches Landesamt NRW, Krefeld.

SKUPIN, K., SPEETZEN, E. & ZANDSTRA, J.G. (1993) *Die Eiszeit in Nordwestdeutschland—Zur Vereisungsgeschichte der Westfälischen Bucht und angrenzender Gebiete*. Geologisches Landesamt NRW, Krefeld.

SMED, P. & EHLERS, J. (1994) *Steine aus dem Norden—Geschiebe als Zeugen der Eiszeit in Norddeutschland*. Bornträger, Berlin and Stuttgart.

SPEETZEN, E. & WEBER, M. (1999) Ein pleistozäner Kalkstein-Schotter bei Holtwick im westlichen Münsterland (Westfalen, NW-Deutschland). *Geol. Paläontol. Westfalen* **52**, 51–58.

STILLE, H. (1904) *Geologische Spezialkarte von Preussen und benachbarten Bundesstaaten—Blatt Etteln* (= new no. 4318 Borchen). Preussische Geologische Landesaufnahme, Berlin.

STILLE, H. (1935a) *Geologische Spezialkarte von Preussen und benachbarten Bundesstaaten—Blatt 2368 Altenbeken* (= new no. 4219 Altenbeken). Preussische Geologische Landesaufnahme, Berlin.

STILLE, H. (1935b) *Geologische Spezialkarte von Preussen und benachbarten Bundesstaaten—Blatt 2441 Lichtenau* (= new no. 4319 Lichtenau). Preussische Geologische Landesaufnahme, Berlin.

TELLER, J.T. (1995) The impact of large ice sheets on continental palaeohydrology. In: *Global Continental Palaeohydrology* (Eds Gregory, K.J., Starkel, L. & Baker, V.R.), pp. 109–129. J. Wiley & Sons, Chichester.

THOME, K.N. (1983) Gletschererosion und -akkumulation im Münsterland und angrenzenden Gebieten. *Neues Jahrb. Geol. Paläontol. Abh.* **166**, 116–138.

Spec. Publs int. Ass. Sediment. (2002) **32**, 291–302

Outlet glaciers of the Pleistocene (LGM) south Tibetan ice sheet between Cho Oyu and Shisha Pangma as potential sources of former megafloods

M. KUHLE

Geographical Institute, Geography and High Mountain Geomorphology, University of Goettingen, Goldschmidtstraße 5, D-37077 Goettingen, Germany (Email: mkuhle@gwdg.de)

ABSTRACT

Field evidence suggests that the Late Pleistocene Bo Chu (*c.* 75 km long) and Kyetrak Chu (*c.* 100 km long) glaciers did not originate in the main Himalayas range, but farther north in southern Tibet. From this location, they flowed down through the Himalayas to the south slope. Ice flow across the local water divide in southern Tibet (Bo Chu glacier) and the Himalayas (Kyetrak Chu glacier) suggests that outlet glaciers formed from a major ice sheet covering the Tibetan plateau. Large lakes developed, dammed by Last Glacial Maximum (LGM) to Late-glacial (*c.* 20–13 ka) Himalayan glaciers on the southern edge of Tibet, as documented by varve-like rhythmites dovetailed with moraine deposits. Late Late-glacial deglaciation resulted in major glacier lake outbursts. The megafloods apparently removed vast amounts of glacigenic sediments from the high transverse valleys of the Himalayas and redeposited them into the Himalayan foreland.

PROBLEM

A controversy exists as to whether an ice sheet covered the Tibetan plateau during the Late Pleistocene and whether meltwater megafloods flowed from its outlets down the southern flank of the Himalayas. A key area to prove or disprove the existence of a major Pleistocene ice sheet in high Asia is the southern margin of Tibet where the upland lies adjacent to the Himalayan peaks that are 3000 m higher (Fig. 1). There the highest snow line (equilibrium line altitude, ELA) runs at latitude 28°N nowadays and probably also during the LGM. So, of all the plateau areas, southern Tibet is climatically farthest away from glaciation now as it was in prehistoric times. If it can be demonstrated that southern Tibet was covered by ice, then this also must have been true for central and northern Tibet because, for planetary reasons, the snow line dips toward the north, barring major differences in aridity. Furthermore, the central plateau is at the same altitude above sea-level or even higher than southern Tibet, and therefore is hypsometrically closer to prehistoric glacial conditions.

Recent glaciers extend from the highest summits of the Himalayas in all directions. On the north slopes, they reach down to the level of the plateaus and into the high valleys of southern Tibet, such as Yepokangara glacier on Shisha Pangma, Rongbuk glacier on Mount Everest and Kyetrak glacier on the north-west flank of the Cho Oyu (Fig. 1). The major transverse valleys that divide the Himalayas into separate massifs are not glaciated at present (Tamur valley, Arun valley, Bote Chu, Marsyandi Khola, Thak Khola, Bheri Khola and Alaknanda valley).

In contrast to the weak traces of glaciation in high plateau areas, the evidence of valley glaciers should be readily identifiable. They would consist of features such as roches moutonnées, polished rocks and glacial striations (the latter only visible on recently exposed surfaces not yet modified by weathering). Furthermore, depositional features such as ground moraine are expected to be present, generally thickening down-valley.

The valleys under study start from the water divide between the Himalayan south side and the Tibetan drainage system. There is a well-developed drainage pattern in southern Tibet running along shallow valleys. The area is thus not a plateau *sensu stricto*, but rather a slightly dissected upland. If covered by an ice sheet, its outlet glaciers must have crossed transfluence

Flood and Megaflood Processes and Deposits: Recent and Ancient Examples. Edited by I. Peter Martini, Victor R. Baker and Guillermina Garzón ISBN: 978-0-632-06404-5

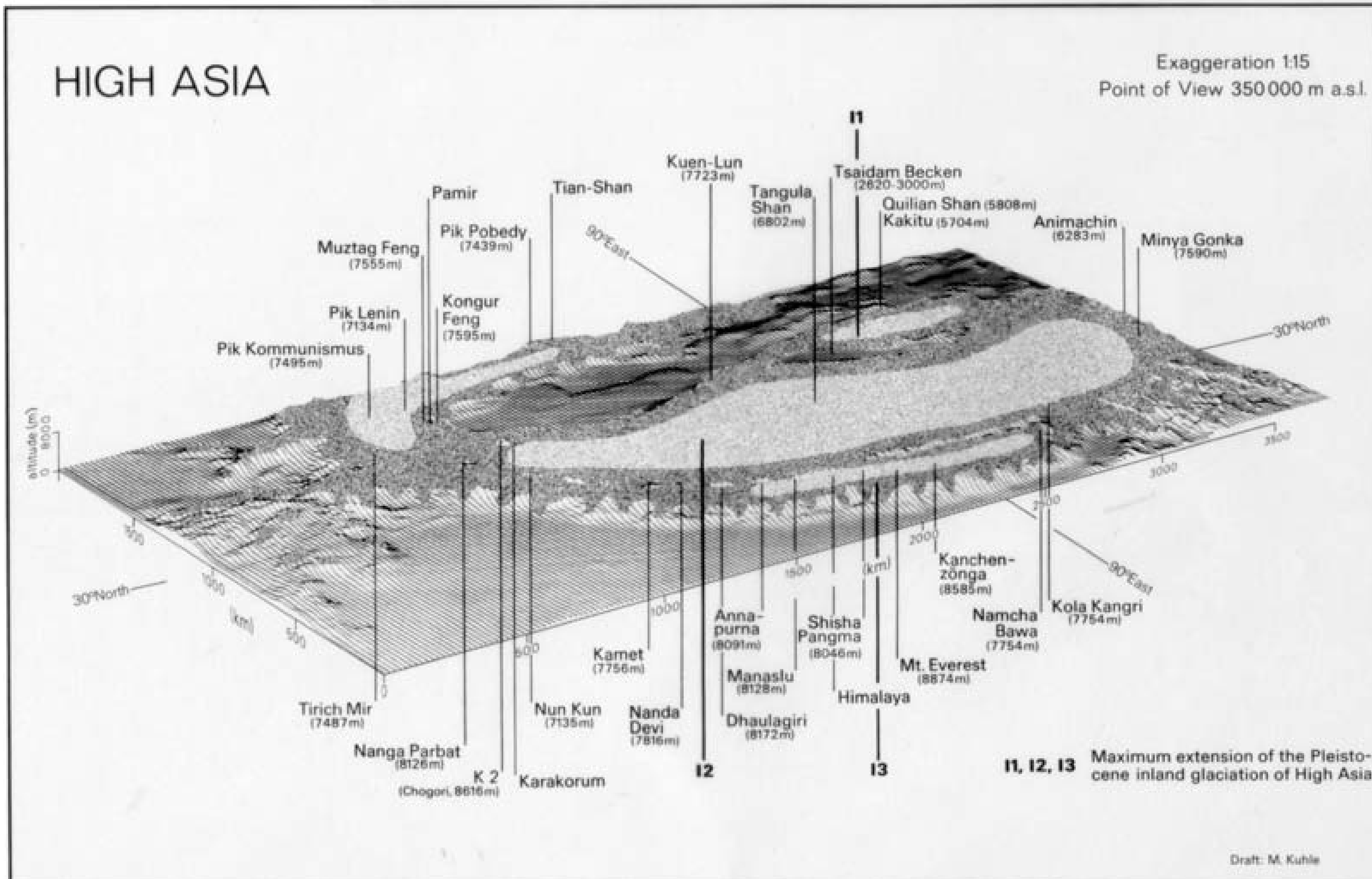

Fig. 1. The LGM Tibetan ice sheet had an extension of more than 2.4 million km^2. The three centres of glaciation I1, I2 and I3 were separated from each other by the Tsaidam lake and the Tsangpo valley.

passes, blocking pre-existing drainage systems. As a consequence, ice-dammed lakes would have formed. Release of the dammed meltwater would have resulted in major floods that swept down steep valleys.

FIELD EVIDENCE

Two valleys between Shisha Pangma and Mount Everest were chosen for detailed investigation (Fig. 1). One is the Bo Chu (Bote Chu; Pa Ho on the Defense Mapping Agency Aerospace Center (1978) Operational Navigational Chart H9, scale 1 : 1 000 000, H91978) that crosses the main ridge of the Himalayas between Shisha Pangma and Chomolung Kang from Yagru Xiong La (Fig. 2, location 25) to Dram (Zhangmu) (Fig. 2, location 1). The second valley is the Kyetrak Chu between Chomolung Kang and Cho Oyu. It rises southward from the settlement of Ting-Jih (Fig. 2, above location 39) in a southerly direction to Nangpa La (location 31). Its axis continues south of this pass in Nangpo Dzangpo to the settlement of Thame on the Himalayan south slope. Both valleys cross local water divides on their way out of southern Tibet. They lead out from the Tibetan dissected upland, cross the Himalayas and slope steeply down to the frontal lowland (Fig. 2). One difference between them is that at the moment, the Kyetrak Valley is still partly glaciated whereas the Bo Chu is not. The present-day Kyetrak glacier flows from the Himalayas (Cho Oyu 8201 m) for 10 km in a northerly direction into Tibet (Fig. 2, locations 31 and 32).

BO CHU (ALSO BOTE CHU, PA HO OR SUN KOSI KHOLA) VALLEY

Lower Bo Chu valley

Earlier investigations have shown that the lower Bo Chu valley was formerly glaciated, and that a Pleistocene Bo Chu glacier reached down to *c*. 700–900 m a.s.l. (Kuhle, 1988).

Further up-valley, where the Bo Chu crosses the main Himalayan ridge, moraine remnants have been largely eroded by monsoon-induced torrents and associated mudflows. One such mudflow (July 1996) brought down morainic material originating from the westerly tributary valley of Jangbo Khola. The mudflow completely destroyed the settlement of Lartza (1300 m a.s.l.) at the bottom of the Bo Chu and 45 people were killed. Granite and augen-gneiss boulders, $3 \times 4 \times 5$ m in size, were incorporated into the mudflow, which derived from the distant massifs of the Shisha Pangma and Rolwaling Himal; that is from the upper catchment area of the Bo Chu. The largest moraine boulder transported by mudflow in this valley section of the Bo Chu is $6.7 \times 11.3 \times 17.7$ m in size. It lies 6 km downstream from the settlement of Kodari, a few metres above the valley bottom. Xu Daoming (1988) refers to this boulder as a displaced moraine component. According to his investigations, the boulder was transported from a locality near locations 3–5 (Fig. 2) by two mudflows caused by outbursts of moraine lakes in the Rolwaling Massif in 1964 and 1981.

Evidence of glaciation in the Bo Chu valley consists mainly of polished bedrock along its flanks between Lartza and Dram (also Khasa or Zhangmu). Particularly impressive is the extensive polishing opposite Dram, reaching up to 400 m above the valley bottom (Fig. 2, location 1). This polishing is well developed on the resistant metamorphic rocks of the Khumbu and Kathmandu covers (KU 1–3; KN 2 and 3, according to Hagen, 1969). This indicates the presence of a thick Pleistocene glacier, with a surface reaching up to about 2400 m a.s.l. However, this Pleistocene valley glaciation of the lower Bo Chu could have arisen just from the Fuqu Chu, originating from the highest glacial catchment area of the Bo Chu, the 8046 m high Shisha Pangma (Fig. 2).

Middle Bo Chu valley

The middle 23-km-long section of the main Bo Chu valley is located between two large western tributary valleys originating from the Shisha Pangma massif. The southern valley is the Fuqu Chu (Fig. 2, location 7), whereas the northern one has no official name (location 20).

Directly opposite the junction with the Fuqu Chu, the surface of the eastern Bo Chu main valley slope is covered partly by ground moraine several metres thick, containing erratic boulders (Fig. 2, location 8). Where this cover is missing, polish on the relatively rapidly weathering rock faces is exposed. This indicates the former presence of a valley glacier with a thickness of at least 500 m, which is further proven by the glacigenic rounding of the valley flank up to its culmination. At the top there is a glacigenic transfluence pass (Fig. 2, location 9).

Another well-preserved example of rock polishing is found on the eastern flank of the Bo Chu valley, between 3670 and 3800 m a.s.l. (location 10, Fig. 2).

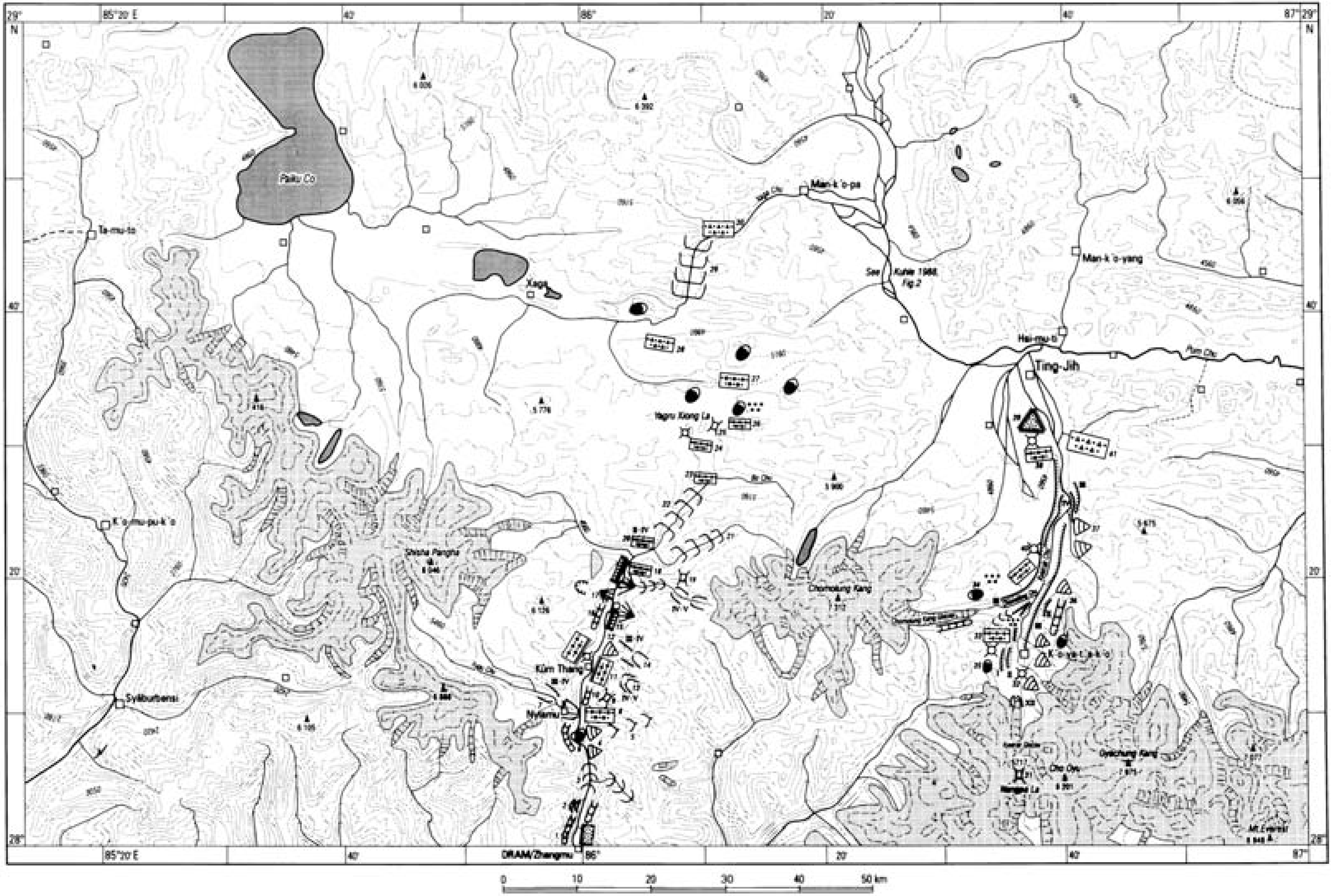

Paiku Co
Ta-mu-to
Xaga
Man-k'o-pa
See Kuhle 1988, Fig.2
Man-k'o-yang
Hai-mu-ti
Ting-Jih
Yagru Xiong La
K'o-mu-pu-k'o
Shisha Pangma
Chomolung Kang
Kûm Thang
Nyalamu
Syilburbensi
Cho Oyu
Gyachung Kang
Mt. Everest
Nangpa La
DRAM/Zhangmu
85°20' E
86°
87°
29°
28°
N
0
10
20
30
40
50 km

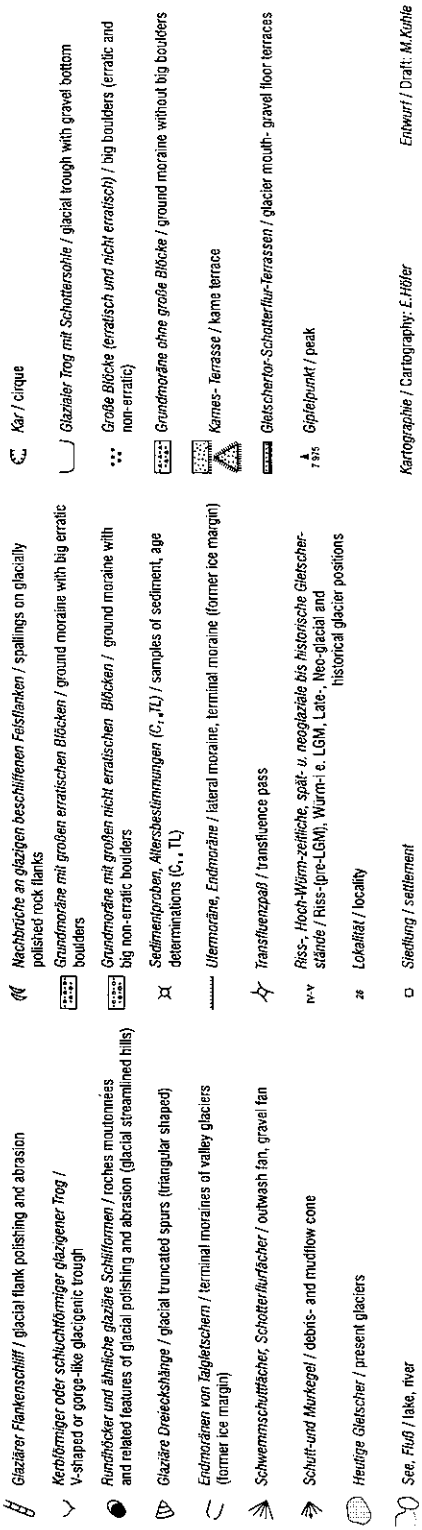

Fig. 2. Quaternary geological and glaciogeomorphological map of southern Tibet with Shisha Pangma and Cho Oyu massifs (for location see I3 in Fig. 1).

On the main valley floor between the settlements of Nylamu and Kum Thang (Milaripas Monastery), a diamicton has been observed, containing isolated far-transported granite and augen-gneiss boulders, sometimes up to a metre in length (3700–4120 m a.s.l., 28°15′20″N, 86°00′30″E; Fig. 2, location 11). Their lithology suggests that they originate from southern Tibet (Kuhle, 1988). The diamicton is interpreted as glaciofluvially altered morainic material. The grain-size distribution is bimodal with a clay mode suggesting a moraine character to the matrix, and the large medium grained sand mode (41%) indicating fluvial reworking of the diamicton (Fig. 3). The low (0.18%) $CaCO_3$ content shows that local carbonate bedrock incorporation was minimal. Morphoscopic analysis of 200 quartz grains shows a predominance of crushed/freshly weathered material (62.5%), typical of ground moraine (Fig. 4, column 21.8.96/1). The remaining (37.5%) quartz grains probably represent the influence of Late-glacial glaciofluvial and Holocene cold-arid processes.

Fresh end moraines in the side (tributary) valleys are evidence of Late-glacial to Neoglacial glaciers. Two of the end moraines reach down to 4100 m a.s.l. (Fig. 2, location 13). A valley glacier descending from a presently unglaciated massif south-west of Chomolung Kang formed them. The inferred ELA depressions of at least 300 m to maximally 700 m suggest an age of *c.* 5500–13 500 yr BP (Kuhle, 1997). Six kilometres to the north there is a junction with another parallel side valley with lateral and end moraines at an altitude of 4100 and 4280 m a.s.l. (Fig. 2, location 14), suggesting an age of *c.* 14 250–13 000 yr BP (Kuhle, 1997). In another tributary valley further north, two

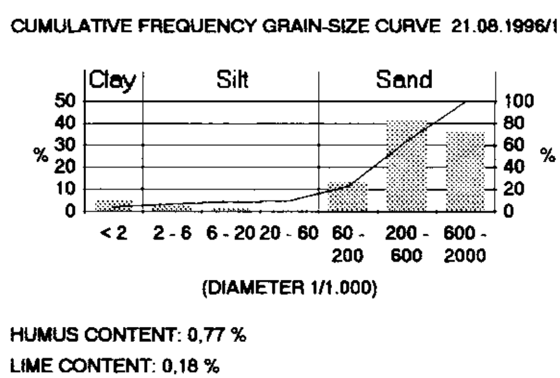

Fig. 3. Typical grain-size distribution of diamictons from Bo Chu and Kyetrak valleys (diamicton, 0.15 m below surface, at 5060 m a.s.l., Yagru Xiong La plateau area (Fig. 2, location 25)).

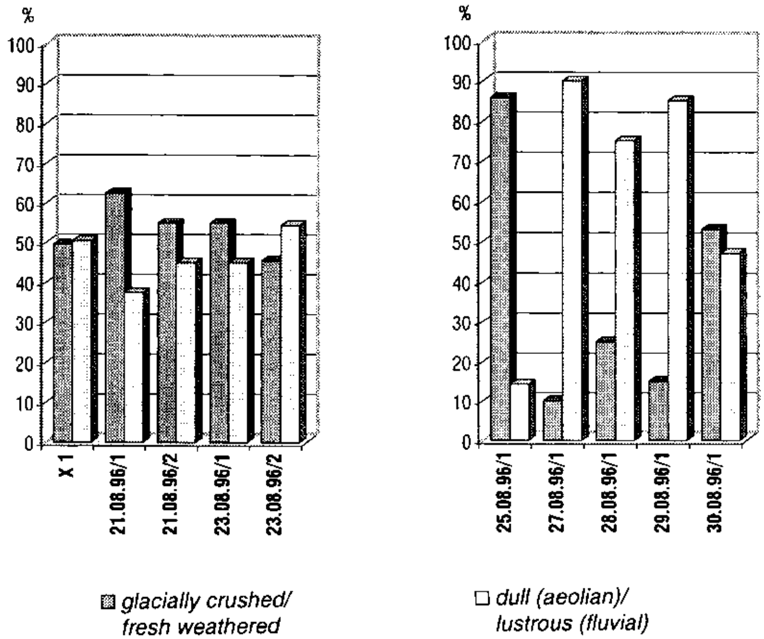

Fig. 4. Morphometric quartz grain analysis of 10 representative samples from southern Tibet. (horizontal scale = date/sample number; vertical scale = number of quartz grains counted in the size range 0.2–0.6 mm).

end-moraine lobes from Late-glacial to Holocene (Neoglacial) periods have been mapped (Fig. 2, IV–V below location 19). The upper catchment area of this west-exposed valley belongs to the Chomolung Kang (7312 m); because of its considerable altitude it is still glaciated.

Further up-valley, a large tributary valley joins the Bo Chu from the west (Fig. 2, location 20). It runs down from the east side of the Shisha Pangma massif, which is still glaciated. At the junction with this side valley, at 4120 m a.s.l, the main Bo Chu valley bottom is covered by a diamicton, probably tens of metres thick. The diamicton contains augen-gneiss boulders about 1 m in diameter. The source rock of these erratics crops out 15–20 km to the west on the Shisha Pangma massif (Kuhle, 1988).

Upper Bo Chu and adjoining parts of the Tibetan Plateau

The upper Bo Chu valley has a typical glacigenic box cross-profile (No. 22) over a distance of more than 20 km. It developed from a broad glacial U-shaped valley covered by till and gravel accumulation at the valley floor. At the upper end of the Bo Chu, a diamicton up to tens of metres thick covers the western slope (28°28′N, 86°09′50″E, 4310 m a.s.l., Fig. 2, location 23), overlying smoothly polished sedimentary bedrock. Exposed bedrock surfaces show parallel striations. Where the moraine mantle was partially eroded laterally by the Sun Kosi-Khola (river), rill erosion and associated earth pillars have developed. The diamicton reaches up to *c.* 400 m above the present valley floor on both sides of the valley. This suggests a minimum altitude of the former glacial ice level of *c.* 4700 m a.s.l. Polishing of the valley flanks, however, is found all the way up to the top of the slopes. This site is right at the edge of the Tibetan plateau. Ice more than 400 m thick in the upper reaches of the Bo Chu (location 23) suggests that it may have been an outlet glacier of the Tibetan ice sheet.

Ice outflow from Tibet can be further verified all along the edge of the plateau. A diamicton was found, containing granite erratics derived from northern source areas (location 24). It overlies sedimentary bedrock. Diamicton interpreted as ground moraine spreads to altitudes far above 5000 m. It uniformly covers the Yagru Xiong La (5060 m, location 25) and also the neighbouring kilometre-wide highland areas of southern Tibet. It contains rounded, facetted, polymictic, mostly erratic boulders that float in a matrix of fine material. The bimodal grain-size distribution suggests a morainic origin of this diamicton, as does morphoscopic quartz grain analysis (Fig. 4, column 21.8.96/2). Two or three kilometres beyond that elevation, streamlined hills are found, carved into the sedimentary bedrock at 4800 m a.s.l. (Fig. 2, above location 26). They are covered by ground moraine with erratic granite boulders (No. 26). Farther to the north, roches moutonnées and large streamlined erosional landforms provide further evidence of former glacial activity. These are the source areas for:

1 the surrounding local moraine (location 27);

2 ground moraine with erratics (location 26) transported in a southerly direction upwards towards the pass (location 25);

3 isolated large erratic granite boulders without moraine cover (above location 26);

4 far-travelled morainic material transported over the Yagru Xiong La into the Bo Chu (location 23).

The unconsolidated sedimentary deposits and the erosive landforms described above are evidence of a complete covering of this part of southern Tibet by a Pleistocene glacier.

Farther north, some 15–18 km north of the local watershed between the upper Bo Chu and a few shallow valleys that run north towards Xaga Chu and into Tibet (location 28), the gentle slopes (8–15°) down to Xaga Chu are completely covered by diamicton one to several metres thick over sedimentary rock substrate. It typically consists of a fine matrix containing isolated, rounded, facetted, polymictic boulders (including granite erratics) that are 10 cm up to a maximum of 30 cm in diameter. The surface of the diamicton is conspicuously shapeless and smooth. It covers the slopes right up to towering hills over 5000 m high, south-east of Xaga Chu, and sometimes it covers even their culminations.

Interpretation

The morphology and sediment cover of the southern edge of the Tibetan high plateau and the upper Bo Chu suggest that an ice sheet completely covered the plateau. Its thickness was sufficient to fill large valleys north of the water divide, such as the Xaga Chu. Large-scale ground moraine cover and the distribution of erratic granite boulders from source areas north of the water divide beyond the Yagru Xiong La, extending in a southerly direction down towards the Bo Chu, are evidence of a prehistoric ice flow from Tibet. Thus, a Bo Chu outlet glacier (Fig. 1, east of Shisha Pangma) arose from the south Tibetan upland ice (Fig. 1, I3). It was channelled through the Bo Chu and drained off through the Himalayan breakthrough valley. In the Himalayas, the Chomolung Kang, the Shisha Pangma and the Rolwaling Himal fed this glacier.

The glaciation history of the Bo Chu valley, including possible development of ice-dammed lakes and their outbursts, can be reconstructed by mapping the ascent of the snowline and associated deglaciation stages from the LGM up to the late Late-glacial. During deglaciation a series of ice-dammed lake outbursts took place. Such floods rushed in a few hours through the Himalayan gorges and dropped 3–4 km in altitude over a distance of no more than 60–80 km. Their geomorphological erosive effect in the highlands and the sedimentology of their down-valley deposits has not been properly evaluated yet.

KYETRAK VALLEY AREA

The Kyetrak Chu located to the north-north-west of the Cho Oyu is another key area for the understanding of the history of glaciation and related events of the region (Fig. 2). Its present-day slope direction is not of much importance, but rather the alignment of its axis is. This area runs north–south through the Himalayas. It ascends first from the settlement of Ting-Jih to the Nangpa La pass (or Khumbu La; Fig. 2, locations 39–31) at an altitude of 5717 m. On the other side of the Himalayan water divide the axis continues along the southern Himalayan slopes (Fig. 2, south of location 31). There, on the other side of the pass, the valley of Nangpo Dzango and, further down, the Dudh Kosi valley both run down through the Khumbu Himal. The glacier terminus probably reached down at least to 1580 m a.s.l. into the valley section of Surke in the Dudh Kosi (Heuberger, 1956, 1974, 1986; Kuhle, 1985, 1987). There, where the two tributaries, the Nangpo Dzango glacier from Nangpa La (location 31) and the Imja Drangka glacier, merged to form the Dudh Kosi glacier (Khumbu glacier) (27°53′N, 86°44′E), the ice apparently still had a thickness of 600–850 m (Kuhle, 1987).

The present-day Kyetrak glacier is 10 km long and flows west of the Cho Oyu (Fig. 5, location 1) from the 5717 m high Nangpa La (Figs 2 (location 31) & 5), in a northerly direction along the bottom of the Kyetrak valley (Fig. 5) down to a level of 4800 m a.s.l. (Fig. 2, below location 32). Investigations of the western valley flank have shown that the sedimentary bedrock (Fig. 5) is covered by diamicton. At 5250 m (Fig. 2, location 33), approximately 600 m above the valley floor (Fig. 5, –5 on the left), diamicton was identified and analysed from an earth pillar located on a mountain ridge. The topographic position of the sample and the bimodal grain-size distribution with a clay fraction

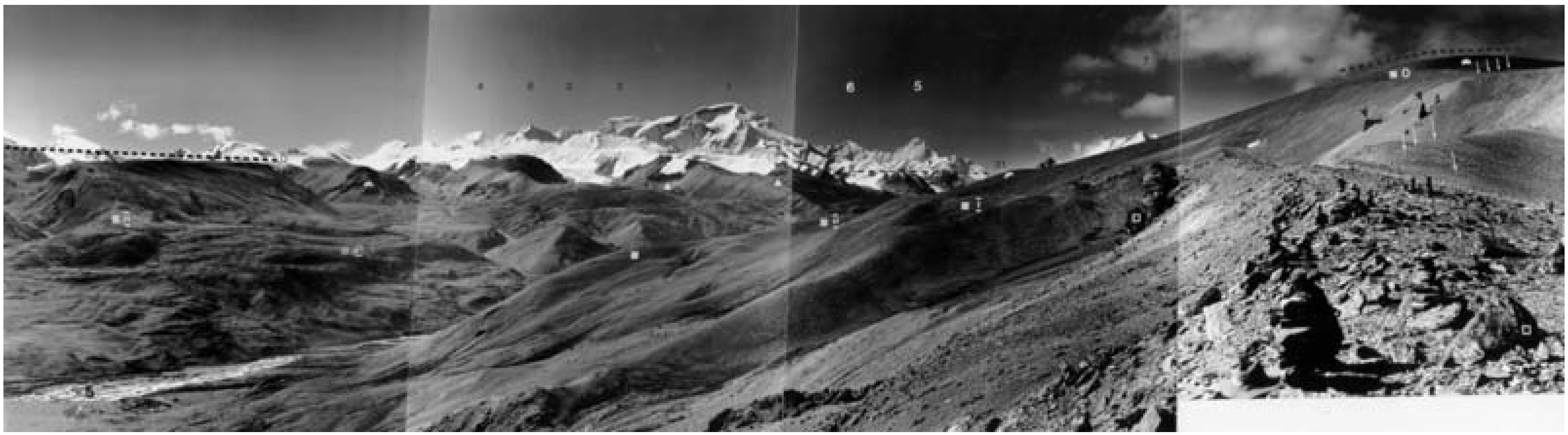

Fig. 5. View from 5250 m a.s.l. across the spur ridge between Kyetrak valley (left-hand) and Chomolung Chu (right-hand) valley slope; named in accordance with information from Tibetan yak nomads, August 1996); right-hand of location 33, Fig. 2. In the background is the Himalaya main ridge with 1 = Cho Oyu, 8201 m; 2 = Gyachung Kang, 7975 m; 3 = Nuptse, 7879 m; 4 = Changtse, 7580 m; 5 = Cho Aui, 7352 m; 6 = 7296 m peak; 7 = 6907 m peak; 8 =Tongqiang peak, 6901 m; (■ = bedrock shists strewn with erratic granite boulders (vertical arrows)). Further up, the erratics are embedded in the ground moraine matrix (■ 0); (Fig. 4 diagram 25.08.96/1);▼ = earth pillars carved from Last Glacial Maximum (LGM) to Late-glacial moraine material (Stadia 0 to I; possibly even younger?). The erratic granite boulders (■ 0) reach up to a height of 5500–5600 m and thus *c.* 700 m above the valley bottom of the Kyetrak Chu (on the left –5). They are the highest accumulative traces of glacial activity in the area. The rounded and polished mountain ridges (- - -0, 0- - -) mark the minimum height of the former ice surface of the Kyetrak Chu outlet glacier (Fig. 3). (■ I, ■II, ■III) are remnants of Late-glacial deposits.▼ = earth pillars in morainic material.; ☗ = mountain ridges rounded by glacial scouring.

(10%) mode suggest a morainic origin. This is confirmed by the predominance (85.7%) in the sample of glacially crushed/freshly weathered quartz grains typical of glacial till (Fig. 4, column 25.8.96/1).

Granite erratics are frequently found, either contained in the diamicton or lying isolated on the sedimentary bedrock (Fig. 5). Boulders and associated diamicton were mapped on the west flank of the Kyetrak Chu over distances of kilometres on slopes, valley shoulders and mountain ridges, covering reddish siltstone and sandstone as well as light-coloured limestone bedrocks (Fig. 2, on the right and diagonally right above location 33; between locations 34 and 40). Their highest occurrence is at about 700 m above the valley floor. Thus, the upper level of the ice of the prehistoric Kyetrak valley glacier reached an altitude of 5500 m a.s.l. The mountain ridges and cupolas above the west flank of the Kyetrak valley are devoid of moraine and/or erratic boulders, but are polished up to altitudes of 5700–5900 m (Figs 2 (locations 34 and 35) & 5). On the opposite east flank of the Kyetrak valley, polished rock has been preserved up to the same altitude (5700–5900 m a.s.l.).

The Kyetrak valley therefore was filled by a glacier at least 1000 m thick during the glacial maximum, the surface of which was inclined opposite to the slope of the valley floor, draining towards the south. It crossed the Himalayan water divide between the Cho Oyu massif and Peak 7 (Fig. 5, between numbers 1, 6, 5 and 7).

It is assumed that during ice build-up, the northward drainage of a small interglacial Kyetrak valley glacier would have been blocked by the formation of an inland ice sheet on the Tibetan plateau to the north (Fig. 1, I3). As a result of continued accumulation the ice would have crossed the col, turning the Kyetrak flow towards the south. During deglaciation of southern Tibet, the drainage of the Kyetrak glacier would have been reversed again. This reverse development from the glacial to the interglacial ice drainage is documented by the moraine ledges on both valley flanks (Fig. 2, I to IV between locations 32 and 38). It is also reflected in till composition. Whereas the oldest till, presumably deposited at the LGM or the early Late-glacial period, contains 17.32% carbonate, the carbonate content in younger tills decreases to 0.15–6.99%.

Six kilometres north of the Late-glacial end moraines (Fig. 2, III to the right of location 38), there is a kame on top of the ground moraine surface of Ting-Jih (location 39, 38°31′N, 86°34′E; basic altitude 4220 m a.s.l.). It stretches from north to south for about 1 km and has a rhombic outline. It is 40 m high and consists of quasi-horizontally layered sand and gravel. It is several kilometres away from the east and west valley flanks of the Kyetrak Chu (Fig. 2, location 39) and is geomorphologically isolated. This kame is interpreted as a sediment body accumulated in a huge moulin (englacial tunnel) in the middle of the outlet glacier.

East of the settlement of Ting-Jih, in the Pum Chu valley (Fig. 2), no clear indication was found of any former glaciation. Therefore an ice-free valley region stretching for a few tens of kilometres towards the east is assumed. This valley contained an ice-dammed lake. The development of the Pum Chu lake is depicted in Fig. 6a–c). During deglaciation, the lake, which was much larger than it was during the LGM (Fig. 6e), broke through the ice barrier and flowed 4000 m to the south-east through the Arun valley into the southern Himalayan foreland (Kuhle, 1988).

CONCLUSIONS

Field evidence suggests that glaciers occupied both the Bo Chu and the Kyetrak Chu valleys during the LGM. The glaciers were 75 and 100 km long and flowed down to about 900–700 m and 1500 m a.s.l., respectively. Thereby, they reached the south Himalayan foothills. The two ice streams originated 30 and 60 km, respectively, north of the Himalayas in Tibet. There they emerged from a more than 1000-m-thick ice sheet at an altitude of 4200–5200 m (Fig. 1, I3 between Shisha Pangma and Mount Everest). The glaciers crossed cols at 5060 m (Yagru Xiong La: Fig. 2, location 25) and at approximately 5300 m (Nangpa rock threshold nowadays called Nangpa La: Fig. 2, location 31). They were therefore south Tibetan outlet glaciers that followed the Bo Chu and the Kyetrak Chu valleys and were joined in their middle sections by local Himalayan glaciers.

The existence of inland ice during the LGM is connected with a snowline (ELA) depression of some 1200–1500 m (Kuhle, 1982, 1988, 1998) (Fig. 1, I3). Figure 7a (ELA = –1200) shows the minimum extent of the corresponding glacier feeding areas of the Tibetan ice sheet. The white surfaces indicate the maximum extent of the intervening ablation areas.

Climatic amelioration in the Late-glacial caused an ELA rise by 500–600 m between *c*. 20 and 13 ka (Fig. 7b, ELA = –600). Correspondingly, major parts of the Tibetan plateau were completely deglaciated. Meltwater was dammed on the down-wasting ice and in ice-free areas forming numerous ice-dammed lakes

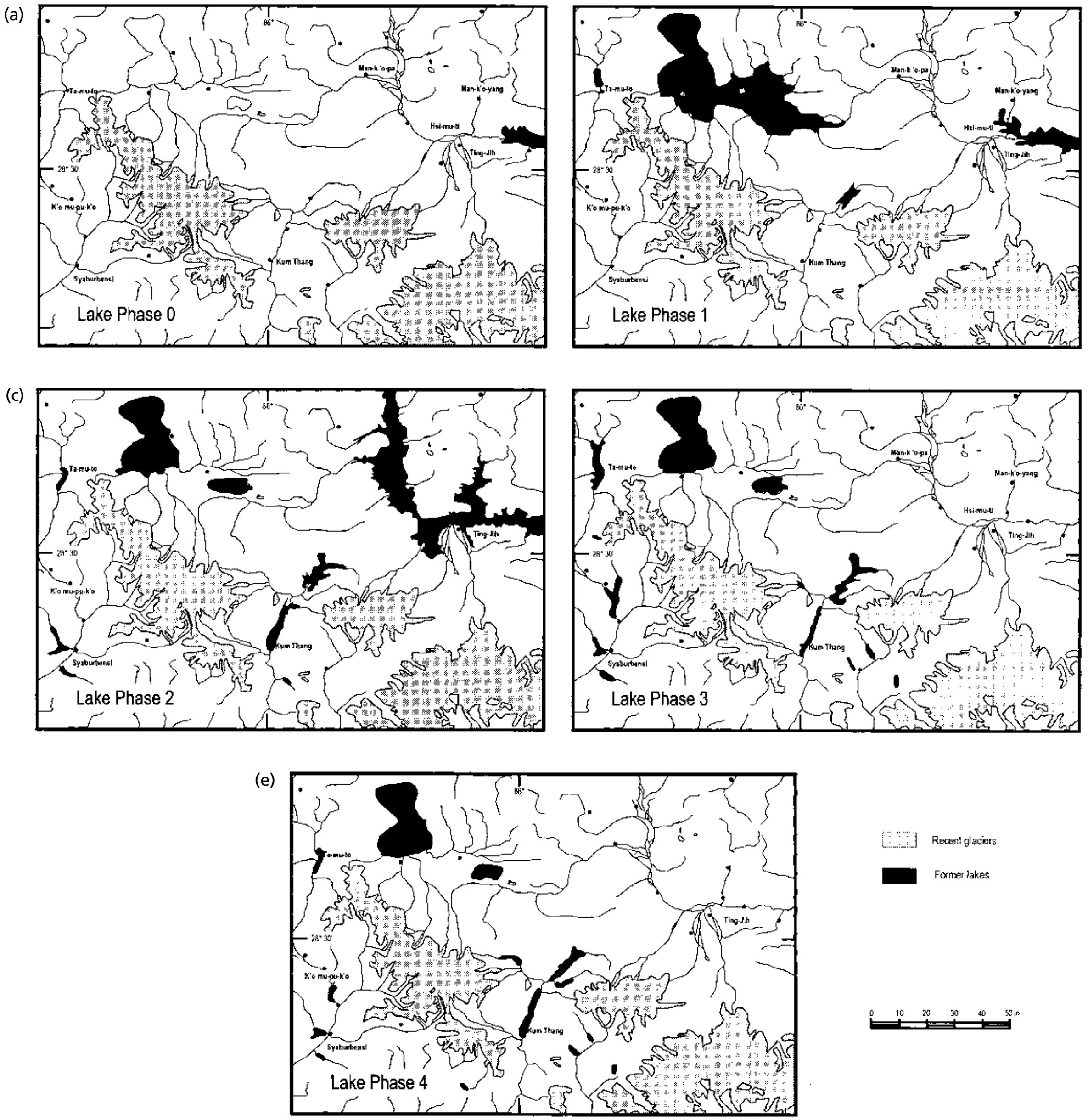

Fig. 6. (a–e) Distribution and build-up of the Last Glacial Maximum (LGM) to Late-glacial ice-dammed lakes in the investigation area. (a) During the LGM (Phase 0), more than 20 ka, there existed a maximum equilibrium line altitude (ELA) depression of at least 1200 m against the relief. From this resulted a nearly complete ice cover with the exception of the Pum Chu ice-dammed lake. (b) During the early Late-glacial (Phase 1) about 17–15 ka, the ELA depression decreased to *c.* 1100 m, so that further ice-dammed lakes were created. (c) During the Late-glacial Phase 2, 15 000–14 250 yr BP, the ELA rose to an ELA depression about 1000 m. The inland ice melted down further and the ice-dammed lake landscape experienced various modifications. (d & e) Modification of ice-dammed lakes as a result of the rising of the ELA to ELA depressions of *c.* 800–900 m in the Late-glacial Phase 3 and of *c.* 700 m in the Late-glacial Phase 4 between *c.* 14 250 and older than 12 870 yr BP. During this time, for instance, the vast Pum Chu ice-dammed lake discharged in a south-east direction through the Arun valley (just outside the map) on to the Himalayan southern slope.

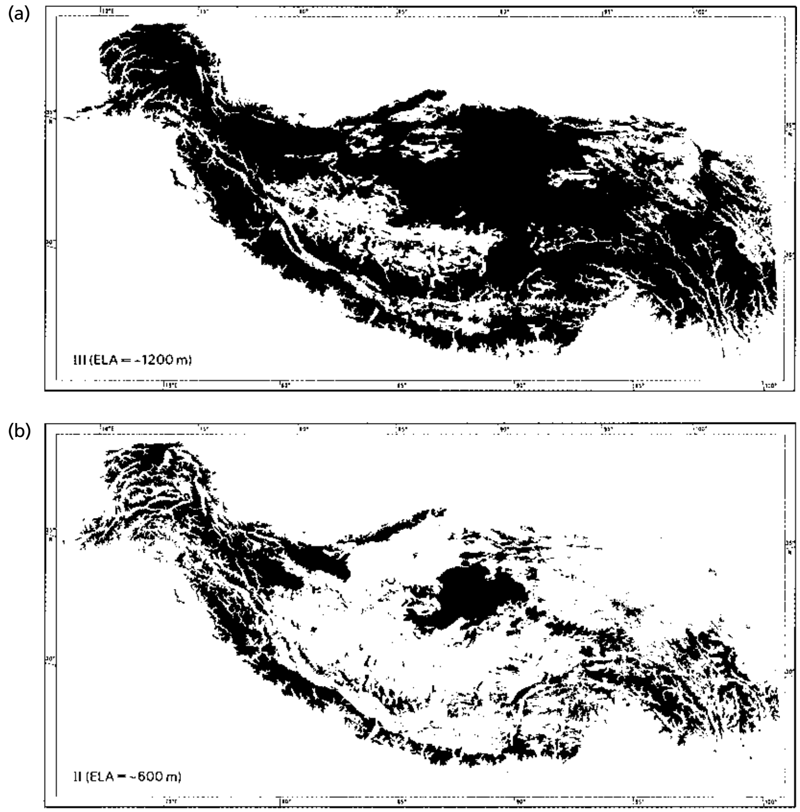

Fig. 7. Simulated effect of changing snowline (equilibrium line altitude—ELA). (a) The ELA lowered 1200 m (*c.* 50–20 ka) from present elevation: most of the Tibetan plateau would be covered by ice. (b) The ELA 600 m (*c.* 17–15 ka) lower than the present: only the highest plateau areas (approximately half of Tibet) would be covered by ice.

of various sizes, up to several hundred metres deep. One of these lakes was the Pum Chu ice-dammed lake mentioned above. The occurrence of further, similar lakes in Tibet is documented by varved clay deposits dovetailed with moraine deposits (Fig. 6a–e; Kuhle, 1988, 1991). It was only during the late Late-glacial, when the ELA rose even further, that the outlet glacier tongues completely melted in the Himalayan cross-valleys, and the glacial lakes eventually drained, at times catastrophically, generating megafloods potentially of enormous dimensions. These floods probably have destroyed or at least strongly remoulded most of the depositional (sedimentary) glacigenic landforms in the valleys, as well as part of the glacigenic erosional features. The megafloods running down from elevations of over 4000 to *c.* 3000 m a.s.l. transported vast amounts of glacial morainic and glaciofluvial sediments down into the Himalayas foreland and redeposited them at altitudes lower than 1000 m a.s.l. These flood deposits await detailed sedimentological analyses.

ACKNOWLEDGEMENTS

The author wishes to thank both Professor Peter Martini for his scientific and linguistic advice during the writing of the manuscript, and Dr Jürgen Ehlers for the comprehensive reworking of the text as well as for the cartographic conversion of Fig. 6a–e. Thanks also are given to E. Höfer for cartography of Fig. 2, O.A. Bauer for sample laboratory analysis, H. Gieseler for plot and calculation program, R. Staschel for area calculations, and E. Höfer and A. Flemnitz for cartography of Fig. 6. All photographs are by M. Kuhle.

REFERENCES

Hagen, T. (1969) Report on the Geological Survey of Nepal. *Denkschr. Schweiz. Naturforschen. Ges.* **86**(I), 1–185 & **86**(II), 1–159.

Heuberger, H. (1956) Beobachtungen über die heutige und eiszeitliche Vergletscherung in Ostnepal. *Z. Gletscherkd. Glazialgeol.* **3**, 349–364.

HEUBERGER, H. (1974) Alpine Quaternary glaciation. In: *Alpine and Arctic Environments* (Eds Ives, J. & Berry, R.G.), pp. 319–338. Methuen, London.

HEUBERGER, H. (1986) Untersuchungen über die eiszeitliche Vergletscherung des Mt. Everest-Gebietes, Südseite, Nepal. *Göttinger Geogr. Abh.* **81**, 29–30.

KUHLE, M. (1982) Der Dhaulagiri- und Annapurna-Himalaya. Ein Beitrag zur Geomorphologie extremer Hochgebirge. *Z Geomorphol. Suppl.* **41**, Bd. I (Text): 1–229; Bd. II (Abb.): 1–183 und Geomorph. Karte 1:85 000.

KUHLE, M. (1985) Ein subtropisches Inlandeis als Eiszeitauslöser. Südtibet- und Mt. Everest-Expedition 1984. *Georgia Augusta, Nachrichten Univ. Göttingen* **42**, 35–51.

KUHLE, M. (1987) Subtropical mountain- and highland-glaciation as Ice Age triggers and the waning of the glacial periods in the Pleistocene. *Geojournal* **14**, 393–421.

KUHLE, M. (1988) Geomorphological findings on the build-up of Pleistocene glaciation in southern Tibet, and on the problem of inland ice. Results of the Shisha Pangma and Mt. Everest Expedition 1984. *Geojournal* **17**, 457–513.

KUHLE, M. (1991) Observations supporting the Pleistocene inland glaciation of High Asia. *Geojournal* **25**, 133–233.

KUHLE, M. (1997) New findings concerning the Ice Age (Last Glacial Maximum) glacier cover of the East-Pamir, of the Nanga Parbat up to the Central Himalaya and of Tibet, as well as the age of the Tibetan inland ice. *Geojournal* **42**, 87–257.

KUHLE, M. (1998) Reconstruction of the 2.4 million km^2 Late Pleistocene ice sheet on the Tibetan Plateau and its impact on the global climate. *Quat. Int.* **45/46**, 71–108. (Erratum **47/48**, 173–182 (1998) included.)

XU DAOMING (1998) Characteristics of debris flow caused by outburst of glacial lakes on the Boqu River Xizang, China. In: *Tibet and High Asia. Results of Sino-German Joint Expedition* (Eds Kuhle, M. & Wenjing, W.). *Geojournal* **17**(4), 569–580.

Index

Page numbers in *italic* refer to figures, those in **bold** refer to tables.

Flood and Megaflood Processes and Deposits: Recent and Ancient Examples. Edited by I. Peter Martini, Victor R. Baker and Guillermina Garzón © 2002 International Association of Sedimentologists. ISBN: 978-0-632-06404-5